

Institut für Theoretische Physik
Fakultät Mathematik und Naturwissenschaften
Technische Universität Dresden

Microscopic Chaos, Fractals, and Transport in Nonequilibrium Steady States

**Mikroskopisches Chaos, Fraktale und Transport
in stationären Nichtgleichgewichtszuständen**

Habilitationsschrift
zur Erlangung des akademischen Grades
Dr. rer. nat. habil.

vorgelegt von
Rainer Klages
Max-Planck-Institut
für Physik komplexer Systeme
geboren am 21. März 1966 in Berlin

Dresden 2004



Eingereicht am 10. November 2003

1. Gutachter: _____

2. Gutachter: _____

3. Gutachter: _____

Contents

Abstract	7
1 *Introduction and outline	9
1.1 Hamiltonian dynamical systems approach to nonequilibrium steady states . .	9
1.2 Thermostated dynamical systems approach to nonequilibrium steady states .	12
1.3 The red thread through this thesis	15
I Fractal transport coefficients	19
2 *Simple maps with fractal diffusion coefficients	25
2.1 A simple model for deterministic diffusion	25
2.2 A fractal parameter-dependent diffusion coefficient	28
2.3 Summary	32
3 Negative and nonlinear response in deterministic drift-diffusion processes	33
3.1 A simple chaotic drift-diffusion model: mathematical definition	34
3.2 ⁺ Calculating deterministic drift and diffusion coefficients	36
3.2.1 Groeneveld's twisted eigenstate method	36
3.2.2 Transition matrix methods	40
3.2.3 Numerical comparison of the different methods	41
3.3 The phase diagram of this two-parameter model	42
3.4 *Summary	49
4 Chaotic and fractal properties of deterministic reaction-diffusion processes ...	51
4.1 A reactive-diffusive multibaker map	51
4.1.1 Deterministic models of reaction-diffusion processes	52
4.1.2 The Frobenius-Perron operator and quasiperiodic boundary conditions	54
4.2 Diffusive dynamics of the multibaker	56
4.2.1 ⁺ Diffusive modes of the dyadic multibaker	56
4.2.2 Diffusion coefficients in parameter-dependent models	57
4.3 Reactive dynamics of the multibaker	62
4.3.1 ⁺ Reactive modes of the dyadic multibaker	62
4.3.2 Reaction rates in the parameter-dependent multibaker	66
4.4 *Summary	71

5	Fractal structures of normal and anomalous diffusion	73
5.1	Fractality of deterministic diffusion in the climbing sine map	73
5.2	+Deterministic diffusion, bifurcations, and periodic windows	78
5.3	*Summary	79
6	Diffusion in randomly perturbed dynamical systems	81
6.1	Suppression and enhancement of diffusion in disordered dynamical systems .	81
6.2	From deterministic to stochastic diffusion in noisy dynamical systems	86
6.3	*Summary	92
7	From simple deterministic diffusive maps to the periodic Lorentz gas	93
7.1	Correlated random walks in one-dimensional maps on the line	93
7.2	Correlated random walks in the periodic Lorentz gas	99
7.3	*Summary	103
8	Deterministic diffusion in the flower-shaped billiard	105
8.1	Why a flower-shaped billiard?	105
8.2	Curvature dependence of the diffusion coefficient	108
8.3	+Machta-Zwanzig approximation for diffusion coefficients	109
8.4	+Further corrections of the Machta-Zwanzig approximation	110
8.5	The Green-Kubo formula approach	114
8.6	*Summary	115
9	Irregular diffusion in the bouncing ball billiard	117
9.1	Phase locking and diffusion in the bouncing ball billiard	117
9.2	+Correlated random walk approximations of the diffusion coefficient	120
9.3	*Summary	123
II	Chaos and transport in thermostated dynamical systems	125
10	Motivation: coupling a system to a thermal reservoir	131
10.1	*Why thermostats?	131
10.2	*Stochastic modeling of thermal reservoirs: the Langevin equation	133
10.3	Equilibrium velocity distribution functions for subsystem and reservoir	137
10.4	The periodic Lorentz gas	142
10.5	*Summary	145
11	*The Gaussian thermostat	147
11.1	Construction of the Gaussian thermostat	147
11.2	Chaos and transport for Gaussian thermostated dynamical systems	150
11.2.1	Phase space contraction and entropy production	150
11.2.2	Lyapunov exponents and transport coefficients	151
11.2.3	Fractal attractors characterizing nonequilibrium steady states	153
11.2.4	Field-dependent electrical conductivity	156
11.3	Summary	160

12 The Nosé-Hoover thermostat	161
12.1 The Liouville equation for dissipative dynamical systems	161
12.2 Construction of the Nosé-Hoover thermostat	163
12.2.1 Heuristic derivation	163
12.2.2 Physics of this thermostat	165
12.3 Properties of the Nosé-Hoover thermostat	167
12.3.1 Fundamental relations between chaos and transport	167
12.3.2 ⁺ Generalized Hamiltonian formalism for the Nosé-Hoover thermostat	168
12.3.3 Chaos, fractal structures, and transport	170
12.4 ⁺ Subtleties and generalizations of the Nosé-Hoover thermostat	174
12.4.1 Necessary conditions and generalizations of this scheme	174
12.4.2 Applying thermal reservoirs to nonequilibrium situations	177
12.5 *Summary	178
13 Summary and criticism of Gaussian and Nosé-Hoover thermostats	181
13.1 Non-Hamiltonian dynamics for nonequilibrium steady states	181
13.2 Phase space contraction and entropy production	184
13.3 Transport coefficients and dynamical systems quantities	188
13.4 Fractal attractors characterizing nonequilibrium steady states	193
13.5 Nonlinear response in the thermostated driven periodic Lorentz gas	195
13.6 *Summary	197
14 Gaussian and Nosé-Hoover thermostats revisited	201
14.1 Non-ideal Gaussian thermostat	201
14.2 Non-ideal Nosé-Hoover thermostat	204
14.3 ⁺ Further alternatives to conventional Gaussian and Nosé-Hoover dynamics	207
14.4 *Summary	208
15 Stochastic and deterministic boundary thermostats	209
15.1 Stochastic boundary thermostats	209
15.2 Deterministic boundary thermostats	211
15.3 ⁺ Stochastic and deterministic boundary thermostats from first principles	212
15.4 Deterministic boundary thermostats for the driven periodic Lorentz gas	216
15.4.1 Phase space contraction and entropy production	217
15.4.2 Attractors, bifurcation diagram and electrical conductivity	219
15.4.3 Lyapunov exponents	221
15.5 Hard disk fluid under shear and heat flow	223
15.5.1 Homogeneous and inhomogeneous modelings of shear and heat flows	224
15.5.2 Shear and heat flows thermostated by deterministic scattering	226
15.6 *Summary	232
16 ⁺Active Brownian particles and Nosé-Hoover thermostats	235
16.1 Generalizing Langevin equations for modeling cell motility	237
16.2 Crater-like velocity distributions	238
16.3 *Summary	243

17 *Concluding remarks	245
17.1 A brief assessment of the main results	245
17.1.1 Fractal transport coefficients in deterministic dynamical systems	245
17.1.2 Universal chaos and transport properties of thermostated systems?	247
17.2 Some important open questions	248
17.2.1 Fractal transport coefficients	249
17.2.2 Thermostated dynamical systems	250
 Acknowledgements	 253
 Bibliography	 255
 Declaration	 297

Abstract

A fundamental challenge is to understand nonequilibrium statistical mechanics starting from microscopic chaos in the equations of motion of a many-particle system. In this thesis we summarize recent theoretical advances along these lines. We focus on two different approaches to nonequilibrium transport: One considers Hamiltonian dynamical systems under nonequilibrium boundary conditions, another one suggests a non-Hamiltonian approach to nonequilibrium situations created by external electric fields and by temperature or velocity gradients.

A surprising result related to the former approach is that in simple low-dimensional periodic models the deterministic transport coefficients are typically fractal functions of control parameters. These *fractal transport coefficients* yield the first central theme of this thesis. We exemplify this phenomenon by deterministic diffusion in a simple chaotic map. We then construct an arsenal of analytical and numerical methods for computing further transport coefficients such as electrical conductivities and chemical reaction rates. These methods are applied to hierarchies of chaotic dynamical systems that are successively getting more complex, starting from abstract one-dimensional maps generalizing a simple random walk on the line up to particle billiards that should be directly accessible in experiments. In all cases, the resulting transport coefficients turn out to be either strictly fractal, or at least to be profoundly irregular. The impact of random perturbations on these quantities is also investigated. We furthermore provide some access roads towards a physical understanding of these fractalities.

The second central theme is formed by a critical assessment of the non-Hamiltonian approach to nonequilibrium transport. Here we consider situations where the nonequilibrium constraints pump energy into a system, hence there must be some thermal reservoir that prevents the system from heating up. For this purpose a *deterministic and time-reversible modeling* of thermal reservoirs was proposed in form of Gaussian and Nosé-Hoover thermostats. This approach yielded simple relations between fundamental quantities of nonequilibrium statistical mechanics and of dynamical systems theory. Our goal is to critically assess the universality of these results. As a vehicle of demonstration we employ the driven periodic Lorentz gas, a toy model for the classical dynamics of an electron in a metal under application of an electric field. Applying different types of thermal reservoirs to this system we compare the resulting nonequilibrium steady states with each other. Along the same lines we discuss an interacting many-particle system under shear and heat. Finally, we outline an unexpected relationship between deterministic thermostats and active Brownian particles modeling biophysical cell motility.

1 *Introduction and outline

Statistical mechanics endeavours to understand the origin of macroscopic properties of matter starting from the microscopic equations of motion of single atoms or molecules. This program traces back to the founders of statistical mechanics, Boltzmann, Maxwell and Gibbs [Bol64, Max65a, Max65b, Gib60], and for many-particle systems in thermal equilibrium it was pursued with remarkable success [Tol38, Ehr59, Wan66, Rei65, Pat88, Hua87]. However, in nonequilibrium situations, that is, for systems under constraints such as external fields or by imposing temperature or velocity gradients, statistical mechanical theories appear to be rather incomplete. In contrast to the equilibrium case there is no generally accepted definition of a nonequilibrium entropy, and correspondingly there is no general agreement on nonequilibrium ensembles that might replace the equilibrium ones [Pen79, Eva90b, Ger99, Rue99b, Gal99].

Fresh input concerning these fundamental problems came from the side of dynamical systems theory, in particular by work of mathematicians like Sinai, Ruelle, Bowen and others over the past decades [Sin91, Sin00, Rue78, Bow75]. Indeed, *SRB measures*¹ appear to be good candidates for taking over the role of the Gibbs ensemble in nonequilibrium [Gas98a, Dor99, Gal99, Rue99b, You02, Gal03]. Additionally, the advent of powerful computers made it possible to numerically solve the nonlinear equations of motion of many-particle systems [All87, Eva90b, Hoo91, Hoo99]. This enabled to investigate the interplay between microscopic chaos in the collisions of single particles and transport properties on macroscopic scales in much more detail than it was possible to the times of the founders of statistical mechanics.

The stage for this work is set by two basic approaches that evolved over the past two decades trying to develop a concise picture of nonequilibrium statistical mechanics by employing methods of dynamical systems theory. In the following two sections we summarize important features of these two directions of research. We then sketch how our present work is embedded into this existing literature, outline its contents and say some words about the style in which it is written. The hurried reader may want to first skip the following two sections, in order to pick up the *red thread through this thesis* provided by Section 1.3.

1.1 Hamiltonian dynamical systems approach to nonequilibrium steady states

In recent work, Gaspard, Nicolis and Dorfman studied nonequilibrium situations by imposing specific boundary conditions onto spatially extended chaotic *Hamiltonian* (-like) dynamical systems. A typical example are diffusion processes due to concentration gradients at the

¹The acronym holds for the initials of Sinai, Ruelle, and Bowen.

boundaries. By this approach the macroscopic transport properties of deterministic dynamical systems could be linked to the underlying microscopic chaos in the equations of motion of the single particles in two ways: The *escape rate approach* considers dynamical systems with absorbing boundaries [Gas90, Gas92c, Gas93, Gas95b, Dor95, Gas95c, Gas98a, Dor99]. Here the escape rate determined by a statistical physical transport equation such as, for example, the diffusion equation, is matched to the one resulting from solving the Liouville equation of the dynamical system. This procedure yields simple formulas linking transport coefficients to dynamical systems quantities, which are here the positive Lyapunov exponents and the Kolmogorov-Sinai entropy of the dynamical system, or respectively the fractal dimension of the associated repeller of the open system.

A second, conceptually related approach applies to closed systems with periodic boundary conditions. It has been worked out for diffusion [Gil01, Gas01] and for reaction-diffusion [Cla02] in low-dimensional models. In this case the decay rate to thermal equilibrium obtained from the (reaction-)diffusion equation is related to the fractal dimension of the corresponding hydrodynamic mode in the Liouville equation of the dynamical system. The transport coefficients can thus be expressed as functions of the system's largest Lyapunov exponent combined with the Hausdorff dimension of this mode. Both approaches can consistently be derived by using Ruelle's thermodynamic formalism [Gas95c, Gas01].

Along similar lines, the origin of nonequilibrium entropy production in chaotic dynamical systems has been investigated. Here the analysis of transport in simple two-dimensional *multibaker maps* introduced by Gaspard [Gas92a] played a crucial role. Multibakers are deterministic versions of simple random walks on the line, where the stochasticity is replaced by microscopic chaos. On the other hand, these maps share generic properties with Hamiltonian particle billiards of which *Lorentz gases* [Lor05] are typical examples. In these models a moving point particle collides elastically with circular scatterers distributed randomly or periodically in space. The periodic version with applied external field is also known as the *Galton board* [Gal77]. Both multibakers and Lorentz gases became paradigmatic models in the field of chaos and transport [Gas98a, Dor99, Hoo99, Sza00, Kar00, Gar02, Vol02].

For nonequilibrium transport in such systems, Tél, Vollmer, Breymann and Matyas [Bre96, Tel96, Vol97, Bre98, Vol98, Tel00, Vol00, Mat01, Vol02, Vol03] as well as Gaspard, Tasaki, Dorfman and Gilbert [Gas97b, Gil99a, Tas99, Tas00, Gil00a, Gil00b, Dor02] have proposed new concepts for defining coarse-grained Gibbs entropies leading to a nonequilibrium entropy production that is in agreement with irreversible thermodynamics. The former group attributed the source of irreversible entropy production to the chaotic mixing of the dynamical system and to the associated loss of information due to coarse graining. The latter authors argued that the singularity of the SRB measures exhibited by these nonequilibrium systems already necessitates a respective coarse graining because of mathematical reasons. In both approaches, the source of irreversible entropy production is thus identified with the fractal character of these SRB measures.

Cohen and Rondoni, on the other hand, criticized both theories starting from the fact that the simple models to which these analyses have been applied consist of moving point particles that do not interact with each other but only with some fixed scatterers [Coh98, Ron00a, Coh02, Ron02b]. In their view these systems are non-thermodynamic models that do not allow to identify local thermodynamic equilibrium or any proper source of thermodynamic entropy production; however, see the counter-arguments of the criticized authors provided in Refs. [Vol02, Dor02, Tel02, Gas02a, Gas03].

Another important topic associated with the Hamiltonian approach to nonequilibrium trans-

port concerns the parameter dependence of transport coefficients. It originated from studying deterministic transport in simple *one-dimensional chaotic maps* periodically continued on the line [Sch89, Kla96, Gas98a, Dor99, Cvi03]. Specific types of such models can be straightforwardly derived from the multibaker maps mentioned above [Gas92a, Gas98a, Dor99].

There exists quite an arsenal of methods to compute deterministic diffusion coefficients for these maps such as transition matrix methods [Gas92a, Cla93, Kla95, Kla96, Kla97, Gas98c, Gas98a, Kla99a, Koz99, Kla02a], systematic evaluations starting from Green-Kubo formulas [Kla96, Dor99, Gas98c, Kla02d, Kor02, Kor03], rigorous mathematical treatments related to kneading sequences [Gro02], cycle expansion methods [Art91, Art93, Art94, Tse94, Che95a, Gas98a, Cvi03] and techniques employing the thermodynamic formalism [Sto94, Sto95a, Sto95c, Sto95b, Rad97]. Using such techniques to calculate the parameter-dependent deterministic diffusion coefficient of a simple one-dimensional map, the result was found to be a fractal function [Kla03a] of a control parameter [Kla95, Kla96, Kla99a]. The origin of this fractality could be traced back to the existence of long-range dynamical correlations in the microscopic dynamics of the moving particle, see, e.g., Ref. [Kla02d]. These correlations are topologically unstable and change in a complicated way under parameter variation, a phenomenon that is known as *pruning* in periodic orbit theory [Cvi03].

Starting from this observation, both the conductivity [Gro02] and the chemical reaction rate [Gas98c] of related maps were found to be fractal functions of control parameters. The drift-diffusion coefficients furthermore exhibited phase locking, and the nonlinear response turned out to be partly negative. The latter fact can be understood by relating the biased model to deterministic ratchets [Kla] for which the existence of current reversals under parameter variation is a characteristic property [Jun96, Hän96, Rei02].

Similar fractal transport properties were detected for phase diffusion in a time-discrete model of a driven nonlinear pendulum [Kor02, Kor03]. In this case bifurcation scenarios generated a complicated interplay between normal and anomalous diffusive dynamics. Analogous equations have been studied in the context of experiments on Josephson junctions [Jac81, Cir82, Mir83, Mar89, Wei00, Tan02d], on superionic conductors [Ful75, Bey76, Mar86], and on systems exhibiting charge-density waves [Bro84].

In view of such experimental situations one may ask to which extent fractal transport coefficients are robust with respect to imposing random perturbations in space and time onto the underlying models. This connects the present line of research to the fields of disordered [Rad96, Rad99, Rad03], respectively noisy [Gei82, Rei94, Rei96a, Rei96b, Fra91, Wac99, Cvi00] dynamical systems. A first answer to this question was provided by Refs. [Kla02b, Kla02c] yielding that the oscillatory structure of the diffusion coefficient of a simple model gradually “smooths out” by increasing the perturbation strength eventually recovering precise agreement with results from stochastic theory.

In order to move fractal transport coefficients to more realistic physical systems, studies of deterministic transport in Hamiltonian particle billiards were put forward. In the periodic Lorentz gas long-range dynamical correlations have again a profound impact on the parameter dependence of the diffusion coefficient [Kla00a, Kla02d]. This effect was found to be even more pronounced in a billiard with scatterers of flower-shaped geometry [Har02] and in a periodically corrugated floor, where particles move under the action of a gravitational force [Har01].

We remark that billiards of Lorentz gas-type can actually be manufactured and studied experimentally in form of semiconductor antidot lattices, where noninteracting electrons

move quasi-classically under application of external electric and magnetic fields [Wei91, Wei95, Wei97]. Indeed, the measured magnetoresistance of such systems is well-known to be a highly irregular function of the field strength. For specific settings this quantity has theoretically been predicted to be fractal [Wie01].

Another link between fractal transport coefficients and physical reality is provided by the *bouncing ball billiard*, which yields a simple model for deterministic diffusion of a granular particle on a vibrating periodically corrugated floor [Mat03, Bar03a]. The analysis of this model revealed again highly irregular diffusion coefficients exhibiting the impact of phase locking and of related resonances. This model was constructed in order to be close to recent experiments on granular material [Far99, Pre02] and could eventually be of practical importance, say, for the transport of screws and related mechanical parts on vibratory conveyor belts [Gro03, Rou04, Gro04].

Finally, as related research we mention the line of both theoretical and experimental work on *fractal conductance fluctuations* in mesoscopic nonlinear dynamical systems, see, e.g., Refs. [Ket96, Heg96, Sac98, Huf01]. However, in this case the fractality is intimately connected with the mixed phase space of the Hamiltonian dynamical systems under study, apart from the fact that the analysis aimed primarily at quantum and semi-classical transport. Whether there is any closer connection between these findings and the purely classical fractality of transport coefficients discussed above forms an open question.

To conclude this outline of a Hamiltonian dynamical systems approach to nonequilibrium steady states we refer to an interesting experiment that was proposed and carried out by Gaspard et al. [Gas98b, Bri01]. Its purpose was to verify the existence of microscopic deterministic chaos in the dynamics of an interacting many-particle system. Long trajectories of a tracer particle suspended in a fluid were recorded, and this data was used for computing a coarse grained entropy that was argued to yield a lower bound for the sum of positive Lyapunov exponents of the system. However, after this work was published non-chaotic counterexamples were constructed yielding almost indistinguishable results for the coarse-grained entropy [Det99b, Gra99, Det00b]. This initiated ongoing discussions and motivated research on transport in non-chaotic models [Lep00, Cen00, Alo02, Gra02, Cec03, Alo03], which complements existing results for chaotic systems.

1.2 Thermostated dynamical systems approach to nonequilibrium steady states

A nontrivial limitation of the Hamiltonian approach to chaotic transport is that it excludes nonequilibrium constraints generating a continuous flux of energy into the system as, for example, the application of external fields.² Such situations necessitate the modeling of an infinite dimensional *thermal reservoir* that is able to continuously absorb energy in order to prevent a subsystem from heating up [Pen79, Rue99b, Gal99, Dor99, Ron02a]. The need to model these situations emerged particularly from *nonequilibrium molecular dynamics computer simulations* that focus on simulating heat or shear flow of many-particle systems or currents under application of external fields [Eva90b, Hoo91, Hes96a, Mor98, Hoo99, Det00a, Mun00, Tuc00].

²Note that the use of *Helfand moments* enables an indirect treatment of such situations similar to the use of equilibrium time correlation functions related to Green-Kubo formulas [Dor95, Gas98a].

A well-known example for modeling thermal reservoirs is provided by the *Langevin equation* [Lan08] yielding the interaction with a heat bath by a combination of Stokes friction and stochastic forces [Wax54, Rei65, Pat88, Kub92, Zwa01]. Indeed, one way to derive generic types of Langevin equations starts from a Hamiltonian formulation for a heat bath consisting of infinitely many harmonic oscillators. This heat bath suitably interacts with a subsystem that consists of a single particle [Zwa73, For87, Kub92, Stu99, Zwa01]. In the course of the derivation the detailed bath dynamics is eliminated resulting in an equation of motion for the subsystem that is *stochastic and non-Hamiltonian*. The Langevin equation thus nicely illustrates Ruelle’s statement “if we want to study non-equilibrium processes we have thus to consider an infinite system or non-Hamiltonian forces” [Rue99a].³

As we will argue in the second part of this work, there is nothing mysterious in modeling thermal reservoirs with non-Hamiltonian equations of motion, see also, e.g., Refs. [Pen79, Sma80, Rue99b, Che95b, Rue96, Che97, Gal99, Lie99a, Ron02a]. In case of thermostated systems the non-Hamiltonianity results straightforwardly from projecting out spurious reservoir degrees of freedom. Early nonequilibrium molecular dynamics computer simulations employed actually stochastic models of heat baths [And80, Cic80, Sch78, Ten82, All87, Nos91], however, very soon people started to look for alternatives. Infinite-dimensional Hamiltonian thermal reservoirs, on the other hand, can very well be modeled and analyzed analytically [Eck99b, Eck99a, Zwa01], but on a computer the number of degrees of freedom must, for obvious reasons, remain finite. These constraints provided a very practical motivation for constructing nonequilibrium steady states on the basis of finite-dimensional, deterministic, non-Hamiltonian equations of motion.

About twenty years ago Hoover et al. [Hoo82] and Evans [Eva83a] independently and simultaneously came up with a strikingly simple non-Hamiltonian modeling of a thermal reservoir, which they coined the *Gaussian thermostat* [Eva83b]. This scheme introduces a (Gaussian) constraint in order to keep the temperature for a given subsystem strictly constant in nonequilibrium at any time step. A few years later Nosé invented a very related non-Hamiltonian thermal reservoir that was able to thermostat the velocity distribution of a given subsystem onto the canonical one in equilibrium, and to keep the energy of a subsystem constant on average in nonequilibrium [Nos84a, Nos84b]. His formulation was simplified by Hoover [Hoo85] leading to the famous Nosé-Hoover thermostat [Eva90b, Hoo91, Hes96a, Mor98, Hoo99, Det00a, Mun00, Ron02a]. Suitable adaptations of these schemes to nonequilibrium situations such as, e.g., shear flows yielded results that were well in agreement with predictions of irreversible thermodynamics and linear response theory [Eva90b, Sar98]. Hence, these thermostats became widely accepted tools for performing nonequilibrium molecular dynamics computer simulations. Eventually, they were successfully applied even to more complex fluids such as, for example, polymer melts, liquid crystals and ferrofluids [Hes96a, Hes96b, Hes97], to proteins in water and to chemical

³For a related statement see, e.g., Smale [Sma80]: “We would conclude that theoretical physics and statistical mechanics should not be tied to Hamiltonian equations so absolutely as in the past. On physical grounds, it is certainly reasonable to expect physical systems to have (perhaps very small) non-Hamiltonian perturbations due to friction and driving effects from outside energy absorption. Today also mathematical grounds suggest that it is reasonable to develop a more non-Hamiltonian approach to some aspects of physics.” In his interesting article Smale further suggests to “revive the ergodic hypothesis via introduction of a dissipative/forcing term” into Hamiltonian equations of motion, since in his view dissipative dynamical systems have a better chance to be ergodic than Hamiltonian ones that usually exhibit profoundly non-ergodic dynamics due to a mixed phase space.

processes in the condensed matter phase [Tuc00].

Soon it was realized that this non-Hamiltonian modeling of thermal reservoirs not only enabled to efficiently construct nonequilibrium steady states on the computer but also that it made them amenable to an analysis by means of dynamical systems theory [Eva90b, Hoo91, Mar92a, Mar97, Tel98, Mor98, Hoo99]. First of all, in contrast to the stochastic Langevin equation Gaussian and Nosé-Hoover thermostats preserve the deterministic nature of the underlying Newtonian equations of motion. Even more, though the resulting dynamical systems are dissipative, surprisingly the thermostated equations of motion are still time-reversible hence yielding a class of systems characterized by the, at first view, contradictory properties of being *time-reversible*, *dissipative* and, under certain circumstances, even being *ergodic* [Che95b, Che97, Hoo96b]. Computer simulations furthermore revealed that subsystems thermostated that way contract onto *fractal attractors* [Hol87, Mor87a, Mor87b, Hoo87, Pos88, Hoo88a, Mor89a, Pos89, Mor89b] with an *average rate of phase space contraction that is identical to the thermodynamic entropy production* [Hol87, Pos88, Che93a, Che93b]. This led researchers to conclude that in thermostated dynamical systems the phase space contraction onto fractal attractors is at the origin of the second law of thermodynamics [Hol87, Rue96, Rue97b, Rue97a, Hoo99, Rue99b, Gal98, Gal99, Rue03].

Interestingly, the average rate of phase space contraction plays the same role in linking statistical physical transport properties to dynamical systems quantities as the escape or decay rates in the Hamiltonian approach to nonequilibrium [Tel96, Rue96, Bre98, Gil01]. The key observation is that, on the one hand, the average phase space contraction rate is identical to the sum of Lyapunov exponents of a dynamical system, whereas, on the other hand, for Gaussian and Nosé-Hoover thermostats it equals the thermodynamic entropy production. For thermostated dynamical systems this again furnishes a relation between transport coefficients and dynamical systems quantities [Mor87a, Pos88, Eva90a, Van92, Bar93, Coh95, Eva00, Aok02]. A suitable reformulation of these equations makes them formally analogous to the ones obtained from the Hamiltonian approach to transport. These results were considered as an indication for the existence of a specific backbone of nonequilibrium transport in terms of dynamical systems theory [Tel96, Bre98, Gas98a, Gil01].

Another interesting feature of Gaussian and Nosé-Hoover thermostated dynamical systems is the existence of *generalized Hamiltonian and Lagrangian formalisms* from which the thermostated equations of motion can be deduced, which involve non-canonical transformations of the phase space variables [Nos84a, Nos84b, Det96b, Det97a, Mor98, Cho98]. Similarly to Hamiltonian dynamics deterministically thermostated systems often share a certain symmetry in the spectrum of their Lyapunov exponents known as the *conjugate pairing rule*, which was widely studied in the recent literature, see, e.g., Refs. [Dre88, Pos88, Eva90a, Coh95, Mor98, Sea98, Rue99b]. That is, all Lyapunov exponents of a given dynamical system can be grouped into pairs such that each pair sums up to the same value, which in nonequilibrium is non-zero.

In most cases Lyapunov exponents of thermostated systems can only be calculated numerically. However, for the periodic Lorentz gas and related systems there is an elegant analytical approach by means of kinetic theory developed by van Beijeren and Dorfman et al. [vB95, vB96, Lat97, vB97, vZ98, vB98, vB00b]. Furthermore, in recent computer simulations of interacting many-particle systems Posch et al. [Mil98a, Pos00a, Mil02, Hoo02c, For03] observed the existence of *Lyapunov modes* in thermal equilibrium indicating that the microscopic contributions to the Lyapunov instability of a many-particle fluid form specific modes of instability, quite in analogy to the well-known hydrodynamic modes governing

macroscopic transport [Eck00, McN01, Tan02c, Tan02a, Mar03].

All these interesting properties inspired mathematicians to look at these systems from a more rigorous point of view. A cornerstone is the proof by Chernov et al. of the existence of Ohm's law for the periodic Lorentz gas driven by an external electric field and connected to a Gaussian thermostat [Che95b, Che97]. Another important development was the *chaotic hypothesis* by Gallavotti and Cohen [Gal95a, Gal95b, Gal98, Gal99], which was motivated by results from computer simulations on thermostated dynamical systems [Eva93a].⁴ This fundamental assumption generalizes Boltzmann's ergodic hypothesis in summarizing some general expectations on the chaotic nature of interacting many-particle systems which, if fulfilled, considerably facilitate calculations of nonequilibrium properties.

Further promising achievements in the field of thermostated dynamical systems are *fluctuation theorems* that establish simple symmetry relations between positive and negative fluctuations of the nonequilibrium entropy production. Again, such laws first came up in the framework of nonequilibrium molecular dynamics computer simulations for thermostated systems, see Evans, Cohen and Morriss [Eva93a]. Later on respective theorems were proven by Gallavotti and Cohen starting from the chaotic hypothesis [Gal95a, Gal95b].⁵ Related theorems for stochastic systems were derived in Refs. [Kur98, Leb99]. In Ref. [Mae99] it was argued that fluctuation theorems can more generally be understood as an intrinsic property of Gibbs measures⁶ defined in nonequilibrium situations. Meanwhile fluctuation theorems have been verified for many different systems in many different ways analytically [Dor99, Rue99b, Ron00b, Jar00, Eva02b, Jep03], by computer simulations [Bon98a, Lep00, Eva02b, Sch03], and in physical experiments [Cil98, Wan02]. It appears that fluctuation theorems belong to the rather few general results characterizing nonequilibrium steady states very far from equilibrium thus generalizing Green-Kubo formulas and Onsager reciprocity relations, which can be derived from them nearby equilibrium [Gal96b, Gal98, Gal99, Eva02b, Gal03].

1.3 The red thread through this thesis

Our thesis focuses on two basic themes that are intimately connected with the two directions of research outlined above: Part I elaborates on the origin, calculation and explanation of fractal transport coefficients in low-dimensional deterministic dynamical systems. Part II deals with the construction and analysis of nonequilibrium steady states in dissipative dynamical systems associated with thermal reservoirs.

For a quick reading we recommend to focus on all parts marked with a star (*), supplemented by studying the introductory remarks preceding all the single chapters. Sections labeled by a plus (+) contain information that may be skipped even for more thorough studies. In any case, if not done so already, one should commence with the previous Sections 1.1 and 1.2. They feature a concise outline of the general field of research into which this thesis is embedded, together with a brief summary of major topics covered by this work. One

⁴The chaotic hypothesis, in its original formulation [Gal95b], states: *A reversible many-particle system in a stationary state can be regarded as a transitive Anosov system for the purpose of computing the macroscopic properties of the system.*

⁵For similarities and differences between Evans-Cohen-Morriss and Gallavotti-Cohen fluctuation theorems see, e.g., Refs. [Coh99, Ron02a, Eva02b].

⁶See, e.g., Refs. [Bec93, Dor99] for introductions to Gibbs measures.

may then go through the series of introductions and summaries corresponding to the single chapters. Here the reader should not miss the two more explicit summaries provided right at the beginnings of Part I and Part II. This short tour through our thesis should evidently be concluded with Chapter 17.

We highly recommend to include Chapter 2 in such a quick reading. This chapter describes the major finding of the author's Ph.D. thesis work, namely the existence of a fractal diffusion coefficient in a rather abstract deterministic model. It furthermore provides a motivation for a deterministic approach towards nonequilibrium transport, by introducing a simple map that became a sort of standard model for the investigations reported in Part I. The central aim of the work compiled in Chapters 3 to 9 originating over the past few years was to bring fractal diffusion coefficients to physical reality. This required a sharpening of our theoretical methods, which goes hand in hand with studying a series of increasingly more complex models. In the course of these efforts, analogous fractal properties were discovered for additional deterministic transport coefficients. Our conclusion is that fractal transport coefficients are typical for a specific class of physical dynamical systems, and that they should be seen in experiments. To systematically argue for this statement is the major theme of Part I.

Concerning Part II, we suggest to go at least through Section 10.1 that motivates the physics of thermal reservoirs in a very intuitive way. The patient reader may wish to consult as well Section 10.2 for a more detailed motivation that starts from the well-known Langevin equation, by pointing towards some fundamental problems in modeling thermal reservoirs. If even more time is left, we recommend to take a look at Chapter 11 that describes a paradigmatic modeling of a deterministic and time-reversible thermal reservoir. Applying this method to a simple model in a nonequilibrium situation, we summarize the resulting chaos and transport properties of the combined system in this chapter. Partly it was argued in the literature that these properties should be universal for thermostated dynamical systems in nonequilibrium steady states altogether, see Chapters 11 to 13. Hence, the main theme of Part II is to critically assess the universality of these results as obtained from a non-Hamiltonian approach to nonequilibrium steady states. In Chapters 14 to 15 we indeed show that there exist thermal reservoirs yielding counterexamples to most of these claims of universality. Chapter 16 finally establishes a previously unexpected relationship between the modeling of deterministic thermal reservoirs and simple models for the motility of biological entities such as, e.g., crawling cells.

As far as the style is concerned in which this thesis is written, we remark that Part I is composed on the basis of the existing publications Refs. [Kla95, Gro02, Gas98c, Kor02, Kla02b, Kla02c, Kla02d, Har02]. However, partly it also draws on unpublished work: Section 3 presents an older draft of Ref. [Gro02], which contains a number of still unpublished results and additional explanations that have been skipped for the printed version. Section 9 features a short paper corresponding to Ref. [Mat03] that has not yet been published.

Part II, on the other hand, contains a single review that has extra been written for this thesis and is currently submitted for publication. It is built around the series of papers Refs. [Kla00b, Rat00b, Wag99, Rat00a, Rat02, Wag00], but, featuring a review, summarizes many other important results in this field that are not due to the author. Like Part I, it includes some yet unpublished results: They consist of the non-ideal Gaussian thermostat Section 14.1 and the relation between Nosé-Hoover thermostats and active Brownian particles Section 16.2.

The different origin of these two fundamental parts is reflected in the degree of difficulty the

non-expert may expect by reading through them: According to the cumulative character of Part I, it should be possible to study all chapters essentially independently, but the style of the whole part is rather advanced. On the other hand, the reader may enjoy learning about fractal transport coefficients along the lines of hermeneutics: That is, reflecting the cooperation of the present author with different colleagues in the course of performing this research, the main models, methods and findings are presented in this part from successively different points of views, thus providing themes and variations which the reader will hopefully find interesting. In contrast, as a review, Part II is written in a rather pedagogical way. Here we try to keep things as simple as possible and do not present more technical details than absolutely necessary. This is reflected by the fact that there are only very few formulas in this part but a lot of text.

Both parts presuppose some basic knowledge of (nonequilibrium) statistical mechanics [Rei65, Hua87] and of dynamical systems theory [Sch89, Eck85, Ott93, Bec93, All97]. We touch upon some rigorous mathematical concepts particularly in Section 3.2.1, otherwise our work represents a generic theoretical physicist's approach towards chaos and transport in nonequilibrium steady states which does not require a too detailed knowledge of mathematical dynamical system's theory. In this respect, we remark that for Part II we do not employ concepts such as SRB measures and Anosov systems, despite the fact that all issues discussed in this part are intimately related to them. We emphasise that these objects do play a crucial role for building up a rigorous mathematical theory of nonequilibrium steady states as outlined, e.g., in Refs. [Gas98a, Dor99, Gal99, Rue99b]. However, in Part II we work on a level that is less rigorous consisting of straightforward physical examples and demonstrations plus some simple calculations and results from computer simulations. It is our hope that this approach still suffices to make the reader familiar with what we believe are some central problems in the field of chaos and transport in thermostated dynamical systems.

Concerning books and reviews that are closely related to the topics covered by this thesis, for Part I we may recommend particularly Refs. [Kla96, Gas98a, Nic98, Dor99, Cvi03] and with respect to Part II Refs. [Eva90b, Hes96a, Mor98, Hoo99, Det00a, Ron02a] for further reading. There exists also a number of conference proceedings and related collections of articles which the reader may wish to consult [Mar92a, Mar97, Tel98, Kar00, Sza00, Gar02, Kla03b]. Concerning more specific references, we restricted ourselves to citing articles that we feel are especially relevant to the problems highlighted in this thesis, still this resulted in quite a large number of references. We furthermore remark that in this thesis we do not intend to give a full historical account of recent developments in chaos theory and nonequilibrium statistical mechanics; for this purpose see, e.g., Refs. [Bru76, Gle88, Cvi03, Uff01, Vol02]. Only on certain occasions we go a little bit more into the historical depth.

Part I

Fractal transport coefficients

In this part we elaborate on the fractal parameter dependence of various transport coefficients by analyzing a variety of low-dimensional deterministic models. We start in Chapter 2 by providing a general motivation for a chaotic dynamical systems' approach to nonequilibrium transport [Kla96, Kla99a]. These theoretical ideas are exemplified by a paradigmatic one-dimensional deterministic model that generalizes the concept of diffusion as a simple random walk on the line [Gro82, Fuj82, Gro83]. The remaining part of this chapter discusses the finding of a fractal [Kla03a] diffusion coefficient for this model. That is, we outline a method for the computation of this quantity as well as an approach that explains its fractal origin [Kla95, Kla96, Kla99a].

In Chapter 3 we consider a straightforward extension of this model in which the symmetry of the system is broken [Gro02]. Hence, we arrive at a simple deterministic drift-diffusion process containing the purely diffusive map of Chapter 2 as a special case. Related biased one-dimensional maps have been studied by Barkai and Klafter on the basis of stochastic methods [Bar97, Bar98] and by Gilbert and Dorfman [Gil04]. After introducing our model in a mathematically rigorous way, we outline a set of methods by which the transport properties for this considerably more difficult dynamical system can be calculated exactly. One class of these methods is mathematically rigorous and yields extremely fast and precise computational schemes for the two transport coefficients [Gro]. The other type of methods is more physically intuitive and enables the computation of some further interesting quantities characterizing the time-dependent dynamics in this map [Kla96, Kla97, Gas98c, Kla02a]. We finally construct what may be called the phase diagram of this two-parameter model and outline the interesting findings of phase locking in both drift and diffusion coefficients, as well as the striking fact that there are currents in this model which run opposite to the applied bias [Gro02].

Chapter 4 deals with a deterministic modeling of reaction-diffusion processes [Els85, Gas98c, Nie98, Cla00, Cla01, Gas02b, Cla02, Cla03]. The first section outlines the relation between multibaker maps and other central models discussed in Part I, which are one-dimensional maps of the type considered in Chapters 2 and 3, and Lorentz gases as covered by Chapters 7 to 9. That way, we motivate the specific model analyzed in this chapter, which is a chemically reactive and diffusive two-dimensional deterministic multibaker map [Gas98c]. In the two remaining sections of this chapter we study successively the diffusive and reactive properties of this model, each time by starting with the most simple case of a control parameter value, by constructing the eigenmodes of the deterministic system [Gas92a, Tas95, Gas93, Gas95a, Gas98a]. We then switch to the full parameter dependence of the reactive-diffusive dynamics by summarizing both existing and new methods for computing the associated transport coefficients [Kla95, Kla96, Kla97, Kla99a, Kla02a, Kla]. Both the diffusion coefficient and the chemical reaction rate turn out to be fractal. Moreover, the parameter-dependent reaction rate features a highly complex scenario of different dynamical phase transitions, which is also reflected in the underlying time-dependent dynamics [Gas98c].

So far we only studied transport in *uniformly hyperbolic* dynamical systems in which all transport coefficients are usually well-defined [Gas98a, Dor99]. Chapter 5 treats diffusive transport in a simple *nonhyperbolic* map [Sch82, Gei82, Gro82, Fuj82] that, in a way, represents a deterministic diffusive counterpart of the famous logistic map which is restricted to the unit interval. This diffusive model yields different dynamical regimes consisting of localization of particles, ballistic flights and normal diffusion depending on the choice of a control parameter. Correspondingly, the deterministic diffusion coefficient displays an interplay between these different types of dynamics by exhibiting three different kinds of

fractal structures. These fractalities can, to some extent, be understood by systematically evaluating a Green-Kubo formula for diffusion, as introduced in Chapter 4. This analysis is supplemented by investigating the bifurcation scenario of this map featuring different sequences of periodic windows [Sch82, Gro82, Fuj82].

Another direction of research going beyond the most simple type of deterministic dynamics is summarized in Chapter 6. Here we investigate the impact of random perturbations both in space [Rad96, Rad99, Rad03] and in time [Gei82, Rei94, Rei96a, Rei96b] onto deterministic diffusion, sometimes called *quenched and annealed disorder* [Bou90]. For a certain type of quenched disorder we find suppression and enhancement of the normal diffusion coefficient as a function of the perturbation strength [Kla02b]. Again, these irregularities just reflect the presence of strong dynamical correlations in the underlying deterministic dynamical model, which is the simple map studied in Chapters 2 and 3. The same explanation for the existence of irregular parameter-dependencies of the diffusion coefficient holds for the case of time-dependent noise, where we observe a transition from deterministic to stochastic diffusion [Kla02c]. That is, there are two different limiting cases of diffusive dynamics depending on the random perturbation strength, the former featuring a fractal diffusion coefficient, whereas the latter yields a completely smooth, monotonic curve as expected from simple random walk theory [Sch82, Gro82, Kla96, Kla97, Kla02a].

The remaining three chapters of Part I elaborate primarily on deterministic diffusion in periodic particle billiards. Chapter 7 establishes the methodological transition from the simple maps studied up to now to this new, more realistic class of time-continuous models [Kla02d]. Here we focus on the systematic approach for calculating and understanding fractal diffusion coefficients which employs the Green-Kubo formula for diffusion, cp. to Chapters 4 and 5. This scheme is worked out both for diffusion in the simple one-dimensional map of Chapters 2 and 3 and for diffusion in the periodic Lorentz gas [Bun80, Bun81, Mac83, Bun91, Gas92c, Bar93, Gas98a, Cvi92, Mor94, Gas95b, Mat97, Kla00a], the model briefly introduced in Chapter 4. Our main point is to show that the periodic Lorentz gas also exhibits an irregular parameter-dependent diffusion coefficient, and that the origin of this fine structure is analogous to the one discussed for one-dimensional maps. The Green-Kubo based method by which we perform our analysis was called *correlated random walk approach* [Kla02d], since it yields both random walk results and exact deterministic dynamical formulas as limiting cases of a respective series expansion for the diffusion coefficient.

This theory is applied to another Hamiltonian particle billiard in Chapter 8, where instead being circular the scatterers are of a flower shape [Har02]. The different geometry induces a more irregular structure for the parameter-dependent diffusion coefficient of this model than observed for the periodic Lorentz gas. Thus, we have identified a mechanism that allows us to construct particle billiards exhibiting more irregular transport coefficients. In order to understand this oscillatory structure we employ a variety of different approximation schemes all starting from a simple random walk approximation, which systematically include higher-order dynamical correlations [Mac83, Kla00a]. We show that these schemes give a convenient explanation of the diffusive irregularities in the flower-shaped billiard in terms of dynamical correlations.

In the final Chapter 9 of Part I we focus on deterministic diffusion in a very simple microscopic model of granular matter. For this purpose we consider a particle bouncing inelastically on a one-dimensional vibrating periodically corrugated floor [Mat03]. Computer simulation results reveal again a highly irregular diffusion coefficient as a function of the frequency of the vibrating floor. The largest peaks are due to the existence of phase locking,

a phenomenon that it is well-known for a for a non-diffusing ball bouncing inelastically on a flat surface [Pie83, Pie88, Kov88, Tuf92, Meh90, Luc93, Lic92, Guc90]. Irregularities on finer scales are explained by employing again the Green-Kubo expansion outlined in Chapters 5 and 7. With this model we hope to stimulate specific experiments on granular matter in order to see fractal diffusion coefficients, in the form of oscillations on finer and finer scales, in real and perhaps rather practical physical system [Far99, Pre02].

2 *Simple maps with fractal diffusion coefficients

We consider chains of one-dimensional, piecewise linear, chaotic maps with uniform slope. We study the diffusive behaviour of an initially nonuniform distribution of points as a function of the slope of the map by solving the Frobenius-Perron equation. For Markov partition values of the slope, we relate the diffusion coefficient to eigenvalues of the topological transition matrix. The diffusion coefficient obtained shows a fractal structure as a function of the slope of the map. This result may be typical for a wide class of maps, such as two-dimensional sawtooth and standard maps.

In Section 2.1 we explain the concept of deterministic diffusion and introduce our model. In Section 2.2 we outline a method of how to calculate the parameter-dependent diffusion coefficient for this dynamical system and discuss the result.

This work has been performed together with J.R. Dorfman and was part of the author's Ph.D. thesis [Kla96]. The first section is based on the introduction of Ref. [Kla99a], the second section draws on Ref. [Kla95]. For further details see Refs. [Kla96, Kla99a]. Related results are published in Refs. [Kla97, Kla99a, Kla02a, Kla02d].

2.1 A simple model for deterministic diffusion

In contrast to the traditional picture of diffusion as an uncorrelated random walk, the theory of dynamical systems makes it possible to treat diffusion as a *deterministic dynamical process*: For this purpose the orbit of a point particle with initial condition x_0 may be generated by a dynamical system

$$x_{n+1} = M(x_n) \quad . \quad (2.1)$$

$M(x)$ is a one-dimensional map that determines how a particle gets mapped at discrete time steps $n \in \mathbb{N}$ from position x_n to position x_{n+1} . A simple example for such a map will be introduced in detail below. Defining $M(x)$ together with Eq. (2.1) gives the *full microscopic equations of motion* of the system. This way, the complete memory of the particle is taken into account.

Hence, the decisive new fact that distinguishes this dynamical process from the one of a simple uncorrelated random walk is that here x_{n+1} is uniquely determined by x_n , rather than having a random distribution of x_{n+1} for a given x_n . If the resulting dynamics of an ensemble of particles, each governed by the same deterministic dynamical system $M(x)$, has the property that the diffusion coefficient D is well defined, this process is denoted as *deterministic diffusion* [Gro82, Fuj82, Gro83, Gei82, Gei84, Gei85, Sch82, Art91, Art93, Art94,

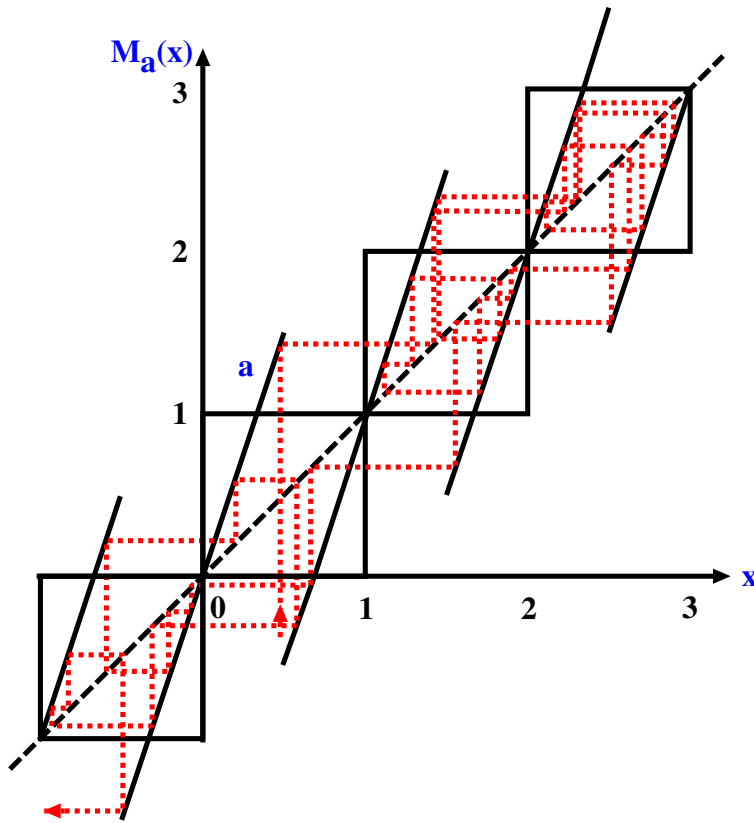


Figure 2.1: A simple model for deterministic diffusion. The dashed line depicts the orbit of a diffusing particle in the so-called cobweb plot [All97]. The slope a , here $a = 3$, serves as a control parameter in the periodically continued piecewise linear map.

[Tse94, Che95a, Gas98a, Kla95, Kla99a, Dor99, Kla96, Cvi03]. The diffusion coefficient may then be defined by the Einstein formula [Ein05, Wax54, Sta89, vK92]

$$D = \lim_{n \rightarrow \infty} \frac{\langle (x_n - x_0)^2 \rangle}{2n} , \quad (2.2)$$

where $\langle \dots \rangle$ represents the average over an initial ensemble of values of x_0 . We will typically choose the initial ensemble as one in which the points are distributed uniformly over a unit interval of the real line. Of course, in order to obtain a representative value for the diffusion coefficient one must argue that D is largely independent of the choice of the initial ensemble.

Fig. 2.1 shows the model which shall largely be studied throughout Part I. As far as we know, this model was first introduced by Grossmann and Fujisaka [Gro82, Fuj82]. It depicts a “chain of boxes” of chainlength $L \in \mathbb{N}$ which continues periodically in both directions to infinity, and the orbit of a moving point particle. Let

$$M_a : \mathbb{R} \rightarrow \mathbb{R} , \quad x_n \mapsto M_a(x_n) = x_{n+1} , \quad n \in \mathbb{N}_0 \quad (2.3)$$

be a map modelling the chain of boxes introduced above, i.e., a periodic continuation of discrete one-dimensional piecewise linear expanding [Bec93] maps with uniform slope. The index a denotes a control parameter, which is the slope of the map. If $|a| > 1$ the map is expanding, and its Lyapunov exponent $\lambda := \ln |a|$ is greater than zero. Thus, $M_a(x)$ is

dynamically unstable and may in this sense be called chaotic [Ott93]. In order for the map to be chaotic and piecewise linear, it cannot be monotonic, so there must be points of discontinuity and/or non-differentiability.

The term “chain” in the characterization of $M_a(x)$ can be made more precise as a *lift of degree one*,

$$M_a(x+1) = M_a(x) + 1 \quad , \quad (2.4)$$

for which the acronym *old* has been introduced [Mis89, Als89b, Kat95]. This means that $M_a(x)$ is to a certain extent translational invariant. Being *old*, the full map $M_a(x)$ is generated by the map of one box, e.g., on the unit interval $0 < x \leq 1$, which will be referred to as the *box map*. In this chapter it shall be assumed that the graph of this box map is point symmetric with respect to the center of the box at $(x, y) = (0.5, 0.5)$. This implies that the graph of the full map $M_a(x)$ is anti-symmetric with respect to $x = 0$,

$$M_a(x) = -M_a(-x) \quad , \quad (2.5)$$

so that there is no “drift” in the chain of boxes. The case with drift will be discussed in Chapter 3. In Fig. 2.1, which contains a section of a simple map of this type, the box map has been chosen to

$$M_a(x) = \left\{ \begin{array}{ll} ax & , \quad 0 < x \leq \frac{1}{2} \\ ax + 1 - a & , \quad \frac{1}{2} < x \leq 1 \end{array} \right\} \quad , \quad a \geq 2 \quad , \quad (2.6)$$

cf. Refs. [Gro82, Gas92c, Ott93]. This example may be classified as a *Lorenz map with escape* [Guc90, Pei92, Gle93, Hub90, Als89a]. The chaotic dynamics of this type of maps is generated by a “stretch-split-merge”-mechanism for a density of points on the real line [Pei92]. For sake of brevity, Eq.(2.6), together with Eqs.(2.3) and (2.4), and trivially fulfilling Eq. (2.5), may be referred to as map \mathcal{L} . Related maps have been discussed in Refs. [Gro82, Fuj82, Art91, Gas92c, Kla96, Gro83, Tho83, Kla97].

It has been proposed [Fuj82] to look at the dynamics in this chain of boxes in analogy to the process of *Brownian motion*: [Wax54, vK92]: If a particle stays in a box for a few iterations, its internal box motion is supposed to get randomized and may resemble the microscopic fluctuations of a Brownian particle, whereas its external jumps between the boxes could be interpreted as sudden “kicks” the particle suffers by some strong collisions. This suggests that “jumps between boxes” contribute most to the actual value of the diffusion coefficient. Brownian motion is usually described in statistical physics by introducing some stochasticity into the equations which model a diffusion process. The main advantage of the simple model discussed here is that diffusion can be treated by taking the full dynamics of the system into account, i.e., the complete orbit of the moving particle is considered, without any additional approximations. This is another way to understand the notion of deterministic diffusion in contrast to diffusion as obtained from stochastic approaches. That is, in the purely deterministic case the orbit of the particle is immediately fixed by determining its initial condition.

One should note that the strength of diffusion, and therefore the magnitude of the diffusion coefficient, are related to the probability of the particle to escape out of a box, i.e., to perform a jump into another box. This escape probability, however, as well as the average distance a particle travels by performing such a jump, changes by varying the system parameter. The problem that will be solved in the following is to develop a general method for computing parameter-dependent diffusion coefficients $D(a)$ for piecewise linear maps on the line. Here

map \mathcal{L} will serve as a simple example. However, the methods to be presented should work as well for any other piecewise linear map of the type introduced above, evidently with analogous results [Kla96, Kla97].

2.2 A fractal parameter-dependent diffusion coefficient

To describe the dynamical behaviour of an arbitrary initial density for a set of particles on some interval of the line $-\infty \leq x \leq \infty$, we will need the Liouville (continuity) equation of the dynamical system, which is usually called *Frobenius-Perron equation* in case of time-discrete maps. This Frobenius-Perron equation is given by [Las94, Ott93, Gas98a, Dor99]

$$\rho_{n+1}(x) = \int dy \rho_n(y) \delta(x - M_a(y)) \quad , \quad (2.7)$$

where $\rho_n(x)$ is the probability density for points on the line, and $M_a(y)$ is the map under consideration. We suppose that the motion takes place on an interval $0 < x < L$, and we impose periodic boundary conditions, i.e. $\rho_n(0) = \rho_n(L)$, or absorbing boundary conditions, $\rho_n(x) = 0$ for $x = 0, L$, for all n [vK92]. Next we use the argument of Gaspard and coworkers [Gas90, Dor95, Gas95c, Gas92a, Gas92b, Gas93, Gas92c] to relate the eigenmodes of the Frobenius-Perron equation to the solution of the diffusion equation

$$\frac{\partial \varrho(x, t)}{\partial t} = D \frac{\partial^2 \varrho(x, t)}{\partial x^2} \quad , \quad (2.8)$$

where $\varrho(x, t)$ is the macroscopic density of particles at a point x at time t , and D is a diffusion coefficient. If for large L , and large n , the first few eigenmodes of the Frobenius-Perron equation are identical to those of the diffusion equation, the diffusion coefficient can be obtained by matching eigenmodes in an appropriate scaling limit. More explicitly, for periodic boundary conditions $\varrho(0, t) = \varrho(L, t)$, one can easily see that for large times $\varrho(x, t)$ has the form

$$\varrho(x, t) = \text{const.} + A \exp(-D(4\pi^2/L^2)t \pm i(2\pi/L)x) \quad . \quad (2.9)$$

Consequently, if one can find a solution of Eq. (2.7), for large L and n , in the form of

$$\rho(x, n) = \text{const.} + A' \exp(-\gamma_p(a)n \pm i(2\pi/L)x) \quad , \quad (2.10)$$

one can relate the decay rate $\gamma_p(a)$ to D by

$$D(a) = \lim_{L \rightarrow \infty} (L/2\pi)^2 \gamma_p(a) \quad . \quad (2.11)$$

For absorbing boundary conditions one links the diffusion coefficient to the escape rate from the system by an equation similar to Eq.(2.11) [Kla96, Kla99a]. The escape-rate formalism of chaotic dynamics shows that the escape rate from a system with absorbing boundaries is equal to the Lyapunov exponent minus the Kolmogorov-Sinai entropy for particles trapped within the system whose trajectories lie on a fractal repeller [Gas90, Dor95, Gas95c]. For the case of maps with slopes of uniform magnitude considered here, the Komolgorov-Sinai entropy for the fractal repeller $h_{KS}(a)$ is identical to the topological entropy of points on the repeller and it can be computed from $\gamma_p(a)$ as $h_{KS}(a) = \log a - \gamma_p/4 + O(L^{-3})$ [Gas92a, Gas92b, Gas93].

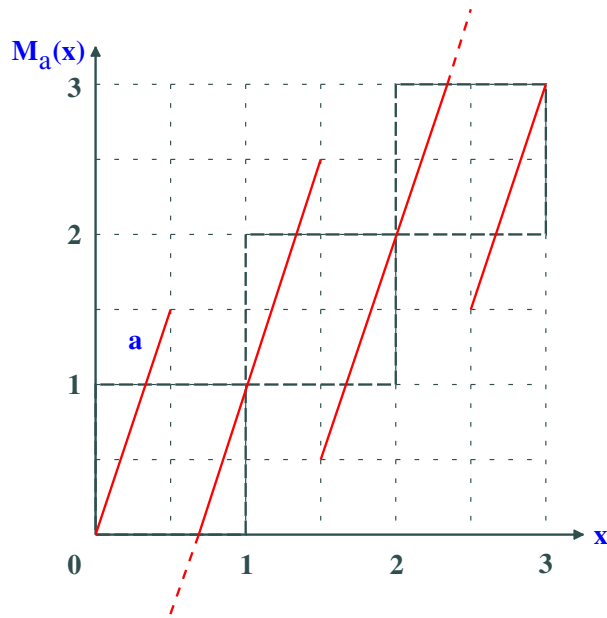


Figure 2.2: Illustration of the dynamical system denoted as map \mathcal{L} , cf. to Eqs. (2.3) to (2.6), for a particular slope, $a = 3$. The Markov partition given by the dashed grid leads to the construction of the transition matrix in Eq. (2.13).

The use of maps with uniform slope is not an essential ingredient in the calculation of $D(a)$ described below, which can be applied to more general linear maps. The main idea is that the Frobenius-Perron equation can be written as a matrix equation whenever the parameters of the map are such that one can construct a Markov partition of the interval $(0, L)$, which has the property that partition points get mapped onto other partition points by the map $M_a(x)$ [Boy79, Boy88, Bec93]. In a related context, these partitions have been discussed in [Hsu85, Bal94]. For such values of a , Eq.(2.7) can be written as

$$\boldsymbol{\rho}_{n+1} = (1/|a|) M \boldsymbol{\rho}_n \quad , \quad (2.12)$$

where $\boldsymbol{\rho}_n$ is a column vector of the probability densities in each of the Markov partition regions at time n , and M is a topological transition matrix whose elements M_{ij} are unity if points in region j can be mapped into region i , and are zero otherwise.

As a simple example we consider the form of the matrix M when $a = 3$ for map \mathcal{L} , and periodic boundary conditions are used on an interval of length L . In this case the regions of the partition are all of length $1/2$, as illustrated in Fig. 2.2. Then M is a $2L \times 2L$ matrix of the form

$$M = \begin{pmatrix} 1 & 1 & 0 & 0 & \cdots & 0 & 0 & 1 & 0 \\ 1 & 1 & 0 & 1 & 0 & 0 & \cdots & 0 & 0 \\ 1 & 0 & 1 & 1 & 0 & 0 & \cdots & 0 & 0 \\ 0 & 0 & 1 & 1 & 0 & 1 & 0 & 0 & \cdots \\ 0 & 0 & 1 & 0 & 1 & 1 & 0 & 0 & \cdots \\ \vdots & & & & \vdots & & & & \vdots \\ 0 & 1 & 0 & 0 & \cdots & 0 & 0 & 1 & 1 \end{pmatrix} . \quad (2.13)$$

In the limit $n \rightarrow \infty$, for any L , and any ‘‘Markov partition’’ value of a , the Frobenius-Perron equation can be solved in terms of the eigenmodes of M for any initial value $\rho_0(x)$

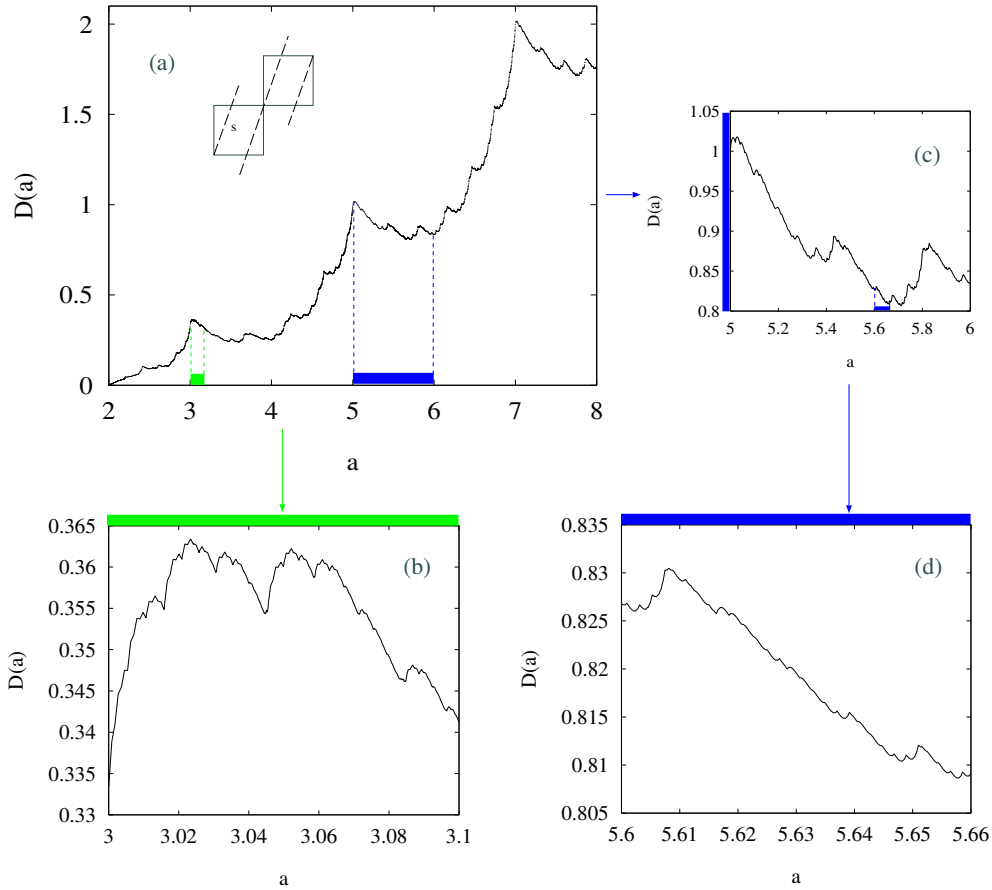


Figure 2.3: Diffusion coefficient $D(a)$ computed for the dynamical system map \mathcal{L} , see Eqs. (2.3) to (2.6), and some enlargements. Graph (a) consists of 7908 single data points. In graph (b)-(d), the dots are connected with lines. The number of data points is 476 for (b), 1674 for (c), and 530 for (d).

which is uniform in each of the Markov partition regions. For periodic boundary conditions, M is always a (block)circulant [Ber52, Dav79], the largest eigenvalue of M is precisely $|a|$ according to the Perron-Frobenius theorem [Gan71], and the corresponding eigenmode is a constant, representing the equilibrium state. The rate of decay to equilibrium, $\gamma_p(a)$, is obtained as $\gamma_p(a) = \log(|a|/\chi_1)$, where χ_1 is the next largest eigenvalue of M [Gas92a, Gas92b, Gas93]. Analytical expressions for $D(a)$ can be derived for all integer values of $a \geq 2$. For even integers, the results of Grossmann and Fujisaka [Gro82, Fuj82] are recovered, $D(a) = (1/24)(a-1)(a-2)$, and for odd integers we find $D(a) = (1/24)(a^2 - 1)$. To obtain $D(a)$ for a general Markov partition value of a , one can use computer methods.¹

Fig. 2.3 (a) shows the results for the diffusion coefficient of the dynamical system map \mathcal{L} , Eqs.(2.3) to (2.6), for values of a in the range $2 \leq a \leq 8$. In Fig. 2.3 (b)-(d), we present magnifications of three small regions in this interval.² One can see clearly that $D(a)$ has a complicated fractal structure with regions exhibiting self-similar like structures.

¹For circulant matrices, standard software packages (NAG, IMSL) do not always give the full spectrum correctly [Bea91], but the results for the first two largest eigenvalues are reliable.

²For a chainlength of $L = 100$, the numerical precision for each $D(a)$ is always better than 0.1% with respect to the limit in Eq.(2.11). Therefore, errorbars do not appear in the diagrams.

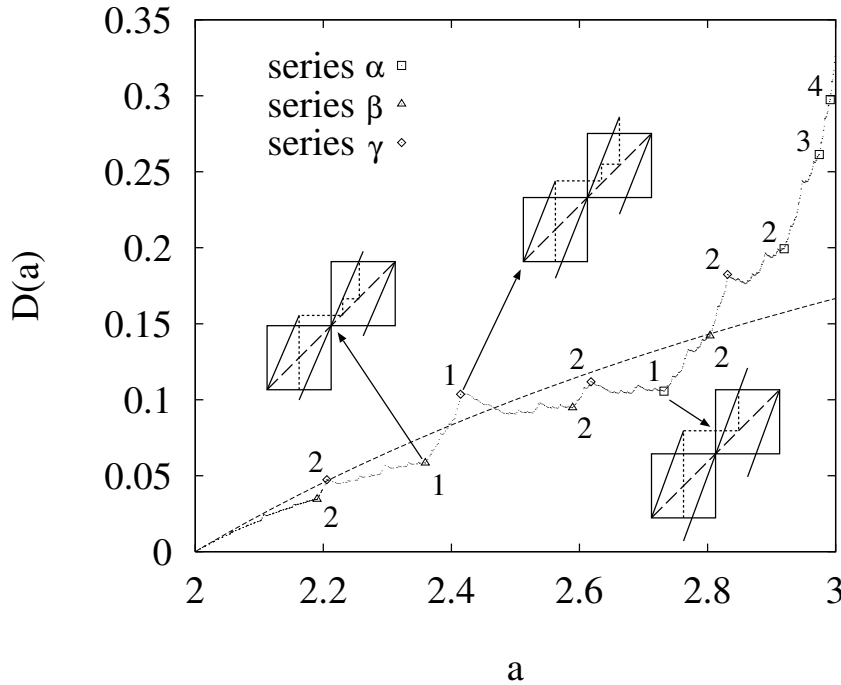


Figure 2.4: Enlargement of the region of slope $a \leq 3$ with the solution for a simple random walk model (dashed line) and labels for the values which are significant for “turnstile dynamics” (see text). For some points, the turnstile coupling is shown by pairs of boxes. The graph consists of 979 single data points.

In Ref. [Kla03a], fractal dimensions of this curve were computed both from the box counting method [Man82, Ott93, Pei92] and by evaluating the autocorrelation function of this graph [Fal90, Tri95]. Both dimensions were found to be fractal for large parameter intervals, with values that are very close to, but different from one. However, even further, both quantities turned out to be themselves fractal functions of the control parameter if computed locally on a uniform grid of small but finite subintervals. This points to the fact that the diffusion coefficient is not a simple, strictly self-similar or self-affine fractal, but exhibits a more intricate type of irregularity. Correspondingly, we characterized the diffusion coefficient displayed in Fig. 2.3 as a *fractal fractal function* [Kla03a].

In Fig. 2.4, we show an enlargement of the region for $2 \leq a \leq 3$. The dashed line is the prediction of $D(a)$ for a simple random-walk model suggested by Schell, Fraser and Kapral [Sch82]. Note that the model correctly accounts for the behaviour of $D(a)$ near $a = 2$. The wiggles in this graph can be understood by considering the transport of particles from one unit interval to another. These regions are coupled to each other by *turnstiles*, where points in one unit interval get mapped outside that particular interval into another unit interval. As in the case of two-dimensional twist maps, such as the sawtooth map, these turnstiles are crucial for large-scale transport [Wig92, Mac84, Che89, Che90, Mei92].

The region $2 \leq a \leq 3$ can be analyzed by studying the interaction of turnstiles. One can recognize three distinct series of values of a , each of which provides a cascade of seemingly self-similar regions of decreasing size, as the limits $a \rightarrow 2$ or $a \rightarrow 3$ are approached. To understand these series, consider the trajectory of a point that starts just to the left at $x = 1/2$. The first iterate of $x = 1/2$ is in the second interval, $(1, 2)$. The *series alpha* values of a are defined by the condition that the second iterate of $x = 1/2$ is at the leftmost point

of the upward turnstile in the second interval $(1, 2)$ ($a = 2.732$), or that the third iterate is at the corresponding point in the third interval ($a = 2.920$), etc. The numbers on the graph refer to the number of intervals the image of $x = 1/2$ has travelled before it gets to the appropriate point on the turnstiles. *Series β* points are defined in a similar way, but they are allowed to have two or more internal reflections within an interval before reaching the left edge of a turnstile. *Series γ* points are defined by the condition that some image of $x = 1/2$ has reached the rightmost edge of an upward turnstile (i.e. some point $x = n + 1/2$, where n is an integer), and consequently an increase in a will lead to a decrease in $D(a)$. These cascades provide a basis for a physical understanding of the features of $D(a)$ in this region: Particles leave a particular unit interval through a turnstile and undergo a number of iterations before they are within another turnstile. Whether they continue to move in the same or the reverse direction at the next and later turnstiles is a sensitive function of the slope of the map. Thus the fractal structure of the $D(a)$ curve is due to the effects of long-range correlations among turnstiles and these correlations lead to changes of $D(a)$ on an infinitely fine scale. A similar argument can be employed to explain, at least qualitatively, the fractal structure of $D(a)$ for higher values of the slope, although more work needs to be done before a full understanding of this curve is obtained.³

2.3 Summary

1. We have motivated a deterministic chaotic approach towards a theory of nonequilibrium transport by generalizing diffusion starting from a simple random walk on the line. As an example, we have introduced a simple piecewise linear one-dimensional deterministic map modeling a diffusion process by using deterministic chaos.
2. For such types of dynamical systems we have developed a method that enables to compute the full parameter-dependent diffusion coefficient numerically exactly. This method is based on solving the eigenvalue problem of the Liouville (Frobenius-Perron) equation of the dynamical system by constructing the Liouville operator in terms of topological transition matrices. The diffusion coefficient can then be related to specific eigenvalues of this matrix. The result turns out to be a *fractal fractal function* of the control parameter of the map, in the sense that the fractal dimension of this curve is itself a fractal function of the control parameter. For a certain parameter region, a heuristic explanation of the self-similar like structure is given in terms of specific microscopic scattering processes that change in a very complicated way under parameter variation.

³These qualitative explanations are not sufficient to get the exact values for all the local extrema of $D(a)$. Compare, e.g., $a = 3, 5, 7, \dots$

3 Negative and nonlinear response in deterministic drift-diffusion processes

We study chaotic transport in a one-dimensional periodic array of scatterers defined by a piecewise linear map on unit intervals. We analyze the dynamics of this simple model under application of a bias. Two methods for calculating the transport coefficients are outlined: One starts from a rigorous mathematical analysis of the cumulant generating function supplemented by twisted boundary conditions. The other one is based on the numerical evaluation of topological transition matrices. We find that our model exhibits a rich phase diagram in the parameter plane: For typical parameter values the current as well as the diffusion coefficient are fractal functions of their two control parameters. Especially at small values of the bias particles may, depending on the other parameter, move on average opposite to the bias, and at infinitesimally small bias there is in general no linear response. Moreover, close to the transition to non-chaotic behavior there are Arnold tongues where the current is fixed to a rational value, and there is no diffusion.

We start in Section 3.1 by defining our model, which consist of the simple map studied in the previous chapter amended by a second parameter mimicking the action of a bias. We then introduce the quantities we want to compute, namely the cumulants which yield in particular the current and the diffusion coefficient as functions of the two control parameters. In Section 3.1 we will outline two basic methods which both enable to compute exactly the values of these quantities for our model system. Section 3.3 is devoted to an analysis of the phase diagram emerging in the parameter plane for our system. Its fundamental structure is explained by simple heuristic arguments. We then numerically evaluate the current and the diffusion coefficient on the basis of our methods and discuss the results with respect to the phase diagram.

As we already mentioned in the introduction Section 1.3, this chapter features an unpublished older draft corresponding to the eventually published article Ref. [Gro02]. We include this version here, because it contains still unpublished results as well as some further, possibly helpful explanations that have been skipped for the completely rewritten published version. Both works have been performed together with J. Groeneveld.

3.1 A simple chaotic drift-diffusion model: mathematical definition

The model studied in the following is defined by a map M of the line \mathbb{R} onto itself having the property that “the translation by M ”, i.e. the function $M(x) - x$, is periodic in x with period one so that it satisfies, for all $x \in \mathbb{R}$, the relation

$$M(x + 1) = 1 + M(x) \quad . \quad (3.1)$$

To such a map M there is associated a map m of a half open/half closed interval or, equivalently, of the circle, onto itself, as can be made precise as follows: We first define within \mathbb{R} two “fundamental sets”, i.e. the two half open/half closed unit intervals $I_0^- = [-\frac{1}{2}, \frac{1}{2})$ and $I_0^+ = (-\frac{1}{2}, \frac{1}{2}]$. To say that such an interval I_0^ϵ is a “fundamental set of \mathbb{R} with respect to its normal subgroup \mathbb{Z} ” only means that any real number $x \in \mathbb{R}$ has the unique decomposition

$$x = y + n \quad (3.2)$$

into an integer $n \in \mathbb{Z}$ and an element $y \in I_0^\epsilon$. Accordingly, we may also decompose, for any fixed $\epsilon = \pm$, a function M satisfying the relation (3.1) uniquely as a sum of a map m of I_0^ϵ onto itself, and an integer valued function z with period one, as follows:

1. For $x \in I_0^\epsilon$ we define $m(x)$ and $z(x)$ by the relation

$$M(x) = m(x) + z(x) \quad (3.3)$$

and the conditions that $m(x) \in I_0^\epsilon$ and $z(x) \in \mathbb{Z}$.

2. This definition is extended to all of \mathbb{R} by imposing the relations $m(x + 1) = 1 + m(x)$ and $z(x + 1) = z(x)$. The result is that Eq.(3.3) holds true for any $x \in \mathbb{R}$. It is now also obvious that m not only follows linearly from M in a unique manner, but also that this is an idempotent operation, i.e. a projection.

We now specialize our M to being piecewise linear, and that of the simplest kind in that the number of its “laps” per unit interval equals one. We then arrive at the following specification of $M(x)$ for $|x| < \frac{1}{2}$:

$$M(x) = ax + b \quad , \quad (3.4)$$

wherein a and b are two real parameters. This definition is completed by assigning to $M(\frac{1}{2})$ a respective value.

Our object of study here is to determine the long-time behavior of the position x_n at time n of a point particle starting at time $n = 0$ at x_0 which moves in discrete time steps $n = 0, 1, \dots$ according to the equation of motion

$$x_{n+1} = M(x_n) \quad . \quad (3.5)$$

The most general case would be to assume for the initial position x_0 any probability distribution or measure μ_0 restricted to either one of the fundamental intervals I_0^ϵ . As a

consequence of Eq.(3.5), x_n will have a distribution μ_n whose time dependence is governed by the Frobenius-Perron operator \mathcal{L}_F corresponding to the map M , symbolically written as

$$\mu_{n+1} = \mathcal{L}_M \mu_n \quad . \quad (3.6)$$

The distribution μ_n of x_n can be gathered from the characteristic function $Q_n(u)$ of μ_n defined by

$$Q_n(u) = \langle e^{ux_n} \rangle_0 \quad (3.7)$$

with $\langle \dots \rangle_0 = \int_{-\infty}^{\infty} d\mu_0 \dots$, wherein u is a complex number the real part $\Re(u)$ of which is sufficiently small so that the integral converges. The above would be equivalent to knowing the logarithm of $Q_n(u)$, which is the cumulant generating function [vK92],

$$\sum_{i=1}^{\infty} u^i K_i(n) = \log Q_n(u) \quad , \quad (3.8)$$

or, equivalently, to knowing the set of cumulants $K_i(n)$ ($i = 1, 2, \dots$) of μ_n . The first two of these are the most important ones to describe particle transport after long times, and are expressed in terms of the moments of x_n as follows:

$$K_1(n) = \langle x_n \rangle_0 \quad , \quad (3.9)$$

and

$$K_2(n) = \langle x_n^2 \rangle_0 - \langle x_n \rangle_0^2 \quad . \quad (3.10)$$

In terms of these the current J and the diffusion coefficient D can be expressed, at least if these limits exist, by

$$J \equiv c_1 = \lim_{n \rightarrow \infty} \frac{1}{n} K_1(n) \quad (3.11)$$

and

$$D \equiv c_2 = \lim_{n \rightarrow \infty} \frac{1}{2n} K_2(n) \quad . \quad (3.12)$$

c_1 was already considered by Poincaré [Poi54, Ito81] and is also known as the “rotation number” or “winding number”. The quantity c_2 for this model at $b = 0$ was studied in detail in Refs. [Kla95, Kla96, Kla99a]. These quantities c_k for any k will be referred to as the *cumulant rates* or *scaled cumulants* [Duf95] of the dynamical system. For $k \geq 3$ they yield the higher-order Burnett coefficients [Dor77].

The limits in Eqs.(3.11) and (3.12) depend in general on the initial measure μ_0 . For example, if μ_0 is chosen to be concentrated on a single point x_0 , then, due to the property of sensitive dependence on initial conditions for $|a| > 1$, stationary measures do not exist and, even worse, the corresponding measures do not represent the physical properties one is interested in. Hence, it seems necessary to restrict the measures we will consider to a smaller class. A minimal requirement for such a class should be the invariance under the Frobenius-Perron operator of the dynamical map M of the problem at hand. In particular, one would like it to contain the natural Lebesgue measure on the space considered, and one would like it to be small enough such that the Frobenius-Perron operator would only have a single invariant vector. In addition, one would like to be able to do analysis, and so one would need a certain topology or even a metric on the function space.

In the present problem there are several choices which meet all these requirements. One choice is the following: We consider the space of probability distributions with piecewise constant densities $\rho(x) : \mathbb{R} \rightarrow \mathbb{R}$, which are related to the measure by

$$d\mu = \rho(x)dx \quad . \quad (3.13)$$

Firstly, this choice is physically reasonable. And secondly, as we can prove [Gro], the values of the above cumulant rates c_1, c_2, \dots do not depend on the particular choice of $d\mu_0$ from this class. Therefore, the values allowed this way are arguably the physical relevant ones.

3.2 ⁺Calculating deterministic drift and diffusion coefficients

In this section we outline two basic methods to compute various dynamical properties of the model, such as the cumulant rates c_k and some time dependent quantities:

1. *Groeneveld's twisted eigenstate method*, which is rigorous and explicit enough so as to allow for further mathematical analysis.
2. The improvements obtained along the lines of the *transition matrix methods* described in Refs. [Kla95, Kla97, Kla96, Kla99a].

We will focus on the essential ideas of these methods only. Further technical details, in particular rigorous mathematical proofs in the case of the first method, will be given elsewhere [Gro, Kla].¹

3.2.1 Groeneveld's twisted eigenstate method

The professed central aim of this method is to obtain the large time behavior of the probability distribution of x_n , which is tantamount to computing the characteristic function $Q_n(u)$ of x_n with respect to the initial measure μ_0 . For this purpose, one takes advantage of the following two basic features:

- 1) The discrete translational symmetry in the problem as given by Eq.(3.1) can be expressed by saying that the map $M(x)$ and the discrete translation operator $T(x) = 1 + x$ commute,

$$MT = TM \quad . \quad (3.14)$$

This allows one to split the function space on which the Frobenius-Perron operator \mathcal{L}_M of Eq. (3.6) acts into eigenspaces of a corresponding translation operator \mathcal{L}_T . The elements of these latter spaces can be reinterpreted as functions on a unit interval with properly modified boundary conditions, which are also called *twisted* boundary conditions in the literature (see Refs. [Fis73, Gro81] and further references therein). In the present case one

¹Here we outline Groeneveld's method as understood by the present author, on the basis of kind explanations by its creator. We emphasize that J.Groeneveld is not responsible for any ambiguities that are contained in this sketch of his method. For a more detailed presentation that is approved by the inventor see Ref. [Gro02].

such space, which is characterized by a complex number u called “twist parameter”, consists of functions satisfying

$$\psi(x + 1) = e^{-u}\psi(x) \quad (3.15)$$

where $\psi(x)$ is a \mathbb{C} -valued function on the real line. In addition, these functions are required to be of bounded variation. The corresponding Frobenius-Perron operator will then be denoted with $\mathcal{L}_M(u)$. It should be remarked that, in the general case of $e^u \neq 1$, probability is no longer conserved globally, although it still is locally. This is expressed by the fact that the stationary eigenstate of $\mathcal{L}_M(u)$ obeying

$$\mathcal{L}_M(u)|\Phi \rangle = \lambda(u)|\Phi \rangle \quad , \quad (3.16)$$

which approaches the equilibrium one if $u \rightarrow 0$, has an eigenvalue $\lambda_0(u)$ which is no longer equal to one. It is just this quantity which contains all information we need to solve our problem, that of calculating the cumulant rates c_k . In fact, one has that their generating function

$$c(u) = \sum_{k=1}^{\infty} u^k c_k \quad (3.17)$$

is given by

$$c(u) = \log \lambda_0(u) \quad , \quad (3.18)$$

where in turn

$$\lambda_0(u) = \lim_{n \rightarrow \infty} \frac{1}{n} \log Q_n(u) \quad . \quad (3.19)$$

2) As a calculational device, which works only in dimension $d = 1$, the problem is reinterpreted in terms of one-dimensional electrostatics: The probability density can then be considered as an electric field strength, and a jump at a discontinuity of such a density is therefore regarded as a charge at that point. This is an entirely equivalent description of the problem, which has the virtue of facilitating the calculations of the spectrum of $\mathcal{L}_M(u)$ of which we need just $\lambda_0(u)$ for our present purpose. Only if we want to calculate time dependent quantities, such as velocity autocorrelation functions, as can also be done within the present formalism, we need the remaining parts of the spectrum of the operator. In this picture, the effect of $\mathcal{L}_M(u)$ on the point charges is to move them according to the map M as if they were particles, and to decrease their strengths by multiplying them with a factor of $1/a$. There is then a simple procedure to obtain an equation which determines $\lambda_0(u)$ uniquely for sufficiently small u and hence all coefficients c_k in Eq.(3.17).

To obtain that crucial formula, the action of \mathcal{L}_M on the set of piecewise constant functions defined above must be translated respectively. We note that the latter are characterized by a set of point charges such that the sum of the positive ones within either of the intervals I_0^\pm is finite, as well as that of the negative ones (the sum of the absolute magnitudes of these two total charges is just the “bounded variation”-norm alluded to earlier). However, before letting the map M act on these charges in the way mentioned above, the Frobenius-Perron operator makes a small modification of such a state:

Step A: modify At every point where M is discontinuous a double layer is introduced consisting of two equal charges of opposite signs such that in-between these charges the electric field (i.e., the probability density) vanishes. This can always be done

and corresponds to shifting charges by an infinitesimal amount only; which implies that our present calculation of an equation for $\lambda_0(u)$ is still rigorous and precise. An important consequence of these modifications is that afterwards the total charge in each unit interval vanishes.

Step B: move and reduce In this next step all charges are moved and reduced in size as explained above.

The action of \mathcal{L}_M in the language of electrostatics then consists of these two parts A and B, or if one wishes: $\mathcal{L}_M(u) = \mathcal{L}_{M,B}(u)\mathcal{L}_{M,A}(u)$. The above techniques allow to derive an equation for $\lambda_0(u)$ which will turn out to determine, together with the condition

$$\lambda_0(u) \rightarrow 1 \quad \text{as} \quad u \rightarrow 0 \quad , \quad (3.20)$$

the function $\lambda_0(u)$ uniquely. The argument can be given in three steps:

1. One assumes that $\lambda \equiv \lambda(u) \neq 0$ is an eigenvalue of $\mathcal{L}_M(u)$ according to Eq.(3.16) and writes down the equations for the coordinates of all the charges which may occur in such an eigenstate, and for their strengths. For this purpose, we recall that $\epsilon = \pm$, $I_0^+ = (-\frac{1}{2}, \frac{1}{2}]$, and $I_0^- = [-\frac{1}{2}, \frac{1}{2})$, and start with

$$y_0^\epsilon = \frac{\epsilon}{2} \quad . \quad (3.21)$$

Next we define for all $r = 0, 1, \dots$ the numbers n_r^ϵ and y_r^ϵ by the relation

$$n_r^\epsilon + y_{r+1}^\epsilon = a y_r^\epsilon + b \quad (3.22)$$

and the conditions $n_r^\epsilon \in \mathbb{Z}$ and $y_r^\epsilon \in I_0^{\epsilon\alpha^{r+1}}$, wherein α is a constant defined by $\alpha = \text{sign}(a)$.

2. The effect of $\mathcal{L}_{M,B}$ on an eigenstate is then just to “normalize” such a state in the sense that it is a projection operator: $\mathcal{L}_{M,B}^2 = \mathcal{L}_{M,B}$. Hence, if $|\Phi\rangle$ is an eigenstate with eigenvalue λ , so then is $\mathcal{L}_{M,B}|\Phi\rangle$.
3. Consequently, the total charge of an eigenstate, as far as located within either of the two fundamental intervals I_0^ϵ , must vanish. The strengths of these charges can be calculated recursively and involves all powers of λ . Requiring their sum to be zero then leads to a consistency equation of the form

$$C(\lambda, u) = 0 \quad . \quad (3.23)$$

The left hand side of this “consistency function” is defined by

$$C(\lambda, u) = \sum_{\epsilon=\pm} \epsilon \sum_{r=0}^{\infty} (\lambda a)^{-r} e^{u N_r^\epsilon} . \quad (3.24)$$

This equation for λ as a function of u is the central formula of our approach. It turns out that the consistency function is analytic in λ and u near the set $\lambda = 1$, $\Re(u) = 0$.

Furthermore, a simple argument shows that this equation has only a single root λ_0 which satisfies the further condition Eq.(3.20). This root turns out to be even analytic in u .

At this point all what remains to be done is to expand Eq.(3.23) into powers of $\log \lambda$ and u . Here one encounters certain “ N -quantities” defined for $r = 0$ by $N_0^\epsilon = -\frac{\epsilon}{2}$ and for $r = 0, 1, \dots$ by

$$N_{r+1}^\epsilon = N_r^\epsilon + n_r^\epsilon. \quad (3.25)$$

We note that $N_r^\epsilon \in \mathbb{Z} + \frac{1}{2}$. In addition, we will encounter certain “ N -moments” defined by

$$N_{k,l} = \frac{1}{k!l!} \sum_{\epsilon=\pm} \epsilon \sum_{r=0}^{\infty} a^{-r} (N_r^\epsilon)^k r^l. \quad (3.26)$$

Expanding into powers of $c \equiv \log \lambda$ and u by taking into account also Eq.(3.17) and Eq.(3.18), the above implicit equation for λ_0 is reduced to an explicit equation for each of the scaled cumulants c_k ($k = 1, 2, \dots$). These expressions turn out to be amenable to iterative calculations on a computer.

Here we display only the resulting formulas for c_1 and c_2 in the case of general (a, b) and for c_2 and c_4 in the bias-free case $b = 0$. They are:

1. For general (a, b) , c_1 and c_2 are given by

$$c_1 = N_{2,0}/N_{1,1} \quad (3.27)$$

$$c_2 = (N_{3,0} - N_{2,1}c_1 + N_{1,2}c_1^2)/N_{1,1} \quad (3.28)$$

2. For $b = 0$, the odd order c_k 's vanish and the expressions for c_2 and c_4 simplify to

$$c_2 = N_{3,0}/N_{1,1} \quad (3.29)$$

$$c_4 = (N_{5,0} - N_{3,1}c_2 + N_{1,2}c_2^2)/N_{1,1} \quad (3.30)$$

There are also alternative expressions in terms of the y -quantities instead of the above ones which are in terms of the N -quantities. Of these we display only the following intriguingly simple one for c_1 . It can be derived from Eq. (3.27) by using the relations (3.22), (3.25) and (3.26),

$$J = c_1 = b + (a - 1)y^{(2)}/y^{(1)} \quad (3.31)$$

wherein the $y^{(k)}$'s are defined, for $k = 1, 2$, by

$$y^{(k)} = \frac{1}{k!} \sum_{\epsilon=\pm} \epsilon \sum_{r=0}^{\infty} a^{-r} (y_r^\epsilon)^k \quad (3.32)$$

Finally, we remark that it follows as a direct consequence of the theorem of Perron-Frobenius that the quantities $N_{1,1}$ and $y^{(1)}$, which are related by

$$(a - 1)N_{1,1} = ay^{(1)} \quad (3.33)$$

are both positive for all real a and b with $|a| > 1$. This is comforting since it shows consistency with the fact that the above expressions require division by just either of these quantities. Hence these divisions can cause no problem.

The above expressions have been reformulated in terms of some simple, fast recursive schemes eminently suitable for numerical computations. Additionally, we remark that by employing the twisted eigenstate method proofs of several important properties of our model can be obtained, such as [Gro]:

- The Markov partition points are dense in the chaotic part ($|a| > 1$) of the parameter plane.
- For typical values of a , the ratio $J(a, b)/b$ has no limit as $b \rightarrow 0$.
- $D(a, 0)$ is continuous in a . That such a thing might be true was originally conjectured in Refs. [Kla95, Kla96, Kla99a] on the basis of detailed numerical evidence.

3.2.2 Transition matrix methods

An alternative way to solve the Frobenius-Perron equation (3.6) for our model, which is perhaps more physically intuitive, starts from writing this equation as a matrix equation, see Eq. (2.12). Here the probability density is given by a column vector at discrete time steps defined with respect to a certain partitioning in phase space, and the Frobenius-Perron operator is formulated in terms of a topological transition matrix. Solutions of the Frobenius-Perron equation can then be obtained either by solving the eigenvalue problem of the transition matrix [Kla95, Kla96, Gas98c, Kla99a], or by numerical iteration of this equation [Kla96, Kla97, Gas98c, Kla02a].

The fundamental problem is how to construct the matrix operator of Eq. (2.12). We elaborate on this by first briefly reviewing a method of construction which employs Markov partitions, cp. to Chapter 2.² We then discuss the limited applicability of this method in case of our two-parameter model. This leads to two improvements of the original method: one which incorporates a more efficient approach to obtain Markov partition points; and a second one which is not restricted to Markov partitions anymore.

1. Markov partition method:

Solving the Frobenius-Perron equation by using Markov partitions is a well-known technique in dynamical systems theory, see, e.g., Ref. [Bec93]. In Chapter 2, respectively in Refs. [Kla95, Kla96, Kla97, Kla99a], this approach has been employed to compute the diffusion coefficient D as a function of the slope a for our map $M_{a,b}$ specialized to the case $b = 0$. Here the fact has been used that for parameters where a Markov partition for the given map exists, the topological transition matrices of Eq. (2.12) can be constructed in a straightforward way. Thus, the applicability of this method, which we call *Markov partition method*, depends, firstly, on whether a Markov partition exists or not; secondly, on whether these partitions are dense in the parameter space; and thirdly, on whether the quantity to be calculated is continuous in the parameters.

Thus, an important sub-problem of this approach is that of finding parameter values corresponding to Markov partitions close enough to the values one is interested in. In case of the one-parameter model at $b = 0$, one can solve this sub-problem by defining a partition via the iteration of the critical point of the map. Markov parameter values of the slope a can then be computed as the roots of algebraic equations corresponding to certain classes of such orbits [Kla96, Kla99a]. However, in case of our two-parameter model considered here, two such algebraic equations must be solved simultaneously. This makes the method technically more difficult and numerically very inefficient. For this reason, a more efficient method was looked for to compute Markov partition parameter values.

²For Markov partitions in one-dimensional maps see [Rue89, dM93, Bow79].

1.a renormalized iteration method:

The basic feature of this method is that it converges to a Markov partition parameter pair nearby an arbitrary initial parameter pair (a, b) . The method starts by constructing transition matrices according to the prescription of the Markov partition method, but stopping this process after a finite number of steps irrespective of whether a Markov partition has been found or not. This implies making a small error in the construction of the matrices such that only an approximate matrix for a given parameter pair is obtained. A consequence is that this approximate matrix in the Frobenius-Perron equation (2.12) is no longer probability conserving. The loss of probability is then compensated by *renormalizing* the Frobenius-Perron equation at each time step. Under numerical iteration the probability density of this renormalized equation converges to the one of a Markov partition parameter pair nearby the original one. The parameter values of this Markov partition can then be easily determined.

A disadvantage of this renormalized iteration method, however, is that it still only solves the Frobenius-Perron equation for Markov partition parameter pairs. Therefore, it was desirable to develop a matrix method which would not be restricted to Markov partitions anymore.

1.b approximate iteration method:

Here, approximate transition matrices are constructed for arbitrary parameter pairs of our model in a way that the norm of the probability density in the Frobenius-Perron equation is preserved. The construction is such that for a given size of the partition, i.e. for a given number of its parts, and by continuously changing the two parameters, the matrices yield suitable interpolations between single Markov partition parameter pairs approximating the exact solution of the Frobenius-Perron equation. However, at any Markov partition parameter pair the method gives the exact results for the respective Markov partition. As can be proven [Gro], the Markov partitions are dense in the chaotic part ($|a| > 1$) of the parameter plane. For this reason, allowing the size of the partition to increase, this method converges everywhere to the exact results. In low order, that is, for small partition size, the method can be applied analytically. In higher order, that is, for larger partitions, it was implemented numerically.

3.2.3 Numerical comparison of the different methods

Both the improved transition matrix methods 1.a and 1.b and the twisted eigenstate method have been implemented numerically for our two-parameter model. The twisted eigenstate method yields analytically exact expressions for the first four cumulant rates c_k , although it is not restricted to these. The two improved transition matrix methods described here, on the other hand, provide a direct picture of the spreading of the probability density in time and space starting from some initial density. In this sense, the matrix methods give access to more information than the twisted eigenstate method, which, at the moment, focuses on the asymptotic behavior of the cumulant rates. That is, via the time dependent probability density all relevant time-dependent quantities can be obtained such as higher cumulant rates and velocity autocorrelation functions [Kla96].

However, the matrix methods are not yet optimized for efficiently computing the values of the cumulant rates in the limit of infinite time. Such an optimization could be obtained by using Green-Kubo formulas, as has been outlined in Refs. [Kla96, Gas98c]. Here the twisted eigenstate method is numerically much more efficient and precise. Apart from that, the

twisted eigenstate method is mathematically rigorous and thus allows one to obtain proofs of important general properties of the present model.

The numerical differences may be illustrated by the following results: We chose some typical values in the parameter plane. We then applied our different methods to compute the first four cumulant rates at these parameters as described above. To iterate transition matrices up to a size of about 2500 x 2500 elements over 40 time steps, the matrix methods required computing times of about 0.4 to 4 CPU seconds per parameter pair on a SUN Ultra-5 and on DEC-Alphas. For the renormalized iteration method 1.a, this yielded a precision of about 12 digits behind the dot in the cumulant rates, for the approximate iteration method 1.b the precision was about 5 digits. The twisted eigenstate method, on the other hand, required for the same parameter values and for a precision of much more than 12 digits behind the dot CPU times in the order of 10^{-3} to 10^{-4} seconds. Through application of these different methods we have verified that the numerical error is less than visible in our following Figs. 3.2, 3.3, 3.6 and 3.7. In case of the other figures, it has been checked via convergence of the data that the numerical error is also less than visible.

3.3 The phase diagram of this two-parameter model

In this section we explore the parameter plane (a, b) of our model. We characterize the different regions in it according to certain topological properties of the map M and by studying the qualitative behavior of certain dynamical order parameters of the system, such as the Lyapunov exponent and the cumulant rates $J = c_1$ and $D = c_2$.

We start by discussing what may be denoted as the *phase diagram* of our two-parameter model, by which we understand a kind of a map indicating the different dynamical phases distinguished by the above criteria, see Fig. 3.1. Since our model $M \equiv M_{a,b}$ obeys the translation symmetry as expressed by $M_{a,b} + 1 = M_{a,b+1}$, cf. Eq.(3.1), and the reflection symmetry as expressed by $M_{a,b}(x) = -M_{a,-b}(x)$, it follows straightforwardly that the cumulant rates $c_k \equiv c_k(a, b)$ satisfy $c_k(a, b + 1) = c_k(a, b) + \delta_{k,1}$ and $c_k(a, -b) = (-1)^k c_k(a, b)$, for $k = 1, 2, \dots$. Keeping these simple relations in mind it follows that one may, without loss of generality, restrict the discussion of the parameter plane to a *fundamental strip*, e.g., to the region defined by $0 \leq b \leq \frac{1}{2}$. In Fig. 3.1 the positive a part of the fundamental strip of the parameter plane is represented.

First, there is the Lyapunov exponent which, for the present model, is equal to $\ln |a|$. This fact implies that the phase diagram can be subdivided into three connected regions according to the sign of the Lyapunov exponent: One *non-chaotic* region given by $|a| < 1$, and two *chaotic* regions defined by $a < -1$ and $a > 1$ respectively. In case of the positive- a part shown in the figure this separation of the parameter plane is indicated by the dotted vertical line at $a = 1$. As will be discussed below, the picture of the various phases in the region close to this transition line turns out to be quite complicated.

A second way of characterizing the dynamical system is in terms of topological invariants: As a first and simplest example we take the property whether or not the movements of the particles are restricted to be possible only in the direction of the bias b . In the case $b > 0$, which we shall without loss of generality assume, this is equivalent to the assumption that our map $M_{a,b}(x)$ satisfies for all x the condition $M(x) > x$. Because of the assumed periodicity with period one of $M(x) - x$, cf. Eq.(3.1), this is equivalent to the condition

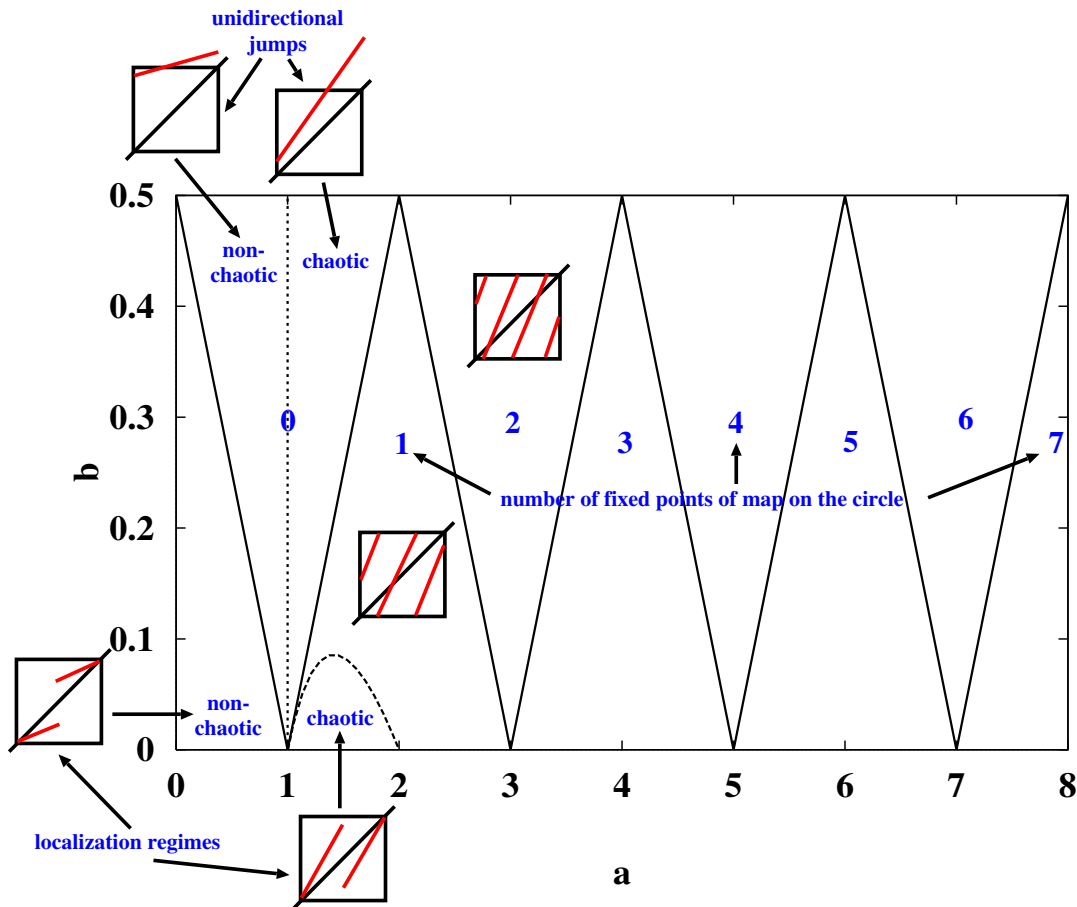


Figure 3.1: The most significant part of the positive a -region of the parameter plane of the map $M_{a,b}$: Parts for other values of b follow by the reflection and translational symmetries of the system. At the zig-zag lines, as parameters are varied, fixed points of the projected map $m_{a,b}$ of the circle onto itself are generated or disappear. These straight lines thus separate regions characterized by a particular value of the number of fixed points of the circle map $m_{a,b}$. Also shown is one of the Arnol'd tongues characterized by $2 > a > 1$ and $J = 0$ for $b \rightarrow 0$.

that for $|x| < \frac{1}{2}$ it is $ax + b > x$, which is equivalent to the condition that

$$2b > |a - 1| \quad . \quad (3.34)$$

The latter inequality defines a region of the parameter plane confined by two straight lines intersecting at $a = 1, b = 0$, as shown in Fig. 3.1. In the positive a -part of the fundamental parameter strip depicted in that figure, regions are then further subdivided by the values attained by a more general topological invariant, *viz.* the number of fixed points of the associated circle map $m_{a,b}$. A simple reasoning shows that the zig-zag lines in that figure can be obtained from the single straight line in the figure given by the equation $2b = 1 - a$, which is just one of the two straight lines determined by Eq.(3.34), by means of the symmetry operations $b \rightarrow b + 1$ (translation symmetry) and $b \rightarrow -b$ (reflection symmetry). It follows that whenever one crosses the zig-zag line shown in the figure, the number of fixed points of the projected map m changes by one. On the other hand, from Fig. 3.2 we observe that just at these lines the surfaces representing the current J and the diffusion coefficient D exhibit certain ridges.

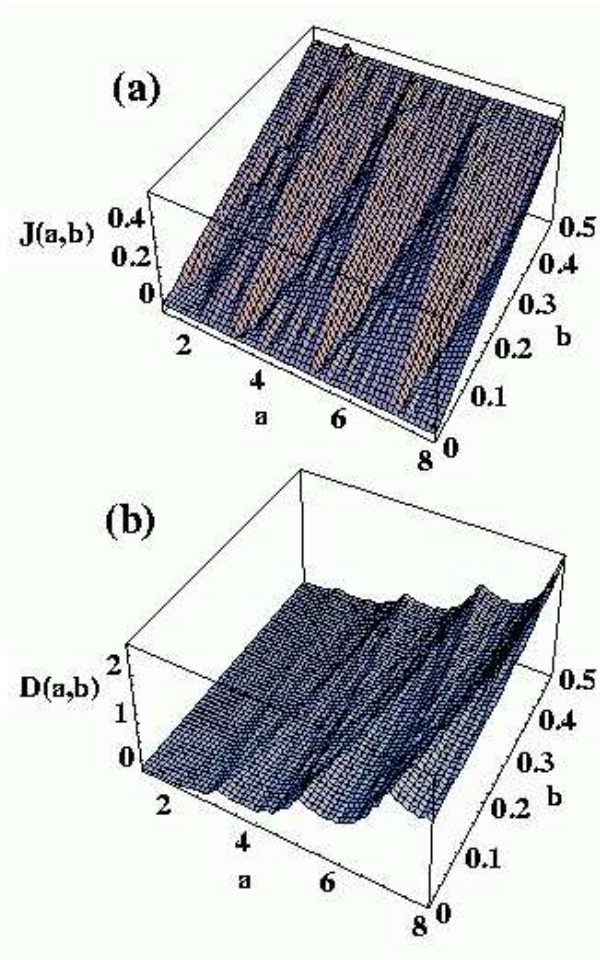


Figure 3.2: Three-dimensional plots of (a) the current $J(a, b)$, and (b) the diffusion coefficient $D(a, b)$, as functions of the control parameters a and b . Computations were performed on the basis of the explicit formulas for these quantities derived by means of the twisted eigenstate method, see Section 3.2. One notices that both surfaces are “scarred” along just the same straight lines as drawn in Fig. 3.1.

These lines are related to the process in which certain Markov partitions are generated [Kla]: In Fig. 3.1, each line of the zig-zag curve corresponds to the situation that one of the two critical points of m is mapped, in a single iteration, onto an endpoint $x = \pm \frac{1}{2}$. Wherever two such curves intersect, as e.g., at $a = 3, 5, 7, \dots$ and $b = 0, 0.5$, one finds oneself in a Markov partition point. Thus, we observe that at places where such a “half-way Markov condition” as meant above is satisfied, this appears to be reflected in the structure of the cumulant rates J and D . In addition, upon closer scrutiny of Fig. 3.2 further such topological subdivisions of the primary regimes of Fig. 3.1 can be detected. Such higher-order topological effects may eventually form the key to understand the full structure in the parameter dependence of the cumulant rates. In this respect we note that in case of $b = 0$ a related argument has been used to understand the complicated structure of the diffusion coefficient $D(a, 0)$ for our model in the region $2 < a < 3$ [Kla95, Kla96, Kla99a], cf. Section 2.2.

We furthermore remark that $J(a, b) = b$ for $a \in \mathbb{N}$ and $J(a, b) = b$ for $2b \in \mathbb{N}$, which yields the exact boundaries in Fig. 3.2 (a). Note that in a small spot near the point $(a = 2, b = 0.5)$ the function $J(a, b)$ goes down far too steeply for it to be visible, in the chosen perspective,

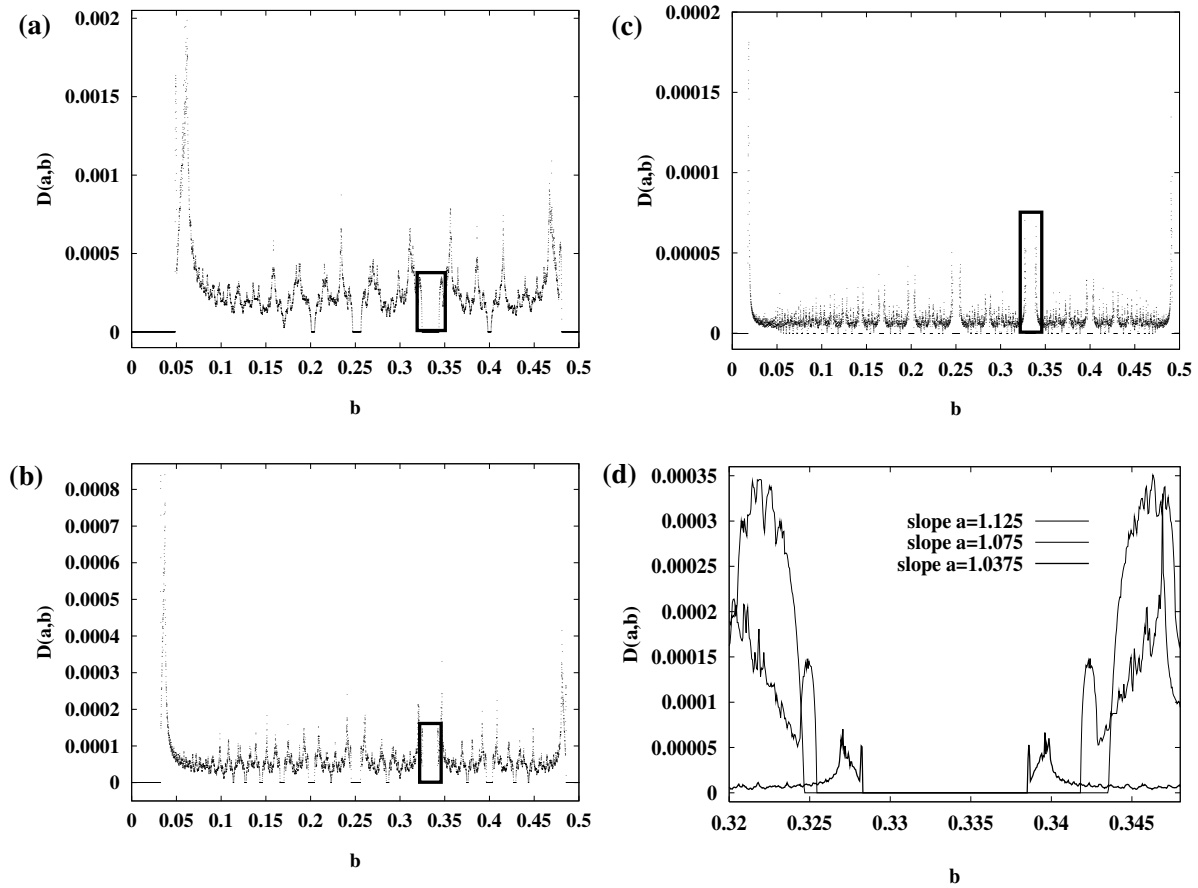


Figure 3.3: Diffusion coefficient $D(a, b)$ as a function of the shift b for three fixed values of the slope a : (a) $a = 1.125$, (b) $a = 1.075$, (c) $a = 1.0375$. With a approaching the line $a = 1$ where a transition to non-chaotic behavior occurs, one observes more and more b -intervals with vanishing diffusion coefficient. In these regions mode locking occurs as is shown in Figs. 3.4 and 3.5. These are the well-known Arnold tongues whose number increases to infinity as $a \rightarrow 1$. Their boundaries can be calculated exactly. The black boxes in subfigures (a), (b) and (c) indicate the region which is magnified in subfigure (d).

that at the boundary it indeed ends up at the value $J(a, 0.5) = 0.5$. At the boundary of Fig. 3.2 (b) at $a = 1$ it is $D = 0$ for all b , and at $a = 8$ it exactly equals $7/4$ for all b , as can easily be verified analytically.

A third way in which we have classified points of the parameter plane, which is more physically relevant but also more difficult than the previous analysis, is a subdivision of the plane according to the qualitative behavior of quantities such as J and/or D . An example of this is the subdivision of the chaotic region for $a < 2$ into Arnold tongues, which are well-known from the sine circle map [Dim87, Hao89]. In these subregions there is no diffusion, and the current J is fixed to a rational value. In Fig. 3.1 we have depicted part of the boundary curve of just one of them, which is easily calculated from an exact algebraic equation.

However, this is only a first example of a region consisting of points for which the corresponding dynamical system has the property that there exist certain intervals on the line from which a particle cannot escape once it is inside them. In these situations the diffusion coefficient evidently vanishes, $D(a, b) = 0$. Further such Arnold tongue regions can be dis-

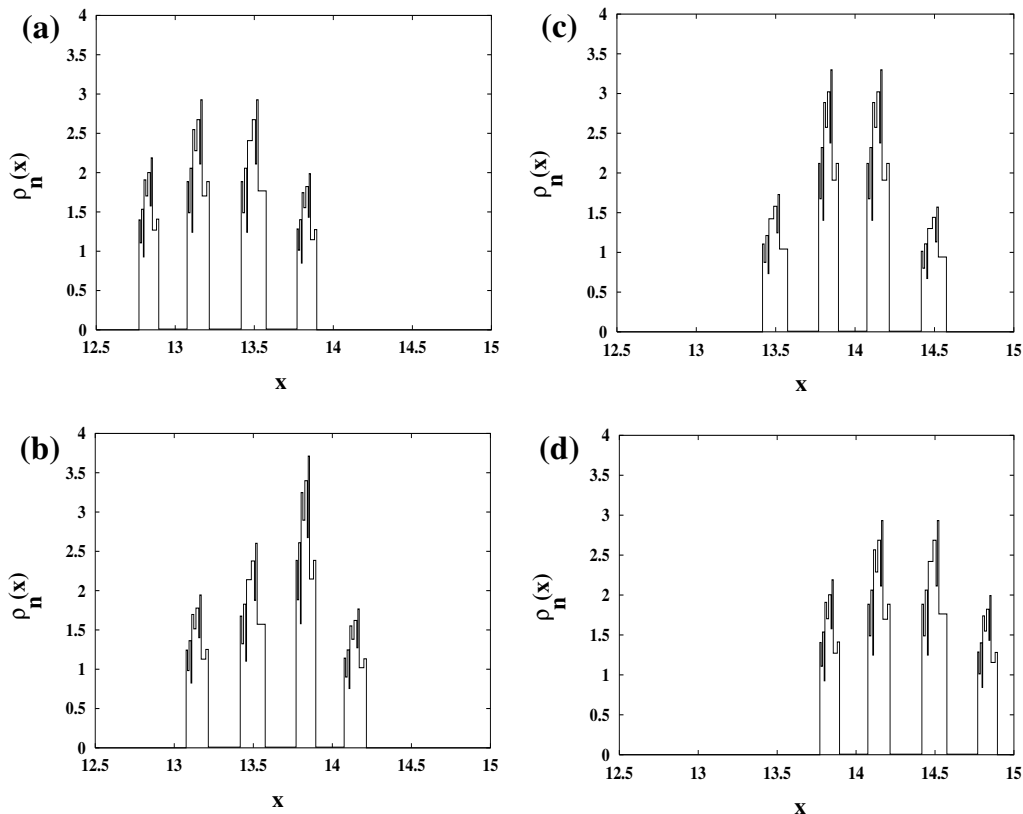


Figure 3.4: Probability density $\rho_n(x)$ at $a = 1.125$ and $b = 0.333$ as obtained from the approximate iteration method described in Section 3.2 after (a) $n = 40$, (b) $n = 41$, (c) $n = 42$, (d) $n = 43$ iterations starting from a uniform density on the unit interval. The order of the partition is 35 parts per unit interval determining the accuracy of the results. Since the parameter pair does not correspond to a Markov partition, the exact solution should have infinitely many “steps”, part of which can be seen in the figure. One furthermore observes that the probability distribution has developed a periodic pattern repeating itself after three time steps, apart from a translation over a distance of one. Hence, the current J is mode locked to the value $1/3$ and the diffusion coefficient vanishes.

cerned in Fig. 3.3 (a) to (c) which display $D(a, b)$ as a function of b for three fixed values of a . The transition line at $a = 1$ is approached in two ways:

1. Almost everywhere in the parameter plane where the diffusion coefficient does not vanish,³ this coefficient appears to be a fractal function (for a definition of a fractal function, cf., e.g., Refs. [Ber80, Kla03a]).
2. The regions with $D = 0$ seem to be getting more and more numerous and more densely packed the closer a gets to one [Gro02].

Note also the critical behavior around these regions as magnified, for a typical example, in Fig. 3.3 (d).

³With “almost everywhere” we mean except at integer values of the slope and multiples of $\frac{1}{2}$ for the bias, in which case the map yields a Bernoulli process.

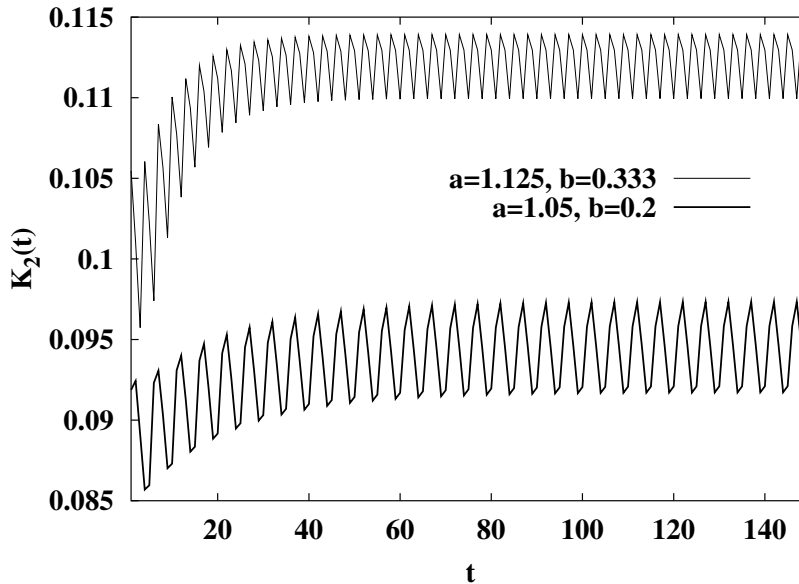


Figure 3.5: Time-dependence of the second cumulant $K_2(t)$ defined by Eq.(3.10) for two specific pairs of parameter values situated in different Arnold tongues. In both cases the initial density was uniform on the unit interval. Both curves appear to remain bounded for all times implying a vanishing diffusion coefficient, and to become periodic (with periods three and five, respectively) as $t \rightarrow \infty$, a sure sign of the phenomenon of mode locking.

The dynamical explanation of these Arnold tongues is displayed in Figs. 3.4 and 3.5, where a uniform probability density on the unit interval was chosen as the initial condition. Fig. 3.4 shows the time evolution of this density in a chain of L boxes after a certain number of iterations. The parameter pair was situated within an Arnold tongue. One observes that this density does not spread out anymore yielding $D = 0$, whereas it continues periodically moving to the right with a non-zero fluctuating velocity. In Fig. 3.5 the second cumulants for two parameter values in different Arnold tongues are displayed as functions of time. They clearly depict the mode locking behavior of the second cumulant $K_2(t)$ implying $D = 0$.

Finally, regions in the parameter plane can be classified with respect to the sign of the current: Fig. 3.6 depicts the current J as a function of the slope a for three different values of the bias b approaching zero. Firstly, one clearly sees the highly irregular structure of the current which becomes wilder and wilder the closer b comes to zero. Again, these irregularities, which persist on finer and finer scales, are suggestive of the current being a fractal function of the two parameters a and b almost everywhere (see footnote 3) in the parameter plane. The region of $a < 2$ with $J = 0$ is the localization region indicated in Fig.3.1. Secondly, for $b \rightarrow 0$, and on a line with constant a , there appear more and more regions where the current becomes negative. These two features, the fractality and the negativity of the current, were first found by Groeneveld [Gro], and were subsequently verified by the author of this thesis [Kla], by respectively using the different methods described in Section 3.2. More recently, they were corroborated in Ref. [Gil04] by studying a related model.

In Fig. 3.7 such regions are explored in more detail for three fixed values of a and by varying b in the region $10^{-8} \leq b \leq 1$. For all three values of a the current J divided by b shows a highly irregular behavior as a function of b which persists on finer and finer scales, and which again points to a fractal structure. In particular, for small b the current appears to

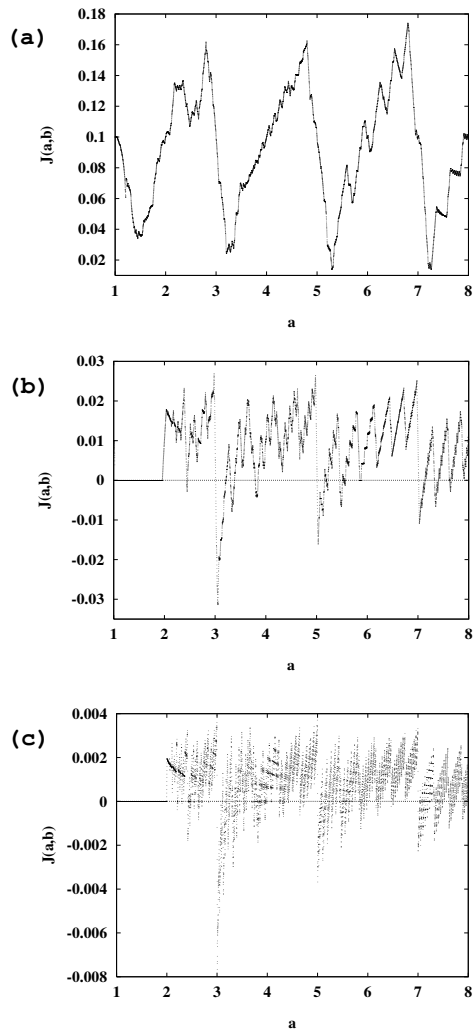


Figure 3.6: The current $J(a, b)$ as a function of the slope a at a fixed bias b for (a) $b = 0.1$, (b) $b = 0.01$, (c) $b = 0.001$. One notices in particular: 1. that the dependence of the current $J(a, b)$ on the slope a appears to have a fractal structure on the entire a -axis; 2. that, contrary to intuition, on considerable portions of the a -axis $J(a, b)$ is negative; and 3. that these two types of irregularities of the current $J(a, b)$ become stronger the closer $b \rightarrow 0$.

remain negative in all three cases. Hence, for these values of a there is no indication of the existence of a regime of linear response for infinitesimally small values of b . On the other hand, for extremely large values of b the current J obviously becomes linear in b . Comparing the plots of the current J as a function of b for $a = 3.0001$ and for $a = 3.01$, the sensitivity of $J(a, b)$ as a function of a becomes apparent. Note in particular that $J(3, b)/b = 1$ exactly for all b , showing that the case $a = 3$ is in a sense “integrable”: in this case the response of J to b is linear on all scales.

More details concerning the origin of these negative currents are shown in Fig. 3.8. The main plot depicts the probability on L coupled boxes starting from a uniform density on a unit interval after iteration of 40 time steps. The parameter pair (a, b) used in this figure yields a Markov partition for the map. Note that, on a coarse scale, the distribution resembles a Gaussian, whereas on a fine scale a periodic fine structure exists. This is a very general feature of this kind of dynamical models not particular to the present one [Kla96]. The center

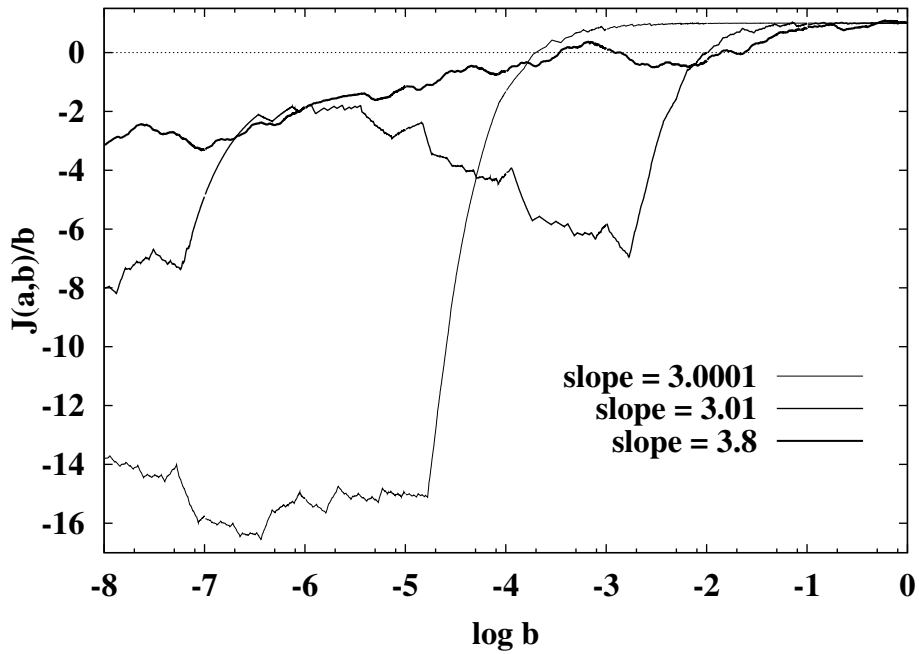


Figure 3.7: Plot of the current $J(a, b)$ divided by the bias b as a function of $\log b$ for three different values of the slope a . These three graphs seem to indicate the following: 1. that $J(a, b)/b$, as a function of b , is nowhere differentiable. The exact expressions of the twisted eigenstate method allow to go further and make the stronger statement, that this function “has fractal behavior”, which refers to a scaling behavior in the limit of infinitely small distances. 2. that $J(a, b)/b$ is sometimes, as, e.g., for these parameter values, negative; 3. that for the three a -values chosen here, the limit $\lim_{b \rightarrow 0} J(a, b)/b$ does not exist; in other words, that the “response J of the system to the bias b ” is not linear in b for small b . This is confirmed as well by the exact results quoted.

of the distribution is moving to the left indicating a current opposite to the bias. This can be seen more clearly in the magnification to the upper right which shows the invariant density for the circle map m . That the invariant density in such maps has a step-like structure has already been noticed by many authors, see, e.g., Refs. [Dör85, Klu90, Ers93]. As sketched in the figure, the fact that $b > 0$ would suggest that, on average, more particles would leave the box to the right. In contrast to that, the probability density has evolved in a way such that after a sufficiently long time, independently of the initial condition there is a higher probability for a particle to leave the box to the left than to the right. This result is typical for parameter values yielding negative currents.

3.4 *Summary

1. We have amended the simple map studied in the previous chapter by introducing a second parameter that breaks the symmetry of the system. Hence, we arrived at a simple deterministic model for a drift-diffusion process, which we defined in mathematical terms.
2. Subsequently, we outlined two basic methods enabling to numerically exactly calculate

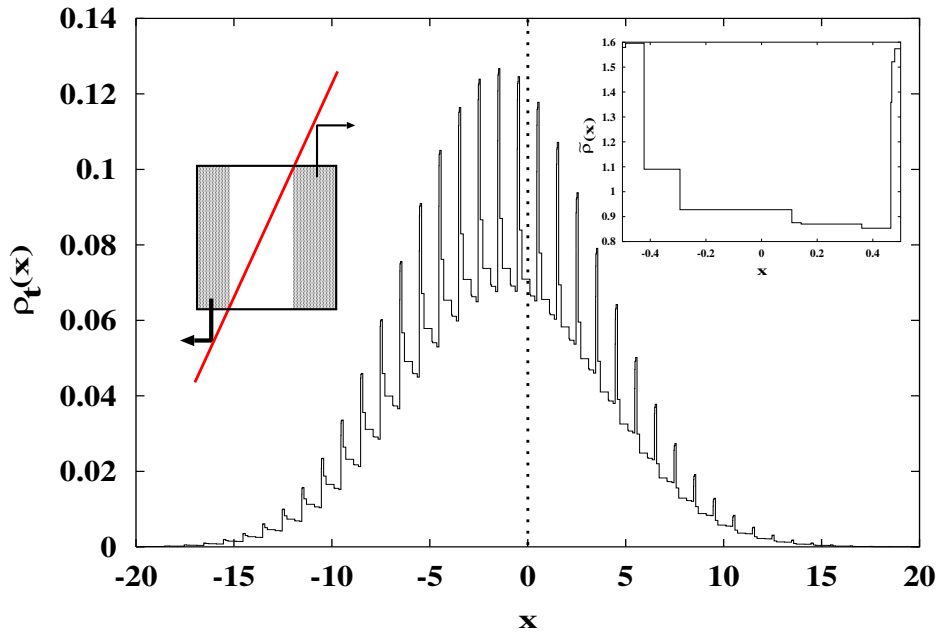


Figure 3.8: Probability density $\rho_n(x)$ at the Markov partition point $a \simeq 3.112987$ and $b \simeq 0.021281$ after $n = 40$ iterations, as computed by means of the renormalized iteration method described in Section 3.2. The order of the Markov partition is here 10 parts per unit interval. The inset in the upper right hand corner shows the invariant probability density on the circle of our projected map $f_{a,b}$ denoted as $\tilde{\rho}(x)$. The corresponding inset to the left illustrates how it can be understood that the escape rate out of any given box on the infinite line is larger towards the left than towards the right, notwithstanding the fact that the bias b is positive. This follows from the fact that the equilibrium density on the left hand side of the basic unit interval is larger than that on the right hand side.

the drift and diffusion coefficients of this model. Groeneveld's rigorous mathematical approach proceeds from the generating function of the system by evaluating it in terms of kneading and related sequences. It eventually arrives at expressing the transport coefficients in form of simple recursive equations. The more physical approach generalizes the idea of using transition matrices as already discussed in Chapter 2 leading to iterative matrix solutions of the complete time-dependent Frobenius-Perron equation. Advantages and drawbacks of both methods are briefly discussed.

3. Finally, we apply all these methods in order to construct and analyze the phase diagram of this model in the parameter plane. Both the drift and the diffusion coefficient are typically fractal functions of the two control parameters. In particular, depending on the choice of parameters the model exhibits different dynamical regimes such as phase locking, and parameter regions with negative currents. The origin of the negative currents is related to strong microscopic backscattering in any box of the periodically continued system.

4 Chaotic and fractal properties of deterministic reaction-diffusion processes

We study the consequences of deterministic chaos for diffusion-controlled reaction. As an example, we analyze a diffusive-reactive deterministic multibaker and a parameter-dependent variation of it. We construct the diffusive and the reactive modes of the models as eigenstates of the Frobenius-Perron operator. The associated eigenvalues provide the dispersion relations of diffusion and reaction and, hence, they determine the reaction rate. For the simplest model we show explicitly that the reaction rate behaves as phenomenologically expected for one-dimensional diffusion-controlled reaction. Under parametric variation, we find that both the diffusion coefficient and the reaction rate have fractal-like dependences on the system parameter.

In Section 4.1, we construct multibaker models of reaction-diffusion by starting from a diffusive-reactive Lorentz gas. In Section 4.2, we focus on the diffusive properties of the multibakers. By employing quasiperiodic boundary conditions we show that for the simplest model the diffusive properties are the same as those of the previously discussed dyadic multibaker of diffusion. We then demonstrate that under parametric variation of this model the diffusion coefficient exhibits a self-similar structure reminiscent of fractal curves. In Section 4.3, we describe the reactive properties. With quasiperiodic boundary conditions, we first study the simplest model and derive the dispersion relation of the chemiodynamic modes. We explicitly construct the phase-space distribution of these modes and define the reaction rate by comparison with phenomenology. We then show that the reaction rate behaves in a highly irregular manner if we consider the parameter-dependent model.

The work presented in this chapter originated in collaboration with P. Gaspard and builds upon Ref. [Gas98c].

4.1 A reactive-diffusive multibaker map

Matter is most often the stage of reactions which evolve on a reactive time scale intermediate between the long time scale of hydrodynamic transport phenomena and the short time scale of microscopic chaos. This chaos is generated by the collisions between the atoms and molecules of the fluid beyond a temporal horizon caused by the Lyapunov instability of motion. Under nonequilibrium conditions, long-time trajectories organize themselves in phase space to form fractal structures and unusual invariant or conditionally invariant measures, the consequences of which have just started to be explored. In this perspective,

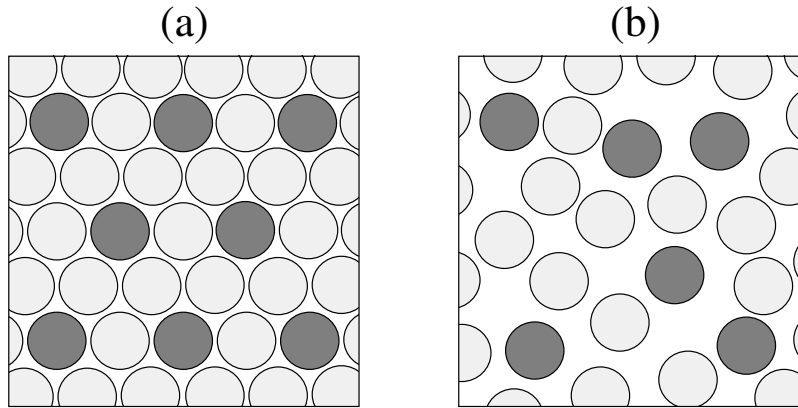


Figure 4.1: Examples of reactive Lorentz-type models: (a) on a regular lattice; (b) on a random lattice.

we study in this chapter simple models of reaction-diffusion processes in order to confront the phenomenology with the new approach based on deterministic chaos.

We shall focus on the simplest reaction-diffusion process with a linear chemical reaction law,



which already provides a nontrivial dynamics. As a vehicle of our study we shall use multi-baker models, which are deterministic versions of discrete Markov processes. The models we propose are spatially extended generalizations of a baker-type model of isomerization previously studied by Elskens and Kapral [Els85].

4.1.1 Deterministic models of reaction-diffusion processes

In order to motivate the introduction of the multibaker models, we first consider a reactive Lorentz gas in which a point particle undergoes elastic collisions on hard disks which are fixed in the plane. The disks may form a regular or a random configuration, see Fig. 4.1. A fraction of the disks are supposed to be catalysts where the point particle changes its state, or color, from A to B or vice versa at the instant of the collision. The mass of the particle is assumed to be the same in both states A and B . The phase space coordinates of each particle are given by its position, its velocity, and its color (x, y, v_x, v_y, c) with $c \in \{A, B\}$. Since energy is conserved at the elastic collisions, the magnitude of the velocity is a constant of motion, $v = \sqrt{v_x^2 + v_y^2}$, so that the coordinates reduce to $(x, y, \varphi, c) = (\mathbf{X}, c)$, where $\varphi = \arctan(v_y/v_x)$ is the angle between the velocity and the x -axis.

The motion induces a time evolution of the phase-space probability densities, or concentrations, for each color,

$$\mathbf{f}(\mathbf{X}) = \begin{pmatrix} f(\mathbf{X}, A) \\ f(\mathbf{X}, B) \end{pmatrix}. \quad (4.2)$$

The mean phase-space density, defined by the average of the concentrations, does not distinguish between the colors. Thus, we may expect that

$$\tilde{f}(\mathbf{X}) = \frac{1}{2}[f(\mathbf{X}, A) + f(\mathbf{X}, B)] \quad (4.3)$$

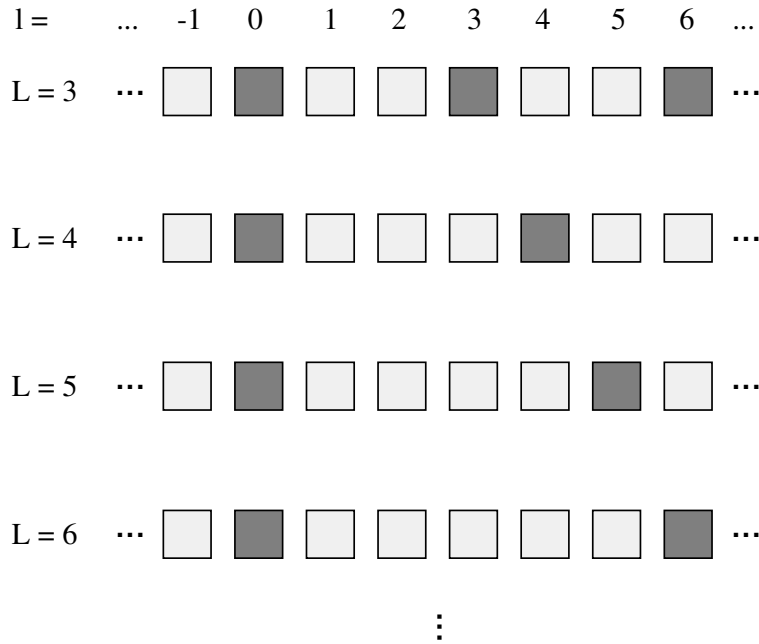


Figure 4.2: Geometry of a reactive multibaker or bakery map.

evolves in time exactly as in the non-reactive Lorentz gas, as studied elsewhere [Bun80, Bun81, Che94, Gas96]. The dynamics of reaction should appear in the difference between the concentrations

$$g(\mathbf{X}) = f(\mathbf{X}, A) - f(\mathbf{X}, B) \quad (4.4)$$

which is expected to follow a macroscopic relaxation toward zero if there is equipartition of particles between both colors.

It has been explained elsewhere that the flow dynamics of the Lorentz gas can be reduced to a Birkhoff mapping from collision to collision [Gas96, Gas98a]. Each collision can be represented by two variables: the angle θ giving the position of impact on the perimeter of the disk as $(x = \cos \theta, y = \sin \theta)$ and the angle ϕ between the velocity after the collision and the normal at impact. The sine of the velocity angle $\varpi = \sin \phi$ together with the position angle θ are the so-called Birkhoff coordinates, in which the mapping is area-preserving. All the collision events with the disk of label l are thus represented by the rectangle

$$\mathcal{R}_l = \{(\theta, \varpi, l) : 0 \leq \theta < 2\pi, -1 \leq \varpi \leq +1\}. \quad (4.5)$$

The dynamics of collisions can therefore be written as the Birkhoff mapping

$$(\theta_{n+1}, \varpi_{n+1}, l_{n+1}, c_{n+1}) = \Phi(\theta_n, \varpi_n, l_n, c_n), \quad (4.6)$$

which is known to be area-preserving, time-reversal symmetric, and of hyperbolic character. A caricature of this mapping is provided by a multibaker model. In Fig. 4.2 we suppose that the rectangular domains Eq. (4.5) representing the disks are replaced by squares

$$\mathcal{S}_l = \{(x, y, l) : 0 \leq x \leq 1, 0 \leq y \leq 1\}, \quad (4.7)$$

where $l \in \mathbb{Z}$ is the label of the square. Each square of the multibaker model corresponds to a disk of the Lorentz gas. Now, the collision dynamics is simplified by replacing the

complicated Birkhoff map Eq. (4.6) by a baker-type map with horizontal stretching by a factor of two, followed by cutting the elongated square into two. The collisions from disk to disk are replaced by jumps of the particle from square to square according to the transition rule $l \rightarrow l - 1$ if $x \leq 1/2$ and $l \rightarrow l + 1$ if $x > 1/2$ between next-neighbouring squares. The squares are arranged such that they form a one-dimensional chain. One out of L squares is assumed to be a catalyst where the color changes from $c = A$ (resp. B) to its complement $\bar{c} = B$ (resp. A). The map of the model is thus

$$\Phi(x, y, l, c) = \begin{cases} \left(2x, \frac{y}{2}, l - 1, c'\right), & 0 \leq x \leq \frac{1}{2}, \\ \left(2x - 1, \frac{y+1}{2}, l + 1, c'\right), & \frac{1}{2} < x \leq 1, \end{cases} \quad (4.8)$$

where $c' = \bar{c}$ if $l = 0, \pm L, \pm 2L, \dots$ and $c' = c$ otherwise. This map is area-preserving, time-reversal symmetric, and chaotic with a positive Lyapunov exponent $\lambda_+ = \ln 2$ and a negative one $\lambda_- = -\ln 2$, such as the multibaker map [Gas92a, Gas93, Gas95a, Tas94, Tas95].

In our model, the reaction is controlled by the diffusion if the reactive sites are diluted in the system. This important case of chemical reactions has been much studied in the literature since Smoluchowski's seminal work [Wei86, Ber88]. It is known that the macroscopic reaction rate is determined by the time taken by particles to diffuse towards the reactive site. A crossover occurs at dimension two which is the Hausdorff dimension of a Brownian path. Accordingly, the flux of reactants toward a catalyst is sensitive to the presence of the next-neighbouring catalysts in less than two dimensions, but not in systems of dimensions higher than two. In particular, in a one-dimensional system the reaction rate should behave as

$$\kappa \sim \frac{D}{L^2}, \quad (4.9)$$

where D is the diffusion coefficient and L is the distance between the reactive sites or catalysts.

A main goal of our work is to investigate the dynamical properties of our reaction-diffusion model in order to know whether this expected macroscopic behavior is confirmed from the microscopic dynamics or not. We shall also consider a parametric variation of this model with a more complicated dynamics. This is due to an extra dependency on a shift parameter which is introduced when the half squares are glued back into the chain. When this continuous parameter varies it induces topological changes in the trajectory dynamics which are reminiscent of the topological changes induced by varying the disk radius in the Lorentz gas [Bun80, Bun81, Che94, Gas96, Kla00a]. The parametric extension of the multibaker model shows that the diffusion coefficient as well as the reaction rate may vary in a highly irregular fashion as a function of a parameter. This is an important consequence of deterministic chaos which already appears on the level of one-dimensional maps, as will be discussed in the following section.

4.1.2 The Frobenius-Perron operator and quasiperiodic boundary conditions

Since Boltzmann's work it is well known that transport and reaction-rate processes should be conceived in a statistical sense because the individual trajectories are affected by the famous

Poincaré recurrences. We therefore consider the time evolution of statistical ensembles of trajectories as represented by the probability densities Eq. (4.2). They evolve in time according to the Frobenius-Perron equation, in general terms reading

$$f_{n+1}(x, y, l, c) = f_n \left[\Phi^{-1}(x, y, l, c) \right] \equiv (\hat{P}f_n)(x, y, l, c) \quad (n \in \mathbb{Z}) . \quad (4.10)$$

We choose quasiperiodic boundary conditions by assuming that the solution of the Frobenius-Perron equation is quasiperiodic on the chain with a wavenumber k . Moreover, we suppose that the solution decays exponentially with a decaying factor $\chi = \exp s$ where $|\chi| \leq 1$ or $\text{Re } s \leq 0$,

$$f_n(x, y, l, c) \sim \chi^n \exp(ikl) . \quad (4.11)$$

The decay rate s is calculated by solving the eigenvalue problem of the Frobenius-Perron operator. We note that the Frobenius-Perron operator is in general non-unitary so that root vectors associated with possible Jordan-block structures may exist beyond the eigenvectors. We shall focus here on the eigenvectors because they control the slowest decay on the longest time scales [Gas93, Gas95a].

For quasiperiodic solutions, the Frobenius-Perron operator reduces to the following Frobenius-Perron operator \hat{Q}_k which depends on the wavenumber k and acts on functions which are defined only in L successive squares of the chain,

$$\hat{Q}_k \equiv \begin{cases} f_{n+1}(x, y, 0, c) = \theta\left(\frac{1}{2} - y\right) f_n\left(\frac{x}{2}, 2y, 1, c\right) + \\ \quad e^{-ikL} \theta\left(y - \frac{1}{2}\right) f_n\left(\frac{x+1}{2}, 2y - 1, L - 1, c\right) , \\ f_{n+1}(x, y, 1, c) = \theta\left(\frac{1}{2} - y\right) f_n\left(\frac{x}{2}, 2y, 2, c\right) + \theta\left(y - \frac{1}{2}\right) f_n\left(\frac{x+1}{2}, 2y - 1, 0, \bar{c}\right) , \\ f_{n+1}(x, y, 2, c) = \theta\left(\frac{1}{2} - y\right) f_n\left(\frac{x}{2}, 2y, 3, c\right) + \theta\left(y - \frac{1}{2}\right) f_n\left(\frac{x+1}{2}, 2y - 1, 1, c\right) , \\ \quad \vdots \\ f_{n+1}(x, y, L - 2, c) = \theta\left(\frac{1}{2} - y\right) f_n\left(\frac{x}{2}, 2y, L - 1, c\right) + \\ \quad \theta\left(y - \frac{1}{2}\right) f_n\left(\frac{x+1}{2}, 2y - 1, L - 3, c\right) , \\ f_{n+1}(x, y, L - 1, c) = e^{ikL} \theta\left(\frac{1}{2} - y\right) f_n\left(\frac{x}{2}, 2y, 0, \bar{c}\right) + \\ \quad \theta\left(y - \frac{1}{2}\right) f_n\left(\frac{x+1}{2}, 2y - 1, L - 2, c\right) . \end{cases} \quad (4.12)$$

We notice that there is a reaction, i.e., a change of color, for particles passing the cell $l = 0$ so that a concentration with $l = 0$ and \bar{c} appears in the second and in the last line. We also notice that there is a factor $\exp(-ikL)$ in the first line for the particle coming from the previous segment of length L in the infinite chain, where the concentration functions are multiplied by the factor $\exp(-ikL)$. On the other hand, there is a factor $\exp(ikL)$ in the last line for the particle coming from the next segment where the concentration functions are multiplied by $\exp(ikL)$. Otherwise, this Frobenius-Perron operator is the same as in the infinite dyadic multibaker model studied in Refs. [Gas92a, Gas93, Gas95a].

As we discussed in the previous section, the presence of two chemical components $c = A$ or B implies that the Frobenius-Perron operator \hat{Q}_k acts on $2L$ functions which can be linearly combined to separate the functional space in two subspaces on which two decoupled Frobenius-Perron operators would act. The first subspace is defined by Eq. (4.3) where the

Frobenius-Perron operator reduces to the diffusive Frobenius-Perron operator of the multi-baker map. The second subspace is defined by Eq. (4.4) which gives a different evolution operator of reactive type. Diffusive properties are studied in the next Section 4.2, while reactive properties will be discussed in Section 4.3.

4.2 Diffusive dynamics of the multibaker

4.2.1 ⁺Diffusive modes of the dyadic multibaker

In this subsection we consider the diffusive dynamics of the dyadic multibaker model Eq. (4.8) with quasiperiodic boundary conditions. The subspace of diffusion is defined by the mean density of Eq. (4.3). For hydrodynamic modes of wavenumber k we thus write

$$\tilde{f}_n(x, y, l) = \frac{1}{2} [f_n(x, y, l, A) + f_n(x, y, l, B)] \equiv \exp \left[i \left(k + 2\pi \frac{\nu}{L} \right) l \right] \eta_n(x, y), \quad (4.13)$$

and the new function obeys the simpler evolution equation

$$\begin{aligned} \eta_{m+1}(x, y) &= (\hat{Q}_k^{(D)} \eta_m)(x, y) \equiv e^{+i(k+2\pi\nu/L)} \theta \left(\frac{1}{2} - y \right) \eta_m \left(\frac{x}{2}, 2y \right) + \\ &e^{-i(k+2\pi\nu/L)} \theta \left(y - \frac{1}{2} \right) \eta_m \left(\frac{x+1}{2}, 2y-1 \right), \end{aligned} \quad (4.14)$$

which is the Frobenius-Perron equation for the dyadic multibaker map based on quasiperiodic boundary conditions [Gas93]. The respective Frobenius-Perron operator has been analyzed in detail elsewhere [Gas93, Gas95a]. Its decay rates are

$$s_{m\nu}(k) = \ln \chi_{m\nu}(k) = -m \ln 2 + \ln \cos \left(k + \frac{2\pi\nu}{L} \right) \quad (4.15)$$

with $m = 0, 1, 2, 3, \dots$, $\nu = 0, 1, 2, \dots, L-1$, and with a degeneracy of $(m+1)$. The eigenvectors

$$(\hat{Q}_k^{(D)} \psi_{m\nu})(x, y; k) = e^{s_{m\nu}(k)} \psi_{m\nu}(x, y; k), \quad (4.16)$$

and some root vectors have been constructed in Refs. [Gas93, Gas95a] in terms of the cumulative functions

$$F_{0\nu}(x, y; k) = \int_0^x dx' \int_0^y dy' \psi_{0\nu}(x', y'; k). \quad (4.17)$$

For small enough wavenumbers k , these cumulative functions are continuous functions which are products of a monomial in x with a nondifferentiable de Rham function in y . Accordingly, the eigenvectors $\psi_{0\nu}$ are complex singular measures for small enough k .

We observe that the decay rate with $m = 0$ and $\nu = 0$ vanishes quadratically as $k \rightarrow 0$ in agreement with the expected diffusive behavior,

$$s_{00}(k) = \ln \cos k = -\frac{k^2}{2} - \frac{k^4}{12} \cdots, \quad (4.18)$$

which shows that the diffusion coefficient is $D = 1/2$.

The nonequilibrium steady states corresponding to a uniform density gradient g for the mean density of Eq. (4.3) have also been constructed [Tas94, Tas95]. It has been shown that the nonequilibrium steady state of the infinite system corresponds to a singular invariant measure represented by a continuous but nondifferentiable cumulative function

$$F_{\text{st. st.}}(x, y, l) = \int_0^x dx' \int_0^y dy' \tilde{f}_{\text{st. st.}}(x', y', l) = g l x y + g x T(y), \quad (4.19)$$

where $T(y)$ is the Takagi function obtained as a solution of the iteration [Hat84]

$$T(y) = \begin{cases} \frac{1}{2} T(2y) + y, & 0 \leq y \leq \frac{1}{2}, \\ \frac{1}{2} T(2y - 1) - y + 1, & \frac{1}{2} < y \leq 1. \end{cases} \quad (4.20)$$

The Takagi function is nondifferentiable because its formal derivative is infinite almost everywhere. It is given by a Lebowitz-McLennan type of formula [Leb59, Mac59, Gas97a]

$$\frac{dT}{dy} = \sum_{n=0}^{\infty} j[M^n(y)], \quad (4.21)$$

where $M(y) = 2y \bmod 1$ and $j(y) = \pm 1$ if $y < 1/2$ or $y > 1/2$, respectively, is the *jump velocity*. The singular character of the diffusive steady state turns out to be a general feature in finite-dimensional deterministic chaos of large spatial extension, as shown elsewhere [Gas96, Tas94, Tas95].

Moreover, this singular character of the steady state measure plays a fundamental role in the explanation of the entropy production of irreversible thermodynamics [Bre96, Tel96, Vol97, Gas97b, Bre98, Vol98, Gil99a, Tas99, Tas00, Gil00a, Gil00b, Tel00, Vol00, Mat01, Dor02, Vol02, Vol03]. In particular, the expected entropy production can be derived from the Takagi function in the case of the multibaker map [Gas97b]. The presence of this singularity solves the famous paradox of the constancy of the Gibbs entropy, which can be set up when we do not recognize that the out-of-equilibrium invariant measure is very different from the equilibrium one on fine scales in phase space. The out-of-equilibrium invariant measure becomes singular if the nonequilibrium constraints are imposed at distances larger than several mean free paths. This is probably a paradoxical aspect of the local equilibrium hypothesis that a nonequilibrium system appears in local equilibrium on the largest scales of phase space although intrinsic correlations exist on finer scales which are due to the chaotic dynamics. The singular character of the invariant measure explains that there is an entropy production in large nonequilibrium systems where the chaotic dynamics removes the signature of determinism down to extremely fine scales in phase space.

4.2.2 Diffusion coefficients in parameter-dependent models

We now study the situation when a system parameter is varied. As discussed in the previous Chapters 2 and 3, under such circumstances the drift and diffusion coefficients of simple one-dimensional maps display fractal structures by changing the parameter. Here we outline yet another method of how to calculate and to understand fractal diffusion coefficients. To study parameter-dependent transport in multibaker models like Eq. (4.8), methods to cope with one-dimensional maps are again crucial, because these maps govern the dynamics of

multibakers projected onto the x -axis. This is exemplified for a two-dimensional parameter-dependent multibaker which we introduce and discuss to the end of this subsection. On this basis we will show later on that the reactive transport properties of our parameter-dependent multibaker exhibit again profound fractal structures. We thus emphasize the striking analogies between the diffusive and the reactive properties in regard to their parametric sensitivity.

Fractal forms in a Green-Kubo formula

As a simple example for a one-dimensional diffusive chaotic map we consider again the model introduced in Section 2.1 denoted as map \mathcal{L} , cf. to Eqs. (2.3) to (2.6), as illustrated in Fig. 2.2. Here we elaborate on its diffusive properties starting from the Green-Kubo formula for diffusion [Kla96, Dor99, Gas92a, Kla02d, Kor02, Kor03]

$$D(a) \equiv \left\langle j_a(x) \sum_{t=0}^{\infty} j_a[M_a^n(x)] \right\rangle - \frac{1}{2} \langle j_a^2(x) \rangle \quad , \quad (4.22)$$

where the average $\langle \dots \rangle \equiv \int_0^1 dx \varrho_a(x) \dots$ has to be taken over the invariant probability density $\varrho_a(x)$ on the unit interval. $j_a(x)$ gives the integer number of boxes a particle has traversed after one iteration starting at position x and is thus the parameter-dependent extension of the jump velocity introduced in Eq. (4.21) above. Thus, the complete microscopic dynamics is divided into two parts in Eq. (4.22): the *intra-cell dynamics*, that is, the dynamics within a single box, which is represented by the invariant probability density, and the *inter-cell dynamics* given by the sum of the jump velocities, which contains the memory of the particles travelling between the single boxes of the chain.

For computing the diffusion coefficient both parts can be treated separately. The invariant probability density is obtained by solving the Frobenius-Perron equation Eq. (4.10), respectively Eq. (2.7), for the map restricted to the unit interval. As outlined in Chapter 2, for this purpose Eq. (2.7) can be written as the matrix equation Eq. (2.12), where the Frobenius-Perron operator has been transformed into a transition matrix [Kla95, Gas92a, Kla96, Bec93, Kla99a]. For maps of the type considered here, exact transition matrices can be constructed whenever a so-called Markov partition exists. This is the case for a dense set of parameter values a on the real line. The invariant probability density can then be calculated either by solving the eigenvalue problem of the transition matrix, which in simple cases can be performed analytically, or by solving the Frobenius-Perron equation by iterating the transition matrices numerically.

In Fig. 4.3 (a) and (b), typical invariant probability densities are plotted at two values of the slope. They are step functions on the unit interval, where the regions of the functions being piecewise constant correspond to the single cells of the respective Markov partitions. For piecewise linear maps, the invariant probability densities should always be step functions, although for arbitrary parameter value they may consist of infinitely many steps [Kla96, Dör85, Ers93, Klu90], cf. also Fig. 3.3. The sum of jump velocities, as the second ingredient of the Green-Kubo formula Eq. (4.22), gives the integer displacement of a particle after n iterations starting at initial position x . Since the system is chaotic, this function is highly irregular in x . To deal with this quantity, it is more convenient to define functions $T_a(x)$ via

$$\frac{dT_a}{dx} \equiv \sum_{t=0}^{\infty} j_a[M_a^n(x)] \quad , \quad (4.23)$$

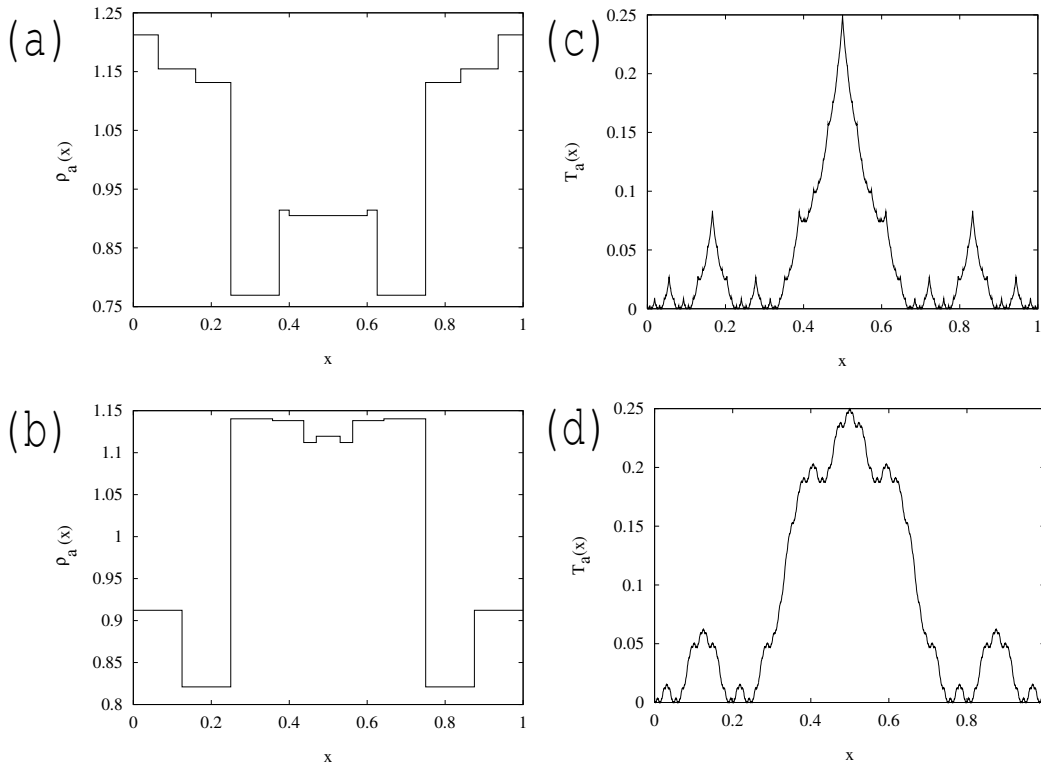


Figure 4.3: (a), (b) Invariant probability densities $\rho_a(x)$ on the unit interval for the map of Fig. 2.1 mod 1. The slope is $a \simeq 2.5004$ for (a) and $a \simeq 3.49997$ for (b). (c), (d) Generalized Takagi functions $T_a(x)$ for the same map at $a = 3$ in (c) and at $a = 4$ in (d).

which is a parametric extension of Eq. (4.21). The functions $T_a(x)$ now give the integral of the displacement of particles which start in a certain subinterval, and they behave much more regular in x than the sums of jumps. Employing $T_a(x) = \lim_{t \rightarrow \infty} T_{a,n}(x)$, it can be shown that these functions are obtained in terms of the recursion relation

$$T_{a,n}(x) = t_a(x) + \frac{1}{a} T_{a,n-1} \left[\tilde{M}_a(x) \right], \quad (4.24)$$

with $t_a(x)$ being determined by $dt_a/dx \equiv j_a(x)$ and by requiring that $T_a(0) = T_a(1) = 0$. $T_a(x)$ can be computed by iterating Eq. (4.24) numerically. For two special values of the slope the results have been plotted in Fig. 4.3 (c) and (d). The functions $T_a(x)$ are self-similar on the unit interval and scale with the slope a . For $a = 2$, Eq. (4.24) appears as a special case of Eq. (4.20). Therefore, functions like $T_a(x)$ may be denoted as *generalized Takagi functions*.

The numerically exact result for the parameter-dependent diffusion coefficient was already shown in Fig. 2.3. Alternatively to the explanation provided in Section 2.2, the fractal [Kla03a] character of $D(a)$ can now be understood by analyzing the Green-Kubo formula Eq. (4.22) [Kla96, Kor02]. From this point of view, two basic components are responsible for the fractality: On the one hand, the diffusion coefficient is given in terms of sums of jumps, which, according to Eq. (4.23), are related to fractal generalized Takagi functions as shown in Fig. 4.3 (a) and (b). This goes together with the jump velocity $j_a(x)$ having a discontinuity which varies with the parameter a and which reveals in a sense the fractal character of the generalized Takagi functions. On the other hand, a second source of irregularity are the

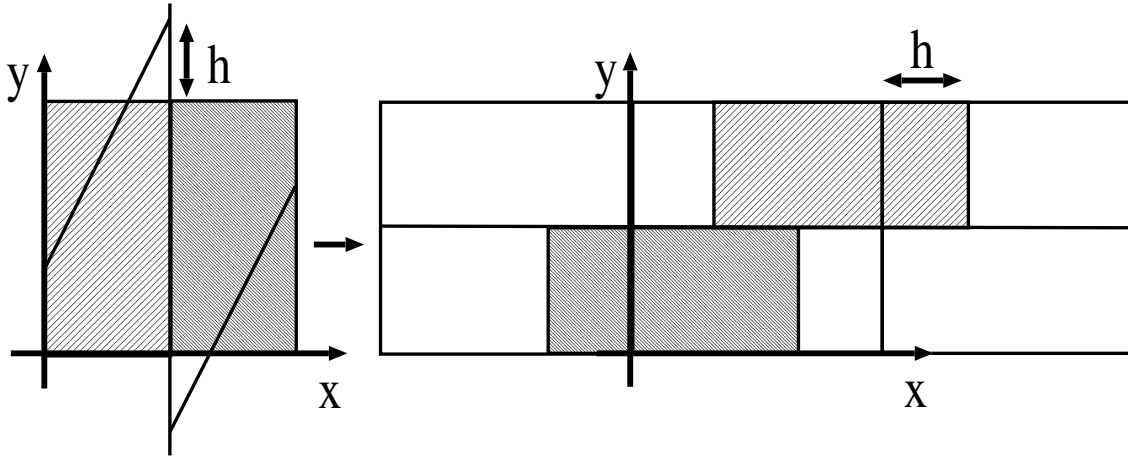


Figure 4.4: Dynamics of one cell of an area-preserving multibaker with a non-trivial parameter-dependence h . Projection of the dynamics onto the horizontal axis reduces the system to the symmetric one-dimensional piecewise linear map shown in the figure to the left which for $h = 0$ is the Bernoulli shift.

stepwise discontinuities in the density of the invariant measure $\varrho_a(x)$ as shown in Fig. 4.3 (c) and (d). The irregular behavior of the diffusion coefficient results from a combination of these effects, which are connected in the Green-Kubo formula via integrating the respective generalized Takagi functions over the respective invariant density [Kla96].

An area-preserving multibaker with fractal diffusion coefficients

The same phenomenon of a fractal diffusion coefficient appears in a parameter-dependent generalization of the diffusive-reactive multibaker model introduced above. This two-dimensional area-preserving map is sketched in Fig. 4.4. Here, the two rectangles of the left and of the right half of the square are “sliding” along the upper and the lower horizontal channel of the periodically continued map governed by a parameter h , as shown in the figure. It should be noted that for $h = 0.5$ and shifting the coordinate system by $\Delta x = 0.5$ the model reduces to the simple dyadic multibaker of Eq. (4.8). The dynamics of the probability density $\tilde{f}_n(x, y, l)$ of the full multibaker $\Phi_h(x, y, l)$ is determined by the Frobenius-Perron equation

$$\tilde{f}_{n+1}(x, y, l) = \tilde{f}_n[\Phi_h^{-1}(x, y, l)] \quad , \quad (4.25)$$

cp. to Eq. (4.10), where $\Phi_h^{-1}(x, y, l)$ is the inverse map. A projection of this two-dimensional Frobenius-Perron equation onto the unstable x -direction by integrating over the stable y -direction via $\varrho_n(x, l) \equiv \int dy \tilde{f}_n(x, y, l)$ [Dor99, Gas92a] shows that the dynamics of the probability density $\varrho_n(x, l)$ is determined by the Frobenius-Perron equation of the simple one-dimensional map included in Fig. 4.4, which is a kind of Bernoulli map shifted symmetrically by a height h . This one-dimensional map governs the dynamics of the multibaker map projected on the x -axis. By extending the system periodically, we recover a chain of one-dimensional maps of the type of the one shown in Fig. 2.1.

Concerning reversibility, we follow the definition that there must exist an involution \mathbf{G} in phase space, $\mathbf{G} \circ \mathbf{G} = 1$, which reverses the direction of time via $\mathbf{G} \circ \Phi \circ \mathbf{G} = \Phi^{-1}$ [Rob92]. For the special case of h taking multiples of $1/2$ involutions \mathbf{G} can be found which are

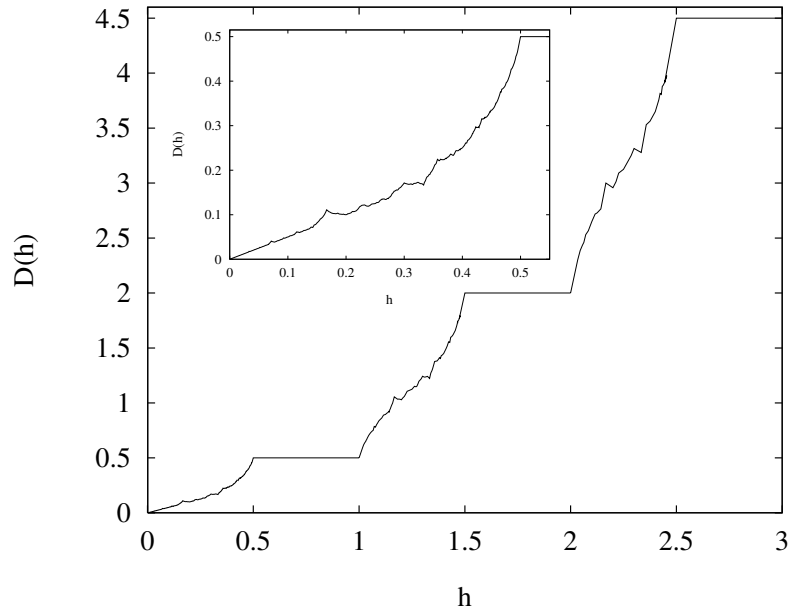


Figure 4.5: Parameter-dependent diffusion coefficient $D(h)$ for the multibaker of Fig. 4.4 and blowup of the initial region. The main graph consists of 638 data points, the magnification of 514. In both cases the single points have been connected with lines, errorbars are too small to be visible.

related to a simple mirroring in phase space.¹ For general h it can be shown that the system has strong reversibility properties, although the existence of an involution \mathbf{G} remains an open question [Rob92].

To compute the parameter-dependent diffusion coefficient of this multibaker we use that the projected dynamics is governed by a one-dimensional map, and thus we apply the same methods as outlined above. The result is shown in Fig. 4.5. The diffusion coefficient is again a non-trivial function of the parameter h and shares many characteristics of the curve presented in Fig. 2.3, for example, a certain random walk-like behavior on a coarse grained scale [Kla97]. But it also exhibits some new features, especially that the diffusion coefficient is constant in intervals $0.5 + m \leq h \leq 1 + m$, $m \in \mathbb{N}_0$. This is due to the fact that the transition matrices corresponding to respective Markov partitions, and thus the respective symbolic dynamics of the map, do not change in this parameter interval.

It is worth mentioning that in contrast to the specific model of Fig. 2.1 the invariant probability density of the projected one-dimensional map here is always uniform for all parameter values of h . Therefore, the only contributions to the fractality of $D(h)$ come from the inter-cell dynamics as described by the Takagi functions $T_a(x)$. We remark that the underlying one-dimensional map and its fractal diffusion coefficient have been reviewed in Ref. [Vol02].

¹If h takes integer values, we find for \mathbf{G} a simple mirroring along the diagonal $x = y$ in each unit cell. If h takes odd multiples of $1/2$, by shifting all unit cells about $\Delta x = 1/2$ we find for \mathbf{G} a mirroring along the diagonal from the upper left to the lower right in each unit cell.

4.3 Reactive dynamics of the multibaker

4.3.1 +Reactive modes of the dyadic multibaker

In this section we turn to the study of the chemiodynamic or reactive modes of our simple dyadic model Eq. (4.8) of diffusion-controlled reaction. Contrary to the total number of particles $N_A + N_B$, which is a constant of motion, the numbers of particles of each chemical species are not conserved. Accordingly, we should not expect that the reactive modes have a vanishing decay rate as $k \rightarrow 0$. This is in contrast to the diffusive modes which are related to the conserved total number of particles and for which the decay rate (4.18) vanishes at $k = 0$.

Here we consider the subspace defined by the difference between the particle concentrations in the multibaker,

$$g(x, y, l) \equiv f(x, y, l, A) - f(x, y, l, B) . \quad (4.26)$$

Thus we employ the fact that the dynamics of the concentration difference can be decoupled from the mean density for this model as has been mentioned before, compare to Eq. (4.4). With quasiperiodic boundary conditions, the difference of chemical concentration evolves in time according to the reactive evolution operator

$$\hat{R}_k \equiv \begin{cases} g_{n+1}(x, y, 0) = \theta\left(\frac{1}{2} - y\right) g_n\left(\frac{x}{2}, 2y, 1\right) + e^{-ikL} \theta\left(y - \frac{1}{2}\right) g_n\left(\frac{x+1}{2}, 2y - 1, L - 1\right) , \\ g_{n+1}(x, y, 1) = \theta\left(\frac{1}{2} - y\right) g_n\left(\frac{x}{2}, 2y, 2\right) - \theta\left(y - \frac{1}{2}\right) g_n\left(\frac{x+1}{2}, 2y - 1, 0\right) , \\ g_{n+1}(x, y, 2) = \theta\left(\frac{1}{2} - y\right) g_n\left(\frac{x}{2}, 2y, 3\right) + \theta\left(y - \frac{1}{2}\right) g_n\left(\frac{x+1}{2}, 2y - 1, 1\right) , \\ \vdots \\ g_{n+1}(x, y, L - 2) = \theta\left(\frac{1}{2} - y\right) g_n\left(\frac{x}{2}, 2y, L - 1\right) + \\ \theta\left(y - \frac{1}{2}\right) g_n\left(\frac{x+1}{2}, 2y - 1, L - 3\right) , \\ g_{n+1}(x, y, L - 1) = -e^{ikL} \theta\left(\frac{1}{2} - y\right) g_n\left(\frac{x}{2}, 2y, 0\right) + \\ \theta\left(y - \frac{1}{2}\right) g_n\left(\frac{x+1}{2}, 2y - 1, L - 2\right) . \end{cases} \quad (4.27)$$

Our goal is now to obtain the eigenvalues and eigenstates of this reactive evolution operator

$$\hat{R}_k \left\{ \Psi(x, y, l) \right\}_{l=0}^{L-1} = e^{s(k)} \left\{ \Psi(x, y, l) \right\}_{l=0}^{L-1} , \quad (4.28)$$

with $\chi(k) = \exp[s(k)]$. We define the cumulative functions

$$G_n(x, y, l) = \int_0^x dx' \int_0^y dy' g_n(x', y', l) , \quad (4.29)$$

which obey a set of equations which can be derived from Eq. (4.27). We suppose that the leading eigenstates are uniform along the unstable direction x , which is justified by the fact that the hyperbolic dynamics smoothens out any heterogeneities along the unstable direction,

$$\Psi(x, y, l) = \mathcal{D}(y, l) , \quad (4.30)$$

where $\mathcal{D}(y, l)$ is a Schwartz distribution. We note that the further eigenstates and root states do depend on x and require a more detailed analysis. The cumulative functions of

the leading eigenstates are thus

$$G_{\text{eigenstate}}(x, y, l) \equiv x C(y, l) \quad \text{with} \quad C(y, l) = \int_0^y dy' \mathcal{D}(y', l). \quad (4.31)$$

Replacing $g_n(x, y, l)$ by $\mathcal{D}(y, l)$ and $g_{n+1}(x, y, l)$ by $\chi \mathcal{D}(y, l)$ in Eq. (4.27) and integrating over the interval $[0, y]$, we obtain the following iterative equations for the new functions $C(y, l)$

$$\begin{aligned} C(y, 0) &= \begin{cases} \frac{1}{2\chi} C(2y, 1), & y < 1/2, \\ \frac{1}{2\chi} [C(1, 1) + \exp(-ikL)C(2y-1, L-1)], & y > 1/2, \end{cases} \\ C(y, 1) &= \begin{cases} \frac{1}{2\chi} C(2y, 2), & y < 1/2, \\ \frac{1}{2\chi} [C(1, 2) - C(2y-1, 0)], & y > 1/2, \end{cases} \\ C(y, 2) &= \begin{cases} \frac{1}{2\chi} C(2y, 3), & y < 1/2, \\ \frac{1}{2\chi} [C(1, 3) + C(2y-1, 1)], & y > 1/2, \end{cases} \\ &\vdots \\ C(y, L-2) &= \begin{cases} \frac{1}{2\chi} C(2y, L-1), & y < 1/2, \\ \frac{1}{2\chi} [C(1, L-1) + C(2y-1, L-3)], & y > 1/2, \end{cases} \\ C(y, L-1) &= \begin{cases} -\frac{\exp(ikL)}{2\chi} C(2y, 0), & y < 1/2, \\ \frac{1}{2\chi} [-\exp(ikL)C(1, 0) + C(2y-1, L-2)], & y > 1/2. \end{cases} \end{aligned} \quad (4.32)$$

The eigenvalue can be obtained by setting $y = 1$ in Eq. (4.32), which leads to the eigenvalue equation

$$\begin{pmatrix} -2\chi & 1 & 0 & 0 & \cdots & 0 & 0 & \exp(-ikL) \\ -1 & -2\chi & 1 & 0 & \cdots & 0 & 0 & 0 \\ 0 & 1 & -2\chi & 1 & \cdots & 0 & 0 & 0 \\ 0 & 0 & 1 & -2\chi & \cdots & 0 & 0 & 0 \\ \vdots & \vdots & \vdots & \vdots & \ddots & \vdots & \vdots & \vdots \\ 0 & 0 & 0 & 0 & \cdots & 1 & -2\chi & 1 \\ -\exp(ikL) & 0 & 0 & 0 & \cdots & 0 & 1 & -2\chi \end{pmatrix} \begin{pmatrix} C(1, 0) \\ C(1, 1) \\ C(1, 2) \\ C(1, 3) \\ \vdots \\ C(1, L-2) \\ C(1, L-1) \end{pmatrix} = 0. \quad (4.33)$$

The characteristic determinant has been calculated for several values of the distance L between the reactive sites,

$$L = 3 : \quad 4\chi^3 + \chi + \cos(3k) = 0, \quad (4.34)$$

$$L = 4 : \quad 8\chi^4 - 2 + 2\cos(4k) = 0, \quad (4.35)$$

$$L = 5 : \quad 16\chi^5 - 4\chi^3 - 3\chi + \cos(5k) = 0, \quad (4.36)$$

$$L = 6 : \quad 32\chi^6 - 16\chi^4 - 6\chi^2 + 1 + \cos(6k) = 0, \quad (4.37)$$

⋮

The corresponding dispersion relations of the reactive modes are depicted in Fig. 4.6 together with those of the diffusive modes. Fig. 4.6 shows that the slowest decay rate which gives

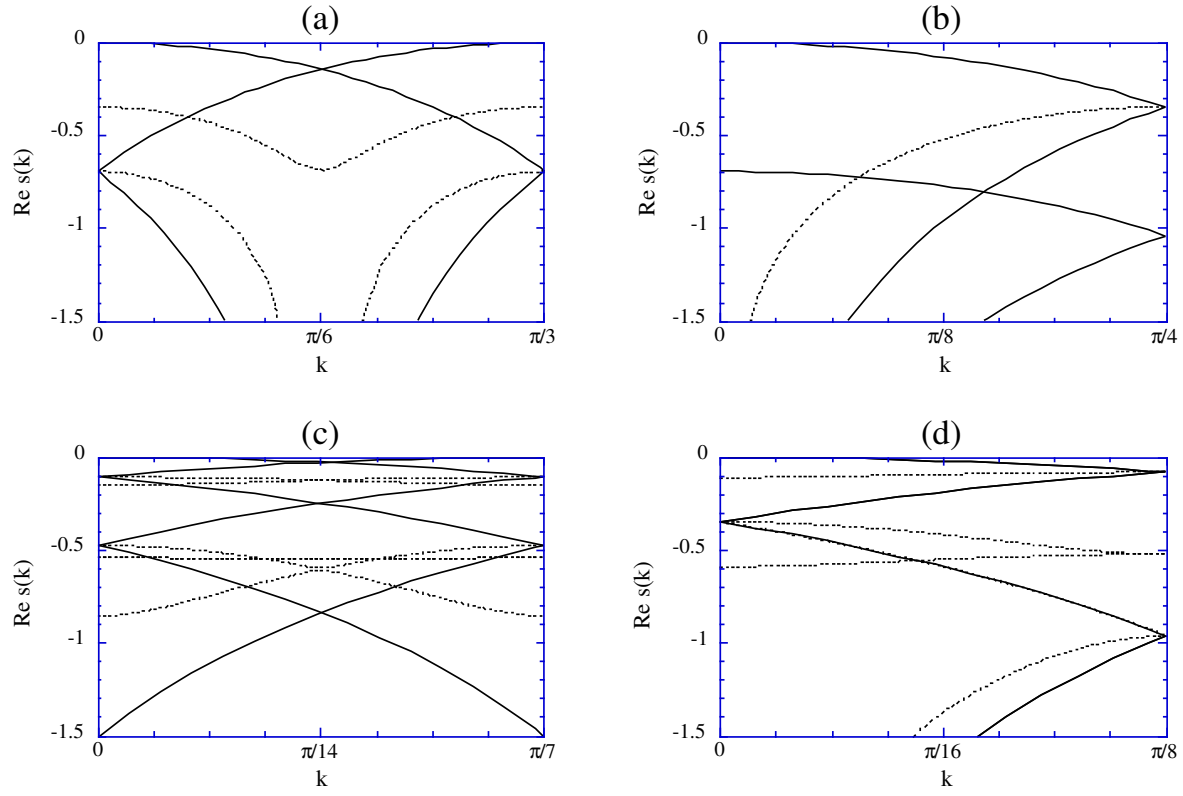


Figure 4.6: Dispersion relations of the diffusive modes (solid lines) and of the reactive modes (dotted lines) for the dyadic reactive multibaker with (a) $L = 3$; (b) $L = 4$; (c) $L = 7$; (d) $L = 8$.

the reaction rate appears at $k = 0$ for L odd and at $k = \pm\pi/L$ for L even. The cumulative functions $\{C(y, l)\}_{l=0}^3$ of the eigenstate corresponding to the reaction rate at $k = 0$ are depicted in Fig. 4.7 for the model with $L = 3$ by solving Eq. (4.32) iteratively. Near its maximum values, the dispersion relation behaves quadratically like

$$L \text{ odd} : s^{(r)}(k, L) = -\tilde{\kappa}(L) - D^{(r)}(L)k^2 + \mathcal{O}(k^4) \text{ at } k = 0, \quad (4.38)$$

$$L \text{ even} : s^{(r)}(k, L) = -\tilde{\kappa}(L) - D^{(r)}(L) \left(k \mp \frac{\pi}{L}\right)^2 + \mathcal{O}\left[\left(k \mp \frac{\pi}{L}\right)^4\right] \text{ at } k = \pm \frac{\pi}{L}. \quad (4.39)$$

An analytical calculation of the reaction rate $\tilde{\kappa}(L)$ and a numerical calculation of the reactive diffusion coefficient $D^{(r)}(L)$ versus L reveal that

$$\tilde{\kappa}(L) = -\ln \cos \frac{\pi}{L} = \frac{\pi^2}{2L^2} + \mathcal{O}(L^{-4}), \quad (4.40)$$

$$D^{(r)}(L) \sim \frac{1}{L}. \quad (4.41)$$

The reaction rate thus behaves as expected for diffusion-controlled reaction in one dimension, compare to Eq. (4.9). These results, combined with the results for the diffusive modes, show

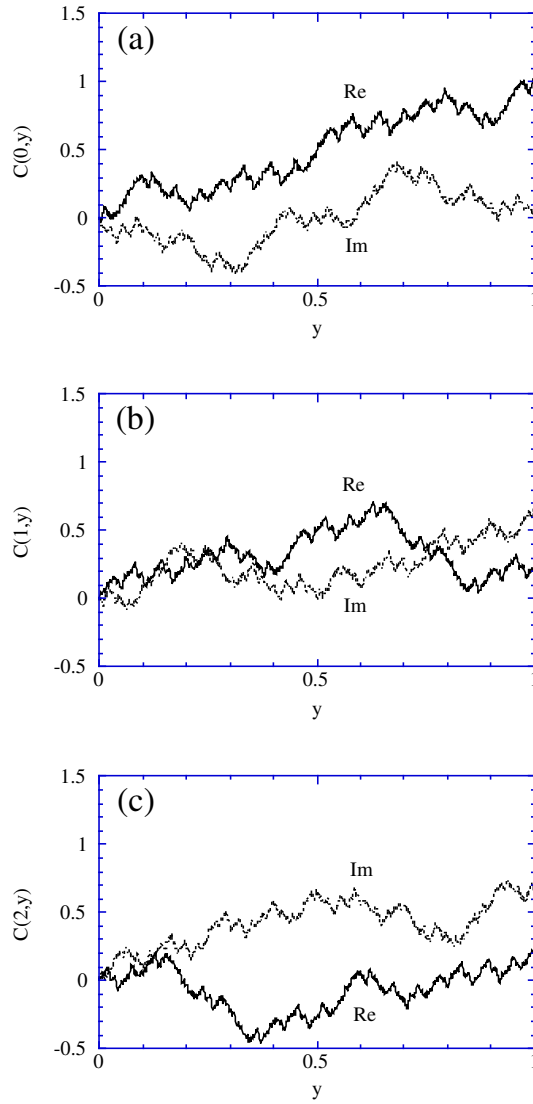


Figure 4.7: Cumulative functions $\{C(y, l)\}$ with $l = 0, 1, 2$ of the reactive eigenstate at vanishing wavenumber $k = 0$ in the reactive multibaker model $L = 3$.

that, on macroscopic scales, the coarse-grained density and the concentration difference

$$\rho(l) = \int_0^1 dx \int_0^1 dy \tilde{f}(x, y, l), \quad (4.42)$$

$$\sigma(l) = \int_0^1 dx \int_0^1 dy g(x, y, l) = G(1, 1, l), \quad (4.43)$$

behave like

$$\text{diffusive mode:} \quad \frac{\partial \rho}{\partial t} \simeq D \frac{\partial^2 \rho}{\partial l^2}, \quad (4.44)$$

$$\text{reactive mode:} \quad \frac{\partial \sigma}{\partial t} \simeq D^{(r)} \frac{\partial^2 \sigma}{\partial l^2} - \tilde{\kappa} \sigma \quad (L \text{ odd}). \quad (4.45)$$

Corrections with higher-order spatial derivatives could also be taken into account in the dynamics of the reactive mode. For a model with L odd, this behavior corresponds to a

macroscopic reaction-diffusion system with

$$\frac{\partial \rho_A}{\partial t} \simeq \frac{D + D^{(r)}}{2} \frac{\partial^2 \rho_A}{\partial l^2} + \frac{D - D^{(r)}}{2} \frac{\partial^2 \rho_B}{\partial l^2} - \frac{\tilde{\kappa}}{2} (\rho_A - \rho_B), \quad (4.46)$$

$$\frac{\partial \rho_B}{\partial t} \simeq \frac{D - D^{(r)}}{2} \frac{\partial^2 \rho_A}{\partial l^2} + \frac{D + D^{(r)}}{2} \frac{\partial^2 \rho_B}{\partial l^2} + \frac{\tilde{\kappa}}{2} (\rho_A - \rho_B), \quad (4.47)$$

where $\rho_A = \rho + \sigma/2$ and $\rho_B = \rho - \sigma/2$. According to these macroscopic equations, the diffusion coefficient of each species is $D_A = D_B = (D + D^{(r)})/2$, the cross-diffusion coefficient is $D_{AB} = D_{BA} = (D - D^{(r)})/2$, while the reaction rate of Eq. (4.1) is given by the logarithm of the absolute value of the leading eigenvalue of the reactive evolution operator as

$$\kappa = \frac{\tilde{\kappa}}{2} = -\frac{1}{2} \ln \cos \frac{\pi}{L} = -\frac{1}{2} \ln |\chi(k=0)|. \quad (4.48)$$

We remark that, according to this microscopic analysis, the macroscopic equations of a reaction-diffusion system do not necessarily follow the simple assumption often carried out that the cross-diffusion coefficients vanish, $D_{AB} = D_{BA} = 0$. This particular case is only recovered if $D = D^{(r)}$, which is not fulfilled here. The origin of this difference holds in the fact that the diffusion coefficient D_A associated with the state A of a particle is in general different from the diffusion coefficient of the particle itself which may be in two possible states A or B . In this regard, the cross-diffusion appears to be of importance in reacting systems.

Besides, the models with L even follow more complicated reaction-diffusion equations where the reactive diffusion coefficient $D^{(r)}$ has a different status because it is associated with a nonvanishing wavenumber $k = \pm\pi/L$. Nevertheless, the part of the reaction-diffusion process which is responsible for the reactive exponential decay is confirmed by the microscopic analysis.

4.3.2 Reaction rates in the parameter-dependent multibaker

We now discuss the parameter-dependent reactive multibaker by taking the shift parameter h into account, as it has already been done for the purely diffusive case, see Fig. 4.4. Thus, in addition to the integer periodicity L of the reaction cells of the multibaker the reaction rate κ will also depend on h . One may then raise the question how the reaction rate $\kappa(h, L)$ changes with respect to varying h for fixed L . Moreover, we will give some illustrative features of the time-dependent dynamics of the reaction process for typical h parameters.

Analogously to the previous section, we start with the difference of chemical concentrations $g(x, y, l)$ as defined in Eq. (4.26). We again use the property that parallel to the x -axis the two-dimensional reactive multibaker can be projected onto a one-dimensional map, as has been pointed out before, cf. Fig. 4.4. The time evolution of the projected reactive part $\zeta_n(x, l) \equiv \int dy g(x, y, l)$ of the multibaker is then determined by the reactive evolution equation of a respective one-dimensional map,

$$\zeta_n(x, l) = \hat{R}^{(1)}(h, L) \zeta_{n-1}(x, l). \quad (4.49)$$

Here $\hat{R}^{(1)}(h, L)$ represents the one-dimensional reactive evolution operator, and $\zeta_n(x, l) \equiv \varrho_n(x, l, A) - \varrho_n(x, l, B)$ is the difference between A and B -particle densities in the corresponding one-dimensional map. As has been done for the purely diffusive case, we again

write this equation as a matrix equation, where instead of $\hat{R}^{(1)}(h, L)$ a topological transition matrix $M(h, L)$ acts onto a particle density vector $\underline{\zeta}_n$. The matrix $M(h, L)$ is structured such that in case of reactive scattering centers the elements in the corresponding columns of the matrix have a negative sign, and thus a particle changes color by leaving a reaction cell. Otherwise, the matrix is the same as outlined for the diffusive case.

We first discuss some details of the time evolution of the reactive modes. By integrating over $\zeta_n(x, l)$ or its respective vector representation we obtain the difference between the total number of A and B -particles at discrete time n which is $\xi_n \equiv \sum_l \int dx \zeta_n(x, l)$. From the corresponding phenomenological time-continuous reaction equation Eq. (4.45) one would expect that for the reactive multibaker ξ_n decays exponentially after a suitable coarse graining according to $\xi_n = \xi_0 \exp(-\tilde{\kappa}t)$. If this is the case, we can define the reaction rate of the reactive multibaker in analogy to the phenomenological equation as $\kappa(h, L) = \tilde{\kappa}/2$.

To compute $\kappa(h, L)$ according to this definition, we solve the matrix formulation of Eq. (4.49) by iterating the transition matrices $M(h, L)$ numerically. As an initial particle density we choose $\zeta_0(x, l)$ to be uniform in one reactive cell of the multibaker, which corresponds to having only A particles in this cell with the number of B particles being locally zero, and we make the chain long enough such that the evolving density is not affected by boundary conditions.

Figs. 4.8 (a) and (b) give two typical examples of $\zeta_n(x, l)$ for certain parameter values of h after $n = 40$ iterations. They show how the ‘‘perturbation’’ $\zeta_0(x, l)$, which is a local initial deviation from the equilibrium state $\zeta_n(x, l) = 0$ ($t \rightarrow \infty$), spreads out along the x -axis by exhibiting a rather complex fine structure with oscillations around zero. Figs. 4.8 (c) and (d) contain half-logarithmic plots of $|\xi_n|$ with respect to the discrete time n . These plots reflect a different dynamical behavior of ξ_n for different magnitudes of the reaction rate. For $\kappa(h, L)$ close to zero, see the upper two curves in Fig. 4.8 (c), ξ_n decays apparently non-exponentially for small times n . Only for larger times it eventually reaches exponential decay. Thus, the system shows that it is close to states of the h parameter where it is non-reacting. For the lowest curve in Fig. 4.8 (c), which corresponds to an intermediate reaction rate, ξ_n provides initially strong periodic fluctuations. They are partly due to the complex deterministic dynamics of the reactive baker in one cell of the chain, as has already been observed and explained for a one-dimensional purely diffusive case [Kla96]. Apart from such strong periodic oscillations on a fine scale, in Fig. 4.8 (d) ξ_n exhibits an interesting crossover between a fast decay for smaller times and a slower decay for larger times, where again it approaches exponential behavior. This may reflect the fact that for larger reaction rates $\kappa(h, L) \gg 0$ the reaction is controlled by the diffusive dynamics. These features of ξ_n should be compared to the characteristics of the respective probability densities $\zeta_n(x, l)$ in the figure.

To obtain quantitative values for the reaction rate, Eq. (4.49) has been analyzed by solving the eigenvalue problem of the corresponding transition matrix $M(h, L)$, analogously to what has been done in the previous section for the dyadic reactive multibaker. In general, the spectra of $M(h, L)$ are extremely complicated [Gas]. However, as has been argued in the previous section for special cases, and supported by our observation of long-time exponential decay of ξ_n for the general case, we expect that, in the limit of infinite time, the reaction in the multibaker will always be governed by the slowest eigenmodes and their respective eigenvalues. This motivates to define the parameter-dependent reaction rate $\kappa(h, L)$ via the

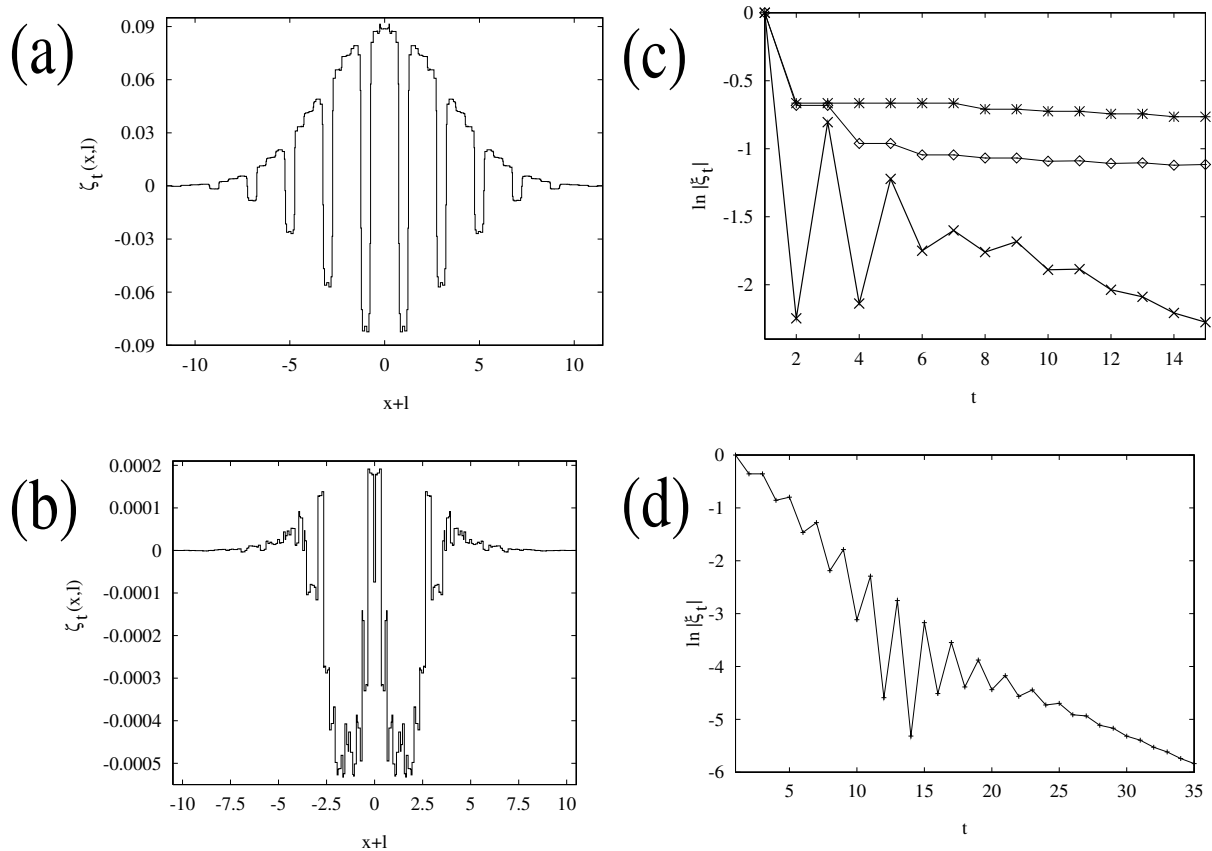


Figure 4.8: (a), (b) Densities corresponding to the difference in the number of A and B -particles per total number of particles after $n = 40$ iterations of the map. In (a) ($L = 2, h \simeq 0.2429$) the reaction rate is close to zero, whereas in (b) ($L = 3, h \simeq 0.1496$) it is locally maximal in h . (c), (d) Half-logarithmic plots of the total difference ξ_n in the number of A and B -particles of the system as it varies in time n . In (c) the corresponding reaction rates $\kappa(h, L)$ are close to zero for the upper two curves ($\kappa < 0.006$), for the lower curve the reaction rate has an intermediate value ($\kappa \simeq 0.02$), whereas in (d) it is locally maximal in h ($\kappa \simeq 0.05$). The parameters for the upper curve in (c) correspond to (a), the curve in the middle is at $L = 3, h \simeq 0.247$, and the lowest one is at $L = 3, h \simeq 0.4472$. Case (d) corresponds to (b).

maximum of the absolute value of the eigenvalues of $M(h, L)$,

$$\kappa(h, L) \equiv -\frac{1}{2} \ln |\chi_{\max}(h, L)| \quad , \quad (4.50)$$

analogously to Eq. (4.48). Numerically, we find that for large regions of the h parameter a certain fundamental domain L_F of the multibaker is sufficient to obtain the correct leading eigenvalue $\chi_{\max}(h, L)$. This domain must always include multiples of two reactive centers, and its length is defined by the number $L_F \equiv 2L \text{Int}(1 + h)$ of cells of the multibaker. In these regions, solutions for the eigenvalue problem of $M(h, L)$ defined on the domain L_F lead to a maximum eigenvalue $\chi_{\max}(h, L)$ as obtained by solving the corresponding eigenvalue problem for longer and longer chain lengths $mL \rightarrow \infty$, $m \in \mathbb{N}$. However, especially for small L and large $\kappa(h, L)$ this fundamental domain only provides an approximation to the exact results which are then obtained by making the chain length mL large enough such that the

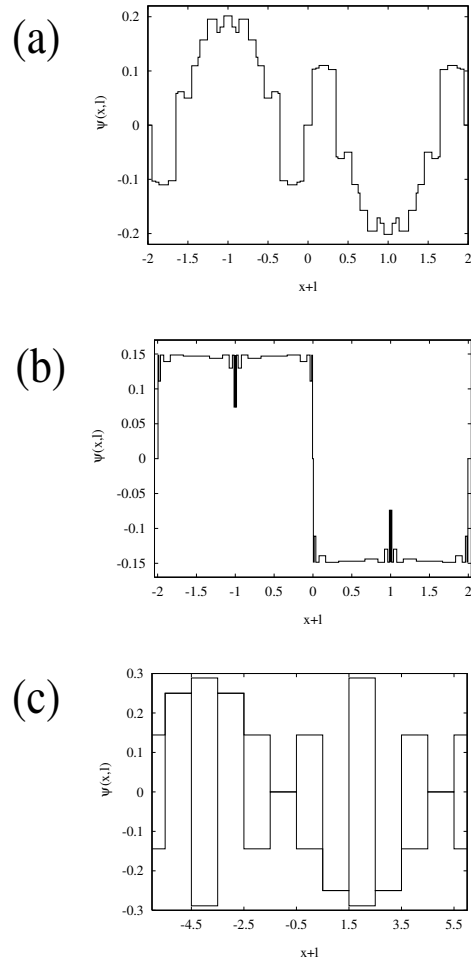


Figure 4.9: Examples of largest eigenmodes $\psi(x, l)$ for the reactive multibaker corresponding to the largest eigenvalue $\chi_{\max}(h, L)$ parallel to the x axis in the fundamental domain L_F as described in the text. For (a) ($L = 2, h \simeq 0.1496$) the reaction rate $\kappa(h, L)$ is very large ($\kappa \simeq 0.12$), for (b) ($L = 2, h \simeq 0.4947$) it is very small ($\kappa \simeq 0.003$). In both cases, there exist only two real largest eigenmodes where the second ones are shifted by a phase. In (c) ($L = 6, h = 1$) both largest eigenmodes have been plotted (thick line for the one and thin line for the other, respectively).

error in $\chi_{\max}(h, L)$ with respect to mL is sufficiently small. Fig. 4.9 shows some typical largest eigenmodes $\psi(x, l)$ on the fundamental domain in cases where it gives the correct corresponding largest eigenvalue $\kappa(h, L)$. For large reaction rates, to a certain respect the largest eigenmodes behave like sine functions, see Fig. 4.9 (a), whereas for smaller reaction rates the largest eigenmodes approach two-periodic step-like functions as shown in Fig. 4.9 (b). Fig. 4.9 (c) depicts the largest eigenmodes for a parameter value of h which is just at the borderline of a non-reacting h region, but where the system is nevertheless already highly reactive. Here, the eigenmodes appear to be especially complicated [Gas].

In Fig. 4.10 (a) the reaction rate $\kappa(h, L)$ as defined via Eq. (4.50) has been computed for a series of reaction center periodicities L . For $h = 0.25$ there is no reaction rate in the system. In this case, the iteration method confirms that the difference in the number of particles ξ_n oscillates periodically around zero instead of decaying exponentially. An analysis of the eigenvalue spectra of the corresponding transition matrices reveals that at this h parameter

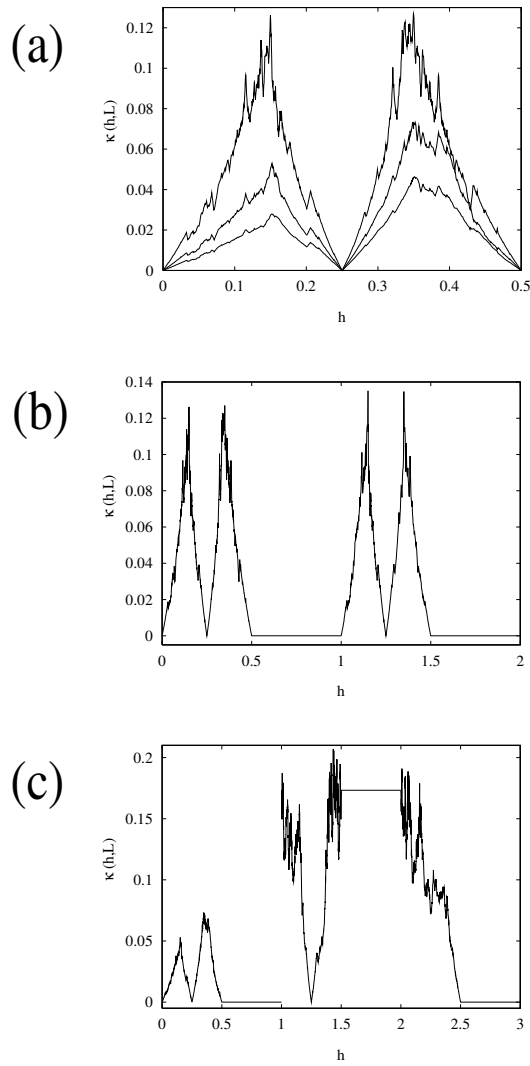


Figure 4.10: (a) Reaction rate $\kappa(h, L)$ at different integer values of the reaction cell periodicity: $L = 2$ (upper curve), $L = 3$ (middle), $L = 4$ (lower curve). (b) Reaction rate for $0 \leq h \leq 2$ at $L = 2$. (c) Reaction rate for $0 \leq h \leq 3$ at $L = 3$. In all cases, error bars are too small to be visible.

the respective reactive multibakers are not ergodic [Gas]. For all other h of the figure the reaction rate is well-defined and shows a complicated structure. By increasing L the reaction rate $\kappa(h, L)$ decreases almost everywhere, as one can expect intuitively, except in certain small parameter regions of h .

Fig. 4.10 (b) gives the full result for $\kappa(h, L)$ at $L = 2$. This structure repeats itself with a periodicity of $2m \leq h \leq 2 + 2m$, $m \in \mathbb{N}_0$. In certain intervals of h the four peaks depicted in the figure are very similar, or even identical, however, there does not appear to be a simple scaling law by which the full peaks can be mapped onto each other. The plateau regions with zero reaction rate correspond to the respective regions observed in Fig. 4.5 for the diffusion coefficient of the system. They share the same characteristics as discussed above for the singular case of $h = 0.25$, except that at $h = 1$ the system is ergodic, but not mixing. Topologically, these regions are of the same origin as explained for the diffusive case.

In Fig. 4.5 (c) the reaction rate has been computed for $L = 3$. In contrast to the two-periodic

case the change from a non-reactive region to a reactive region occurs for $L = 3$ apparently discontinuously in the reaction rate by varying h around 1. This corresponds to the system at $h = 1$ and $L = 3$ being mixing, whereas for the same h and $L = 2$ it was ergodic, but not mixing. We note that for $L = 4$ there are even two of such discontinuous transitions. The detailed irregular structure of the curves, as well as the phase-transition like behavior shown in Fig. 4.10 (c), can be understood in more detail by analyzing the eigenvalue spectra of the reactive evolution operator and how they change under parameter variation, as will be discussed elsewhere [Gas].

Apart from varying h , other parameter dependencies can be studied in this reactive multibaker as well. For example, the distance between the single reaction centers could be changed by allowing L to be continuous, the positions of the reaction centers could be shifted by keeping L fixed, and the size of the reaction centers could be increased or decreased. In all these cases we expect non-trivial parameter dependences to be typical which are similar to the one depicted in Fig. 4.10 [Gas].

4.4 *Summary

1. Starting from the Lorentz gas, we motivated multibaker maps that yield another important class of models for deterministic transport. In particular, we introduced a reactive-diffusive multibaker exhibiting a non-trivial parameter dependence. We outlined in which way its reactive-diffusive dynamics is determined by the Frobenius-Perron (continuity) equation governing the probability density of this dynamical system.
2. We then focused on the purely diffusive dynamics of the model. Keeping the control parameter of the map fixed onto a trivial value, we first constructed the diffusive eigenmodes of the system and established a relation of the associated nonequilibrium steady states with fractal Takagi functions.

We proceeded with a brief review of another basic method to calculate and to understand fractal diffusion coefficients, which starts from a Green-Kubo formula for diffusion. Along these lines, the fractal diffusion coefficient could be linked again to fractal, in this case generalized, Takagi functions. This set the stage for computing the parameter-diffusion coefficient of the reactive-diffusive multibaker again yielding a fractal function, however, being of a slightly different type than the one discussed previously.

3. Finally, we studied the reactive properties of our model. We started by constructing the reactive modes, again for a specific parameter value, and by computing the dispersion relation for both the diffusive and the reactive modes. We also outlined the relation of this model to macroscopic reaction-diffusion equations in terms of a coupled set of differential equations.

The last section displayed results for the parameter-dependent reaction rate of the model. For this purpose the equations governing the one-dimensional projected multibaker dynamics have been solved numerically by suitably adapting the set of methods for one-dimensional maps discussed previously. We detected highly complex structures in the time-dependent spreading of the particle densities and in the reactive

eigenmodes cumulating in a fractal parameter-dependence of the chemical reaction rate. All these quantities exhibited furthermore a complicated interplay between different dynamical phases resulting from specific changes in the topological properties of the underlying chaotic dynamical system subject to parameter variations.

5 Fractal structures of normal and anomalous diffusion

A paradigmatic nonhyperbolic dynamical system exhibiting deterministic diffusion is the smooth nonlinear climbing sine map. We find that this map generates fractal hierarchies of normal and anomalous diffusive regions as functions of the control parameter. The measure of these self-similar sets is positive, parameter-dependent, and in case of normal diffusion it is connected with a fractal diffusion coefficient. By using a Green-Kubo formula we link these fractal structures to the nonlinear microscopic dynamics in terms of fractal Takagi-like functions.

In Section 5.1 we introduce the basic model of this chapter, the climbing sine map, calculate its parameter-dependent diffusion coefficient and analyze its structure by means of a Green-Kubo formula for diffusion. Section 5.2 provides a more detailed analysis of the bifurcation scenarios exhibited by this system in terms of periodic windows.

The research presented in this chapter originated in collaboration with the author's Ph.D. student N. Korabel. The short account of results included here corresponds to Ref. [Kor02], more details can be found in Ref. [Kor03].

5.1 Fractality of deterministic diffusion in the climbing sine map

A simple model for anomalous diffusion is provided by the one-dimensional *climbing sine map*¹ [Gei82, Gro83, Rei94, Sch82, Gro82, Fuj82]. It can be obtained from driven nonlinear pendulum equations [Chi79, Hub80, Mir85, Bla96, Sak02, Fes02, Tan02d] in the limit of strong dissipation via discretization of time [Kog83, Boh84, Bak85]. The climbing sine is a typical example of a *nonhyperbolic* dynamical system that exhibits a rich dynamics consisting of chaotic diffusive motion, ballistic dynamics and localized orbits. Under parameter variation these dynamical regimes are highly intertwined resulting in complex scenarios related to the appearance of periodic windows [Sch82, Gro82, Fuj82].

It is elucidating to relate the climbing sine map to one-dimensional *hyperbolic* maps [Kor03]. As we have shown in the previous chapters, for these maps the transport coefficients usually exist and are fractal [Kla03a] functions of control parameters [Kla95, Kla99a, Kla96]. Hence, a crucial question is whether the origin of normal and anomalous diffusion in the broad class of nonhyperbolic systems is as well of a fractal nature. In this chapter we argue that

¹If restricted to the circle, this map reduces to the “sine circle map” [Ott93]. However, here we are interested in the spatially continued “lifted” circle map that was coined “climbing sine” in the literature [Gei82, Gro83, Rei94, Sch82, Gro82, Fuj82].

nonhyperbolic behavior not only amplifies such fractal structures but generates even more complex fractal characteristics of deterministic diffusion under parameter variation.

The climbing sine map is defined by

$$x_{n+1} = M_a(x_n), \quad M_a(x) := x + a \sin(2\pi x), \quad (5.1)$$

where $a \in \mathbb{R}$ is a control parameter, $x \in \mathbb{R}$, and x_n is the position of a point particle at discrete time n . Obviously, as in case of map \mathcal{L} , cf. Eqs. (2.4) and (2.5) of Chapter 2, $M_a(x)$ possesses translation and reflection symmetry,

$$M_a(x + p) = M_a(x) + p, \quad M_a(-x) = -M_a(x). \quad (5.2)$$

The periodicity of the map naturally splits the phase space into different cells $(p, p + 1]$, $p \in \mathbb{Z}$. We will focus on parameters $a > 0.732644$ for which the extrema of the map exceed the boundaries of each cell for the first time indicating the onset of diffusive motion.

The bifurcation diagram of the associated circle map $m_a(x) := M_a(x) \bmod 1$, consists of infinitely many periodic windows, see Fig. 5.1. Whenever there is a window the dynamics of Eq. (5.1) is either ballistic or localized [Sch82, Gro82, Fuj82]. Fig. 5.1 demonstrates that this scenario has a strong impact on the diffusion coefficient defined by $D(a) := \lim_{n \rightarrow \infty} \langle x_n^2 \rangle / (2n)$, where the brackets denote an ensemble average over moving particles. For localized dynamics orbits are confined within some finite interval in phase space implying subdiffusive behavior for which the diffusion coefficient vanishes, whereas for ballistic motion particles propagate superdiffusively with the diffusion coefficient being proportional to n . Only for normal diffusion $D(a)$ is nonzero and finite. At the boundaries of each periodic window there is transient intermittent-like behavior eventually resulting in normal diffusion with $D(a) \sim a^{(\pm 1/2)}$ [Gei82, Gro83, Rei94, Sch82, Gro82, Fuj82].

Here we are interested in the complete parameter-dependent diffusion coefficient. For this purpose we compute $D(a)$ from numerical simulations by using the Green-Kubo formula for maps [Gas98a, Dor99, Kla02d, Kla95, Kla99a, Gas98c, Gro02], cf. Eq. (4.22) rewritten in form of

$$D_n(a) = \langle j_a(x_0) J_a^n(x) \rangle - \frac{1}{2} \langle j_a^2(x_0) \rangle, \quad (5.3)$$

where the angular brackets denote an average over the invariant density of the circle map, $\langle \dots \rangle := \int_0^1 dx \rho(x) \dots$. The jump velocity j_a is defined by $j_a(x_n) := [x_{n+1}] - [x_n] \equiv [M_a(x_n)]$, where the square brackets denote the largest integer less than the argument. The sum $J_a^n(x) := \sum_{k=0}^n j_a(x_k)$ gives the integer value of the displacement of a particle after n time steps that started at some initial position $x \equiv x_0$ called *jump velocity function*. Eq. (5.3) defines a time-dependent diffusion coefficient which, in case of normal diffusion, converges to $D(a) \equiv \lim_{n \rightarrow \infty} D_n(a)$. In our simulations we truncated $J_a^n(x)$ after having obtained enough convergence for $D(a)$, that is, after 20 time steps. The invariant density was obtained by solving the continuity equation for $\rho(x)$ with the histogram method of Ref. [Lic92].

The highly non-trivial behavior of the diffusion coefficient in Fig. 5.1 can qualitatively be understood as follows: As we explained in Section 4.2, the Green-Kubo formula Eq. (5.3) splits the dynamics into an inter-cell dynamics, in terms of integer jumps, and into an intra-cell dynamics, as represented by the invariant density. We first approximate the invariant density in Eq. (5.3) to $\rho(x) \simeq 1$ irrespective of the fact that it is a complicated function of x and a [Sch82, Gro82, Fuj82]. This approximate diffusion coefficient we denote with a superscript in Eq. (5.3), $D_n^1(a)$. The term for $n = 0$ is well-known as the stochastic random

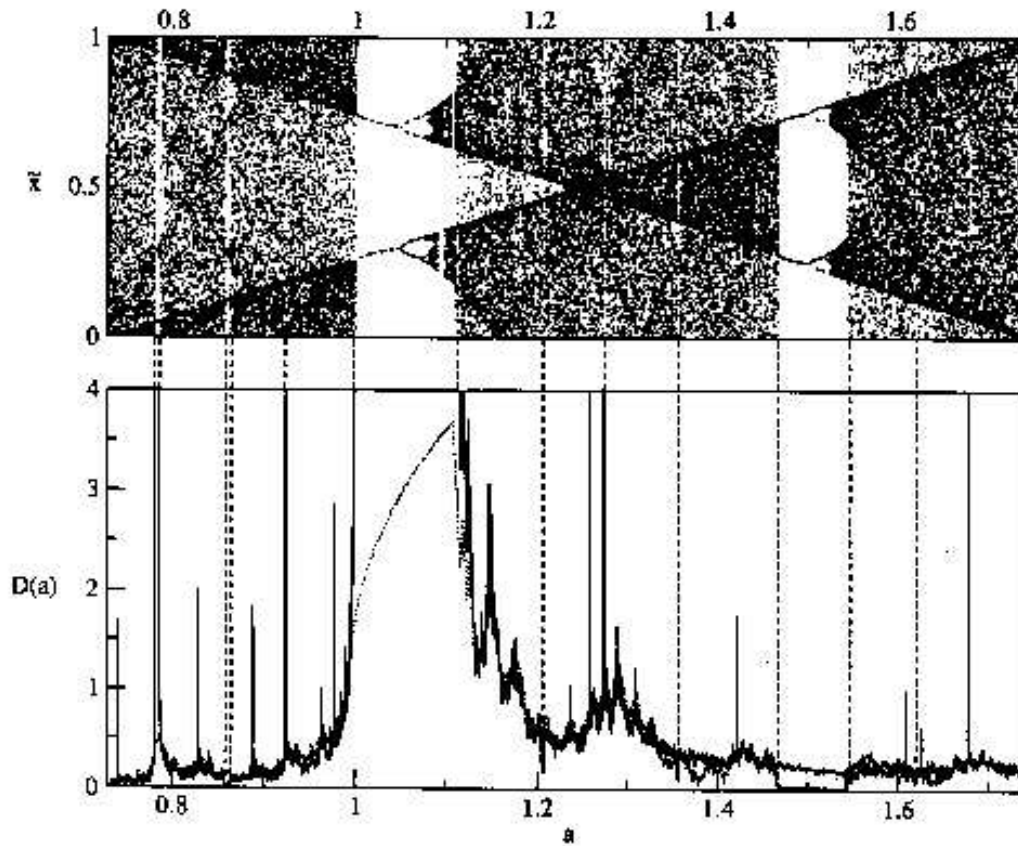


Figure 5.1: Upper panel: bifurcation diagram for the climbing sine map. Lower panel: diffusion coefficient from simulations as a function of the control parameter a in comparison with the correlated random walk approximation $D_{10}^1(a)$ (dots). The dashed vertical lines connect regions of anomalous diffusion, $D(a) \rightarrow \infty$ or $D(a) \rightarrow 0$, with ballistic and localized dynamics in respective windows of the bifurcation diagram. All quantities here and in the following figures are without units.

walk approximation for maps, which excludes any higher-order correlations [Gei82, Gro83, Rei94, Sch82, Gro82, Fuj82, Kla96, Kla02a]. The generalization $D_n^1(a)$, $n > 0$ was called *correlated random walk approximation* [Kla02d]. For hyperbolic maps it will be discussed in detail in Chapter 7. We now use this systematic expansion to analyze the diffusion coefficient of the climbing sine map in terms of higher-order correlations.

In Fig.5.2 (a) we depict results for $D_n(a)$ at $n = 1, \dots, 10$. One clearly observes convergence of this approximation in parameter regions with normal diffusion. Indeed, a comparison of $D_{10}^1(a)$ with $D(a)$, as shown in Fig.5.1, demonstrates that there is qualitative agreement on large scales. On the other hand, for parameters corresponding to ballistic motion the sequence of $D_n^1(a)$ diverges, in agreement with $D(a) \rightarrow \infty$, whereas for localized dynamics it alternates between two solutions. This oscillation is reminiscent of the dynamical origin of localization in terms of certain period-two orbits. That these solutions are non-zero is due to the fact that the invariant density was approximated. In regions of normal diffusion this approximation nicely reproduces the irregularities in the diffusion coefficient. Even more importantly, the magnifications in Fig.5.2 give clear evidence for a self-similar structure of the diffusion coefficient.

We now further analyze the dynamical origin of these different structures. According to its

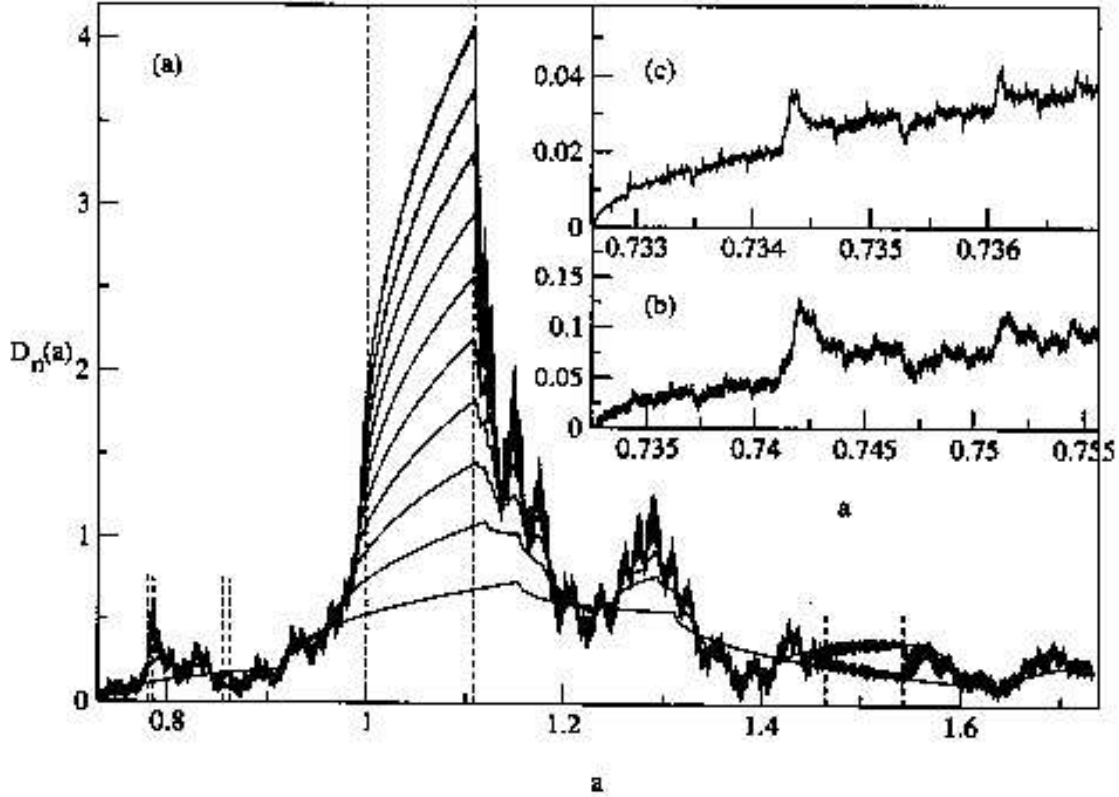


Figure 5.2: (a) Sequence of correlated random walks $D_n^1(a)$ for $n = 1, \dots, 10$. The dashed lines define the same periodic windows as in Fig. 5.1. The inserts (b) and (c) contain blowups of $D_{10}^1(a)$ in the initial region of (a). They show self-similar behavior on smaller and smaller scales.

definition, the time-dependent jump velocity function $J_a^n(x)$ fulfills the recursion relation

$$J_a^n(x) = j_a(x) + J_a^{n-1}(m_a(x)) . \quad (5.4)$$

$J_a^n(x)$ is getting extremely complicated after some time steps, thus we introduce the more well-behaved function

$$T_a^n(x) := \int_0^x J_a^n(z) dz, \quad T_a^n(0) \equiv T_a^n(1) \equiv 0 \quad , \quad (5.5)$$

cp. to Eq. (4.23). Integration of Eq. (5.4) then yields the recursive functional equation

$$T_a^n(x) = t_a(x) + \frac{1}{m_a'(x)} T_a^{n-1}(m_a(x)) - I(x) \quad (5.6)$$

containing the integral term

$$I(x) := \int_0^{m_a(x)} dz g''(z) T_a^{n-1}(z) , \quad (5.7)$$

where $t_a(x) := \int dz j_a(z)$, $m_a'(x) := dm_a(x)/dx$ and $g''(z)$ is the second derivative of the inverse function of $m_a(x)$.² For piecewise linear hyperbolic maps $I(x)$ simply disappears and

²In order to define an inverse of $m_a(x)$, we split the unit interval into subintervals on which this function is piecewise invertible.

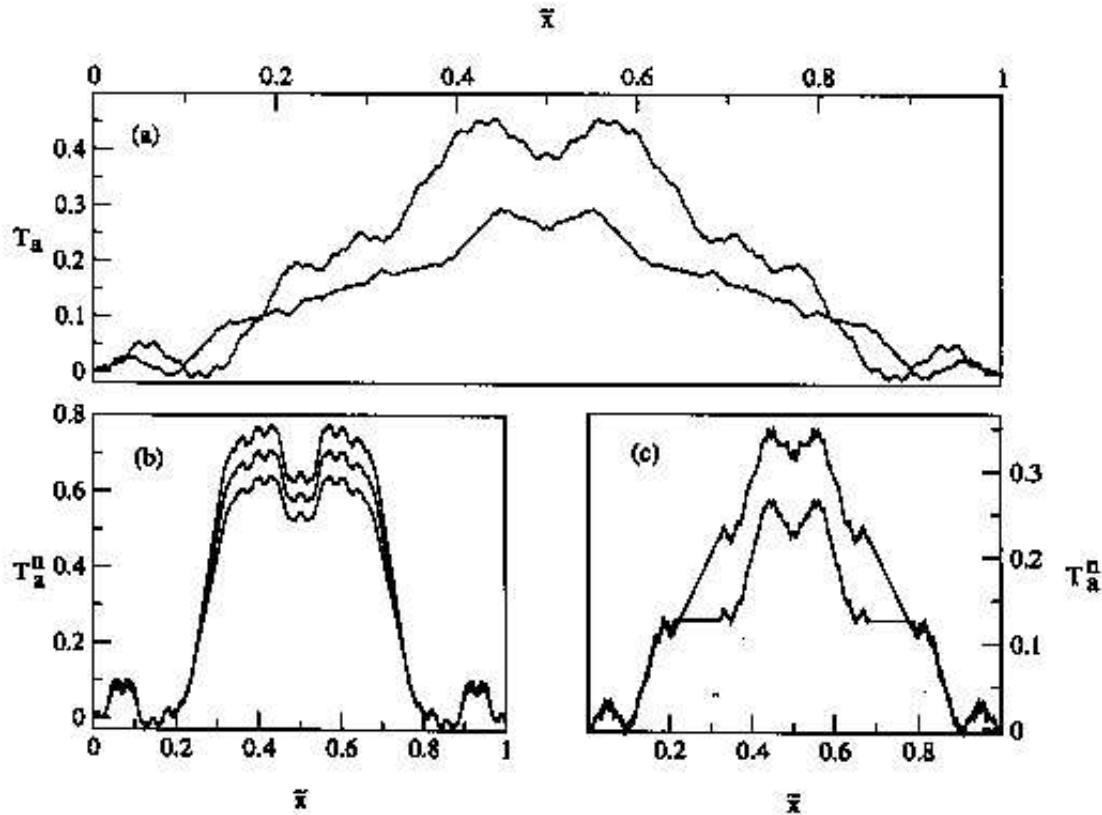


Figure 5.3: Functions $T_a^n(x)$ for the climbing sine map as defined by Eqs. (5.4)-(5.7). (a) diffusive dynamics at $a = 1.2397$ (upper curve) and at $a = 1.7427$ (lower curve), (b) ballistic dynamics at $a = 1.0$, and (c) localized dynamics at $a = 1.5$. In (a) the limiting case $n \rightarrow \infty$ is shown, in (b) and (c) it was $n = 5, 6, 7$.

the derivative in front of the second term reduces to the local slope of the map thus recovering ordinary de Rham-type equations such as Eq. (4.24) [Gas98a, Dor99, Kla96, Gas98c, Gro02]. It is not known to us how to directly solve this generalized de Rham-equation for the climbing sine map, however, solutions can alternatively be constructed from Eq. (5.5) on the basis of simulations. Results are shown in Fig. 5.3. For normal diffusive parameters the limit $T_a(x) = \lim_{n \rightarrow \infty} T_a^n(x)$ exists, and the respective curve is fractal over the whole unit interval somewhat resembling (generalized) fractal Takagi functions [Gas98a, Dor99, Kla96, Gas98c, Gro02]. In case of periodic windows $T_a^n(x)$ either diverges due to ballistic flights, or it oscillates indicating localization. Interestingly, in these functions the corresponding attracting sets appear in form of smooth, non-fractal regions on fine scales, whereas the other regions look fractal.

The diffusion coefficient can now be formulated in terms of these fractal functions by integrating Eq. (5.3). For $a \in (0.732644, 1.742726]$ we get

$$D(a) = 2[T_a(x_2)\rho(x_2) - T_a(x_1)\rho(x_1)] - D_0^p(a), \quad (5.8)$$

where x_i , $i = 1, 2$, is defined by $[M_a(x_i)] := 1$ and $D_0^p(a) := \int_{x_1}^{x_2} dx \rho(x)$. Our previous approximation $D_n^1(a)$ is recovered from this equation as a special case.

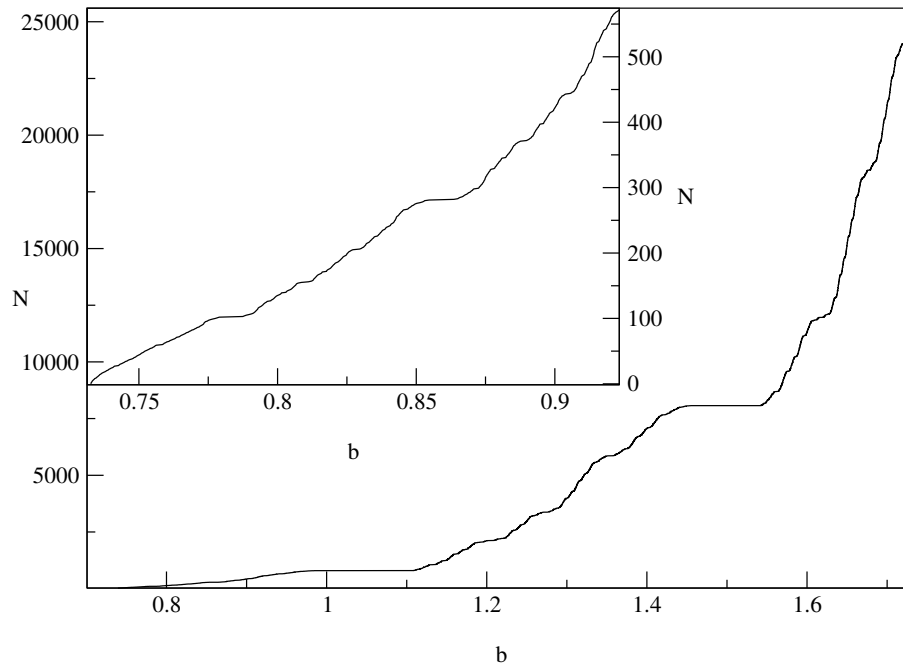


Figure 5.4: Devil's staircase-like structure formed by the distribution of periodic windows as a function of the control parameter. N is the integrated number of period six-windows. The inset shows a blowup of the initial region.

5.2 ⁺Deterministic diffusion, bifurcations, and periodic windows

The intimate relation between periodic windows and the irregular behavior of the diffusion coefficient motivates us to investigate the structure of the periodic windows in the climbing sine map in more detail. The appearance of windows was analyzed quite extensively for non-diffusive unimodal maps [Met73, Jac78, Fei78, Fei79, Fei83], whereas for diffusive maps on the line, apart from the preliminary studies of Refs. [Sch82, Gro82, Fuj82], nothing appears to be known. The windows are generated by certain periodic orbits, consequently there are infinitely many of them, and they are believed to be dense in the parameter set [Ott93]. Windows with ballistic dynamics are born through tangent bifurcations, further undergo Feigenbaum-type scenarios and eventually terminate at crises points. Windows with localized orbits only occur at even periods. They start with tangent bifurcations and exhibit a symmetry breaking at slope-type bifurcation points.

In order to analyze the structure of the regions of anomalous diffusion, we sum up the number of period six-windows as a function of the parameter, that is, the total number is increased by one for any parameter value at which a new period six-window appears. This sum forms a Devil's staircase-like structure in parameter space indicating an underlying Cantor set-like distribution for the corresponding anomalous diffusive region, see Fig. 5.4. The (Lebesgue) measure of periodic windows is obviously positive, hence this set must be a fat fractal [Yor85]. Its self-similar structure can quantitatively be assessed by computing the so-called fatness exponent [Far85].

We are furthermore interested in the parameter dependence of this fractal structure, therefore we divide the parameter line into subsets labeled by the integer value of the map

maximum on the unit interval, $[M_a(x_{max})] = j$, $j \in \mathbb{Z}$. For $j = 1, 2, 3$ we obtain a fatness exponent of 0.45 with errors of 0.03, 0.04, and 0.05 for the different j . We mention that this value was conjectured to be universal and was also obtained for non-diffusive unimodal maps [Far85].

We now study the measure of the windows as a function of the parameter. For this purpose we computed all windows up to period six for the first subset, up to period five for $j = 2, 3$, and we summed up their measures in the respective subsets. We find that the total measure decays exponentially as a function of j while oscillating with odd and even values of j on a finer scale [Kor03]. This oscillation can be traced back to windows generated by localized dynamics that only appear at even periods thus contributing only periodically to the total measure. However, different measures of ‘ballistic’ and ‘localized’ windows decay with the same rate. We have furthermore computed the complementary measure C_j of diffusive dynamics in the j th subset of parameters. We find that $C_1 = 0.783$, $C_2 = 0.898$, and $C_3 = 0.932$ with an error of ± 0.002 , so the measure of the diffusive regions is always non-zero and seems to approach one with increasing parameter values.

5.3 *Summary

1. The climbing sine map defines a simple one-dimensional nonhyperbolic dynamical system exhibiting both normal and anomalous diffusive behavior. We calculated the parameter-dependent diffusion coefficient of this model and showed that it exhibits a highly non-trivial interplay between normal and anomalous diffusive parameter regions. The normal diffusion coefficient again turned out to be fractal. Using a Green-Kubo formula, both normal and anomalous dynamics could be linked to generalized fractal Takagi functions, for which a functional recursion relation was derived.
2. In order to better understand the structure of the anomalous diffusive regions as functions of the control parameter we studied the emergence of periodic windows in this map. We found two different series of windows, one related to localization of particles and another one displaying ballistic flights leading to superdiffusion. Both types of windows form fractal sets in the normal diffusive regions as functions of the control parameter. However, the Lebesgue measure of the normal diffusive region eventually appears to approach one in the limit of large parameter values.

6 Diffusion in randomly perturbed dynamical systems

The impact of space- and time-dependent disorder on deterministic diffusion in chaotic dynamical systems is studied. As an example, we consider a periodic array of scatterers defined by a chaotic map on the line. In computer simulations we find a crossover from deterministic to stochastic diffusion under variation of the perturbation strength related to different asymptotic laws for the diffusion coefficient. Typical signatures of this scenario are multiple suppression and enhancement of normal diffusion. These results are explained by simple theoretical approximations showing that the oscillations emerge as a direct consequence of the unperturbed diffusion coefficient, which is known to be a fractal function of a control parameter.

In Section 6.1 we study the impact of a specific type of spatial disorder onto deterministic diffusion. Section 6.2 deals with the case of putting noise onto the same type of system.

Both outlines are compiled from the publications Refs. [Kla02b, Kla02c].

6.1 Suppression and enhancement of diffusion in disordered dynamical systems

The field of *disordered dynamical systems* tries to bring together two at first view very different directions of research [Rad96, Rad99, Rad03, Bun03a]:¹ Diffusion on disordered lattices with quenched (static) randomness is a traditional problem of statistical physics, which can be studied by probabilistic methods being developed in the theory of stochastic processes [Hau87, Wei94, Bou90, Keh98]. However, as discussed in the previous chapters, diffusion can also be generated from deterministic chaos in nonlinear equations of motion [Gei82, Sch82, Gro82, Fuj82] making it possible to assess chaotic and fractal properties of diffusion by methods of dynamical systems theory [Lic92, Gas98a, Cvi03, Dor99].

Understanding the dynamics of disordered dynamical systems hence poses the challenge of suitably combining these different concepts and ideas. To our knowledge, only very few cases of respective models have been studied so far. Examples include random Lorentz gases for which Lyapunov exponents have been calculated by means of kinetic theory and by computer simulations [Dor99, vB95, Del95c, vB98], numerical studies of diffusion on disordered rough surfaces and in disordered deterministic ratchets [Pop98, Pop00, Ari01], as well as numerical and analytical studies of chaotic maps on the line with quenched disorder [Rad96, Rad99, Tse99, Tse00, Rad03].

¹see also the conference on “Disordered Dynamical Systems” at the MIPPKS Dresden, organized by G.Radons (1998); cf. <http://www.mpipks-dresden.mpg.de/~dds/>.

In this section we will focus again on the most simple example in the latter class of models, which are piecewise linear maps on the line. In case of mixing dynamics, unperturbed maps of this type exhibit normal diffusion [Gro82, Fuj82, Art91, Tse94, Che95a, Kla95, Kla99a, Kla96, Kla97]. However, adding quenched disorder in form of a local bias with globally vanishing drift profoundly changes the dynamics leading to subdiffusion in a complicated potential landscape [Rad96, Rad99, Tse99, Tse00]. Here we will consider a different type of static randomness which is multiplicative, preserves the local symmetry of the model, and is not related to Lévy distributions [Bar00] thus not resulting in anomalous diffusion. Consequently, here we denote with suppression and enhancement of diffusion the variation of the *normal* diffusion coefficient.

Another important aspect is that in previous work the disordered maps always exhibited the Bernoulli property [Rad96, Rad99, Tse99, Tse00], therefore the diffusive properties were in agreement with expectations from stochastic theory. In our case we start from the unperturbed model coined map \mathcal{L} in Chapter 2 which, as we have shown in the previous chapters, exhibits strong dynamical correlations resulting in a fractal [Kla03a] diffusion coefficient as a function of control parameters [Kla95, Kla99a, Kla96, Kla97, Gro02]. Adding uncorrelated static randomness enables to study in which way these dynamical correlations survive, or are getting destroyed, as a function of the perturbation strength, and to which extent simple random walk theory may still be applicable for understanding perturbed chaotic diffusion.

The unperturbed model map \mathcal{L} as defined in Chapter 2, see Eqs. (2.3) to (2.6), obeys the equation of motion

$$x_{n+1} = M_a(x_n) \quad . \quad (6.1)$$

We now modify this system by adding a random variable $\Delta a(i)$, $i \in \mathbb{Z}$, to the slope a on each interval $[i - 1/2, i + 1/2)$ yielding $M_a^{(i)}(x) = (a + \Delta a(i))x$. We assume that the random variables $\Delta a(i)$ are independent and identically distributed according to a distribution $\chi_\alpha(\Delta a)$, where α is again a control parameter. In the following we will consider two different types of such distributions, namely random variables distributed uniformly over an interval of size $[-\alpha, \alpha]$,

$$\chi_\alpha(\Delta a) = \Theta(\alpha + \Delta a)\Theta(\alpha - \Delta a)/(2\alpha) \quad , \quad (6.2)$$

and dichotomous or δ -distributed random variables,

$$\chi_\alpha(\Delta a) = (\delta(\alpha + \Delta a) + \delta(\alpha - \Delta a))/2 \quad . \quad (6.3)$$

Since $|\Delta a| \leq \alpha$, we denote α as the perturbation strength. As an example, we sketch in Fig. 6.1 the map resulting from the disorder of Eq. (6.2) as applied to the slope $a = 3$.

In the absence of any bias, the diffusion coefficient is defined as $D(a, \alpha) = \lim_{n \rightarrow \infty} \langle x_n^2 \rangle / (2n)$, where the brackets denote an ensemble average over moving particles for a given configuration of disorder. An additional disorder average is not necessary because of self-averaging [Bou90]. Note that for locally symmetric quenched disorder and $(a - \alpha) > 2$ there is no physical mechanism leading to infinitely high reflecting barriers as they are responsible for Golosov localization [Rad96, Rad99, Rad03, Bou90]. Thus diffusion must be normal, as is confirmed by computer simulations. Hence, the central question is what happens to the parameter-dependent diffusion coefficient $D(a, \alpha)$ under variation of the two control parameters a and α .

For the unperturbed case $\alpha = 0$ the diffusion coefficient has been computed in Chapters 2 to 4 [Kla95, Kla99a, Kla96, Gro02] showing that $D(a, 0)$ is a fractal function of the slope a as

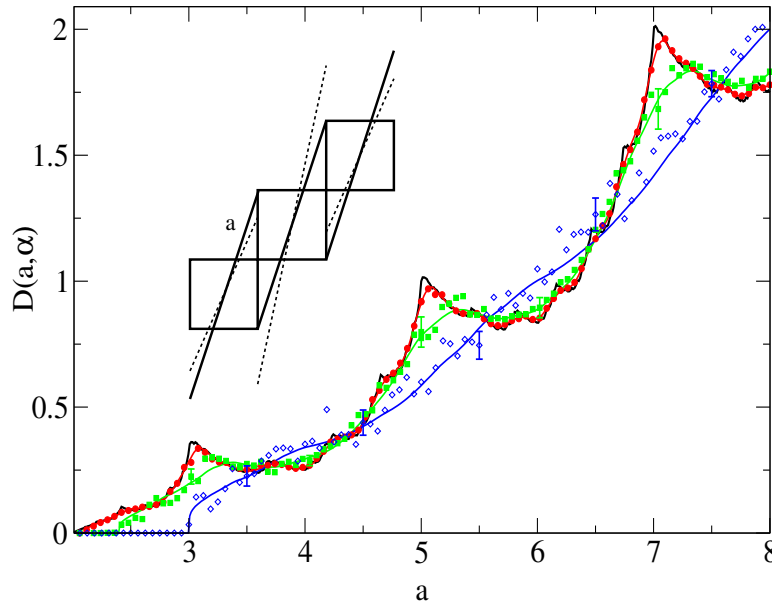


Figure 6.1: Diffusion coefficient $D(a, \alpha)$ for the piecewise linear map shown in the figure. The slope a is perturbed by static disorder of maximum strength α as defined in Eq. (6.2). The bold black line depicts $D(a, 0)$. The symbols represent computer simulation results for $\alpha > 0$, the corresponding lines are obtained from the theoretical approximation Eq. (6.5) The parameter values are: $\alpha = 0.1$ (circles), $\alpha = 0.4$ (squares), $\alpha = 1.0$ (diamonds).

a control parameter. This function is depicted in Fig. 6.1, as well as results from computer simulations for different values of the perturbation strength α in case of uniform disorder.² As expected, this irregular structure gradually disappears by increasing α . However, it is remarkable that even for large perturbation strength α oscillations are still visible as a function of a indicating that the underlying dynamical correlations are very robust against this type of perturbations. Note furthermore the non-analytical behavior of $D(a, \alpha)$ for $\alpha > 0$ and small a thus indicating the existence of a dynamical phase transition which was not present in the unperturbed case.

Before we proceed to more detailed simulation results we briefly repeat what is known for diffusion in lattice models with random barriers [Hau87, Wei94, Bou90, Keh98, Zwa82, Der83, Lyo85]. In the most simple version, the quenched disorder is defined on a one-dimensional periodic lattice with transition rates between neighbouring sites i and $i + 1$ having the symmetry $\Gamma_{i,i+1} = \Gamma_{i+1,i} \equiv \Gamma_k$ for a given random distribution of Γ_k . In this situation an exact expression for the stochastic diffusion coefficient has been derived reading [Keh98, Zwa82, Der83, Lyo85]

$$d = \{1/\Gamma\}^{-1} l^2 \quad , \quad (6.4)$$

with the brackets defining the disorder average $\{1/\Gamma\} = 1/N \sum_{k=0}^N 1/\Gamma_k$ at chain length N and for a distance l between sites. The double-inverse demonstrates that the highest barriers dominate diffusion in one dimension, thus $\Gamma_k \rightarrow 0$ naturally leads to a vanishing

²In the unperturbed case the numerical error is less than visible [Kla95, Kla99a, Kla96, Gro02]. In case of perturbations, for each point a maximum of 1,000,000 particles has been iterated up to 50,000 time steps each; representative error bars are included in all figures.

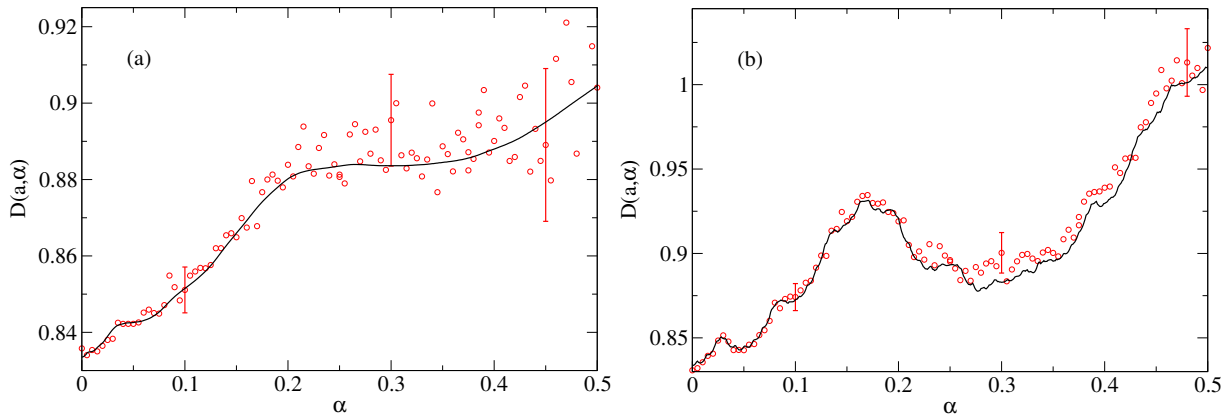


Figure 6.2: Diffusion coefficient $D(a, \alpha)$ as a function of the perturbation strength α at slope $a = 6$: (a) disorder distribution Eq. (6.2), (b) disorder distribution Eq. (6.3). The circles represent results from computer simulations, the lines are obtained from the approximation Eq. (6.5).

diffusion coefficient. This scenario is translated to the map under consideration as follows: Eq. (6.1) can be understood as a time-discrete Langevin equation, $x_{n+1} = x_n - \partial V(x_n)/\partial x_n$ [Rad96, Rad99, Rad03, Gro82, Fuj82]. Under proper integration of $M_a^{(i)}(x)$ the corresponding potential $V(x)$ is reminiscent of a random barrier model with the perturbation strength α determining the highest barriers. Hence, simple random walk theory predicts suppression of diffusion for the chaotic map *viz.* $D(a, \alpha)$ being a monotonously decreasing function of α .

To check this hypothesis, we choose fixed values of a corresponding to the two extreme situations of starting from a local maximum or minimum, respectively, of the unperturbed $D(a, 0)$ in Fig. 6.1. We first focus on the local minimum at $a = 6$ for $\alpha \leq 0.5$ with uniform and dichotomous disorder, see Fig. 6.2. In sharp contrast to the prediction of the simple random walk theory outlined above, in both cases we observe enhancement of diffusion as a function of α . Moreover, this enhancement does not appear in form of a simple functional dependence on α : In (a), smoothed-out oscillations are visible on smaller scales, whereas in (b) the resulting function is clearly non-monotonous and wildly fluctuating exhibiting multiple suppression and enhancement in different parameter regions. Results on larger scales of α are depicted in Fig. 6.3 for dichotomous disorder. Fig. 6.3 (b) shows that choosing a at a local maximum of $D(a, 0)$ leads to suppression of diffusion for $\alpha < 1.0$, whereas a local minimum generates enhancement in the same parameter region of α . We emphasize that in both cases the diffusion coefficient decreases on a very coarse scale by increasing α thus recovering qualitative agreement with the simple random walk prediction Eq. (6.4).³ Indeed, for $(a - \alpha) \rightarrow 2$ barriers are formed which a particle cannot cross anymore implying the existence of localization.

To theoretically explain the simulation results, we modify Eq. (6.4) in a straightforward way such that it can be applied to our disordered deterministic map under consideration. We first note that for uniform transition rates $\Gamma_k = \text{const.}$ it is $d(\Gamma_k, l) = \Gamma_k l^2$. Using this familiar expression for the random walk diffusion coefficient on the unperturbed lattice

³Simulations have also been carried out for uniform disorder Eq. (6.2) essentially yielding smoothed-out versions of the curves shown in Fig. 6.3 [Kla02c].

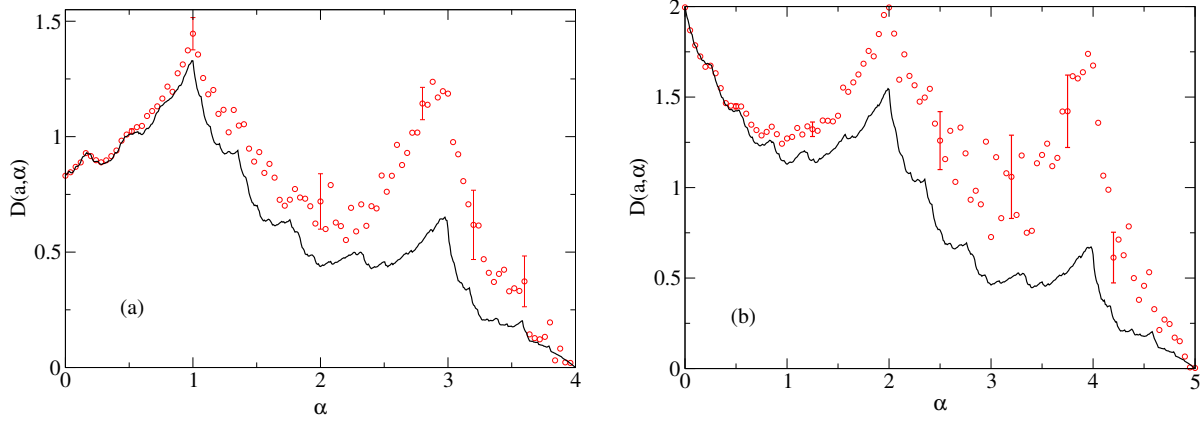


Figure 6.3: Diffusion coefficient $D(a, \alpha)$ as a function of the perturbation strength α for dichotomous disorder Eq. (6.3) at two different slopes a : (a) $a = 6$, (b) $a = 7$. The circles represent results from computer simulations, the lines are obtained from the approximation Eq. (6.5).

we rewrite Eq. (6.4) as $d = \{1/d(\Gamma_k, l)\}^{-1}$. In case of our map, the transition rates and the distance between sites are both somewhat combined in the action of the slope a as a control parameter. Therefore, the unperturbed diffusion coefficient is correctly rewritten by replacing $d(\Gamma_k, l) \equiv d(a)$.

The key question is now what function shall be used for the parameter-dependent diffusion coefficient $d(a)$ in case of deterministic dynamics. Here we propose to *identify the function $d(a)$ with the exact, unperturbed deterministic diffusion coefficient* previously defined as $D(a, 0)$. Providing this information, the exact formula Eq. (6.4) for stochastic dynamics becomes an *approximation* which can straightforwardly be applied to deterministic dynamics in disordered systems. If the disorder distributions $\chi_\alpha(\Delta a)$ are bounded by the perturbation strength α , and by taking the continuum limit for the random variable, our final result reads

$$D_{app}(a, \alpha) = \left[\int_{-\alpha}^{\alpha} d(\Delta a) \frac{\chi_\alpha(\Delta a)}{D(a + \Delta a, 0)} \right]^{-1}. \quad (6.5)$$

The results obtained from this central formula are depicted in Figs. 6.1 to 6.3 in form of lines. For small enough α the agreement between theory and simulations is excellent thus confirming the validity of this equation. For larger α our theory still correctly predicts the oscillations generated from dichotomous disorder, however, since Eq. (6.5) is approximate it should not be surprising to detect quantitative deviations.

We now show that this formula provides a physical explanation for the complex dependence of the diffusion coefficient on the perturbation strength. For $\alpha \rightarrow 0$ Taylor expansion leads to

$$D_{app}(a, \alpha) = \int_{-\alpha}^{\alpha} d(\Delta a) \chi_\alpha(\Delta a) D(a + \Delta a, 0). \quad (6.6)$$

As will be shown in the following section, Eq. (6.6) can be proven without advocating Eq. (6.5) by starting from the definition of the diffusion coefficient [Kla02c]. In this limit the perturbed diffusion coefficient reduces to an average of the exact diffusion coefficient over the neighbourhood $[a - \alpha, a + \alpha]$ weighted by the respective disorder distribution $\chi_\alpha(\Delta a)$. Consequently, if a is chosen at a local minimum the result must be enhancement of diffusion

by increasing α , and suppression at a local maximum, respectively.⁴ On these grounds it is clear that the fractal parameter dependence of $D(a, 0)$ must reappear in the perturbed diffusion coefficient hence leading to multiple suppression and enhancement on all scales.

6.2 From deterministic to stochastic diffusion in noisy dynamical systems

Understanding diffusion in *noisy maps*, that is, in time-discrete dynamical systems where the deterministic equations of motion are perturbed by noise, figures as a prominent problem in recent literature. The most simple example of such models are again one-dimensional chaotic maps on the line. In seminal contributions by Geisel and Nierwetberg [Gei82], and by Reimann et al. [Rei94, Rei96a, Rei96b], scaling laws have been derived for the diffusion coefficient yielding suppression and enhancement of diffusion with respect to variation of the noise strength. Related results have been obtained in Refs. [Fra91, Wac99, Eck03].

However, all these studies apply only to the onset of diffusion where the scaling laws are reminiscent of a dynamical phase transition, and not much appears to be known far away from this transition point. In such more general situations, only perturbations by a nonzero average bias have been studied [Bar97, Bar98]. Related models are deterministic Langevin equations, in which the interplay between deterministic and stochastic chaos has been analyzed [Bec87, Bec95, Bec96, Kan98], however, without focusing on diffusion coefficients. Non-diffusive noisy maps have furthermore been investigated by refinements of cycle expansion methods [Cvi00].

Deterministic diffusion refers to the asymptotically linear growth of the mean square displacement in a purely deterministic, typically chaotic dynamical system [Gei82, Rei94, Rei96a, Rei96b, Wac99, Kla95, Kla99a, Kla96], whereas by *stochastic diffusion* we denote the respective behavior of the same quantity in a system driven by uncorrelated random noise. In this work we study the transition scenario from deterministic to stochastic diffusion in the most simple type of chaotic dynamical systems, which are piecewise linear maps on the line. Particularly, we are searching for signatures of deterministic and stochastic dynamics in the diffusion coefficient as a function of the strength of time-dependent stochastic noise. In this aspect our work appears to be related to the recent dispute on a possible distinction between chaotic and stochastic diffusion in experiments [Gas98b, Bri01, Gra99, Det99b, Det00b, Cen00], where some of the theoretical models studied are very similar to the one introduced below.

We start from the same unperturbed system as considered in the previous section, that is, map \mathcal{L} as defined in Chapter 2, see Eqs. (2.3) to (2.6). However, here we apply two types of *annealed* disorder [Bou90] to the map, namely

(i) noisy slopes [Rei94, Rei96a, Rei96b, Wac99]: we add the random variable Δa_n , $n \in \mathbb{N}$, to all slopes a making them time-dependent in form of

$$M_{a+\Delta a_n}(x) = (a + \Delta a_n)x, \quad (6.7)$$

or (ii) noisy shifts [Gei82, Rei94, Rei96a, Rei96b, Fra91]: we add the random variable Δb_n ,

⁴Based on this heuristical argument, these phenomena have already been conjectured in Ref. [Kla96], see p. 65.

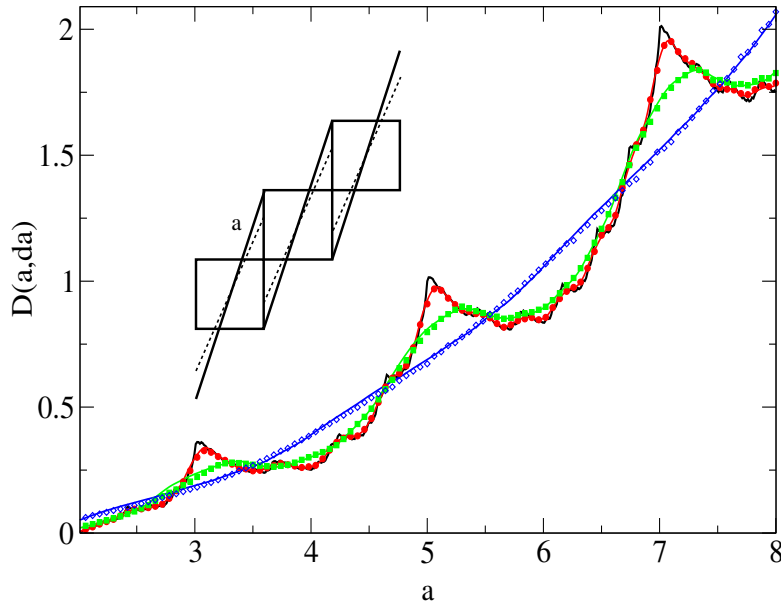


Figure 6.4: Diffusion coefficient $D(a, da)$ for the piecewise linear map shown in the figure. The slope a is perturbed by the uniform noise of maximum strength da of Eq. (6.9). The bold black line depicts numerically exact results for the unperturbed diffusion coefficient at $da = 0$. Computer simulation results for $da \neq 0$ are marked with symbols, the corresponding lines are obtained from the approximation Eq. (6.13). The parameter values are: $da = 0.1$ (circles), $da = 0.4$ (squares), $da = 1.0$ (diamonds).

$n \in \mathbb{N}$, as a time-dependent uniform bias yielding

$$M_{a, \Delta b}(x) = ax + \Delta b_n . \quad (6.8)$$

In both cases we assume that the random variable $\Delta_n \in \{\Delta a_n, \Delta b_n\}$ is independent and identically distributed according to a distribution $\chi_d(\Delta_n)$, where $d \in \{da, db\}$ is again a control parameter. We consider two different types of such distributions, namely random variables distributed uniformly over an interval of size $[-d, d]$ [Fra91, Wac99],

$$\chi_d(\Delta_n) = \frac{1}{2d} \Theta(d + \Delta_n) \Theta(d - \Delta_n) \quad , \quad (6.9)$$

and dichotomous or δ -distributed random variables [Rei94, Rei96a, Rei96b, Wac99],

$$\chi_d(\Delta_n) = \frac{1}{2} (\delta(d - \Delta_n) + \delta(d + \Delta_n)) \quad . \quad (6.10)$$

Since $|\Delta_n| \leq d$, we denote d as the perturbation strength. As an example, we sketch in Fig. 6.4 our model for noisy slopes. We now define the diffusion coefficient as

$$D(a, d) = \lim_{n \rightarrow \infty} \frac{1}{2n} (\langle x_n^2 \rangle_{\rho_0} - \langle x_n \rangle_{\rho_0}^2) , \quad (6.11)$$

with

$$\langle x_n^k \rangle_{\rho_0} = \int dx \int d(\Delta_0) d(\Delta_1) \dots d(\Delta_{n-1}) \rho_0(x) \chi(\Delta_0) \chi(\Delta_1) \dots \chi(\Delta_{n-1}) x_n^k , \quad (6.12)$$

where $\rho_0(x)$ denotes the initial distribution of an ensemble of moving particles, $x_0 \equiv x$, $k \in \mathbb{N}$, and $\Delta_j, j \in \{1, \dots, n-1\}$, is the random variable. $D(a, d)$ has been computed by iterating Eqs.(6.7), (6.8) numerically for an ensemble of moving particles. Because of self-averaging [Bou90], it suffices to generate single series of random variables from Eqs.(6.9), (6.10) instead of evaluating all the integrals in Eq. (6.12). To obtain better numerical convergence, for noisy shifts the first moment squared in Eq. (6.11) was subtracted while Eqs. (6.9), (6.10) imply that the long-time average over the random variable Δ_n does not yield any bias. In Refs. [Kla95, Kla99a, Kla96] it was shown that the unperturbed map \mathcal{L} exhibits normal diffusion if $a > 2$, and the same was found by adding a bias b [Gro02]. Correspondingly, for the types of perturbations defined above diffusion should always be normal if $(a - da) > 2$, as was confirmed in simulations. Hence, the central question is what happens to the parameter-dependent diffusion coefficient $D(a, d)$ under variation of the two control parameters a and d in case of the above two types of noise.

For $da = 0$ it was shown that $D(a, 0)$ is a fractal [Kla03a] function of the slope a as a control parameter [Kla95, Kla99a, Kla96], see Fig. 6.4. Included are results from computer simulations for uniformly distributed noisy slopes at different values of the perturbation strength da .⁵ As expected, the irregular structure gradually disappears by increasing da . Qualitatively the same result is obtained by applying noisy shifts [Kla]. Fig. 6.4 may be compared to the corresponding result for *quenched* slopes Fig. 6.1. Apart from numerical uncertainties, there are clear differences in the critical behavior close to the onset of diffusion. However, for small enough perturbation strength and large enough a the results look qualitatively similar indicating that in this limit quenched and annealed diffusion may be treated on the same footing.

This statement is corroborated by a trivial approximation for the perturbed diffusion coefficient, which we motivate starting from dichotomous noisy slopes. Naive reasoning suggests that, at arbitrary fixed parameters a and da , the *perturbed* diffusion coefficient $D(a, da)$ can be approximated by simply averaging over the *unperturbed* diffusion coefficient $D(a, 0)$ at respective values of the slopes $a - da$ and $a + da$ yielding $D_{\text{app}}(a, da) = (D(a - da, 0) + D(a + da, 0))/2$. It is straightforward to extend this heuristic argument to any other type of uncorrelated noise yielding the generalized expression

$$D_{\text{app}}(\mathbf{p}, \mathbf{d}) = \int d(\mathbf{\Delta}) \chi_d(\mathbf{\Delta}) D(\mathbf{p} + \mathbf{\Delta}, 0). \quad (6.13)$$

Here \mathbf{p} is a vector of control parameters such as $\mathbf{p} = \{a, b\}$ in case of the map above, \mathbf{d} is the corresponding vector of perturbation strengths, and $\mathbf{\Delta}$ is the vector of perturbations such as $\mathbf{\Delta} = \{\Delta a, \Delta b\}$ for noisy shifts and slopes. Further generalizations of this equation, for example, to arbitrary moments as defined in Eq. (6.12), are straightforward. Applying this formula to the case of quenched slopes discussed in the previous section [Kla02b] reproduces the diffusion coefficient approximation Eq. (6.6). The corresponding approximations for uniform noisy slopes are depicted in Fig. 6.4 as lines. They show that even for $da = 1$ the agreement between theory and simulations is excellent. This confirms that, in the limit described above, quenched and annealed disorder generating normal diffusion can indeed approximately be treated in the same way.

Let us now look at the diffusion coefficient for a given value of a as a function of da . Fig. 6.4 shows that approximately at integer slopes the fractal diffusion coefficient $D(a, 0)$ exhibits

⁵A maximum of 1,000,000 particles has been iterated up to 50,000 time steps each. In figures without error bars, the numerical error is less than the size of the symbols.

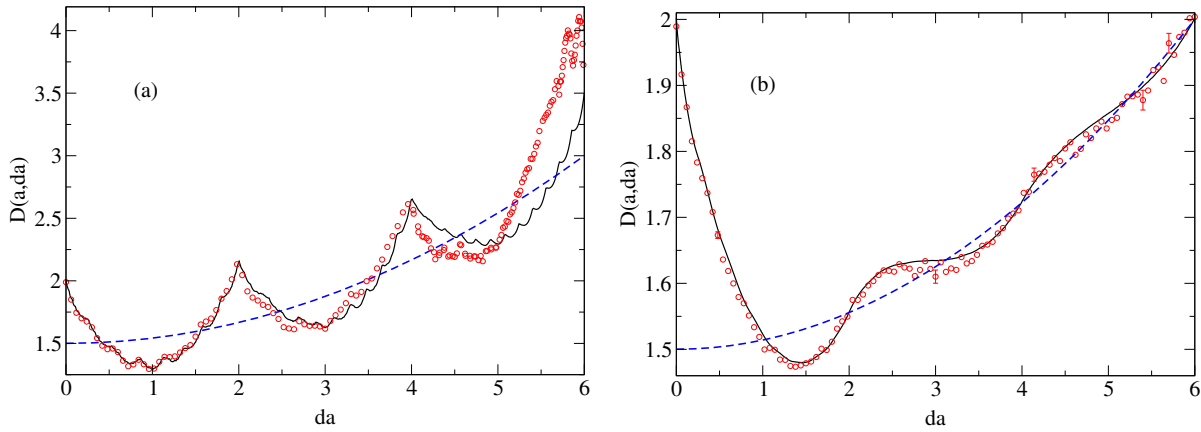


Figure 6.5: Diffusion coefficient $D(a, da)$ as a function of the perturbation strength da at slope $a = 7$ for noisy slopes distributed according to: (a) dichotomous noise Eq. (6.10), (b) uniform noise Eq. (6.9). The circles represent results from computer simulations, the bold lines are obtained from the approximation Eq. (6.13), the dashed lines represent the stochastic limit for the diffusion coefficient Eq. (6.18).

local extrema. Since Eq. (6.13) represents an average over the unperturbed solution in a local environment $[a - da, a + da]$ it predicts local suppression and enhancement of diffusion at odd and even integer slopes, respectively, under variation of the perturbation strength da . This has already been conjectured in Ref. [Kla96] and has been verified in the previous section [Kla02b] for quenched slopes.

We first check this hypothesis for noisy slopes around the local maximum of $D(a, 0)$ at $a = 7$ distributed according to Eqs. (6.9), (6.10). Figs. 6.5 (a), (b) depict again results obtained from computer simulations in comparison to Eq. (6.13). As predicted, in both cases there is suppression of diffusion for small enough da . For dichotomous noise the perturbed diffusion coefficient increases on a coarse scale by exhibiting multiple, fractal-like suppression and enhancement on finer scales. For uniform perturbations there is a pronounced crossover from suppression to enhancement on a coarse scale, by again exhibiting oscillations on a fine scale. In both cases the agreement between simple theory and simulations is excellent for small enough da , whereas systematic deviations particularly in case of dichotomous noise are visible for larger da . Related non-monotonicities for a deterministic diffusion coefficient perturbed by noise have been reported by Eckhardt et al. [Eck03].

Note that if $a - \Delta a_n < 2$ particles are getting trapped within a box at a respective time step n , and that for $a - \Delta a_n < 1$ the map is non-chaotic. In the first case simulations and simple reasoning suggest that the perturbed map still exhibits normal diffusion. However, as soon as $a - da < 1$ numerical results indicate that there is no normal diffusion anymore [Kla]. This appears to be due to the contracting behavior of the non-chaotic map resulting in localization of particles. The oscillatory behavior of the diffusion coefficient in Fig. 6.5 (a) just below this transition point is not yet understood.

Employing Eq. (6.13) we now analyze noisy shifts. The unperturbed two-parameter diffusion coefficient $D(a, b, 0)$ has been calculated numerically exactly for the map under consideration in Chapter 3 [Gro02]. Results for the perturbed diffusion coefficient $D(a, db) \equiv D(a, 0, db)$ are presented in Fig. 6.6 (a) for dichotomous noise and in (b) for uniform perturbations, both starting from $D(a, 0)$ at $a = 6$. In both cases the perturbed diffusion coefficient exhibits

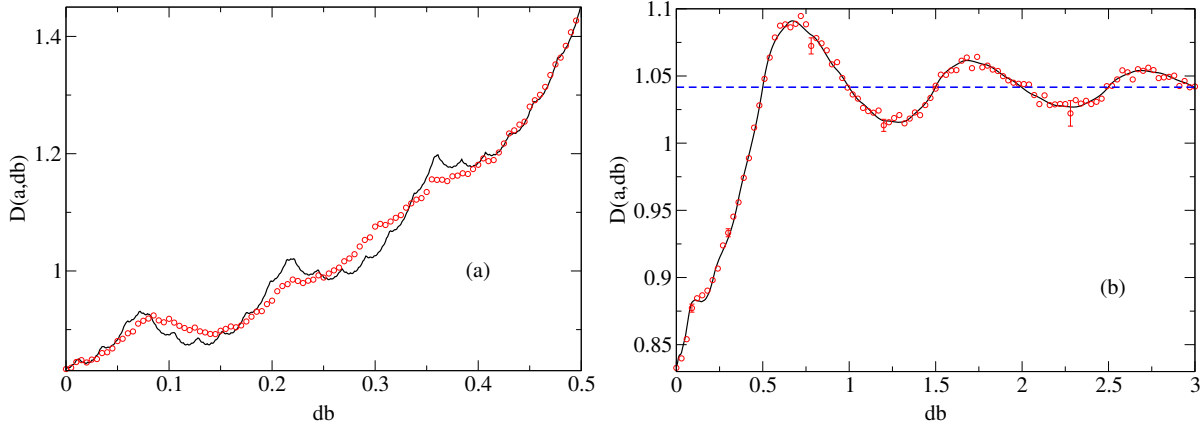


Figure 6.6: Diffusion coefficient $D(a, db)$ as a function of the perturbation strength db at slope $a = 6$ for noisy shifts distributed according to: (a) dichotomous noise Eq. (6.10), (b) uniform noise Eq. (6.9). The circles represent results from computer simulations, the bold lines are obtained from the approximation Eq. (6.13), the dashed line represents the stochastic limit for the diffusion coefficient Eq. (6.17).

strong enhancement of diffusion for $da \rightarrow 0$ due to the fact that the unperturbed diffusion coefficient at $a = 6$ is approximately identical with a local maximum in the (a, b) parameter plane [Gro02]. For dichotomous perturbations it suffices to show results for $0 < db < 0.5$ only. Translation and reflection symmetry of the map imply that this function is mirrored in the interval from $0.5 < db < 1$, and that the full sequence in $0 < db < 1$ is periodically repeated for higher values of db , cf. Chapter 3. As in the corresponding case of noisy slopes, the perturbed diffusion coefficient increases on a coarse scale by exhibiting multiple fractal-like suppression and enhancement on a fine scale. In case of uniform perturbations there is a pronounced crossover to an approximately constant diffusion coefficient for larger db .

Before calculating the stochastic limit of the diffusion coefficient we provide an analytical justification for the heuristic approximation Eq. (6.13). For sake of simplicity, we demonstrate it only for noisy slopes, $\Delta_n \equiv \Delta a_n$. Noisy shifts as well as quenched disorder can be treated along the same lines [Kla]. Let us start from the definition of the diffusion coefficient Eq. (6.11) where $\langle x_n \rangle = 0$. Let Δa_n be uniformly distributed in $[-da, da]$, $\Delta a_0 \equiv \Delta a$. In case of $da \rightarrow 0$ all random variables are bounded by $\Delta a_n = \Delta a + \epsilon$, $-2da \leq \epsilon \leq 2da$. We now put this expression into the perturbed equation of motion Eqs. (6.7), (6.8), as contained in Eq. (6.11), which we write as $x_{n+1, a+\Delta a_n} = M_{a+\Delta a_n}(x_n)$. As a first step we now take the limit $\epsilon \rightarrow 0$ resulting in the expression for the mean square displacement

$$\begin{aligned}
 \langle x_n^2 \rangle &= \int dx \int d(\Delta a) d(\Delta a_1) \dots d(\Delta a_{n-1}) \rho_0(x) \chi(\Delta a) \chi(\Delta a_1) \dots \chi(\Delta a_{n-1}) x_{n, a+\Delta a_{n-1}}^2 \\
 &= \int dx \int d(\Delta a) \rho_0(x) \chi(\Delta a) x_{n, a+\Delta a}^2 (\epsilon \rightarrow 0).
 \end{aligned} \tag{6.14}$$

As a second step we exchange the time limit contained in Eq. (6.11) with the integration

over $d(\Delta a)$ yielding

$$\begin{aligned}
D_{app}(a, da) &= \lim_{n \rightarrow \infty} \frac{\langle x_n^2 \rangle}{2n} \\
&= \int d(\Delta a) \chi_{da}(\Delta a) \lim_{n \rightarrow \infty} \int dx \rho_0(x) \frac{x_{n,a+\Delta a}^2}{2n} \\
&= \int d(\Delta a) \chi_{da}(\Delta a) D(a + \Delta a, 0), \tag{6.15}
\end{aligned}$$

where we have used that the unperturbed diffusion coefficient was defined as

$$D(a, 0) = \lim_{n \rightarrow \infty} \int dx \rho_0(x) x_{n,a}^2. \tag{6.16}$$

We have thus verified our previous approximation Eq. (6.13) for noisy slopes in the limit of small perturbation strength. A similar derivation can be carried out for noisy shifts arriving again at Eq. (6.13) in case of very small perturbation strength. For quenched shifts it is known that a normal diffusion coefficient does not exist [Rad96], thus any approximation by Eq. (6.13) must fail. Indeed, it turns out that in this case taking the limit $\epsilon \rightarrow 0$ fundamentally changes the properties of the dynamical system and is thus no valid operation [Kla].

Finally, we calculate the parameter-dependent stochastic diffusion coefficient related to the map with noisy slopes. Starting from the definition Eq. (6.16) the complete loss of memory in the unperturbed map is modeled by [Kla96, Kla97]

- (i) replacing the distance x_n a particle travels by n times the distance a particle travels at any single time step, $n\Delta x = n(M_a(x) - x)$, and
- (ii) neglecting any memory effects in the probability density on the unit interval by assuming $\rho_0(x) = 1$. Then Eq. (6.16) yields

$$D_{rw}(a) = \frac{(a-1)^2}{24}. \tag{6.17}$$

As was shown in Refs. [Kla96, Kla97], this equation correctly describes the asymptotic parameter dependence of the deterministic diffusion coefficient for $a \rightarrow \infty$ thus explaining the increase of $D(a, 0)$ in Fig. 6.4 on a coarse scale. On this basis, the corresponding result for noisy slopes is easily calculated by using Eq. (6.17) as the functional form for $D(a+\Delta a, 0)$ in the approximation Eq. (6.15) reading

$$D_{rw}(a, da) = D_{rw}(a, 0) + \Delta a^2/c, \tag{6.18}$$

where $c = 24$ for dichotomous noise Eq. (6.10) and $c = 72$ for uniform noise Eq. (6.9). Eq. (6.18) thus confirms the common sense expectation that noise should typically enhance diffusion and represents the *stochastic limit* of the diffusion coefficient. This equation is depicted in Fig. 6.5 (a), (b) in form of dashed lines. In case of dichotomous noise the correlations are obviously large enough such that even for large perturbation strength da there is no transition to the stochastic limit, whereas in case of uniform noisy slopes the diffusion coefficient approaches the stochastic solution asymptotically in da thus verifying the existence of a transition from deterministic to stochastic diffusion. That such a distinct transition behavior exists in these models was already conjectured in Ref. [Kla96]. Analogous

calculations for noisy shifts yield Eq. (6.17) for all values of db reflecting the fact that for large enough a the stochastic diffusion coefficient should not depend on the bias. This result is shown in Fig. 6.6 (b) and again confirms an asymptotic approach of the diffusion coefficient to the stochastic limit under variation of db .

Based on the known result of the existence of a fractal diffusion coefficient for the unperturbed $D(a, b, 0)$ we conjecture that the typical transition scenario in this type of systems consists of (multiple) suppression and enhancement of diffusion. We finally note that Eqs. (6.17), (6.18) are closely related to the approximation outlined in Ref. [Gei82], and to the simple heuristic argument given by Reimann [Rei94, Rei96a, Rei96b] by which he explains the suppression of deterministic diffusion by noise in the climbing sine map near a crisis; more details will be discussed elsewhere [Kla].

6.3 *Summary

1. We started this chapter by studying the impact of spatial, locally symmetric disorder on deterministic diffusion in a model exhibiting a fractal diffusion coefficient. For two different types of independent and identically distributed random perturbations computer simulations yielded, as expected, that the fractal diffusion coefficient gradually “smooths out” as a function of the perturbation strength. Interestingly, we observed a kind of phase transition for small enough control parameters in the perturbed system. Looking at diffusion for a fixed control parameter as a function of the perturbation strength we found complex scenarios of suppression and enhancement of normal diffusion which are again due to strong dynamical correlations. All these numerical results are well explained by a simple heuristic approximation that employs a well-known random walk formula for diffusion on disordered lattices, which we suitably transfer to our case of deterministic diffusion in a random environment.
2. Alternatively, we put time-dependent random perturbations, or “noise”, onto the same unperturbed map. The distributions of random variables were the same as studied before, however, here we investigated both the impact of random slopes and random shifts, the latter breaking the symmetry of the system at a fixed time step. As before, computer simulations showed that the fractal diffusion coefficient changed into a smooth oscillatory structure by applying these types of noise, by eventually crossing over to a monotonically increasing function that is in full agreement with ordinary random walk theory. This crossover from deterministic to stochastic diffusion was displayed more clearly in the diffusion coefficient as a function of the perturbation strength. However, as in case of quenched disorder the noise-dependent diffusion coefficient is no monotonous function but exhibits suppression and enhancement on small and large scales depending on the specific choice of control parameters. Again, we provided a simple analytical approximation for the randomly perturbed diffusion coefficient explaining these findings in relation to the unperturbed fractal diffusion coefficient. This approximation could be derived exactly.

7 From simple deterministic diffusive maps to the periodic Lorentz gas

Low-dimensional periodic arrays of scatterers with a moving point particle are ideal models for studying deterministic diffusion. For such systems the diffusion coefficient is typically an irregular function under variation of a control parameter. Here we propose a systematic scheme of how to approximate deterministic diffusion coefficients of this kind in terms of correlated random walks. We apply this approach to two simple examples which are a one-dimensional map on the line and the periodic Lorentz gas. Starting from suitable Green-Kubo formulas we evaluate hierarchies of approximations for their parameter-dependent diffusion coefficients. These approximations converge exactly yielding a straightforward interpretation of the structure of these irregular diffusion coefficients in terms of dynamical correlations.

In Section 7.1 we exemplify this approach for the piecewise linear map \mathcal{L} on the line introduced in Chapter 2 and studied in subsequent chapters. In Section 7.2 we develop a suitably adapted version of this theory for billiards and demonstrate its application to diffusion in the periodic Lorentz gas.

The work reported here was assisted by N. Korabel and got published in Ref. [Kla02d]. For closely related studies on diffusion in the periodic Lorentz gas see Ref. [Kla00a].

7.1 Correlated random walks in one-dimensional maps on the line

We first work out our theory for one-dimensional diffusive maps of the type of map \mathcal{L} , see Chapter 2, defined by the equation of motion $x_{n+1} = M_a(x_n)$. Let

$$m_a(x) := M_a(x) \pmod{1} \quad (7.1)$$

be the reduced map related to $M_a(x)$. This map governs the dynamics on the unit interval according to $x_n = m_a^n(x)$. Let $\rho_n(x)$ be the probability density on the unit interval of an ensemble of moving particles starting at initial conditions $x \equiv x_0$, which evolves according to the Frobenius-Perron continuity equation Eq. (2.7).

Again, we focus on the deterministic diffusion coefficient defined by the Einstein formula Eq. (2.2). As was already employed in Chapters 4 and 5, the Einstein formula for diffusion can be exactly transformed onto the Green-Kubo formula for maps [Dor99, Kla96, Fuj82, Gas92a], cp. to Eqs. (4.22), (5.3), which for convenience we rewrite here in form of

$$D_n(a) = \sum_{k=0}^n c_k \langle j(x_0)j(x_k) \rangle \quad , \quad (7.2)$$

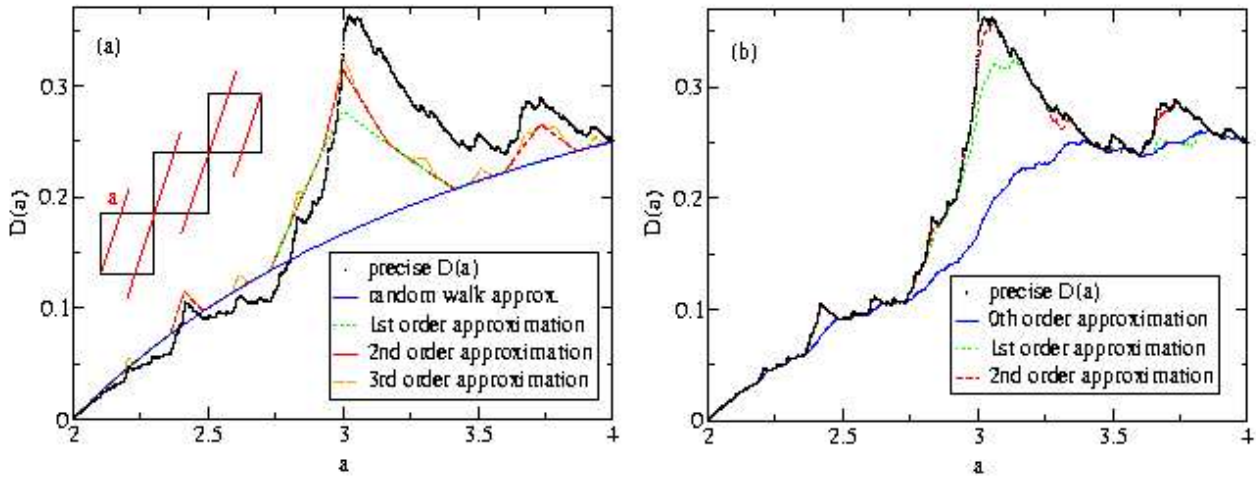


Figure 7.1: Diffusion coefficient $D(a)$ for the one-dimensional map shown in the upper left part of (a), where a is the slope of the map. The dots are obtained from the method of Refs. [Kla95, Kla96, Kla99a, Gas98c, Gro02], the different lines correspond to different levels of approximations based on the Green-Kubo formula Eq. (7.2). In (a) the approximations were computed from Eq. (7.7) assuming a constant invariant density, in (b) they are from Eq. (7.8) which includes the exact invariant density. Any error bars are smaller than visible. All quantities here and in the following figures are without units.

with $D(a) \equiv \lim_{n \rightarrow \infty} D_n(a)$ and

$$c_k = \begin{cases} \frac{1}{2} & , \quad k = 0 \\ 1 & , \quad k \geq 1 \end{cases} . \quad (7.3)$$

Like in Chapters 4, 5, the jump velocity

$$j(x_n) := [x_{n+1}] - [x_n] \quad , \quad (7.4)$$

$[x]$ being the largest integer less than x , takes only integer values and denotes how many unit intervals a particle has traversed after one iteration starting at x_n .

In the following we shall specialize again onto map \mathcal{L} defined by Eqs. (2.3) to (2.6), which is sketched in Fig. 7.1 (a). This figure furthermore depicts a magnification of the parameter-dependent diffusion coefficient of the map, cp. to Fig. 2.3, in the regime of $2 \leq a \leq 4$ as calculated in Chapters 2 to 4 [Kla95, Kla96, Kla99a, Gas98c, Gro02] by means of a numerical implementations of analytical methods.

As explained in Chapters 4 and 5, for an analysis of this fractal diffusion coefficient Eq.(7.2) forms a suitable starting point, because it distinguishes between two crucial contributions of the dynamics to the diffusion process. These are (1) the motion of the particle on the unit interval $x_n \bmod 1$ generating the invariant density $\rho_a^*(x)$, and (2) the integer jumps from one unit interval to another one as related to $j(x_n)$. In Chapter 4 [Kla96, Gas98c] it was argued that both parts provide independent sources of fractality for the diffusion coefficient. However, there Eq. (7.2) was only discussed in the limit of infinite time. Chapter 5 [Kor02, Kor03], in turn, provided an analysis of this formula for intermediate time steps, but only for the complicated case of intertwined normal and anomalous diffusion as it exists in the climbing sine map.

In this chapter we start with the Green-Kubo expansion in a more tutorial way by demonstrating it for the more simple example of map \mathcal{L} . We elucidate the specific contributions of the single terms to the fractality of the normal diffusion coefficient step by step detail, by analyzing how the Green-Kubo formula eventually converges to the exact diffusion coefficient. For this purpose we build up hierarchies of approximate diffusion coefficients. These approximations are defined such that the different dynamical contributions to the diffusion process are properly filtered out. Another issue is how to evaluate the single terms of the Green-Kubo expansion on an analytical basis. In this section we show in detail how to do this for map \mathcal{L} . In the next section we apply the same idea to billiards such as the periodic Lorentz gas.

We start by looking at the first term in Eq.(7.2). For $a < 4$ the absolute value of the jump velocity $j(x_n)$ is either zero or one. Assuming that $\rho_a^*(x) \simeq 1$ for $a \rightarrow 2$ and cutting off all higher order-terms in Eq. (7.2), the first term leads to the well-known *random walk approximation* of the diffusion coefficient [Kla96, Fuj82, Gei82, Sch82, Kla97, Kla02a]

$$D_0(a) = \frac{1}{2} \int_0^1 dx j^2(x) \quad , \quad (7.5)$$

which in case of the map Eq. (2.6) reads

$$D_0(a) = (a - 2)/(2a) \quad . \quad (7.6)$$

This solution is asymptotically correct in the limit of $a \rightarrow 2$. More generally speaking, the reduction of the Green-Kubo formula to the first term only is an exact solution for arbitrary parameter values only if all higher-order contributions from the velocity autocorrelation function $C(n) := \langle j(x_0)j(x_n) \rangle$ are strictly zero. This is only true for systems of Bernoulli type [Fuj82]. Conversely, the series expansion in form of Eq. (7.2) systematically gives access to higher-order corrections by including higher-order correlations, or memory effects. This leads us to the definition of two hierarchies of correlated random walk diffusion coefficients: (1) Again, we make the approximation that $\rho_a^*(x) \simeq 1$. We then define

$$D_n^1(a) := \sum_{k=0}^n c_k \int_0^1 dx j(x)j(x_k) \quad , \quad n > 0 \quad , \quad (7.7)$$

with $D_0^1(a) \equiv D_0(a)$ given by Eq. (7.5). Obviously, this series cannot converge to the exact $D(a)$.

(2) By using the exact invariant density in the averages of Eq.(7.2) we define

$$D_n^\rho(a) := \sum_{k=0}^n c_k \int_0^1 dx \rho_a^*(x)j(x)j(x_k) \quad , \quad n > 0 \quad , \quad (7.8)$$

here with $D_0^\rho(a) = \frac{1}{2} \int_0^1 dx \rho_a^*(x)j^2(x)$, which must converge exactly. The approximations $D_n^1(a)$ and $D_n^\rho(a)$ may be understood as time-dependent diffusion coefficients according to the Green-Kubo formula Eq. (7.2). According to their definitions, $D_n^1(a)$ enables us to look at contributions coming from $j(x_n)$ only, whereas $D_n^\rho(a)$ assesses the importance of contributions resulting from $\rho_a^*(x)$. The rates of convergence of both approximations give an estimate of how important higher-order correlations are in the different parameter regions of the diffusion coefficient $D(a)$.

Similarly to Eq. (7.6), Eq. (7.7) can easily be calculated analytically to first order reading

$$D_1^1(a) = \begin{cases} (a-2)/(2a) & , \quad 2 < a \leq 1 + \sqrt{3} \quad \text{and} \quad 2 + \sqrt{2} < a \leq 4 \\ 3/2 - 3/a - 2/a^2 & , \quad 1 + \sqrt{3} < a \leq 3 \\ -1/2 + 3/a - 2/a^2 & , \quad 3 < a \leq 2 + \sqrt{2} \end{cases} . \quad (7.9)$$

Further corrections up to order $n = 3$ were obtained from computer simulations, that is, an ensemble of point particles was iterated numerically by using the equations of motion. All results are contained in Fig. 7.1 showing that this hierarchy of correlated random walks generates a self-affine structure which resembles, to some extent, the one of the well-known Koch curve. Fig. 7.1 (a) illustrates that this structure forms an important ingredient of the exact diffusion coefficient $D(a)$ thus explaining basic features of its fractality. Indeed, a suitable generalization of this approach in the limit of time to infinity leads to the formulation of $D(a)$ in terms of fractal generalized Takagi functions as discussed in Chapters 4 and 5 [Kla96, Gas98c, Kor02, Kor03].

Fig. 7.1 (b) depicts the results for the series of $D_n^p(a)$ up to order $n = 2$ as obtained from computer simulations. This figure illustrates that there exists a second source for an irregular structure related to the integration over the invariant density, as explained above. In the Green-Kubo formula Eq.(7.2) both contributions are intimately coupled with each other via the integration over phase space.

We now perform a more detailed analysis to reveal the precise origin of the hierarchy of peaks in Fig. 7.1. For this purpose we redefine Eq. (7.7) as

$$D_n^1(a) = \int_0^1 dx j(x) J_n(x) - \frac{1}{2} \int_0^1 dx j^2(x) , \quad n > 0 \quad , \quad (7.10)$$

where we have introduced the *jump velocity function*

$$J_n(x) := \sum_{k=0}^n j(x_k) \quad , \quad (7.11)$$

again with $x \equiv x_0$. From Eq. (7.4) it follows $J_n(x) = [x_{n+1}]$, that is, this function gives the integer value of the displacement of a particle starting at some initial position x .

In Fig. 7.2 we depict some representative results for $J_1(x)$ under variation of the control parameter a . Because of the symmetry of the map we restrict our considerations to $0 < x < 0.5$. Eq. (7.10) tells us that the product of this function with $j(x)$ determines the diffusion coefficient $D(a)$. The shaded bar in Fig. 7.2 marks the subinterval in which $j(x) = 1$, whereas $j(x) = 0$ otherwise, thus an integration over $J_1(x)$ on this subinterval yields the respective part of the diffusion coefficient. One can now relate the four diagrams (a) to (d) in Fig. 7.2 to the functional form of $D_1^1(a)$ in Fig. 7.1 (a) thus understanding where the large peak in $D_1^1(a)$ for $2.732 < a < 3.414$ comes from: For $a < 2.732$, $J_1(x)$ does not change its structure and the interval where particles escape to other unit intervals increases monotonously, therefore $D(a)$ increases smoothly. However, starting from $a = 2.732$ particles can jump for the first time to next nearest neighbours within two time steps, as is visible in $J_1(x)$ taking values of 2 for x close to 0.5. Consequently, the slope of $D(a)$ increases drastically leading to the first large peak around $a = 3$. Precisely at $a = 3$, backscattering sets in meaning that particles starting around $x = 0.5$ jump back to the original unit interval within two time steps, as is reminiscent in $J_1(x)$ in form of the region $J_1(x) = 0$ for x close to 0.5. This leads to

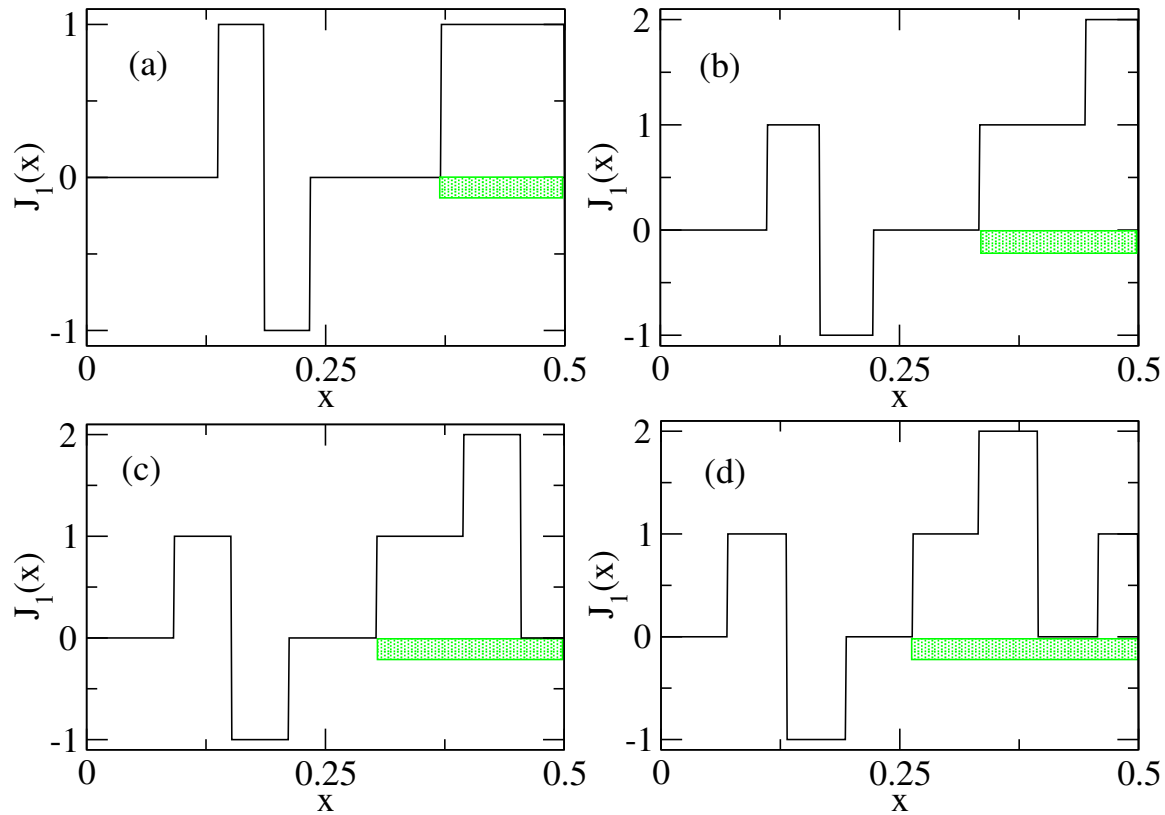


Figure 7.2: Jump velocity function $J_1(x)$ as defined by Eq. (7.11) which gives the integer value of the displacement of a particle starting at some initial position x . Shown are results for different values of the slope a . It is (a) $a = 2.7$, (b) $a = 3.0$, (c) $a = 3.3$, (d) $a = 3.8$. The shaded bar marks the subinterval where the jump velocity $j(x_n)$ defined in Eq. (7.4) is equal to one.

the negative slope in $D(a)$ above $a = 3$. Finally, particles starting around $x = 0.5$ jump to nearest neighbour unit intervals by staying there during the second time step instead of jumping back. This yields again a monotonously increasing $D(a)$ for $a > 3.414$.

Any higher-order peak for $D_n^1(a)$, $n > 1$, follows from analogous arguments. Thus, the source of this type of fractality in the diffusion coefficient is clearly identified in terms of the topological instability of the function $J_1(x)$ under variation of the control parameter a . Indeed, this argument not only quantifies two previous heuristic interpretations of the structure of $D(a)$ as outlined in Refs. [Kla95, Kla96, Kla99a], it also explains why, on a very fine scale, there are still deviations between these results and the precise location of the extrema in $D(a)$, cp. to the “overhang” at $a = 3$ as an example. The obvious reason is that contributions from the invariant density slightly modifying this structure are not taken into account.

Looking at the quantities $J_n(x)$ furthermore helps us to learn about the rates of convergence of the approximations $D_n^1(a)$ to $D(a)$ at fixed values of a , as is illustrated in Fig. 7.3 (a) to (d). Here we have numerically calculated $J_n(x)$ at $a = 3.8$ for $n = 0, 1, 2, 3$. Again, the shaded bar indicates the region where $j(x) = 1$ enabling $J_n(x)$ to contribute to the value of the diffusion coefficient according to Eq. (7.10). In fact, $J_n(x)$ may also be interpreted as the *scattering function* of an ensemble of particles starting from the unit interval, since it

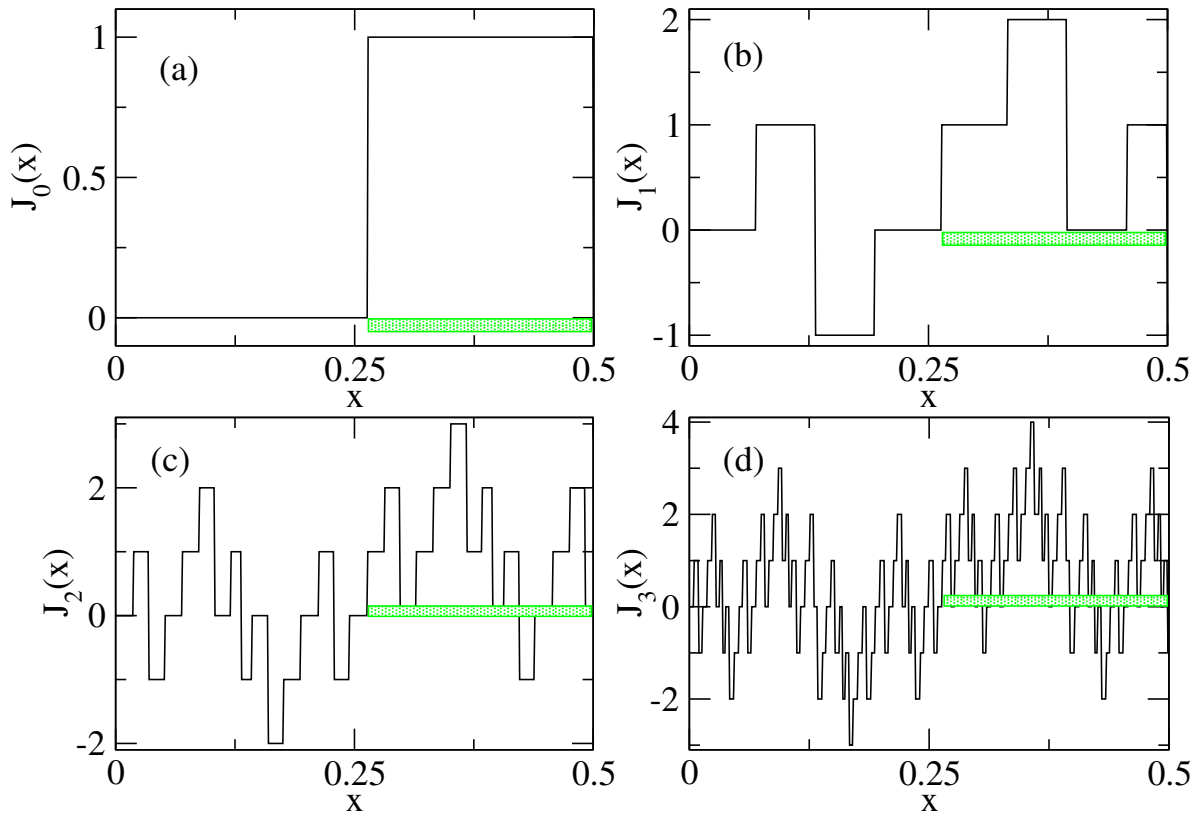


Figure 7.3: Jump velocity function $J_n(x)$ as defined by Eq. (7.11) at the fixed parameter value $a = 3.8$ for the different number of time steps (a) $n = 0$, (b) $n = 1$, (c) $n = 2$, (d) $n = 3$. Again, the shaded bar marks the subinterval where the jump velocity $j(x_n)$ defined in Eq. (7.4) is equal to one.

sensitively measures the final position to which a particle moves within n time steps under variation of its initial position x . One can clearly see that, with larger n , $J_n(x)$ develops more and more discontinuities eventually leading to a highly singular and irregular function of x . Integration over further and further refinements of $J_n(x)$ determines the convergence of the series of $D_n^1(a)$ to a fixed value $D_\infty^1(a)$, cp. to Fig. 7.1 (a). To obtain quantitative values for the associated rates of convergence with respect to parameter variation is an open question.

As was pointed out in Chapters 4 and 5, a suitable integration over the functions $J_n(x)$ leads to the definition of fractal generalized Takagi functions, which can be calculated in terms of de Rham-type functional recursion relations [Kla96, Gas98c, Kor02, Kor03]. In a way, the integration over jump velocity functions such as the one shown in Fig. 7.3 (d) is similar to the integration over Cantor set structures leading to Devils' staircase-type functions [Man82]. Our results presented so far thus bridge the gap between understanding the coarse functional behavior of $D(a)$ on the basis of simple random walk approximations only, and analyzing its full fractal structure in terms of Takagi-like fractal forms, in combination with an integration over a complicated non-uniform invariant density. We now show that essentially the same line of argument can be successfully applied to more physical dynamical systems such as particle billiards.

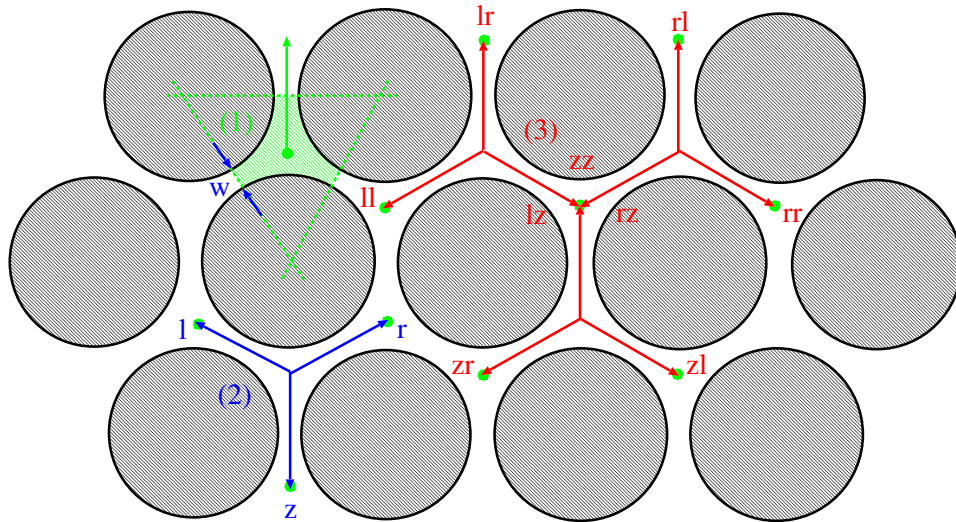


Figure 7.4: Geometry of the periodic Lorentz gas with the gap size w as a control parameter. The hatched area related to (1) marks a so-called trapping region, the arrow gives the lattice vector connecting the center of this trap to the next one above. In (2) three lattice vectors are introduced and labeled with the symbols l, r, z . They indicate the positions where particles move along the hexagonal lattice of Wigner-Seitz cells, starting from the trap z , within two time steps of length τ . (3) depicts the situation after three time steps τ with the different lattice vectors associated to symbol sequences of length two.

7.2 Correlated random walks in the periodic Lorentz gas

The class of two-dimensional billiards we want to discuss here is described as follows: A point particle undergoes elastic collisions with obstacles of the same size and shape whose centers are fixed on a triangular lattice. There is no external field, thus the equations of motion are defined by the Hamiltonian $H = mv^2/2$ supplemented by geometric boundary conditions as induced by the scatterers. A standard example is the periodic Lorentz gas for which the scatterers consist of hard disks of radius R , see Fig. 7.4 [Lor05, Gas98a, Dor99]. In the following we choose $m = 1$, $v = 1$, $R = 1$, and as a control parameter we introduce the smallest inter disk distance w such that the lattice spacing of the disks is $2 + w$. w is related to the number density n of the disks by $n(w) = 2/[\sqrt{3}(2 + w)^2]$. At close packing $w = 0$ the moving particle is trapped in a single triangular region formed between three disks, see Fig. 7.4, part (1). For $0 < w < w_\infty = 4/\sqrt{3} - 2 = 0.3094$, the particle can move across the entire lattice, but it cannot move collision-free for an infinite time. For $w > w_\infty$ the particle can move ballistic-like in form of arbitrarily far jumps between two collisions. The diffusion coefficient for this particle billiard can be defined by the two-dimensional time-continuous equivalent of the Einstein formula Eq. (2.2) reading

$$D(w) = \lim_{t \rightarrow \infty} \langle (\mathbf{x}(t) - \mathbf{x}(0))^2 \rangle / (4t) \quad , \quad (7.12)$$

where, again, the average is taken over the equilibrium distribution of particles with position coordinates $\mathbf{x}(t)$. It can be proven that in the regime of $0 < w < w_\infty$ the parameter-dependent diffusion coefficient $D(w)$ exists [Bun80]. The full parameter-dependence of this function was discussed particularly in Ref. [Kla00a] showing that, on a fine scale, $D(w)$ is

an irregular function of the parameter w similarly to the diffusion coefficient of the one-dimensional map $D(a)$ as discussed above. Whether $D(w)$ is indeed fractal, or maybe C^1 but not C^2 in contrast to the one-dimensional map discussed above, is currently an open question.

The main issue we want to focus on in this section are quantitative approximations for the full parameter dependence of $D(w)$, and to check for the importance of memory effects. A first simple analytical approximation for the diffusion coefficient was derived by Machta and Zwanzig in Ref. [Mac83]. This solution was based on the assumption that diffusion can be treated as a Markovian hopping process between the triangular trapping regions indicated in Fig. 7.4. For random walks on two-dimensional isotropic lattices the diffusion coefficient then reads

$$D = \ell^2/(4\tau) \quad , \quad (7.13)$$

where $\ell = (2 + w)/\sqrt{3}$ is the smallest distance between two centers of the traps, and τ^{-1} is the average rate at which a particle leaves a trap. This rate can be calculated by the fraction of phase space volume being available for leaving the trap divided by the total phase space volume of the trap thus leading to the Machta-Zwanzig random walk approximation of the diffusion coefficient

$$D_{\text{MZ}}(w) = \frac{w(2 + w)^2}{\pi[\sqrt{3}(2 + w)^2 - 2\pi]} \quad . \quad (7.14)$$

Indeed, this approximation is precisely the billiard analogue to the one-dimensional random walk diffusion coefficient for maps Eqs.(7.5), (7.6). Similarly, this approximation is asymptotically exact only for $w \rightarrow 0$, as is shown in comparison to computer simulation results in Fig. 7.5 [Kla00a, Mac83].

In Ref. [Kla00a], Eq. (7.14) was systematically improved by including higher-order correlations. Two basic approaches were presented both starting from the idea of Machta and Zwanzig of looking at diffusion in the Lorentz gas as a hopping process on a hexagonal lattice of “traps” with frequency τ^{-1} . This picture was quantified by introducing a simple symbolic dynamics for a particle moving from trap to trap as indicated in Fig. 7.4.

Let us follow a long trajectory of a particle starting with velocity \mathbf{v} parallel to the y -axis, cp. part (1) in Fig. 7.4. For each visited trap we label the entrance through which the particle entered with z , the exit to the left of this entrance with l , and the one to the right with r , see part (2) in Fig. 7.4. Thus, a trajectory in the Lorentz gas is mapped onto words composed of the alphabet $\{z, l, r\}$. One can now associate transition probabilities to these symbol sequences reading, for a time interval of 2τ , $p(z), p(l), p(r)$. $p(z)$ corresponds to the probability of backscattering, whereas $p(l) = p(r) = (1 - p(z))/2$ indicates forward scattering. For a time interval of 3τ , we have nine symbol sequences each consisting of two symbols leading to the probabilities $p(zz), p(zl), p(zr), p(lz), p(ll), p(lr), p(rz), p(rl), p(rr)$, and so on.

Beside this hierarchy of conditional probabilities defined on a symbolic dynamics there is a different type of probability that a particle leaving a trap jumps without any collision directly to the next nearest neighbour trap. As was shown in Ref. [Kla00a], Eq. (7.14) can be corrected by analytically including all these probabilities. Alternatively, lattice gas computer simulations were performed by using the probabilities as associated to the symbol sequences.

These heuristic corrections of Eq. (7.14) led to a satisfactory explanation of the overall behavior of $D(w)$ on a coarse scale, however, the convergence was not exact. The lattice gas

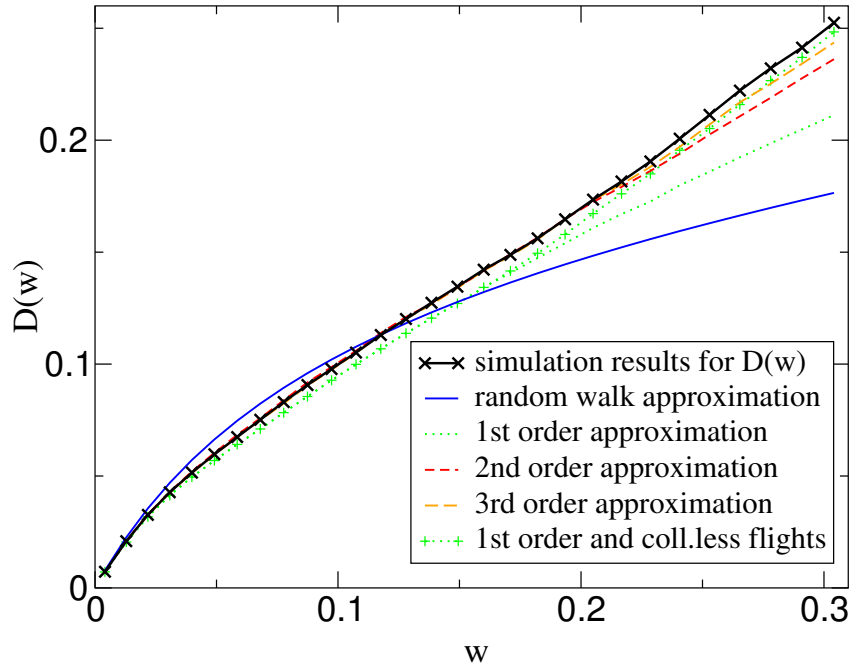


Figure 7.5: Diffusion coefficient $D(w)$ for the periodic Lorentz gas as a function of the gap size w as a control parameter. The computer simulation results for $D(w)$ are from Ref. [Kla00a], error bars are much smaller than the size of the symbols. The other lines correspond to different levels of the approximation Eq. (7.16), the last approximation (again with symbols) is from Eq. (7.20).

simulations, on the other hand, were converging exactly, however, here a proper analytical expression for the diffusion coefficient approximations in terms of the associated probabilities was not available.

In analogy to the procedure as outlined for the one-dimensional map, that is, starting from a suitable Green-Kubo formula, we will now define a third approximation scheme that we expect to be generally applicable to diffusion in particle billiards. Compared to the two existing approaches mentioned above the advantage of the new method is two-fold, namely (1) that by using the set of symbolic probabilities the respective Green-Kubo formula can be evaluated according to an analytical scheme, and (2) that the resulting approximations converge exactly to the computer simulation results.

In the appendix of Ref. [Kla02d] it is proven that, starting from the Einstein formula Eq. (7.12), quite in analogy to the one-dimensional case a Green-Kubo formula can be derived that is defined for an ensemble of particles moving on the hexagonal lattice of traps depicted in Fig. 7.4. The final formula reads

$$D(w) = \frac{1}{2\tau} \sum_{k=0}^{\infty} c_k \langle \mathbf{j}(\mathbf{x}_0) \cdot \mathbf{j}(\mathbf{x}_k) \rangle \quad , \quad (7.15)$$

again with c_k as defined in Eq. (7.3). Here $\mathbf{j}(\mathbf{x}_k)$ defines jumps at the k th time step in terms of the lattice vectors $\ell_{\alpha\beta\gamma\dots}$ associated to the respective symbol sequence of the full trajectory on the hexagonal lattice, cp. to Fig. 7.4. Let us start with $\mathbf{j}(\mathbf{x}_0) = \ell/\tau$, $\ell := (0, \ell)^*$. The next jumps are then defined by $\mathbf{j}(\mathbf{x}_1) = \ell_{\alpha}/\tau$, $\alpha \in \{l, r, z\}$, and so on. The averages indicated in Eq. (7.15) by the brackets are calculated by weighting the respective scalar products of lattice vectors with the corresponding conditional probabilities $p(\alpha\beta\gamma\dots)$.

Note that Eq. (7.15) is the honeycomb lattice analogue to the Green-Kubo formula derived by Gaspard for the Poincaré-Birkhoff map of the periodic Lorentz gas [Gas98a, Gas96]. The Poincaré-Birkhoff version is very efficient for numerical computations, however, according to its construction it fails to reproduce the Machta-Zwanzig approximation Eq. (7.14). Consequently, it does not appear to be very suitable for diffusion coefficient approximations of low order. More details will be discussed elsewhere [Har]. We remark that, in terms of using a symbolic dynamics, there is also some link between Eq. (7.15) and respective diffusion coefficient formulas obtained from periodic orbit theory [Cvi95, Cvi92].

We now demonstrate how Eq. (7.15) can be used for systematic improvements of the diffusion coefficient on the lattice of traps by including dynamical correlations: As in case of one-dimensional maps we start by looking at the first term in Eq. (7.15) and cut off all higher order contributions. Obviously, the first term is again the random walk expression for the diffusion coefficient on the hexagonal lattice of traps that, by including the respective solution for the jump frequency τ^{-1} , boils down to Eq. (7.14). For calculating higher-order corrections we now define the hierarchy of approximations

$$D_n(w) = \frac{l^2}{4\tau} + \frac{1}{2\tau} \sum_{\alpha\beta\gamma\dots} p(\alpha\beta\gamma\dots) \boldsymbol{\ell} \cdot \boldsymbol{\ell}(\alpha\beta\gamma\dots), \quad n > 0 \quad , \quad (7.16)$$

with $D_0(w)$ given by Eq. (7.14). To our knowledge yet there is no method available to analytically calculate the conditional probabilities $p(\alpha\beta\gamma\dots)$. Our following evaluations are therefore based on the data presented in Ref. [Kla00a] as obtained from computer simulations. In terms of the formal probabilities it is now easy to calculate the solution for the first order approximation at time step 2τ to

$$D_1(w) = D_0(w) + D_0(w)(1 - 3p(z)) \quad . \quad (7.17)$$

For a comparison of this formula with the simulation data $D(w)$ see Fig. 7.5. We remark that the corresponding solution in Ref. [Kla00a] as obtained from a heuristical correction of Eq. (7.14) reads $D_{1,MZ}(w) = D_0(w)3(1-p(z))/2$. Indeed, one can show that the new formula Eq.(7.17) is closer to $D(w)$ for large w , whereas for small w the previous approximation is somewhat better. It is straightforward to calculate the two approximations of next higher order to

$$D_2(w) = D_1(w) + D_0(w) (2p(zz) + 4p(lr) - 2p(ll) - 4p(lz)) \quad (7.18)$$

and to

$$\begin{aligned} D_3(w) = & D_2(w) + D_0(w) [p(llr) + p(llz) + p(lrl) + p(lrr) + p(lzl) + p(lzz) + p(rll) \\ & + p(rlr) + p(rrl) + p(rrz) + p(rzr) + p(rzz) + p(zll) + p(zlz) + p(zrr) + p(zrz) \\ & + p(zzl) + p(zzr) - 2(p(lll) + p(lrz) + p(lzr) + p(rlz) + p(rrr) + p(rzl) + p(zlr) \\ & + p(zrl) + p(zzz))] \quad . \quad (7.19) \end{aligned}$$

All results are shown in Fig. 7.5 demonstrating that the series of approximations defined by Eq. (7.16) converges quickly and everywhere to the simulation results. Our new scheme thus eliminates the deficiency of the semi-analytical approximation proposed in Ref. [Kla00a] that was based on heuristically correcting the Machta-Zwanzig approximation Eq. (7.14). By comparing this new scheme with the lattice gas simulations of the same reference, on the other hand, it turns out that the rate of convergence of the lattice gas approach is

still a bit better. In any case, all these three methods unambiguously demonstrate that for achieving a complete understanding of the density-dependent diffusion coefficient in the periodic Lorentz gas it is unavoidable to take higher-order correlations, or the impact of memory effects, properly into account.

We finally remark that a very good low-order approximation for the diffusion coefficient can already be obtained by combining Eq. (7.17) with the probability of collisionless flights $p_{\text{cf}}(w)$ mentioned above, that is, by taking into account the possibility of next nearest neighbour jumps. The correction of $D_0(w)$ as given by Eq. (7.14) according to collisionless flights only was already calculated in Ref. [Kla00a] and read $D_{0,\text{cf}}(w) = D_0(w)(1 + 2p_{\text{cf}}(w))$. Adding now the second term of Eq. (7.17) to this expression by just following the Green-Kubo scheme yields

$$D_{1,\text{cf}}(w) = D_0(w)(2 + 2p_{\text{cf}}(w) - 3p(z)) \quad . \quad (7.20)$$

This solution is also depicted in Fig. 7.5 and shows that this approximation indeed significantly improves Eq. (7.17) for large w yielding a function that is qualitatively and quantitatively very close to $D(w)$. We know of no better approximation for $D(w)$ based on information such as $p(z)$ and $p_{\text{cf}}(w)$ only. The successful application of Eq. (7.20) suggests that collisionless flights form an important mechanism to understand the full diffusive dynamics of this billiard. However, somewhat surprisingly they are not explicitly contained neither in the Green-Kubo expansion Eq. (7.16) nor in the lattice gas simulations of Ref. [Kla00a]. In both cases exact convergence is achieved by following the hierarchy of symbol sequence probabilities only in which collisionless flights are not apparent.

7.3 *Summary

1. In this chapter we proposed a rigorous, systematic approach to understand the irregular structures of parameter-dependent diffusion coefficients. For this purpose we employed, respectively derived, suitable Green-Kubo formulas for diffusion on periodic lattices. Since our theory recovers simple random walk approximations for diffusion in lowest order, but enables to systematically improve these approximation by including higher-order terms, we called it *correlated random walk approximation*. We first outlined this approach for our standard model of a one-dimensional diffusive map on the line. For this map we discussed in full detail the origin of the fractal structure in the diffusion coefficient by evaluating analytically and numerically the single terms of the Green-Kubo expansion. Particularly, we focused on the contribution eventually related to fractal generalized Takagi functions that were already discussed in previous chapters. We showed that the convergence of the Green-Kubo series expansion intimately depends on the choice of parameters reflecting the existence of intricate long-range dynamical correlations.
2. The big advantage of this theory is that it can be straightforwardly generalized to understand irregular diffusion in particle billiards such as the periodic Lorentz gas. The main point is to derive a suitable Green-Kubo formula for billiards that recovers the well-known Machta-Zwanzig random walk approximation for diffusion in lowest order. We show that such a formula can then be evaluated along similar lines as in case of the one-dimensional maps discussed before. Again, the convergence of this series expansion yields evidence for an irregular structure of the diffusion coefficient in the

periodic Lorentz gas on fine scales. These irregularities can be physically understood in terms of sequences of forward- and backward scattering whose existence depends sensitively upon parameter variations.

8 Deterministic diffusion in the flower-shaped billiard

We propose a flower-shaped billiard in order to study the irregular parameter dependence of chaotic normal diffusion in a simple Hamiltonian system. Our model consists of periodically distributed obstacles of flower shape, and it is strongly chaotic for almost all parameter values. We compute the parameter-dependent diffusion coefficient of this model from computer simulations and analyze its functional form by different schemes all generalizing the simple random walk approximation of Machta and Zwanzig. The improved methods we use are based either on heuristic higher-order corrections to the simple random walk model, on lattice gas simulation methods, or they start from a suitable Green-Kubo formula for diffusion. We show that dynamical correlations, or memory effects, are of crucial importance to reproduce the precise parameter dependence of the diffusion coefficient.

In Section 8.1 we introduce the flower-shaped billiard. Numerical results depicting the non-trivial parameter dependence of the diffusion coefficient are shown in Section 8.2. In Sections 8.3, 8.4 and 8.5, we briefly review different approaches to understand the parameter dependence of diffusion coefficients in deterministic dynamical systems, i.e., the Machta-Zwanzig approximation, further systematic corrections of it, as well as the approach based on a suitable Green-Kubo formula for diffusion, by applying them to the flower-shaped billiard.

This work originated in collaboration with T. Harayama and P. Gaspard, see Ref. [Har02]. For related work we refer to Refs. [Kla00a, Kla02d].

8.1 Why a flower-shaped billiard?

One of the main drawbacks concerning the analysis of diffusion in the standard periodic Lorentz gas as described in the previous chapter is that the parameter range of normal diffusion is very limited. In this small region the irregular behavior of the parameter dependent diffusion coefficient shows up on very fine scales and appears to be rather smooth within the range of precision available from computer simulations [Kla00a, Har]. Consequently, the question about the existence of a truly *fractal* diffusion coefficient similar to the one existing in simple one-dimensional maps is very difficult to answer for this model. As the main reason for this behavior it might be suspected that the topological instability of the standard periodic Lorentz gas under parameter variation is not strong enough to generate more pronounced irregularities in this region.

The main purpose of this chapter is therefore to propose a billiard which is very similar to the standard periodic Lorentz gas, but which has a geometry, and an associated range of control parameters exhibiting normal diffusion, with stronger topological instabilities. This

way, we intend to learn more about the emergence of possible fractal structures for diffusion coefficients in billiards. As we will show, our model indeed generates a considerably stronger irregular parameter dependence of the diffusion coefficient than in the standard Lorentz gas. By applying the set of approximation methods mentioned above we argue that long-range dynamical correlations, or memory effects of orbits, are again at the origin of this irregularity, as in case of simple one- and two-dimensional maps.

The two-dimensional class of billiards we consider here consists of a point particle of mass m moving in a plane such that its Hamiltonian is

$$H = \frac{1}{2m}p_x^2 + \frac{1}{2m}p_y^2, \quad (8.1)$$

where x and y denote the Cartesian coordinates of the position in the plane while p_x and p_y are the corresponding momenta. The point particle undergoes elastic collisions with obstacles that are fixed in the plane. All the obstacles have the same shape, and their centers are situated on a triangular lattice according to

$$\mathbf{x}_c = m_c \boldsymbol{\ell}_1 + n_c \boldsymbol{\ell}_2, \quad (8.2)$$

as defined in terms of the fundamental translation vectors of the triangular lattice

$$\boldsymbol{\ell}_1 = (0, 1) \quad (8.3)$$

and

$$\boldsymbol{\ell}_2 = \left(\frac{\sqrt{3}}{2}, \frac{1}{2} \right), \quad (8.4)$$

where m_c and n_c are integers.

If all the pairs of integers are selected, we fill the whole triangular lattice with hard wall obstacles, and the billiard is invariant under the group of spatial translations generated by the vectors Eq. (8.2). Accordingly, the whole lattice can be mapped onto a so-called Wigner-Seitz cell with periodic boundary conditions. The elementary Wigner-Seitz cell of the triangular lattice is a hexagon of area

$$A_{WS} = |\boldsymbol{\ell}_1 \times \boldsymbol{\ell}_2| = \frac{\sqrt{3}}{2}. \quad (8.5)$$

Here we propose an open billiard consisting of flower-shaped obstacles instead of disks, which belongs to the general class of periodic Lorentz gases whose normal diffusion has been proven by Bunimovich, Sinai and Chernov [Bun80, Bun81, Bun91, Che99]. The mixing property and the extension of such billiards to higher-dimensional gases have been studied by Chernov [Che94]. As shown in Fig. 8.1, the space between the obstacles forms the two-dimensional domain of the billiard where the point particle moves freely and collides with the obstacles obeying the law of elastic reflection.

A single scatterer of our billiard is defined as follows: First, we consider the inner hexagon whose vertices are on the middle points of the sides of the hexagon of the elementary Wigner-Seitz cell, as depicted by the dotted lines in Fig. 8.2. Next, we join six arcs which have the same radii and touch the inner hexagon. Then we obtain the flower-shaped obstacle shown in Fig. 8.2. Note that the radius r of one arc which consists in a petal of the flower-shaped obstacle can be changed from $1/(4\sqrt{3})$ to infinity. According to this construction,

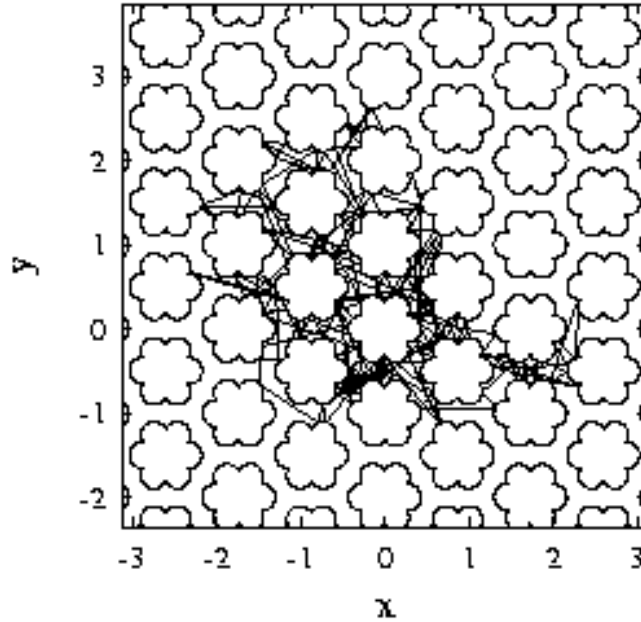


Figure 8.1: The modified Lorentz gas composed of a point particle moving freely in the spaces between the flower-shaped obstacles, which scatters elastically with the obstacles. In our case, mass $m = 1$ and velocity $v = 1$. The quantities plotted in this and in the following figures are dimensionless.

the position space forms a two-dimensional torus. The motion of the point particle in the infinite lattice is unbounded so that transport by diffusion is *a priori* possible. Indeed, we will show that the diffusion of point particles in the billiard of the flower-shaped obstacles is normal.

When the dynamics is reduced to the Wigner-Seitz cell, the position of the particle inside this cell must be supplemented by a lattice vector of the type of Eq. (8.2) in order to determine the actual position of the particle in the infinite lattice. This lattice vector changes in discrete steps at each crossing of the border of the elementary Wigner-Seitz cell.

A billiard whose obstacles are disks, or, in higher dimensions, spheres, is called a periodic Lorentz gas, cf. Chapters 4 and 7. This model serves as a typical example for studying deterministic diffusion [Bun80, Bun81, Bun91, Che99, Mac83, Che94, Gas95b]. The diffusion coefficient of the standard periodic Lorentz gas has been studied in various ways both analytically and numerically. Recent work focused particularly on its density dependence, see Refs. [Kla00a, Kla02d] and further references therein.

In order to describe the dynamics in billiards, let us introduce the Liouville equilibrium invariant measure given by

$$d\mu_e = I(x, y)\delta(H - E)dx dy dp_x dp_y, \quad (8.6)$$

where $I(x, y)$ is the indicator function of the billiard domain, and E is the energy of the point particle. Averages over this invariant measure are denoted by $\langle \dots \rangle$. This measure is normalizable for the reduced dynamics in an elementary Wigner-Seitz cell where the area of the billiard domain takes a finite value. In this finite case, the Liouville invariant measure

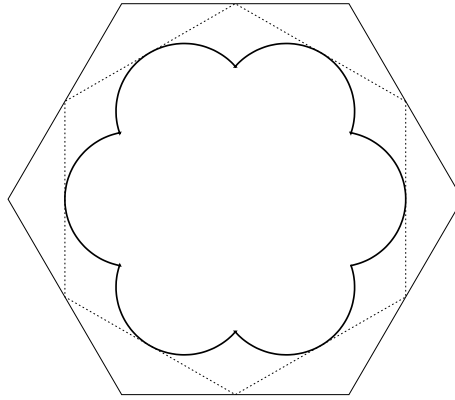


Figure 8.2: Definition of a flower-shaped obstacle. The bigger hexagon (bold lines) is the elementary Wigner-Seitz cell. The arc always touches the smaller hexagon (dotted lines), which prohibits any infinite horizon.

is a probability measure which defines the microcanonical ensemble of equilibrium statistical mechanics.

The flower-shaped billiard belongs to the class of dispersing billiards whose hyperbolicity has been proven by Sinai [Sin70]. Consequently, it is known that the motion of the point particle in the elementary Wigner-Seitz cell of our billiard is hyperbolic in the sense that all orbits are unstable of saddle type with nonvanishing Lyapunov exponents, and time averages are equal to averages over the Liouville equilibrium invariant measure.

8.2 Curvature dependence of the diffusion coefficient

Since the system of flower-shaped obstacles is fully chaotic, and by working in the regime of finite horizon, we may expect that diffusion is normal in the sense that the position is asymptotically a Gaussian random variable with a variance growing linearly in time. Consequently, the diffusion coefficient exists and is finite [Bun80, Bun81, Bun91, Che99, Che94]. Indeed, we checked numerically that the variance is proportional to time after sufficiently long time evolution.

The diffusion coefficient D may be defined by the Einstein formula Eq. (7.12). According to this formula the diffusion coefficient was calculated from computer simulations in the flower-shaped billiard, where the curvature κ of the petals is varied from 0 to its maximum $4\sqrt{3}$. The results are depicted in Fig. 8.3. In this figure we observe a non-trivial structure depending on the curvature κ of the arc defining the petal of the flower-shaped obstacles.

The gross features of the curvature dependence for the diffusion coefficient can qualitatively be explained as follows: When the curvature of the petal of the flower-shaped obstacle is zero, the inner hexagon shown by the dotted lines in Fig. 8.2 connects to the six hexagons surrounding it. In this case, the point particle remains forever localized in compact domains bounded by the three neighbouring hexagons. For this specific value of the control parameter, the motion of the point particle is completely predictable because the compact domain is an equilateral triangle, and the system is integrable.

When the curvature becomes positive, the point particle can run away from the compact domain and diffusion occurs. As already explained, at all positive curvatures of the petal,

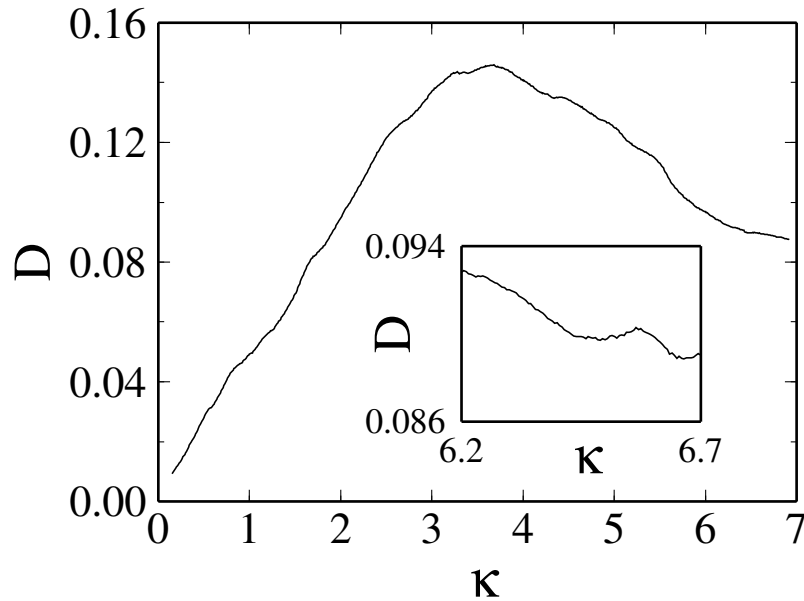


Figure 8.3: Diffusion coefficient D (solid line) versus the curvature κ of the petal of the flower-shaped obstacles. The diffusion coefficient increases approximately linearly for small enough κ until reaching a global maximum. Inset: Zoom on the curve of the diffusion coefficient for larger κ showing the irregularity of this curve on fine scales.

even if they are very small, the motion of the point particle is fully chaotic and the horizon is finite, hence diffusion is expected to be normal. The diffusion coefficient starts to increase from zero according to the linear increase of the curvature of the petal, and related to the fact that the space between petals also increases.

When the radius of the petal is equal to $R_L = \sqrt{3}/4 \simeq 0.433$, which is the distance between the center of the hexagon and the tangent point to the hexagon, the obstacle becomes a disk of radius R_L , that is, for this parameter value our billiard is precisely the same as the conventional periodic Lorentz gas. This point corresponds to the curvature $\kappa \simeq 2.309$ in Fig. 8.2.

When the radius r of the curvature of the petal decreases below R_L , the point particle is much more likely to be trapped in the space between two obstacles. This appears to be due to the formation of wedges between any two petals of a flower-shaped obstacle.

The inset of Fig. 8.3 depicts a zoom on the curve showing the fine structure on smaller scales with respect to curvature. We remark that the apparently continuous fluctuations therein are within the numerical errors, that is, we confirmed the convergence of our results within a precision of order 10^{-4} by taking an average over 10^{10} initial conditions. Unfortunately, with our computational power it is impossible to check whether this oscillatory behavior persists on even finer scales.

8.3 +Machta-Zwanzig approximation for diffusion coefficients

As we already outlined in the previous chapter, in Ref. [Mac83] Machta and Zwanzig have obtained a simple analytical approximation for the diffusion coefficient of the periodic Lorentz

gas which yields asymptotically correct results in the limit of small gaps between disks. In this case, the particle is somewhat trapped in the triangular regions between three adjacent scatterers for a long time. Hence, the particle is supposed to lose the memory of its past itinerary due to the multiple scattering in the trap region, and the transition probabilities to the neighbouring triangular cells are assumed to be equivalent. As was shown in Ref. [Mac83], the average rate τ^{-1} of such transitions can be calculated from the fraction of phase space available for leaving the trap divided by the total phase space volume of the trap leading to

$$\tau = \pi A / (3W), \quad (8.7)$$

where A is the area of the trap and W the width of the gap between the disks.

The flower-shaped billiard has similar types of traps as the periodic Lorentz gas. Accordingly, the Machta-Zwanzig approximation can be applied to the flower-shaped billiard as well, and Eq. (8.7) holds again for the average trapping time. Hence, we only need to calculate the area of the trap and the gap between the petals from simple geometrical considerations yielding

$$A = \frac{3\sqrt{3}}{4} - 3h \left[\sqrt{3}h + \sqrt{r^2 - h^2} \right] \quad (8.8)$$

and

$$W = \frac{1}{2} - \left[\sqrt{3}h + \sqrt{r^2 - h^2} \right], \quad (8.9)$$

where

$$h = \frac{1}{2} \left(\frac{\sqrt{3}}{4} - r \right). \quad (8.10)$$

In the above, r denotes the radius of the curvature of the petal.

The distance l between the centers of the flower-shaped obstacles is $1/\sqrt{3}$. Assuming that the gap size W is very narrow leads to the Machta-Zwanzig random walk approximation for the diffusion coefficient

$$D_{MZ} = \frac{l^2}{4\tau} \quad (8.11)$$

with τ being given by Eq. (8.7) and supplemented by Eqs. (8.8)-(8.10) for the flower-shaped case. As is shown in Fig. 8.4, the Machta-Zwanzig approximation works very well in the vicinity of zero curvature of the petal only.

8.4 + Further corrections of the Machta-Zwanzig approximation

As we have briefly sketched in the previous chapter, the Machta-Zwanzig approximation for the standard periodic Lorentz gas can be further generalized by taking memory effects of orbits into account [Kla00a]. This generalization was based on the observation that, except in the asymptotic limit of narrow gap sizes, the diffusive dynamics is not a simple Markov process, in the sense that there exist non-vanishing dynamical correlations. By mapping the orbit of a particle onto a suitable symbolic dynamics the probabilities to obtain certain symbol sequences of finite length were numerically calculated. Increasing the length of these symbol sequences yielded systematic corrections of the Machta-Zwanzig approximation.

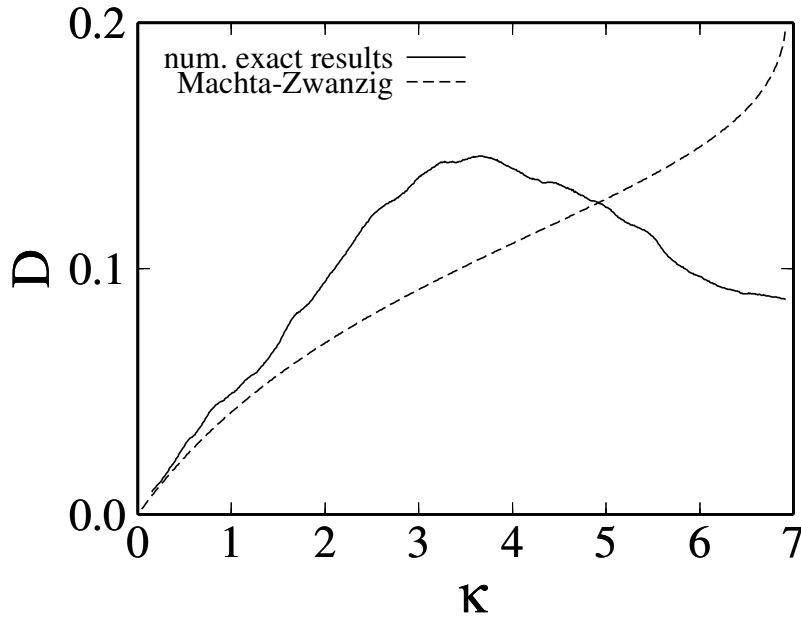


Figure 8.4: Diffusion coefficient D (solid line) versus the curvature κ of the petal of the flower-shaped obstacle. The solid curve correspond to the numerically exact results while the dotted curve yields the Machta-Zwanzig random walk approximation Eq. (8.11).

In Ref. [Kla00a], two schemes directly emerging from this approach were discussed, one suggesting simple heuristic corrections to the simple random walk model of diffusion Eq. (8.11), and another one employing lattice gas computer simulations defined by these probabilities. In this section we apply these two methods to the flower-shaped billiard in order to systematically correct the Machta-Zwanzig approximation. A third scheme starting from a Green-Kubo formula for diffusion will be discussed in Section 8.5.

The Machta-Zwanzig approximation assumes that a particle jumps from one trap to a neighbouring trap situated on the hexagonal lattice of traps. However, there exist non-vanishing probabilities that a particle can jump to next nearest neighbours, or even farther, without collisions. Accordingly, we should correct the Machta-Zwanzig approximation for the flower-shaped billiard by using the probabilities p_{cf1} and p_{cf2} of those collisionless flights which lead from one cell directly to its second nearest neighbours, or to the third nearest neighbours, respectively. The distances l_1 and l_2 between the centers of a trap to respective second and third neighbours are

$$l_1 = \sqrt{3}l, \quad l_2 = \sqrt{7}l. \quad (8.12)$$

The diffusion coefficient D_{cf} with corrections due to these collisionless flights then reads

$$\begin{aligned} D_{cf} &= (1 - p_{cf1} - p_{cf2})D_{MZ} + p_{cf1}\frac{l_1^2}{4\tau} + p_{cf2}\frac{l_2^2}{4\tau} \\ &= (1 + 2p_{cf1} + 6p_{cf2})D_{MZ}. \end{aligned} \quad (8.13)$$

Next we take memory effects of orbits due to backscattering into account. For this purpose, orbits are coded by labeling the entrance through which a particle enters a trap with z , the exit to the left of this entrance with l , and the one to the right with r , cf. Section 7.2. Thus, an orbit can be mapped onto a sequence of symbols z, l , and r . For example, $p(z)$ is the

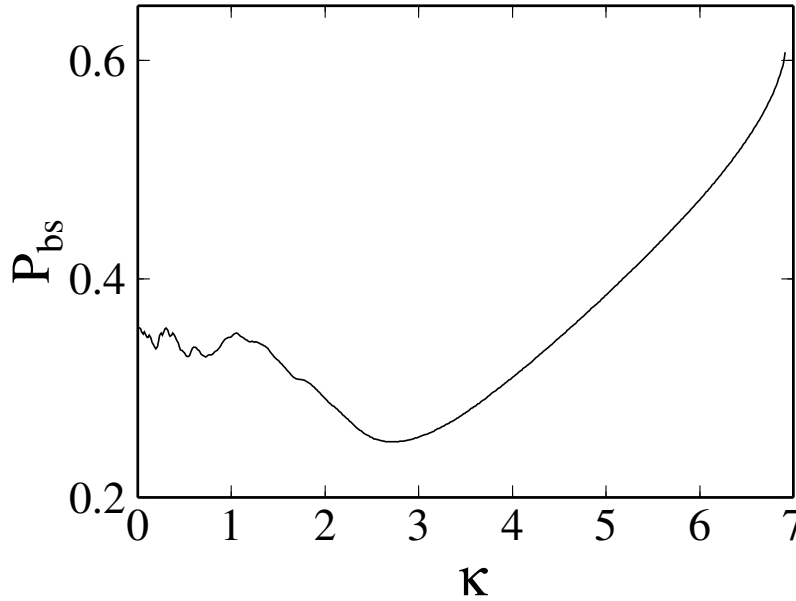


Figure 8.5: Backscattering probability $p_{bs} \equiv p(z)$ (solid line) versus the curvature κ of the petal of the flower-shaped obstacle. In the case of a Markovian process it is equal to $1/3$.

backscattering probability p_{bs} , which is the probability of the moving particle to leave the trap through the same gate where it entered. The Machta-Zwanzig approximation assumes that $p(z) = p(l) = p(r) = 1/3$. However, in general $p(z)$ is not close to $1/3$ as shown in Fig. 8.5, because the actual orbits do not lose their memory during their itineraries.

A more profound explanation for the complicated functional form of $p(z)$ may be provided in terms of the theory of chaotic scattering: Chaotic scattering systems with multiple exit modes typically have fractal phase space boundaries separating the sets of initial conditions (basins) going to the various exits. However, open systems such as a three-disk scatterer of the periodic Lorentz gas possess the even stronger property of being *Wada*, that is, any initial condition which is on the boundary of one exit basin is also simultaneously on the boundary of all the other exit basins [Poo96, JA01]. Changing the curvature κ sensitively affects the highly irregular structure of these basin boundaries. Consequently, Fig. 8.5 may be understood as reflecting the topological instability of Wada basins under parameter variation, and as we will now show this is reflected in the parameter dependence of the diffusion coefficient.¹

Modifying the Machta-Zwanzig random walk by including the backscattering probability $p(z)$ we obtain the diffusion coefficient

$$D_{BS} = \frac{(1 - p(z))l_2^2}{4(2\tau)} = (1 - p(z))\frac{3}{2}D_{MZ}. \quad (8.14)$$

Combining the effects of collisionless flights and backscattering yields as a first order approximation

$$D_1 = \frac{3}{2}(1 - p(z))(1 + 2p_{cf1} + 6p_{cf2})D_{MZ}. \quad (8.15)$$

¹We remark that a more detailed analysis of the chaotic scattering process for the periodic Lorentz gas as contained in the draft version of Ref. [Kla00a], see the note in this reference, was largely deleted in the printed version, upon explicit request of the editor to shorten our article in order to be included into a Special Issue. Quite the same analysis formed the starting point of the more recent Ref. [Agu03].

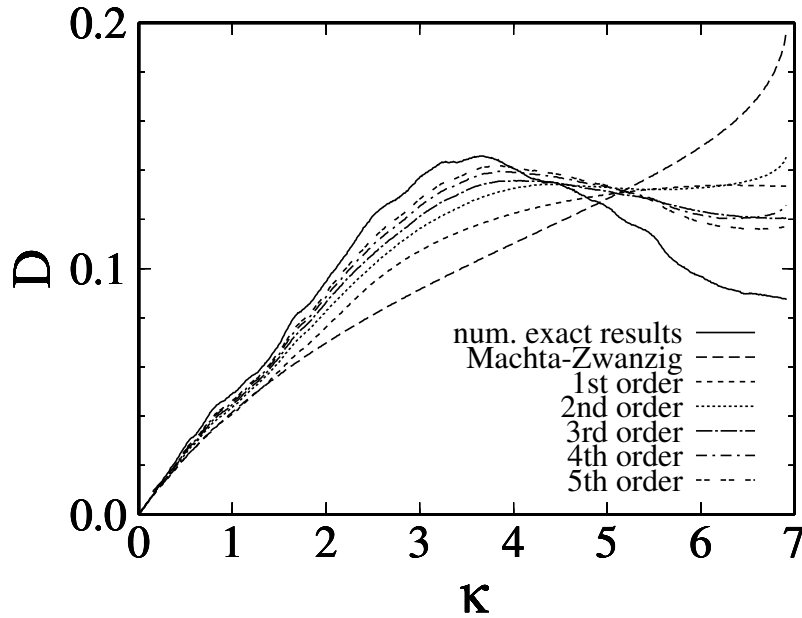


Figure 8.6: Diffusion coefficient of higher-order approximations due to including higher-order backscattering probabilities. The solid curve corresponds to numerically exact results while the other curves represent approximate solutions.

Higher-order approximations of the diffusion coefficient, as related to longer symbol sequences and respective probabilities such as $p(lrz\dots)$, can be derived in the same way [Kla00a]. For the flower-shaped billiard, respective results are shown in Fig. 8.6.

The above correction methods assume that all orbits follow higher-order Markov processes, where correlations are present in form of initial transient times before the variance becomes linear in time. This dynamics appears to be more suitably represented in form of lattice gas simulations on a honeycomb lattice, where the sites of the lattice represent the traps. Indeed, for the periodic Lorentz gas such lattice gas simulations were performed in Ref. [Kla00a] confirming fast convergence to the numerically exact results. Compared to that scheme, the convergence of the intuitive correction method described above is firstly slower, and secondly it is not everywhere converging to the numerically exact results, which is due to the fact that this approach was purely of a heuristic nature.

We also performed lattice gas simulations in case of the flower-shaped billiard according to the following prescription: Particles hop from site to site with a frequency τ^{-1} , which is identical to the hopping frequency used in the Machta-Zwanzig approximation. The hopping probabilities are given by the backscattering probability $p(z)$ and by those corresponding to respective longer symbol sequences. The diffusion coefficient is then obtained from the Einstein formula Eq. (7.12) in the limit when the variance is getting proportional to time. The correlations in the actual orbits are thus systematically and exactly filtered out according to the length of the symbol sequences.

In Fig. 8.7, the results of such higher-order approximations according to lattice gas simulations are shown. One can see that the convergence to the numerically exact results is not only much better than in Fig. 8.6, but even exact. Strong memory effects are clearly visible especially after the diffusion coefficient curve takes its maximum. In the previous heuristic modifications to the simple random walk model, the dynamics was only modeled for a limited number of time steps as a Markov process. Fig. 8.6 suggests that correlations as

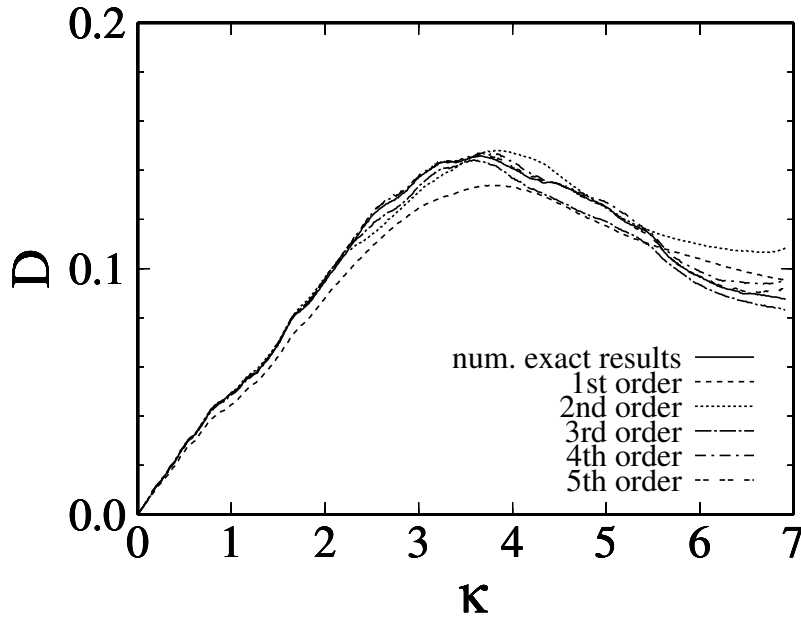


Figure 8.7: Diffusion coefficient as obtained from lattice gas simulations based on higher-order backscattering probabilities. The solid curve corresponds to numerically exact results while the other curves yield higher-order approximations.

contained in the symbol sequences are more suitably represented by higher-order iterations in form of lattice gas simulations. However, a disadvantage is that the lattice gas scheme requires a second round of computations which is put on top of the previous simulations, by again looking at the time evolution of an initial ensemble of points.

8.5 The Green-Kubo formula approach

The main drawbacks of the two methods described above were, firstly, that the heuristic corrections of the Einstein formula were not converging exactly to the numerically exact results, and, secondly, that the lattice gas simulations were merely a numerical scheme without being represented in form of analytical approximations. These deficiencies were essentially resolved, as outlined in Section 7.2 [Kla02d], by the derivation of the Green-Kubo formula Eq. (7.15) that employs the symbolic dynamics on the hexagonal lattice of traps introduced in Section 8.4, respectively in Section 7.2. In case of the flower-shaped billiard the first term of Eq. (7.15) yields Eq. (8.11) amended by Eqs. (8.8)-(8.10). Higher-order corrections can then be calculated by using the hierarchy of approximations D_n defined by Eq. (7.16), again with $D_0 \equiv D_{MZ}$ given by Eq. (8.11) plus supplements.

The impact of dynamical correlations on the diffusion coefficient can now be understood by analyzing the single contributions in terms of the correlation function

$$C_n := \langle \mathbf{j}(\mathbf{x}_0) \cdot \mathbf{j}(\mathbf{x}_n) \rangle \quad (8.16)$$

as contained in the Green-Kubo formula Eq. (7.15). In fully chaotic systems such as the periodic Lorentz gas and the flower-shaped billiard, the velocity correlation function decays exponentially, which is in agreement to the results depicted in Fig. 8.8. By comparing this figure to Fig. 8.9 one can learn how the irregularities of the correlation function determine the parameter dependent diffusion coefficient.

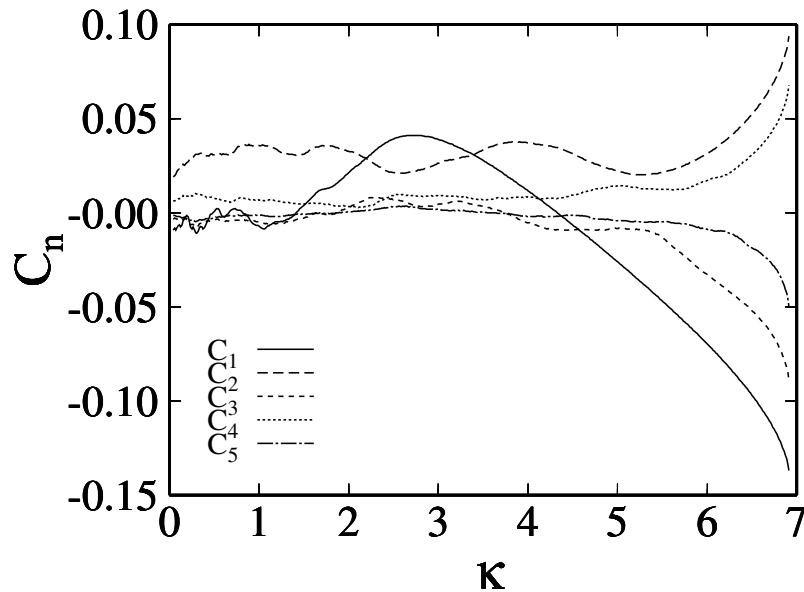


Figure 8.8: Parameter dependence of the time-dependent correlation function C_n , see Eq. (8.16), defined with respect to the symbolic dynamics on the hexagonal lattice of traps. At any parameter C_n decays exponentially related to the fact that the Green-Kubo formula Eq. (7.15) is a convergent series. The speed of the convergence depends on the curvature. Obviously, in the large curvature region the correlation function decays more slowly than for small curvature.

Let us start with the first-order approximation of Eq. (7.15) reading $D_1 = D_0 + D_0(1 - 3p(z))$, cf. Eq. (7.17). The functional form of $p(z)$ in Fig. 8.5 thus qualitatively explains the position of the global maximum of the diffusion coefficient, because at this value of the curvature the probability of backscattering is minimal. Adding up the three-jump contributions coming from C_2 furthermore yields the most important quantitative contributions in this region of the curvature.

In the region of large curvature the diffusion coefficient decays monotonically according to the effect of two-hop correlations covered by C_1 . However, note the large fluctuations of the correlation function C_n as well as of the diffusion coefficient approximations D_n in this regime both indicating the dominant effect of long-range higher-order correlations. Studying the detailed convergence of the approximations depicted in Fig. 8.9 shows that correlations due to orbits with longer symbol sequences yield irregularities in the parameter dependence of the diffusion coefficients on finer and finer scales.

8.6 *Summary

1. The idea to construct a diffusive Hamiltonian particle billiard with flower-shaped scatterers emerged from the fact that the irregularities in the parameter-dependent diffusion coefficient of the periodic Lorentz gas were not too pronounced. Identifying the topological instability of the dynamical system as the origin of the irregular parameter-dependence suggested to define scatterers exhibiting a stronger curvature dependence thus leading to the flower shape. A precise definition of this model was given in the first section of this chapter.

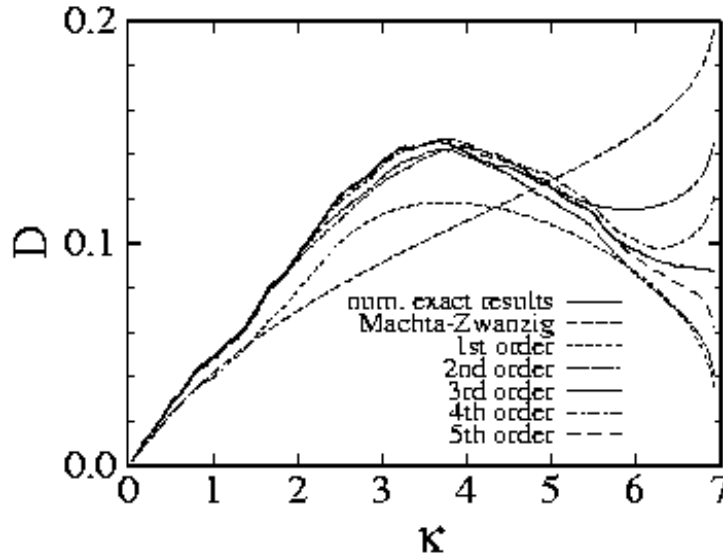


Figure 8.9: Diffusion coefficients as obtained from the Green-Kubo formula Eq. (7.15). The solid curve correspond to the asymptotic, numerically exact results while the other curves yield the respective hierarchy of approximations.

2. We then obtained the diffusion coefficient of this model as a function of the curvature of the scatterers from computer simulations. The result showed again a non-monotonous curve with irregularities on finer scales. Whether this structure is eventually fractal could not be resolved numerically. The coarsest functional form of this diffusion coefficient could be roughly understood by means of simple physical arguments.
3. More fine-tuned explanations were provided by different types of approximation: Firstly, we worked out the random-walk formula for diffusion, known as the Machta-Zwanzig approximation, for the flower-shaped billiard. However, as in case of the periodic Lorentz gas this formula is only asymptotically correct in the limit of small diffusion coefficients. Further corrections to this result could be obtained by means of simple heuristic improvements based on including non-Markovian forward and backward-scattering probabilities. Having a series of higher order probabilities of this type at hand, one can alternatively obtain approximations from computer simulations on a honeycomb lattice. The most suitable approximation scheme is provided by the Green-Kubo expansion already outlined in the previous chapter as applied to the flower-shaped billiard.

9 Irregular diffusion in the bouncing ball billiard

We consider a particle that is subject to a constant vertical force and scatters inelastically on a vibrating periodically corrugated floor. This model we call the *bouncing ball billiard*. Computer simulations show that the diffusion coefficient of this seemingly simple granular system exhibits maxima as a function of the driving frequency whenever there are resonances between the vibration period and the average time of flight of the particle. By evaluating a Green-Kubo formula for diffusion we verify further irregularities on fine scales pointing towards a fractal structure of this curve.

In Section 9.1 we motivate our model and briefly review results on phase locking for a ball bouncing on a flat vibrating plate. We furthermore display results for the diffusion coefficient as a function of the vibration frequency computed from simulations and explain the apparent largest irregularities with respect to phase locking. A more refined analysis in terms of a Green-Kubo expansion corroborates the existence of further irregularities on fine scales, see Section 9.2.

The research outlined in this chapter has been performed together with L. Matyas, who was working with the author as a postdoc. Here we present a yet unpublished summary of the long article Ref. [Mat03] being in press. Further work on the bouncing ball billiard is currently in preparation [Bar03a].

9.1 Phase locking and diffusion in the bouncing ball billiard

Concluding the first part of this thesis, we propose to bring the theory of fractal transport coefficients and experiments together by studying what we call the *bouncing ball billiard*. From the theoretical side, our model is motivated by the work of Harayama and Gaspard (HG) [Har01], who analyzed a Hamiltonian billiard where a particle subject to a constant vertical field jumps onto a periodically corrugated floor. Again, the diffusion coefficient of the HG billiard turned out to be fractal, here as a function of the particle energy.

Interestingly, the geometry of this model is the same as the one used in a recent experiment on granular material [Pre02], where a granular gas was driven by a vibrating surface coated with a periodic grid of small steel balls. A somewhat related, ratchet-like setup was studied theoretically and experimentally in Ref. [Far99]. Consequently, we modify the HG system by including some friction at the collisions while compensating the loss of energy by vibrating the corrugated floor periodically. The geometry of this model is depicted in the inset of Fig. 9.1. The resulting bouncing ball billiard mimicks the experimental situation in Ref.

[Pre02], however, the dissipative dynamics of this model is now inherently different from the Hamiltonian one of the HG system. This becomes obvious for the limiting case of a flat vibrating surface for which our model reduces to the famous bouncing ball problem where a particle with a restitution coefficient α bounces vertically on a vibrating floor in the gravitational field g [Pie83, Pie88, Kov88, Tuf92, Meh90, Luc93, Lic92, Guc90].

Focusing first onto the non-diffusing bouncing ball, we assign the position $y = A \sin(\omega t)$ to the floor at time t with amplitude A and vibration frequency ω . The parameters A , ω and g can be grouped together into $\Gamma = A\omega^2/g$ so that there are only two control parameters Γ and α . A fundamental property of this system is the existence of *phase locking* [Pie83, Pie88, Kov88, Tuf92, Meh90, Luc93, Lic92, Guc90], that is, if the time of flight between two collisions is k times the period of the vibration the bouncing ball exhibits a $k/1$ -resonance. The corresponding regions in the parameter space are bounded by [Meh90, Luc93]

$$\pi k \frac{1-\alpha}{1+\alpha} < \Gamma < \pi \left\{ \left[\frac{1-\alpha}{1+\alpha} k \right]^2 + \left[\frac{2(1+\alpha^2)}{\pi(1+\alpha)^2} \right]^2 \right\}^{1/2}. \quad (9.1)$$

In the following we study the impact of these resonances on diffusion in the bouncing ball billiard. The parameters of the system are chosen in order to be close to a possible experimental setup [Pre02]. The corrugated floor is constructed by circular scatterers with curvature $K = 0.04\text{mm}^{-1}$. This value was chosen for the surface to be sufficiently flat such that the bouncing ball resonances Eq. (9.1) survive the dynamical instability generated by the geometry. The intersection of any two arcs form wedges, whose centers are at a distance of $d = 2\text{mm}$ on a line. We applied periodic boundary conditions after one arclength. For the amplitude of the vibrations we chose $A = 0.1\text{mm}$. Between two inelastic collisions at the surface the motion of a particle is a free flight in the gravitational field $g \simeq 9.81\text{m/s}^2$. The inelasticity is modeled by the perpendicular and tangential restitution coefficients α and β yielding the collision rules

$$v_{\perp n}^+ - v_{ci\perp n} = \alpha (v_{ci\perp n} - v_{\perp n}^-) \quad (9.2)$$

and

$$v_{\parallel n}^+ - v_{ci\parallel n} = \beta (v_{\parallel n}^- - v_{ci\parallel n}) \quad , \quad (9.3)$$

where v_{ci} is the velocity of the vibrating floor and v_{\perp} (v_{\parallel}), $v_{ci\perp}$ ($v_{ci\parallel}$) denote the perpendicular (tangential) component of the particle's, respectively the floor's velocity with respect to the surface at the scattering point. The value of the normal restitution coefficient is fixed to $\alpha = 0.5$. According to Eq. (9.1) at this value of α at most one $k/1$ -resonance is possible for any Γ . By setting the horizontal restitution coefficient to $\beta = 0.99$ long horizontal *creeping orbits*, where a particle moves over many scatterers in form of directed sequences of very tiny hops, are eventually eliminated. However, short creeps, being considerably smaller than one arclength, are still possible. Hence, for the set of parameters chosen above the dynamics of the bouncing ball billiard should be strongly determined by the resonances, which allows to study how this phenomenon affects the diffusive properties of the model.

The diffusion coefficient was computed numerically according to the Einstein formula Eq. (7.12) restricted to one dimension, that is, with a factor of two instead of four in the denominator, cf. Eq. (2.2). The ensemble of points which was simulated consisted of 10^3 initial conditions distributed uniformly over the phase space region $0 \leq s \leq 2.0004\text{mm}$,

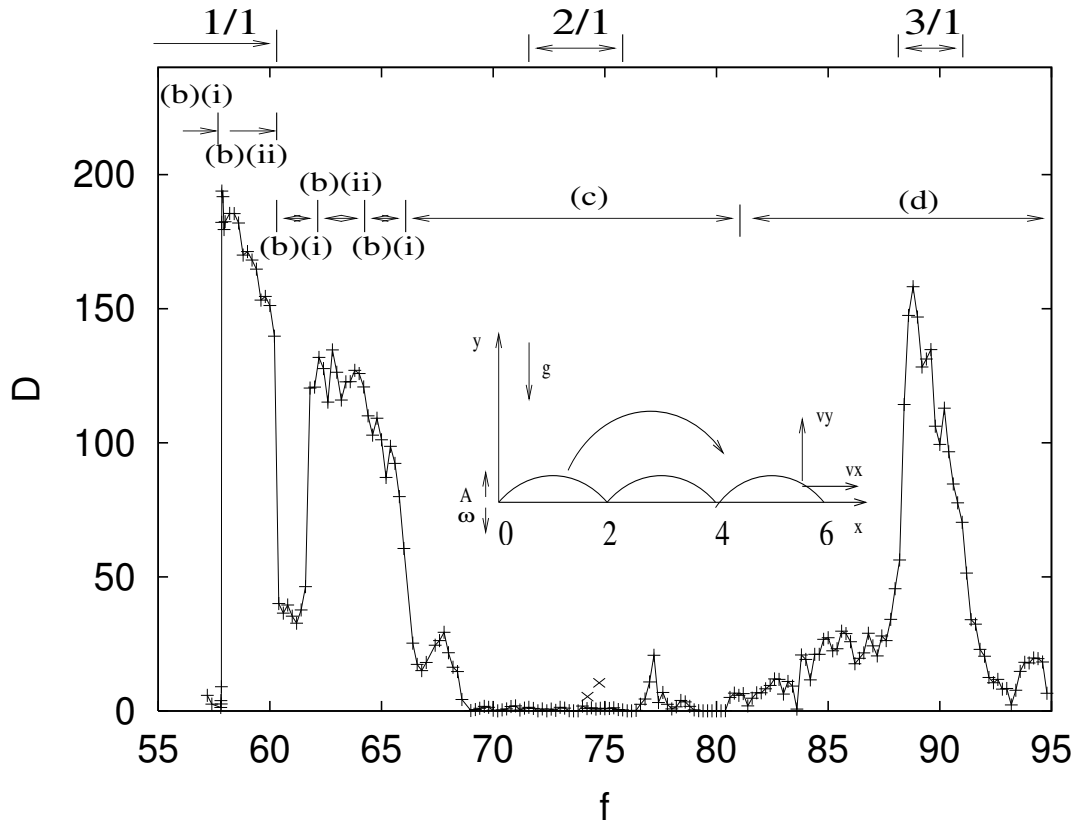


Figure 9.1: The inset shows a sketch of the bouncing ball billiard. The main figure presents computer simulation results for the diffusion coefficient as a function of the vibration frequency of the floor. It is strongly enhanced by the resonances of the bouncing ball problem Eq. (9.1), whose intervals at $\alpha = 0.5$ are shown above the frame. Further dynamical regimes are indicated by different labels, see text. The second resonance is related to specific initial conditions and is depicted by the two cross (\times) symbols at the frequencies 74.0Hz and 74.5Hz. The standard deviation errors are smaller than the magnitude of the symbols. In this and in the following figures the diffusion coefficient D is in units of mm^2/s , the frequency f is in Hz .

$|v_x^+| \leq 40\text{mm/s}$, $0 < v_y^+ \leq 40\text{mm/s}$ defined by the clockwise arclength at the impact s and the horizontal and vertical velocities v_x^+ and v_y^+ just after a collision. In spite of the fact that at resonant frequencies the dynamics may be nonergodic [Tuf92] the average kinetic and total energy converged to constant values after transient times indicating the existence of a nonequilibrium steady state.

Fig. 9.1 shows a complex scenario of different dynamical regimes under variation of the vibration frequency:

(a) If $\Gamma < 1$ the maximal acceleration of the surface is smaller than the gravitational force, i.e., $A\omega^2 < g$. Consequently, for $f < 49.77\text{Hz}$ once a particle sticks to the surface it never leaves it again. The first frequency at which for any initial condition a particle moves out of a wedge is $f = 58.0\text{Hz}$ denoting the onset of diffusion.

(b) In the interval $f \in [58.0, 65.6]\text{Hz}$ the 1/1-resonance strongly determines the dynamics and we identify two different dynamical regimes: (i) parameter regions where the system has two attractors corresponding to $f \in [57.0, 57.8]\text{Hz}$, $f \in [60.3, 61.8]\text{Hz}$ and $f \in [63.4, 65.6]\text{Hz}$.

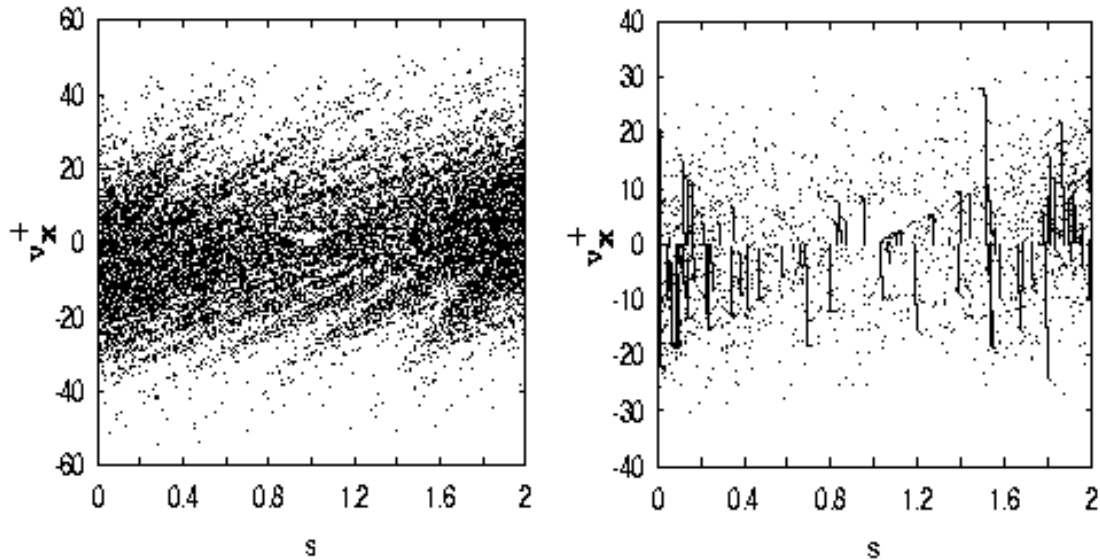


Figure 9.2: Projections of the phase space in (s, v_x^+) coordinates, where s is the position of the colliding particle on the arc and v_x^+ is the horizontal velocity after a collision. The left figure depicts the attractor at $f = 58.0\text{Hz}$, for which Fig. 9.1 indicates a 1/1-resonance. The right half shows that in case of nonresonant motion at $f = 85.2\text{Hz}$ the particle may partly exhibit “creepy motion”. The position s is in units of mm , the velocity v_x^+ in mm/s .

In these regions some initial conditions lead to the 1/1-resonance, whereas other ones generate a time-to-time creeping motion on the surface. (ii) The other dynamical regime exhibits only one attractor with all initial conditions leading to the same resonant behavior, which occurs for $f \in [57.9, 60.2]\text{Hz}$ and $f \in [61.9, 63.3]\text{Hz}$. This resonant motion becomes regular only in the vertical direction where it is very similar to the 1/1-phase locking of the bouncing ball, while in the horizontal direction the system shows a highly irregular normal diffusive dynamics. In this regime the interaction with the surface consists only of regular collisions without any creeps, see the attractor of Fig. 9.2.

(c) For $f \in [67.2, 81.0]\text{Hz}$ the escape from the wedges takes long times due to long creeps. In the vicinity of 74.0Hz the 2/1-resonance shows up, however, it is only exhibited by a few initial conditions with $v_y^+ > 100\text{m/s}$. Hence, it is considerably weaker than the previous one.

(d) The last dynamical regime we study here is in the interval $f \in [81.1, 95.0]\text{Hz}$ demonstrating a significant increase of the diffusion coefficient over a larger frequency interval. The corresponding attractor reveals a from time-to-time “creepy motion”, see the almost vertical lines in Fig. 9.2 indicating collisions with the surface at almost any time step and with decreasing velocity.

9.2 + Correlated random walk approximations of the diffusion coefficient

We now quantitatively analyze the irregular structure of the diffusion coefficient by applying the theoretical approach developed in the previous two chapters. That is, we derive some simple analytical and numerical approximations starting with a prediction from random

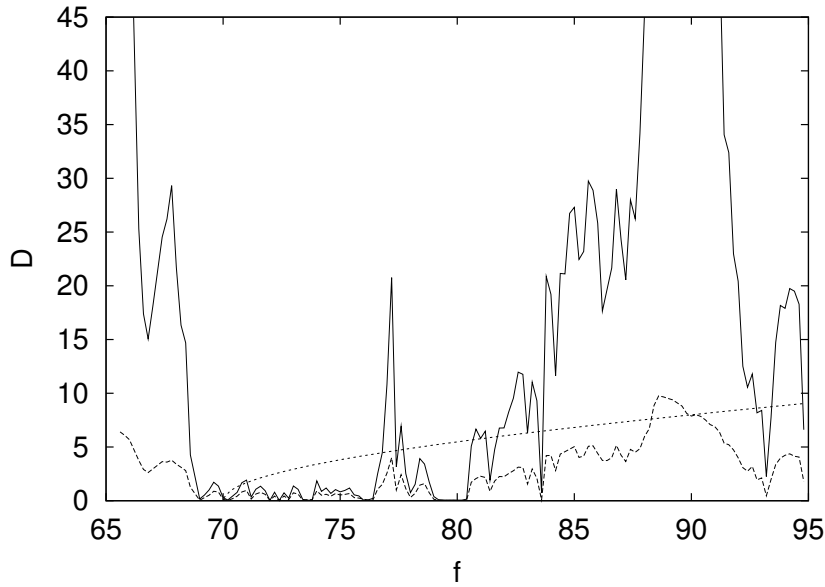


Figure 9.3: Evaluations of the random walk formula Eq. (9.4) for the diffusion coefficient with frequencies $f > 65.6\text{Hz}$. The solid line corresponds to the diffusion coefficient of Fig. 9.1. The dotted monotonously increasing curve represents the analytical formula Eq. (9.6), the dashed irregular curve close to zero depicts Eq. (9.4) with the escape time computed numerically.

walk theory.

For frequencies where diffusion is small the wedges of the billiard are like traps for the bouncing particle. In this case the diffusion coefficient is determined by the average escape time τ needed to leave a trap leading to the Machta-Zwanzig random walk formula [Mac83]

$$D_{\text{rw}}(f) = \frac{d^2}{2\tau(f)}, \quad (9.4)$$

cp. to Eqs. (7.13), (8.11) and supplements, where d is the distance between two traps. An analytical estimate of the average escape time is obtained by employing the average kinetic energy E_x ,

$$\tau \simeq \frac{d}{\langle v_x \rangle} \simeq \frac{d}{\sqrt{2E_x}}, \quad (9.5)$$

where $\langle v_x \rangle$ is the average velocity in the horizontal direction. E_x can be calculated from the energy balance $E_x = E - E_y - mg\bar{y}$ in which E_y stands for the average kinetic energy related to v_y and $mg\bar{y}$ denotes the average potential energy of the particle. The total average energy E is approximated with respect to the harmonically oscillating surface to $E \simeq A^2\omega^2/2$, where the average height is set equal to the amplitude of the vibrations.¹ Computer simulations indicate that only a small percentage of the energy pumped vertically into the system is transferred into the horizontal direction, $E_y \simeq 19E_x$. With this input the energy balance yields $2E_x \simeq A^2\omega^2/20 - mgA/10$ and combining Eq. (9.5) with Eq. (9.4)

¹A simplified model with sawtooth vibrations supports the fact that the total average energy scales with ω^2 , cf. Ref. [War95]. That its prefactor is most conveniently chosen to be identical to the one of a particle oscillating harmonically in a quadratic potential appears to be, as far as we can tell, a mere coincidence.

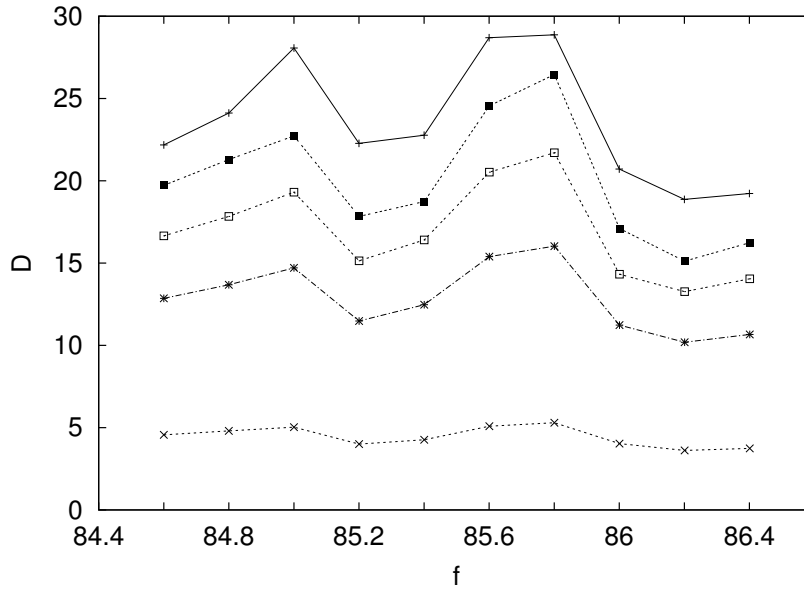


Figure 9.4: Blowup of the frequency interval $f \in [84.6, 86.4]$ Hz in Fig. 9.1. The solid line on top shows the respective diffusion coefficient, the lowest dotted line depicts the random walk approximation Eq. (9.4) with the escape time computed numerically. The other lines show the approximations $D_n(f)$ obtained from the one-dimensional version of the Green-Kubo formula Eq. (7.16) for $n = 0, 2, 4$ and 7 (from bottom to top).

leads to the diffusion coefficient

$$D_c(f) \simeq \frac{d}{2} \sqrt{2E_x} \simeq \frac{d}{2} \sqrt{\frac{A^2 \omega^2}{20} - \frac{mgA}{10}}. \quad (9.6)$$

Fig. 9.3 shows that this result is close to the one for which τ in Eq. (9.4) was obtained from computer simulations. Note that Eq. (9.6) indicates the onset of a monotonously increasing diffusion coefficient, as one would expect from stochastic theory if the resonances were not present. The numerical approximation of Eq. (9.4) roughly follows this coarse functional form while qualitatively being more similar to the numerically exact values. However, quantitatively it is much too small indicating the existence of long-range dynamical correlations that go beyond a simple random walk picture.

Such higher order memory effects can systematically be taken into account by using the Green-Kubo formula for diffusion in billiards discussed in Chapters 7 and 8 [Kla02d]. As in case of the Einstein formula, the one-dimensional formula is obtained from the two-dimensional result simply by multiplying Eq. (7.15) with a factor of two. Correspondingly, for the bouncing ball billiard $j(x_k)$ denotes jumps at the k th time step τ on a one-dimensional lattice with sites at a distance d . Approximations D_n of order n , where these diffusion coefficients are functions of the frequency f , are now defined by the respective one-dimensional version of Eq. (7.16). For this hierarchy of approximations $D_n(f)$ one can numerically compute the conditional probabilities $p(\alpha\beta\gamma\dots)$ contained in Eq. (7.16). As in Chapters 7 and 8, the random walk solution Eq. (9.4) is represented by the first term, and the higher order corrections yield information about the impact of dynamical correlations on the diffusion coefficient.

Fig. 9.4 shows that the convergence of this sum is not monotonous in the frequency thus

confirming the existence of irregularities on fine scales and clearly identifying their origin in terms of long-time dynamical correlations. This behavior is well-known from related systems exhibiting deterministic diffusion [Kla95, Kla99a, Kla96, Gro02, Gas98c, Kor02, Kla00a, Har02, Kla02d, Har01, Kla02a, Kla03a] and points to a possible fractal structure of the diffusion coefficient in the bouncing ball billiard.

9.3 *Summary

1. In order to bring the phenomenon of fractal transport coefficients to physical reality, we have proposed a simple model for diffusion of a granular particle on a vibrating surface subject to an external gravitational field. In analogy to the dynamical systems studied previously, this surface was equipped with a periodic grid of circular scatterers with which the moving particle collided inelastically. Computing the frequency-dependent diffusion coefficient for this model we obtained again a highly irregular curve. We showed that the largest maxima of this function are due to phase locking as known for a ball bouncing inelastically on a flat vibrating plate. We furthermore numerically analyzed the phase space of the dynamical system exhibiting different specific types of dynamics which change under parameter variation in a complicated fashion.
2. We finally applied the correlated random walk approximation for billiards, as discussed in the previous two chapters, to the frequency-dependent diffusion coefficient. We first heuristically derived a simple random walk approximation for our model that qualitatively matched well to our results from computer simulations. By successively working out the first terms of the associated Green-Kubo series expansion, we argued that, again, irregularities on fine scales detected in simulations are largely due to long-time dynamical correlations. With this model we hope to stimulate experimental work on related, existing physical systems trying to corroborate an irregular structure in respective diffusion coefficients.

Part II

Chaos and transport in thermostated dynamical systems

The second part of this thesis focuses on the non-Hamiltonian approach to nonequilibrium steady states outlined in the introductory Section 1.2. As mentioned in Section 1.3, it features a review that has specifically been written for this thesis. The main objective is to summarize recent developments in the construction of deterministic, time-reversible thermal reservoirs, and to analyze the chaos and transport properties of the nonequilibrium steady states resulting from their application in nonequilibrium situations. The findings we present were believed to form a backbone for a general theory of nonequilibrium transport in dissipative dynamical systems starting from microscopic chaos. Chapters 10 to 13 mostly review the respectively existing literature while Chapters 14 to 16 elaborate more specifically on the author's and collaborators' contributions to this subject.

Reflecting the pronounced review character of this part, our presentation attempts to be more pedagogical than the one of Part I: In Chapter 10 we motivate thermostats in a very intuitive way that is particularly directed to non-experts. This motivation is supplemented by a more detailed analysis of the Langevin equation [Lan08, Rei65, Wax54, vK92, Pat88, Gal99] from the point of view of modeling thermal reservoirs [Zwa01]. We then sketch briefly how to compute velocity distribution functions for a subsystem interacting with a thermal reservoir that consists of arbitrarily many degrees of freedom [Kla00b, Rat00b]. This basic problem of equilibrium statistical mechanics illustrates the importance of suitably projecting out reservoir degrees of freedom. The results will be used in Chapter 15 for systematically constructing thermal reservoirs modeling an arbitrary number of degrees of freedom, as well as in Chapter 16.

In the final section of Chapter 10 we define in much detail the periodic Lorentz gas [Lor05], a standard model for chaotic transport [Gas98a, Dor99, Sza00]. In contrast to Part I, for Part II this simple model will be driven by an external electric field [Gal77] and thermalized [Mor98, Dor99, Hoo99, Det00a] by applying some generic types of thermostats that we introduce step by step. The corresponding nonequilibrium steady states will be numerically constructed and analyzed concerning their statistical and chaotic dynamical properties. Applying a variety of different thermal reservoirs to the same model enables us to inquire about possible universal chaos and transport properties of nonequilibrium steady states generated by different thermostats. The question to which extent such universal properties exist forms the main theme of our review.

This discussion is put forward in Chapter 11 by introducing the *Gaussian thermostat*, which is the most simple and prominent example for modeling a deterministic and time-reversible thermal reservoir [Eva90b, Mor98, Dor99, Hoo99, Rue99b, Det00a]. Note that this scheme constrains the energy directly in the interior of a subsystem and not at some boundaries, hence it is called a *bulk thermostat*. We summarize what we consider to be the crucial properties of this class of thermostats as far as connections between transport properties and dynamical systems quantities are concerned.

Chapter 12 features a discussion of the *Nosé-Hoover thermostat* [Eva90b, Hoo91, Hes96a, Mor98, Hoo99, Det00a, Mun00, Ron02a], from which the Gaussian one is obtained as a special case, and some generalizations of it. We motivate the Nosé-Hoover thermostat starting from the (generalized) *Liouville equation* for dissipative dynamical systems [Lio38, Ger73, Ste79, Ste80, And86, Eva90b, Dor99, Ram02, Ser03] which we briefly derive. The Nosé-Hoover scheme is conceptually analogous to the Gaussian one thus yielding analogous formulas relating chaos to transport. However, despite this formal analogy the fractal structure of the attractor of the Nosé-Hoover thermostated Lorentz gas changes differently under parameter variation in comparison to the Gaussian thermostated model. This

is reflected in different bifurcation diagrams, and correspondingly we obtain different field dependencies of the electrical conductivity for both models.

In Chapter 13 we present a critical assessment of chaos and transport properties of nonequilibrium steady states generated by these two well-known and widely used thermostating schemes as presented up to this point. A key feature is that the models of thermal reservoirs discussed so far exhibit a built-in identity between phase space contraction and thermodynamic entropy production. We take this opportunity to elaborate on the striking formal analogy between three formulas relating transport coefficients to dynamical systems quantities [Gas98a, Gil01, Rue96, Bre96, Det00a]. Two of them are resulting from the Hamiltonian approach to transport for closed and open systems, one is emerging from the thermostated systems approach.

This enables us to pose more clearly the central question of this review, namely, whether there are universal statistical and chaotic dynamical properties of nonequilibrium steady states which are independent from the specific type of thermostat used. Partly this issue has been discussed in the literature under the label of *equivalence of nonequilibrium ensembles* related to different thermostats [Eva85b, Eva90b, Lie92, San92, Eva93b, Che95b, Gal96a, Che97, Gal97, Coh98, Sar98, Rue99b, vZ99, Det00a, Eva02a, Bon02, Hoo03, Gal03]. Additionally, there is a line of work arguing for an equivalence of ensembles between thermostated and non-thermostated time-discrete maps as far as nonequilibrium entropy production is concerned [Bre96, Tel96, Mor96b, Vol97, Bre98, Vol98, Gil99a, Gil99b, Tel00, Vol00, Vol02, Vol03].

Our critical discussion of standard thermostating schemes motivates to look for alternative models of thermal reservoirs, which will be introduced in the remaining chapters. The main idea is to construct thermal reservoirs that do not by default exhibit an identity between phase space contraction and entropy production. In order to be comparable to Gaussian and Nosé-Hoover schemes these alternative models must as well be deterministic and time-reversible, and one has to show that they generate well-defined nonequilibrium steady states. Sharing these properties they would provide counterexamples to the claimed universality of the identity as concluded from the analysis of standard Gaussian and Nosé-Hoover thermostats. Consequently, in this case also the relations between transport coefficients and dynamical systems quantities as derived for Gaussian and Nosé-Hoover thermostats would become different.

A first class of such counterexamples is presented in Chapter 14 by what we call *non-ideal Gaussian and Nosé-Hoover thermostats* [Rat00a]. It follows a detailed discussion of their chaos and transport properties, again for the example of the driven periodic Lorentz gas. Chapter 15 starts by reviewing a well-known thermostat acting only at the boundaries of a subsystem instead of in the bulk, which is known under the name of *stochastic boundary conditions* [Leb78, Cic80, Ten82, Gol85, Che95b, Che97, Hoo98c, Pos98]. In order to compare this thermal reservoir to Gaussian and Nosé-Hoover thermostats we make stochastic boundaries deterministic and time-reversible leading to *thermostating by deterministic scattering*, a scheme that contains stochastic boundaries as a special case [Kla00b, Rat00b, Wag99, Rat02, Wag00]. As before, we first apply this deterministic thermal reservoir to the driven periodic Lorentz gas. However, in the final section of this chapter we also review results for shear and heat flow in a many-particle hard-disk fluid thermostated by deterministic scattering [Wag99, Wag00].

We will show that thermostating by deterministic scattering defines a second class of systems exhibiting nonequilibrium steady states in which phase space contraction is not nec-

essarily equal to thermodynamic entropy production. Consequently, as in case of non-ideal Gaussian and Nosé-Hoover thermostats, there are no unique relations between transport coefficients and dynamical systems quantities anymore. Furthermore, related to the fact that this scheme defines boundary thermostats the spectra of Lyapunov exponents of dynamical systems thermostated that way yield properties that are rather different from the ones obtained for systems thermostated in the bulk by using Gaussian or Nosé-Hoover thermostats. Further systems with nonequilibrium steady states in which phase space contraction is not equal to entropy production have been explored in Refs. [Gas97b, Coh98, Eck99a, Dae99, Gas98a, Ben01, Ron02a].

We finish our discussion in Chapter 16 by pointing towards a surprising connection between Nosé-Hoover thermostats and *active Brownian particles* as introduced by Schweitzer and Ebeling et al. [Sch98, Ebe99, Til99, Erd00]. The latter models are thought to mimic, among others, the crawling of isolated biological cells on rough surfaces which can be measured experimentally [Fra90, Sto91, Sch93, Har94, Die03]. Active Brownian dynamics is modeled by Langevin equations with velocity-dependent friction coefficients that enable a Brownian particle to convert internal into kinetic energy and *vice versa*. By using heuristic arguments we show that limiting cases of such models reduce to conventional Nosé-Hoover dynamics. Establishing this link to deterministic thermostats sheds some light onto the origin of so-called crater-like velocity distribution functions as they were previously observed in computer simulations for active Brownian particles. We argue that they may emerge as superpositions of canonical and microcanonical velocity distributions, a phenomenon that is nicely exemplified by the Nosé-Hoover thermostat under parameter variations.

The main conclusion of our review, summarized in Chapter 17, is that *from a dynamical systems point of view* conventional Gaussian and Nosé-Hoover thermostats provide only a very specific access road to the modeling of nonequilibrium steady states. A fundamental problem of these thermal reservoirs is that they furnish a default identity between the rates of average phase space contraction and thermodynamic entropy production, which is at the heart of linking nonequilibrium thermodynamics to dynamical systems theory in case of non-Hamiltonian equations of motion. Our analysis shows that alternative, different types of thermostats lead to different such relations. Correspondingly, the associated fractal attractors, the Lyapunov spectra and even the field-dependent electrical conductivities may exhibit very different properties. The last result concerning transport coefficients, on the other hand, is contrasted by our example of an interacting many-particle system under shear and heat flow thermostated at the boundaries. Here all transport properties are very well in agreement with predictions from irreversible thermodynamics and linear response theory. Still, almost all of the chaotic dynamical properties of this system are profoundly different compared to systems that were thermostated by Gaussian or Nosé-Hoover schemes.

Consequently, one may suspect that the variety of different transport properties obtained for the driven periodic Lorentz gas when thermalized with different thermostats rather reflects the simplicity and the low dimensionality of the model. In other words, for simple systems consisting of non-interacting particles modifications of the equations of motion, e.g., by applying different thermostats, may indeed profoundly change their macroscopic transport properties. This aspect is particularly significant when the dynamical systems are *topologically unstable* leading, for example, to the fractal transport coefficients discussed in Part I, which are at variance with common expectations from nonequilibrium thermodynamics. In contrast, for interacting many-particle systems at least the *thermodynamic* properties appear to be rather independent from the type of thermostat used pointing towards

an equivalence of ensembles as discussed by other authors. However, we emphasize that we do *not* find such an equivalence as far as the detailed *chaotic dynamical* properties of many-particle systems are concerned.

We thus conclude that the quest for universal characteristics of nonequilibrium steady states in dissipative chaotic dynamical systems is not yet over. At the moment the only candidate for a universal property of *deterministically thermostated systems*, as far as chaos properties are concerned, appears to be the *fractal structure of attractors*, whereas any further chaos and, depending on the simplicity of the model, even transport property might reflect the choice of the thermostat. This poses a challenge to find more general relations between chaos and transport properties in thermostated dynamical system than discussed up to now. For such an endeavor one may want to start from some suitably coarse-grained nonequilibrium entropy that does not measure details of phase space contraction which appear to be spurious if compared to, say, the Clausius entropy for which nothing else counts than the heat flux into the thermal reservoir. Despite the obvious importance of entropy production we avoid detailed discussions concerning the origin of the second law of thermodynamics. We believe this goes considerably beyond the level of this review, apart from the fact that there already exists a lot of profound literature on this subject, see, e.g., Refs. [Ger99, Bri95, Lie99b] and much further work mentioned in the course of Part II.

We finally remark that particularly Section 10.3, Chapter 14 and Chapter 15 draw on the series of articles Refs. [Kla00b, Rat00b, Wag99, Rat00a, Rat02] published by the author together with G.Nicolis, K.Rateitschak, C.Wagner and W.G.Hoover. Refs. [Kla00b, Rat00b, Rat00a, Rat02] formed the core of K.Rateitschak's Ph.D. thesis pursued under the author's scientific guidance at the Free University of Brussels [Rat01]. Section 14.1 and Section 16.2 contain results that have not yet been published.

10 Motivation: coupling a system to a thermal reservoir

In this chapter we introduce some basic concepts, models and notations as they will be used throughout Part II. We first outline, in a very heuristic way and from a very physical point of view, what thermal reservoirs or so-called “thermostats” are and explain why they are indispensable for studying steady states under typical nonequilibrium conditions.

We then briefly remind the reader of the well-known Langevin equation that may also be thought of modeling the interaction of a subsystem (in this case a single Brownian particle) with a thermal reservoir (the surrounding fluid). In particular, we outline a short derivation of the Langevin equation from Hamiltonian equations of motion in which the thermal reservoir is modeled as a collection of non-interacting harmonic oscillators. This way we exemplify two extreme cases of modeling thermal reservoirs, namely either by purely Hamiltonian dynamics or, alternatively, in terms of some simple but dissipative, irreversible and stochastic equations of motion.

After this discussion of the detailed microscopic dynamics we elaborate on the general functional forms of the velocity distribution functions of subsystem plus thermal reservoir in thermal equilibrium. By means of very simple statistical physical arguments we sketch how to calculate velocity distributions for a subsystem of d_s degrees of freedom which interacts with a d_r -dimensional thermal reservoir in an ideal equilibrium situation. In case of $d_r \rightarrow \infty$ these velocity distributions converge to their canonical counterparts. This simple problem illustrates the importance of projecting out reservoir degrees of freedom. The obtained information will be used later on in order to construct thermal reservoirs, and for finding necessary conditions concerning the existence of bimodal velocity distributions.

To the end of this chapter we define the periodic Lorentz gas, a standard model in the field of chaos and transport, as already partly discussed in Part I, and give some indication of its physical interpretations. In the remaining chapters we will apply different types of thermal reservoirs to the periodic Lorentz gas under nonequilibrium situations. The resulting nonequilibrium steady states we will compare with each other concerning their statistical and chaotic dynamical properties.

10.1 *Why thermostats?

A common problem of thermostating is how to cool down a bottle of beer on a hot summer day [Rei65]. One option is to simply put the bottle of beer in a swimming pool. Microscopically, there emerges a transfer of energy between the molecules in the bottle of beer composing a fluid at temperature T_B and the water molecules in the swimming pool at temperature $T_P < T_B$. Here we define temperature operationally on the basis of equipartitioning

of energy onto all available degrees of freedom [Rei65, Hua87] connecting temperature with the average kinetic energy of a system. Under the assumption that the water molecules are properly interacting with each other, in the sense that such an equipartitioning can properly be established, on average the excess energy related to the temperature difference $T_B - T_P$ will flow across the surface of the beer bottle into the surrounding fluid. Under the very same assumption, it will furthermore equally distribute onto all the water molecules. However, since the number of water molecules is extremely large the increase of the average temperature of the pool, in terms of the average kinetic energy per particle, will be negligibly small.

What we have sketched here is just the well-known process of classical thermal equilibration between a sufficiently small subsystem and a surrounding thermal reservoir, where both systems are initially at two different temperatures. After equilibration both systems will be approximately at the same temperature, $T_B \simeq T_P$. However, so far we have only discussed the simple case of relaxation to thermal equilibrium when subsystem and reservoir together form a closed system.

As a second, slightly more complicated example, think of a nonequilibrium situation in an open system such as a light bulb connected to a battery. The applied voltage will generate a current, and as an Ohmic resistance the thread in the bulb will exhibit some Joule heating. In a naive microscopic picture this heating may be understood as follows: The applied electric field will on average accelerate the electrons in the resistance. Consequently, if there were no mechanism for reducing their average kinetic energy the gas of electrons simply heats up, and no stationary current exists. On the other hand, the single electrons will collide with the atoms constituting the resistance. During these collisions they will exchange energy with the atoms, possibly in terms of exciting lattice modes and eventually causing the whole resistance to heat up. However, across its surface the resistance allows an average flow of energy into the surrounding medium by collisions between the atoms of the thread and the atoms or molecules of the gas. In case of the light bulb this flow of energy just causes the gas around the thread to glow.

The dissipation of energy into a thermal reservoir thus properly counterbalances the pumping of energy into the system by the external electric field and enables the system to evolve into a *nonequilibrium steady state (NSS)*. With that we mean that the statistical physical parameters describing the system on macroscopic scales are constant in time, despite the fact that the system is no longer in thermal equilibrium [dG62]. In case of our example, the existence of a NSS implies that under the nonequilibrium condition of applying an external electric field the electron gas eventually exhibits a stationary current and that the temperature is constant. We note in passing that the proper definition of a nonequilibrium temperature is a subtle problem in itself [Rug97, Mor99], but operationally, again, the principle of equipartitioning of energy might be used [Pos88, Eva90b, Mor98, Hoo99]. If the existence of a NSS is due to the action of a thermal reservoir we say the system is properly *thermostated*.

In other words, thermostats are mechanisms by which the internal energy of a many-particle system, and thus its temperature, can be tuned onto a specific value. Any thermostat may be thought of being associated with some thermal reservoir consisting of an infinite number of degrees of freedom thus being large enough to absorb any amount of energy pumped into the system. Thermostats can be applied in order to achieve equilibration to a global thermal equilibrium or for sustaining a NSS in a nonequilibrium situation where there is a flux of energy through the system, such as induced by external fields or by imposing temperature or

velocity gradients. In a similar vein, other constraints instead of fixing the temperature may be imposed onto a system leading, e.g., to constant pressure or constant stress ensembles [All87, Eva90b, Nos91, Hes96a, Tuc00].

The first question we must focus on before we elaborate on NSS is therefore: How can we suitably amend Newton's equations of motion in order to model an energy dissipation into a thermal reservoir? The basic problems involved here will be exemplified by means of the well-known Langevin equation. At this level of discussion restrict ourselves to equilibrium situations where the construction of thermal reservoirs may appear to be a rather technical problem. However, our main objective is to eventually apply thermal reservoirs as defined in equilibrium to nonequilibrium situations yielding NSS. In later chapters we will inquire to which extent the detailed properties of NSS depend on the detailed modeling of different thermal reservoirs, and to which extent they might be universal.

10.2 *Stochastic modeling of thermal reservoirs: the Langevin equation

The Langevin equation [Lan08] provides a simple theoretical framework for describing what is known as *Brownian motion*: A sufficiently small particle immersed in a fluid performs irregular motion resulting from the collisions between the atoms or molecules of the medium and the particle [Rei65, Wax54, vK92, Pat88, Gal99]. For coal dust particles on the surface of alcohol this phenomenon was observed by the Dutch physician J. Ingenhousz in 1785. However, it became known more widely only later on by the work of the Scottish botanist R. Brown in 1827, who reported similar irregular movements of pollen grains under a microscope. The name Brownian motion was coined by A. Einstein in his famous work from 1905 describing this irregular motion in terms of diffusion processes. A related approach was already proposed by the French mathematician L. Bachelier in 1900 in order to understand the dynamics of stock values. Einstein's work led J.B. Perrin to the experimental measurement of the Avogadro number in 1908 and also motivated P. Langevin's modeling of Brownian motion published in the same year.¹ We first briefly summarize some fundamental features of Langevin's stochastic approach to Brownian motion. In the following chapters we will repeatedly come back to these characteristic properties by discussing to which extent they are reproduced in deterministic chaotic models of Brownian motion.

According to Langevin a Brownian particle is randomly driven by instantaneous collisions with the surrounding particles. On the other hand, energy is removed from the system by some bulk friction. In one dimension this dynamics is modeled by amending Newton's equations of motion to

$$\begin{aligned} \dot{r} &= v \\ \dot{v} &= -\alpha v + \mathcal{F}(t) \quad , \end{aligned} \tag{10.1}$$

where r and v denote the position and the velocity of the Brownian particle. For convenience, here and in the following we set constants like the mass m of the particle and the Boltzmann constant k equal to one. \mathcal{F} holds for white noise, that is, a δ -correlated stochastic force with zero mean modeling the random collisions with the fluid particles, whereas α is a Stokes

¹For this short historical note on Brownian motion we largely followed the nice presentation in Ref. [Met00]; for more details see, e.g., Refs. [Bru76, Sta89].

friction coefficient. In a steady state the molecular stochastic forces and the friction balance each other leading to the fluctuation-dissipation theorem [Rei65, Wax54, Pat88, Zwa01]

$$\alpha = \frac{1}{2T} \int_{-\infty}^{\infty} dt \langle \mathcal{F}(0)\mathcal{F}(t) \rangle \quad , \quad (10.2)$$

where $\langle \dots \rangle$ denotes an ensemble average over the noise acting on the moving particles. The expression $C_{\mathcal{F}}(t) := \langle \mathcal{F}(0)\mathcal{F}(t) \rangle$ is an example of a correlation function. α is in turn related to the diffusion coefficient D of the Brownian particle according to the Einstein relation

$$D = T/\alpha \quad , \quad (10.3)$$

where T is the temperature obtained from equipartitioning of energy, $T = \langle v^2 \rangle$. D is defined independently via the mean square displacement,

$$D := \lim_{t \rightarrow \infty} \frac{\langle [x(t) - x(0)]^2 \rangle}{2t} \quad . \quad (10.4)$$

Here the angular brackets denote an equilibrium ensemble average over moving particles. Alternatively, D can be obtained from the Green-Kubo formula for diffusion

$$D = \int_0^{\infty} dt \langle v(0)v(t) \rangle \quad , \quad (10.5)$$

which is an exact transformation of Eq. (10.4) [Zwa01].

The Green-Kubo formula Eq. (10.5) and the fluctuation-dissipation theorem Eq. (10.2) are formally analogous in relating a macroscopic quantity characterizing the fluid to an integral over some correlation function. $C_v(t) := \langle v(0)v(t) \rangle$ is called the velocity autocorrelation function of the moving particle. As can easily be shown by solving the Langevin equation Eq. (10.1) for C_v , the velocity autocorrelation function decays exponentially in time thus ensuring that, in terms of the Green-Kubo formula Eq. (10.5), the diffusion coefficient exists. If one considers the Brownian particle as a subsystem and the surrounding particles as an infinite dimensional thermal reservoir, the Langevin equation precisely models the situation where a subsystem suitably interacts with a thermal reservoir. However, so far we have motivated this equation purely heuristically. It is therefore interesting to discuss a simple derivation of the above Langevin equation that actually starts from a fully Hamiltonian modeling of subsystem plus thermal reservoir in which the heat bath consists of an infinite number of harmonic oscillators [Zwa73, For87, Kub92, Stu99, Zwa01].² It nicely demonstrates what kind of simplifying assumptions one has to make, starting from first principles, in order to arrive at the simple modeling of thermal reservoirs in terms of Eq. (10.1).

Let the Hamiltonian of the Brownian particle be

$$H_s = \frac{v^2}{2} \quad (10.6)$$

and let the heat bath of harmonic oscillators be

$$H_B = \sum_j \left(\frac{v_j^2}{2} + \frac{\omega_j^2}{2} \left(x_j - \frac{\gamma_j}{\omega_j^2} v_j \right)^2 \right) \quad , \quad (10.7)$$

²In Ref. [Stu99] this model was attributed to Ford and Kac [For87], however, it already appears at least in the paper by Zwanzig [Zwa73]; see also further references in Ref. [For87].

where the oscillators exhibit a special coupling to the subsystem. Here ω_j is the frequency of the j th oscillator and γ_j the strength of the coupling between the Brownian particle and the j th oscillator. The Hamiltonian equations of motion for the combination of subsystem plus thermal reservoir then read

$$\begin{aligned}\dot{x} &= v \\ \dot{v} &= \sum_j \gamma_j \left(x_j - \frac{\gamma_j}{\omega_j^2} x \right)\end{aligned}\quad (10.8)$$

$$\begin{aligned}\dot{x}_j &= v_j \\ \dot{v}_j &= -\omega_j^2 x_j + \gamma_j x \quad .\end{aligned}\quad (10.9)$$

The formal solution of the inhomogeneous differential equation of second order Eq. (10.9) reads

$$x_j(t) = x_j(0) \cos(\omega_j t) + v_j(0) \frac{\sin(\omega_j t)}{\omega_j} + \gamma_j \int_0^t ds x(s) \frac{\sin(\omega_j(t-s))}{\omega_j} \quad . \quad (10.10)$$

Performing integration by parts for the latter integral and thereafter putting Eq. (10.10) into Eq. (10.8) yields the formal Langevin equation

$$\dot{v}(t) = - \int_0^t ds K(s) v(t-s) + F(t) \quad . \quad (10.11)$$

By comparing this equation to the former stochastic Langevin equation Eq. (10.1) the first term on the right hand side is identified as some nonlinear, non-Markovian friction containing the memory function

$$K(t) = \sum_j \frac{\gamma_j^2}{\omega_j^2} \cos(\omega_j t) \quad . \quad (10.12)$$

The second term on the right hand side of Eq. (10.11) must consequently yield the “noise”, which is given explicitly by

$$F(t) = \sum_j \gamma_j v_j(0) \frac{\sin(\omega_j t)}{\omega_j} + \sum_j \gamma_j \left(x_j(0) - \frac{\gamma_j}{\omega_j^2} x(0) \right) \cos(\omega_j t) \quad . \quad (10.13)$$

Note that $F(t)$ is fully deterministic in depending on the initial conditions of all heat bath variables.

In order to recover Eq. (10.1) both expressions are now simplified as follows: If the spectrum of frequencies ω_j is thought to be continuous, the memory function Eq. (10.12) may be written as a Fourier integral. By assuming convenient functional forms for the density of states of ω_j and for the coupling coefficients γ_j the memory function can be replaced by a delta function, $K(t) \sim \delta(t)$. In this special case the Langevin equation Eq. (10.11) is Markovian and the ordinary Stokes friction of Eq. (10.1) is recovered.

As far as the “noise” is concerned, according to Eq. (10.13) $F(t)$ is a linear function of the initial positions and velocities of all bath oscillators that are furthermore independent degrees of freedom. Hence, there are no correlations between these variables. If all initial conditions are *sampled randomly* from a canonical distribution one can show that the fluctuation-dissipation theorem takes the form [Zwa01]

$$\langle F(t)F(t') \rangle = TK(t-t') \quad . \quad (10.14)$$

Under the above assumption that the memory function is Markovian this equation boils down to Eq. (10.2), or in other words, the fluctuations induced by $F(t)$ turn out to be white noise. We see that, in this case, the noise is put in “by hand” into Eq. (10.11) by assuming a suitable distribution of initial conditions for the heat bath variables.

In summary, we have discussed the connection between two extreme versions of modeling the interaction of a subsystem consisting of a single particle with a thermal reservoir: One employs the fully Hamiltonian, i.e., deterministic, time-reversible and phase space preserving equations of motion Eqs. (10.6) and (10.7). To start this way may be considered convenient from a microscopic point of view. However, note that the statistical properties of the harmonic oscillator heat bath are pre-determined by the choice of initial conditions supplemented by the specific form of the memory kernel in Eq. (10.14). The latter yields the decay of the force correlations, hence the problem of introducing randomness is shifted towards choosing a proper initial distribution for the oscillator variables. A realistic heat bath, on the other hand, should generate a (canonical) equilibrium distribution of position and velocity variables in a self-contained way, that is, due to the action of the dynamical system defining the bath and irrespective of any specific initial conditions. That this is not the case for the harmonic oscillator heat bath one may consider as quite a deficiency of the model. Another more practical disadvantage becomes clear in nonequilibrium situations, where the sum over harmonic oscillators in Eq. (10.7) must be infinite in order to allow for the existence of a NSS. Though taking this limit does not pose any crucial difficulty for analytical investigations, the Hamiltonian scheme thus becomes very inconvenient for computer simulations.

The alternative type of modeling consists of the very intuitive linear and Markovian Langevin equation Eq. (10.1). However, according to its derivation from the harmonic oscillator heat bath strictly speaking these nice properties emerge only because of profound approximations. Even more, the dynamics eventually turns out to be non-Hamiltonian, that is, stochastic, irreversible and, as a consequence of Stoke’s friction, on average phase space contracting; see also Ref. [Hoo99] for related arguments.

Hence, both types of heat bath models do not really capture the whole essence of the problem. Correspondingly, there is plenty of room for generalizations of modeling thermal reservoirs, in two directions: On the one hand, starting from some Hamiltonian equations of motion or respective toy models of dynamical systems one may wish to put the derivation of equations modeling the action of a heat bath onto a small subsystem onto more general, rigorous grounds. This approach was pursued, e.g., in a line of work by Beck et al. [Bec87, Bec95, Bec96]. Here the analysis starts from a time-discrete version of the Langevin equation Eq. (10.1) in which randomness is generated by a deterministic chaotic map thus trying to understand to which extent deterministic chaos modeling reservoir degrees of freedom can mimic stochastic noise. In a similar vein, Just and Kantz et al. considered chaotic dynamical systems with time scale separation where the fast degrees of freedom may be related to the action of a thermal reservoir [Jus01, Jus03, Kan03]. Note that similar to Beck’s approach they modeled thermal reservoirs by dynamical systems that consist of only very few degrees of freedom exhibiting a chaotic dynamics. By using projection operator techniques for the phase space densities of the dynamical system variables they studied to which extent the fast degrees of freedom can be replaced by stochastic noise acting on the slow variables of respective subsystems, and how the resulting equations of motion for the subsystems look like. A related problem was investigated by Eckmann et al., who mathematically analyzed the nonequilibrium properties of a chain of anharmonic oscillators

coupled to two heat baths at different temperatures modeled by Hamiltonian wave equations [Eck99b, Eck99a].

As far as we can tell it is extremely hard to derive rigorous results for the dynamical properties of thermal reservoirs and the associated subsystems, even in equilibrium situations, by starting from first principles. We are not aware that yet there is a general theory for this problem. A major difficulty appears to be that the precise characteristics of the thermal reservoirs depend to quite some extent on the detailed nonlinear and non-Markovian properties of the underlying equations of motion. Thus, typically one has to employ profound approximations in order to come up with some general statistical description, as was already indicated above. In nonequilibrium situations the problem of characterizing steady states with respect to their chaotic and dynamical properties becomes even more peculiar, which connects to our respective discussion in the introduction.

As an alternative to a rigorous bottom-up approach one may therefore construct a variety of simple and successively more sophisticated models of thermal reservoirs, with the purpose to learn about the detailed statistical and dynamical properties of the associated equilibrium and nonequilibrium steady states generated by these models. One may then inquire about general characteristics that are valid for all these models. We emphasize that this top-to-bottom approach, of course, bears other risks. In particular, one may too quickly conclude from the fascinating properties of a specific toy model concerning universal features. But this can be cured by trying to construct counterexamples.

Of course, this bottom-up approach towards the physics of steady states is of a very heuristic nature. Still, in order to qualify as thermal reservoirs all models have to fulfill certain basic criteria. In the following we will require that, like ordinary equations of motion of moving particles, they are deterministic, time-reversible, and that they are able to generate a NSS under nonequilibrium conditions.

However, some details are still missing. So far we have focused on the equations of motion of subsystem plus thermal reservoir only. We did not explicitly discuss the detailed properties of the associated probability densities of subsystem and thermal reservoir and how they should look like, at least in equilibrium situations. This will be performed in the following section.

10.3 Equilibrium velocity distribution functions for subsystem and reservoir

In this part we shall look at a subsystem that is coupled to a thermal reservoir from a purely statistical point of view. That is, we do not assume any detailed knowledge about the underlying equations of motion. We are interested only in the probability densities for the velocities of the subsystem and of the thermal reservoir, which we call velocity distribution functions, in the general case of thermal equilibrium. We do not discuss the probability densities for the associated position coordinates of the degrees of freedom, since the action of the thermal reservoir primarily concerns an exchange of energy related to the velocities. Our goal is to assess how different dimensionalities of subsystem and thermal reservoir, if the reservoir is first thought to be finite dimensional, affect the functional forms of the corresponding velocity distribution functions.

In order to illustrate the general case we start by discussing the most trivial example, where

subsystem and thermal reservoir each consist of only one degree of freedom. Afterwards we switch to the general situation in which there is a subsystem with d_s degrees of freedom interacting with a thermal reservoir of d_r degrees of freedom, where typically $d_s < d_r$ and where the total number of degrees of freedom is $d = d_s + d_r$.³

Let us consider a large collection of points in the full phase space of the system, which in general may be restricted by some boundary conditions. The equilibrium velocity distribution function $\rho \equiv \rho(v_1, v_2)$ for $d = 2$ is then defined with respect to this ensemble of points, which move according to the same equations of motion. It is the number of points one can find in the phase space volume element $dv_1 dv_2$ centered around the velocity vector (v_1, v_2) at time t divided by the size of this volume element and by the total number of points N of the ensemble. By integrating over the whole accessible phase space the velocity distribution is properly normalized to one.

Let us now assume that we are in an equilibrium situation where equipartitioning of energy holds between all degrees of freedom and that the total energy of subsystem plus reservoir is conserved. For sake of simplicity we may assume that there is only kinetic energy as, e.g., in a gas of hard spheres. Hence, all points in velocity space should be uniformly distributed on a circle of radius $v := \sqrt{v_1^2 + v_2^2}$, where for convenience we set $v \equiv 1$, see Fig. 10.1 for an illustration. Subsystem plus reservoir thus obey the microcanonical distribution

$$\rho(v_1, v_2) \sim \delta(1 - v_1^2 - v_2^2) \quad . \quad (10.15)$$

It is now straightforward to calculate the velocity distribution functions of the subsystem, respectively of the thermal reservoir, which are obviously identical, by projecting out one of the two degrees of freedom from this microcanonical distribution. One way of how to do this is by using polar coordinates, $v_1 = \cos \phi$ and $v_2 = \sin \phi$, where ϕ denotes the polar angle in velocity space depicted in Fig. 10.1. The probability density corresponding to ϕ is then simply $\rho(\phi) = \text{const.}$ On the other hand, v_1 is a function of ϕ . According to conservation of probability the probability densities for v_1 and ϕ are related to each other by

$$\rho(\phi)|d\phi| = \rho(v_1)|dv_1| \quad . \quad (10.16)$$

Hence, $\rho(v_1)$ is easily calculated in terms of $\rho(\phi)$ by differentiating v_1 leading to

$$\rho(v_1) = \frac{1}{\pi\sqrt{1 - v_1^2}} \quad , \quad (10.17)$$

where the prefactor is obtained from normalization. As indicated in Fig. 10.1, this result matches to physical intuition: By projecting the uniform distribution of points on the circle onto the v_1 -axis it is clear that there must be a higher density of points nearby the values of $v_2 = 0$ on the circle, whereas around $v_1 = 0$ the density of points must be minimal.

The main message of this trivial example is that non-uniform probability densities, which may otherwise be considered as an indicator of some non-Hamiltonian average phase space contraction, may very well coexist with a uniform, microcanonical one as it characterizes ordinary Hamiltonian dynamical systems. The obvious reason is that *one degree of freedom got projected out* respectively, so we neglected some information by not looking at the full combination of subsystem plus thermal reservoir.

³This problem has been posed as an exercise in the book of van Kampen on p.11 [vK92].

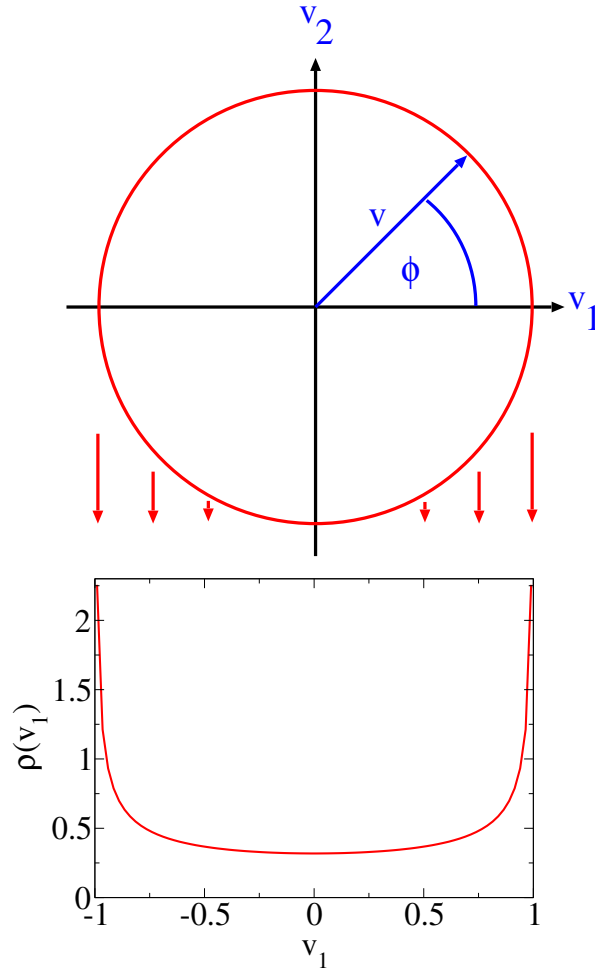


Figure 10.1: Projection of the two-dimensional microcanonical velocity distribution Eq. (10.15) onto one component. The density of points is uniform on a circle of radius $v = 1$. The velocity vector is composed of the two velocity components v_1 and v_2 , and its direction is determined by the polar angle ϕ . The lower figure represents the one-component velocity distribution $\rho(v_1)$ Eq. (10.17) calculated from projecting out v_2 from Eq. (10.15).

Along the same lines and under the same conditions as described above, i.e., by assuming thermal equilibrium, equipartitioning of energy and a constant total kinetic energy E , the general case of a d_s -dimensional subsystem interacting with a d_r -dimensional thermal reservoir can now be studied. In this case the full velocity distribution function for subsystem plus thermal reservoir obeys the microcanonical distribution

$$\rho(v_1, \dots, v_d) \sim \delta(2E - v_1^2 - \dots - v_d^2) \quad (10.18)$$

with $d = d_s + d_r$ and $v_k, k = 1, \dots, d$, as all the velocities. That is, all points in velocity space are uniformly distributed on a hypersphere with radius $\sqrt{2E}$. How do the corresponding velocity distributions of subsystem and reservoir now look like for arbitrary numbers of degrees of freedom d , d_s and d_r ? Again, in order to calculate these distribution functions one has to project out the respective number of degrees of freedom from Eq. (10.18). Here we wish to focus on eliminating $d - 1$ or $d - 2$ degrees of freedom only. The solutions may be obtained along the same lines as in the two-dimensional case by using generalized spherical

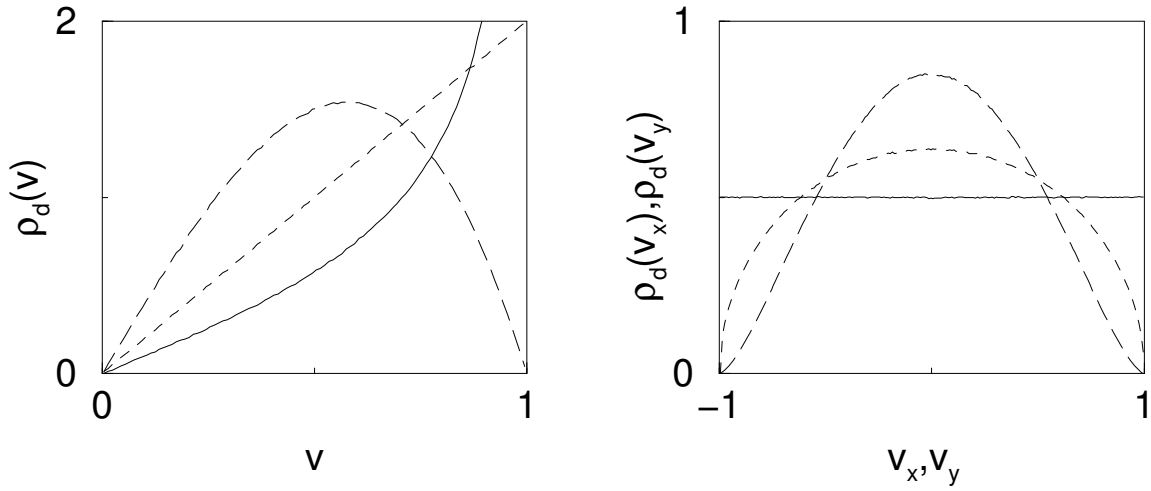


Figure 10.2: Left: equilibrium velocity distribution function $\rho_d(v)$ for the absolute value v of the velocity vector (v_x, v_y) , which may be thought to represent a subsystem with two degrees of freedom coupled to a $(d - 2)$ -dimensional thermal reservoir. Shown are $d = 3$ (solid curve), 4 (dashed curve) and 6 (long dashed curve) at a kinetic energy of $E = 0.5$ as calculated from Eq. (10.20). Right: analogous results for the single velocity components v_x , respectively v_y , calculated from Eq. (10.19).

coordinates. However, we skip the calculations that are technically a bit more involved [Rat00b]. The results are as follows: By projecting out $d - 1$ dimensions the probability density for one velocity component v_1 is calculated to

$$\rho_d(v_1) = \frac{\Gamma(\frac{d}{2})}{\sqrt{\pi}\Gamma(\frac{d-1}{2})} \frac{(2E - v_1^2)^{\frac{d-3}{2}}}{(2E)^{\frac{d-2}{2}}}, \quad (10.19)$$

where $\Gamma(x)$ stands for the gamma function. This solution was already known to Maxwell and Boltzmann [Max79, Has09], however, in their calculation they took a different starting point; for an alternative derivation see also Ref. [Mil98b]. Projecting out $d - 2$ dimensions yields the probability density for the absolute value of the velocity vector of two components v_1 and v_2 with $v = \sqrt{v_1^2 + v_2^2}$ reading

$$\rho_d(v) = (d - 2)v \frac{(2E - v^2)^{\frac{d-4}{2}}}{(2E)^{\frac{d-2}{2}}}. \quad (10.20)$$

These solutions are depicted in Fig. 10.2 for $d = 3, 4, 6$. As can be seen, for $d \gg 1$ both types of velocity distributions start to converge towards their canonical counterparts. This can be made precise by taking the limit of $d \rightarrow \infty$ in Eqs. (10.19) and (10.20). Using equipartitioning of energy, $E = \sum_{k=1}^d v_k^2/2 = Td/2$, where T is the temperature and $k_B \equiv 1$, we arrive at the well-known results

$$\lim_{d \rightarrow \infty} \rho_d(v_1) = \frac{1}{\sqrt{2\pi T}} e^{-v_1^2/2T}, \quad (10.21)$$

respectively

$$\lim_{d \rightarrow \infty} \rho_d(v) = \frac{1}{T} v e^{-\frac{v^2}{2T}}. \quad (10.22)$$

We have thus rederived the canonical distributions for v_1 and for v starting from the microcanonical one of subsystem plus thermal reservoir by projecting out an infinite number of reservoir degrees of freedom. Altogether the above equations yield the full information how, according to elementary equilibrium statistical mechanics, the velocity distribution functions of a subsystem consisting of d_s degrees of freedom shall look like if it experiences ideal interactions with a d_r -dimensional thermal reservoir.

We remark that the velocity distribution Eq. (10.21) is reproduced by an ensemble of particles obeying the stochastic Langevin equation Eq. (10.1) in the limit of $t \rightarrow \infty$. The corresponding Markov process modeling the stochastic behavior of the velocity of a Brownian particle, which is characterized by a stationary Gaussian velocity distribution, is well-known in more mathematical terms as an Ornstein-Uhlenbeck process [vK92, Wax54].

An interesting question is now to which extent the above ideal functional forms of equilibrium velocity distributions are obtained for deterministic dynamical systems of d degrees of freedom when one looks at a respective smaller number of degrees of freedom $d_s < d$. A very popular example of this type of problem is the one- or two-dimensional harmonic oscillator coupled to a suitable deterministic thermal reservoir. If the reservoir mimicks an infinite number of degrees of freedom $d \rightarrow \infty$ the above derivations suggest that the harmonic oscillator velocities should simply approach canonical distributions. However, for such a behavior it is necessary that the thermostated subsystem exhibits at least an ergodic dynamics, because only in this case a single subsystem trajectory samples the whole phase space appropriately in order to possibly generate a canonical distribution. If the phase space is not uniquely accessible because of non-ergodicities the resulting velocity distributions will strongly depend on initial conditions and are typically not canonical. This discussion again indicates how sensitively the interplay between subsystem and thermal reservoir may depend on the detailed properties of the involved dynamical systems; for further details see Section 12.4.

As we already mentioned, the emphasis of this work is on nonequilibrium situations, and here thermal reservoirs are used as a tool to generate NSS representing transport properties of the associated dynamical system. Unfortunately, there is yet no analogue of microcanonical or canonical ensembles for nonequilibrium processes. In other words, nothing is known about how velocity distribution functions shall generally look like in nonequilibrium situations. The standard approach is therefore to define a thermal reservoir in an equilibrium situation by “gauging” it according to the requirement that it generates a microcanonical or a canonical velocity distribution for a respective subsystem connected to it. If this applies, a suitable nonequilibrium situation may be created.

For arbitrary deterministic dynamical subsystems it is by no means obvious or guaranteed that the thermal reservoir still properly “works” under these constraints, which intimately depends on the ergodic and chaotic dynamical properties of subsystem and thermal reservoir. If it does, the reservoir should generate a NSS that is characterized by specific nonequilibrium velocity distribution functions. This way, one can learn something about the variety of different velocity distributions that may exist in different nonequilibrium systems under application of specific models of thermal reservoirs, rather than the other way around. Unless there is a general theory of NSS starting from first principles, which at the moment is not the case, no other approach appears to be feasible here. Of course, for modeling nonequilibrium situations the associated thermal reservoirs must always mimick an infinite number of degrees of freedom in order to prevent a subsystem from heating up.

We finally remark that the above results for equilibrium velocity distributions of subsystems

plus finite-dimensional thermal reservoirs will be used in Chapter 15 in order to systematically construct a specific class of deterministic, time-reversible thermal reservoirs that dissipate energy according to inelastic collisions at the boundaries of a subsystem. Furthermore, we will use these results in Chapter 16 by discussing the origin of crater-like velocity distribution functions in models of active Brownian particles.

10.4 The periodic Lorentz gas

As we just discussed, whether or not thermal reservoirs are able to generate a specific velocity distribution for moving particles depends to quite some extent on the detailed dynamical properties of the subsystem to which it is applied. As an alternative to the problematic harmonic oscillator one may wish to choose a subsystem that is by default chaotic thus providing a more suitable starting point for the action of a thermal reservoir. Though chaotic one may wish that, nevertheless, this system is well analyzed in the mathematical literature.

Such a paradigmatic toy model is the *Lorentz gas* that was also discussed in Chapters 4 and 7. The two-dimensional *periodic* version of it is sketched in Fig. 10.3 and consists of hard disks of radius R at density n whose centers are fixed on a triangular lattice in a plane. Between the scatterers a point particle moves with velocity \mathbf{v} and mass m by performing a free flight, whereas at collisions it exhibits specular reflections with the disks. If no further external constraints are applied the kinetic energy of the moving particle is constant, whereas the direction of the velocity changes according to the collisions with the scatterers. The phase space thus consists of the four variables (x, y, v_x, v_y) . However, because of energy conservation there are only three independent variables, where one may replace v_x and v_y by the angle of flight of the particle with the x -axis. For sake of simplicity we set $R = m = v \equiv 1$.

In the original work by H.A. Lorentz [Lor05], to whom the model is commonly attributed, the Lorentz gas consists of *randomly* distributed *hard spheres*. It was invented by him in 1905 in order to model the motion of classical electrons in metals, where the electrons do not interact with each other but scatter elastically only with hard spheres mimicking the atoms of the metal. However, as a laboratory device the two-dimensional periodic version of this system was, in a way, already introduced about 30 years earlier by Sir Francis Galton in 1877 [Gal77]. Hence, this model is also sometimes referred to as the *Galton board*.

Galton used his device, which he called *the quincunx*, in lectures for demonstrating the existence of a binomial distribution that results when particles falling under the influence of a gravitational field are moving left or right through a periodic board of scatterers. He actually claimed that the same probabilistic laws existed in form of typical laws of heredity within populations of animate beings [Gal77]. His theme is therefore very different from Lorentz' intention, who used his model to verify Drude's theory of classical electronic transport in metals [Dru00] by adding nonequilibrium constraints such as an electric field and a gradient of temperatures.

Though Drude's and Lorentz' work provide some heuristic microscopic derivation of Ohm's law, and of the law by Wiedemann and Frantz, it is well-known that this classical approach is not suitable to yield explanations for other fundamental properties of metals such as, e.g., their specific heat, which can only be understood by using quantum mechanics [Iba96]. On the other hand the two-dimensional Lorentz gas, the scatterers equipped with

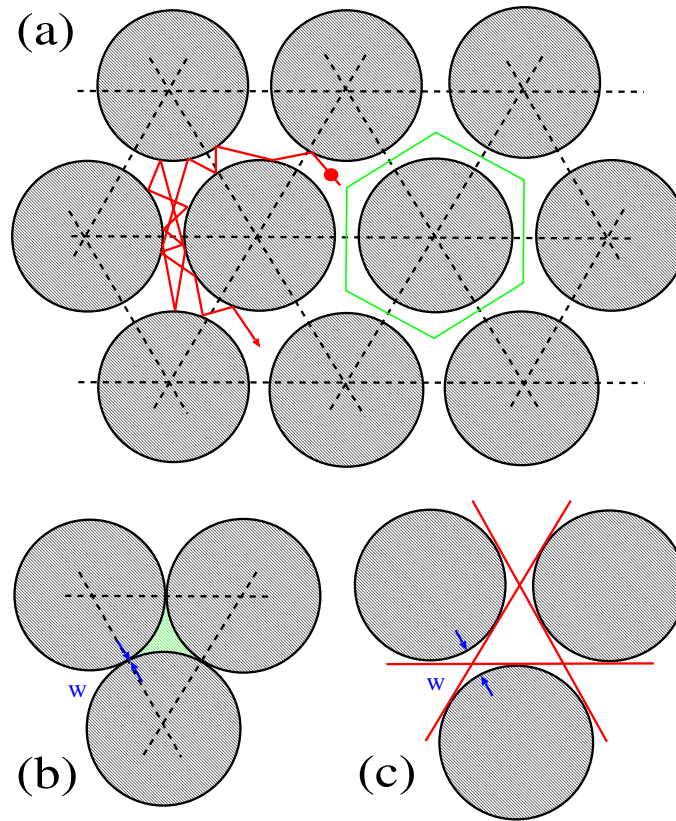


Figure 10.3: Sketch of the two-dimensional periodic Lorentz gas where hard disks of unit radius are situated on a triangular lattice. (a) contains the hexagonal fundamental cell, or Wigner-Seitz cell, of this system. It also shows the trajectory of a point particle moving with a constant velocity and scattering elastically with the disks. (b) represents the limiting case of the highest density of scatterers where the minimal distance w between two scatterers is zero. That is, the scatterers touch each other and there is no diffusion. (c) depicts the other limiting case at a lower density where, for a specific value of w , for the first time trajectories exist along which a particle can move collision-free for an infinite time and thus sees an “infinite horizon”. In this case the dynamics is ballistic and the diffusion coefficient is infinite.

smooth potentials, turned out to be very useful for understanding electronic transport in *antidot lattices* under the action of electric and magnetic fields. These low-dimensional semiconductor devices can be manufactured with scatterers distributed both randomly and periodically in a plane. For small enough field strength the Fermi wavelength is smaller than the lattice constant. Hence, an electron exhibits an essentially classical transport process, where in good approximation the single electrons do not interact with each other; see Refs. [Wei91, Lor91, Wei97] for some experimental as well as Refs. [Gei90, Fle92] for corresponding theoretical work. We thus emphasize that much care has to be taken regarding the physical significance of the Lorentz gas concerning a general understanding of transport in real matter. The usefulness of this model for physically realistic situations should best be assessed from case to case.

In the following chapters we focus on the two-dimensional version of the Lorentz gas on a triangular lattice, so if not said otherwise with “Lorentz gas” we denote precisely this

configuration of scatterers. The unit cell of this dynamical system, which is called *Wigner-Seitz cell* in solid state physics, is a hexagon, see Fig. 10.3 (a). Note that alternatively the scatterers may also be put on a square lattice, in which case the unit cell is sometimes called a *Sinai billiard* [Sin70]. If no further external constraints are added there is only one control parameter, which is the density of scatterers n or alternatively the smallest distance between two scatterers, the gap size w , as depicted in Fig. 10.3 (b) and (c). In the triangular case three different dynamical regimes are identified:

1. Particles are localized in space, i.e., they cannot leave a unit cell, since all disks touch each other, see Fig. 10.3 (b). This is the high density regime with a minimal gap size w between two adjacent disks of $w = 0$, and the diffusion coefficient is trivially zero.
2. There exist trajectories along which particles can move ballistically and collision-free for an infinite time, i.e., under certain initial conditions particles see “infinite horizons” in the Lorentz gas as indicated by Fig. 10.3 (c). This happens for $w > 4/\sqrt{3} - 2 \simeq 0.3094$ and marks the onset of a low-density regime in which the diffusion coefficient is infinite.
3. In-between these two regimes the horizon for the moving particles is finite. As has been proven in Refs. [Bun80, Bun81, Bun91, Che99], in this case a central limit theorem for the velocities exists and the diffusion coefficient is finite. This is related to an exponential decay of the velocity autocorrelation function of the moving particle [Mac83, Mat97] from which the existence of a diffusion coefficient follows according to the Green-Kubo formula for diffusion Eq. (10.5).

On this occasion we may refer to a further simple physical interpretation of the periodic Lorentz gas reflecting these three different dynamical regimes: The scattering of a point particle with a Lorentz gas disk may be looked at as a two-body problem, where a particle of a reduced mass μ moves with a relative velocity \mathbf{v} and scatters, in this case, with a hard core potential $V(R)$. By suitably rescaling the radii of the moving particle and of the fixed scatterer, whose sum should be constant, and by periodically continuing the unit cell including the moving particle, the dynamics may be considered as the collective motion of some lattice modes in a periodic medium such as a crystal. In this case the periodic Lorentz gas was coined the *correlated cell model* [Ald63, Del96a].

According to the three different regimes discussed above there are also three different regimes of lattice modes: In case 1 the lattice modes are again localized, in case 2 dislocations are possible, whereas case 3 may be interpreted as some kind of “melting”. This relation of the periodic Lorentz gas to the correlated cell model was used to prove the existence of a shear and a bulk viscosity in what was called a “two-particle fluid” [Bun96]. Note also that, in kinetic theory, the random Lorentz gas is well-known as a model for a gas mixture of heavy and light particles, where the difference of the masses is large enough such that the heavy particles, in good approximation, can be considered to be immobile with respect to the light particles [Cha70].

The periodic Lorentz gas exhibits a number of important “nice” dynamical properties.⁴ First of all, it is Hamiltonian and thus deterministic, area-preserving and time-reversible.

⁴For readers that are not too familiar with dynamical systems theory this paragraph may be skipped; alternatively, for respective definitions of dynamical systems quantities we refer to Refs. [Sch89, Ott93, Gas98a, Dor99].

Secondly, it has been proven that the Lorentz gas is a K-system, which implies that it is mixing and ergodic [Bun80, Bun81, Bun91, Che99]. Furthermore, due to the defocusing character of the hard disks⁵ the Lorentz gas is a hyperbolic, chaotic dynamical system. However, because of the hard walls it is not differentiable, as is exemplified by the existence of tangent collisions, and therefore strictly speaking it is not Anosov or Axiom A [Gas96, Gas98a]. Finally, corresponding to the three independent variables of the periodic Lorentz gas there are three different Lyapunov exponents reflecting its hyperbolic behavior: One is zero, which is the one parallel to the flow, the other two are smaller respectively larger than zero, and because the system is phase space preserving all Lyapunov exponents trivially sum up to zero.

We remark that for random configurations of scatterers in two and three dimensions the Lyapunov exponents have been computed analytically by means of kinetic theory, partly in comparison with results from computer simulations [vB95, Lat97, vB97, Del97b, vB98]. For the two-dimensional periodic Lorentz gas both on a quadratic and on a triangular lattice computer simulation results for the Lyapunov exponents were presented in Refs. [Gas95b, Gas98a]. Random and periodic Lorentz gases are prototypical models of so-called *particle billiards* that have been widely studied in the field of chaos and transport both from the physical as well as from the mathematical side of dynamical systems theory. Hence there exists a large literature that the reader may wish to consult in order to learn about more detailed properties, see, e.g., Refs. [Gas98a, Dor99, Sza00] and further references therein.

10.5 *Summary

1. We started this chapter by elaborating on the physical meaning of a thermal reservoir. This discussion was performed on a very elementary heuristic level. The action of a thermal reservoir on a subsystem was first outlined for thermal equilibrium. In nonequilibrium situations thermal reservoirs are generally indispensable in order to generate NSS.
2. As a well-known example for modeling thermal reservoirs we have heuristically introduced the simplest form of a stochastic Langevin equation. We have also briefly summarized some of its most important properties. It was then shown how this Langevin equation can be derived starting from Hamiltonian equations of motion, where the heat bath is modeled by a collection of non-interacting harmonic oscillators. On this basis we have discussed deficiencies of both schemes as far as the modeling of thermal reservoirs is concerned, and we have mentioned some more recent approaches that try to go beyond this simple modeling.
3. On a more statistical level, we have outlined how to calculate the equilibrium velocity distribution functions for a single velocity component as well as for the absolute value of two velocity components for a subsystem that is coupled to a d_r -dimensional thermal reservoir. In the limit of $d_r \rightarrow \infty$ we recovered the corresponding well-known canonical distributions, as was to be expected. We indicated that these “ideal” velocity distribution functions, according to equilibrium statistical mechanics, may not by default be properly reproduced by an arbitrary deterministic dynamical subsystem

⁵This type of scatterers is said to be *convex*, or *dispersing*.

such as the harmonic oscillator, coupled to some model of a thermal reservoir. Related problems for modeling NSS were also briefly discussed.

4. Finally, we explicitly defined the periodic Lorentz gas, which exhibits “nice” dynamical properties in an equilibrium situation by being, among others, Hamiltonian, mixing and fully chaotic. We started with a brief history of the (periodic) Lorentz gas, discussed its physical significance and some possible physical interpretations as far as physical reality is concerned. We classified its three different dynamical regimes and very briefly summarized its most important mathematical properties. In the following, the periodic Lorentz gas will serve as our standard model in order to compare the action of different thermal reservoirs with each other, particularly in nonequilibrium situations.

11 *The Gaussian thermostat

We now introduce a very popular deterministic and time-reversible modeling of a thermal reservoir which is known as the *Gaussian thermostat*. We assign this thermostating scheme to the periodic Lorentz gas driven by an external electric field and summarize what we consider to be the most important features of the resulting model from a dynamical systems point of view. The properties we report are to a large extent typical for Gaussian thermostated systems altogether. Specifically, we review a connection between thermodynamic entropy production and the average phase space contraction rate as well as a simple functional relationship between Lyapunov exponents and transport coefficients. Furthermore, there exists a fractal attractor in the Gaussian thermostated Lorentz gas which changes its topology under variation of the electric field strength. Correspondingly, the electrical conductivity is an irregular function of the field strength as a control parameter. We also briefly elaborate on the existence of linear response in this model.

11.1 Construction of the Gaussian thermostat

In the following chapters the periodic Lorentz gas serves as a standard model to which different thermal reservoirs are applied. A big advantage of the Lorentz gas, say, in comparison to the harmonic oscillator is that it exhibits deterministic chaos, which is a consequence of the defocusing geometry of the scatterers. Hence, in contrast to the Langevin dynamics of Eq. (10.1) we do not need to impose a stochastic force onto this model in order to enforce Brownian motion-like spatial fluctuations for a moving particle.¹ Instead, some random-looking trajectories in position space are generated due to the intrinsic Lyapunov instability of the system, see again Fig. 10.3. This is in turn intimately related to the mixing and ergodic properties of the Lorentz gas. We thus replace stochasticity by deterministic chaos in order to generate a Brownian motion-like dynamics, cp. also to our discussion in Section 10.2.

As was outlined in the previous chapter, in a certain regime of densities of scatterers the periodic Lorentz gas exhibits normal diffusion related to an exponential decay of the velocity autocorrelation function, in analogy to the diffusive properties of Langevin dynamics. In the present Part II we do not study how the Lorentz gas dynamics changes under variation of the density of scatterers, see Refs. [Kla00a, Kla02d]. Instead, we simply choose one specific parameter value for the minimal distance between two scatterers, $w \simeq 0.2361$, as it is standard in the literature to ensure that a diffusion coefficient exists [Mor87a, Llo94, Llo95, Del95a, Mor96a, Det96a].

¹On the other hand, without applying an external field the absolute value of the velocity for the moving particle is yet constant in the Lorentz gas, which is at variance to ordinary Langevin dynamics. However, see Chapter 12 for respective further modifications of the Lorentz gas.

In order to drive this model out of equilibrium we apply an external electric field that, if not said otherwise, is parallel to the x -axis. However, as explained before, if there were no interaction with a thermal reservoir any moving particle would on average be accelerated by the external field consequently leading to an ongoing increase of energy in the system, and there were no NSS. Therefore the model must be connected to some thermal reservoir. In other words, it must be thermostated. The periodic Lorentz gas amended by an external field and coupled to a suitable thermal reservoir is called the *driven periodic Lorentz gas*. This model has been widely studied in the literature over the past fifteen years [Mor87a, Hoo88a, Hoo89b, Hoo92, Van92, Che93a, Che93b, Bar93, Lue93, Llo94, Llo95, Det95, Del95a, Mor96a, Det96a, Det97b, Det97c, Bon97, Coh98, Mor98, Hoo98c, Hoo99, Dor99, Tel00, Bon00, Det00a, MM01, Bon02, Vol02, Lar03].

Following our discussion of the Langevin equation one may remove energy from the field-driven Lorentz gas according to

$$\begin{aligned}\dot{\mathbf{r}} &= \mathbf{v} \\ \dot{\mathbf{v}} &= \boldsymbol{\varepsilon} - \alpha(\mathbf{v})\mathbf{v} \quad ,\end{aligned}\tag{11.1}$$

supplemented by the geometric boundary conditions imposed by the Lorentz gas scatterers. With $\alpha \equiv \alpha(\mathbf{v}) = \text{const.}$ we have an ordinary Stokes friction term, and the equations represent a deterministic variant of the stochastic Langevin equation Eq. (10.1) amended by an external electric field $\boldsymbol{\varepsilon}$. Here and in the following the electric charge q of the particle is set equal to one. This viscous Lorentz gas has been studied by computer simulations in Ref. [Hoo92].

For numerical solutions one has to discretize Eqs. (11.1) in time. The second of the above two equations then reads

$$\mathbf{v}(t + \Delta t) = \boldsymbol{\varepsilon}\Delta t + \tilde{\alpha}\mathbf{v}(t) \quad , \quad 0 < \Delta t \ll 1 \quad ,\tag{11.2}$$

with $\tilde{\alpha} := 1 - \alpha\Delta t$. For small enough Δt there is $0 < \tilde{\alpha} < 1$, and by keeping the time interval fixed the viscous force amounts to a rescaling of the velocity periodically in time with a constant scaling factor $\tilde{\alpha}$. This procedure can be made more efficient by replacing $\tilde{\alpha}$ according to

$$\tilde{\alpha}(\mathbf{v}) := \sqrt{\frac{E}{E(t)}} \quad ,\tag{11.3}$$

where E is the target kinetic energy of the system and $E(t)$ the measured kinetic energy at time t . The scaling factor now depends on the velocity of the moving particle and may thus fluctuate in time. This elementary but rather convenient numerical method to keep the energy fixed became well-known for molecular dynamics computer simulations under the name of *velocity rescaling* [Eva83a, All87, Hol87, Hol95, Hes96a, Hes96b, Hoo97, Det00a]. Note that both the Lorentz gas with a Stokes friction coefficient and with rescaled velocities is deterministic but not time-reversible.

In order to further improve the efficiency of these thermostating mechanisms one may start directly from a velocity-dependent friction coefficient in Eq. (11.1), $\alpha \equiv \alpha(\mathbf{v})$. Requiring energy conservation at any time step implies $d\mathbf{v}^2/dt = 0$ as a constraint on the functional form of $\alpha(\mathbf{v})$ and yields

$$\alpha(\mathbf{v}) = \boldsymbol{\varepsilon} \cdot \mathbf{v}/v^2 \quad .\tag{11.4}$$

This method of thermostating was proposed simultaneously and independently by Hoover and coworkers [Hoo82] and by Evans [Eva83a] in 1982. Performed in the limit of $\Delta t \rightarrow 0$, the velocity rescaling Eqs. (11.2), (11.3) is identical to the combination Eqs. (11.1), (11.4) [Eva83a, Hol87, Hol95, Hes96a, Hoo97, Det00a].

In contrast to ordinary Stokes friction that only reduces the kinetic energy, the velocity-dependent version Eq. (11.4) pumps energy into the system whenever the particle is moving opposite to the field. This friction is maximal when the velocity is parallel to the field, and it is zero when velocity and electric field are perpendicular to each other. Trivially, it is zero when the electric field is zero due to the fact that in the equilibrium periodic Lorentz gas a particle is moving with a constant absolute value of the velocity anyway. Still, in comparison to the friction of the deterministic, generalized Langevin equation Eq. (10.11) that was obtained starting from the heat bath of harmonic oscillators, such a generalization of ordinary Stokes friction may not be considered physically unreasonable.

Alternatively, Eq. (11.4) can be derived from Gauss' principle of least constraints [Eva83b, Eva90b, Mor98, Ron02a], which is a fundamental principle of classical mechanics.² For this reason a velocity-dependent friction force that keeps the energy of a particle constant at any time step was coined the *Gaussian thermostat* [Eva83b]. Correspondingly, the Gaussian thermostat applied to the driven periodic Lorentz gas generates a microcanonical-like distribution in velocity space [Mor98].³

In fact, here we are constraining only the kinetic energy of the moving particle, therefore this version is sometimes further classified as the *Gaussian isokinetic thermostat*. For soft particles one may fix alternatively the total internal energy consisting of the sum of kinetic plus potential energy yielding the *Gaussian isoenergetic thermostat*, see Refs. [Eva90b, Mor98, Det00a, Ron02a] for these denotations. Suitably amended versions of the Gaussian thermostat can also be applied, for example, to many-particle systems under shear, see Chapter 15 for further discussions.

Similar to the case of Stoke's friction which models the loss of energy of a moving particle into a surrounding viscous fluid one may associate with the Gaussian friction variable Eq. (11.4) some imaginary thermal reservoir that acts at any instant of time. Thus the Gaussian thermostat is another example of a so-called *bulk thermostat*. We remark that this physical picture contradicts the specific interpretation of the driven periodic Lorentz gas as a model for noninteracting electrons moving in a periodic crystal. Here one may expect that energy is only dissipated at the collisions with a scatterer and not during a free flight. However, the action of the Gaussian thermostat is conceptually fine if the Lorentz gas is considered as a two-particle fluid that is immersed into another fluid serving as a thermal reservoir. Let us furthermore remark that in Chapter 15 we will introduce boundary thermostats for the Lorentz gas, where a particle exchanges energy with a thermal reservoir only at the collisions with a scatterer. On this occasion we will discuss similarities and differences to what we find for the Gaussian thermostated case summarized below.

Surprisingly, the equations of motion Eqs. (11.1) supplemented by Eq. (11.4) are time-reversible consequently modeling the, at first view, seemingly contradictory situation of a deterministic, time-reversible, dissipative dynamical system [Hoo96b]. As will be outlined

²In contrast to d'Alembert's principle, for the Gaussian version the virtual displacements are acceleration terms instead of the positions of a moving particle.

³Note that in nonequilibrium the distribution of points on the energy shell is not uniform anymore reflecting the existence of an average current.

in the following, under certain conditions the Gaussian thermostated driven Lorentz gas furthermore exhibits an ergodic and chaotic particle dynamics and corresponding well-defined NSS. In contrast to standard Stoke's friction and to stochastic thermostats the Gaussian scheme thus enables to elaborate on the fundamental problem how time-reversible, deterministic, microscopic equations of motion may generate macroscopic irreversible transport in nonequilibrium situations associated with energy dissipation.

11.2 Chaos and transport for Gaussian thermostated dynamical systems

We now analyse the Gaussian thermostated driven periodic Lorentz gas from a dynamical systems point of view and summarize what we consider to be the characteristic chaos and transport properties of this class of dynamical systems.

11.2.1 Phase space contraction and entropy production

A first fundamental property of Gaussian thermostated systems is obtained from computing their *average phase space contraction rate* defined by

$$\kappa := \langle \nabla \cdot \mathbf{F}(\mathbf{r}, \mathbf{v}) \rangle, \quad (11.5)$$

where $\mathbf{F}(\mathbf{r}, \mathbf{v})$ stands for the equations of motion of the system Eqs. (11.1) and the brackets denote an ensemble average. A straightforward calculation, by taking into account that α is a function of \mathbf{v} , yields

$$\kappa = - \langle \alpha \rangle \quad (11.6)$$

with α defined by Eq. (11.4), where $\kappa < 0$. Let us now rewrite this equation by introducing a nonequilibrium temperature T . If we want to do so by using equipartitioning of energy [Eva90b, Mor98, Hoo99] we need to know about the number of degrees of freedom of the system. The velocity space is two-dimensional, but one may argue that the energy constraint eliminates one degree of freedom of the system. However, this argument is debatable, and actually there is quite an ambiguity in defining a temperature for the driven Lorentz gas [Che93a, Che93b].⁴ By assuming that there is one degree of freedom only we arrive at

$$v^2 = T, \quad (11.7)$$

with $k_B \equiv 1$. We can now write

$$- \kappa = \varepsilon \cdot \langle \mathbf{v} \rangle / T, \quad (11.8)$$

where the right hand side is the familiar expression related to the Joule heating derived from irreversible thermodynamics. Alternatively, one could have started from Clausius' definition of entropy production in terms of the heat transfer dQ between subsystem and thermal reservoir, $\Delta S = \int dQ/T$ [dG62, Hua87, Det00a, Gal03], yielding the same equation.⁵ We

⁴If we switch back to the Lorentz gas without an external field we also, trivially, have energy conservation. However, here nobody would claim that the number of degrees of freedom is reduced respectively.

⁵In the d -dimensional case and for N particles there is a prefactor of $Nd - 1$ on the right hand side of Eq. (11.6), but this factor cancels with a respective prefactor on the right hand side of Eq. (11.7) such that the identity is preserved [Coh98]. Note also that the Clausius form is only valid for quasistatic processes in, at least, local thermodynamic equilibrium.

thus arrive at the fundamental result that, for Gaussian thermostated systems, there is an *identity between the absolute value of the average rate of phase space contraction and thermodynamic entropy production* [Hol87, Pos87, Pos88, Eva90b, Che95b, Che97, Che93a, Che93b, Vol97, Bre98, Gil99a, Hoo99, Det00a, Vol03]. A third way to obtain this identity starts from Gibbs' definition of entropy production, as will be discussed in Chapter 13.

11.2.2 Lyapunov exponents and transport coefficients

Note that Eq. (11.8) provides a crucial link between dynamical systems properties, in terms of phase space contraction, and thermodynamics, in terms of entropy production. By employing this link a second fundamental property for Gaussian thermostated systems is easily derived as follows: First of all, there is an identity between the average phase space contraction of a dynamical system and the sum of Lyapunov exponents [Eck85, Gas98a]. For the driven Lorentz gas under consideration two Lyapunov exponents are zero, due to the energy constraint and assessing the neutral direction parallel to the trajectory of a moving particle. From the remaining two exponents one is positive and one is negative, at least for small enough field strength, see, for example the numerical results of Refs. [Llo95, Del95b, Det95, Det96a, Mor96a, Mor98]. Consequently we have

$$\kappa = \lambda_+ + \lambda_- \quad . \quad (11.9)$$

Let us now replace the average current by introducing the field-dependent electrical conductivity $\sigma(\varepsilon)$ according to⁶

$$\langle \mathbf{v} \rangle =: \sigma(\varepsilon) \boldsymbol{\varepsilon} \quad , \quad (11.10)$$

where ε stands for the absolute value of the field strength. For sake of simplicity here we consider only the case of the field being parallel to the x -axis. Because of the symmetry of the two-dimensional model $\sigma(\varepsilon)$ is then a scalar quantity, whereas for general direction of the field strength one has to employ a tensorial formulation [Llo95]. Replacing the average current $\langle \mathbf{v} \rangle$ on the right hand side of Eq. (11.8) by Eq. (11.10) and the average phase space contraction rate κ on the other side by Eq. (11.9) we arrive at a simple relation between the conductivity $\sigma(\varepsilon)$ and the sum of Lyapunov exponents of the dynamical system,

$$\sigma(\varepsilon) = -\frac{T}{e^2}(\lambda_+(\varepsilon) + \lambda_-(\varepsilon)) \quad . \quad (11.11)$$

This important connection between transport coefficients and dynamical systems quantities was first reported by Posch and Hoover for a many-particle system with an external field [Pos88] and was called the *Lyapunov sum rule* later on [Eva90a]. For the driven periodic Lorentz gas its existence was rigorously proven in Refs. [Che93a, Che93b]. Eq. (11.11) can also be related to periodic orbits [Van92] and was studied in much detail numerically [Bar93, Llo95, Del95b]. Functional forms that are completely analogous to Eq. (11.11) also hold for many-particle systems and for other transport coefficients such as viscosity [Eva90a, Eva90b, Coh95, Sar98] and thermal conductivity [Aok02] under the necessary condition that heat is dissipated by Gaussian and related thermostats [Mor98].

⁶Strictly speaking this quantity may rather be called the *mobility* of a particle, in distinction from the conductivity that involves the charge and the density per unit volume of the mobile electrons of a conductor [Wan66, Rei65]. However, in our case there is no difference.

The Lyapunov sum rule moved particularly into the center of interest starting from the work by Evans, Cohen and Morriss [Eva90a] who introduced a further simplification of it for systems with many degrees of freedom. The observation was that for dissipative many-particle systems the spectrum of Lyapunov exponents may exhibit a remarkable symmetry property [Pos88, Mor89a, Eva90a]. This was first reported for the case of a uniform viscous damping by Dressler [Dre88] and was later on called the *conjugate pairing rule*: If all non-zero Lyapunov exponents are ordered according to their values they can be grouped into pairs such that each pair sums up to precisely the same value [Dre88, Pos88, Eva90a, Sar92, Gup94, Coh95, Det95, Del96b, Det96c, Lat97, Del97b, Del97a, Det97a, Mor98, Sea98, Bon98b, vB98, Woj98, Rue99b, vB00b, Dol00, Pan02c, Pan02b, Pan02a, Mor02, Tan02b]. This pairing rule is well-known for Hamiltonian dynamical systems, however, here the Lyapunov exponents appear in pairs that always sum up to zero. Indeed, in phase space preserving dynamical systems it can be shown that conjugate pairing is a direct consequence of the symplecticity of the Hamiltonian [Eck85, Mei92, Abr94, Gas98a].

If conjugate pairing holds for the very different class of dissipative, thermostated systems it enables to replace the sum over the full spectrum of Lyapunov exponents which appears on the right hand side of Eq. (11.11) by the sum over one pair of exponents only. For higher-dimensional dynamical systems this drastically simplifies the computation of transport coefficients according to Eq. (11.11), since the total number of different exponents is here extremely large and the full spectrum is very hard to extract numerically. Instead, for a conjugate pair one may just choose the largest and the smallest Lyapunov exponent, where the largest exponent is typically not too difficult to get [Ben80, Wol85, Ott93]. The smallest one, in turn, is best computed by reversing the direction of time [Hoo88b, Eva90a, Coh95, vB96, Lat97, Sar98, Sea98, Tan02b].

However, note that the reversed trajectories still have to be constrained to the invariant set associated with the forward dynamics. As we will further explain in the following section, in dissipative systems this set is usually a *fractal attractor* that becomes a *fractal repeller* under time reversal, and it requires some additional numerical efforts to keep the trajectories in this now unstable region. From a computational point of view the Lyapunov sum rule Eq. (11.11) supplemented by conjugate pairing thus does not appear to provide a more efficient mean for computing transport coefficients than other existing standard procedures. For example, along the lines of Eq. (11.11) it were easier to compute the average value of the thermostating variable instead of any Lyapunov exponent, see Eqs. (11.6) and (11.9).

Conjugate pairing was analytically proven to hold under certain conditions that particularly concern the specific form of the interparticle potential and the special type of deterministic thermostat used [Det96c, Det97a, Mor98, Woj98, Rue99b, Pan02a]; see also the kinetic theory calculations for the three-dimensional Gaussian isokinetically thermostated driven random Lorentz gas in Refs. [Lat97, vB98, vB00b] and the respective comparison to computer simulations [Del97b]. Conjugate pairing in the three-dimensional driven periodic Lorentz gas, again connected to a Gaussian isokinetic thermostat, was numerically corroborated in Refs. [Det95, Mor96a].

For interacting many-particle systems under shear the situation concerning the validity of conjugate pairing appears to be considerably less clear, see Refs. [Eva90a, Coh95, Gup94, Mor98] and the very recent discussion in Refs. [Mor02, Tan02b, Pan02b, Pan02c]; see also Refs. [Del96b, Sar92, Sea98] for numerical studies of various thermostated systems in which conjugate pairing appears to hold, respectively does not appear to hold. Generally, it seems to be easier to give sufficient conditions under which conjugate pairing does *not*

hold: one example is a three-dimensional periodic Lorentz gas under electric and magnetic fields for which there is, or is not, conjugate pairing depending on the specific direction of the two fields [Dol00]. Another generic class of counterexamples to conjugate pairing is provided by systems that are thermostated at the boundaries [Pos88, Del97a, Wag00]. The latter models indicate that conjugate pairing is intimately related to the thermostat acting homogeneously and ‘democratically’ on all particles in the bulk of a system [Mor98, Eva00], whereas inhomogeneous thermostating at the boundaries prevents the Lyapunov exponents to come in conjugate pairs. In Chapter 15 we will more explicitly discuss counterexamples of the latter type.

11.2.3 Fractal attractors characterizing nonequilibrium steady states

How does it fit together that *time-reversible* microscopic equations of motion yield *irreversible* macroscopic transport in a NSS? As was first discussed by Hoover et al. [Hol87, Mor87a] and by Morriss [Mor87b], for this type of driven thermostated systems reversibility and irreversibility are intimately linked to each other by the existence of a *fractal attractor* in phase space; see Refs. [Mor87b, Mor89b, Eva90b, Pet94] for a sheared two-particle system, Refs. [Pos87, Pos88, Mor89a, Pos89, Hoo94, Del97a, Wag00] for many-particle systems under various nonequilibrium conditions, Refs. [Mor87a, Hoo88a, Hoo89b, Van92, Hoo92, Che93a, Che93b, Lue93, Llo94, Llo95, Del95a, Det96a, Det97c, Mor98, Hoo98c, Kla00b, Rat00b, Rat00a, Rat02] for the driven periodic Lorentz gas and Refs. [Hol87, Kus90, Hoo91, Tel96, Pos97, Pos98, Gil99a, Gil99b, Hoo99, Tel00, Vol02] for related models.⁷

We now outline characteristic features of the attractor of the driven periodic Lorentz gas. For convenience the temperature of the thermostat is fixed at $T = 1$. In order to simplify the analysis a Poincaré surface of section is considered. That is, we introduce a further constraint in position space by representing the dynamics in terms of the phase space coordinates at a collision with a disk only. These collisions are defined by the position on the circumference of the disk according to the angle β and by the impact angle γ related to the direction of the velocity of the moving particle, see Fig. 11.1. The set $(\beta, \sin \gamma)$ forms the *Birkhoff coordinates* of a particle billiard [Gas96, Gas98a], see also Section 4.1. A convenient property of the Birkhoff coordinates is that in the Hamiltonian case at field strength $\varepsilon = 0$ the invariant probability density $\rho(\beta, \sin \gamma)$ associated with these coordinates is simply uniform in the whole accessible phase space.

In contrast to that, Fig. 11.2 shows that in case of dissipation generated by an electric field and counterbalanced by a Gaussian thermostat the phase space density contracts onto a complicated fractal-looking object. Numerical analysis provides evidence that the attractor shown in Fig. 11.2 is *multifractal* [Ott93, Bec93, Lev89]: Although the two-dimensional phase space spanned by the Birkhoff coordinates is fully covered for small enough field strength

⁷Here we are using the term *attractor* according to the operational definition of Eckmann and Ruelle [Eck85]: Let there be points in phase space generated by the equations of motion of a dynamical system. The attractor is the set on which these points accumulate for large times. For more rigorous mathematical definitions see, e.g., Refs. [Eck85, Gas98a, Guc90, Dev89]. Sometimes the additional term *strange* is employed to further characterize attractors [Rue71]. However, its use appears to be quite ambiguous in the literature, partly indicating the existence of a chaotic dynamics on the attracting set [Bec93, Sch89, Eck85, Lev89], partly being synonymous for the attractor exhibiting a fractal structure [Ott93, Gre84]. Hence, here we avoid this denotation.

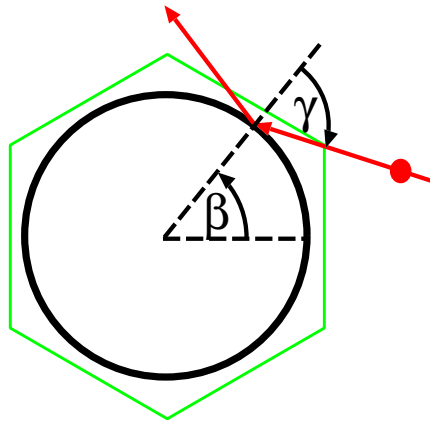


Figure 11.1: Phase space coordinates describing the collision of a point particle with a disk in case of the two-dimensional periodic Lorentz gas. β denotes the position of the colliding particle on the circumference of the disk, whereas the impact angle γ is related to the direction of the velocity of the moving particle before the collision.

yielding a box-counting dimension of two in computer simulations, the higher-order Renyi dimensions such as the information dimension and the correlation dimension are non-integer and slightly smaller than two indicating an inhomogeneous fractal folding of the phase space [Hoo89b, Det96a, Det00a].

However, note that here we are discussing the attractor in the reduced phase space defined by the Poincaré surface of section only. As far as the whole accessible phase space corresponding to the three independent phase space variables of the model is concerned there is a proof that the Hausdorff dimension of this fractal set is less than three and identical to the information dimension for non-zero but small enough field strength [Che93a, Che93b], which appears to be consistent with computer simulation results [Del95a].

The basic structure of the attractor shown in Fig. 11.2 can roughly be understood as follows: points in phase space with an impact angle of $\gamma = \pm\pi/2$ are reminiscent of *tangent collisions* where a moving particle just passes a disk. These points are due to the hard disk geometry and yield discontinuities in the equations of motion which separate regions in phase space corresponding to different types of trajectories.⁸ Calculating higher iterates of these lines of discontinuity from the equations of motion yields complicated boundaries in phase space which match to the structures depicted in Fig. 11.2, see Refs. [Gas96, Gas98a] for the field-free Lorentz gas and Refs. [Mor87a, Hoo88a, Bon00] for the driven case. We remark that this procedure is intimately related to the construction of *Markov partitions* for the periodic Lorentz gas [Bun80, Bun81, Bun91, Che99]. Note that the topology of these structures changes under parameter variation, which has direct consequences for physical quantities such as the electrical conductivity of the system, as we will discuss in the following section. The bifurcation diagram Fig. 11.3 indicates how the attractor changes by increasing the field strength ε [Mor87a, Hoo89b, Llo94, Llo95, Det96a, Mor98]. Here we show results for the angle θ which is the angle between the horizontal x -axis and the velocity of the

⁸With different types of trajectories we mean that trajectories of different regions hit different scatterers in the spatially extended periodic Lorentz gas, as can be quantitatively assessed in terms of a symbolic dynamics by assigning different symbols to different scatterers, see, e.g., Refs. [Llo94, Llo95, Gas96, Gas98a, Mor98] for further details.

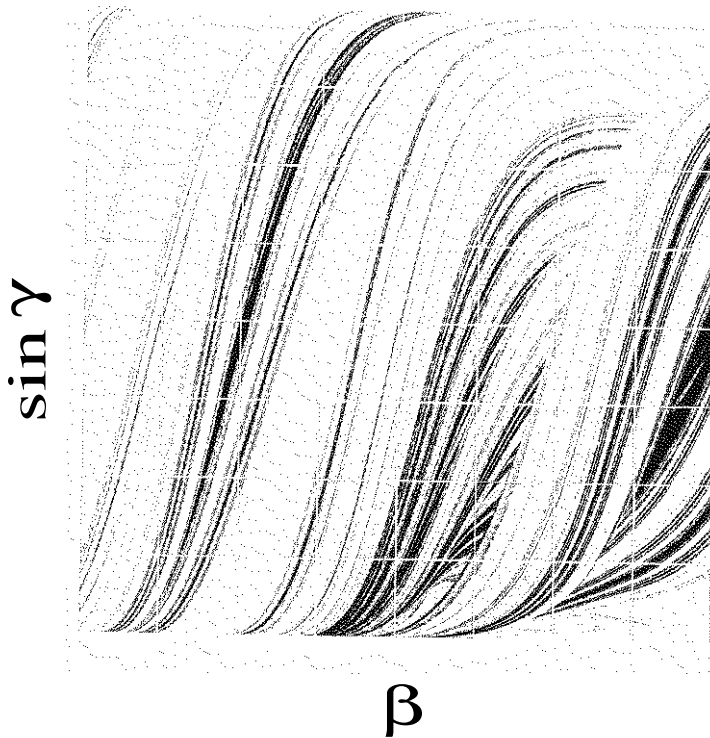


Figure 11.2: Attractor for the Gaussian thermostated periodic Lorentz gas driven by an electric field of strength $\varepsilon = 1.5$ which, here, is parallel to the y -axis. The temperature is $T = 1$, β and $\sin \gamma$ are defined in Fig. 11.1. The figure, originally being a 1m-square, is from Ref. [Hoo89b]. For related results see Refs. [Mor87a, Hoo88a, Del95a, Hoo99].

moving particle after the collision. Consequently, θ is a simple function of the coordinate γ . Results for β and γ are analogous. This figure reveals a complicated bifurcation scenario: By increasing the field strength the attractor first experiences a *crisis* [Ott93] at which it suddenly collapses onto a subset in phase space [Llo94, Llo95, Det96a, Mor98]. For higher values of the field strength there are Feigenbaum-like bifurcations showing a complicated interplay between periodic windows and chaotic parameter regions. Around $\varepsilon = 2.4$ there is even an example of an elliptic fixed point in phase space.

Note that for small enough field strength, that is, before the first crisis occurs, the system is ergodic, see Refs. [Mor87a, Hoo89b, Llo94, Llo95, Det96a, Mor98] for numerical explorations and Refs. [Che93a, Che93b] for a proof. In the course of the bifurcations the system exhibits a complex transition scenario from ergodic and chaotic to non-ergodic and non-chaotic behavior. For high enough field strength the attractor eventually collapses onto a single periodic orbit. This orbit is such that a particle moves parallel to the field during a free flight, whereas at a collision it “creeps” along the circumference of a disk [Mor87a, Llo94, Llo95].

For Gaussian-type thermostated dynamical systems the existence of multifractal attractors in respective Poincaré sections appears to be typical. This applies not only to a single-particle dynamics but also to interacting many-particle systems under general nonequilibrium conditions, see the long list of references cited at the beginning of this section for some examples. The fractality also survives in chaotic dynamical systems where the single particles interact with each other via smooth potentials [Pos87, Pos88, Pos89, Mor89a, Pos97,

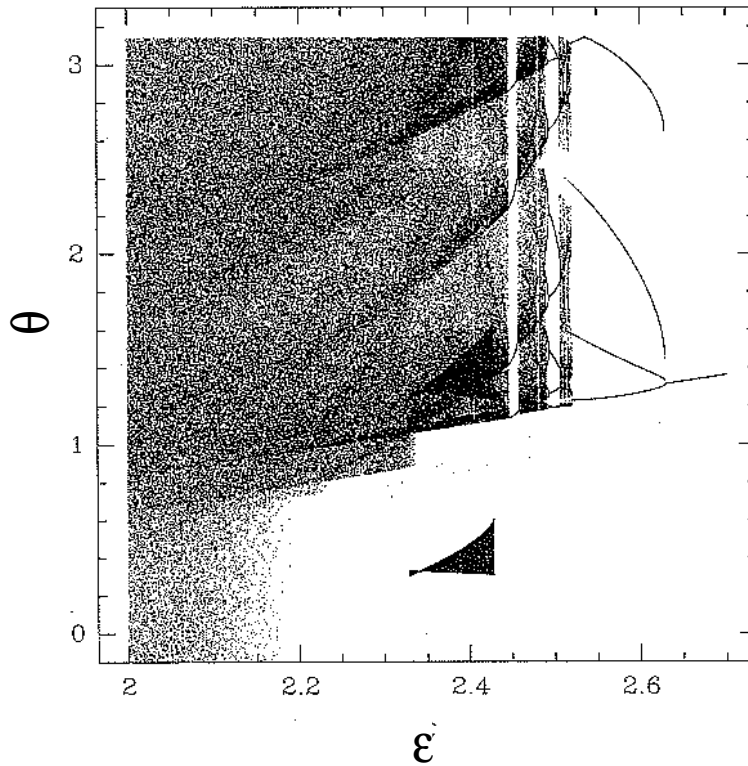


Figure 11.3: Bifurcation diagram for the Gaussian thermostated periodic Lorentz gas driven by an electric field of strength ε which, here, is again parallel to the x -axis. θ is the angle between the x -axis and the velocity of the moving particle after the collision and is a simple function of γ as defined in Fig. 11.1. The temperature is set to $T = 1$. The figure is from Refs. [Llo94, Llo95, Mor98].

[Hoo97] and in systems that are thermostated by a Stokes friction coefficient [Hoo92] or by some constant restitution coefficient at the collisions with a scatterer [Lue93]. Important questions are whether the existence of fractal attractors is a universal property of NSS in chaotic dynamical systems connected to thermal reservoirs, irrespective of the specific thermostat used, and to which extent the structure of the attractor depends on the specific type of thermostat.

11.2.4 Field-dependent electrical conductivity

In the final part of this chapter we focus on the transport properties of the Gaussian thermostated driven periodic Lorentz gas by studying the electrical conductivity $\sigma(\varepsilon)$ introduced in Eq. (11.10). Here we only discuss the ergodic regime of the model at field strengths $\varepsilon \ll 2$ for which $\sigma(\varepsilon)$ is uniquely defined. In this case it can be obtained from computer simulations in form of the time average over the velocity of a single particle sampled from a long trajectory. If the system is non-ergodic the situation is more complicated, since the values for the conductivity then depend on the choice of initial conditions in phase space. Results for $\sigma(\varepsilon)$ in the ergodic regime calculated from computer simulations [Llo95] are shown in Fig. 11.4. Related results have been obtained, also from simulations, in

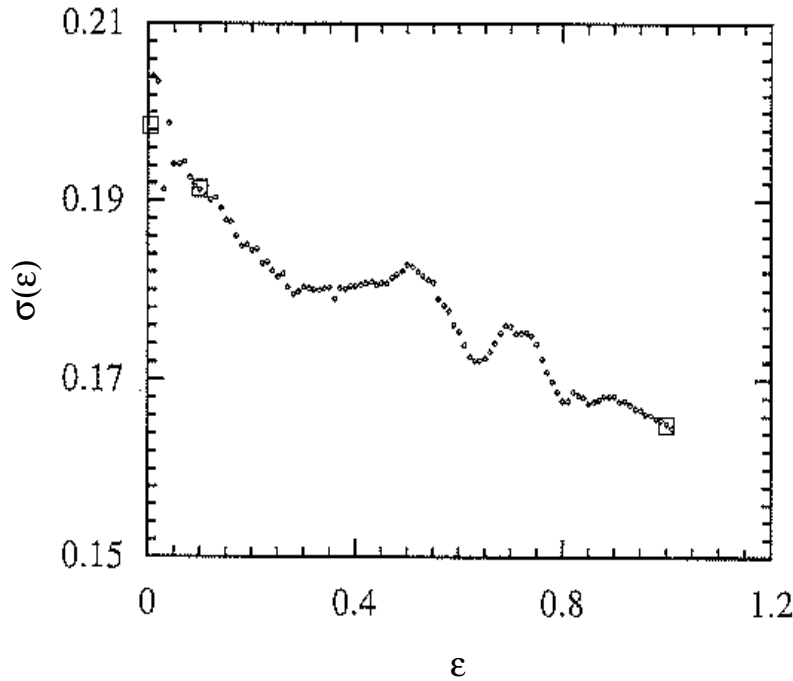


Figure 11.4: Electrical conductivity $\sigma(\varepsilon)$ for the Gaussian thermostated periodic Lorentz gas driven by an electric field of strength ε which is parallel to the x -axis. The temperature is again $T = 1$. The small diamonds are data points computed from higher precision simulations, see Ref. [Llo95] for further details which also contains the original figure. Note the nonlinear response of this quantity and the irregular structure on fine scales.

Refs. [Mor87a, Del95a, Bon00, Det00a]; for calculations based on periodic orbits see Refs. [Van92, Det97b], for the conductivity of a driven Lorentz gas thermostated by a Stokes friction coefficient see Ref. [Hoo92], and for conduction in a modified many-particle Lorentz gas see Refs. [Bar93, Bon97, Bon02].

Two aspects are remarkable in this figure: first of all, the validity of Ohm's law implies that the field-dependent conductivity is simply constant, $\sigma(\varepsilon) \equiv \text{const}$. However, here this quantity clearly decreases on average thus indicating that, for the range of field strengths shown in the figure, the response is already in the nonlinear regime. Indeed, even for the smallest values of the field strength which are accessible to simulations no linear response behavior is visible in this figure. These results [Llo95] are in agreement with simulations performed by other authors [Mor87a, Del95a, Bon00, Det00a]. On the other hand, in the limit of $\varepsilon \rightarrow 0$ the conductivity appears to converge to the correct value of the diffusion

coefficient obtained from the Einstein formula⁹

$$D/T = \sigma(\varepsilon) \quad (\varepsilon \rightarrow 0) \quad , \quad (11.12)$$

which is $D \simeq 0.196$ for $T = 1$ [Mac83, Bar93, Gas95b, Mor94, Del95a, Bon00, Kla00a]. This numerically corroborates the analytical proof of the Einstein relation presented in Refs. [Che93a, Che93b]. For sake of completeness let us remark that the conductivity also depends on the density of scatterers. As expected, for higher densities the response appears to be getting more linear in the regime of field strengths shown in Fig. 11.4 [Del95a]. However, to decide about linearity or nonlinearity is still very ambiguous, since this depends on the scale according to which the results are plotted; see also Fig. 4 in Ref. [Det00a].

A second fact makes the situation even more complicated, namely the existence of irregularities in the conductivity as a function of the field strength in form of non-monotonocities on fine scales, as was first reported in Ref. [Mor87a]. The existence of such irregularities has also been verified by cycle expansion calculations for higher values of the field strength [Det97b] and by other computer simulations [Llo95, Del95a, Bon00], hence they are not artifacts representing numerical imprecisions. Indeed, this phenomenon relates the explicit discussion of irregular and fractal transport coefficients of Part I [Kla95, Kla96, Kla99a, Gas98c, Har01, Gro02, Kor02, Kla02a] to the case of thermostated systems: by using Birkhoff coordinates the periodic Lorentz gas can be linked to maps having the same properties as the ones exhibiting fractal transport coefficients, as discussed in Part I [Gas96, Gas98a, Gil99b, Gas98c, Tel00, Vol02]. It was thus early conjectured that the field-dependent conductivity of the driven Lorentz gas too exhibits fractal properties [Kla95, Kla96, Kla99a].

For one-dimensional maps with broken symmetry yielding drift-dependent currents it was shown in Chapter 3 that the conductivity is typically¹⁰ a nonlinear fractal function of control parameters [Gro02, Gil04]. Similar results were obtained numerically for the parameter-dependent diffusion coefficient in the field-free periodic Lorentz gas, see Chapter 7 [Kla00a, Kla02d], and in related billiards of Lorentz-gas type, see Chapter 8 [Har02]. However, to rigorously prove the existence of irregular structures in transport coefficients is generally a hard task, even for the most simple systems [Gro02], as is exemplified by a recent analysis for the driven Lorentz gas that was not conclusive in this respect [Bon00].

Apart from these numerical assessments of the Lorentz gas conductivity there are seminal mathematical results proving Ohm's law for this model [Che93a, Che93b]. However, this proof does not yield any precise upper bound for the validity of the range of linear response and may thus rather be considered as an existence proof. Indeed, simple heuristic arguments quantifying such bounds as discussed in Refs. [Dor99, Che93b] lead to wrong values for the driven periodic Lorentz gas in comparison to simulation results [Rat00b]. According to these mathematical and numerical analyses one may conclude that a regime of linear response exists in the driven periodic Lorentz gas which, however, is so small in the field strength that, up to now, it could not properly be detected in computer simulations. Even then, an open problem is the possible existence of fractal-like irregularities on fine scales, which for

⁹This equation is easily obtained from the Einstein relation Eq. (10.3) if an external electric field ε is added to the (one-dimensional) Langevin equation Eq. (10.1). In a NSS the average over the time derivative of the velocity on the left hand side of Eq. (10.1) must be zero and the average over the noise on the right hand side is by definition also zero, hence $E - \alpha < v \rangle = 0$. By using Eq. (11.10) one arrives at $\sigma = 1/\alpha$ [Rei65, Pat88]. Note that for the Gaussian thermostated driven Lorentz gas Eqs. (11.1), (11.4) the validity of these relations is not obvious.

¹⁰i.e., for all control parameters except of Lebesgue measure zero

the driven Lorentz gas one may expect to persist as well in the limit of $\varepsilon \rightarrow 0$ [Gro02]. If this is the case Ohm's law may strictly speaking only hold with respect to performing a suitable coarse graining for the conductivity over small but finite subintervals of the field strength.

These problems strongly remind of the famous van Kampen objections against linear response theory [vK71]. It is not our goal here to give a full account of the debate around van Kampen's arguments. For that we may refer, e.g., to Refs. [Mor89c, Eva90b, Kub92, Che93b], to the nice outline in Ref. [Dor99] and to further references therein. Instead, we will highlight certain points that we believe are important for an understanding of the interplay between chaos and transport in the driven periodic Lorentz gas.

Van Kampen criticizes derivations of the laws of linear response that assume microscopic linearity in the equations of motion. By taking this assumption serious he arrives at a simple estimate for the range of validity of linear response which is 10^{-18}V/cm for electrons in a conductor.¹¹ Van Kampen uses this unrealistically small value to illustrate his point that *linearity of the microscopic motion is entirely different from macroscopic linearity*. In other words, the question is how to reconcile the ubiquitous microscopic nonlinearity in the equations of motion of a dynamical system with the macroscopic linearity in the response of the same system. According to van Kampen *it is the randomization of the microscopic variables that enables one to eliminate them from the macroscopic picture, whereas in linear response theory the previous history is not forgotten through randomization, but ignored through linearization*. Curiously enough, van Kampen discusses just the Galton board under external forces as an example. By formally solving the Boltzmann equation that is based on Boltzmann's *molecular chaos* assumption he concludes that *the nonlinear deviations of the microscopic motions somehow combine to produce a linear macroscopic response*; see also Refs. [Che93b, Coh98, Kla00a] on discussions of that point.

To us, the existence proof of linear response for the driven periodic Lorentz gas given in Refs. [Che93a, Che93b] exemplifies how to reconcile macroscopic linearity with microscopic nonlinearity. On the other hand, results from computer simulations and related work [Mor87a, Llo95, Del95a, Det97b, Bon00] still point back to van Kampen's first objection how to quantitatively identify the regime of validity of linear response. Thus, the driven periodic Lorentz gas appears to provide a good illustration for the difficulty formulated by van Kampen that both the existence and the size of the regime of linear response may not be trivially guaranteed in a nonlinear dynamical system; see also Chapter 3 [Gro02] for another example which is even more drastic but also more abstract than the Lorentz gas. A proper theoretical approach thus needs to take into account that, for microscopic chaotic dynamics, the macroscopic response of the system may very sensitively depend on the special character of the system. However, let us emphasize that the periodic Lorentz gas shares specific properties such as being low-dimensional and spatially periodic, which may not be considered to be typical for gases or fluids that are generally composed of many interacting particles. In random Lorentz gases, or in systems with more degrees of freedom, there is no evidence that the response exhibits problems of the type as described by van Kampen.

¹¹We remark that in Ref. [Bon00] a number for the range of validity has been given for the driven periodic Lorentz gas, "possibly as small as of 10^{-20} ", whose order of magnitude is close to the original estimate by van Kampen [vK71], however, without indicating how this value was calculated for this specific system.

11.3 Summary

1. Using the mixing and chaotic periodic Lorentz gas as a simple model system saves us from adding noise in order to generate Brownian motion-like trajectories of a moving particle. This model thus provides an alternative to analyzing the interplay between subsystems and thermal reservoirs by means of stochastic Langevin equations. By furthermore making the friction coefficient velocity-dependent, under the constraint that the total kinetic energy of the system is constant at any time step, we arrive at the formulation of the *Gaussian thermostat* for the periodic Lorentz gas driven by an external electric field. Surprisingly, this combination of subsystem plus modeling of a thermal reservoir is still deterministic and time-reversible. It is also non-Hamiltonian reflecting that the resulting dynamical system is dissipative. The Gaussian thermostat is an example of a thermal reservoir that instantaneously acts in the bulk of a dynamical system.
2. For Gaussian thermostated dynamical systems in nonequilibrium situations there is an identity between the absolute value of the rate of phase space contraction and thermodynamic entropy production in terms of the Clausius entropy, respectively in terms of Joule's heat, by applying an external electric field. This identity represents a crucial link between dynamical systems quantities related to phase space contraction and thermodynamic quantities related to irreversible entropy production.
3. As a consequence of this identity the electrical conductivity is a simple function of the sum of Lyapunov exponents of the dynamical system, which is known as the *Lyapunov sum rule*. Similar formulas hold for other transport coefficients. Gaussian thermostated dynamical systems with more degrees of freedom, such as interacting many-particle systems, may furthermore exhibit a specific symmetry in the spectrum of Lyapunov exponents, which enables to split the spectrum into *conjugate pairs* of exponents all summing up to the same value. If conjugate pairs exist the Lyapunov sum rule can be drastically simplified. However, a necessary condition for this symmetry appears to be that the thermostat acts in the bulk of the system, whereas for boundary thermostats there are no such conjugate pairs. And even for bulk thermostats the precise conditions under which conjugate pairing holds are not perfectly clear and under active discussion.
4. Gaussian thermostated dynamical systems are characterized by the existence of *multifractal attractors* in the Poincaré sections of the phase space. For the Gaussian thermostated driven periodic Lorentz gas the fractal structure of the attractor is particularly determined by sequences of tangent collisions reflecting strong dynamical correlations. Under variation of the external electric field strength the topology of the attractor changes exhibiting a complex bifurcation scenario.
5. Computer simulations yield that the electrical conductivity of this model is a nonlinear function of the electric field strength, which furthermore displays irregularities on fine scales that might be of a fractal origin. Ohms law is proven to hold for sufficiently small field strengths which supposedly were not yet accessible to computer simulations. The problem of detecting the regime of linear response reminds to some of van Kampen's objections against the validity of linear response in chaotic dynamical systems.

12 The Nosé-Hoover thermostat

We construct and analyse a second fundamental form of deterministic and time-reversible thermal reservoirs known as the *Nosé-Hoover thermostat*. To motivate this scheme we need a Liouville equation that also holds for dissipative dynamical systems, which we introduce at the beginning of this chapter. We then focus on the chaos and transport properties of the Nosé-Hoover thermostated driven periodic Lorentz gas by characterizing the associated NSS. For this purpose we first check whether there holds an identity between the average phase space contraction rate and thermodynamic entropy production as it was obtained for the Gaussian thermostat. We then discuss computer simulation results for the attractor and for the electrical conductivity of the Nosé-Hoover driven periodic Lorentz gas by comparing them to their Gaussian counterparts. Finally, we briefly elaborate on subtleties resulting from the construction of the Nosé-Hoover thermostat, and we outline how this scheme can be generalized leading to a variety of additional, similar thermal reservoirs.

12.1 The Liouville equation for dissipative dynamical systems

Here we particularly follow the presentations of Refs. [Eva90b, Dor99]. For sake of simplicity we shall formally restrict ourselves to the case of a one-particle system such as the Lorentz gas. Let the position \mathbf{r} and the velocity \mathbf{v} of the point particle be defined by some equations of motion. We wish to consider an ensemble of particles moving in the same dynamical system. That is, we take a large collection of points in the accessible phase space of the system, which in general may be restricted by (geometric) boundary conditions, cp. also to Section 10.3 for related definitions. Let $\rho \equiv \rho(t, \mathbf{r}, \mathbf{v})$ be the distribution function, or probability density, associated with the ensemble of moving particles. It is the number of points of the ensemble which one can find in the phase space volume element $d\mathbf{r}d\mathbf{v}$ centered around the position (\mathbf{r}, \mathbf{v}) at time t divided by the size of this volume element and by the total number of points N of the ensemble. By integrating over the whole accessible phase space this function is properly normalized to one. Let us consider the fraction $N(t)/N$, where $N \equiv N(0)$ is the number of ensemble members at time zero while $N(t)$ is the number of points at time t . The total change of this fraction of ensemble points in a volume element V with surface A in the phase space obeys the balance equation

$$\frac{d}{dt} \frac{N(t)}{N} = \int_V d\mathbf{r}d\mathbf{v} \frac{\partial \rho}{\partial t} + \int_A d\mathbf{A} \cdot (\mathbf{F}\rho) \quad , \quad (12.1)$$

where $(\dot{\mathbf{r}}, \dot{\mathbf{v}})^* = \mathbf{F} \equiv \mathbf{F}(\mathbf{r}, \mathbf{v})$ stands for the flux given by the equations of motion of a dynamical system such as, e.g., Eqs. (11.1), and $*$ denotes the transpose. The first integral

stands for the source and the second one for the flux term. If we assume that once an ensemble of particles is chosen the number of points is conserved by the equations of motion, i.e., that there is no vanishing of points in phase space due to chemical reactions or related mechanisms, the left hand side must be zero at any instant of time. Applying Gauss' divergence theorem to the flux term, $\int_A d\mathbf{A} \cdot (\mathbf{F}\rho) = \int_V d\mathbf{r}d\mathbf{v} \nabla \cdot (\mathbf{F}\rho)$ with $\nabla := (\partial\mathbf{r}, \partial\mathbf{v})^*$, enables us to combine both integrals of Eq. (12.1) leading to the differential formulation [Pat88, Dor99, Eva90b]

$$\frac{\partial\rho}{\partial t} + \nabla \cdot (\mathbf{F}\rho) = 0 \quad (12.2)$$

or alternatively

$$\frac{d\rho}{dt} + \rho(\nabla \cdot \mathbf{F}) = 0 \quad . \quad (12.3)$$

Note that the continuity equation Eq. (12.1) formulates only the conservation of the *number of points* in phase space. Hence, Eqs. (12.2), (12.3) are valid even if the dynamical system is not phase space *volume* preserving. In turn, for Hamiltonian dynamical systems it is $\nabla \cdot \mathbf{F} = 0$ and the well-known Liouville equation for volume-preserving dynamics is recovered [Rei65, Hua87, Pat88, Dor99],

$$\frac{d\rho}{dt} = 0 \quad . \quad (12.4)$$

This equation expresses the fact that according to Hamiltonian dynamics an ensemble of points moves like an incompressible fluid in phase space, which is often referred to as the *Liouville theorem* in the literature [Rei65, Hua87].

On this occasion some historical remarks are necessary. In his original work [Lio38] Liouville did not care at all about Hamiltonian dynamics. He just started from the equations of motion for an arbitrary dynamical system and derived the evolution equation for its Jacobian determinant, from which Eq. (12.3) follows in a straightforward way. Hence, as pointed out by Andrey [And86],¹ Eq. (12.3) should rather simply be called “the Liouville equation”. However, in textbooks usually only Eq. (12.4) is derived and called “the Liouville equation” [Rei65, Hua87], probably because Liouville's work was mainly applied to Hamiltonian dynamics. Respectively, in the more specialized literature Eq. (12.3) is often denoted as “the generalized Liouville equation” [Ger73, Ste79, Ste80, And85, Ram86, Hoo99, Ram02]. In this thesis we will stick to the historically correct denotation and simply call Eq. (12.3) “the Liouville equation”.

Alternative derivations of the Liouville equation in its most general form can be found in Refs. [Ger73, Ste79, Ste80, And86, Ram02, Ser03], where we should highlight the seminal work of Gerlich [Ger73]. Recently Tuckerman et al. [Tuc97, MT99] derived a seemingly different (generalized) Liouville equation by claiming that Eq. (12.3) is not correct, see Refs. [Mun00, Tuc00] for summaries of this approach. The resulting controversy about the correct form of the Liouville equation [Hoo98a, Rei98, Tuc98b, Eva98, Tuc98a, MT99] was eventually resolved by Ramshaw [Ram02] starting from the observation that Eq. (12.3) is not covariant [Ram86]. However, covariance can be achieved by incorporating a respective coordinate transformation into the Liouville equation, which is generally a function of the metric. Along these lines the connection between Eq. (12.3) and the form of the Liouville equation considered in Refs. [Tuc97, Tuc98b, MT99] can be established. Applying this

¹see also the footnote on p.69 of Ref. [Gas98a] for a related brief historical note

transformation both formulations turn out to be completely equivalent, however, for many purposes Eq. (12.3) appears to be the more convenient choice [Ram02, Ser03].

The Gaussian thermostated driven Lorentz gas provides a simple example where the divergence in Eq. (12.3) does not disappear. It may thus be replaced by Eq. (11.6) leading to

$$\frac{\partial \rho}{\partial t} = \alpha \rho \quad . \quad (12.5)$$

By employing this equation the *Gibbs entropy production* for the Gaussian thermostated driven Lorentz gas can be computed right away, which furnishes an alternative derivation of the identity Eq. (11.8) between phase space contraction and thermodynamic entropy production [Dor99, Det00a]. This and further important implications of the Liouville equation concerning irreversibility and entropy production will be discussed in Section 13.2.

We are now set up to introduce a second fundamental type of deterministic thermal reservoirs generalizing the Gaussian scheme. For this construction the Liouville equation Eq. (12.3) will be used as a convenient starting point.

12.2 Construction of the Nosé-Hoover thermostat

12.2.1 Heuristic derivation

As a crucial property of the Gaussian thermostated driven Lorentz gas the velocity distribution of the moving particle is intimately related to the microcanonical one, that is, the system is constrained onto an energy shell in phase space. Here we introduce a generalized thermostating scheme that, under certain conditions, enables to transform the velocities of a dynamical system onto a *canonical distribution* in thermal equilibrium. Our heuristic derivation follows the presentations in Refs. [Hoo85, Hoo91]; see also a respective short note in Ref. [Hol86] and a formal generalization of this argument in Refs. [Kus90, Bul90a]. We remark that quantum mechanical formulations of deterministic and time-reversible thermal reservoirs can be obtained along the same lines [Kus93, Men01, Kus02, Men03].

Let us start again from the driven Lorentz gas equations of motion Eqs. (11.1) that already exhibit a coupling with a thermal reservoir in form of the friction variable α . Let us now assume that α is not necessarily a simple analytical function of \mathbf{v} like the Gaussian thermostat Eq. (11.4), but that it is determined by some unknown differential equation instead. Formally, the equations of motion then read

$$(\dot{\mathbf{r}}, \dot{\mathbf{v}}, \dot{\alpha})^* = \mathbf{F}(\mathbf{r}, \mathbf{v}, \alpha) \quad , \quad (12.6)$$

and the generalized Liouville equation Eq. (12.3) can be written as

$$\frac{\partial \rho}{\partial t} + \dot{\mathbf{r}} \frac{\partial \rho}{\partial \mathbf{r}} + \dot{\mathbf{v}} \frac{\partial \rho}{\partial \mathbf{v}} + \dot{\alpha} \frac{\partial \rho}{\partial \alpha} + \rho \left[\frac{\partial \dot{\mathbf{r}}}{\partial \mathbf{r}} + \frac{\partial \dot{\mathbf{v}}}{\partial \mathbf{v}} + \frac{\partial \dot{\alpha}}{\partial \alpha} \right] = 0 \quad . \quad (12.7)$$

In contrast to the Gaussian thermostat, which was designed to keep the kinetic energy constant at any time step specifically in nonequilibrium, here our strategy is to define the thermostating mechanism first in thermal equilibrium. The goal is to come up with a dissipation term that transforms the velocity distribution of the subsystem onto the canonical one. In a second step we then create a nonequilibrium situation. Here we will check whether our thermostat is able to generate a NSS, and if so we will study what its precise properties

are. In other words, our goal is to find a differential equation for α that is consistent with the existence of a canonical velocity distribution for an ensemble of subsystem particles. For this purpose we make the ansatz [Nos84a, Nos84b, Pos88, Pos89, Eva90b, Mor98, Hoo99]

$$\rho(t, \mathbf{r}, \mathbf{v}, \alpha) \equiv \text{const.} \exp \left[-\frac{v^2}{2T} - (\tau\alpha)^2 \right] \quad , \quad (12.8)$$

where both the distribution for the velocities of the subsystem and for the thermal reservoir variable α are assumed to be canonical, cp. to Eq. (10.21).² According to equipartitioning of energy T is identified as the temperature of the desired canonical distribution, and in thermal equilibrium this temperature should be identical to the temperature of the associated thermal reservoir. Furthermore, since α has a dimension of $1/\text{second}$ we needed to introduce the new quantity $\tau > 0$ with $[\tau] = s$ in order to make the exponent of the second term dimensionless.

We now combine Eq. (12.8) with the equations of motion for a single free particle, see Eqs. (11.1) with $\varepsilon = 0$. Feeding these equations as well as the ansatz for ρ into Eq. (12.3) yields for α the differential equation

$$\alpha \frac{v^2}{T} - \alpha \dot{\alpha} 2\tau^2 - 2\alpha + \frac{\partial \dot{\alpha}}{\partial \alpha} = 0 \quad . \quad (12.9)$$

This equation can be further simplified by *ad hoc* restricting to the case $\partial \dot{\alpha} / \partial \alpha = 0$. We then arrive at the simple solution

$$\dot{\alpha} = \frac{v^2 - 2T}{\tau^2 2T} \quad . \quad (12.10)$$

This differential equation for the thermostating variable α , together with the equations of motion Eqs. (11.1), defines the so-called *Nosé-Hoover thermostat* for the driven periodic Lorentz gas. The first version of such a thermostat transforming onto canonical distributions was developed by Nosé in 1984 [Nos84a, Nos84b]. His original derivation proceeded along different lines by starting from a generalized Hamiltonian formalism, see Section 12.3.2. Furthermore, it featured an at least for practical purposes spurious differential equation related to another reservoir variable, which was eliminated by Hoover [Hoo85]. This simplified version of the Nosé thermostat was coined the Nosé-Hoover thermostat [Eva85b]. In first explorations it was particularly applied to the harmonic oscillator, and the combined system was respectively called the *Nosé-Hoover oscillator* [Hoo85, Pos86, Hol86, Mar92b, Nos93, Hoo96a, Pos97, Hoo97, Lai03].

As for the Gaussian thermostat, the Nosé-Hoover scheme can be used *isokinetically* by only constraining the kinetic energy of particles, see above, or *isoenergetically* by constraining the total internal energy of soft particles consisting of kinetic plus potential energy [Mor98, Det00a, Ron02a]. It can also be adapted to drive interacting many-particle systems under nonequilibrium conditions into NSS [Nos84a, Nos84b, Pos88, Pos89, Eva90b, Hoo91, Hes96a, Mor98, Hoo99, Det00a, Mun00, Ron02a]. The results obtained from such simulations are typically well in agreement with predictions from irreversible thermodynamics and linear response theory [Eva90b, Sar98]. Hence, like the Gaussian modeling of a thermal reservoir

²For an N -particle system with d degrees of freedom the exponent compiling the total energy of subsystem and thermal reservoir reads respectively $E_{total}/T = (\sum_i v_i^2/2 + NdT\tau^2\alpha^2/2)/T$ [Nos84a, Nos84b, Pos88, Pos89, Eva90b, Mor98, Hoo99].

the Nosé-Hoover scheme became a widely accepted useful tool for performing nonequilibrium molecular dynamics computer simulations not only of simple but also of more complex fluids such as polymer melts, liquid crystals and ferrofluids [Hes96a, Hes96b, Hes97], of proteins in water and of chemical processes in the condensed matter phase [Tuc00].

12.2.2 Physics of this thermostat

First of all, like the equations of motion Eqs. (11.1), (11.4) of the Gaussian thermostated Lorentz gas the Nosé-Hoover counterparts Eqs. (11.1), (12.10) are as well deterministic and time-reversible but non-Hamiltonian. However, in contrast to the microcanonical Gaussian thermostat Nosé-Hoover was constructed for generating a canonical velocity distribution. More than Gaussian constraint dynamics, Nosé-Hoover thermostated systems may thus be considered as deterministic and time-reversible variants of Langevin dynamics, cp. Eqs. (11.1), (12.10) with Eq. (10.1).

For interacting many-particle systems the Nosé-Hoover thermostat conveniently works in thermal equilibrium [Nos84a, Eva85b, Pos89]. However, similar to the Gaussian thermostat this is not the case for the Lorentz gas without external fields, which is due to a malfunctioning of the friction coefficient related to the hard disk collisions [Rat00a]. Nevertheless we are safe in studying the driven Lorentz gas because, in analogy to the Gaussian thermostat, as soon as an electric field is added this problem disappears.

Following this comparison with Langevin dynamics one may inquire about the existence of a fluctuation-dissipation theorem such as Eq. (10.2) for equilibrium Nosé-Hoover dynamics. But as we already discussed in Section 11.1, for dissipative deterministic dynamical systems such as the Gaussian or the Nosé-Hoover thermostated Lorentz gas there is no separation between stochastic forces and dissipation matching to the respective terms in the Langevin equation Eq. (10.1). Actually, for both deterministic thermostats the velocity-dependent friction coefficient is itself a fluctuating variable, in addition to the fact that the position space Lorentz gas dynamics is also nonlinear and fluctuating. Hence, a balance equation like Eq. (10.2) between a constant friction coefficient and stochastic forces cannot exist; however, for more general fluctuation-dissipation relations in case of deterministic dynamics see Ref. [Rue99b].

In order to better understand the action of the Nosé-Hoover frictional force let us look at the ensemble averaged version of Eq. (12.10),

$$\langle \dot{\alpha} \rangle = \frac{\langle v^2 \rangle - 2T}{\tau^2 2T} . \quad (12.11)$$

If the thermostat acts properly in equilibrium the average of the fluctuations of the thermostating variable α must be zero and consequently $\langle v^2 \rangle = 2T$ on the right hand side, which corresponds to equipartitioning of energy for a system with two degrees of freedom.³ T thus serves as a control parameter representing the temperature of the thermal reservoir. Choosing some T the thermostat variable α acts accordingly in order to thermalize the subsystem onto the same temperature. Consequently, in contrast to the Gaussian thermostat the proper temperature is not attained instantaneously but with respect to an ensemble average over a canonical velocity distribution, as we stipulated with our ansatz Eq. (12.8).

³Since here we do not have Gaussian constraints we may safely assume the existence of two degrees of freedom for the subsystem.

That is, for a Lorentz gas particle the kinetic energy is allowed to fluctuate in time around a mean value of $\langle v^2 \rangle / 2$.

As in case of the Gaussian thermostat, α supplemented by the respective dynamics for this variable represents both the coupling of the subsystem to the thermal reservoir as well as the action of the thermal reservoir itself. In a way, one may think of α as a dynamical variable on which all hypothetical degrees of freedom of the thermal reservoir are projected upon just for the purpose of dissipating energy from the subsystem. Along this line of reasoning τ may then be interpreted as the *reservoir response time* with respect to exchanging energy between the subsystem and the thermal reservoir. τ thus serves as another control parameter determining the efficiency of the interaction. Note that this control parameter does not exist for the Gaussian thermostat.

Let us look at the two limiting cases of Eq. (12.8) with respect to a variation of τ : For $\tau \rightarrow \infty$ obviously $\alpha \rightarrow \text{const.}$, and one recovers the familiar case of Newton's *irreversible* equations of motion with constant Stokes' friction. On the other hand, making τ smaller implies that there is a more immediate response of the reservoir to fluctuations of the kinetic energy in the subsystem. Consequently, in the limit of $\tau \rightarrow 0$ there must eventually be instantaneous control leading back to the constraint of keeping the kinetic energy constant at any time step as formulated by the Gaussian thermostat. This can be seen by moving τ^2 from the denominator on the right hand side of Eq. (12.10) to the left hand side and performing the limit $\tau \rightarrow 0$ enforcing $v^2 = 2T$.⁴ For more detailed studies of how Nosé-Hoover dynamics depends on the value of the coupling constant τ see Refs. [Nos84b, Hoo85, Eva85b, Hol86, Nos91, Nos93, Hol95, Kus90].

The Gaussian thermostat may furthermore be classified as a feedback mechanism that is *differential* in time, reflecting the existence of an explicit functional form for the velocity-dependent friction coefficient. The Nosé-Hoover equations can be seen as an *integral* version according to the formal solution of the differential equation for the friction variable

$$\alpha(t) = \alpha(0) + \int_0^t ds \dot{\alpha}(s) \quad (12.12)$$

with $\dot{\alpha}$ being determined by Eq. (12.10) [Hol86, Hol87, Hol95]. Interestingly, the existence of these two limiting cases shows up in the specific functional form of the velocity distribution under variation of τ : For $\tau \rightarrow 0$ and small enough field strength ε this function must evidently approach a microcanonical velocity distribution $\rho(v) \sim \delta(2E - v^2)$, whereas for $\tau \rightarrow \infty$ it yields a canonical one. Consequently, between these two limiting cases there must exist a superposition of the two different shapes in form of a *crater-like* velocity distribution with a dip at the place of the former maximum of the canonical distribution.

Indeed, right this transition is depicted in Fig. 12.1 where $\rho(v_x)$ for a Nosé-Hoover thermostated driven periodic Lorentz gas is represented for three different values of τ [Rat00a]; for related results concerning another, different dynamical system thermostated by Nosé-Hoover see Ref. [Nos91]. Note the symmetry breaking in Fig. 12.1 because of the external electric field, however, one clearly recognizes the approach towards a microcanonical dis-

⁴However, note that for a vanishing external field $\varepsilon = 0$ the friction coefficient of the Gaussian thermostat Eq. (11.4) is by default zero, at least for the driven periodic Lorentz gas. Without external forces the respective solution for Nosé-Hoover should therefore also go to zero for $\tau \rightarrow 0$. Thus, in detail the relation between the Gaussian and the Nosé-Hoover thermostat is more intricate, see also the discussion in Chapter 16.

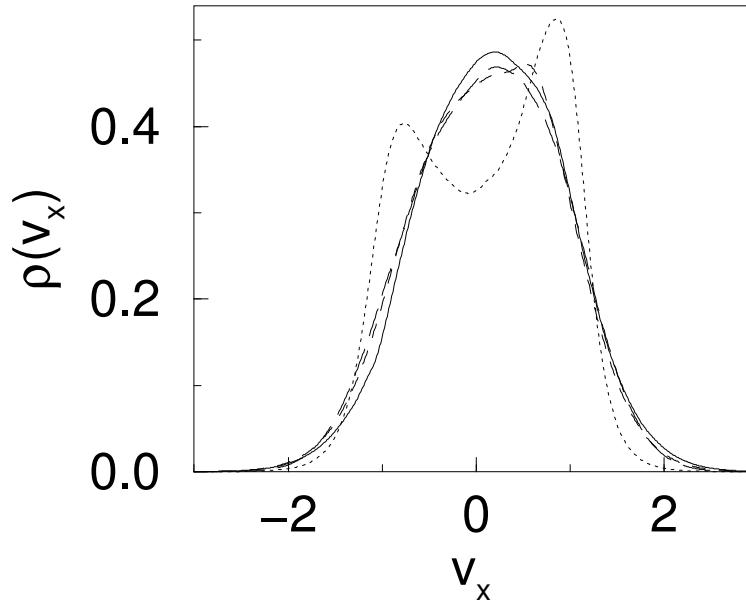


Figure 12.1: Velocity distributions $\varrho(v_x)$ for an ensemble of moving point particles in the thermostated driven periodic Lorentz gas for an electric field of strength $\varepsilon = 0.5$, which is parallel to the x -axis, at temperature $T = 0.60029$: Nosé-Hoover thermostat with a reponse time of the thermal reservoir of $\tau^2 = 0.01$ (dotted curve), $\tau^2 = 1$ (dashed curve), $\tau^2 = 1000$ (long dashed curve) in comparison to the application of the deterministic boundary thermostat (“thermostating by deterministic scattering”) discussed in Chapter 15 (solid curve). Note the transition from a microcanonical-like to a canonical distribution under variation of τ . The figure is from Ref. [Rat00a].

tribution for $\tau \rightarrow 0$.⁵ We will come back to a more explicit discussion of this interesting point in Chapter 16, where it will be shown that crater-like velocity distribution functions that are very similar to the one discussed here play an important role for so-called active Brownian particles which are thought to model, among others, biological cell motility.

12.3 Properties of the Nosé-Hoover thermostat

12.3.1 Fundamental relations between chaos and transport

For the Gaussian thermostated driven Lorentz gas the crucial relation linking thermodynamics to dynamical systems theory was the identity Eq. (11.8) between the average phase space contraction rate and the thermodynamic entropy production in form of Joule’s heat. Let us now check whether the Nosé-Hoover thermostat fulfills this identity as well. For this purpose we calculate the energy balance between subsystem and thermal reservoir [Pos88, Rat00a] by starting from the Hamiltonian for the combined system, see the exponent in Eq. (12.8),

$$H = v^2/2 + T\tau^2\alpha^2 \quad . \quad (12.13)$$

⁵Curiously, in case of *non-ergodic* Nosé-Hoover dynamics similar microcanonical-like and canonical-like distributions can be obtained with respect to different choices of initial conditions for the ensemble of particles, see the preprint of Ref. [Rat00a] for an example.

If the system is properly thermostated yielding a NSS, the average of the time derivative of the total energy must be zero, $\langle dH/dt \rangle = 0$. Differentiating Eq. (12.13) and replacing the derivatives by the equations of motion Eqs. (11.1), (12.10) yields

$$\frac{\langle \boldsymbol{\varepsilon} \cdot \mathbf{v} \rangle}{T} = 2 \langle \alpha \rangle \quad (12.14)$$

The right hand side equals minus the average phase space contraction rate κ defined by Eq. (11.5), whereas the left hand side is obviously Joule's heat. We have thus corroborated the identity Eq. (11.8) for Nosé-Hoover dynamics.

Alternatively, in order to check for the identity one may start directly from the Nosé-Hoover equations of motion Eqs. (11.1), (12.10). Multiplying the differential equation for the velocity with \mathbf{v} and replacing the velocity squared on the right hand side by Eq. (12.10) one arrives at

$$\dot{\mathbf{v}} \cdot \mathbf{v} = \boldsymbol{\varepsilon} \cdot \mathbf{v} - \alpha(\dot{\alpha}\tau^2 2T + 2T) \quad . \quad (12.15)$$

One may now collect all terms related to fluctuations on the left hand side by considering their statistical averages,

$$\left\langle \frac{d}{dt} \left(\frac{1}{2}v^2 + \tau^2 T \alpha^2 \right) \right\rangle = \langle \boldsymbol{\varepsilon} \cdot \mathbf{v} - \alpha 2T \rangle \quad . \quad (12.16)$$

The left hand side is just identical to the average of the Hamiltonian Eq. (12.13) and must be zero in a NSS, see above, hence the right hand side yields again the identity. This derivation is useful if the Hamiltonian related to the thermostat is not known in advance, see Section 14.3 for some examples.

Based on the identity Eq. (12.14) the Lyapunov sum rule can be derived in the same way as explained in Section 11.2.2. For four nontrivial phase space variables it reads

$$\sigma(\varepsilon) = -\frac{T}{\varepsilon^2} \sum_{i=1}^4 \lambda_i(\varepsilon) \quad . \quad (12.17)$$

Hence, with respect to relations between chaos and transport the Nosé-Hoover thermostat belongs to precisely the same class of thermal reservoirs as the Gaussian one.

12.3.2 + Generalized Hamiltonian formalism for the Nosé-Hoover thermostat

A crucial feature of Hamiltonian systems is that the dynamics is phase space volume preserving, which follows from their symplectic structure [Mei92, Abr94]. On the other hand, as was shown for the Gaussian thermostat in Section 11.2.1 and as we just verified for the Nosé-Hoover thermostat, the application of such deterministic thermostating mechanisms leads to an average phase space contraction in nonequilibrium. From that point of view it is surprising that for Gaussian and Nosé-Hoover dynamics a *generalized Lagrangian and Hamiltonian formalism* exists in which this dynamics is phase space volume preserving. Here we outline some main ideas of the Hamiltonian approach for the example of the isokinetic Nosé-Hoover thermostat.

Let us consider the very general case of a subsystem where a particle of unit mass moves under the influence of a potential $u(\mathbf{x})$. Let the microscopic dynamics of this particle be

described by the phase space coordinates (\mathbf{r}, \mathbf{v}) . The dynamics of the thermal reservoir is modeled by only one degree of freedom in terms of the coordinates (r_0, v_0) . All these representations may be called *physical* coordinates, since (\mathbf{r}, \mathbf{v}) represents the actual position and the velocity of some particle. For the *decoupled* system the formal Hamiltonian is

$$H_0(\mathbf{r}, \mathbf{v}, r_0, v_0) = E(\mathbf{v}, v_0) + U(\mathbf{r}, r_0) \quad , \quad (12.18)$$

where $E(\mathbf{v}, v_0) = m\mathbf{v}^2/2 + Qv_0^2/2$ stands for the kinetic energy of particle plus reservoir and $U(\mathbf{r}, r_0) = u(\mathbf{r}) + 2Tr_0$ for the potential energy of both systems. In formal analogy to the particle's kinetic energy, the new quantity Q is sometimes called the *mass* of the reservoir, and T is identified with the reservoir temperature.⁶ The Hamiltonian equations of motion for the decoupled system then read

$$\begin{aligned} \dot{\mathbf{r}} &= \mathbf{v} \\ \dot{\mathbf{v}} &= -\frac{\partial u}{\partial \mathbf{r}} \\ \dot{r}_0 &= Qv_0 \\ \dot{v}_0 &= -2T \quad . \end{aligned} \quad (12.19)$$

The problem is now two-fold: firstly, to find a Hamiltonian that generalizes Eq. (12.18) in suitably representing the *coupled* system, and secondly, to derive the Nosé-Hoover equations of motion, such as the special case Eqs. (11.1), (12.10) for the driven Lorentz gas, from this new Hamiltonian. In a slightly modified setting, this problem first appeared in Nosé's groundbreaking work [Nos84a, Nos84b] leading to the formulation of the so-called Nosé Hamiltonian. Here we follow a simplified approach as it was proposed later on in Refs. [Det97a, Cho98].

Since the Nosé-Hoover equations of motion are not Hamiltonian it is clear that a Hamiltonian formulation of this dynamics can only be achieved by choosing a new set of *generalized* coordinates, for which we may write (\mathbf{R}, \mathbf{V}) in case of the subsystem and (R_0, V_0) in case of the reservoir. Now we implement the so-called *exponential coupling ansatz* for the Hamiltonian in these generalized coordinates,

$$H(\mathbf{R}, \mathbf{V}, R_0, V_0) := e^{-R_0} E(\mathbf{V}, V_0) + e^{R_0} U(\mathbf{R}, R_0) \quad . \quad (12.20)$$

These exponential prefactors define a *nonlinear, multiplicative coupling* between subsystem and thermal reservoir in generalized coordinates. Physically speaking, they suitably rescale the total energy of the system thus serving to keep the energy of the full system constant on average, whereas in nonequilibrium it would increase to infinity otherwise. The different signs of the exponents are adjusted to the different types of kinetic and potential energy. We can now derive Hamilton's equations of motion from this new Hamiltonian to

$$\begin{aligned} \dot{\mathbf{R}} &= e^{-R_0} m \mathbf{V} \\ \dot{\mathbf{V}} &= -e^{R_0} \frac{\partial u}{\partial \mathbf{R}} \\ \dot{R}_0 &= e^{-R_0} Q V_0 \\ \dot{V}_0 &= 2(e^{-R_0} E(\mathbf{V}, V_0) - e^{R_0} T) \quad , \end{aligned} \quad (12.21)$$

⁶Strictly speaking the choice of the potential term for the reservoir, and fixing the number of degrees of freedom associated with it, is a bit more subtle [Cho98, Mor98].

where we have imposed that $H(\mathbf{R}, \mathbf{V}, R_0, V_0) \equiv 0$. Matching the first two equations to the corresponding ones in physical coordinates Eqs. (12.19) suggests the following transformation between physical and generalized coordinates of the subsystem,

$$\begin{aligned}\mathbf{R} &= \mathbf{r} \\ \mathbf{V} &= e^{R_0} \mathbf{v} \quad .\end{aligned}\tag{12.22}$$

Making the same choice for the reservoir coordinates,

$$\begin{aligned}R_0 &= r_0 \\ V_0 &= e^{R_0} v_0 \quad ,\end{aligned}\tag{12.23}$$

we obtain a complete set of equations for transforming between physical and generalized coordinates. Identifying $Q \equiv 2T\tau^2$ and $\alpha \equiv v_0 Q$ the Nosé-Hoover equations Eqs. (11.1), (12.10) for the driven Lorentz gas are precisely recovered from Eqs. (12.21). Let us emphasize at this point that the transformation between the different coordinates given by Eqs. (12.22), (12.23) is strictly *noncanonical* not preserving the phase space volume. Therefore, one should carefully distinguish between traditional Hamiltonian formulations of classical mechanics and the *generalized* Hamiltonian formalism outlined above.

The idea to use a generalized Hamiltonian formalism in order to define the action of a thermal reservoir was pioneered by Nosé [Nos84a, Nos84b] who constructed his thermostating mechanism along these lines. In Refs. [Nos91, Nos93, Hoo85, Eva85b, Pos86, Eva90b] this scheme was applied to different types of subsystems. Later on Dettmann and Morriss showed that there also exist generalized Hamiltonian formulations for the Gaussian isokinetic [Det96b] and isoenergetic [Det99a] thermostat, see Ref. [Hoo88a] for a pre-version of this approach. They also came up with a modified Nosé Hamiltonian leading more straightforwardly to the Nosé-Hoover equations than starting from Nosé's original formulation [Det97a, Hoo99], as is sketched in the derivation above. The generalized Lagrangian approach was outlined by Choquard in Ref. [Cho98], see also this reference as well as Refs. [Mor98, Det00a] for nice summaries concerning the subject of this section. There are furthermore interesting studies to formulate non-Hamiltonian dynamics by using Lie-Poisson [Kus92], generalized Poisson [Ser01, Ser03], or Dirac brackets [Ron02a]. We remark that the symplectic properties of these generalized Hamiltonians appear to be intimately related to the validity of the conjugate pairing rule discussed in Section 11.2.2.

12.3.3 Chaos, fractal structures, and transport

As we have shown in Sections 11.2.1 and 12.3.1, both the Gaussian and the Nosé-Hoover thermostated driven Lorentz gas exhibit an identity between the average phase space contraction rate and thermodynamic entropy production. For the Nosé-Hoover case we now discuss further chaos and transport properties, which are the fractality of the corresponding attractor, the structure of the associated bifurcation diagram and the response to an electric field in terms of the field-dependent conductivity. Particularly, we elaborate on similarities and differences of these properties in comparison to the respective figures shown for the Gaussian thermostat. The computer simulation results for the Nosé-Hoover thermostated driven periodic Lorentz gas presented here are from Ref. [Rat00a].

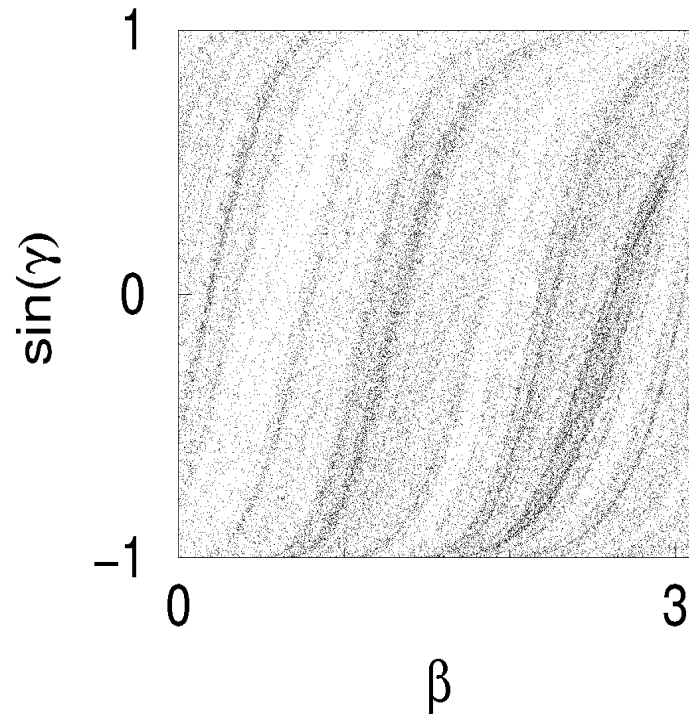


Figure 12.2: Attractor for the Nosé-Hoover thermostated periodic Lorentz gas driven by an electric field of strength $\varepsilon = 1$ which is parallel to the x -axis. β and $\sin \gamma$ are the same as in Fig. 11.2 and are also defined in Fig. 11.1. The temperature is $T = 0.7740645$. The reservoir coupling parameter τ , see Eq. (12.10), has the value 0.1. The results are from Ref. [Rat00a].

Fig. 12.2 depicts a projection of the attractor of the Nosé-Hoover thermostated driven periodic Lorentz gas onto the phase space in Birkhoff coordinates.⁷ Some repeated folding in phase space is clearly visible indicating that, as in case of the Gaussian thermostat, most probably this attractor is again of a multifractal nature. However, for Nosé-Hoover yet no values for a (fractal) dimension quantitatively assessing this structure were computed.⁸ By comparing this attractor to the one obtained from Gaussian thermostating Fig. 11.2 one realizes that the structure of both sets is essentially the same. This is not too surprising since both systems share the same geometry, and as we discussed in Section 11.2.3 the main features of this structure are induced by the geometry of the scatterers. That the Nosé-Hoover thermostat attempts to transform the system onto a canonical distribution explains why the attractor related to the Nosé-Hoover thermostat appears to be a smoothed-out version of the Gaussian counterpart. These results suggest that the appearance of fractal attractors is also typical for Nosé-Hoover thermostated systems. Numerical computations of fractal dimensionality losses in many-particle systems thermostated by Nosé-Hoover confirm

⁷Note that, in contrast to the Gaussian thermostated driven periodic Lorentz gas, Fig. 12.2 does not represent a Poincaré surface of section: For Nosé-Hoover the kinetic energy is not kept constant but fluctuates, hence this plot is composed of points with different absolute values of the velocity of the colliding particle.

⁸but see Section 15.4.2 for a very similar attractor for which the Kaplan-Yorke dimension was found to be fractal

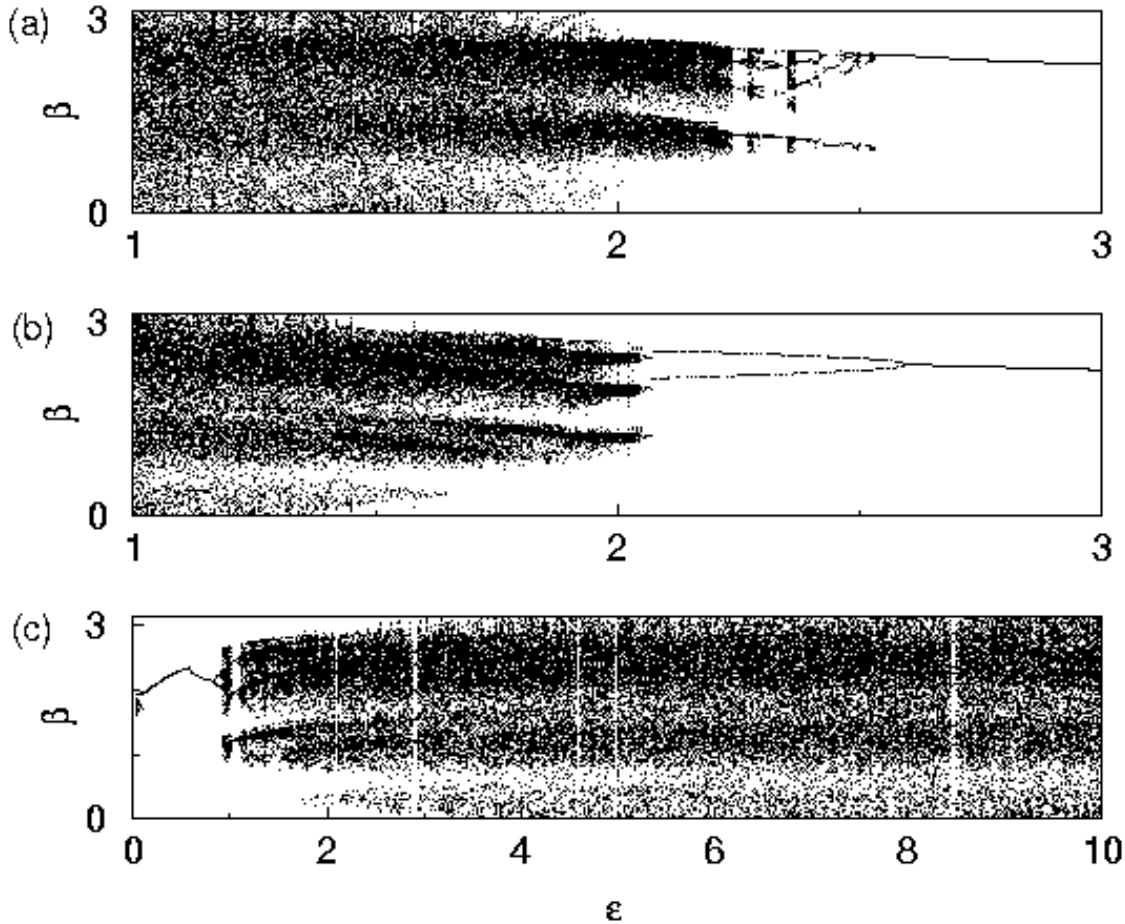


Figure 12.3: Bifurcation diagrams for the Nosé-Hoover thermostated periodic Lorentz gas driven by an electric field of strength ε which is parallel to the x -axis. β is defined in Fig. 11.1. The temperature is fixed to $T = 0.5$ and the values of the reservoir coupling parameter τ , see Eq. (12.10), are: (a) $\tau = 0.1$, (b) $\tau \simeq 31.6$ ($\tau^2 = 1000$) and (c) the dissipative limit of $\tau \rightarrow \infty$ corresponding to a constant friction coefficient α whose value was chosen to be 1. The figure is from Ref. [Rat00a].

this statement [Hol87, Pos88, Pos89, Aok02, Kus02, Hoo02b, Pos03].

Fig. 12.3 contains bifurcation diagrams for the Nosé-Hoover thermostated driven periodic Lorentz gas at three different values of the reservoir coupling constant τ , see Eq. (12.10). For quick response of the reservoir, $\tau \ll 1$, the attractor is phase space filling up to $\varepsilon < 2$, which is reminiscent of the results for the Gaussian thermostated Lorentz gas presented in Fig. 11.3. Note that Fig. 11.3 depicts the angle θ as a function of the field strength ε , whereas Fig. 12.3 displays the angle β , respectively. However, both bifurcation diagrams exhibit qualitatively the same behavior. This is in agreement with the discussion of Section 11.2.2 where we argued that the Nosé-Hoover thermostat yields Gaussian constraint dynamics in the limit of $\tau \rightarrow 0$.

Matching to a naive physical reasoning, by making the response time of the reservoir larger the attractor collapses onto periodic orbits at smaller field strengths than for smaller response times, see Fig. 12.3 (b). However, in detail the situation is much more intricate [Rat00a], as is already indicated by Fig. 12.3 (c) that displays the dissipative limit of

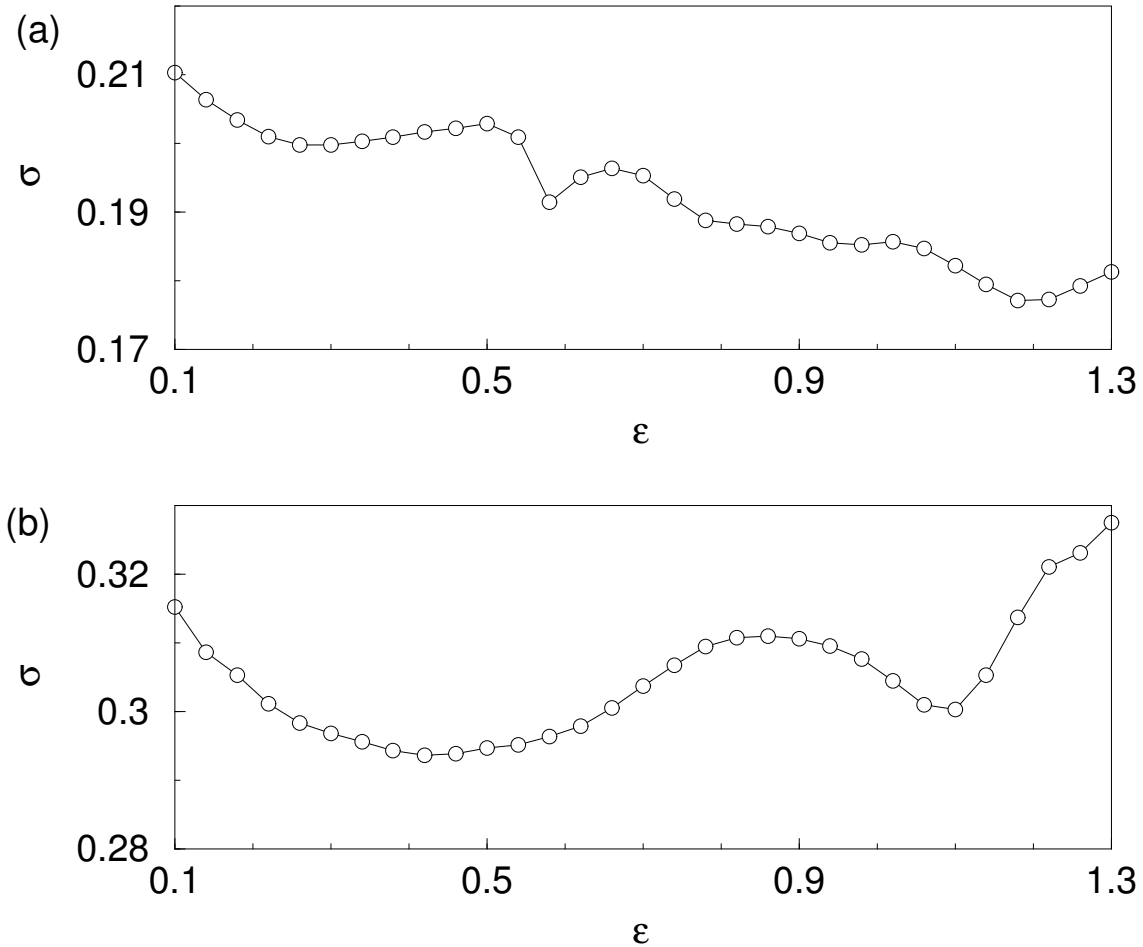


Figure 12.4: Electrical conductivity $\sigma(\epsilon)$ for the Nosé-Hoover thermostated periodic Lorentz gas driven by an electric field of strength ϵ which is parallel to the x -axis. The temperature is $T = 0.5$ and the values of the reservoir coupling parameter τ , see Eq. (12.10), are: (a) $\tau = 0.1$ and (b) $\tau \simeq 31.6$ ($\tau^2 = 1000$). The numerical uncertainty of each point is less than the symbol size. The figure is from Ref. [Rat00a].

$\tau \rightarrow \infty$. Here the bifurcation diagram depends on the value for the constant friction coefficient α . In any case, for all values studied numerically one observes a kind of inverted bifurcation scenario compared to the Gaussian thermostated model and to Figs. 12.3 (a) and (b) in that the attractor starts with periodic orbits and covers the whole accessible phase space only for higher field strengths [Rat00a]. Fig. 12.3 thus shows that for the Nosé-Hoover thermostated driven periodic Lorentz gas the specific structure of the fractal attractor sensitively depends on the choice of the reservoir coupling parameter τ ; see also Refs. [Nos84b, Hoo85, Eva85b, Hol86, Nos91, Nos93, Hol95, Kus90] for studies concerning the variation of τ in other systems and for the impact on dynamical systems properties.

As one might suspect already with respect to these bifurcation diagrams, there is no unique result for the field-dependent electrical conductivity $\sigma(\epsilon)$ at different values of the response time τ either, not even for small field strengths $\epsilon \ll 2$. Fig. 12.4 presents computer simulation results for the two parameter values of τ studied in Figs. 12.3 (a) and (b). The conductivity for $\tau = 0.1$ looks like a smoothed-out version of the Gaussian thermostat con-

ductivity depicted in Fig. 11.4, whereas the curve at $\tau \simeq 31.6$ appears to be more stretched out along the ε -axis. In the latter case it is not even clear whether the conductivity is globally decreasing or increasing. There is little to say concerning the validity of the Einstein relation Eq. (11.12) in the limits of $\tau > 0$ and $\varepsilon \rightarrow 0$ as discussed for the Gaussian version in Section 11.2.4, since the Nosé-Hoover thermostat does not work properly for the Lorentz gas in thermal equilibrium, see Section 12.2.2. Hence, the field-free diffusion coefficient cannot be computed independently.

That both field-dependent Nosé-Hoover conductivities are significantly less irregular than the Gaussian thermostat result of Fig. 11.4 may be understood with respect to the more “stochastic” nature of the Nosé-Hoover thermostat. According to its definition it modifies the billiard dynamics more profoundly than in case of the Gaussian constraint by transforming onto canonical velocity distributions, see again Fig. 12.1 for the probability densities at these parameters. Nevertheless, both conductivities still exhibit pronounced irregularities in form of non-monotonocities, and there are no indications for a regime of linear response, at least not in the numerically accessible region of $\varepsilon > 0.1$. In other words, even the Nosé-Hoover thermostat featuring a canonical velocity distribution does not lead to a more profound appearance of a regime representing Ohm’s law.

In summary, from a statistical mechanical point of view we have the rather unpleasant result that not only dynamical systems properties such as bifurcation diagrams but also transport properties such as the field-dependent electrical conductivity of the deterministically thermostated, driven periodic Lorentz gas strongly depend on details of the specific way of thermostating. However, as in case of the discussion of van Kampen’s criticism in Section 11.2.4 one may speculate that this is rather a consequence of the small number of degrees of freedom and of the spatial periodicity of this model.

12.4 + Subtleties and generalizations of the Nosé-Hoover thermostat

12.4.1 Necessary conditions and generalizations of this scheme

As we briefly discussed in Sections 11.1 and 12.2.2, both the Gaussian and the Nosé-Hoover thermostat do not work properly for the periodic Lorentz gas without external fields: In this case the Gaussian thermostat is trivially non-existent, since the kinetic energy of the moving particle is conserved by definition anyway, whereas the Nosé-Hoover thermostat does not act appropriately because of the hard disk collisions. Controlling the two velocity variables *separately* by Nosé-Hoover eliminates this problem [Rat00a]. In any case, as outlined in the previous sections for both thermostats a small electric field resolves these intricacies leading to well-defined NSS. Apart from that, for interacting many-particle systems it was confirmed numerically that both the Gaussian [Hoo82, Eva83b, Pos88] and the Nosé-Hoover thermostat [Nos84a, Eva85b, Pos89] work correctly even in thermal equilibrium. These examples suggest that the thermostated subsystem must fulfill certain necessary conditions in order attain canonical velocity distributions.

In the literature this problem became well-known by studying both the *Nosé-Hoover oscillator*, which is a harmonic oscillator subject to a Nosé-Hoover thermostat, and a respectively thermalized particle moving in a double-well potential. Already in early computer simulations of the Nosé-Hoover oscillator it was observed that this system did not attain a

canonical velocity distribution in thermal equilibrium [Hoo85, Pos86, Hol86]. This is due to the fact that the unperturbed harmonic oscillator is non-chaotic and perfectly integrable. Hence, under application of some thermal reservoir its regular phase space structure may just be getting deformed, and there is no reason why the resulting subsystem should become fully ergodic.

However, if such a previously regular subsystem is not driven to ergodic behavior by the action of some thermostat the whole phase space will not be sampled appropriately. As a consequence, the resulting velocity distribution may strongly depend on initial conditions and is typically not the canonical one [Hoo85, Pos86, Hol86, Kus90, Bul90a, Ham90, Hoo91, Win92, Mar92b, L'H93, Nos93, Win95, Hoo96a, Hoo97, Mun00, Liu00, Hoo01, Ser01, Lai03]. The same applies to the Nosé-Hoover thermostated double-well potential [Kus90, L'H93, Win95, Bar03b]. Jellinek and Berry [Jel88a, Jel89] and Kusnezov et al. [Kus90, Bul90a] thus emphasized that chaos and ergodic behavior are necessary conditions in order to thermalize a subsystem onto a canonical velocity distribution. This indicates that a thermostated subsystem should strictly speaking be mixing [Arn68, Sch89, Gas98a, Dor99] implying ergodicity and, under rather general conditions, also chaotic behavior [Dev89, Ban92].

These difficulties motivated the construction of a large variety of generalizations of the original Nosé-Hoover thermostat [Hoo89a, Kus90, Bul90a, Bul90b, Ham90, Hoo91, Win92, Mar92b, L'H93, Win95, Hoo96a, Pos97, Hoo97, Bon99, Mun00, Liu00, Lai03, Bra00a, Bra00b, Hoo01, Ser01, Bar03b]. The formal basis for these efforts was laid out again by Jellinek and Berry [Jel88a, Jel88b] and by Kusnezov et al. [Kus90, Bul90a]: Jellinek and Berry showed that there is the additional freedom of changing the *multiplicative* coupling between subsystem and thermal reservoir in generalized coordinates while still being consistent with Nosé's basic idea of transforming onto canonical distributions.⁹ Kusnezov et al., in turn, pointed out that further *additive* contributions to Hamilton's equations of motion in generalized variables, see Eqs. (12.21), are possible, again without contradicting the existence of canonical velocity distributions. Both approaches will typically lead to thermostated equations of motion that are still time-reversible but more nonlinear than the ones corresponding to the original Nosé-Hoover scheme. Thus Nosé-Hoover represents just one choice of infinitely many for modeling a deterministic thermal reservoir transforming onto canonical distributions.

Starting from this important conclusion alternatives to Gaussian and Nosé-Hoover dynamics were explored by many authors. Their strategy was to improve the Nosé-Hoover scheme by constructing a thermostat that is able to conveniently thermalize the harmonic oscillator, or the double-well problem, onto a canonical velocity distribution in equilibrium. A straightforward generalization along the lines of Nosé-Hoover is the thermalization of higher even moments of the subsystem's velocity distribution onto the canonical ones by means of additional thermostating variables [Hoo89a, Jel89, Hoo96a, Pos97, Hoo97, Liu00]. Another formal option is to thermalize the position coordinates of a moving particle leading to the cubic coupling scheme [Kus90, Bul90a]. Enforcing the virial theorem, Hamilton used a linear scaling of the position coordinates [Ham90], which later on was combined with some multiplicative coupling [L'H93]. A thermalization of odd and even particle velocities, partly supplemented by using higher powers of the corresponding friction coefficients, was

⁹In more detail, starting from the Nosé Hamiltonian they showed that changing the scaling rules between the physical and the generalized variables, cp. to Eqs. (12.22), (12.23), plus possibly also changing a time scaling between physical and generalized time (that we did not discuss in Section 12.3.2) is not at variance with canonical velocity distributions being the solutions of the respective Liouville equation Eq. (12.3).

also explored and was argued to represent a deterministic, time-reversible analogue of the stochastic Langevin equation [Bul90b]. More recently, a directional thermostat called *twirler* stirring the angular momentum of a moving particle was introduced and applied in suitable combination with Gaussian and Nosé-Hoover thermostats [Hes02, Hes03].

Another scheme that became rather popular is the Nosé-Hoover chain thermostat [Mar92b, Tuc00] that couples the differential equation for the Nosé-Hoover friction coefficient additively to another Nosé-Hoover friction coefficient, and so on. However, this solution was assessed to be unstable out of equilibrium [Eva98, Bra00a] leading to another modification of it [Bra00a]. Some multiplicative extensions of Nosé-Hoover along the lines of Jellinek's formalism have been worked out by Winkler et al. [Win92, Win95] and became further amended in Ref. [Bra00b]. Another, in a way, multiplicative variant was discussed in Ref. [Ser01].

We finally mention the so-called Nosé-Poincaré method representing a scheme that is in-between the original approaches by Nosé and Nosé-Hoover. The resulting dynamics is identical to Nosé-Hoover, however, it is generated by symplectic equations of motion that enable the application of symplectic integration algorithms, which considerably increases the numerical precision [Bon99, Bar03b]. A further extension of this approach allowing to model generalized types of Nosé-Hoover dynamics along these lines, which appears to share quite some similarities with Jellinek's ideas [Jel88a, Jel88b], was recently proposed in Ref. [Lai03].

It is not the purpose of this work to give a full account of the specific physical and numerical advantages and disadvantages of all these different thermostating schemes. Here we may refer, e.g., to Refs. [Jel88a, Hoo96a, Pos97, Hoo97, Bra00a] that partly review and criticize these more recent methods. Following Jellinek, Branka and Wojciechowski [Bra00b] particularly endeavored to systematically explore the numerical practicability and efficiency of these different classes of thermostats. They arrived at essentially ruling out many of the up to now existing solutions. Further, more physical constraints contradicting some of the methods mentioned above will be briefly summarized in the following section.

However, in our view one may even go so far to question the philosophy underlying most of these novel constructions in that a 'good' thermostat should, by all means, enforce a canonical velocity distribution even for regular dynamical systems such as the harmonic oscillator. The other way around, one may argue that the harmonic oscillator is rather unsuited to be properly thermalized at all just because of its inherent regularity. Correspondingly, a successful transformation of this dynamics onto a canonical velocity distribution indicates that the original dynamics of this system is profoundly destroyed according to the action of the thermal reservoir. This raises the question to which extent the resulting dynamics represents merely the action of the thermostat and whether anything is left at all of the original characteristics of the previously regular subsystem. Nevertheless, we suspect that for practical computational purposes it is still desirable to have a thermostat at hand which is capable to always create a canonical velocity distribution irrespective of the detailed properties of the original dynamical system to which it is applied.

This discussion clearly demonstrates that the world of deterministic and time-reversible thermostats does not only consist of Gaussian and Nosé-Hoover thermostats. Obviously, there exists a microcosmos of variants of them. This should be taken into account if one attempts to come to general conclusions concerning the second law of thermodynamics and the universality of chaotic and transport properties of NSS based on the analysis of Gaussian and Nosé-Hoover thermostats only.

12.4.2 Applying thermal reservoirs to nonequilibrium situations

In Section 10.3 we have argued that thermal reservoirs should generally be constructed in equilibrium situations. In this case the statistical ensembles are well-defined and the corresponding velocity distribution functions for subsystem and thermal reservoir are known exactly. After their definition in thermal equilibrium one may apply these reservoirs for thermalizing a subsystem under nonequilibrium constraints, by expecting that the respective thermostat still works sufficiently well such that a proper NSS is created. One may now learn something new about the NSS resulting for a particular subsystem by analyzing the corresponding nonequilibrium distribution functions as well as the associated chaos and transport properties, which are generally not known in advance.

However, first of all, it is not guaranteed that a thermal reservoir which properly acts in thermal equilibrium also functions in nonequilibrium by generating a NSS. Actually, it appears that most of the generalizations of the Nosé-Hoover thermostat listed above have only been tested in thermal equilibrium so far. Some of them have already been criticized for not working properly under nonequilibrium constraints [Eva98, Bra00a, Bra00b]. Apart from that, only a few studies of nonequilibrium situations are available for these generalized reservoirs [Pos97, Hoo97, Bra00a, Bra00b]. The same applies to the chaotic dynamical properties of subsystems connected to these different thermal reservoirs even in thermal equilibrium, see only Refs. [Kus90, Mar92b, Pos97, Hoo01] for results of some specific cases.

Secondly, a thermal reservoir should always remain in thermal equilibrium, even if the subsystem is under nonequilibrium constraints, and it should only control the temperature of the subsystem, or possibly respective higher moments of it. Consequently, a thermal reservoir should only act on the even moments of the velocity distribution of a subsystem. If a thermal reservoir were defined to also control odd moments of the velocity its action goes beyond simple temperature control and may change the dynamics of the subsystem profoundly. For example, in the driven periodic Lorentz gas the first moment of the velocity yields the current of the subsystem in nonequilibrium. Thus, a thermostat that constrains this quantity would simply pre-determine the current.¹⁰ In the same vein, a thermal reservoir acting onto position coordinates may pre-determine, or at least profoundly influence, the respective moments of the position coordinates hence affecting transport coefficients like diffusion and higher-order Burnett coefficients. Consequently, on the basis of physical grounds one may wish to constrain the action of thermal reservoirs to even velocity moments only. If one follows this argumentation, this already rules out schemes such as the ones presented in Refs. [Kus90, Bul90b, Bul90a, Ham90, L'H93].

In conclusion, all what one can demand is that a thermal reservoir properly acts in a thermal equilibrium situation by thermalizing a subsystem onto a pre-determined velocity distribution. In nonequilibrium the general requirement should be the existence of a NSS at a certain temperature, whose properties as resulting from the action of this thermal reservoir may then be studied respectively.

¹⁰Note, however, that a thermal reservoir may be defined such that it is comoving with the current, in order to thermalize the subsystem onto the proper temperature in the comoving frame; see Refs. [Pos88, Sea98] and also the discussion of a thermostated shear flow in Section 15.5, respectively Refs. [Wag99, Wag00].

12.5 *Summary

1. Starting from the conservation of the number of points in phase space we have derived the Liouville equation for dissipative dynamical systems. The Hamiltonian version of this Liouville equation, which typically appears in textbooks, is obtained from it under the additional assumption of conservation of phase space volume.
2. By employing the general form of the Liouville equation and by requiring that canonical distributions for the velocities of a subsystem and for a reservoir variable exist, we arrived at a simple differential equation determining the velocity-dependent friction coefficient. This equation defines the action of the *Nosé-Hoover thermostat*, supplemented by a respective friction term in the original equations of motion of the subsystem.

In complete analogy to the Gaussian thermostat, Nosé-Hoover thermostated equations of motion are deterministic and time-reversible but non-Hamiltonian. However, in contrast to the Gaussian reservoir the Nosé-Hoover scheme, by construction, attempts to transform the subsystem velocities onto a canonical distribution in thermal equilibrium. Hence, it yields a dynamics that is more similar to Langevin's theory than the one resulting from the Gaussian constraint of constant energy. Another difference of the Nosé-Hoover thermostat compared to the Gaussian one is the appearance of an additional control parameter that may be interpreted as the response time of the thermal reservoir regarding its interaction with a subsystem. In case of infinitely slow response the Stokes friction coefficient is recovered, whereas for infinitesimally quick response the Gaussian constraint is approached. A variation of this control parameter changes the shapes of the corresponding velocity distributions that may accordingly be composed of superpositions of microcanonical and canonical densities.

3. The Nosé-Hoover thermostat belongs to the same class of deterministic and time-reversible thermal reservoirs as the Gaussian one as far as an identity between the average rate of phase space contraction and thermodynamic entropy production is concerned. Respectively, there is also an analogous relation between transport coefficients and Lyapunov exponents for Nosé-Hoover dynamics.

For both thermal reservoirs there exist generalized Hamiltonian and Lagrangian formulations. For the isokinetic Nosé-Hoover thermostat we have outlined how to derive the respective equations of motion from a Hamiltonian in generalized variables via non-canonical transformations.

Like the Gaussian thermostated driven periodic Lorentz gas, the Nosé-Hoover version is as well characterized by a fractal attractor of a similar type. The specific structure of this attractor depends on the value of the reservoir response time. For large enough response times the bifurcations displayed by this fractal attractor are typically very different from the ones observed for the Gaussian reservoir. The same applies to the field-dependent electrical conductivities in case of Nosé-Hoover, which still show irregularities on fine scales and no indication of linear response in the numerically accessible regime of the field strength.

4. Finally, we have summarized problems with Gaussian and particularly with Nosé-Hoover thermostats in equilibrium and nonequilibrium situations. For regular dynam-

ical systems such as the harmonic oscillator or a particle moving in a double-well potential it is well-known that the standard Nosé-Hoover thermostat is not able to thermalize these systems onto canonical velocity distributions in thermal equilibrium. A necessary condition is that the thermostated system must be mixing, respectively chaotic and ergodic. In order to achieve this goal the Nosé-Hoover scheme can be generalized yielding more nonlinear equations of motion than the original method. However, such “stronger” thermostating forces affecting more profoundly the original dynamics of the subsystem to be thermostated pose the question to which extent the original dynamics of the subsystem still plays a role at all. In any case, our discussion clearly shows that a great variety of deterministic and time-reversible thermal reservoirs exists. This fact one may particularly want to take into account with respect to suspected universalities of NSS as concluded from applications from Gaussian and Nosé-Hoover thermostats only.

13 Summary and criticism of Gaussian and Nosé-Hoover thermostats

The approach to nonequilibrium transport reviewed in the previous chapters of this part yields NSS on the basis of non-Hamiltonian equations of motion. This dynamics results from employing deterministic and time-reversible thermal reservoirs that control the temperature of a subsystem under nonequilibrium constraints. The Gaussian and the Nosé-Hoover thermostat constructed before serve as two famous examples of such mechanisms. Both reservoirs have been applied to the periodic Lorentz gas driven by an external electric field, and the resulting NSS have been analyzed with respect to their chaos and transport properties. In the following we focus onto what we consider to be generic properties of NSS associated with Gaussian and Nosé-Hoover dynamics. Our summary is accompanied by a critical discussion of these fundamental features as far as a possible universal description of NSS, irrespective of the specific type of thermostat, is concerned. This assessment will set the scene for the subsequent two chapters.

13.1 Non-Hamiltonian dynamics for nonequilibrium steady states

Constructing NSS requires either to start from a Hamiltonian that models a thermal reservoir of infinitely many degrees of freedom or to use non-Hamiltonian equations of motion, see Section 1.2. As an example, in Section 10.2 we have derived the stochastic Langevin equation from a Hamiltonian defining a thermal reservoir that consists of infinitely many harmonic oscillators. The resulting equation turned out to be dissipative, non-deterministic and non time-reversible thus providing a well-known example of non-Hamiltonian dynamics. This dynamics particularly results from the fact that the equations of motion of the infinitely many reservoir degrees of freedom were eliminated in the course of the derivation, supplemented by some further approximations.

Actually, as we have demonstrated in Section 10.3, projecting out spurious reservoir degrees of freedom typically¹ yields a non-uniform probability density for the thermostated subsystem while the combined distribution of subsystem plus thermal reservoir is still uniform, respectively microcanonical. The non-uniformity of the projected equilibrium density may be taken as an indication of some phase space contraction in the associated variables which is not present in the original phase space volume preserving Hamiltonian dynamics of the full system. Indeed, in case of the Langevin equation and for Gaussian and Nosé-Hoover

¹A counterexample was provided by subsystem and reservoir living altogether in three dimensions and projecting out two of them, see Fig. 10.2.

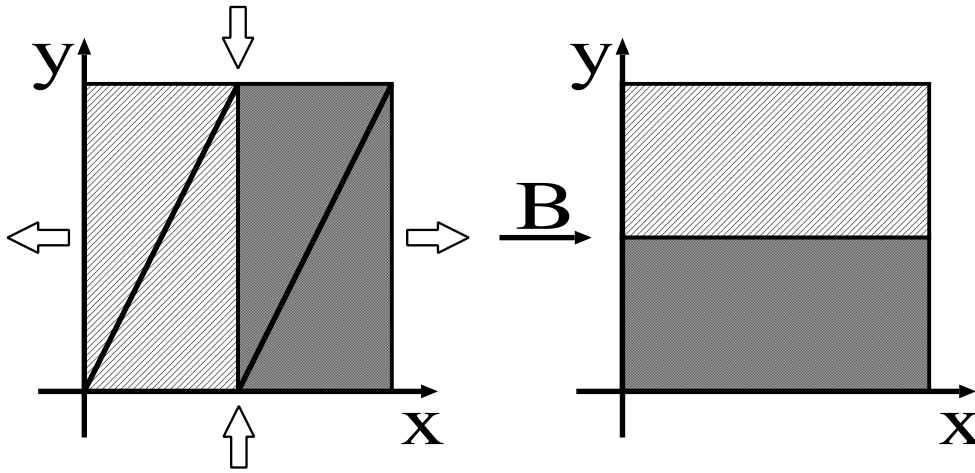


Figure 13.1: Sketch of the baker map defined by Eq. (13.1): a unit square is stretched horizontally and squeezed vertically by preserving its unit area. The resulting rectangle is cut in the middle, and both parts are put on top of each other forming again a unit square. The two diagonal lines in the left part of the figure represent the one-dimensional Bernoulli shift acting onto the x variable only, which determines the dynamics of the baker map along the horizontal axis.

dynamics the equations of motion of the respectively thermostated subsystem are always non-Hamiltonian.

We thus argue that the non-Hamiltonian character results from conveniently simplifying the equations of motion of subsystem plus reservoir by considering the relevant degrees of freedom only while neglecting others. Hence, such a non-Hamiltonian formulation is in principle very well compatible with a Hamiltonian description of the complete combination of subsystem plus reservoir.

Since the use of non-Hamiltonian dynamics for modeling NSS was [Eyi92, Coh92] and is [Lar03] often criticized, we illustrate our arguments by means of a very simple example. Let us consider the two-dimensional baker map acting onto the unit square, cp. to Chapter 4,

$$B(x, y) = \begin{cases} (2x, (y + 1)/2) & , \quad 0 \leq x < \frac{1}{2} \\ (2x - 1, y/2) & , \quad \frac{1}{2} \leq x \leq 1 \end{cases} . \quad (13.1)$$

This map squeezes the unit square along the vertical direction while stretching it horizontally such that the area is preserved. The resulting rectangle is cut in the middle, and both parts are put on top of each other yielding the dynamics depicted in Fig. 13.1. The corresponding equations of motion read

$$(x_{n+1}, y_{n+1}) = B(x_n, y_n) \quad , \quad (13.2)$$

where $n \in \mathbb{N}$ holds for the discrete time.

As already remarked in Refs. [Gas98a, Gas03], it appears that the baker map was first defined and studied by Seidel in 1933 [Sei33] who, in turn, gives informal credit to Birkhoff for its invention. Later on this map was considered by Hopf [Hop37]. Eventually, it became very popular starting from the discussion by Arnold and Avez [Arn68], who also coined the name.² The baker map is one of the most simple chaotic dynamical systems serving as a standard model in many textbooks on nonlinear dynamics, see, e.g., Refs. [Sch89, Ott93,

²Both Seidel and Hopf used the baker map as an example for a system that is metrically transitive,

[Gas98a, Dor99]. Starting from the work by Gaspard [Gas92a] the baker dynamics became extremely popular in form of an analytically tractable model for nonequilibrium transport, the spatially extended so-called *multibaker map* already introduced and studied in Chapter 4 [Gas93, Tas95, Tel96, Vol97, Gas97b, Bre98, Vol98, Gas98c, Gil99a, Gil99b, Tas99, Tas00, Vol00, Ron00b, Gil00b, Gil00a, Tel00, Gil01, Vol02, Woj02, Gar02, Gil04, Gas03, Woj03b, Vol03].³ Even so-called thermostated multibaker maps have been constructed and analyzed from the point of view of mimicking the action of Gaussian and Nosé-Hoover thermostats [Tel96, Vol97, Bre98, Vol98, Gil99a, Gil99b, Vol00, Ron00b, Gil00a, Vol03]. However, in this work we restrict ourselves to the original formulation of Gaussian and Nosé-Hoover dynamics in terms of differential equations only. Corresponding time-discrete dissipative models are reviewed particularly in Refs. [Tel00, Vol02, Dor99].

That the baker map Eq. (13.1) is area-preserving can be confirmed by computing its Jacobian determinant. The map is furthermore invertible and, even more, shares a specific symmetry property that is usually referred to as *reversibility* in time-discrete maps, cf. Section 4.2.⁴ These properties are analogous to respective features in time-continuous Hamiltonian dynamical systems.⁵ It is not our purpose to give a detailed account concerning the dynamical systems properties of the baker map.⁶ We just wish to convey that it is a widely studied standard model mimicking, at least to some extent, a Hamiltonian chaotic dynamical system on the level of time-discrete equations of motion.

In order to illustrate our above discussion about the origin of non-Hamiltonian dynamics we now project out one variable of the baker map. This can be performed starting from the Liouville equation for the baker map⁷ by simply integrating over the y -variable, see Ref. [Dor99] for the detailed calculation. However, x and y are already nicely decoupled in Eq. (13.1) with respect to the direction of the projection. One may therefore immediately conclude that the time-discrete Liouville equation determining the evolution of the probability density along the x -axis only must be governed by the action of the one-dimensional map

$$x_{n+1} \equiv B_x(x_n) = 2x_n \pmod{1} \quad , \quad (13.3)$$

This *Bernoulli shift* is included in Fig. 13.1. Its Jacobian determinant is equal to two, hence this map is uniformly expanding and does not preserve the phase space volume. The baker

or mixing, respectively. Arnold and Avez proved that this map is Bernoulli exhibiting the property of a K-system with positive metric entropy. Seidel originally discussed a baker with stretching/squeezing factors of 10, respectively 1/10.

³For multibaker maps the unit cell of the baker map is periodically continued along the x -axis. The single cells are then coupled with each other by mapping, say, the left vertical strip of the left part in Fig. 13.1 into the next cell to the right while mapping the right vertical strip into the next cell to the left, and so on.

⁴A map B is called *reversible* if there exists an involution $G, GG = 1$, in phase space reversing the direction of time, $BGB = G$ [Rob92]. Thus reversibility in maps is more than the existence of an inverse. However, note that such a reversibility does not necessarily imply time-reversibility [Dol00] and that there is a controversy of how to define time-reversibility in maps [Rob92, Tas95, Hoo96b, Hoo98b, Bre98, Gil99b, Gas98a, Vol02].

⁵However, note that the baker map does not share the property of being symplectic, in contrast, for example, to the standard map [Ott93, Mei92].

⁶Let us mention only some very basic characteristics: Apart from being mixing and a K-system implying chaotic behavior the baker map is also hyperbolic [Dor99]. Strictly speaking it is not Anosov because it is not differentiable at the point of discontinuity [Gas98a].

⁷The time-discrete Liouville equation is usually called *Frobenius-Perron equation* in dynamical systems theory [Dor99, Gas98a, Ott93].

map thus provides a simple example of a system whose complete two-dimensional dynamics is area-preserving, whereas by projecting out one variable the associated one-dimensional equations of motion are dissipative.

Curiously, the equilibrium density of the Bernoulli shift is still uniform, as for the original baker map, whereas in Section 10.3 the probability densities obtained from projecting out reservoir degrees of freedom were typically non-uniform. In order to more closely connect to these results one may simply rotate the unit square of the baker map by 45 degrees [Hoo98b]. Now the density projected upon the horizontal line by integrating over the vertical axis will be non-uniform, whereas the full baker map is still area-preserving. Unfortunately, in contrast to the non-rotated case here the dynamics along the horizontal, respectively the vertical axes are not decoupled anymore,⁸ and it is not straightforward to extract equations of motion governing the dynamics along the x -axis only.

This simple example demonstrates again that non-Hamiltonian dynamics may fit very well together with Hamiltonian equations of motion for the complete system consisting of subsystem plus thermal reservoir. In such a case a non-Hamiltonian dynamics just results from conveniently projecting out superfluous (reservoir) degrees of freedom such as the passive y -variable in the baker map, see also Rondoni et al. [Ron02a, Eva02a] for an analogous argumentation. In our view a non-Hamiltonian description thus emerges very naturally in equations designed to model NSS, and in this respect Gaussian and Nosé-Hoover thermostats are not particularly artificial or unusual.

On the other hand, one should keep in mind that Gaussian and Nosé-Hoover reservoirs have not been derived starting from a purely Hamiltonian dynamics, see, e.g., again the derivation of the Langevin equation in Section 10.2 for comparison. Moreover, in contrast to the projected baker dynamics and to the Langevin equation the former two types of dynamics are even time-reversible. Of course, for Gauss and Nosé-Hoover there exists the generalized Hamiltonian approach discussed in Section 12.3.2, however, it only represents a formal analogy and not a rigorous Hamiltonian derivation. We therefore emphasize again that Gaussian and Nosé-Hoover dynamics yield only a *heuristic modeling* of NSS rather than providing a theory starting from first principles. Hence, one cannot rule out in advance that the properties of dynamical systems thermostated that way may depend on specificities of these thermal reservoirs. This should be taken into account when searching for universal properties of NSS along the lines of this approach.

13.2 Phase space contraction and entropy production

The periodic Lorentz gas driven by an external electric field yielded NSS after connecting this model to either the Gaussian or to the Nosé-Hoover thermostat. Both types of thermostated systems were characterized by an identity between the absolute value of the average rate of phase space contraction and the thermodynamic entropy production in terms of Joule's heat, see Sections 11.2.1 and 12.3.1. This identity represents a basic property of ordinary Gaussian and Nosé-Hoover dynamics and furnishes a crucial link between dynamical systems quantities and transport properties. Interestingly, even the stochastic Langevin equation Eq. (10.1) supplemented by an external electric field exhibits this identity, as one can easily verify. However, in contrast to Gaussian and to Nosé-Hoover dynamics this equation is less

⁸This is related to the fact that we are not projecting onto the unstable manifold only, which is usually the adequate choice for performing a projection.

amenable to an analysis in terms of dynamical systems theory because of the stochastic forces involved.

We now show that this identity is in fact linked to a more general relationship between phase space contraction and entropy production, which holds irrespective of the specific type of dynamical system considered. In our presentation we follow Ref. [And85], for other derivations see particularly Refs. [Eva85a, Eva90b, Gas97b, Dor99, Gal99, Rue99b, Det00a, Eva02a].

Let us start from the general dynamical system

$$\dot{\mathbf{x}} = \mathbf{F}(\mathbf{x}) \quad , \quad (13.4)$$

where \mathbf{x} and \mathbf{F} denote vectors in a k -dimensional phase space $\Gamma \subset \mathbb{R}^k$, $k \in \mathbb{N}$. For convenience here we shall not distinguish between position and velocity components. One may now inquire about the average rate of entropy production in this system by using *Gibbs definition of entropy* [Pen79, Eva90b, Rue99b, Gas98a, Det00a]

$$S_G := - \int_{\Gamma} d\Gamma \rho \ln \rho \quad . \quad (13.5)$$

Here $\rho \equiv \rho(x_1, x_2, \dots, x_k)$ denotes the distribution function of the *complete* dynamical system Eq. (13.4) determined by the Liouville equation Eq. (12.2) and $d\Gamma := dx_1 dx_2 \dots dx_k$ represents a volume element of the phase space Γ . In order to calculate the Gibbs entropy production we differentiate Eq. (13.5) by employing the Leibnitz rule, which yields

$$\frac{dS_G}{dt} = - \int_{\Gamma} d\Gamma (1 + \ln \rho) \frac{\partial \rho}{\partial t} - \sum_i \int_{\Gamma'} d\Gamma' \rho \ln \rho F_i|_{\partial\Gamma_i} \quad (13.6)$$

with $d\Gamma' := dx_1 \dots dx_{i-1} dx_{i+1} \dots dx_k$ and F_i defined at the boundary $\partial\Gamma_i$. The derivative $\partial\rho/\partial t$ can be substituted by using the Liouville equation Eq. (12.2) leading to

$$\frac{dS_G}{dt} = \int_{\Gamma} d\Gamma \rho \nabla \cdot \mathbf{F} + \int_{\Gamma} d\Gamma \rho \ln \rho \nabla \cdot \mathbf{F} + \int_{\Gamma} d\Gamma (1 + \ln \rho) \mathbf{F} \cdot \nabla \rho - \sum_i \int_{\Gamma'} d\Gamma' \rho \ln \rho F_i|_{\partial\Gamma_i} \quad . \quad (13.7)$$

Performing integration by parts the second term on the right hand side of the above equation precisely cancels with the last two terms in the same equation. The final result thus reads

$$\frac{dS_G}{dt} = \int_{\Gamma} d\Gamma \rho \nabla \cdot \mathbf{F} \quad , \quad (13.8)$$

which means that the rate of Gibbs entropy production is always identical to the average rate of phase space contraction defined by Eq. (11.5). This important identity was noted by Gerlich [Ger73] and was subsequently discussed in various settings by other authors [Dob76a, Dob76b, Ste79, And82]. A very lucid and clear statement of this identity is due to Andrey [And85]. In the context of Gaussian and Nosé-Hoover dynamics the importance of the relationship Eq. (13.8) was particularly emphasized in Refs. [Eva85a, Bre96, Hol87, Hoo87, Pos88, Rue96, Rue97a, Gal99, Rue99b, Hoo99, Dor99, Rue03].

As we have mentioned at the beginning of Chapter 1, it appears that there is no generally accepted definition of a thermodynamic entropy in nonequilibrium situations. Some authors considered the Gibbs entropy Eq. (13.5) to be a suitable candidate for such a nonequilibrium

entropy [Eva90b, Gal99, Rue99b, Hoo99]. However, in our view using this concept causes a number of problems.

First of all, Eq. (13.8) tells us that for phase space volume preserving dynamics the Gibbs entropy production is strictly zero. This fact is problematic [Nic98, Det00a], for example, in case of diffusion in Hamiltonian dynamical systems under concentration gradients imposed by flux boundary conditions [Gas97b, Gas98a], see also Ref. [Eck99a] for a Hamiltonian modeling of a heat flow under temperature gradients. In both nonequilibrium situations there is a well-defined irreversible entropy production while the Gibbs entropy production is strictly zero, since there is no non-Hamiltonian thermostating.

Secondly, dissipative dynamical systems usually exhibit a *negative* average rate of phase space contraction. Specific examples are provided by the Gaussian and the Nosé-Hoover thermostated driven Lorentz gas, see Eqs. (11.6) and (12.14). According to Eq. (13.8) the Gibbs entropy production is also negative reflecting a contraction of the system onto a subset in phase space such as a fractal attractor. The decrease of the Gibbs entropy thus measures the fact that the dynamical system is getting “more ordered” in phase space. However, a negative thermodynamic entropy production in NSS appears to be in contradiction with the second law of thermodynamics.

In our earlier derivations of Sections 11.2.1 and 12.3.1, which specifically concerned the Gaussian and the Nosé-Hoover thermostated Lorentz gas, we circumvented this sign problem, since we did not start from the Gibbs entropy production. Instead, we directly computed the average rates of phase space contraction by realizing afterwards that the *absolute* values yielded the thermodynamic entropy production in form of Joule’s heat. This enabled us to “invert the sign” and to establish the identity without entering into the discussion concerning a negative Gibbs entropy production.

A more physical interpretation of the sign reversal may be obtained as follows [Che93a, Rue96, Dor99, Hoo99]: Let us consider a balance equation for the total entropy production of a subsystem under nonequilibrium conditions, in analogy to Eq. (12.1). The source term stands for the entropy production within the subsystem, whereas the flow term holds for the average heat transfer from the subsystem to the thermal reservoir. The reservoir fully absorbs the entropy produced by the subsystem such that in a NSS the average entropy production of subsystem plus thermal reservoir is zero. Hence, from the side of the thermal reservoir the entropy flux must be *positive* causing a positive entropy production in the reservoir. This entropy production may be identified as the relevant one in the sense of irreversible thermodynamics thus yielding the sign reversal. However, in detail this explanation is debatable [Nic96, Gas97b, Gas98a, Nic98, Gil99a, Dae99], because we did not identify a positive entropy production *within* the subsystem itself.

More refined approaches resolve the sign problem by using methods of coarse graining for the phase space densities as they enter into the definition of the Gibbs entropy Eq. (13.5) [Bre96, Nic96, Vol97, Gas97b, Vol98, Bre98, Nic98, Gil99a, Tas99, Dae99, Gas98a, Gil00b, Gil00a, Tas00, Tel00, Dor02, Vol02, Mae03a, Vol03]. Such a coarse grained formulation may be motivated by a second basic deficiency of the Gibbs entropy [Nic96, Gas97b, Dae99, Gil99a, Gas98a]: As we have shown in Sections 11.2.3 and 12.3.3, in deterministically thermostated systems the phase space density typically contracts onto fractal attractors. However, the fractal structure implies that the probability densities characterizing the associated NSS must be singular and non-differentiable. Consequently, they are no well-defined

mathematical objects anymore.⁹ Correspondingly, the integration in Eq. (13.5) is also not well-defined anymore.¹⁰ As a consequence of the formation of these fractal structures it was thus proposed by many authors to use *coarse-grained* Gibbs entropies in order to arrive at a suitable concept of a nonequilibrium entropy, see the long list of references cited above. Up to now these methods have mostly been worked out for time-discrete dynamical systems such as multibaker-maps for which different types of coarse graining have been explored. Concerning further details we may refer, e.g., to Refs. [Gil99a, Gas98a, Tel00, Vol02] providing recent summaries of this issue.

In the light of this criticism it may appear rather surprising that for the Gaussian and for the Nosé-Hoover thermostated driven Lorentz gas the ordinary Gibbs entropy production can nevertheless be fully identified with the thermodynamic entropy production in terms of Joule's heat subject to a sign reversal. A related fact that further contributes to this surprise is that Gibbs' formulation assesses the entropy of a system with respect to *all* phase space variables and with respect to their *complete* deterministic dynamics in time. This is at variance to concepts like coarse-grained Gibbs entropies or Boltzmann entropies. Here there is already a loss of information, because these quantities are not employing the complete phase space densities or respective probability measures as determined by the Liouville equation. In a similar vein, a heat flux from a subsystem to a thermal reservoir will usually involve only a specific fraction of all phase space variables. From the point of view of Clausius definition of entropy production, see Section 11.2.1, the Gibbs entropy may thus measure spurious contributions in comparison to a thermodynamic entropy production by assessing phase space coordinates that are not involved in any heat transfer to a thermal reservoir.

All these physical arguments support again the use of a respectively coarse grained entropy that only assesses the physically relevant contributions to a thermodynamic entropy production. We believe that such a formulation of a nonequilibrium entropy should be compatible with the one of Clausius in terms of a heat transfer. From that point of view there is no reason why phase space contraction, or the respective Gibbs entropy production, should always be identical to the thermodynamic one. One may suspect that such an identity may rather be characteristic of the specific family of thermostats investigated so far.

This hypothesis will be verified by presentings generic families of counterexamples where the identity between phase space contraction and thermodynamic entropy production, respectively between Gibbs and thermodynamic entropy production, is not fulfilled. In order to qualify as counterexamples alternative models of thermal reservoirs must share some basic physical properties with Gaussian and Nosé-Hoover thermostats, such as being dissipative, deterministic and time-reversible. Furthermore, there should be an adequate physical interpretation of the thermostating mechanism. Such counterexamples will be introduced and analyzed in the following two chapters.

⁹In contrast, the corresponding probability *measures* may still be well-defined. Typically, these are SRB measures being smooth along unstable but fractal along stable manifolds [Gas98a, Dor99, Gal99, Rue99b, You02, Gal03].

¹⁰In this case the integral should be replaced by a Lebesgue-Stieltjes integral over the invariant measure [Dor99, Gas98a].

13.3 Transport coefficients and dynamical systems quantities

If there exists an identity between the average phase space contraction rate and thermodynamic entropy production, it is straightforward to link transport coefficients with dynamical systems quantities. Interestingly, for the field-dependent conductivity $\sigma(\varepsilon)$ of both the Gaussian and the Nosé-Hoover thermostated driven periodic Lorentz gas one obtains the same functional relationship reading

$$\sigma(\varepsilon) = -\frac{T}{\varepsilon^2} \sum_{i=1}^N \lambda_i(\varepsilon) \quad , \quad (13.9)$$

cp. to Eqs. (11.11) and (12.17), where N denotes the total number of field-dependent Lyapunov exponents $\lambda_i(\varepsilon)$ and T stands for the temperature. The existence of such a simple functional relationship between chaos quantities and transport coefficients is typical for Gaussian and Nosé-Hoover thermostated dynamical systems, see Sections 11.2.2 and 12.3.1 for further details.

Surprisingly, by using the escape rate approach to chaotic transport outlined in Section 1.1, independently very similar formulas were derived for the very different class of *open Hamiltonian* dynamical systems, where there is an escape of phase space points due to absorbing boundaries. This second fundamental approach to NSS does not require any modeling of thermal reservoirs, hence by default it does not involve any phase space contraction. We will now provide a brief summary concerning formulas linking transport coefficients to dynamical systems quantities as they emerge from both the escape rate and the thermostated systems approach. The resulting different but related formulas will be compared in detail and possible crosslinks between them will be critically assessed.

For sake of simplicity we mainly restrict ourselves again to the periodic Lorentz gas. We start with the driven Lorentz gas under application of a Gaussian thermostat for which $N = 2$ in Eq. (13.9). In order to connect to the escape rate approach we reformulate this equation as follows [Gas98a, Gil01, Rue96]: For the Gaussian thermostated Lorentz gas the sum of Lyapunov exponents on the right hand side consists only of a positive one, $\lambda_+(\varepsilon)$, and a negative one, $\lambda_-(\varepsilon)$, see Eq. (11.11). Both Lyapunov exponents are defined with respect to the invariant measure of the dynamical system which is concentrated on the field-dependent fractal attractor \mathcal{A}_ε . We now indicate this dependence explicitly by writing $\lambda_\pm(\varepsilon) \equiv \lambda_\pm(\mathcal{A}_\varepsilon)$.

As was proven in Refs. [Che93a, Che93b], under certain conditions there is the *Pesin identity* [Eck85, Ott93, Bec93, Gas98a, Dor99] between the Kolmogorov-Sinai entropy $h_{KS}(\mathcal{A}_\varepsilon)$ and the positive Lyapunov exponent on the attractor, $h_{KS}(\mathcal{A}_\varepsilon) = \lambda_+(\mathcal{A}_\varepsilon)$, for the Gaussian thermostated driven Lorentz gas. Having this in mind we rewrite the right hand side of Eq. (13.9) as

$$\begin{aligned} -\sum_{i=1}^2 \lambda_i(\mathcal{A}_\varepsilon) &= -\lambda_+(\mathcal{A}_\varepsilon) - \lambda_-(\mathcal{A}_\varepsilon) \\ &= -h_{KS}(\mathcal{A}_\varepsilon) - \lambda_-(\mathcal{A}_\varepsilon) \\ &= |\lambda_-(\mathcal{A}_\varepsilon)| - h_{KS}(\mathcal{A}_\varepsilon) \end{aligned} \quad (13.10)$$

The domain of the escape rate approach is particularly the description of diffusion processes, see Section 1.1. Accordingly, since the Einstein relation Eq. (11.12) holds for the Gaussian thermostated driven Lorentz gas [Che93a, Che93b] the electrical conductivity $\sigma(\varepsilon)$ on the left hand side of Eq. (13.9) may be replaced by the diffusion coefficient D , $D = T\sigma(\varepsilon)$ ($\varepsilon \rightarrow 0$). This yields as a final result [Gas98a, Gil01, Rue96, Bre96]

$$D = \lim_{\varepsilon \rightarrow 0} \left(\frac{T}{\varepsilon} \right)^2 (|\lambda_-(\mathcal{A}_\varepsilon)| - h_{KS}(\mathcal{A}_\varepsilon)) \quad . \quad (13.11)$$

A corresponding formula from the escape rate approach to chaotic diffusion is obtained as follows [Gas90, Gas92c, Gas93, Gas95b, Dor95, Gas95c, Kla96, Kla99a, Gas98a, Dor99]: We consider a slab of the periodic Lorentz gas with reflecting or periodic boundaries, say, in the vertical direction while in the horizontal direction we use absorbing boundaries a distance L apart from each other. We do not apply any external field but just look at the diffusion of an initial ensemble of point particles along the x -axis. Choosing the density of scatterers such that the periodic Lorentz gas is normal diffusive, see Section 10.4, we expect an exponential decrease of the number N of particles in time t according to

$$N(t) = N(0) \exp(-\gamma_{esc}t) \quad , \quad (13.12)$$

where $N(0)$ stands for the initial number of particles at time zero. Solving the one-dimensional diffusion equation with absorbing boundary conditions yields

$$D = \lim_{L \rightarrow \infty} \left(\frac{L}{\pi} \right)^2 \gamma_{esc} \quad , \quad (13.13)$$

that is, the diffusion coefficient is obtained in terms of the *escape rate* which strictly speaking depends on L , $\gamma_{esc} \equiv \gamma_{esc}(L)$. Let us now assume that the *Pesin identity for open systems* holds for the open periodic Lorentz gas,¹¹

$$\gamma_{esc} = \lambda_+(\mathcal{R}_L) - h_{KS}(\mathcal{R}_L) \quad . \quad (13.14)$$

Here $\gamma_{esc} \equiv \gamma_{esc}(\mathcal{R}_L)$ denotes the *escape rate* of particles with respect to the fractal repeller \mathcal{R}_L . Combining this equation with Eq. (13.13) leads to the fundamental result

$$D = \lim_{L \rightarrow \infty} \left(\frac{L}{\pi} \right)^2 (\lambda_+(\mathcal{R}_L) - h_{KS}(\mathcal{R}_L)) \quad . \quad (13.15)$$

Obviously, the functional forms of Eqs. (13.11) and (13.15) are just the same. However, we emphasize again that both the types of dynamical systems considered and the approaches by which these equations have been derived are very different.

On the other hand, for both derivations the key was to identify a quantity providing a link between chaos and transport properties. For thermostated systems this role is played by the average phase space contraction rate κ defined in Eq. (11.5). In case of open Hamiltonian systems the escape rate γ_{esc} serves for the same purpose. This analogy was first seen by Breyman, Tél and Vollmer [Bre96] and by Ruelle [Rue96]. These authors suggested to define a Gibbs entropy for open dynamical systems, in parallel to the Gibbs entropy of

¹¹So far this identity is only proven for Anosov diffeomorphisms, see, e.g., Refs. [Eck85, Bec93, Dor99, Gas98a] for outlines concerning this generalization of Pesin's identity and further references therein.

closed but thermostated, phase space contracting dynamical systems, related to the concept of conditionally invariant measures. Here the probability measures of particles remaining in the system, respectively the corresponding probability densities, are renormalized in time in order to make up for the loss of absorbed particles. Along these lines the Gibbs entropy production for open systems can be identified with the escape rate, $dS_G/dt = \gamma_{esc}$. On the other hand, for closed systems we have shown in the previous section that the Gibbs entropy production is equal to the average rate of phase space contraction, see Eq. (13.8). Hence, if the rates of Gibbs entropy production for closed and open systems were the same both Eqs. (13.11) and (13.15), that apply to very different dynamical systems, yielded the same transport coefficients in terms of dynamical systems quantities. This was indeed shown to be the case for some simple model systems, that is, (multi)baker maps, under periodic, absorbing and flux boundary conditions thus suggesting an equivalence of these very different nonequilibrium ensembles [Mor96b, Vol97, Vol98, Gil99a, Gil99b, Gil00a, Tel00, Vol02, Vol03].

Tél et al. have furthermore considered the situation of a hybrid system that is both open and dissipative [Tel96, Tel00, Vol02]. By solving the corresponding Fokker-Planck equation with absorbing boundaries and employing again the Pesin identity for open systems they arrived at the generalized formula (see also Ref. [Gas98a])

$$D \left(\frac{\pi}{L} \right)^2 + \frac{\sigma^2 \varepsilon^2}{4D} = \sum_{\lambda_i > 0} \lambda_i(\mathcal{R}_L) - h_{KS}(\mathcal{R}_L) \quad (L \rightarrow \infty, \varepsilon \rightarrow 0) \quad . \quad (13.16)$$

Carrying out the limit of $\varepsilon \rightarrow 0$ eliminates the second term on the left hand side yielding precisely Eq. (13.15) of the escape rate approach if applied to the Lorentz gas. On the other hand, performing $L \rightarrow \infty$ eliminates the first term on the left hand side. The conductivity may then be replaced again by Einstein's formula Eq. (11.12). Taking into account that for the Gaussian thermostat the temperature T should be replaced by $T \equiv T/2$, see Section 11.2.1, and assuming that in the limit of $\varepsilon \rightarrow 0$ the spectrum of Lyapunov exponents exhibits conjugate pairing, $\sum_{\lambda_i > 0} \lambda_i = \sum_{\lambda_i < 0} |\lambda_i|$, one recovers the result for the thermostated Lorentz gas Eq. (13.11).

We finally outline a third basic approach linking transport coefficients to dynamical systems quantities as recently formulated by Gilbert et al. [Gil01, Gas01, Cla02]. Here particularly diffusion in closed volume-preserving dynamical systems has been considered. Starting from the diffusion equation with periodic boundary conditions the solution for the diffusion coefficient reads

$$D = \lim_{L \rightarrow \infty} \left(\frac{L}{2\pi} \right)^2 \gamma_{dec} \quad . \quad (13.17)$$

This result is in formal analogy to Eq. (13.13), however, here γ_{dec} denotes the *decay rate* by which an equilibrium state is approached. By solving the Liouville equation of the respective dynamical system γ_{dec} can be related to the second largest eigenvalue of the Liouville operator associated with the corresponding hydrodynamic mode of diffusion of the dynamical system, see, e.g., Refs. [Kla96, Kla99a]. The crucial observation is now that this eigenvalue is linked to the Hausdorff dimension of the respective mode. Thus, the diffusion coefficient in Eq. (13.17) can be written as a function of the fractal dimension of the second largest eigenmode of the Liouville equation [Gil01, Gas01]. For systems with two degrees of

freedom which are periodically continued in one direction over a length L one gets

$$D = \lim_{L \rightarrow \infty} \left(\frac{L}{2\pi} \right)^2 \lambda_+ (d_H(2\pi/L) - 1) \quad , \quad (13.18)$$

where the Hausdorff dimension d_H is a function of the length of the system, or respectively of the wavenumber $k = 2\pi/L$ of the corresponding hydrodynamic mode. λ_+ denotes again the positive Lyapunov exponent of the system. This approach has been worked out in detail for a multibaker map [Gil01] as well as for diffusive and reactive-diffusive billiards of Lorentz gas type [Gas01, Cla02].

In order to compare Eq. (13.18) with the previous two formulas Eqs. (13.11) and (13.15) one may employ the Kaplan-Yorke formula, respectively Young's formula, which in case of the two-dimensional periodic Lorentz gas with a constrained kinetic energy reads [Eck85, Ott93, Gil01, Che93a]¹²

$$d_I = 2 + h_{KS}/|\lambda_-| \quad . \quad (13.19)$$

This formula links the information dimension d_I of a fractal set to the Kolmogorov-Sinai entropy h_{KS} and to the negative Lyapunov exponent λ_- of the corresponding dynamical system. By using this equation Eq. (13.11) can be rewritten as

$$D = \lim_{\varepsilon \rightarrow 0} \left(\frac{T}{\varepsilon} \right)^2 \lambda_+(\mathcal{A}_\varepsilon) (3 - d_I(\mathcal{A}_\varepsilon)) \quad . \quad (13.20)$$

It appears that this formula was first derived in Ref. [Eva00]. Analogously, Eq. (13.15) reads

$$D = \lim_{L \rightarrow \infty} \left(\frac{L}{\pi} \right)^2 \lambda_+(\mathcal{R}_L) (3 - d_I(\mathcal{R}_L)) \quad . \quad (13.21)$$

In both cases the information dimension d_I is furthermore identical to the Hausdorff dimension d_H of the respective fractal set and may be replaced respectively [Che93a, Che93b, Gas95b].

In conclusion, all three equations Eqs. (13.18), (13.20) and (13.21) relate the diffusion coefficient to the largest positive Lyapunov exponent of the corresponding dynamical system times a term containing the information dimension of the associated fractal structure, which in Eq. (13.18) is a fractal hydrodynamic mode, in Eq. (13.20) a fractal attractor and in Eq. (13.21) a fractal repeller.¹³ Hence, on this level there is quite a formal analogy even between all three approaches. One may thus indeed wonder whether these formulas form a kind of general backbone of nonequilibrium transport in terms of dynamical systems theory [Bre96, Tel96, Rue96]. We remark that, in addition, there exist very interesting, simple formulas by which transport coefficients can be calculated in terms of periodic orbits, see, e.g., Ref. [Van92] for the electrical conductivity and Refs. [Cvi95, Cvi92, Gas98a, Cvi03] for the diffusion coefficient. However, these formulas are conceptually rather different from the ones discussed above. Therefore we do not discuss them here by instead referring to the respective literature, see, e.g., Ref. [Cvi03] for an overview.

¹²We remark that so far this formula has only been proven for two-dimensional Anosov diffeomorphisms with an ergodic measure on compact manifolds, see Refs. [Eck85, Ott93] for further literature.

¹³In order to make this analogy even closer one may further introduce partial codimensions for the fractal structures in Eqs. (13.20) and (13.21), however, this does not appear to be possible for the hydrodynamic mode in Eq. (13.18) [Gil01].

Despite their striking formal analogy one may not overlook that all three equations concern very different physical settings [Coh92, Det00a, Gil01]: Eq. (13.21) applies to diffusion in open Hamiltonian dynamical systems without external fields, where the link between chaos and transport is formed by the rate assessing the escape from the fractal repeller. Eq. (13.18) concerns diffusion in closed Hamiltonian dynamical systems, again without using external fields, however, here there is no repeller. Instead, the fractality of the hydrodynamic mode of diffusion is assessed. In contrast to these two relations, Eq. (13.20) originally started from the current generated in a non-Hamiltonian dynamical system under application of external fields in combination with a specific thermostat. Here the link between chaos and transport is provided by the average phase space contraction rate onto the fractal attractor. Particularly in case of Eqs. (13.20) and (13.21) the physical situations involved remain inherently different.

That both equations can nevertheless be derived from a ‘master formula’ is nicely demonstrated by the hybrid equation Eq. (13.16). However, the left hand side of this equation represents obviously just the sum of the left hand sides of Eqs. (13.11) and (13.15) supplemented by the prefactors from the respective right hand sides. If we add the prefactor-free right hand sides of these two equations as well we obtain, by using the original formulation in the first line of Eq. (13.10) instead of the right hand side of Eq. (13.11), $-\lambda_+(\mathcal{A}_\varepsilon) - \lambda_-(\mathcal{A}_\varepsilon) + \lambda_+(\mathcal{R}_L) - h_{KS}(\mathcal{R}_L)$ ($L \rightarrow \infty, \varepsilon \rightarrow \infty$). By assuming that, in the above limits, $\lambda_\pm(\mathcal{A}_\varepsilon) = \lambda_\pm(\mathcal{R}_L)$ and that, as before, conjugate pairing holds, $\lambda_+ = -\lambda_-$, we recover the right hand side of Eq. (13.16) for the periodic Lorentz gas. Hence, one may argue that Eq. (13.16) represents an additive combination of both formulas. That a more intricate, common root of these two formulas going beyond this equation exists, possibly even combining these two relations with the third one in terms of hydrodynamic modes, appears to be very unlikely to us.

We may furthermore emphasize again that the validity of Eq. (13.11) stands and falls with the existence of the identity between phase space contraction and thermodynamic entropy production. In the previous section we have already casted doubt on the general validity of this identity for dissipative systems. Indeed, the two key quantities linking thermodynamics to chaotic dynamics discussed above measure quite different physical processes: The escape rate merely assesses the absorption of the number of phase space points, or particles, at some boundary, whereas the phase space contraction rate is defined with respect to the full details of the dynamical system in all variables. As we have outlined to the end of the previous section it is thus conceivable that the phase space contraction rate contains spurious information as far as thermodynamic entropy production and transport processes are concerned. We are not aware that yet there are any counterexamples questioning the validity of the formulas emerging from the escape rate and the closed Hamiltonian systems approach. However, as we will argue in the remaining chapters, for the thermostated systems approach the situation appears to be much more delicate.

Concerning practical applications for the calculation of transport coefficients it seems that these three formulas do not provide more efficient computational schemes than, say, Einstein formulas or Green-Kubo relations. As far as we can tell, in most cases dynamical systems quantities such as Lyapunov exponents and Kolmogorov-Sinai entropies are more difficult to compute than statistical averages defined within the framework of common nonequilibrium statistical mechanics only. With respect to a simplification of the Lyapunov sum rule Eq. (13.9) for higher-dimensional dynamical systems we may recall that the conjugate pairing rule of Lyapunov exponents is not universal for NSS in dissipative dynamical systems.

Boundary thermostats and systems under electric and magnetic fields provide counterexamples, see Section 11.2.2 for more details.

Irrespective of these rather practical concerns, we may emphasize that the existence of these three formulas linking transport coefficients to dynamical systems quantities provides highly interesting results from a fundamental physical and dynamical systems point of view, and the formal similarity of these different equations remains very remarkable.

13.4 Fractal attractors characterizing nonequilibrium steady states

Another crucial property of Gaussian and Nosé-Hoover thermostated systems is the existence of fractal attractors underlying NSS. These objects form a fundamental link between the microscopic non-Hamiltonian equations of motion that are, for this type of systems, still deterministic and time-reversible while irreversible transport is exhibited on macroscopic scales. Quantitatively, the existence of these attractors manifests itself in the average phase space contraction rate serving as a link between chaos and transport in dissipative systems, see our discussion in the previous sections.

In Sections 11.2 and 12.3 we have studied the Gaussian and the Nosé-Hoover thermostated driven periodic Lorentz gas as paradigmatic examples for this class of thermostated systems. For the Gaussian type numerical and analytical results provided evidence that in the full accessible phase space the Hausdorff dimension of the attractor is non-integer. In Poincaré surfaces of section, or in respective projections of the phase space, the attractor turned out to be even multifractal; see Figs. 11.2 and 12.2 for plots depicting the associated fractal folding. Supported by results for many other Gaussian and Nosé-Hoover thermostated systems it was thus conjectured that the existence of fractal attractors, and of the associated singular probability measures, is generic for non-Hamiltonian dynamical systems in NSS subject to deterministic and time-reversible thermal reservoirs.

How the topology of these attractors changes under variation of the electric field strength was assessed by means of bifurcation diagrams, as discussed in the same sections. For this purpose the positions of the colliding particles at the Lorentz gas disk were plotted as functions of the electric field strength, see Figs. 11.3 and 12.3. For both the Gaussian and the Nosé-Hoover thermostated driven periodic Lorentz gas these diagrams revealed intricate bifurcation scenarios. On the other hand, the specific form of these scenarios depends intimately on the type of thermal reservoir used and is already very different for Gaussian and Nosé-Hoover dynamics. Even more, in case of Nosé-Hoover thermostating different bifurcation diagrams were obtained for different values of the coupling strength between subsystem and thermal reservoir. Hence, there is no universality concerning the specific change of the topology of these attractors under variation of the field strength. Whether the mere existence of bifurcations, at least, is typical for the thermostated driven periodic Lorentz gas will be clarified in the following two chapters.

However, instead of applying Gaussian and Nosé-Hoover schemes, thermal reservoirs can be mimicked by introducing *stochastic interactions* between subsystem and reservoir particles. Here we briefly sketch various existing numerical and analytical methods of how to model this second fundamental class of thermostats. We then connect to our discussion concerning the possible universality of fractal attractors in NSS.

One way to introduce a stochastic reservoir is by using a Langevin equation, as was discussed in detail in Section 10.2. For molecular dynamics computer simulations this approach was first implemented by Schneider and Stoll [Sch78], see also later work in Ref. [Nos91, Pos00b]. Andersen [And80] proposed a variant of this stochastic bulk thermostat by considering an interacting many-particle system, where at certain time intervals the velocity of a randomly selected particle is chosen randomly from a canonical velocity distribution [All87, Jel88a]. Alternatively, a stochastic sampling of velocities from canonical velocity distributions can be performed at the boundaries of a subsystem. Such *stochastic boundary conditions* were proposed by Lebowitz and Spohn in order to mathematically analyze a three-dimensional random Lorentz gas under a temperature gradient [Leb78]. For molecular dynamics computer simulations this thermostating scheme was implemented by Ciccotti and Tenenbaum [Cic80], again in order to model thermal gradients, see also Refs. [Ten82, Che95b, Che97, Pos98, Wag99] for later use of this method in the context of computer simulations. Stochastic boundary conditions will be introduced in full detail later on in Section 15.1. However, for the following discussion it is not necessary to know about such technical details.

A particularly important result for the class of stochastic boundary thermostated models was reported by Goldstein, Kipnis and Ianiro [Gol85]. They studied a system of Newtonian particles maintaining a heat flux due to a temperature field that is modeled by stochastic boundaries and varies with the position at the boundary. A mathematical analysis of this system yielded that there exists a unique invariant probability measure that is absolutely continuous [Eck85, Dor99] with respect to the Lebesgue measure. In other words, in this case the measure is not singular and hence not fractal. This result was claimed to be generic for stochastically thermostated systems [Eyi92, Coh92] thus contradicting the universality of fractal attractors as conjectured from studying Gaussian and Nosé-Hoover thermostated systems [Hol87, Hoo99].

The claim that the physically relevant probability measures are generally smooth in stochastically thermostated systems has been doubted by Hoover et al. on the basis of numerical explorations: In Ref. [Hoo98c] these authors studied a driven periodic Lorentz gas thermalized by a ‘hybrid’ thermostat consisting of deterministic and stochastic boundaries. Computations of the information dimension of the fractal attractor by evaluating phase space projections such as Fig. 12.2 indicated a slight deviation from an integer value. Furthermore, they considered a one-dimensional Hamiltonian model for heat conduction (the *ding-a-ling* model) with reservoirs defined by stochastic boundaries [Pos98]. They also investigated an interacting many-particle system under an external field [Pos00b] (the *color conductivity model* [Eva90b]). In the latter two cases they computed the information dimension according to the Kaplan-Yorke conjecture, respectively Young’s formula, cp. to Eq. (13.19) of the previous section. The numerical results yielded again deviations from integer values. However, this dimension formula relies on the computation of Lyapunov exponents that in turn necessitate to define a Jacobian quantifying the interaction of the subsystem with the stochastic boundaries. To us it appears that the definition which these authors used for the Jacobian is generally ill-defined, hence we cannot consider the numerical results of Refs. [Pos98, Pos00b] to be conclusive.¹⁴ Thus, whether attractors in stochastically thermostated

¹⁴In Ref. [Hoo98c] the phase space contraction at a stochastic boundary is defined by the second equation below Fig. 2. For this purpose an equality between phase space contraction and entropy production has been *stipulated* for this type of system. On the other hand, a natural assumption is just the conservation of phase space probability (or points in phase space) at the boundary, $drdv\rho(r, v) = dr'dv'\rho(r', v')$, where (r, v) represent position and velocity of a particle before a collision, (r', v') the same variables after a collision, and

systems are generally smooth or fractal, and to which extent this property depends on the specific type of subsystem considered, still remains a very open question to us.

Apart from these considerations we may emphasize again that both types of thermal reservoirs define very different classes of dynamical systems: Gaussian and Nosé-Hoover thermostats keep the dynamics deterministic and time-reversible, whereas stochastically thermostated systems render the equations of motion non-deterministic and non-time reversible. The controversy [Gol85, Eyi92, Coh92, Hoo98c, Pos98, Pos00b, Gal03] concerning the type of invariant measure that emerges under application of these two very different types of thermal reservoirs thus boils down to the question which type of thermostat one considers to be more ‘physical’. We furthermore remark that, connected to our discussion in Section 13.1, Nicolis and Daems [Nic96, Nic98, Dae99] and Ruelle [Rue97b] argued for the positivity of the thermodynamic entropy production in stochastically thermostated systems.

13.5 Nonlinear response in the thermostated driven periodic Lorentz gas

According to the numerical results for the thermostated driven periodic Lorentz gas the topology of the attractors does not only depend on the specific type of thermal reservoir that has been applied, but it is also very sensitive to variations of the external field. From that point of view it is not too surprising that also the field-dependent electrical conductivities of the Gaussian and the Nosé-Hoover thermostated Lorentz gas are not the same, as we have discussed in Sections 11.2.4 and 12.3.3, see Figs. 11.4 and 12.4. Furthermore, even for Nosé-Hoover only the Lorentz gas conductivities still depend on the value for the coupling parameter between subsystem and reservoir, in the same way as the bifurcation diagrams of the different attractors.

On the other hand, all conductivities jointly exhibit a profoundly nonlinear response for the numerically accessible values of the field strength $\varepsilon > 0$. For the Gaussian thermostated Lorentz gas there must exist a regime of linear response in the limit of very small fields according to the mathematical proof by Chernov et al. However, the respective range of field strengths close to zero appears to be so small that up to now computer simulations could not really corroborate its existence. This reminds to some extent to van Kampen’s objections concerning the validity of linear response, who argued that a linear response is not trivially guaranteed for nonlinear chaotic dynamical systems. He emphasized that there might be a nontrivial interplay between microscopic nonlinearity and macroscopic linearity yielding a quantitatively negligibly small regime of linear response.

In addition to these problems concerning coarse functional forms, all field-dependent conductivities exhibit irregularities on fine scales that are not due to numerical errors. As was

ρ is the respective probability distribution. A Jacobian at the collision is then straightforwardly defined by $|J| = |dr'dv'/drdv| = \rho(r, v)/\rho(r', v')$. If one follows this argument one arrives at the result of Ref. [Hoo98c] *only* (i) if both distributions before and after the collisions are identified with canonical distributions which is natural after a collision, but which is not so clear before a collision, cp., e.g., to Ref. [Wag99]; and (ii) if both distributions before and after a collision have precisely the same variance in terms of a temperature, $T = T'$. However, both distribution are only expected to be the same, with the same temperature, in the hydrodynamic limit, whereas systems of finite length as handled on the computer one may expect to exhibit temperature jumps [Kus02]. For this reason we consider the validity of the results reported in Refs. [Pos98, Pos00b] concerning the information dimension to be debatable.

shown in Part I of this thesis, such irregular transport coefficients are in fact well-known from very related classes of dynamical systems, which share the properties of the periodic Lorentz gas of being deterministically chaotic, low-dimensional and spatially periodic. For very simple types of such systems it could be shown that these transport coefficients are even of a fractal nature. For thermostats of Nosé-Hoover type the irregularities appear to be smoothed-out, which may be understood with respect to the fact that here the kinetic energy fluctuates according to a canonical velocity distribution. Imposing instead a constant kinetic energy onto the system by means of a Gaussian thermostat these irregularities look considerably more “fractal-like”.

In summary, to us it still remains an open question to *quantitatively* identify a regime of linear response in the Gaussian thermostated driven periodic Lorentz gas, either analytically or numerically. One may furthermore ask whether such a regime of linear response may also be expected for applications of the Nosé-Hoover and possibly of other types of thermostats. On the other hand, one may suspect that the existence of irregularities on finer scales of the field-dependent conductivity is rather typical for deterministically thermostated driven periodic Lorentz gases. To which extent this holds true, and particularly how this goes together with the expected linear response for very small fields, are important open questions.

This points back again to the question concerning the equivalence of nonequilibrium ensembles. Unfortunately, in low-dimensional deterministic and periodic dynamical systems like the Lorentz gas the conductivity obviously reflects the specific type of thermal reservoir that has been applied. This appears to be at variance with such an equivalence that is expected to yield the same conductivities. Related findings have been reported in Ref. [Bon02]. In order to get more clear about this point it will be important to apply further types of thermal reservoirs to the Lorentz gas dynamics in order to check for similarities and differences, which we will do in the following two chapters.

Finally, as for the hotly debated fractality of attractors in NSS one may expect that the irregular or even fractal structure of parameter-dependent transport coefficients may be getting more regular by imposing stochasticity onto the system. This can be performed by either distributing the scatterers randomly in space, by using a stochastic thermal reservoir as discussed above, or by imposing additional noise onto a deterministic system. For thermostated driven *random* Lorentz gases field- and density-dependent Lyapunov exponents and diffusion coefficients have indeed already been calculated analytically and numerically [vB95, vB96, Lat97, Del97b, vB97, vB98, vB00b] verifying such a smooth dependence on parameters. Additionally, for simple low-dimensional maps it has been studied how the fractal structure of a parameter-dependent diffusion coefficient is affected while imposing different types of perturbations on them in time or in space, see Chapter 6 [Kla02b, Kla02c]. As expected the fractality on arbitrarily fine scales disappears, however, irregularities still survive in form of smoothed-out oscillations. This irregular structure turns out to be very persistent against random perturbations, that is, typically rather strong random perturbations are needed to make the transport completely random walk-like.¹⁵

Hence, there may be complicated scenarios between the two limiting cases of completely deterministic and completely stochastic diffusion, and the application of external randomness significantly affects fractal properties of the type as discussed above. Generally, one

¹⁵An interesting exception is provided by a specific type of quenched disorder leading to a Golosov random walk. In this case an originally normal diffusive process may immediately become anomalous, that is, a diffusion coefficient does not exist anymore [Rad96].

may expect that problems with linear response and the irregularity of parameter-dependent transport coefficients are rather specific to low-dimensional dynamical systems. For interacting many-particle systems, for example, it is natural to assume that all transport coefficients are smooth in their physical parameters and that there are broad regimes of linear response, as predicted by standard nonequilibrium thermodynamics. Examples of such systems will be discussed in Chapter 15.

13.6 *Summary

1. Gaussian and Nosé-Hoover dynamics provide prominent examples for a non-Hamiltonian modeling of NSS. By employing the well-known baker map we demonstrated how volume-preserving “Hamiltonian” dynamics may go together with dissipative equations of motion and corresponding non-uniform probability densities. The key is the elimination of reservoir degrees of freedom by projecting out respective variables from the full equations of motion. Thus, there is nothing mysterious about using a non-Hamiltonian description of NSS.
2. Gaussian and Nosé-Hoover thermostats typically feature an identity between thermodynamic entropy production and the average rate of phase space contraction. However, there exists an even more general identity relating phase space contraction to entropy production in terms of the Gibbs entropy which is completely independent of the type of modeling. On the other hand, in case of a Hamiltonian approach to NSS the Gibbs entropy production is simply zero. For this and other reasons one may doubt whether the Gibbs entropy should be considered as a correct definition of a nonequilibrium entropy being compatible with nonequilibrium irreversible thermodynamics.

Dissipative dynamical systems in NSS exhibit a negative average rate of phase space contraction. Due to the abovementioned identity the Gibbs entropy production is negative as well. This appears to be at variance with the second law of thermodynamics. However, here the Gibbs entropy can be saved by applying methods of coarse graining leading to an inversion of the sign.

To consider a coarse grained entropy production is furthermore suggested by the fact that the invariant measures of deterministically thermostated systems are typically singular. Still, the decisive question is whether the Gibbs entropy always yields the correct thermodynamic entropy production in nonequilibrium as, for example, compared to the Clausius entropy. For Gaussian and Nosé-Hoover thermostats this holds true, but there is no reason why this should generally apply to other types of thermal reservoirs.

3. Having an identity between phase space contraction and entropy production at hand enables one to link transport coefficients to dynamical systems quantities. Surprisingly, the escape rate approach to Hamiltonian dynamical systems yields a formula that is very analogous to the one obtained for dissipative dynamics: In both cases a transport coefficient is related to a difference between sums of Lyapunov exponents and the Kolmogorov-Sinai entropy on some fractal structure. In case of thermostated systems this structure consists of a fractal attractor, whereas for open Hamiltonian systems it is a fractal repeller.

There is even a third formula of a similar type derived for closed Hamiltonian dynamical systems, which connects the Hausdorff dimension of the hydrodynamic mode governing a transport process and a respective Lyapunov exponent to the corresponding transport coefficient. By performing suitable transformations the previous two formulas can be compared to the latter one. All resulting equations involve fractal dimensions of respective fractal sets and Lyapunov exponents thus revealing a striking formal analogy.

On the other hand, these equations are obtained from three very different approaches to NSS, and correspondingly the physical meaning of the involved quantities is rather different. We described a ‘master formula’ linking two of the three equations, however, its additivity suggests that there is no further reduction onto a common ‘root’. In addition, the formula derived for thermostated systems stands and falls with the validity of the identity between phase space contraction and entropy production, which in turn appears to be doubtful. In this respect the formulas emerging from the two Hamiltonian approaches seem to be on safer grounds.

4. We commented upon the suspected typicality of fractal attractors in dissipative NSS. For Gaussian and Nosé-Hoover thermostated systems there is a wealth of work corroborating the fractality of attractors. However, at least for the driven periodic Lorentz gas the topology of these fractal structures depends not only on the type of thermal reservoir used, but also on the variation of control parameters such as the coupling strength between subsystem and reservoir and the electric field strength. This is exemplified by bifurcation diagrams exhibiting complicated bifurcation scenarios for the attractor under variation of these parameters.

Alternatives to deterministic and time-reversible thermal reservoirs are provided by the stochastic Langevin equation and by stochastic boundary conditions. For a specific stochastically thermostated system it has been proven that the associated invariant measure is smooth hence contradicting the ubiquitous existence of fractal attractors in NSS. This was contrasted by numerical computations for other stochastically thermostated systems yielding again fractal objects, however, partly the numerical concepts employed appear to be debatable. Whether attractors in stochastically thermostated systems are typically smooth or fractal, or whether this actually depends on the specific type of system, remains an important open question.

5. A similar reasoning applies to the field-dependent conductivities of the thermostated driven periodic Lorentz gas. As in case of attractors, their functional forms reflect the specific type of thermal reservoir that has been applied. Numerically, no regimes of linear response could be detected for the driven periodic Lorentz gas, despite a proof for the existence of such a regime in the Gaussian thermostated case. In addition, all conductivities showed pronounced irregularities on finer scales as functions of the field strength which partly may be of a fractal origin. How the latter property goes together with a suspected linear response and to which extent all these properties hold for arbitrary thermal reservoirs remains to be clarified.

From a thermodynamic point of view these intricate dependencies of transport properties on parameter variations and on the type of reservoir are rather undesirable questioning the equivalence of nonequilibrium ensembles. One may thus attribute

such nontrivial characteristics to the simplicity and low dimensionality of the model. This does not imply that the model itself is unphysical, since systems with these properties very well exist in nature. Imposing randomness onto such dynamics indeed smoothes out these irregularities. Considering a higher-dimensional system composed of interacting many particles is expected to yield the same consequences.

In summary, a major question concerning the theory of transport in dissipative systems might be formulated as follows: How general are the results obtained from Gaussian and Nosé-Hoover thermostats for NSS of dissipative dynamical systems? That is, to which extent are these properties universal in that they hold for other thermostating schemes as well, or do they depend on the specific way of thermostating?

The remaining chapters of Part II will be devoted to shed further light onto this fundamental question. Our approach will be carried out in two steps: A first step is to invent alternative, possibly more general thermostating schemes which are not fully identical to the previous class of methods but share certain characteristics with them, such as being deterministic and time-reversible and leading to NSS. In the following we present two generic examples of such methods. In a second step we study whether, by using these schemes, the same results for quantities characterizing chaos and transport are obtained as exemplified by Gaussian and Nosé-Hoover thermostats.

14 Gaussian and Nosé-Hoover thermostats revisited

In our previous discussions we have identified important crosslinks between chaos and transport in Gaussian and Nosé-Hoover thermostated models. Some authors even conjectured these relations to be universal for dissipative dynamical systems altogether. It is thus illuminating to look at simple generalizations of ordinary Gaussian and Nosé-Hoover dynamics, which we define again for the driven periodic Lorentz gas. We then analyze these thermostating schemes along the same lines as discussed previously, that is, by analytically and numerically studying the transport and dynamical systems properties of the respectively thermostated driven periodic Lorentz gas. Finally, we compare the results obtained from our analysis to the ones characterizing conventional Gaussian and Nosé-Hoover schemes as discussed in Chapters 11 to 13.

14.1 Non-ideal Gaussian thermostat

Consider again the Gaussian thermostated driven periodic Lorentz gas defined by Eqs. (11.1), (11.4) with an external field that is parallel to the x direction, $\varepsilon \equiv (\varepsilon_x, 0)^*$. We now distinguish between the interactions of subsystem and thermal reservoir parallel and perpendicular to the field direction by making the parallel coupling field-dependent,

$$\begin{aligned}\dot{r}_x &= v_x \\ \dot{v}_x &= \varepsilon_x - \alpha v_x - \alpha \varepsilon_x v_x \\ \dot{r}_y &= v_y \\ \dot{v}_y &= -\alpha v_y \quad ,\end{aligned}\tag{14.1}$$

where $\alpha \equiv \alpha(v_x, v_y)$.¹ The difference to the Gaussian case is reminiscent by the third term on the right hand side of the second equation. This additional term conveniently adjusts the action of the thermostat to the anisotropy of the external field thus providing a physical justification for its introduction. Correspondingly, one may expect that this version thermalizes the driven Lorentz gas more efficiently than the conventional, as we may now call it, Gaussian thermostat Eqs. (11.1), (11.4). Formally, this generalization just amounts in making the conventional coupling constant field-dependent and then expanding it in the

¹The careful reader may suspect some mismatch of units in the second of the four equations listed above. However, we replaced the Stokes friction coefficient by $\alpha(1 + \varepsilon_x/|\varepsilon_0|)$, where ε_0 is some arbitrary field strength by which we make the field term dimensionless. As before with the masses, the charge, and the Boltzmann constant, we set $\varepsilon_0 \equiv 1$.

field strength ε_x in form of a power series, $\alpha \equiv (1 + \varepsilon_x)\alpha$. The conventional Gaussian case is obviously recovered in zeroth order while Eqs. (14.1) include the first order.

The explicit functional form for α can be calculated in complete analogy to Section 11.1 from the requirement of energy conservation yielding

$$\alpha(v_x, v_y) = \frac{\varepsilon_x v_x}{v^2 + \varepsilon_x v_x^2} . \quad (14.2)$$

Comparing this result to the corresponding one for the conventional Gaussian thermostat Eq. (11.4) identifies the second term in the denominator as a new contribution. By using the definition of Eq. (11.5) the average phase space contraction rate is calculated to

$$\kappa = - \langle \alpha \rangle - \left\langle \frac{2\varepsilon_x^2 v_x v_y^2}{(v^2 + \varepsilon_x v_x^2)^2} \right\rangle . \quad (14.3)$$

Again, a comparison of κ with the result for the conventional Gaussian thermostat Eq. (11.6) is instructive: apart from the correction already contained in α , Eq. (14.3) features a second term for the phase space contraction rate. All these additional terms become negligible in the limit of $\varepsilon_x \rightarrow 0$ thus approximately recovering the conventional Gaussian thermostat. But the point is that according to Eq. (14.3) there is clearly no identity between phase space contraction and thermodynamic entropy production anymore. Indeed, some entropy production related to Joule's heat, $dS = \varepsilon_x \langle v_x \rangle / T$, see Eq. (11.8), is still reminiscent in Eqs. (14.2), (14.3), however, it does not show up in form of a simple functional relationship to the average phase space contraction rate.

We may thus refer to the coupling in terms of the conventional Gaussian thermostat defined by Eqs. (11.1), (11.4) as an *ideal coupling*, in the sense that it yields this simple identity, whereas we call the coupling Eqs. (14.1), (14.2) *non-ideal* in that it does not preserve the identity. Consequently, we call the thermostating scheme defined by Eqs. (14.1), (14.2) the *non-ideal Gaussian thermostat*.²

We now discuss computer simulation results for the driven periodic Lorentz gas thermostated that way [Kla99b]. Note that for technical reasons here the field of strength ε was chosen to be parallel to the y -axis, $\varepsilon \equiv \varepsilon_y$,³ by adjusting the thermostating scheme in Eqs. (14.1) respectively. Fig. 14.1 (a) shows results for the conductivity $\sigma(\varepsilon)$ of the non-ideal Gaussian thermostated driven Lorentz gas. The fluctuations on small scales are less irregular than for the conductivity of the conventional Gaussian thermostat Fig. 11.4, which probably reflects the more efficient coupling with respect to the direction of the field. However, the oscillations seem to be less smooth than the ones for the Nosé-Hoover case shown in Fig. 12.4. Again there is no visible regime of linear response for $\varepsilon \rightarrow 0$. Curiously, the nonlinearities conspire to form an approximately linear response regime at intermediate values of the field strength; see, e.g., Ref. [Coh98] for a brief appreciation of such phenomena. Reassuringly, for small enough field strength the conductivity approaches the value indicated by a star, which was calculated from the respective diffusion coefficient in the field-free case according to the Einstein formula Eq. (11.12), see Section 11.2.4.

Fig. 14.1 (b) depicts numerical results for the average phase space contraction rate Eq. (14.3) and for the thermodynamic entropy production according to $dS(\varepsilon) = \langle \varepsilon v_y / v^2 \rangle = \sigma(\varepsilon) \varepsilon^2 / T$.

²This scheme was orally presented on occasion of the conference on *Microscopic chaos and transport in many-particle systems* in Dresden, August 2002 [Kla].

³Numerical results indicated that for $\varepsilon \parallel x$ the dynamics suffered from more creeping orbits than for $\varepsilon \parallel y$.

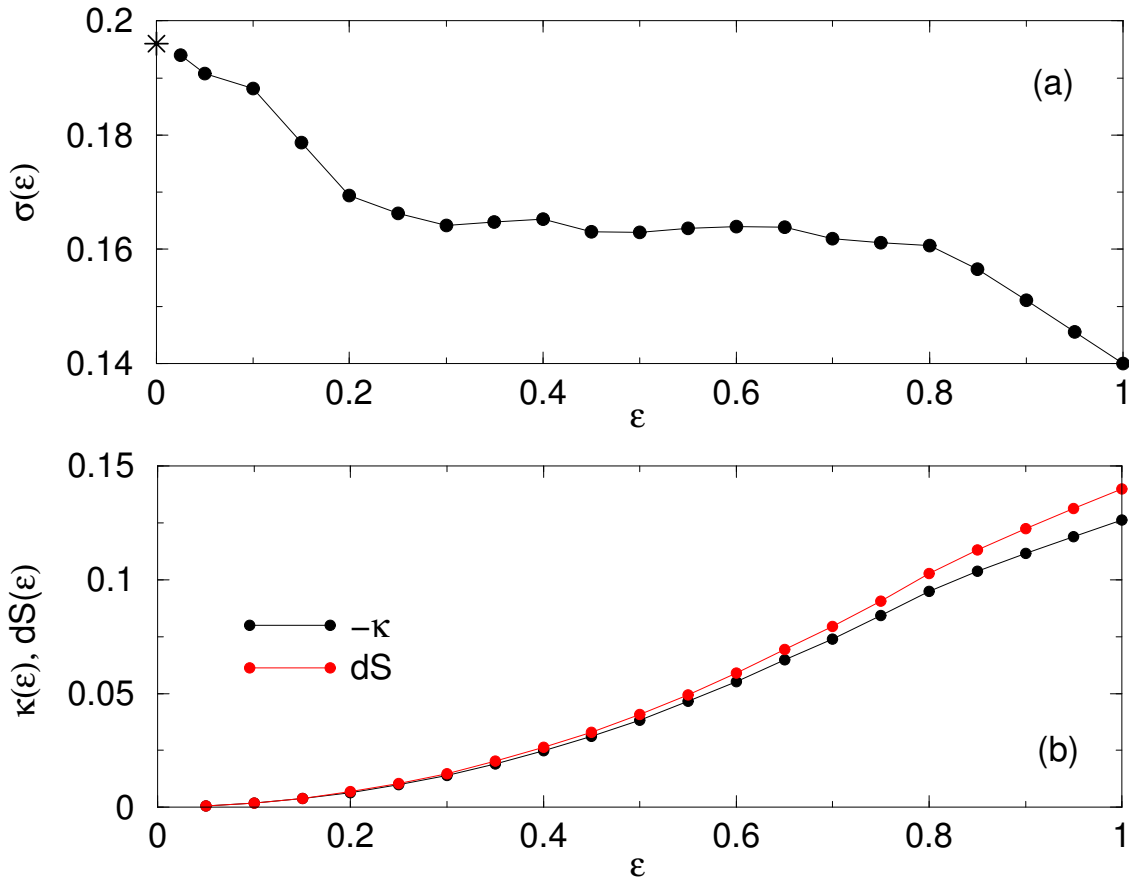


Figure 14.1: Computer simulation results for the driven periodic Lorentz gas equipped with the non-ideal Gaussian thermostat Eqs. (14.1) at the temperature $T = 1$: (a) Field-dependent conductivity $\sigma(\varepsilon)$ as a function of the field strength $\varepsilon \equiv \varepsilon_y$. The star denotes the result in the limit of $\varepsilon \rightarrow 0$ according to the Einstein formula Eq. (11.12). (b) Comparison between the average phase space contraction rate $\kappa(\varepsilon)$ and the thermodynamic entropy production $dS(\varepsilon)$.

These results quantitatively confirm the non-identity between both quantities as already suggested by Eq. (14.3). Note that in analogy to the irregularity of $\sigma(\varepsilon)$ at least the entropy production $dS(\varepsilon)$ should yield irregularities on fine scales as well. However, this structure might be largely suppressed by the quadratic factor in ε . It would be interesting to investigate whether κ and dS exhibit different types of such irregularities corresponding to more intricate higher-order deviations between them.

Since there is no identity between phase space contraction and entropy production there is trivially no simple relation between the conductivity and the Lyapunov exponents such as the Lyapunov sum rule Eq. (11.11), cp. to its derivation for the conventional Gaussian thermostat in Section 11.2.2. Indeed, for the average phase space contraction rate Eq. (14.3) it is not even obvious how to single out the conductivity without performing suitable approximations. For the two-dimensional Lorentz gas a conjugate pairing of Lyapunov exponents is guaranteed by default. However, one may conjecture that this property also holds in case of higher-dimensional non-ideal Gaussian thermostated systems. It is furthermore natural to assume that a fractal attractor exists for the respectively thermostated driven periodic

Lorentz gas which is qualitatively of the same type as the one for the conventionally Gaussian thermostated model Fig. 11.2. These questions as well as how the respective non-ideal bifurcation scenario looks like remain to be investigated.

14.2 Non-ideal Nosé-Hoover thermostat

Precisely the same reasoning as for the non-ideal Gaussian thermostat can be applied for constructing a non-ideal Nosé-Hoover scheme. We illustrate this by summarizing results from Ref. [Rat00a]. Without loss of generality the coordinate system is chosen such that the direction of the field with strength ε is parallel to the x -axis. Indeed, with $\alpha \equiv (1 + \varepsilon_x)\alpha$ it is easy to see that the heuristic derivation for the conventional case provided in Section 12.2.1 must not be repeated, since all other functional forms remain precisely the same. This implies that even with a field-dependent α the respectively thermostated system is still transformed onto the same canonical distribution Eq. (12.8) as in case of the conventional Nosé-Hoover thermostat.

For our definition of the non-ideal Nosé-Hoover thermostat we thus simply combine Eqs. (14.1) with α defined by Eq. (12.10) yielding

$$\begin{aligned} \dot{r}_x &= v_x \\ \dot{v}_x &= \varepsilon_x - \alpha v_x - \alpha \varepsilon_x v_x \\ \dot{r}_y &= v_y \\ \dot{v}_y &= -\alpha v_y \\ \dot{\alpha} &= \frac{v^2 - 2T}{\tau^2 2T} . \end{aligned} \quad (14.4)$$

The conventional Nosé-Hoover thermostat Eqs. (11.1), (12.10) is recovered from these equations as a special case in thermal equilibrium, $\varepsilon_x \rightarrow 0$.

That the strength of the coupling between particle and reservoir is indeed properly adjusted to the anisotropy induced by the field is made more explicit as follows: Eqs. (14.4) can be rewritten by defining two field-dependent friction coefficients, $\alpha_x = (1 + \varepsilon_x)\alpha$ and $\alpha_y \equiv \alpha$, governed by

$$\dot{\alpha}_x = (v^2/2T - 1)(1 + \varepsilon_x)/\tau^2 \quad (14.5)$$

and

$$\dot{\alpha}_y = (v^2/2T - 1)/\tau^2 , \quad (14.6)$$

respectively. For each velocity component there is consequently a separate reservoir response time according to $\tau_x := \tau/\sqrt{1 + \varepsilon_x}$ and $\tau_y \equiv \tau$. Correspondingly, with increasing field strength the response time parallel to the field decreases thus making the action of the thermostat parallel to the field more efficient compared to the coupling perpendicular to the field.

In analogy to the previous section and to Sections 11.2, 12.3, we shall now discuss the chaos and transport properties of the non-ideal Nosé-Hoover thermostated driven periodic Lorentz gas. Starting from Eq. (11.5) the phase space contraction rate of this thermostated system is obtained to

$$\kappa = -(2 + \varepsilon_x) \langle \alpha \rangle . \quad (14.7)$$

ε	$\tau = 1$	$\tau \simeq 31.6$		
	$-\kappa$	dS	$-\kappa$	dS
0.5	0.152	0.145	0.145	0.147
1.0	0.547	0.561	0.567	0.592
1.5	1.240	1.366	1.256	1.391

Table 14.1: Average phase space contraction rate κ , see Eq. (14.7), and thermodynamic entropy production $dS = \varepsilon \langle v_x \rangle / T$, $\varepsilon \equiv \varepsilon_x$, for the non-ideal Nosé-Hoover thermostated driven periodic Lorentz gas Eqs. (14.4). As a value for the temperature we have $T = 0.5$. The numerical error is about ± 0.001 . The data are from Ref. [Rat00a].

Performing an analogous calculation as in Section 12.3.1, i.e., starting from the energy balance Eq. (12.13) and requiring that the average time derivative of the total energy is zero, by using Eqs. (14.4) we arrive at the equation

$$\frac{\varepsilon_x \langle v_x \rangle}{T} = 2 \langle \alpha \rangle + \frac{\varepsilon_x \langle v_x^2 \alpha \rangle}{T}, \quad (14.8)$$

which should again be compared to the result of the conventional case Eq. (12.14). Obviously, as in case of the non-ideal Gaussian thermostat Eq. (14.3) there is a new second term that does not allow for an identity between the average phase space contraction rate and thermodynamic entropy production. In fact, if v_x^2 and α were independent quantities and if equipartition of energy were fulfilled, $\langle v_x^2 \rangle = T$, then the identity would be recovered from Eq. (14.8). However, first of all, according to computer simulations v_x^2 and α are no independent quantities. Secondly, $\langle v_x^2 \rangle = T$ is only strictly fulfilled in thermal equilibrium, thus the identity cannot hold.

Some numerical results for the phase space contraction rate κ and for the thermodynamic entropy production dS are presented in Table 14.1 at different values of τ and $\varepsilon \equiv \varepsilon_x$ yielding quantitative evidence for these deviations. An interesting aspect is that both functions apparently cross each other, which is at variance with the numerical results for the non-ideal Gaussian thermostat shown in Fig. 14.1, where $-\kappa$ appears to provide a lower bound for dS . The reason for this phenomenon is not yet understood and may deserve further investigations.

In analogy to the non-ideal Gaussian thermostat, Eq. (14.8) does not allow to recover the Lyapunov sum rule Eq. (12.17) as it holds for the conventional Nosé-Hoover thermostat: The electrical conductivity may be suitably introduced on the left hand side of Eq. (14.8), and by using Eq. (14.7) one may also replace the average friction coefficient in the first term on the right hand side by the average phase space contraction rate, respectively by the sum of Lyapunov exponents. Still, there remains the friction coefficient in the second term on the right hand side, which cannot be eliminated without making further assumptions. In any case, the resulting expression is significantly different from any ordinary Lyapunov sum rule as it holds for conventional Gaussian and Nosé-Hoover thermostats. Thus, the non-ideal Nosé-Hoover thermostat provides another counterexample against the universality of simple relations between chaos and transport in dissipative dynamical systems as discussed specifically in Section 13.3.

No Lyapunov exponents have yet been computed for the non-ideal Nosé-Hoover thermostated driven periodic Lorentz gas. However, since this scheme defines also a bulk thermostat we

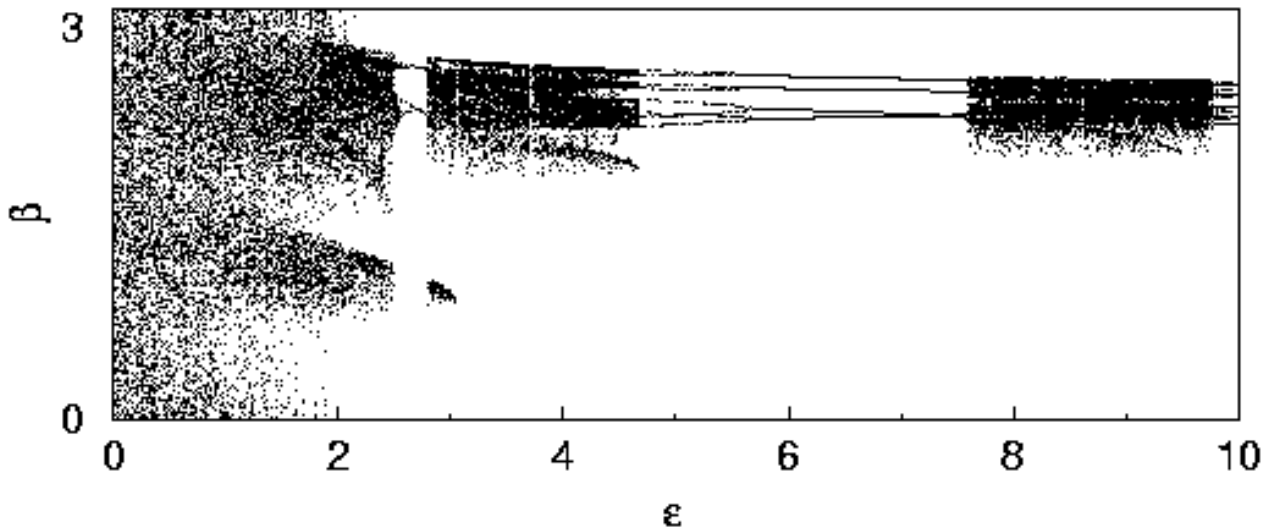


Figure 14.2: Bifurcation diagram for the non-ideal Nosé-Hoover thermostated periodic Lorentz gas driven by an electric field of strength ε which is parallel to the x -axis. β is defined in Fig. 11.1. The temperature is $T = 0.5$, the reservoir coupling parameter $\tau = 1$. The figure is from Ref. [Rat00a].

would expect that conjugate pairing holds for the four Lyapunov exponents of this system. In Section 12.3.2 we have outlined a generalized Hamiltonian formalism for the conventional Nosé-Hoover thermostat. Along similar lines a derivation for the non-ideal Nosé-Hoover thermostat can be performed [Kla]. The same holds for the non-ideal Gaussian thermostat in comparison to the conventional one. But these appear to be rather technical aspects such that we do not go into further detail here.

The structure of the attractor of the non-ideal Nosé-Hoover thermostated Lorentz gas, if projected onto Birkhoff coordinates, see Section 11.2.3, is qualitatively more “smoothed out” than the one of the conventionally Gaussian thermostated version Fig. 11.2. On the other hand, it is still a bit more detailed than the one corresponding to the attractor of the conventional Nosé-Hoover thermostat Fig. 12.2. Here we do not show the attractor generated by Eqs. (14.4) but refer to Ref. [Rat00a] for a respective figure and for further details.

Instead, we present a bifurcation diagram for the non-ideal Nosé-Hoover thermostated driven periodic Lorentz gas. Fig. 14.2 may be compared to the one of the conventionally Nosé-Hoover thermostated case Fig. 12.3 (a). Although the response time τ is one order of magnitude smaller for the conventional case than for the non-ideal version thus indicating a more efficient coupling to the thermal reservoir, the action of the non-ideal version appears to be similarly efficient concerning a full covering of the phase space, which in both cases breaks down approximately at $\varepsilon \simeq 2$. This is in full agreement with the physical motivation for introducing the field-dependent coupling as discussed in the previous section in that it should enhance the efficiency of the thermostat’s action compared to conventional schemes. A bifurcation diagram for the conventional Nosé-Hoover case at $\tau = 1$ can be found in the material accompanying Ref. [Rat00a] and confirms our above assessment.

The parameter-dependent electrical conductivity for the non-ideal version has not yet been computed, however, based on our discussion of the previous cases it is not unreasonable to expect that the results will just yield another highly nonlinear, irregular curve.

14.3 ⁺Further alternatives to conventional Gaussian and Nosé-Hoover dynamics

In order to conclude this chapter we summarize whether various mechanisms generating NSS fulfill the identity between the average rate of phase space contraction and thermodynamic entropy production discussed before. To a large extent, these mechanisms have already been encountered on previous occasions, see in particular Sections 12.4 and 13.2.

Cohen and Rondoni showed that even the Gaussian *isoenergetic* thermostat applied to a many-particle system provides an identity between phase space contraction and entropy production only in the thermodynamic limit of a large number of particles [Coh98, Ron02a]. Benettin and Rondoni introduced a specific time-reversible rescaling of the single velocity components of a moving particle at the boundary of a system while keeping the total kinetic energy fixed [Ben01, Ron02a]. This mechanism may be considered as an intermediate case between a straightforward velocity rescaling, see Section 11.1, and an ordinary Gaussian isokinetic thermostat. The complete dynamical system is defined such that it exhibits a symmetry breaking thus generating a current in a NSS. Similarly to the non-ideal thermostats discussed in the previous two sections, for small enough bias the average phase space contraction rate is getting proportional to the thermodynamic entropy production while for larger bias this relationship becomes inherently nonlinear. Related dissipation mechanisms have been introduced earlier by Zhang and Zhang [Zha92] and in particular by Chernov and Lebowitz [Che95b, Che97], see also Section 15.5.1 where we will discuss the example of a shear flow in a NSS. However, Chernov and Lebowitz argued for an identity according to their method.

As far as the generalized Nosé-Hoover thermostats sketched in Section 12.4 are concerned, whether or not they exhibit an identity can easily be checked by following the second approach outlined in Section 12.3.1 for the example of the conventional Nosé-Hoover thermostat. It turns out that controlling higher even moments along the lines of Nosé-Hoover [Hoo89a, Jel89, Hoo96a, Pos97, Hoo97, Liu00], the Nosé-Hoover chain thermostat [Mar92b, Hoo97, Tuc00] and the deterministic formulation of a Langevin-like equation according to Bulgac and Kusnezov [Bul90b] all preserve the identity. All these schemes are furthermore time-reversible thus sharing fundamental properties with the class of conventional Gaussian and Nosé-Hoover thermostats.

The cubic coupling scheme proposed by Kusnezov et al. [Kus90, Bul90a], on the other hand, is time-reversible but does not show the identity. This is due to a thermalization of the position coordinates creating an additional phase space contraction that does not contribute to a Joule heating. In a way, this method exemplifies our assessment formulated in Section 13.2 that the phase space contraction of a dynamical system may involve contributions that, from the point of view of a thermodynamic entropy production, do not matter. Unfortunately, as we discussed already in Section 12.4.2 the physical interpretation of thermalizing position coordinates in the cubic coupling scheme remains unclear. Hence, this modeling may not be considered as an unambiguous counterexample concerning the identity.

The generalized Nosé-Hoover thermostats introduced by Hamilton et al. [Ham90, L'H93] and by Winkler et al. [Win92, Win95] are all time-reversible but do not fulfill the identity either. However, here it is not yet clear whether these schemes work conveniently in nonequilibrium situations. The methods proposed by Branka et al. [Bra00a, Bra00b] and by Sergi et al. [Ser01] are already not time-reversible and hence do not qualify as counterexamples for

Gaussian and Nosé-Hoover dynamics.

Apart from considering the action of thermal reservoirs leading to dissipative dynamical systems we may recall that there are other ways in order to create NSS which do not involve any phase space contraction thus also providing counterexamples concerning an identity. For example, Gaspard studied diffusion under concentration gradients, respectively dynamical systems under flux boundary conditions [Gas97b, Gas98a]. Eckmann et al. considered a model for a heat flow by using a fully Hamiltonian thermal reservoir consisting of infinitely many planar waves [Eck99a]. All these studies are reminiscent of the Hamiltonian approach to NSS. In the latter case the system actually reminds of the infinite Hamiltonian modeling of the Langevin equation, see Section 10.2, rather than the thermostating approach. In any case, in both situations there is by default no phase space contraction and consequently no identity. Similarly, van Beijeren and Dorfman argued for a non-existence of this identity by using a Lorentz gas model for a heat flow [vB00a], however, their argument appears to be debatable.

Finally, Nicolis and Daems analyzed the general setting of dynamical systems perturbed by noise by deriving a balance equation for the entropy production [Nic96, Nic98, Dae99]. They found correction terms to an identity between phase space contraction and entropy production which they identified as functions of the noise strength. But in this case the dynamical systems considered are again not time-reversible anymore because of the noise and thus belong to a different class than conventional Gaussian and Nosé-Hoover thermostats.

14.4 *Summary

1. We introduced a straightforward generalization of the conventional Gaussian thermostat, again for the example of the driven periodic Lorentz gas. This thermostating scheme is by default deterministic and time-reversible but is constructed such that it does not yield an identity between the average rate of phase space contraction and thermodynamic entropy production. We coined this method the *non-ideal Gaussian thermostat*. Since there is no identity there is also no Lyapunov sum rule relating transport coefficients to dynamical systems quantities. The field-dependent conductivity of this model is again highly nonlinear and different from the one found in other thermostated driven periodic Lorentz gases.
2. In the same vein, we introduced a *non-ideal Nosé-Hoover thermostat* that also does not exhibit the identity and hence no Lyapunov sum rule. In both cases, the non-identity resulted from modifying the coupling between subsystem and thermal reservoir by suitably adjusting it to the symmetry breaking caused by the external electric field. This even increased the efficiency of the non-ideal thermostats compared to their conventional colleagues as could be seen, for example, by means of matching bifurcation diagrams.
3. We finally summarized various other existing approaches towards the construction of NSS by inquiring whether or not they feature an identity between phase space contraction and entropy production. Apart from Hamiltonian modelings of NSS, it appears that there are many other examples of thermostating schemes not providing such an identity. However, in most cases they have not yet been studied respectively in nonequilibrium situations.

15 Stochastic and deterministic boundary thermostats

Gaussian and Nosé-Hoover schemes belong to the class of so-called *bulk thermostats*, that is, they remove energy from a subsystem during the originally free flight of a particle. *Boundary thermostats*, on the other hand, change the energy of a particle only at the collisions with the boundaries of the subsystem.¹

In this chapter we construct and analyze fundamental types of the latter class of thermostats. We start with well-known stochastic versions, which are so-called *stochastic boundary conditions* as they have already been mentioned in Section 13.4. We then show how to make stochastic boundaries deterministic and time-reversible by using a simple chaotic map. This recent, new modeling of a thermal reservoir was called *thermostating by deterministic scattering* in the literature. The equations of motion resulting from this method are still deterministic and time-reversible hence sharing fundamental properties with Gaussian and Nosé-Hoover schemes. However, both the construction of this deterministic boundary thermostat and the dynamics associated with it are generally very different in comparison to conventional bulk thermostats.

An analysis of models thermostated by deterministic scattering thus enables us to learn more about possible universal properties of nonequilibrium steady states in dissipative dynamical systems. We demonstrate this by studying again the transport and dynamical systems properties of a respectively thermostated driven periodic Lorentz gas. Our findings are compared to the ones reported previously for Gaussian and Nosé-Hoover thermostats. We finally briefly discuss results for a hard-disk fluid under nonequilibrium conditions, which is also thermostated at the boundaries.

15.1 Stochastic boundary thermostats

Let us consider a point particle moving in a plane, which interacts with a thermal reservoir through collisions at a flat wall, see Fig. 15.1. If the reservoir is in thermal equilibrium at a certain temperature, the reservoir degrees of freedom will be distributed according to a canonical distribution. Consequently, the subsystem particle will be thermalized at the collision with respect to a Gaussian velocity distribution. If we assume that the memory of the particle is completely lost at the collision, the velocity after the collision can be randomly sampled from the respective velocity distribution of the thermal reservoir. This

¹Of course, the action of Gaussian and Nosé-Hoover thermostats can be restricted to some boundary layers of a subsystem thus bridging the gap between bulk and boundary thermostats as has been done in Ref. [Pos89].

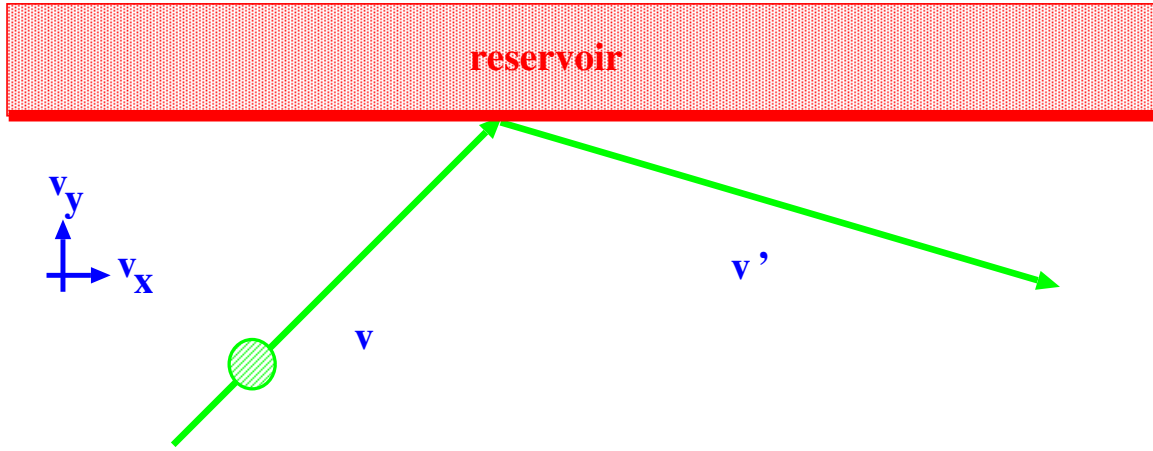


Figure 15.1: Setup for defining stochastic boundary conditions: a point particle of mass $m = 1$ moving with velocity \mathbf{v} collides inelastically with a flat wall. The velocity after the collision is denoted by \mathbf{v}' . The difference in the kinetic energy $(v'^2 - v^2)/2$ is transferred to, or from, a thermal reservoir associated with the wall. \mathbf{v}' is obtained according to Eq. (15.3), see the text.

is the physical essence of what is called *stochastic boundary conditions*, see also our brief account of them in Section 13.4.

Casting this physical picture into an equation it must be taken into account that an impenetrable wall breaks the symmetry of the subsystem. That is, there are different velocity distributions parallel and perpendicular to the wall: Parallel to the wall the particle's outgoing velocity component v'_x , see Fig. 15.1, should be sampled simply from the Gaussian distribution for reservoir velocities parallel to the wall. However, in the perpendicular direction an observer who is sitting at the wall will measure a non-zero average flux of reservoir, respectively subsystem particles to the wall. This flux is due to the fact that all these particles can approach the impenetrable wall from one side only. Consequently, the symmetry of the corresponding distributions of velocity components perpendicular to the wall is broken as well. This is properly modeled by multiplying the bulk velocity distribution of reservoir, respectively subsystem, with the absolute value of the perpendicular velocity component, $|v_y|$.

In summary, if the velocity distribution of the thermal reservoir is canonical at temperature T an observer at the boundary measures for the two velocity components $v_x \in [-\infty, \infty)$, $v_y \in [0, \infty)$ of a reservoir particle colliding with the boundary [Leb78, Cic80, Ten82, Che95b, Che97, Wag99]

$$\rho(v_x, v_y) = (2\pi T^3)^{-1/2} |v_y| \exp\left(-\frac{v_x^2 + v_y^2}{2T}\right) . \quad (15.1)$$

The subsystem particle must then exhibit precisely the same distribution of outgoing velocities, under the conditions that its velocities before and after the collision are not correlated and that the reservoir distribution is not modified.

In practice, these scattering rules are implemented as follows [Wag99]: draw two independently and identically distributed random numbers $\zeta, \xi \in [0, 1]$ from a uniform density $\rho(\zeta, \xi) = 1$ by using a suitable random number generator. The transformation rules of how to get from these uniform distributions to the Gaussian ones of Eq. (15.1) can be

calculated from the requirement of phase space conservation.² For the outgoing velocities $v'_x, v'_y \in [0, \infty)$ this condition reads

$$\begin{aligned} \rho(\zeta)\rho(\xi) \left| \frac{d\zeta d\xi}{dv'_x dv'_y} \right| &= \sqrt{\frac{2}{\pi T^3}} |v'_y| \exp\left(-\frac{v'^2_x + v'^2_y}{2T}\right) \\ &= \left| \frac{\partial \mathcal{T}(v'_x, v'_y)}{\partial v'_x \partial v'_y} \right| \end{aligned} \quad (15.2)$$

Integration yields for the transformation \mathcal{T} the functional form

$$\begin{aligned} (v'_x, v'_y) &= \mathcal{T}^{-1}(\zeta, \xi) \\ &= \sqrt{2T} \left(\operatorname{erf}^{-1}(\zeta), \sqrt{-\ln(\xi)} \right) \end{aligned} \quad (15.3)$$

which completes the algorithm.

15.2 Deterministic boundary thermostats

From the point of view of dynamical systems theory the problem with stochastic boundaries is that they are not deterministic and time-reversible. Consequently, they do not enable a detailed analysis of transport and dynamical systems properties of dissipative systems as outlined in the previous chapters. However, this problem can rather straightforwardly be resolved as follows [Kla00b, Rat00b, Wag99]: Let $\mathcal{M} : [0, 1] \rightarrow [0, 1]$, $(\zeta, \xi) \rightarrow \mathcal{M}(\zeta, \xi)$ be a two-dimensional deterministic map with an inverse \mathcal{M}^{-1} . Loosely speaking, the random number generators in Eq. (15.3) are then replaced by the action of this map, however, in form of the following scattering rules

$$(|v'_x|, |v'_y|) = \begin{cases} \mathcal{T}^{-1} \circ \mathcal{M} \circ \mathcal{T}(|v_x|, |v_y|) & ; v_x \geq 0 \\ \mathcal{T}^{-1} \circ \mathcal{M}^{-1} \circ \mathcal{T}(|v_x|, |v_y|) & ; v_x < 0 \end{cases} \quad (15.4)$$

with $\mathcal{T}^{-1} : [0, 1] \times [0, 1] \rightarrow [0, \infty) \times [0, \infty)$. This prescription is not yet complete. First of all, we have to further specify the sign of the outgoing velocities. We do this for the geometry presented in Fig. 15.1 by requiring that particles going in with positive (negative) tangential velocity go out with positive (negative) tangential velocity. For the perpendicular component we require that v_y always changes its sign. This distinction between positive and negative velocities, supplemented by the respective use of \mathcal{M} and \mathcal{M}^{-1} in the equations, renders the collision process time-reversible. This is easily verified by using the collision rules Eq. (15.4) and reversing the direction of time after a collision. Finally, to avoid any artificial symmetry breaking in numerical experiments, the application of \mathcal{M} and \mathcal{M}^{-1} in Eq. (15.4) should be alternated with respect to the position of the scattering process at the wall.

It remains to characterize the map \mathcal{M} of this equation in more detail. In order to compare with Gaussian and Nosé-Hoover thermostats we require that this map is deterministic and reversible; for a definition of the latter property see footnote 4. Furthermore, \mathcal{M}

²For a two-dimensional Gaussian without a flux term the same reasoning in polar coordinates leads to the well-known Box-Müller algorithm [Pre92].

should be mixing [Arn68, Sch89, Gas98a, Dor99] implying ergodicity and, under rather general conditions, also chaotic behavior [Dev89, Ban92] in the sense of exhibiting a positive Lyapunov exponent [Ott93]. Preferably, the map should also be uniformly hyperbolic [Eck85, Ott93, Gas98a, Dor99], and for convenience it should generate a uniform probability density in phase space. All these properties, except the last one, are necessary conditions for enabling a proper thermostating. That is, the whole phase space of the map should be sampled such that, in combination with the transformation \mathcal{T} according to Eq. (15.4), the canonical distribution can be reproduced completely on the basis of these scattering events; see also Section 12.4.1 for a related discussion of necessary conditions regarding a proper functioning of deterministic thermostats.

Apart from these constraints the precise functional form of the map appears to be arbitrary. By choosing different maps one may model different particle-wall interactions. In this respect the map \mathcal{M} together with the transformation \mathcal{T} plays the role of a scattering function containing detailed information about the microscopic scattering process of a particle. Fixing the functional form of the map completes our set of scattering rules, which has been called *thermostating by deterministic scattering* [Kla00b, Rat00b, Wag99, Rat02].

If not indicated otherwise, in the following we will choose for \mathcal{M} the probably most simple example of a map fulfilling all of the above requirements. This is the two-dimensional *baker map* as it has been introduced and explicitly discussed in Section 13.1, see Eq. (13.1) and the corresponding Fig. 13.1. However, we remark that other simple maps such as the cat map, respectively for general values of the control parameter the sawtooth map, as well as the standard map [Sch89, Ott93, Mei92, All97], both for large enough values of their control parameters, have also been used within this scheme already [Wag99, Kla99b, Wag00].

15.3 + Stochastic and deterministic boundary thermostats from first principles

There are two crucial ingredients in the approach outlined above leading to stochastic and deterministic boundary thermostats: Firstly, the knowledge of the equilibrium velocity distribution functions of a thermal reservoir with infinitely many degrees of freedom is required. Secondly, the energy transfer at the boundaries must be defined in form of suitable microscopic collision rules.

In both respects specifically our derivation of thermostating by deterministic scattering is quite heuristic. That is, we started from essentially pre-defined stochastic boundaries and conveniently modified them by choosing new collision rules. However, a systematic construction from first principles should rather proceed the other way around by first leading to the general solution, which is the deterministic case, and then recovering the stochastic case by eliminating any correlations at the collisions with the wall. Such an approach should provide more insight into the detailed mechanism and into the conditions for a proper functioning of this thermostat. Here we outline in three steps how such a systematic construction is performed [Kla00b, Rat00b]:

1. equilibrium velocity distribution functions:

Our first goal is to construct a model for a thermal reservoir consisting of an arbitrary but finite number of degrees of freedom. For this purpose we need to know the velocity

distribution functions of a subsystem consisting of d_s degrees of freedom, which interacts with a thermal reservoir of $d_r < \infty$ degrees of freedom in thermal equilibrium. With $d = d_s + d_r$ we denote the total number of degrees of freedom, where $d_s < d_r$, and we may assume that there is only kinetic energy. In Section 10.3 we have summarized how to calculate the finite-dimensional velocity distributions of the subsystem by giving some exact results; see Eq. (10.19) for the equilibrium distribution of one velocity component v_1 and Eq. (10.20) for the distribution of the absolute value of the velocity vector of two components v_1 and v_2 with $v = \sqrt{v_1^2 + v_2^2}$.

Note that the corresponding distribution functions are bulk distributions only, whereas, for defining a boundary thermostat, we need to know the functional forms of these distributions at the boundaries of the thermal reservoir, respectively of the subsystem. This bulk-boundary transformation may be performed heuristically such as outlined in the previous section. Ref. [Rat00b] provides a more microscopic derivation of this relation by means of calculating the average time of flight between two collisions and the average collision length. In any case, all these arguments eventually amount in a multiplication of the finite-dimensional bulk densities Eqs. (10.19), (10.20) with a “flux” factor of v_1 , respectively of v , supplemented by a suitable renormalization of the associated velocity distributions.

2. defining a proper coupling:

Knowing these fundamental functional forms of the subsystem’s boundary equilibrium velocity distribution functions, the next step is to define a suitable microscopic coupling between subsystem and thermal reservoir. The coupling should be such that it establishes an energy transfer between subsystem and reservoir degrees of freedom, which generates the desired velocity distribution. In order to preserve the Hamiltonian character of the microscopic equations of motion of the subsystem to be thermostated we demand that this coupling is deterministic and time-reversible. In some sense, there should furthermore be conservation of phase space volume, as will be explained later on.

A first idea of how such a coupling may look like can be obtained from the *rotating disk model*: Let us consider a unit cell of the field-free periodic Lorentz gas, see the geometry of Fig. 10.3, where the fixed disk rotates with an angular velocity ω . Altogether we have thus three degrees of freedom, two for the moving point particle and one for the rotating disk. Assuming that the particle is elastically reflected perpendicular to the disk reduces the problem of an energy transfer between particle and disk to the problem of two elastically colliding masses on a line. The corresponding equations of motion can easily be derived and are of the form of a nonlinear two-dimensional map governing the exchange between translational and rotational energy.

This rotating disk model was originally proposed in Ref. [Rat00b] but became more popular only later on by applying it to a periodic Lorentz gas under a temperature gradient, see Ref. [MM01] and more recent studies in Refs. [Lar03, Bun03b]. Here all disks of the spatially extended Lorentz gas rotate with different angular velocities thus mimicking a thermal reservoir of, in principle, arbitrary dimensionality. Interactions between these different rotational degrees of freedom are provided by the moving particle carrying energy from one disk to another. To some extent, this Hamiltonian modeling of a thermal reservoir reminds of the one employing an arbitrary number of harmonic oscillators which was used for deriving the stochastic Langevin equation, see Section 10.2. It thus suffers from the same deficiency that, at least numerically, it cannot conveniently be applied to nonequilibrium situations involving external fields, because in this case an infinite number of reservoir degrees of

freedom is needed in order to continuously remove energy from the subsystem.

Hence we follow a different path leading to a more abstract and more general model of a thermal reservoir. This approach is further motivated by a second problem with the rotating disk model: Computer simulations for a single rotating disk under periodic boundary conditions show that only for specific values of the associated control parameters this coupling reproduces the equilibrium velocity distributions Eqs. (10.19), (10.20) at $d = 3$ [Rat00b, Lar03]. This reflects the fact that generally the dynamics of this system is very complicated indicating non-ergodic behavior in a mixed phase space consisting of islands of stability and chaotic layers. As a consequence, not for all values of the control parameters there is equipartitioning of energy, which is needed for a microcanonical distribution for subsystem plus thermal reservoir [Rei65]. In turn, only the presence of equipartitioning appears to guarantee a proper energy transfer between subsystem and reservoir degrees of freedom providing a proper thermalization.

In other words, an arbitrary map \mathcal{M} defining the collision rules of a moving particle with a disk, such as provided by the rotating disk model, must generally be *enforced* to yield equipartitioning of energy, respectively the desired equilibrium velocity distributions for reservoir and subsystem.³ This can be achieved by, first of all, choosing a map \mathcal{M} that is sufficiently ‘nice’, in the sense of fulfilling the list of necessary conditions already provided in the previous section. The map must further be combined with a second map \mathcal{T} according to Eq. (15.4) in order to ensure that the desired functional forms of the equilibrium velocity distributions are attained. This map \mathcal{T} is defined in complete formal analogy to Eqs. (15.2), (15.3) in replacing the Gaussian of Eq. (15.2) by the finite-dimensional “target” velocity distribution function determined by Eq. (10.19).

As an example, let us consider a single Lorentz gas scatterer under periodic boundary conditions. We modify the collision rules according to the above reasoning such that this system mimicks a rotating disk-like situation with $d_s = 2$ for the moving particle and $d_r = 1$ associated with the disk, thus $d = 3$ altogether. For the map \mathcal{M} we choose again the baker map Eq. (13.1). The target equilibrium velocity distributions are determined by Eqs. (10.19), (10.20) at $d = 3$. The transformation \mathcal{T} is then calculated from the prescription used in Eq. (15.2) if the Gaussian of this equation is replaced by the respective functions of Eqs. (10.19), (10.20) at $d = 3$. Here one needs to make a choice concerning the coordinate system in which the velocity variables shall be defined. For the Lorentz gas disk one may choose, e.g., a local coordinate system with respect to the point at the collision. Some further details are explained in the following section. The resulting expression for \mathcal{T} is finally combined with the map \mathcal{M} according to Eq. (15.4). Computer simulations of this inelastic Lorentz gas scatterer provide evidence that, indeed, the desired velocity distributions are generated by this model [Rat00b].

Obviously, the general idea underlying this method is not restricted to $d = 3$. According to the transformation \mathcal{T} , all what we need to know is the proper equilibrium distribution function of a thermal reservoir associated with d_r degrees of freedom while interacting with a subsystem of d_s degrees of freedom. In other words, we do not need to care about any explicit equations of motion defining d_r degrees of freedom in order to model a thermal reservoir. From now on we therefore carefully distinguish between the *number of degrees of freedom* of the thermal reservoir that we mimick, and the *number of dynamical variables* which are

³In Ref. [Lar03] it was argued that relating different rotational degrees of freedom to different disks also resolves this problem.

actually involved in modeling this reservoir. For the collision rules that we are currently discussing the action of the thermal reservoir may be represented by one dynamical variable only: Let k represent the absolute value of the velocity vector of all reservoir degrees of freedom. The value of k is then defined via energy conservation for subsystem plus reservoir, $E = v^2/2 + k^2/2$, where v is the absolute value of the velocity of a subsystem particle before a collision. Accordingly, the value v' after a collision is generated by the collision rules Eq. (15.4), with a suitable choice for \mathcal{T} , and the corresponding value k' of the reservoir variable is again obtained from energy conservation. Thus, $\Delta k := k' - k$ yields the energy transfer between subsystem and reservoir at a collision.

We add that this general formalism might be used to obtain deterministic and time-reversible collision rules for two colliding granular particles instead of using normal and tangential restitution coefficients according to which the microscopic dynamics is dissipative, non-Hamiltonian, and not reversible. A finite-dimensional thermal reservoir then mimicks d_r internal degrees of freedom of some granular material storing kinetic energy from which it can be restored at a collision, compare, e.g., to microscopic models of inelastic collisions as discussed in Refs. [Asp98, Bri96]. However, note that we did not yet arrive at the transformation represented by Eq. (15.3), since our collision rules still concern a finite dimensional thermal reservoir only.

3. modeling an infinite dimensional reservoir:

In a general nonequilibrium situation only a thermal reservoir consisting of an infinite number of degrees of freedom is able to continuously absorb energy and to possibly generate a NSS. For the equilibrium velocity distributions Eqs. (10.19), (10.20) this implies that we need to take the limit of $d \rightarrow \infty$. As was shown in Section 10.3, employing equipartitioning of energy we then arrive at the well-known canonical distributions Eqs. (10.21), (10.22). In this limit the total energy of the thermal reservoir is not well-defined anymore, consequently it cannot be represented by a dynamical variable k as introduced for the finite-dimensional case discussed above. However, this variable can easily be dropped, since it does not appear explicitly in the collision rules.

By using now the canonical velocity distribution Eq. (10.21) we arrive at Eq. (15.2) in order to define the transformation \mathcal{T} . Neglecting any correlations in the map \mathcal{M} before and after a collision, the stochastic boundary conditions Eqs. (15.3) are recovered from their deterministic counterpart Eq. (15.4) as a special case. Hence, we may say that this approach provides a derivation of stochastic boundaries from first principles. In fact, thermostatting by deterministic scattering was first constructed by following this bottom-up approach [Kla00b, Rat00b]. Only subsequently it was realized that the final outcome may be considered as a deterministic generalization of stochastic boundaries along the top-to-bottom approach of Section 15.1 [Wag99]. This completes our derivation of a modeling of stochastic and deterministic boundaries “from first principles”.

We conclude this section by taking up the thread from Sections 10.3 and 13.1, in which we provided a simple explanation for the origin of an average phase space contraction in thermostated nonequilibrium systems. In fact, the previous bottom-up approach towards deterministic boundary thermostats nicely illustrates the respective reasoning as follows: Let us start in an equilibrium situation with constant total energy and let the number $d = d_s + d_r$ of degrees of freedom of subsystem plus thermal reservoir for a moment again be finite. As we explained in Section 10.3, in this case an ensemble of points representing

the combination of subsystem plus reservoir is uniformly distributed on a hypersphere in velocity space indicating that there is no average phase space contraction. However, the projected-out velocity distributions of the subsystem are typically not uniform anymore, cp. to Eqs. (10.19), (10.20).

Correspondingly, by calculating the Jacobian determinant for the collision rules Eqs. (15.4) *only* on the basis of respective functional forms of \mathcal{T} for given d , one finds that the subsystem dynamics alone is not phase space conserving at a single collision [Kla]. This should not come as a surprise, since at any collision there is an exchange of kinetic energy with the reservoir. Nevertheless, in case of an equilibrium situation the *average* phase space contraction rate for the subsystem is still zero reflecting the fact that on average there is no energy transfer between subsystem and reservoir. This was also confirmed numerically for the respectively modified Lorentz gas.

The apparent phase space contraction at a collision simply results from the fact that so far we looked at the dynamics of the subsystem only. In a complete analysis the dynamics of the thermal reservoir must be taken into account as well. This dynamics is adequately represented by the variable k , which, here, is well-defined again because of $d < \infty$ and can be obtained via energy conservation. The complete dynamics thus actually consists of the set of variables (\mathbf{v}, k) . By looking at the Jacobian determinant of the combined system (\mathbf{v}, k) one can indeed verify that the complete dynamics is always locally phase space conserving. Consequently, there is no contradiction between a locally dissipative dynamics of the subsystem alone and a phase space preserving Hamiltonian character of the full equations of motion for subsystem plus thermal reservoir.

Let us now apply these arguments to a nonequilibrium situation, e.g., by imposing an external field onto the subsystem. The field will continuously increase the kinetic energy of a particle moving in the subsystem, and the thermal reservoir will continuously absorb this energy through collisions by storing it onto infinitely many degrees of freedom according to equipartitioning of energy. During the free flight of the particle there is no action of the thermal reservoir, and the subsystem is trivially Hamiltonian. At a collision we are using precisely the same collision rules as defined above for which we have argued, in case of $d < \infty$, that there is no loss of phase space volume either. Consequently, by properly looking at subsystem *plus* thermal reservoir we conclude that the whole dynamics is phase space conserving, and in this respect Hamiltonian-like, in nonequilibrium as well. This is not in contradiction to the fact that there is an average flux of energy from the subsystem to the thermal reservoir, which counterbalances the generation of an average current parallel to the external field. These arguments should also be valid by making the number of reservoir degrees of freedom arbitrarily large, that is, in the limit of $d \rightarrow \infty$.

We finally remark that, although for thermostating by deterministic scattering the equations of motion appear to be compatible with a Hamiltonian dynamics, as argued above, a Hamiltonian formulation of this scheme is currently not known.

15.4 Deterministic boundary thermostats for the driven periodic Lorentz gas

Let us now apply the scheme of thermostating by deterministic scattering to the periodic Lorentz gas by modeling a thermal reservoir mimicking an *infinite number* of degrees of

freedom as outlined in the previous section. That is, the originally elastic collisions of the moving particle with the hard disk are made *inelastic* allowing for an energy transfer at a collision without changing the geometry of the system. Note that the unit cell with a single scatterer is periodically continued by applying periodic boundary conditions. In physical terms one may thus think of the arbitrarily many degrees of freedom that we are now going to associate with the disk as mimicking, e.g., different lattice modes in a crystal, which remove energy from a colliding particle.

This modification of the standard Lorentz gas is performed by adapting the collision rules Eqs. (13.1), (15.3) and (15.4) to the circular geometry of a Lorentz gas disk. For this purpose we replace the usual Cartesian coordinates by the tangential, respectively the normal component of the velocity of the colliding particle in a local coordinate system at the scattering point. That is, we write $v_{\parallel} \equiv v_x$ and $v_{\perp} \equiv v_y$ in Eqs. (15.3), (15.4). Alternatively, one may wish to choose local polar coordinates [Kla00b, Rat00b].

We are now prepared to study the chaos and transport properties of the driven periodic Lorentz gas thermostated by deterministic scattering and to compare the results with the previous ones obtained for ideal and non-ideal Gaussian and Nosé-Hoover thermostats. Note that thermostating by deterministic scattering was constructed in order to generate a canonical velocity distribution in thermal equilibrium. In this respect this boundary thermostat forms a counterpart to the Nosé-Hoover thermostat acting in the bulk. In fact, our previous Fig. 12.1 depicts some representative nonequilibrium velocity distribution functions for the driven periodic Lorentz gas thermostated both by Nosé-Hoover and by deterministic scattering. For moderate to large response times the Nosé-Hoover distributions are indeed very similar to the one obtained from thermostating by deterministic scattering.

Concerning other chaos and transport properties we will show in the following that a comparison is more non-trivial. First we check analytically for an identity between phase space contraction and entropy contraction. We then show numerical results for the attractor both resulting from deterministic and from stochastic boundary thermostats. In the deterministic case we further discuss the associated bifurcation diagram as well as the electrical conductivity. Finally, we elaborate on the spectrum of Lyapunov exponents. In this section we particularly summarize results published in Refs. [Kla00b, Rat00b, Rat02].

15.4.1 Phase space contraction and entropy production

In contrast to bulk thermostats such as Gauss or Nosé-Hoover, for a driven periodic Lorentz gas thermostated at the boundaries the phase space volume is conserved during free flights between collisions. As was briefly mentioned in the previous section, any phase space contraction can thus only be generated by the collision rules defined in terms of the composition of maps Eqs. (13.1), (15.3) and (15.4). For maps any change of the phase space volume is assessed by the Jacobi determinant, see Section 13.1. In case of thermostating by deterministic scattering adapted to the Lorentz gas geometry this quantity may be denoted by $|dv'_{\parallel} dv'_{\perp}|/|dv_{\parallel} dv_{\perp}|$. Here the numerator is composed of the two velocity components after a collision and in the denominator there are the corresponding velocity components before a collision with the disk. If a particle collides $n \in \mathbb{N}$ times the product of Jacobian

determinants evolves in time according to

$$\begin{aligned} \prod_{i=1}^n \frac{|dv'_{i,\parallel} dv'_{i,\perp}|}{|dv_{i,\parallel} dv_{i,\perp}|} &\equiv \exp \left(\sum_{i=1}^n \ln \frac{|dv'_{i,\parallel} dv'_{i,\perp}|}{|dv_{i,\parallel} dv_{i,\perp}|} \right) \\ &= \exp \left(n \left\langle \ln \frac{|dv'_{\parallel} dv'_{\perp}|}{|dv_{\parallel} dv_{\perp}|} \right\rangle \right) . \end{aligned} \quad (15.5)$$

For the last step it was assumed that the system is ergodic, which enables to replace the time average by an ensemble average over colliding particles. In this expression

$$\kappa_b := \left\langle \ln \frac{|dv'_{\parallel} dv'_{\perp}|}{|dv_{\parallel} dv_{\perp}|} \right\rangle \quad (15.6)$$

is denoted as the average exponential rate of phase space contraction per unit time, where the index b indicates the definition at a boundary. This quantity is obviously zero if the map is volume preserving and deviates from zero otherwise. Hence, for time-discrete dynamics such as the collision map Eq. (15.4) under consideration κ_b replaces the average phase space contraction rate κ of time-continuous dynamics defined by Eq. (11.5).⁴

For the periodic Lorentz gas thermostated by deterministic scattering κ_b can be calculated from the collision rules Eqs. (13.1), (15.3) and (15.4) to [Rat02]

$$\kappa_b = \frac{\langle v'^2 \rangle - \langle v^2 \rangle}{2T} , \quad (15.7)$$

where v' and v are the absolute values of the velocities after and before a collision, respectively. κ_b is thus identical to minus the average outward flux of kinetic energy to the reservoir $dQ := (\langle v^2 \rangle - \langle v'^2 \rangle)/2$ divided by the temperature T , where T derives from Eq. (15.3). This result holds in equilibrium as well as in nonequilibrium. As in case of Gaussian and Nosé-Hoover thermostats, Eq. (15.7) may now be compared to the entropy production $dS = dQ/T_r$ in terms of the heat transfer between subsystem and thermal reservoir, cp. to Section 11.2.1, where T_r denotes the temperature of the thermal reservoir, leading to

$$\kappa_b = -\frac{T_r}{T} dS \quad . \quad (15.8)$$

In this case, the question concerning an identity between dS and κ_b boils down to the problem whether the temperature T coming from Eq. (15.3) can always be identified with the actual temperature of the thermal reservoir T_r . In equilibrium, that is, without applying an external field ε , it is $T = T_r$ for the periodic Lorentz gas, which follows from the definition of this thermostating scheme outlined in Section 15.1 to 15.3. However, in this situation Eq. (15.8) is trivially zero on both sides anyway.

On the other hand, to define a proper temperature in a nonequilibrium situation is very problematic, see also our brief discussion in Section 10.1. For our model one can argue at least along two different lines in order to define a proper reservoir temperature: One

⁴More explicitly, κ_b naturally shows up in the formal solution for the probability distribution function of the time-discrete Liouville (Frobenius-Perron) equation in dissipative maps. This is in full analogy to solving the time-continuous Liouville equation Eq. (12.3), where the average of the divergence plays the same role.

reasoning is that the temperature of a thermal reservoir consisting of an infinite number of degrees of freedom should never change under whatsoever nonequilibrium conditions and, hence, should always be the same as in thermal equilibrium [Hoo02a]. This implies $T_r \equiv T$ and according to Eq. (15.8) the identity between phase space contraction and entropy production, as discussed for ideal Gaussian and Nosé-Hoover thermostats, holds as well.

However, for all thermostats analyzed in Part II it is well-known that generally the nonequilibrium temperature of the subsystem, if defined via the kinetic energy of the moving particle on the basis of equipartitioning of energy, is not necessarily equal to the equilibrium reservoir temperature T that is contained in the equations of motion [Pos88, Pos89, Eva90b, Sea98, Rat00a]. In case of boundary thermostats this implies that identifying T_r with T typically yields temperature jumps at the boundaries [Kus02]. Such discontinuities in the temperature profile are at variance with a local equipartitioning of energy between the reservoir degrees of freedom and the degrees of freedom of the colliding particle.

In contrast to the first definition outlined above, this motivates to simply *assume* such an existence of a local equipartitioning of energy in a NSS. Under this assumption the reservoir temperature can be defined by computing the average kinetic energy of a particle at the moment of the collision [Wag99, Kla00b, Rat00b, Rat02]. This definition of a nonequilibrium temperature thus amounts in smoothly extrapolating the temperature profile from the bulk of the subsystem to the boundary of the reservoir. An application of this method to the boundary thermostated driven periodic Lorentz gas yields $T_r > T$ for an electric field with strength $\varepsilon > 0$ [Rat02]. Consequently, by following a temperature definition that is based on a no temperature-slip assumption at the boundary the identity is not recovered. In our view, both definitions of a reservoir temperature can be defended. Therefore, the issue about the existence or non-existence of the identity may be considered as undecided in this case.

As far as the Lyapunov sum rule introduced in Section 11.2.2 is concerned, the situation is simpler. Replacing κ_b on the left hand side of Eq. (15.8) by the sum of Lyapunov exponents we may employ $dS = \varepsilon < v_x > / T_r$ on the right hand side, which is the Joule heat that the particle gains during a free flight. Using furthermore $\sigma(\varepsilon) = < v > / \varepsilon$ we obtain

$$\sigma(\varepsilon) = -\frac{T}{\varepsilon^2} \sum_{i=1}^4 \lambda(\varepsilon) \quad , \quad (15.9)$$

which, formally, is precisely the Lyapunov sum rule derived for the ideal Gaussian and Nosé-Hoover thermostats, cp. to Eqs. (11.11), (12.17). The only ambiguity is, again, whether T shall be identified with the temperature of the thermal reservoir or whether it shall be considered as a parameter in nonequilibrium by which the reservoir temperature T_r can be tuned accordingly, as discussed above. In any case, whether or not there holds an identity between phase space contraction and entropy production, here there exists a simple relation between the conductivity and the Lyapunov exponents of the system.

15.4.2 Attractors, bifurcation diagram and electrical conductivity

Fig. 15.2 shows two attractors for the driven periodic Lorentz gas thermostated at the boundaries, where all results presented for this thermostat are at $T = 0.5$. Part (a) displays simulation results for the deterministic boundaries Eqs. (13.1), (15.3) and (15.4) adapted to the Lorentz gas geometry. Part (b) shows analogous results for stochastic boundaries,

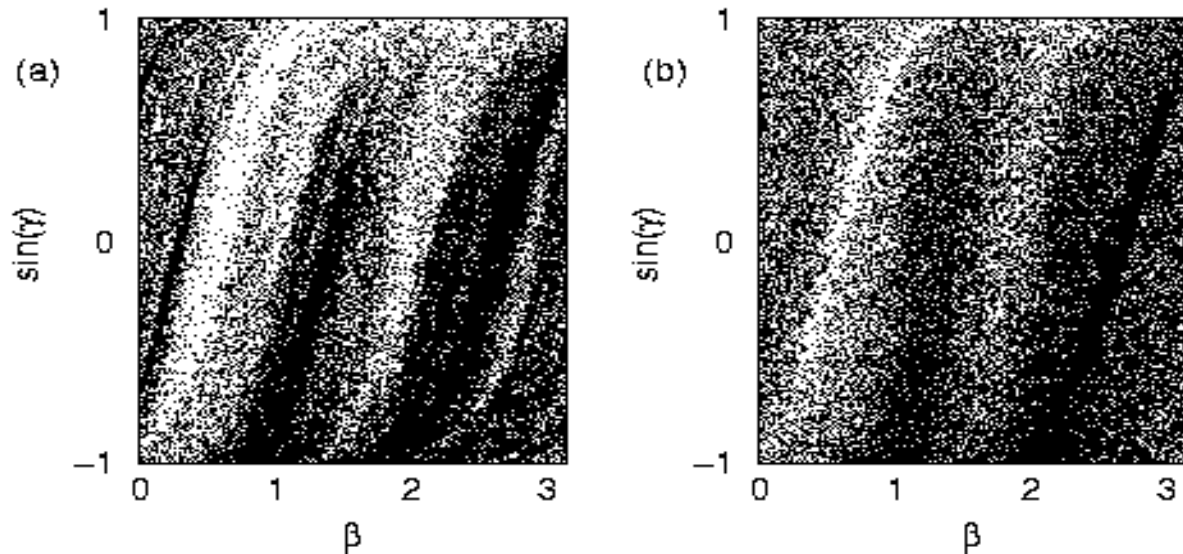


Figure 15.2: Attractor for the periodic Lorentz gas driven by an electric field of strength $\varepsilon = 1$ which is parallel to the x -axis. The reservoir equilibrium temperature is $T = 0.5$, β and $\sin \gamma$ are defined in Fig. 11.1. In (a) the system is thermostated by deterministic scattering, see Eqs. (13.1), (15.3) and (15.4), in (b) it is thermostated by stochastic boundaries, see Eq. (15.3) and explanations. The results are from Refs. [Kla00b, Rat00b].

where the baker map Eq. (13.1) has been replaced by a random number generator. Both figures may be compared to the previous attractors Fig. 11.2 for the Gaussian thermostated Lorentz gas and Fig. 12.2 for Nosé-Hoover.

Clearly, the deterministic boundary solution exhibits a fractal-like folding, in analogy to the ones displayed for the Gaussian and for the Nosé-Hoover thermostat. In Fig. 15.2 (a) this structure just appears to be a bit more smoothed-out than for the Nosé-Hoover case. On the other hand, apart from a few non-uniformities on a coarse scale no fine structure is visible anymore for the attractor obtained from stochastic boundaries suggesting that Fig. 15.2 (b) does not represent a fractal set.

For deterministic boundaries the dimensionality of the attractor in the four-dimensional phase space was computed numerically by means of the field-dependent Kaplan-Yorke dimension $D_{KY}(\varepsilon)$ that was briefly mentioned in Section 13.3 [Rat02]. The results show that the dimensionality monotonously decreases from $D_{KY}(0) = 4$ to $D_{KY}(1) \simeq 3.7$ quantitatively confirming the fractality of the attractor in Fig. 15.2 (a). For Fig. 15.2 (b) respective computations are more subtle⁵ and remain to be done. We emphasize that such computations would be very interesting, since according to our discussion in Section 13.4 it is not yet clear whether or not stochastically thermostated systems typically exhibit fractal attractors. The bifurcation diagram for the driven periodic Lorentz gas thermostated by deterministic boundaries is depicted in Fig. 15.3. Again, it should be compared to the previous counterparts Fig. 11.3 for the ideal Gaussian thermostat, Fig. 12.3 for the ideal Nosé-Hoover and Fig. 14.2 for the non-ideal Nosé-Hoover thermostat. Remarkably, in case of deterministic

⁵The Kaplan-Yorke dimension requires the computation of the full spectrum of Lyapunov exponents. Therefore, in case of stochastic boundaries one has to compute Lyapunov exponents for a stochastically perturbed dynamics; see also our discussion in Section 13.4 for respective difficulties.

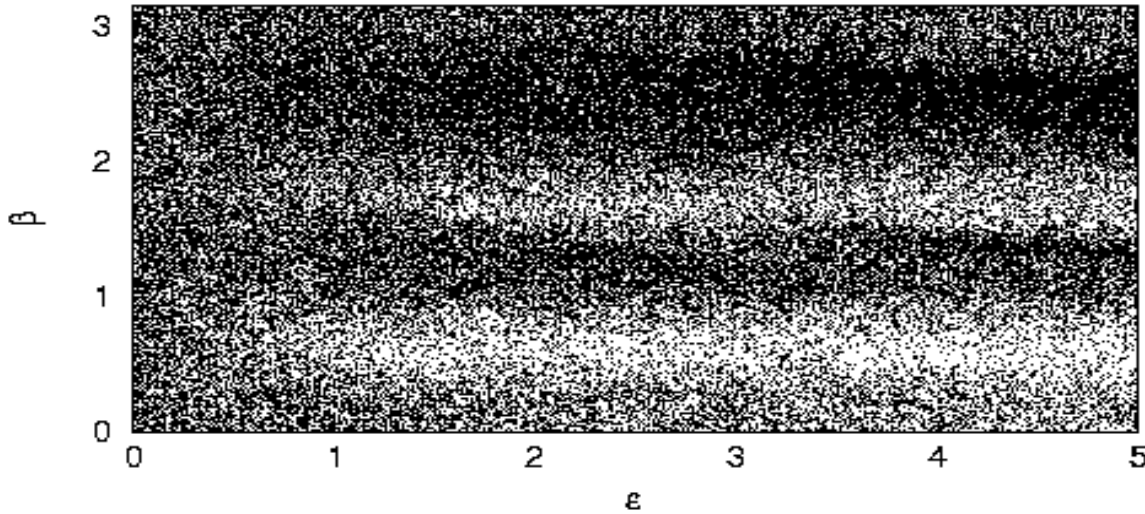


Figure 15.3: Bifurcation diagram for the periodic Lorentz gas thermostated by deterministic scattering and driven by an electric field of strength ε which is parallel to the x -axis. The reservoir equilibrium temperature is $T = 0.5$, β is defined in Fig. 11.1. The figure is from Refs. [Kla00b, Rat00b].

scattering there is no bifurcation scenario at all. That is, Fig. 15.3 neither shows a contraction of the attractor onto periodic orbits nor a breakdown of ergodicity for higher field strengths as it occurs for Gauss and Nosé-Hoover. Similar results have been obtained for other choices of projections in phase space as discussed in Ref. [Rat00b]. These results indicate that deterministic boundaries more strongly regularize the dynamics of the subsystem than Gauss and Nosé-Hoover. Furthermore, the different bifurcation diagrams clearly show that for simple systems such as the periodic Lorentz gas the deformations of the attractor under variation of the field strength intimately depend on the specific type of thermostating. Fig. 15.4 finally contains the field-dependent electrical conductivity for the driven periodic Lorentz gas deterministically thermostated at the boundaries. In comparison to the conductivities corresponding to the ideal Gaussian, Nosé-Hoover and to the non-ideal Nosé-Hoover thermostats shown in Figs. 11.4, 12.4 and 14.1 (a), respectively, this curve looks rather smooth. As in the other cases, there is no indication of a regime of linear response in the numerically accessible regime of field strengths above $\varepsilon \geq 0.1$. On the other hand, again some wiggles on fine scales are visible suggesting that even for a bifurcation diagram such as Fig. 15.3 the corresponding conductivity might be, to some extent, an irregular function on fine scales. Note that the diffusion coefficient of the field-free periodic Lorentz gas thermostated by deterministic scattering may be different from the one for fully elastic scatterers and has not yet been computed. Hence, we do not know the prospective limiting value of $\sigma(\varepsilon)$ for $\varepsilon \rightarrow 0$ according to the Einstein formula Eq. (11.12).

15.4.3 Lyapunov exponents

By applying our deterministic boundary thermostat the kinetic energy is not kept constant at any instant of time, in analogy to Nosé-Hoover, but in contrast to the Gaussian thermostat. Consequently, this system is characterized by four Lyapunov exponents in the two-dimensional periodic Lorentz gas thermostated by deterministic scattering. Numerical

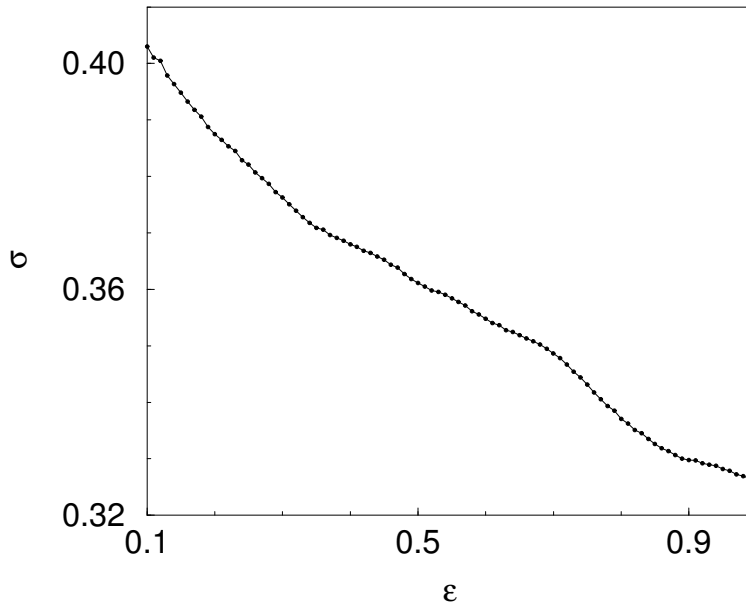


Figure 15.4: Electrical conductivity $\sigma(\epsilon)$ for the periodic Lorentz gas thermostated by deterministic scattering and driven by an electric field of strength ϵ which is parallel to the x -axis. The reservoir equilibrium temperature is $T = 0.5$. Each point has a numerical uncertainty that is less than the symbol size. The results are from Refs. [Kla00b, Rat00b].

computations of this spectrum of Lyapunov exponents turn out to be rather delicate due to the inelasticity at the collisions and require some more intricate adjustments compared to standard methods [Rat02].

For zero field numerical results corroborate that conjugate pairing holds with two zero, one negative and one positive Lyapunov exponent. However, in nonequilibrium there is no pairing of Lyapunov exponents anymore as shown in Fig. 15.5. This is in sharp contrast to the Lyapunov spectrum associated with bulk thermostats such as Gauss and Nosé-Hoover but appears to be typical for boundary thermostats, see our discussion in Section 11.2.2. More precisely, one Lyapunov exponent is zero reflecting phase space conservation parallel to the flow. Two become negative and decrease monotonously in the field strength similar to power laws. Their functional forms remind of the non-zero exponents associated with the Gaussian thermostated driven Lorentz gas [Mor96a]. Indeed, as we have shown, for both thermostats there holds the Lyapunov sum rule, see Eqs. (11.11), (15.9). This equation, in turn, requires that the Lyapunov exponents are quadratic at least for small enough field strength.

The single positive Lyapunov exponent, on the other hand, displays a more intricate non-monotonous behavior under variation of the field strength. According to Pesin's theorem, see Section 13.3, it must be equal to the Kolmogorov-Sinai entropy suggesting the following heuristic understanding of its functional form [Rat02]: For small field strength the particle attempts to move parallel to the field, hence the Kolmogorov-Sinai entropy decreases. However, by increasing the field strength the system starts to heat up in the bulk, consequently the Kolmogorov-Sinai entropy increases again. Such a behavior was not observed for the Gaussian thermostated Lorentz gas, where the Kolmogorov-Sinai entropy always decreases monotonically [Del95a, Det95], which is probably due to constraining the energy in the bulk.

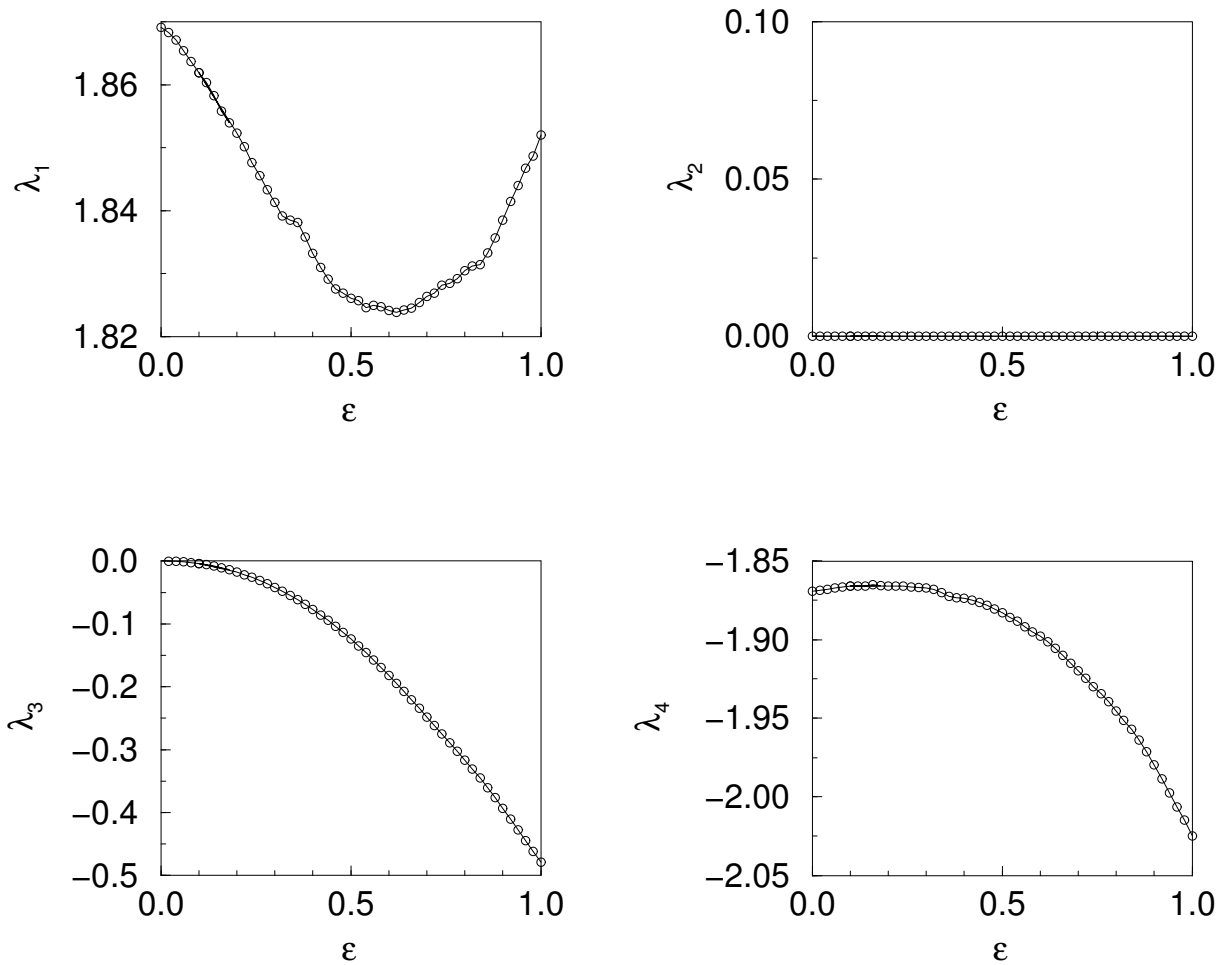


Figure 15.5: The four Lyapunov exponents $\lambda_i(\varepsilon)$ for the periodic Lorentz gas thermostated by deterministic scattering and driven by an electric field of strength ε which is parallel to the x -axis. The reservoir equilibrium temperature is $T = 0.5$. The numerical uncertainty of each point is less than $5 \cdot 10^{-4}$. The results are from Ref. [Rat02].

15.5 Hard disk fluid under shear and heat flow

Up to now we have applied different schemes of thermostating to the driven periodic Lorentz gas only, which is a one-particle system that derives its statistical properties from the chaotic scattering of a moving point particle with a fixed hard disk. We deliberately chose a very simple model in order to focus on the impact that different thermostats have on this system. From this point of view, an important question is to which extent our findings concerning relations between chaos and transport still hold for many-particle systems that include interactions between different moving particles. Suitably amended periodic Lorentz gases of this type were already investigated in Refs. [Bar93, Bon97, Bon02]. Here we skip this intermediate step and immediately consider interacting many-particle systems for which hard disk fluids under nonequilibrium conditions are typical examples.

In a way, by looking at these systems we are back to the roots of thermostating: As explained in Section 1.2 and Chapters 10 to 11, deterministic thermostats were originally designed as efficient tools within the framework of molecular dynamics computer simulations for driving

large, interacting many-particle systems into well-defined NSS that are consistent with the laws of thermodynamics. That deterministically thermostated systems furthermore exhibit interesting chaos properties was only realized later on and subsequently motivated more specific studies of simple models such as the Nosé-Hoover oscillator and the thermostated driven Lorentz gas.

Here we move the other way around from simple to more complex systems. Particularly, we want to check whether for interacting many particles there is an identity between phase space contraction and entropy production, whether there are simple equations relating transport coefficients to Lyapunov exponents, and whether NSS are still characterized by the existence of fractal attractors.

As an example, we discuss a hard disk fluid under shear and heat flow. We start by briefly sketching various known methods for modeling a shear flow. A well-known example are the *SLLOD* equations of motion representing the application of the conventional Gaussian thermostat for obtaining a sheared NSS. We then outline the construction of *Maxwell daemon boundaries* for modeling a hard disk fluid under shear. Finally, we discuss in more detail results for heat and shear flows generated according to thermostating by deterministic scattering, where we draw upon Refs. [Wag99, Wag00]. Interesting questions are whether these systems yield an identity between phase space contraction and thermodynamic entropy production and, correspondingly, whether there are Lyapunov sum rules for the respective transport coefficients. We furthermore summarize numerical results for the Lyapunov spectrum and for the Kolmogorov-Sinai entropy of this system.

15.5.1 Homogeneous and inhomogeneous modelings of shear and heat flows

Modeling and understanding shear and heat flows features as a prominent problem in nonequilibrium statistical mechanics. This is reminiscent by the existence of a huge literature on this subject. It is certainly not our goal to give a full account of all these works, in particular since many important aspects are nicely summarized in a number of reviews [All87, Eva90b, Hes96a, Hes96b, Hoo99, Mun00]. However, by mainly focusing on shearing we briefly describe at least some important approaches that have been pursued and to give a short account of investigations along the lines of connecting chaos and transport.

Probably the most naive way to shear a many-particle system is by using walls that move with certain velocities [Hes96a, Mun00]. Early attempts along these lines trace back to work by Hoover and Ashurst, see, e.g., Ref. [Hoo75] and also Refs. [Lie92, San92] for later investigations. Posch and Hoover used such *sliding boundaries* in combination with a Nosé-Hoover thermostat restricted to these boundaries [Pos89].

In contrast to this inhomogeneous driving from the boundaries, *Lees-Edwards* or *sliding brick* boundary conditions act homogeneously in the bulk of the system [All87, Eva90b, Hes96a, Hes96b, Hoo99, Mun00, Coh95]. The idea is to suitably displace copies of a unit cell of particles in space such that a linear shear profile is imposed onto the system. Lees-Edwards boundaries alone already yield a planar Couette flow for not too high shear rates. However, it turned out that this method could be improved by combining it with a Gaussian thermostat. In fact, the need to conveniently simulate sheared fluids and solids originally motivated the invention of the Gaussian scheme, cp. also to Section 11.1 [Hoo82, Eva83a]. Further refinements of the approach consisting of homogeneous shearing and Gaussian bulk

thermostating eventually led to the formulation of the *SLLOD*⁶ equations of motion [Eva90b, Eva90a, Sar92, Coh95, Hes96a, Mor89c, Sar98, Sea98, Mun00].

Curiously, by applying these shear flow algorithms to fluids consisting of hard spheres shear-induced microstructures were emerging in the simulations for high enough shear rates. That is, the particles were aligning themselves parallel to the direction of the flow in form of strings, or blocks (“plugs”). These orderings became known as the *string phase*, [Eva86, Eva90b, Mun00], respectively the *plug phase* [Loo90, Hes90, Hes96b, Hes97]. Partly it was argued that these phases represent artifacts of the homogeneous thermostating algorithms described above, since by construction these methods are adapted to the shear flow profile in a self-contained way [Eva86, Eva90b]. This led to the invention of more refined *profile unbiased* thermostating schemes (*PUT*) for which, partly, such structures were not observed anymore. Further refinements of *PUT* thermostats, on the other hand, reproduced these flow-induced positional orderings again [Loo90, Hes90]. To some extent, this problem reminds of our previous discussion starting from Chapter 11, where we have shown that the application of different thermostats to the driven periodic Lorentz gas may yield different NSS. Here we appear to have a similar situation in the nonlinear regime of a sheared and thermostated many-particle system.

More recent work focused onto the connection between momentum transport and chaos properties of shear flows. It may not come as a surprise that, again, the *SLLOD* equations furnish an identity between phase space contraction and entropy production [Coh97]. Consequently, there is also a Lyapunov sum rule as already discussed in Section 11.2.2 [Eva90a]. The most simple sheared systems allowing more detailed analyses are two-particle systems [Lad85] for which the existence of a shear viscosity could be proven [Bun96]. Morriss et al. [Mor87b, Mor89a, Mor89b, Pet94] extensively computed the complete spectra of Lyapunov exponents for such systems by showing that the phase space in these models contracts onto fractal attractors. Further numerical computations of Lyapunov spectra for sheared many-particle systems under application of conventional thermostating algorithms have been performed in Refs. [Pos89, Eva90a, Sea98, Sar92, Eva00]. Note that the existence of a conjugate pairing rule even in homogeneously thermostated shear flows appears to be very delicate topic, as we have already outlined in Section 11.2.2. We finally mention that even a multibaker map modeling a shear flow has been constructed and analyzed in Refs. [Tel01, Mat01].

Alternatively, Chernov and Lebowitz [Che95b, Che97] proposed a many-particle shear flow model exhibiting a well-defined NSS without using a conventional thermostat. They considered a two-dimensional system of hard disks confined in a square box of length L with periodic boundary conditions along the x -axis, i.e., the left and right sides at $x = \pm L/2$ are identified. At the top and bottom sides of the box, $y = \pm L/2$, they introduced rigid walls where the disks are reflected according to certain scattering rules. The disks interact among themselves by impulsive hard collisions so that the bulk dynamics is purely conservative.

Shear is now introduced by imposing collision rules at the boundaries which turn the angle θ that the velocity vector of a particle moving towards the wall forms with the wall into an outgoing angle $\theta' := c\theta$, $0 < c < 1$. These “Maxwell daemon-like” boundaries mimic the impact of a shear force at the particle-wall interaction and enforce that particles move favorably parallel to the wall. Since energy is conserved by this operation the total energy of

⁶Concerning the origin of this name, which is not an acronym, see, e.g., Ref. [Mun00] and further references therein.

the particles is strictly kept constant thus reminding of the action of a Gaussian thermostat. Similar constraints have also been studied by other authors in different settings [Zha92, Ben01].

Chernov and Lebowitz used both time-reversible and irreversible formulations of such scattering rules. In both cases the resulting NSS of the hard disk-fluid were in full agreement with hydrodynamics. As a consequence of the specific scattering rules at the boundaries again the total phase space volume was not conserved. However, in this case the authors argued for an identity between phase space contraction and entropy production. Subsequent numerical studies of the dynamical instability of this system performed by other authors [Del97b] clearly showed that, as usual for boundary thermostats, the model exhibited no conjugate pairing rule. On the other hand, by using the full spectrum of Lyapunov exponents again evidence was provided for the existence of a fractal attractor in nonequilibrium. In further work the fluctuations of the entropy production of this model were investigated [Bon98a, Bon01].

As far as heat flows are concerned, general approaches to model the application of temperature gradients are summarized in Refs. [Hoo75, Hoo99, Eva90b, All87, Sar98, Kus02, Hoo03]. A mathematical analysis of Fourier's law in some simple stochastic and Hamiltonian systems was provided in Refs. [Leb78, Eck99b, Eck99a, Mae03b]. Numerical implementations considered both stochastic [Ten82, Cic80] and deterministic boundaries, see, e.g., Refs. [Pos98, Hoo02b, Aok02, Kus02, Hoo03, Pos03]. Bulk thermostats were tested in Refs. [Hoo84, Hoo86]. In more recent work even a heat flow in a periodic Lorentz gas with rotating disks was studied [MM01, Lar03]. We remark that, apart from these works, there exists a vivid discussion about the validity of Fourier's law in more simple models, partly also elaborating on the role of microscopic chaos, see Ref. [Lep03] and further references therein. However, here we will touch the heat flow case only very briefly by restricting ourselves to a specific many-particle system.

In the following we present results for a system consisting of a large number of hard disks that collide elastically with each other. This hard disk fluid is sheared and thermostated at the boundaries. The shear is modeled by moving walls, or sliding boundaries, imposing a local shear force onto the particles. In order to pump energy out of this system we use thermostating by deterministic scattering at the walls.

15.5.2 Shear and heat flows thermostated by deterministic scattering

We consider N hard disks that are confined between two flat walls as described above for the Maxwell daemon model. However, here we change the scattering rules at both walls according to Eqs. (13.1), (15.3) and (15.4), cp. to Fig. 15.1 and the respective discussion. Associating different temperatures T^u and T^d to the upper and the lower wall, respectively, enables us to study the case of a heat flow from a hot to a cold reservoir [Wag99].

For the simulations the length of the box was chosen to be $L = 28$ implying that the volume fraction occupied by $N = 100$ hard disks of radius $r = 1/2$ is $\rho = 0.1$. The temperature gradient was set according to $T^d = 1$ with $T^u = 1.5$ or $T^u = 2$. In both cases the temperature profile was found to be approximately linear, apart from boundary effects, and the kinetic energy of the particles was equipartitioned between the two degrees of freedom. As discussed in Section 15.4.1, assigning T^u and T^d as they appear in Eq. (15.3) to be the reservoir temperatures yields temperature jumps at the walls. This can be avoided by redefining the two reservoir temperatures according to smoothly extrapolating from the bulk to the

boundaries under the assumption of equipartitioning of energy at the walls. In the following we take the latter point of view. Computing the thermal conductivity from simulations, the numerical results matched well to the predictions from Enskog's kinetic theory [Ris96, Gas71]. This agreement improved by driving the system into the hydrodynamic limit. Hence, thermostating by deterministic scattering is able to generate a heat flow in a linear response regime that is in full agreement with hydrodynamics.

In a next step, the identity between phase space contraction and thermodynamic entropy production was checked for this situation. We do not go into too much detail at this point, see Ref. [Wag99] for an explicit discussion. However, there was good agreement between both quantities as obtained from computer simulations, which again improved in the hydrodynamic limit, so in this case the identity was confirmed. We furthermore note that the ingoing and outgoing fluxes at the walls were approaching local thermodynamic equilibrium in the hydrodynamic limit.

Starting from the same setup we now want to model the case of a shear flow. For this purpose we choose $T^u = T^d \equiv 1$. In addition, we wish that the upper and lower wall move with constant velocities d , respectively $-d$, opposite to each other. At a collision a hard disk must then experience the shear force

$$\mathcal{S}_d(v_x, v_y) = (v_x + d, v_y) \quad (15.10)$$

with d being positive (negative) at the upper (lower) wall. The main problem is to suitably combine S_d with the action of the thermal reservoir at the wall. In Ref. [Wag99] three different options for linking S_d with the thermostating rules Eqs. (13.1), (15.3) and (15.4) were explored. We first discuss

$$(v'_x, v'_y) = \begin{cases} \mathcal{S}_d \circ \mathcal{T}^{-1} \circ \mathcal{M} \circ \mathcal{T} \circ \mathcal{S}_d(v_x, v_y) & ; v_x \geq \pm d \\ \mathcal{S}_d \circ \mathcal{T}^{-1} \circ \mathcal{M}^{-1} \circ \mathcal{T} \circ \mathcal{S}_d(v_x, v_y) & ; v_x < \pm d \end{cases} . \quad (15.11)$$

Requiring time-reversibility enforces us to apply S_d symmetrically before and after the thermalization. Performing simulations for $d = 0.05$ and $d = 0.1$ the analysis proceeded along the same lines as for the heat flow: It was found that the system exhibited a linear shear profile for the average velocity parallel to the x -direction and a quadratic temperature profile between the walls, both as expected from hydrodynamics. Again, there were temperature jumps at the walls if the reservoir temperature T_r in nonequilibrium was identified with the equilibrium reservoir temperature T . A comparison of the viscosity computed from simulations with Enskog's theory [Gas71, Che95b, Che97] yielded good agreement in the hydrodynamic limit, which is demonstrated in Table 15.1. Thus, the combined mechanism of boundary thermostating and shear Eq. (15.11) generated a shear flow exhibiting a linear response regime in agreement with hydrodynamics.

We are now prepared to discuss the relation between phase space contraction and entropy production for this model. The average phase space contraction rate κ_b at the walls is defined in complete analogy to Eq. (15.6),

$$\kappa_b := \left\langle \ln \frac{|dv'_x dv'_y dx' dy'|}{|dv_x dv_y dx dy|} \right\rangle . \quad (15.12)$$

Calculating the Jacobian determinant from the collision rules Eq. (15.11) yields

$$\begin{aligned} \kappa_b^{u/d} &= \frac{1}{2T^{u/d}} \left\langle v_x'^2 + v_y'^2 - v_x^2 - v_y^2 - \langle v_x' \rangle^2 + \langle v_x \rangle^2 \right\rangle \\ &+ \frac{1}{2T^{u/d}} \left\langle \langle v_x' \rangle^2 - \langle v_x \rangle^2 - 2d(v_x' + v_x) \right\rangle , \end{aligned} \quad (15.13)$$

	N=100	N=200	N=400	N=800
$d=0.05$	0.9616	0.9904	1.0081	1.0382
$d=0.1$	0.9702	1.001	1.0226	1.0232

Table 15.1: Results for the fraction η_{exp}/η_{th} in a sheared fluid consisting of N hard disks. The shear viscosity η_{exp} was obtained from computer simulations, whereas η_{th} was calculated from Enskog's kinetic theory. The system is driven by boundaries moving with velocities $\pm d$ and thermostated by deterministic scattering at these walls, see Eq. (15.11). The values are from Ref. [Wag99].

where the angular brackets denote ensemble averages over moving particles. The temperatures $T^{u/d}$ are the reservoir equilibrium temperatures at the upper (lower) walls defined in Eq. (15.11).

Eq. (15.13) was already decomposed such that it can be compared to the thermodynamic entropy production of this system. For this purpose we consider again the Clausius form of entropy production in terms of the average heat transfer at the walls reading

$$dS = -\frac{1}{2T_r^{u/d}} \langle v_x'^2 + v_y'^2 - v_x^2 - v_y^2 - \langle v_x' \rangle^2 + \langle v_x \rangle^2 \rangle \quad . \quad (15.14)$$

Here $T_r^{u/d}$ stands for the reservoir temperature in nonequilibrium computed from the assumption that there is no temperature slip at the walls. Obviously, apart from the minus sign dS is formally identical to the first bracketed term in Eq. (15.13). As in Section 15.4.1, the issue is just whether one may identify the reservoir equilibrium temperature $T^{u/d}$ with the reservoir temperature $T_r^{u/d}$ under nonequilibrium conditions. Irrespective of this problem, the second term in Eq. (15.13) yields a contribution to the phase space contraction at the walls that has nothing to do with the thermodynamic entropy production of Eq. (15.14). We may inquire whether this term has a possible physical interpretation. For the scattering rules Eq. (15.11) the average over in- and outgoing velocities parallel to the walls $u_w := (\langle v_x' \rangle + \langle v_x \rangle)/2$ is not necessarily identical to d . By assuming that it is at least some linear function of d the second line in Eq. (15.13) yields some correction of order d^2 . This contribution might be interpreted as a phase space contraction due to a friction parallel to the walls and may be thought of representing properties of a wall like roughness, or anisotropy of the wall scatterers.

In this respect our shear flow collision rules are very close again to the modifications that led to the non-ideal Gaussian and Nosé-Hoover thermostats discussed in Section 14.1 and 14.2. Note that for the latter types of thermostats the identity was destroyed due to what we called a *non-ideal coupling* between subsystem and reservoir. That is, we generalized the way subsystem and reservoir interact with each other by taking into account additional terms going beyond standard Gaussian and Nosé-Hoover frictional forces. Similarly, the above collision rules allow to incorporate further specificities into the microscopic subsystem-reservoir coupling. We conclude that such generalizations may lead to phase space contraction rates that are arbitrarily more complicated than the entropy production expected from thermodynamics.

That indeed the identity between phase space contraction and entropy production does not hold is quantitatively assessed by Table 15.2. Here computer simulation results are presented

	N=100	N=200	N=400	N=800
$d=0.05$	0.6761	0.5882	0.5023	0.4230
$d=0.1$	0.6457	0.5761	0.4934	0.4275

Table 15.2: Computer simulation results for the fraction $-dS/\kappa_b$ in a sheared fluid consisting of N hard disks. The system is driven by boundaries moving with velocities $\pm d$ and thermostated by deterministic scattering at these walls, see Eq. (15.11). The entropy production dS was numerically computed from Eq. (15.14), the average phase space contraction rate κ_b from Eq. (15.13). The values are from Ref. [Wag99].

for the fraction $-dS/\kappa_b$ of the entropy production dS , Eq. (15.14), divided by the average phase space contraction rate κ_b , Eq. (15.13). Clearly, the absolute values of both quantities are not the same, and the situation is getting even worse by approaching the hydrodynamic limit.

We remark that the entropy production in the bulk according to hydrodynamics [Che95b, Che97] was also computed from the simulations. The result was again compared to the entropy flux across the walls in terms of the Clausius entropy yielding good agreement by approaching the hydrodynamic limit. In order to sort out the possibility that the non-identity specifically depends on the choice of the baker map in the collision rules Eqs. (15.11), the same simulations were carried out by replacing the baker with the standard map mentioned in Section 15.2, which was tuned such that its dynamics was approximately hyperbolic. However, instead of recovering the identity here the mismatch between phase space contraction and entropy production got even more profound [Wag99].

A more microscopic understanding concerning the origin of this inequality can be obtained by looking at the velocity distributions of the in- and outgoing particles at the walls. Fig. 15.6 shows that the two velocity components coming in from the bulk are nice Gaussian distributions at the wall. Indeed, the outgoing velocity distribution parallel to y is essentially indistinguishable from its ingoing counterpart. However, in sharp contrast to that the outgoing velocity distribution parallel to x exhibits a very irregular structure with some discontinuities. The explanation is that, according to the collision rules Eqs. (15.11), there will always be more out- than ingoing particles with $v_x \geq d$ at the upper wall (and with $v_x \leq d$ at the lower wall). Thus, due to normalization the two Gaussian halves in Fig. 15.6 (b) will never match to a full, nice Gaussian even in the hydrodynamic limit. Correspondingly, the associated in- and outgoing fluxes at the walls will never come close to a local thermodynamic equilibrium.

This motivates to check for the importance of local thermodynamic equilibrium at the walls concerning an identity between phase space contraction and entropy production. For this purpose a second set of time-reversible collision rules was constructed [Wag99] yielding local thermodynamic equilibrium at the walls in the hydrodynamic limit. However, the analytical result for the average phase space contraction rate already provided an equation that, again, was not identical to the entropy production Eq. (15.14), not even in the hydrodynamic limit. Computer simulations confirmed that, quantitatively, there is no identity either. Hence, these collision rules establish no identity even in case of local thermodynamic equilibrium at the walls.

Eventually, a third set of collision rules was considered, again generating local thermodynamic equilibrium at the walls, however, by breaking time-reversal symmetry [Wag99].

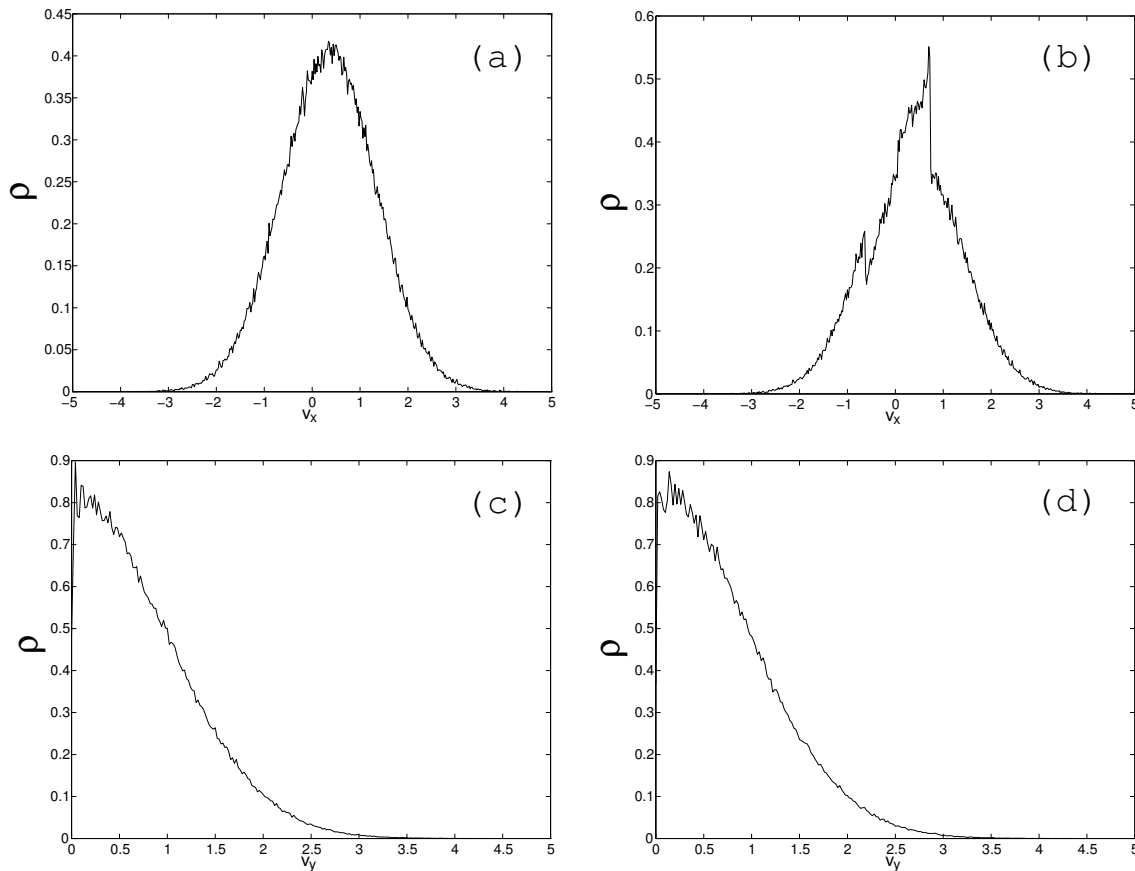


Figure 15.6: Velocity distributions ρ at the walls for a sheared fluid consisting of N hard disks. The system is driven by boundaries moving with velocities $\pm d$ and thermostated by deterministic scattering at these walls, see Eq. (15.11). Shown are results for the velocity components v_x parallel and v_y perpendicular to the upper wall of the sheared system. (a) and (c) depict the distributions of velocities before the collisions with the wall, (b) and (d) the same after the collisions. The results are from Ref. [Wag99].

In this case both the analytical expressions and the computer simulation results showed an identity between phase space contraction and entropy production in the hydrodynamic limit. Consequently, time-reversibility cannot be a necessary condition for an identity between phase space contraction and entropy production. This was already stated in Refs. [Che95b, Che97, Nic98, Dae99] but seems to be at variance with conclusions drawn from the analysis of simple multibaker maps [Vol97, Bre98, Vol98, Tel00, Vol02]; see also Ref. [Mae03a] for a discussion of the relation between time-reversibility and entropy production on the basis of Gibbs states.

Typically, the existence or non-existence of the identity will have direct consequences for the validity of the Lyapunov sum rule as it was discussed in Sections 11.2.2, 12.3.1, 14.1 and 14.2. An exception to the rule was the driven periodic Lorentz gas thermostated by deterministic scattering where the identity was ambiguous, however, where in any case formally a Lyapunov sum rule was recovered, see Section 15.4.1. In other words, the identity is a sufficient condition for the validity of the Lyapunov sum rule but not necessary.

For the heat flow case outlined above the identity holds, hence there is a Lyapunov sum

rule. On the other hand, a numerical computation of the Lyapunov spectrum shows [Wag00] that there is no conjugate pairing of Lyapunov exponents, as expected for a system that is thermostated at the boundaries. A computation of the Kaplan-Yorke dimension corroborates the existence of a fractal attractor. It might be interesting to construct collision rules that do not yield an identity for a heat flow, which should be possible along the lines as performed for the shear flow.

As far as the latter is concerned, for sake of comparison we first state the Lyapunov sum rule for the SLLOD equations. Here the identity holds and the shear viscosity η can be computed to [Eva90a, Coh95]

$$\eta(\gamma) = -\frac{T}{L^2\gamma^2} \sum_i \lambda_i(\gamma) \quad , \quad (15.15)$$

where T is the temperature of the thermal reservoir, respectively the temperature predetermined in the Gaussian thermostat, $\gamma := dv_x(y)/dy$ stands for the shear rate and L is again the system size.

For thermostating by deterministic scattering this relation may look rather different, depending on whether the identity holds. Let us consider the model for a boundary-driven shear flow Eqs. (15.11) explicitly discussed above for which there is no identity. By using the hydrodynamic relation $dS = L^2\gamma^2\eta/T_r$ and Eqs. (15.13), (15.14) one can nevertheless relate the viscosity of this model to the Lyapunov exponents arriving at

$$\eta(\gamma) = -\frac{T}{L^2\gamma^2} \left(\sum_i \lambda_i(\gamma) + O(d^2) \right) \quad . \quad (15.16)$$

Here we have abbreviated the second line in Eq. (15.13) by the expression $O(d^2)$. Note that, in contrast to the non-ideal Gaussian and Nosé-Hoover thermostats of Sections 14.1 and 14.2, in this case we could at least establish an explicit relation between viscosity and Lyapunov exponents. Still, the viscosity is no simple function of Lyapunov exponents anymore thus providing a counterexample against a universality of the Lyapunov sum rule in thermostated interacting many-particle systems.

Fig. 15.7 shows Lyapunov spectra for the shear flow generated from Eq. (15.11) in case of a system with 36 hard disks at a volume fraction of $\rho \simeq 0.47$, where the particles are in a quadratic box of length $L \simeq 7.746$. Depicted are results from simulations at three different shear forces d [Wag00]. The overall shape of these spectra is quite typical for sheared many-particle fluids [Mor89a, Mor89b, Pos89, Eva90a, Sar92, Del97a, Sea98]. However, note the asymmetry particularly between the largest positive and negative exponents. The sum of pairs of respectively ordered exponents is also included in the figure showing that, as in case of the heat flow, there is no conjugate pairing rule for the Lyapunov exponents.

Finally, we present results for the Kolmogorov-Sinai entropy of this system, which, according to Pesin's theorem, is identical to the sum of positive Lyapunov exponents. In Fig. 15.8 this quantity is plotted as a function of the shear rate γ for the same model parameters as in Fig. 15.7 above. The figure may be compared to the respective result for the driven periodic Lorentz gas thermostated by deterministic scattering, see λ_1 in Fig. 15.5. There is quite an analogy in that h_{KS} exhibits a global minimum by increasing the driving force. Curiously, for the non time-reversible collision rules of the third model discussed above there is no such local minimum. Furthermore, the respective results for the heat flow of both models also do not exhibit a local minimum, see Ref. [Wag00] for further details.

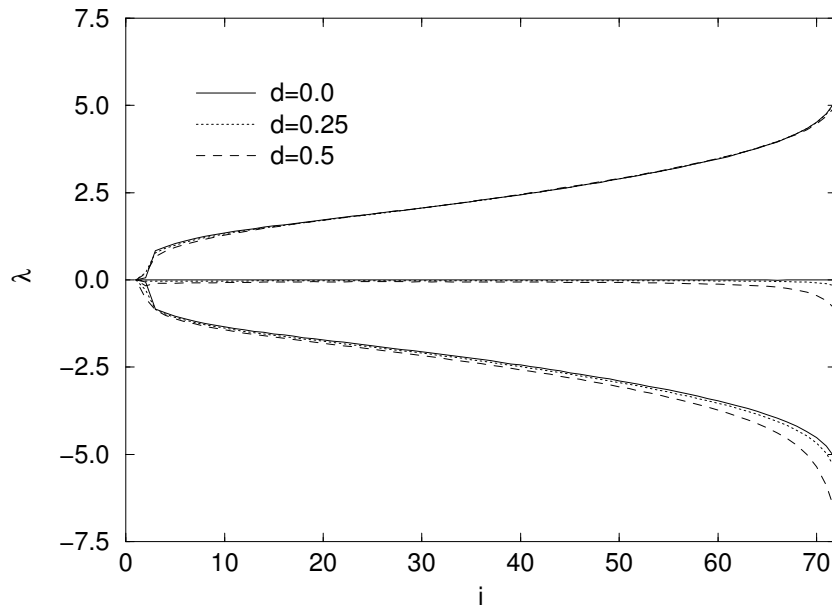


Figure 15.7: Spectra of Lyapunov exponents λ for a sheared fluid consisting of 36 hard disks at a volume fraction of $\rho \simeq 0.47$. The system is driven by boundaries moving with velocities $\pm d$ and thermostated by deterministic scattering at these walls, see Eq. (15.11). Shown are results for three different driving forces as indicated in the figure. The lines in the middle represent the sums of conjugated pairs of Lyapunov exponents. The figure is from Ref. [Wag00].

Computations of the Kaplan-Yorke dimension for the first and the third shear flow model yielded again evidence for the existence of fractal attractors. For a total of 144 phase space variables the associated loss of phase space dimensionality went up to about 6 at shear rates around $\gamma = 0.5$. Assessing the magnitude of the dimensionality loss became an active recent topic particularly by applying Gaussian and Nosé-Hoover thermostats restricted to boundary layers, after it was realized that the dimensionality loss may significantly exceed the number of constrained variables [Hoo02b, Aok02, Kus02, Pos03].

15.6 *Summary

1. Modeling a stochastic thermal reservoir at the boundaries of a system is well-known in form of *stochastic boundary conditions*. The precise collision rules were briefly reviewed at the beginning of this chapter.
2. These stochastic collision rules can easily be made deterministic and time-reversible by using a deterministic map. The map should exhibit certain properties in order to enable a proper thermalization. The resulting deterministic and time-reversible boundary thermostat has been called *thermostating by deterministic scattering*.
3. Both types of boundary thermostats can be derived from first principles in three steps: Firstly, the precise functional forms of the equilibrium velocity distribution functions for arbitrarily many reservoir degrees of freedom are required, as they have been

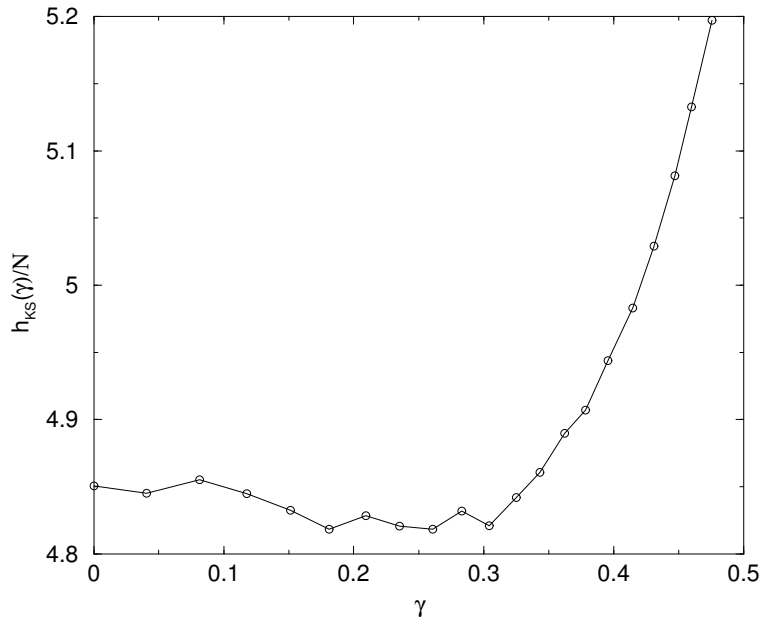


Figure 15.8: The Kolmogorov-Sinai entropy h_{KS} per particle as a function of the shear rate γ for a fluid consisting of $N = 36$ hard disks at a volume fraction of $\rho \simeq 0.47$. The system is driven by boundaries moving with velocities $\pm d$ and thermostated by deterministic scattering at these walls, see Eq. (15.11). The figure is from Ref. [Wag00].

calculated earlier according to elementary equilibrium statistical mechanics. Secondly, one must define some coupling between subsystem and thermal reservoir. One then has to check whether the chosen coupling reproduces the correct velocity distribution functions. For arbitrary couplings this will not hold, typically. In this case one should enforce that the correct target velocity distributions are attained by suitably modifying the collision rules. For a nonequilibrium situation one needs to consider the limit of infinitely many reservoir degrees of freedom. Following this construction step by step sheds light again onto the origin of phase space contraction in thermostated systems, along similar lines as already elucidated previously.

4. As an example for the application of a deterministic boundary thermostat again the driven periodic Lorentz gas has been analyzed. Here the identity between phase space contraction and entropy production is ambiguous and depends on the definition of the temperature of the thermal reservoir. In any case, there is a Lyapunov sum rule for the electrical conductivity.

The attractor for the driven periodic Lorentz gas deterministically thermostated at the boundaries exhibits a fractal structure that is quite analogous to the previous ones resulting from ideal and non-ideal Gaussian and Nosé-Hoover thermostats. For stochastic boundaries this structure is not present anymore suggesting that the corresponding attractor is possibly not fractal. However, this conjecture remains to be verified quantitatively. In contrast to previous thermostated driven Lorentz gases the bifurcation diagram for the deterministic boundary thermostat is phase space covering for all values of the electric field strength. The electrical conductivity shows a nonlinear field dependence that is also different from the one obtained for other thermostats,

being more smooth than in previous cases. Still, there are some irregularities on fine scales.

As is typical for boundary thermostated systems, there is no conjugate pairing rule of Lyapunov exponents for this model. The Kolmogorov-Sinai entropy related to the single positive Lyapunov exponents shows an interesting, non-monotonous behavior as a function of the field strength which has not been observed for bulk thermostats.

5. Finally, we have briefly summarized existing schemes that model shear flows for interacting many-particle systems, such as sliding boundaries, Less-Edwards 'sliding brick' boundary conditions, applying the Gaussian thermostat to shear in form of SLLOD equations of motion and refinements leading to PUT thermostats. For ideal Gaussian thermostats applied to modeling shear and heat flows there hold the usual relations between chaos and transport such as the identity between phase space contraction and entropy production and the Lyapunov sum rule. An alternative scheme was invented in form of Maxwell daemon boundaries and was argued to share the same properties. We also briefly outlined some conventional models of heat flows.

We then focused onto a hard disk fluid under shear and heat flow thermostated by deterministic scattering. For a heat flow this system exhibited linear response and yielded again an identity between phase space contraction and entropy production. For modeling a shear flow three different versions of a deterministic boundary thermostat were discussed. All of them generated a linear response regime. Two of them did not yield an identity and consequently no Lyapunov sum rule. One of them was not time reversible but reproduced the identity. Two of the shear flow models were analyzed in further detail showing that there was no conjugate pairing rule, as expected for thermostats acting at the boundaries. However, both models exhibited a fractal attractor. The latter properties are shared by the heat flow case. As in case of the respectively thermostated driven periodic Lorentz gas, the Kolmogorov-Sinai entropy displayed an interesting non-monotonous behavior as a function of the shear rate.

16 ⁺Active Brownian particles and Nosé-Hoover thermostats

In this chapter we return first to the Langevin equation reviewed in Section 10.2. Langevin’s theory of Brownian motion presupposes that a Brownian particle is only *passively* driven by collisions from the surrounding particles. This input of energy is removed from the system by Stokes friction in the bulk leading to a balance between molecular stochastic forces and friction as formulated by the fluctuation-dissipation theorem.

Surprisingly, the Langevin equation can also be used to describe the motility of biological cells crawling on substrates, at least if the cell dynamics is sampled on large enough time scales. For experiments on moving cells such as granulocytes¹ and other types of crawling cells see Refs. [Fra90, Sto91, Sch93, Har94, Die03]; see also Refs. [Gru94, Rie00, Upa01] for related work where the cells move in more complex environments. In order to illustrate that cells may behave like Brownian walkers Fig. 16.1 depicts an experimentally measured trajectory of an isolated epithelial² cell moving on a substrate.

However, biological entities such as cells or bacteria may not really comply with the physical assumption of being particles that move only because of stochastic environmental forces. In order to sustain their motion such organisms rather need some external supply of ‘fuel’ that may be stored internally, and one may think of some metabolic activity converting the fuel into motion. This picture motivated to suitably amend conventional Langevin equations arriving at *active* Brownian particles that are able to take up energy from the environment, to store it onto internal degrees of freedom, and to convert it into kinetic energy [Sch98, Ebe99, Til99, Erd00]. Earlier models of active Brownian particles featured a response of these entities to environmental changes leading to pattern formation processes on a macroscopic scale [Sch94, SG95]. Other recent work further generalizes active Brownian particles in order to describe confined systems with rotational excitations [Erd02, Ebe03].

In the following we will argue that limiting cases of Langevin equations modeling active Brownian particles contain ingredients that trace back to the conventional Nosé-Hoover thermostat discussed in Chapter 12. This may not come too much as a surprise if one simply reinterprets the thermal reservoir associated with the Nosé-Hoover dynamics as the internal energy of a crawling cell. That is, instead of assuming the thermal reservoir to be ubiquitous and stationary one now deems it to be locally co-moving with the respective biological entity. Note that this merely amounts in suitably adapting the physical interpretation of the equations of motion, without requiring any reformulation of them.

Similarly to deterministic thermostats, in our view such equations for cell motility may be

¹These cells are attracted to sites of inflammation to destroy microorganisms and invaded cells.

²An epithelial cell is one of the closely packed cells forming the epithelium, which is a thin layer of tissue that covers organs, glands, and other structures within the body.

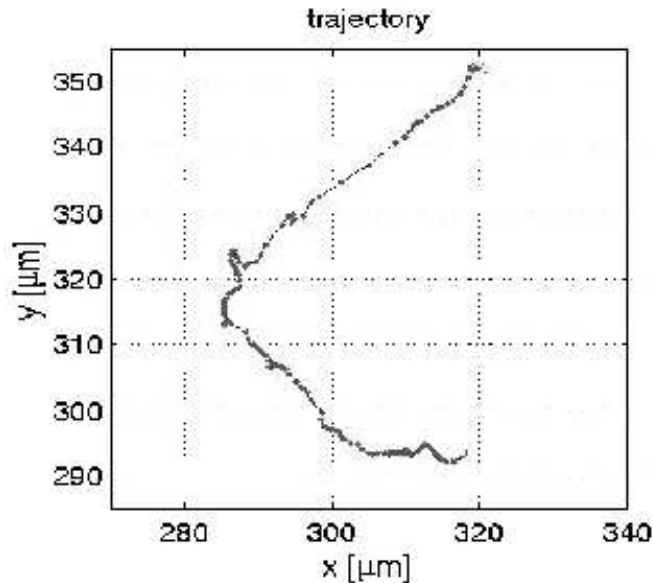


Figure 16.1: Experimental results for the migration of an isolated renal epithelial MDCK-F (Madin-Darby canine kidney) cell on a substrate. The positions x and y were extracted from microscopic phase contrast images taken at time intervals of one minute and acquired for periods of two to four hours [Die03].

considered as simple toy models that are proposed “top-to-bottom” on the basis of heuristic theoretical arguments rather than starting “bottom-up” from a detailed analysis of biological experiments. However, this approach may be useful for learning along which lines ordinary Langevin equations need to be modified in order to model the detailed dynamics of moving cells.

Here we review the formulation of active Brownian particles in terms of generalized Langevin equations. We show that a particularly simple limiting case of such equations exhibits formal analogies with the Nosé-Hoover thermostat. On the basis of the existing literature we then briefly summarize similarities and differences between active Brownian particles and Nosé-Hoover thermostats from a dynamical systems point of view.

In the second section we outline some essential features of the velocity distribution functions of active Brownian particles. We argue that the appearance of crater-like structures in their profile may be understood in connection with Nosé-Hoover thermostats. By employing the general functional forms of the equilibrium velocity distribution functions discussed in Section 10.3 we finally state some necessary conditions for the appearance of such crater-like structures.

16.1 Generalizing Langevin equations for modeling cell motility

The ansatz for modeling active Brownian particles which we review here starts from the generalized two-dimensional Langevin equation [Sch98, Ebe99, Til99, Erd00]

$$\begin{aligned}\dot{\mathbf{r}} &= \mathbf{v} \\ \dot{\mathbf{v}} &= -\alpha\mathbf{v} + \mathcal{F}(t) \quad ,\end{aligned}\tag{16.1}$$

where \mathcal{F} is white noise, that is, a δ -correlated stochastic force of strength S with zero mean value,

$$\langle \mathcal{F}(0)\mathcal{F}(t) \rangle = S\delta(t) \quad .\tag{16.2}$$

The noise strength S can be straightforwardly associated with the friction coefficient α according to the fluctuation-dissipation theorem Eq. (10.2) and with the diffusion coefficient D by using the Einstein relation Eq. (10.3),

$$\frac{S}{2T} = \alpha = \frac{T}{D} \quad .\tag{16.3}$$

Let us now assume that there is a generalized friction coefficient α in form of

$$\alpha = \alpha_0 - de \quad .\tag{16.4}$$

Here α_0 holds for ordinary Stokes friction, the variable e denotes the internal energy of the moving entity, and the constant $d > 0$ yields the rate of conversion from internal into kinetic energy. e is in turn obtained from a suitable balance equation for which different choices have been discussed. A general ansatz, denoted in the following as *case 1*, reads [Sch98, Ebe99, Til99]

$$\dot{e} = \frac{1}{\mu}(q - e(c + dv^2)) \quad .\tag{16.5}$$

In this equation $q \geq 0$ describes a constant take-up of energy, which generally may be space-dependent, and c models some constant internal loss of energy. Note that d could be velocity-dependent, however, in Eq. (16.5) we stick to the most simple assumption that the prefactor of e is only quadratic in v . μ determines the rate of change of the internal energy e and thus plays a role similar to τ^2 in the Nosé-Hoover thermostat, see Eq. (12.10). In case of very fast feedback $\mu \rightarrow 0$ Eq. (16.5) boils down to the fixed point *case 2*,

$$e = \frac{q}{c + dv^2} \quad .\tag{16.6}$$

Combining this equation with Eq. (16.4) yields the velocity-dependent friction coefficient

$$\alpha = \alpha_0 \frac{v^2 - v_0^2}{\frac{q}{\alpha_0} + v^2 - v_0^2}\tag{16.7}$$

with $v_0^2 := q/\alpha_0 - c/d$. A special case of this type of friction is obtained by assuming $v^2 \ll v_0^2$, or alternatively $c/d \gg v^2$, in the denominator only leading to *case 3*

$$\alpha = \alpha_1 \frac{v^2 - v_0^2}{v_0^2}\tag{16.8}$$

with $\alpha_1 := -\alpha_0 + qd/c$. This equation is sometimes called the *Rayleigh-type model*, because a similar ansatz for a velocity-dependent friction coefficient has been introduced by Rayleigh in the context of the theory of sound [Erd00]. Eq. (16.8) looks strikingly similar to Eq. (12.10) defining the Nosé-Hoover thermostat. However, note that the former represents the explicit functional form for α , whereas the latter is a differential equation with a time-derivative for α on the left hand side.

Motivated by this formal similarity, one may ask to which extent models of active Brownian particles can exhibit dynamical systems properties as outlined in Chapter 12 for the Nosé-Hoover thermostat. A fundamental difference between active Brownian particles and Nosé-Hoover thermostats is that the former have been introduced for modeling the energetic aspects of moving biological entities on a microscopic level, without knowing in advance about the velocity distributions generated by these models. In contrast to that, Nosé-Hoover thermostats have been constructed for generating, under suitable conditions, specifically canonical velocity distributions, see Section 12.2.1. A further difference already resulting from the Stokes friction coefficient is that the equations of motion for active Brownian particles are irreversible. But even more, according to ordinary Langevin dynamics these equations include noise, which is in contrast to the concept of Nosé-Hoover and other deterministic thermostats.

In order to bring active Brownian particles and deterministic thermostats closer together, thus making the three models introduced above more amenable to methods of dynamical systems theory, one may replace the white noise term by deterministic chaos, as we already briefly described in Section 10.2. Another option is to generate deterministic chaos by choosing a suitable potential in configuration space such as the geometry of the periodic Lorentz gas, see the beginning of Section 11.1. Yet we do not know anything about the velocity distributions for deterministic active Brownian particles and there is still the lack of time-reversibility. Hence, there is no reason why for these models one should expect an identity between phase space contraction and entropy production to hold. Similarly, there is no reason why by default equipartitioning of energy should be fulfilled. Whether fractal attractors exist for this class of dissipative dynamical systems and whether Lyapunov sum rules and conjugate pairing rules hold, as they typically do for ideal Nosé-Hoover thermostats, are further interesting questions that have not been studied so far. However, we remark that for so-called canonical-dissipative systems containing active Brownian particles as a special case generalized Hamiltonian equations have been constructed that remind of the generalized Hamiltonian formalism developed for Gaussian and Nosé-Hoover thermostats outlined in Section 12.3.2 [Ebe00].

16.2 Crater-like velocity distributions

Let us now summarize what is known about the velocity distribution functions for the three different cases of active Brownian particles discussed above. In this framework we shall also discuss connections with the Nosé-Hoover thermostat.

In all cases, the most obvious solution for the velocity distribution is obtained at $e = \text{const}$. This is the Stokes limit of constant friction for which the velocity distribution is well-known to be purely canonical, see Section 10.3.

For *case 1*, Eqs. (16.1), (16.4) and (16.5), not much appears to be known regarding general combinations of parameters in Eq. (16.5).

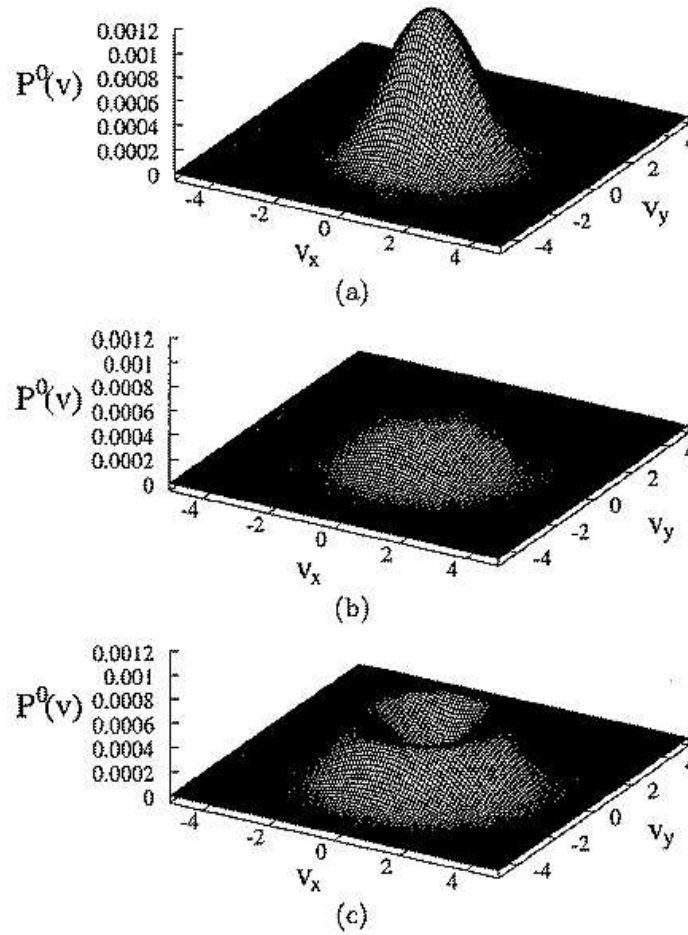


Figure 16.2: Transition from canonical to *crater-like* velocity distributions in the model of active Brownian particles called *case 2*, see Eq. (16.6) in combination with Eqs. (16.1), (16.4). The figure displays the analytical solution $\rho(v) \equiv P^0(v)$ of Eq. (16.9). The parameters are $c = 1$, $q = 10$, $S = 4$, $\alpha_0 = 2$ and (a) $d = 0.07$, (b) $d = 0.2$, (c) $d = 0.7$. The figure is from Ref. [Erd00].

For the special *case 2* the situation is much better: Here the analytical solution for the velocity distribution function can be obtained from solving the corresponding Fokker-Planck equation and reads [Til99, Erd00]

$$\rho(v) = C \left(1 + \frac{dv^2}{c} \right)^{q/S} \exp \left(-\frac{\alpha_0}{S} v^2 \right) \quad , \quad (16.9)$$

where C is a normalization constant. Interestingly, as shown Fig. 16.2 this velocity distribution displays a transition from canonical to more microcanonical-like under variation of d or related parameters. Such *crater-like* velocity distributions exhibiting a dip at the place of the former maximum of the canonical distribution appear to be quite typical for active Brownian particles [Erd00, Sch01, Ebe01, Erd02, Ebe03].

Fig. 16.2 should be compared to our previous Fig. 12.1 displaying velocity distributions for the Nosé-Hoover thermostated driven periodic Lorentz gas. Apart from the asymmetry

due to the external electric field the scenario is completely the same as in Fig. 16.2: By tuning the reservoir coupling parameter τ the Nosé-Hoover velocity distribution clearly shows a transition from canonical to microcanonical-like. The advantage of the Nosé-Hoover thermostat is that due to its construction the origin of these different functional forms is rather well-understood, as already outlined in Section 12.2.2: In the limiting case of $\tau \rightarrow 0$ the Nosé-Hoover thermostat generates a microcanonical velocity distribution, whereas in the limit of Stokes friction for $\tau \rightarrow \infty$ it yields a canonical one. Hence, there must be a transition between canonical and microcanonical for intermediate τ parameters. This transition is represented by a superposition of these two different velocity distributions.

For Fig. 16.2 and *case 2* a very similar explanation might thus be employed: The canonical velocity distribution is probably reminiscent of passive motion of the Brownian particles driven by the noise term in Eq. (16.1). The appearance of microcanonical-like features must then be due to the deterministic, velocity-dependent friction coefficient appearing in the equations of motion. This interplay may result in a transition from a canonical to a microcanonical(-like) distribution which is quite analogous to the one displayed by the Nosé-Hoover system. In contrast to Nosé-Hoover, however, for active Brownian particles this transition may rather reflect a change from noise-driven, passive motion to more active dynamics as determined by the deterministic, nonlinear part of the equations of motion.

On the other hand, we also have this formal analogy between the Nosé-Hoover equations of motion and at least *case 3* of active Brownian particles as noted in the previous section. If this link could be made more explicit one might argue that, irrespective of stochastic contributions in the equations governing active Brownian particles, there should as well be a Nosé-Hoover like transition in the velocity distributions which is purely generated by a tuning of the deterministic, velocity-dependent friction coefficient. This leads us to the conclusion that in case of active Brownian particles there may actually be two rather analogous transitions between canonical and microcanonical distributions, one that is of a purely deterministic origin and another one that is due to the interplay between deterministic and stochastic forces. To which extent the one or the other is exhibited by the dynamics may then depend on the specific choice of the control parameters.

We further remark at this point that an at first view analogous transition from unimodal to bimodal distributions has been reported for the stationary states of a nonlinear oscillator driven by Lévy noise [Che02, Che03]. However, the detailed dynamical origin of this transition appears to be very different from the two scenarios discussed above thus demonstrating that there may actually be a larger number of different dynamical mechanisms generating such bifurcations in the velocity distributions.

In order to undermine these arguments and before discussing the velocity distribution function of *case 3* in detail, let us analyze the transition between microcanonical and canonical distributions for the Nosé-Hoover thermostat more explicitly. Note that in the following we consider a purely deterministic equilibrium dynamics without any external field. We recall that the equation governing the velocity-dependent Nosé-Hoover friction coefficient α , Eq. (12.10), read

$$\dot{\alpha} = \frac{v^2 - 2T}{\tau^2 2T} \quad . \quad (16.10)$$

In the limit of $\tau \rightarrow 0$ the Nosé-Hoover thermostat approaches the Gaussian one for which the kinetic energy is strictly kept constant at any time step. This suggests that the fluctuations of the friction coefficient α triggered in Eq. (16.10) by the remaining equations of motion

should be getting smaller and smaller for larger times when the system is evolving into a steady state. Expanding Eq. (16.10) linearly in time yields

$$\alpha(t + \Delta t) = \frac{v^2 - 2T}{\tau^2 2T} \Delta t + \alpha(t) \quad (\tau \rightarrow 0, \Delta t \ll 1) \quad . \quad (16.11)$$

As desired for thermalizing onto a steady state this equation has a fixed point that in the limit of $\tau \rightarrow 0$ is associated with the Gaussian thermostat constraint $v^2 = 2T$. However, if the first term on the right hand side of Eq. (16.11) were a non-zero constant the system cannot reach a steady state, since $\alpha(t) \rightarrow \pm\infty$. Hence, in this case $\alpha(t) = 0$ is the only steady state solution. For $\tau \ll 1$ small but finite $\alpha(t)$ fluctuates around zero corresponding to the time-dependence of v as induced by the other equations of motion. According to our above argument, for $\tau \ll 1$ these fluctuations may be suitably approximated by setting $\alpha(t) = 0$ on the right hand side of Eq. (16.11) thus recovering the functional form of the Rayleigh friction Eq. (16.8). Note that in the other extreme of $\tau \rightarrow \infty$ the friction coefficient α can be an arbitrary constant thus recovering Stokes friction, which in this equilibrium situation corresponds to zero velocity. We thus have a Hopf-like bifurcation scenario [Ott93] from $v = 0$ for $\tau \rightarrow \infty$ to a limit cycle behavior with $v = \text{const.}$ for $\tau \rightarrow 0$.

On the basis of this approximation, let us study what happens in the limit of small but finite $\tau \ll 1$ for the equilibrium velocity distribution function Eq. (12.8) of Nosé-Hoover reading

$$\rho(t, \mathbf{r}, \mathbf{v}, \alpha) = \text{const.} \exp \left[-\frac{v^2}{2T} - (\tau\alpha)^2 \right] \quad . \quad (16.12)$$

The approximation Eq. (16.11) enables us to eliminate $\alpha(t)$ from the above equation yielding

$$\rho(v) = C \exp \left(-\frac{v^2}{2T} - \frac{(v^2 - 2T)^2 (\Delta t)^2}{4\tau^2 T^2} \right) \quad (16.13)$$

$$= C \delta_\tau \left(\frac{(v^2 - 2T)}{2T} \right) \exp \left(-\frac{v^2}{2T} \right) \quad (\tau \ll 1, \Delta t \ll 1) \quad (16.14)$$

For the second line we have used the definition of the δ -function as a series of exponentials in τ [Rei65], where C is a normalization constant. We thus indeed arrive at the limiting case of a crater-like Nosé-Hoover velocity distribution composed of a canonical and a microcanonical contribution.

This solution may finally help to analyze the velocity distribution that was obtained for the active Brownian particle *case 3* [Erd00, Erd02],

$$\rho(v) = C \exp \left(\frac{\alpha_1}{S} v^2 - \frac{\alpha_2}{2S} v^4 \right) \quad (16.15)$$

with $\alpha_2 := \alpha_0 d/c$. The functional form matches nicely to Eq. (16.13) and there should be a respective decomposition into a canonical and into a microcanonical component in analogy to Eq. (16.14). However, there is the subtlety that Eq. (16.15) represents the solution for a stochastic system as is reminiscent by the strength S of the stochastic force. We therefore have to inquire whether this stochasticity is a crucial ingredient fundamentally distinguishing this distribution from the formally completely analogous but deterministic Nosé-Hoover solution Eq. (16.13).

Let us assume that in a suitable *case 3* system both the fluctuation-dissipation theorem and the Einstein relation are valid. According to Eq. (16.3) S is then a trival function

of the temperature T and the diffusion coefficient D . The temperature T may be defined by furthermore assuming equipartitioning of energy, $T = \langle v_0^2 \rangle / 2$, where $\langle v_0^2 \rangle$ is the average kinetic energy of the active Brownian particle. The diffusion coefficient D might be thought of being generated deterministically. We therefore argue that Eq. (16.15) also holds in a purely deterministic modeling of *case 3* thus establishing the connection to the Nosé-Hoover dynamics analyzed before. Under these conditions, *case 3* must exhibit the very same transition in the velocity distributions as Nosé-Hoover.

For sake of completeness we remark that in the limit of small velocities and by expanding the prefactor of the velocity distribution Eq. (16.9) of *case 2*, Eq. (16.15) of *case 3* is recovered again. Along these lines one may understand a transition such as the one depicted in Fig. 16.2 also on the basis of Nosé-Hoover dynamics.

To summarize, in all three cases of active Brownian particles discussed above there exists Stokes limit of constant friction yielding canonical velocity distributions irrespective of any stochastic contributions. We therefore conjecture that, in analogy to Nosé-Hoover dynamics, for *purely deterministic* active Brownian particles there exists a completely analogous transition from canonical to microcanonical velocity distributions under suitable parameter variation yielding intermediate crater-like velocity distributions. One choice for such a parameter variation should be varying μ in *case 1*, but other combinations of parameters, in analogy to varying τ in Nosé-Hoover dynamics, should be possible as well. For stochastic active Brownian particles defined in the framework of ordinary Langevin dynamics, *in addition* there should be a transition from a canonical velocity distribution function generated by the stochastic forcing to a microcanonical-like counterpart that, again, is due to a suitably tuned deterministic friction coefficient. This theoretical prediction still needs to be verified by computer simulations.

Finally, we briefly comment on two important necessary conditions limiting the range of existence of crater-like velocity distributions. For this purpose we remind again of the derivation of velocity distributions via projection from a microcanonical one outlined in Section 10.3. Let us assume that the velocity space of the moving particle has a dimension of $d \equiv d_s$, in order to be consistent with our previous notations. Let us furthermore assume that the d_s -dimensional velocity distribution of the moving particle is microcanonical as, for example, resulting from the application of a Gaussian thermostat, or in the limit of Nosé-Hoover dynamics for $\tau \rightarrow 0$. The central formula is then Eq. (10.19) telling us that *not* for any dimensionality d_s a one-dimensional projection $\rho(v_x) \equiv \rho(v_1)$ exhibits a crater-like minimum in its functional form.

More precisely, Fig. 10.2 shows that for $d_s \geq 3$ the particle's one-component equilibrium velocity distribution does not display a global minimum anymore. However, this eliminates any possibility for the generation of crater-like velocity distributions. That is, creating a transition from a projection of a microcanonical distribution to a canonical one (by noise, or by tuning τ in the Nosé-Hoover thermostat) for $d_s < 3$ cannot generate any non-monotonocities in intermediate distributions. In other words, for moving particles with more than two degrees of freedom there cannot be any transition between microcanonical and canonical one-component velocity distributions anymore featuring crater-like intermediate functional forms.

An analogous argument holds if the dimensionality d_r of an associated thermal reservoir can be changed as discussed, e.g., for thermostating by deterministic scattering in Section 15.3. For such a combination of subsystem and reservoir one can straightforwardly check [Kla], again by using Eq. (10.19) with $d \equiv d_s$, respectively with $d \equiv d_s + d_r$, that non-monotonous

velocity distributions only appear if $d_s + d_r \geq 3$. These two bounds put therefore quite a window on the existence of crater-like velocity distributions.

Our discussion thus shows how deterministic thermostats such as Gauss, Nosé-Hoover and thermostating by deterministic scattering may help to understand the origin of velocity distributions in, at first view, seemingly quite different systems that may even be amenable to physical and biological experiments.

16.3 *Summary

1. Results from experimental measurements on the motility of isolated cells moving on substrates can be understood, to some extent, by using conventional Langevin equations. Amended versions of such equations modeling the storage of internal energy of biological cells lead to the formulation of *active Brownian particles*.
2. We briefly reviewed three fundamental versions of active Brownian particles in which the friction coefficient of ordinary stochastic Langevin equations has been suitably generalized. The most simple model shared a striking formal similarity with the Nosé-Hoover dynamics discussed before. However, *per se* active Brownian particles and deterministic thermostats belong to the fundamentally different classes of stochastic, respectively deterministic dynamical systems.
3. We then discussed the origin of crater-like velocity distributions both for deterministic Nosé-Hoover dynamics and for stochastic active Brownian particles in thermal equilibrium. In case of Nosé-Hoover this transition is triggered by the tuning of the reservoir response time yielding a superposition between a microcanonical and a canonical distribution, as already mentioned in Section 12.2.2. Here we analyzed this scenario in more detail starting from the Nosé-Hoover equations of motion. Based on formal similarities of the underlying equations, we concluded that the same scenario must be present for active Brownian particles.

However, in addition the latter class of systems appears to feature a second mechanism leading to crater-like velocity distribution functions. In this case they result from a superposition between a stochastically generated canonical distribution and a microcanonical(-like) one related to the action of the deterministic friction coefficient.

Finally, we gave two necessary conditions concerning the involved number of degrees of freedom which must be fulfilled in order to generate transitions that are characterized by crater-like velocity distributions.

17 *Concluding remarks

The final chapter of this thesis consist of two parts: Following the two central themes of this work, we first summarize our main results. We then conclude with a list of what we believe are important open problems.

17.1 A brief assessment of the main results

There are currently two fundamental approaches aiming at a general theory of NSS starting from microscopic chaos in the equations of motions of suitable model systems: One of them proceeds along the lines of Hamiltonian dynamics supplemented by suitable (nonequilibrium) boundary conditions. The other one applies to nonequilibrium situations where a coupling to some kind of thermal reservoir is needed in order to sustain stationary solutions for statistical physical quantities. Typically, the latter approach renders the dynamical systems under consideration non-Hamiltonian due to a respective modeling of thermal reservoirs. We have briefly outlined these two theories of chaotic NSS in our general introduction Chapter 1. Correspondingly, this thesis consisted of two major parts. We now elaborate on the essential themes and results of both parts one after the other.

17.1.1 Fractal transport coefficients in deterministic dynamical systems

Chapters 2 to 9 focused on the phenomenon of irregular, respectively fractal transport coefficients in certain types of chaotic dynamical models. The different facettes of the analysis associated with this theme we summarize as follows:

1. We developed an **arsenal of methods** suitable for computing parameter-dependent transport coefficients of deterministic, chaotic dynamical systems. One type of these methods starts from the fact that, under certain conditions, the Liouville (Frobenius-Perron) operator of dynamical systems can be cast into the form of topological transition matrices. One may then either solve the eigenvalue problems of these matrices, by relating transport coefficients to respective eigenvalues of the Liouville operator, or one may simply iterate these matrices numerically hence obtaining the complete time-dependent solution of the Liouville equation. A rigorous mathematical solution for calculating deterministic transport coefficients of a simple model was, secondly, obtained by Groeneveld. It started from the generating function of the system and succeeded by expressing the transport coefficients in form of some coupled recursion relations. A third method employs Green-Kubo formulas for diffusion and relates diffusion coefficients to a combination of invariant probability densities and fractal

generalized Takagi functions. The latter can be computed by again solving functional recursion relations, whereas the former are still obtained by some matrix method. Of course, these are not the only methods being available for doing such calculations but just the ones used by us, as outlined in Part I.

2. These methods were applied to a **variety of models** exhibiting deterministic transport. Our models were constructed such that they exhibited an increasing degree of complexity, by approaching physical reality. We started with simple one-dimensional, piecewise linear maps on the line yielding rather abstract, but on the other hand exactly solvable models. We then studied a multibaker map representing a two-dimensional extension of such one-dimensional systems. For truly nonlinear one-dimensional maps no exact results could be obtained anymore, and instead we employed computer simulations. The same applies to randomly perturbed one-dimensional maps as well as to deterministic diffusion in Hamiltonian and non-Hamiltonian particle billiards.
3. Studying these models with the set of methods outlined above, we found that they all exhibit **irregular, respectively fractal transport coefficients**. That is, we provided examples for drift coefficients, or conductivities, diffusion coefficients and chemical reaction rates that are all irregular, respectively fractal functions of control parameters. In case of one-dimensional maps it could be shown, qualitatively and quantitatively, that these transport coefficients are strictly fractal. The diffusion coefficients of the three different particle billiards we investigated also displayed irregularities on large and fine scales, however, whether they are of a fractal origin remains an open question.
4. We explored **different ways of understanding these fractal structures**. What we coined turnstile approach relates parameter-dependent irregularities in a transport coefficient to specific microscopic orbits of particles, which originate at specific parameter values. These orbits change in a complicated way under parameter variation due to the topological instability of the chaotic dynamical system hence transferring this instability to the associated transport coefficients. A second approach used the fact that Green-Kubo formulas provide convenient series expansions for, at least, deterministic diffusion coefficients. In these equations the first term is reminiscent of random walk approximations well-known from stochastic theory, whereas higher-order terms feature dynamical correlations of increasingly high order. By looking at the convergence of such a series one can thus identify contributions to fractal diffusion coefficients in terms of specific higher-order dynamical correlations.

In the light of the discussion presented in Part II, one may raise the question to which extent the fractal transport coefficients of Part I may be considered to be “universal” for transport in nonequilibrium steady states. In Chapter 6 we demonstrated that random perturbations smooth out these fractal structures, as expected from naive physical reasoning. We believe that, in a similar way, in high-dimensional dynamical systems large numbers of degrees of freedom counteract to any pronounced fractal parameter-dependence of transport coefficients. This would also reconcile a deterministic dynamical systems’ approach towards non-equilibrium transport with well-known results from nonequilibrium thermodynamics such as linear response theory. On the other hand, irregular, respectively fractal transport

coefficients were shown to exist for all the models studied in this thesis which, however all shared certain properties. Hence, we arrive at the conclusion that fractal transport coefficients are typical for a specific class of physical dynamical systems exhibiting the properties of being deterministically chaotic, spatially periodic, and low-dimensional.

17.1.2 Universal chaos and transport properties of thermostated systems?

The major theme of Part II was to explore to which extent the description of NSS generated by conventional Gaussian and Nosé-Hoover dynamics is universal. In this endeavour Chapter 13 played a crucial role, where we summarized what we consider to be the most important links between chaos and transport resulting from Gaussian and Nosé-Hoover dynamics. We now briefly go through this list again and, on the basis of the analysis provided in Chapters 14 to 16, come to final conclusions.

1. **non-Hamiltonian dynamics for NSS:** In our view, this type of dynamics yields a rather natural description of NSS due to external forces. As we argued on many occasions, the non-Hamiltonian character of thermostated systems such as Langevin, Gaussian or Nosé-Hoover dynamics can be understood with respect to projecting out spurious reservoir degrees of freedom. From this point of view we do not see any reason to insist on a Hamiltonian modeling of NSS.
2. **phase space contraction and entropy production:** Conventional Gaussian and Nosé-Hoover thermostats display a default identity between these two quantities, which is at the heart of linking thermodynamics to dynamical systems theory in dissipative dynamical systems. However, it is not too difficult to construct counterexamples of deterministic and time-reversible thermal reservoirs generating well-defined NSS but not exhibiting this identity. We just mention non-ideal Gaussian and Nosé-Hoover thermostats and sheared hard-disk fluids thermostated by deterministic scattering. Care should therefore be taken exploring the second law of thermodynamics on the basis of this identity.
3. **transport coefficients and dynamical systems quantities:** Conventional Gaussian and Nosé-Hoover dynamics features the Lyapunov sum rule linking transport coefficients to Lyapunov exponents. However, the existence of such a simple functional relationship is intimately connected with the existence of the abovementioned identity. Hence, it is not surprising that this relation between chaos quantities and transport coefficients is not universal either. Non-ideal thermostats and thermostating by deterministic scattering yield again explicit counterexamples. We furthermore emphasize that there are broad classes of thermostated dynamical systems not exhibiting a conjugate pairing of Lyapunov exponents.
4. **fractal attractors characterizing NSS:** In all deterministically thermostated dynamical systems analyzed in this review the resulting attracting sets were characterized by fractal structures. This fractality is thus a very promising candidate for a universal property of NSS associated with deterministic and time-reversible thermal reservoirs. As it stands, it is also the only surviving one of the list of possibly universal characteristics discussed so far. However, note that the detailed topology of the attracting

sets still intimately depends on the type of thermal reservoir applied. This is represented by the different types of bifurcation diagrams for the driven periodic Lorentz gas connected to different thermal reservoirs.

5. **nonlinear response in the thermostated driven periodic Lorentz gas:** Despite a mathematical proof for the existence of linear response in the Gaussian thermostated driven periodic Lorentz gas, no clear signs of a regime of linear response could be detected in computer simulations for the Gaussian as well as for other thermostated Lorentz gases. Even worse, applying different thermostats yielded significantly different results for the field-dependent electrical conductivity of this model. We must therefore conclude that there is no equivalence of nonequilibrium ensembles for the thermostated driven periodic Lorentz gas in this regime of field strengths. In case of a thermostated hard disk fluid the situation appears to be better in that, at least, there is an equivalence of nonequilibrium ensembles as far as thermodynamic properties are concerned. However, we emphasize that on the level of chaos quantities there is no equivalence either.

We thus conclude that, from the point of view of nonequilibrium thermodynamics, the periodic Lorentz gas seems to be a rather delicate dynamical system. This appears to be due to the low dimensionality of the dynamics featuring a single moving point particle only. In this case statistical properties arise from the chaotic collisions of the particle with the fixed scatterers and contain intricate dynamical correlations in time and space.

The different results for the field-dependent electrical conductivity presented in this review demonstrate the limits of standard thermodynamic descriptions applied to the thermostated model. However, in many other respects both the periodic Lorentz gas with and without external fields still exhibits “nice” thermodynamic behavior. And even the existence of irregularities in the field-dependent electrical conductivity should not be deemed “unphysical”: Interacting many-particle systems typically display thermodynamic behavior due to their intrinsic statistical properties, whereas chaotically moving single particles may exhibit very intricate dynamical phenomena reflecting specific nonlinearities in their equations of motion.

To us it appears that the periodic Lorentz gas, as well as multibaker maps, are right in-between these two large classes of high and low-dimensional, interacting and non-interacting many-particle systems. Such intermediate dynamics may thus display both ordinary thermodynamic behavior as well as specific chaotic dynamical properties. This assessment leads back again to our discussion of fractal transport coefficients summarized in the previous section. An adequate theoretical description thus needs to develop a well-balanced combination of both statistical and dynamical systems methods in order to adequately assess both the chaos and transport properties of this highly interesting type of dynamical systems.

17.2 Some important open questions

Here we list some central problems that we consider worth to be studied in further research. More detailed open questions were already mentioned in the course of this thesis on various occasions.

17.2.1 Fractal transport coefficients

1. **further sharpening the methods for computing fractal transport coefficients:** As we mentioned above, for more non-trivial models such as the nonlinear climbing sine map and particle billiards, so far transport coefficients could only be computed on the basis of computer simulations, or by extremely simple and insufficient analytical random walk approximations. It would thus be highly desirable to further improve the available theoretical methods in order to obtain exact results for such systems. Our personally preferred approach would be to proceed along Green-Kubo formulas by evaluating both generalized Takagi functions in more general settings, combined with improved matrix methods for computing invariant densities. Such methods may eventually also be applied to highly non-trivial Hamiltonian dynamical systems such as sawtooth [Dan89b, Dan89a], standard [Rec80, Rec81] and Harper [Leb98] maps, as well as to periodic Lorentz gases under electric and magnetic fields [Gei90, Fle92, Fle95]. For all these types of models irregular transport coefficients are well-known to exist theoretically, however, they have not yet been analyzed with respect to a possible fractal origin. Furthermore, these models are close to various experiments, as we will further elaborate below.
2. **more fractal transport coefficients:** We strongly believe that other transport coefficients such as, for example, viscosities and thermal conductivities will also turn out to be fractal for specific classes of physical dynamical systems. Concerning viscosities one may study the simple two-particle fluid of Refs. [Bun96, Vis03a, Vis03b], for thermal conduction one may consider a periodic Lorentz gas under a temperature gradient similar to Refs. [MM01, Lar03].
3. **fractal transport coefficients in experiments?** This is of course a crucial issue that still asks for some pioneering, particularly experimental work to be performed. First of all, we do not suggest that “true” fractal functions may really be observable in experiments. Evidently, random perturbations and limits of experimental resolutions will always be apparent smoothing out such curves on finer scales, as discussed in Chapter 6. However, the same chapter suggests that such a fractal behavior may be at the origin of smoothed-out oscillations on very fine scales of transport coefficients, and these oscillations may very well be observable in experiments. Promising candidates of experimentally accessible systems in which irregular transport coefficients, supposedly indicating a fractal origin, may be detected are ratchets exhibiting drift-diffusion processes [Jun96, Rei02], antidot lattices showing electric and magneto-transport [Wei91, Wei95, Wei97, Wie01], Josephson junctions displaying phase diffusion [Gei85, Wei00, Tan02d], and granular systems consisting of a diffusing bouncing ball as discussed in Chapter 9 [Far99, Pre02, Gro03, Rou04, Gro04].
4. **fractal transport coefficients and quantum mechanics?** An interesting question would be whether, or to which extent, classical fractal transport coefficients survive in quantum mechanical dynamical systems of the type discussed in Part I. An appropriate model to start with is provided by the purely diffusive multibaker map exhibiting a fractal diffusion coefficient as presented in Chapter 4. This model has recently been quantized at a certain parameter value [Woj02, Woj03b, Woj03a]. Similarly, a very interesting issue is to investigate whether there is any connection

between the type of fractality of transport coefficients discussed here and the one revealed for the quantum mechanical mesoscopic Hamiltonian dynamical systems of Refs. [Ket96, Heg96, Sac98, Huf01].

5. **some more specific open questions:** One issue related to the recent discussion of the role of deterministic chaos for nonequilibrium transport [Gas98b, Bri01, Det99b, Gra99, Det00b] would be whether there are also fractal transport coefficients in non-chaotic models [Lep00, Cen00, Alo02, Gra02, Cec03, Alo03]. It might be that chaos is not really a necessary condition for generating such fractal parameter dependencies, and that topological instabilities may also be produced by alternative, non-chaotic mechanisms.

One could furthermore suspect that fractal transport coefficients may not only be related to spatial periodicities, but that periodicities in time such as oscillating external fields can also induce fractal parameter variations.

Another promising direction of research concerns fractal transport properties of anomalous dynamical systems, as already started, to some extent, in Chapter 5. Here one may particularly compare with results from the so-called continuous time random walk theory representing a stochastic approach towards nonequilibrium transport.

Finally, it would be valuable to have a mathematical proof for our heuristically derived formula Eq. (6.5) approximating deterministic diffusion under quenched disorder.

17.2.2 Thermostated dynamical systems

1. **defining a nonequilibrium entropy:** This is of course a central question of nonequilibrium statistical mechanics altogether. From our point of view it is not enough to construct a theory of NSS starting from the ordinary Gibbs entropy. A proper definition of a nonequilibrium entropy should yield results that are compatible with standard nonequilibrium thermodynamics. In case of the driven Lorentz gas we think here of entropy production in terms of Clausius' entropy combined with Joule's heat. To us it appears that, apart from other problems, the Gibbs entropy may contain spurious contributions compared to a thermodynamic entropy production, since it samples the complete phase space which is at variance to an entropy production in terms of a heat transfer. This problem may be eliminated by using a revised definition of the Gibbs entropy based on a suitable coarse-graining. It might be interesting to apply such recent methods of coarse-grained entropies to our examples of thermostated dynamical systems not yielding an identity between phase space contraction and entropy production. One may hope that starting from such an amended Gibbs entropy ordinary thermodynamics can again be recovered even for our more general examples.
2. **fluctuation theorems:** We have said very little about this recent and very active research topic that concerns symmetry relations in the fluctuations of nonequilibrium entropy production. Apart from the fractality of attractors, fluctuation theorems currently feature as another important candidate for universal results characterizing NSS in dissipative dynamical systems. However, up to now fluctuation theorems have only been tested in thermostated dynamical systems furnishing an identity between phase space contraction and entropy production. It would thus be important to check

for their existence in thermostated systems not featuring this identity, such as the ones described in our review. Interestingly, the existence of a certain class of fluctuation theorems is intimately linked to the validity of the chaotic hypothesis mentioned in the introduction. Hence, testing these fluctuation theorems one also studies, to some extent, the validity of the chaotic hypothesis. We furthermore suggest to look for fluctuation theorems in experiments on cell motility.

3. **existence of fractal attractors in stochastically perturbed dynamical systems:** As we have outlined on previous occasions, this important question is still not settled. In order to solve this problem one may study, for example, the driven periodic Lorentz gas or a hard disk fluid under shear supplemented by stochastic boundaries. It might then be elucidating to compare the respective results to the ones obtained from thermostating by deterministic scattering.
4. **analyzing NSS for generalized Nosé-Hoover thermostats and for active Brownian particles:** Following the philosophy of Nosé-Hoover there emerged a large collection of generalized deterministic and time-reversible thermostats for which it is still not clear to which extent they are functioning under nonequilibrium constraints. If they do, they may provide further access roads towards an analysis of chaos and transport properties of NSS going beyond ordinary Gaussian and Nosé-Hoover dynamics. The same reasoning applies to active Brownian particles that may be considered as another type of thermostated dynamical systems.
5. **quantum-mechanical formulations of thermal reservoirs:** In this thesis we did not say anything about extensions of classical deterministic and time-reversible thermostats towards the quantum regime. It seems that this field is currently evolving, see Refs. [Gri89, Kus93, Kus95, Men01, Kus02, Men03] and further references therein. Eventually, it might be interesting to study to which extent these approaches furnish links between chaos and transport being analogous to their classical counterparts.

Acknowledgements

I would like to express my sincere appreciation and gratitude to Profs. S.Hess, J.R.Dorfman, T.Tél, P.Gaspard, and G.Nicolis, who allowed me to learn from them as a diploma student, as a Ph.D. student, and as a postdoc. This work owes very much to their guidance. I furthermore wish to thank Prof. P.Fulde, not only for profoundly supporting my research activities at the MPIPKS Dresden all the time, but also for advising me concerning my intended habilitation at the TU Dresden. Concerning the latter endeavour, I would also like to thank Prof. U.Bahr for providing indispensable advice and support.

Sincere thanks go to Drs. J.Groeneveld, T.Harayama, P.Dieterich, A.Chechkin as well as to Profs. C.Dellago and W.G.Hoover, with whom I had, or have, the great pleasure to collaborate on the subjects presented in this thesis. I also thank my former Ph.D. student Dr. K.Rateitschak as well as my very recent, or present, coworkers Mr. N.Korabel, Dr. L.Matyas, Mr. T.Klauss and Dr. I.F.Barna for performing joint research with me on chaotic transport.

It was furthermore a great pleasure to organize an international conference on the field of research partly covered by this thesis, which was pursued together with Profs. H.van Beijeren, P.Gaspard, and J.R.Dorfman. Thanks go to all of them for their great enthusiasm, help and advice, as well as to Ms. M.Lochar for her kind and efficient administrative support. Profs. P.Cvitanovic, W.Ebeling, C.Grebogi, D.J.Evans, P.Hänggi, H.Kantz, A.Pikovsky, H.A.Posch, G.Radons, E.Schöll, I.M.Sokolov as well as Drs. C.Dettmann, K.Gelfert, W.Just, A.Riegert, F.Schmüser, D.Panja and Ms. N.Baba helped profoundly with many valuable hints and discussions during my research. Particularly, Drs. A.Riegert, K.Rateitschak and Mr. N.Korabel invested a lot of time for working themselves through a first version of the second part of this thesis, by providing many helpful hints. Great thanks to all of them!

I wish to express my gratitude to the directors, to the staff, and to all the other members at the Max-Planck-Institute for the Physics of Complex Systems in Dresden for providing excellent working conditions and a fantastic working atmosphere. This thesis was written while I was a *distinguished postdoctoral fellow* at this institute. Previous financial support of my research by postdoctoral fellowships of the DFG and of the EU is also gratefully acknowledged.

Finally, I want to thank my parents U. and G.Klages and my brother M.Klages for supporting in many different ways my sometimes a bit strenuous life as a traveling physicist.

Bibliography

- [Abr94] R. Abraham and J.E. Marsden, *Foundations of mechanics*. (Addison-Wesley, Reading, 1994). (Cited on pages [152](#) and [168](#).)
- [Agu03] J. Aguirre and M.A.F. Sanjuan, *Limit of small exits in open Hamiltonian systems*. Phys. Rev. E **67**, 056201/1–7 (2003). (Cited on page [112](#).)
- [Ald63] B.J. Alder, W.G. Hoover and T.E. Wainwright, *Cooperative motion of hard disks leading to melting*. Phys. Rev. Lett. **11**, 241–243 (1963). (Cited on page [144](#).)
- [All87] M.D. Allen and D.J. Tildesley, *Computer simulation of liquids*. (Clarendon Press, Oxford, 1987). (Cited on pages [9](#), [13](#), [133](#), [148](#), [194](#), [224](#) and [226](#).)
- [All97] K.T. Alligood, T.S. Sauer and J.A. Yorke, *Chaos - An introduction to dynamical systems*. (Springer, New York, 1997). (Cited on pages [17](#), [26](#) and [212](#).)
- [Alo02] D. Alonso, A. Ruiz and I. de Vega, *Polygonal billiards and transport: diffusion and heat conduction*. Phys. Rev. E **66**, 066131/1–15 (2002). (Cited on pages [12](#) and [250](#).)
- [Alo03] D. Alonso, A. Ruiz and I. de Vega, *Transport in Polygonal Billiards*. in print for the Physica D Special Issue Ref. [\[Kla03b\]](#), 2003. (Cited on pages [12](#) and [250](#).)
- [Als89a] L. Alsedà and J. Llibre, *Kneading theory of Lorenz maps*. in: Dynamical Systems and Ergodic Theory, volume 23 of Banach Center Publications, pages 83–89. (Polish Scientific Publishers, Warszawa, 1989). (Cited on page [27](#).)
- [Als89b] L. Alsedà, J. Llibre, M. Misiurewicz and C. Tresser, *Periods and entropy for Lorenz-like maps*. Ann. Inst. Fourier, Grenoble **39**, 929–952 (1989). (Cited on page [27](#).)
- [And80] H.C. Andersen, *Molecular dynamics simulations at constant pressure and/or temperature*. J. Chem. Phys. **72**, 2384–3173 (1980). (Cited on pages [13](#) and [194](#).)
- [And82] L. Andrey, *Ideal gas in empty space*. Il Nuovo Cimento **69B**, 136–144 (1982). (Cited on page [185](#).)
- [And85] L. Andrey, *The rate of entropy change in non-Hamiltonian systems*. Phys. Lett. **111A**, 45–46 (1985). (Cited on pages [162](#) and [185](#).)
- [And86] L. Andrey, *Note concerning the paper “The rate of entropy change in non-Hamiltonian systems”*. Phys. Lett. **114A**, 183–184 (1986). (Cited on pages [127](#) and [162](#).)

- [Aok02] K. Aoki and D. Kusnezov, *Lyapunov exponents, transport and the extensivity of dimensional loss*. preprint arXiv.nlin.CD/0204015, 2002. (Cited on pages [14](#), [151](#), [172](#), [226](#) and [232](#).)
- [Ari01] C.M. Arizmendi, F. Family and A.L. Salas-Brito, *Quenched disorder effects on deterministic inertia ratchets*. Phys. Rev. E **63**, 061104/1–5 (2001). (Cited on page [81](#).)
- [Arn68] V.I. Arnold and A. Avez, *Ergodic problems of classical mechanics*. (W.A. Benjamin, New York, 1968). (Cited on pages [175](#), [182](#) and [212](#).)
- [Art91] R. Artuso, *Diffusive dynamics and periodic orbits of dynamical systems*. Phys. Lett. A **160**, 528–530 (1991). (Cited on pages [11](#), [26](#), [27](#) and [82](#).)
- [Art93] R. Artuso, G. Casati and R. Lombardi, *Periodic orbit theory of anomalous diffusion*. Phys. Rev. Lett. **71**, 62–64 (1993). (Cited on pages [11](#) and [26](#).)
- [Art94] R. Artuso, *Recycling deterministic diffusion*. Physica D **76**, 1–7 (1994). (Cited on pages [11](#) and [26](#).)
- [Asp98] T. Aspelmeier, G. Giese and A. Zippelius, *Cooling dynamics of a dilute gas of inelastic rods: a many-particle simulation*. Phys. Rev. E **57**, 857–865 (1998). (Cited on page [215](#).)
- [Bak85] P. Bak, T. Bohr and M.H. Jensen, *Mode-locking and the transition to chaos in dissipative systems*. Physica Scripta **T9**, 531–539 (1985). (Cited on page [73](#).)
- [Bal94] N.J. Balmforth, E.A. Spiegel and C. Tresser, *Topological entropy of one-dimensional maps: approximations and bounds*. Phys. Rev. Lett. **72**, 80–83 (1994). (Cited on page [29](#).)
- [Ban92] J. Banks, J. Brooks, G. Cairns, G. Davis and P. Stacey, *On Devaney’s definition of chaos*. Am. Math. Monthly **99**, 332–334 (1992). (Cited on pages [175](#) and [212](#).)
- [Bar93] A. Baranyai, D.J. Evans and E.G.D. Cohen, *Field-dependent conductivity and diffusion in a two-dimensional Lorentz Gas*. J. Stat. Phys. **70**, 1085–1098 (1993). (Cited on pages [14](#), [22](#), [148](#), [151](#), [157](#), [158](#) and [223](#).)
- [Bar97] E. Barkai and J. Klafter, *Crossover from dispersive to regular transport in biased maps*. Phys. Rev. Lett. **79**, 2245–2248 (1997). (Cited on pages [21](#) and [86](#).)
- [Bar98] E. Barkai and J. Klafter, *Deterministic transport in biased maps: Crossover from dispersive to regular transport*. Phys. Rev. E **57**, 5237–5246 (1998). (Cited on pages [21](#) and [86](#).)
- [Bar00] E. Barkai, V. Fleurov and J. Klafter, *One-dimensional stochastic Lévy-Lorentz gas*. Phys. Rev. E **61**, 1164–1169 (2000). (Cited on page [82](#).)
- [Bar03a] I.F. Barna, R. Klages and L. Matyas. unpublished, 2003. (Cited on pages [12](#) and [117](#).)

- [Bar03b] E.J. Barth, B.B. Laird and B.J. Leimkuhler, *Generating generalized distributions from dynamical simulation*. J. Chem. Phys. **118**, 5759–5768 (2003). (Cited on pages [175](#) and [176](#).)
- [Bea91] R.M. Beam and R.F. Warming, *The asymptotic spectra of banded Toeplitz and quasi-Toeplitz matrices*. Technical Memorandum 103900, NASA Ames Research Center, Moffett Field, California, 1991. (Cited on page [30](#).)
- [Bec87] C. Beck and G. Roepstorff, *From dynamical systems to the Langevin equation*. Physica A **145**, 1–14 (1987). (Cited on pages [86](#) and [136](#).)
- [Bec93] Chr. Beck and F. Schlögl, *Thermodynamics of Chaotic Systems*, volume 4 of Cambridge nonlinear science series. (Cambridge University Press, Cambridge, 1993). (Cited on pages [15](#), [17](#), [26](#), [29](#), [40](#), [58](#), [153](#), [188](#) and [189](#).)
- [Bec95] C. Beck, *From the Perron-Frobenius equation to the Fokker-Planck equation*. J. Stat. Phys. **79**, 875–894 (1995). (Cited on pages [86](#) and [136](#).)
- [Bec96] C. Beck, *Dynamical systems of Langevin type*. Physica A **233**, 419–440 (1996). (Cited on pages [86](#) and [136](#).)
- [Ben80] G. Benettin, L. Galgani, A. Giorgili and J.-M. Strelcyn, *Lyapunov characteristic exponents for smooth dynamical systems: A method for computing all of them. Part 2: numerical application*. Meccanica **15**, 21–29 (1980). (Cited on page [152](#).)
- [Ben01] G. Benettin and L. Rondoni, *A new model for the transport of particles in a thermostatted system*. Mathematical Physics Electronic Journal **7**, 1–22 (2001). (Cited on pages [129](#), [207](#) and [226](#).)
- [Ber52] T.H. Berlin and M. Kac, *The spherical model of a ferromagnet*. Phys. Rev. A **86**, 821–835 (1952). (Cited on page [30](#).)
- [Ber80] M.V. Berry and Z.V. Lewis, *On the Weierstraß-Mandelbrot fractal function*. Proc. R. Soc. Lond. A **370**, 459–484 (1980). (Cited on page [46](#).)
- [Ber88] B.J. Berne, M. Borkovec and J.E. Straub, *Classical and modern methods in reaction rate theory*. J. Phys. Chem. **92**, 3711–3725 (1988). (Cited on page [54](#).)
- [Bey76] H.U. Beyeler, *Cationic Short-Range Order in the Hollandite $K_{1.54}Mg_{0.77}T_{7.23}O_{16}$: Evidence for the Importance of Ion-Ion Interactions in Superionic Conductors*. Phys. Rev. Lett. **37**, 1557–1560 (1976). (Cited on page [11](#).)
- [Bla96] J.A. Blackburn and N. Grønbech-Jensen, *Phase diffusion in a chaotic pendulum*. Phys. Rev. E **53**, 3068–3072 (1996). (Cited on page [73](#).)
- [Boh84] T. Bohr, P. Bak and M.H. Jensen, *Transition to chaos by interaction of resonances in dissipative systems. II. Josephson junctions, charge-density waves, and standard maps*. Phys. Rev. A **30**, 1970–1981 (1984). (Cited on page [73](#).)
- [Bol64] L. Boltzmann, *Lectures on Gas Theory*. (Univ. of Cal. Press, Berkeley, 1964). (Cited on page [9](#).)

- [Bon97] F. Bonetto, G. Gallavotti and P.L. Garrido, *Chaotic principle: an experimental test*. Physica D **105**, 226–252 (1997). (Cited on pages [148](#), [157](#) and [223](#).)
- [Bon98a] F. Bonetto, N.I. Chernov and J.L. Lebowitz, *(Global and local) Fluctuations of phase space contraction in deterministic stationary nonequilibrium*. Chaos **8**, 823–833 (1998). (Cited on pages [15](#) and [226](#).)
- [Bon98b] F. Bonetto, E.G.D. Cohen and C. Pugh, *On the validity of the conjugate pairing rule for Lyapunov exponents*. J. Stat. Phys. **92**, 587–627 (1998). (Cited on page [152](#).)
- [Bon99] S.D. Bond, B.J. Leimkuhler and B.B. Laird, *The Nosé-Poincaré method for constant temperature molecular dynamics*. J. Comput. Phys. **151**, 114–134 (1999). (Cited on pages [175](#) and [176](#).)
- [Bon00] F. Bonetto, D. Daems and J.L. Lebowitz, *Properties of stationary nonequilibrium states in the thermostatted periodic Lorentz gas. I. The one particle system*. J. Stat. Phys. **101**, 35–60 (2000). (Cited on pages [148](#), [154](#), [157](#), [158](#) and [159](#).)
- [Bon01] F. Bonetto and J.L. Lebowitz, *Thermodynamic entropy production fluctuation in a two-dimensional shear flow model*. Phys. Rev. E **64**, 056129/1–9 (2001). (Cited on page [226](#).)
- [Bon02] F. Bonetto, D. Daems, J.L. Lebowitz and V. Ricci, *Properties of stationary nonequilibrium states in the thermostatted periodic Lorentz gas: The multiparticle system*. Phys. Rev. E **65**, 051204/1–9 (2002). (Cited on pages [128](#), [148](#), [157](#), [196](#) and [223](#).)
- [Bou90] J.-P. Bouchaud and A. Georges, *Anomalous diffusion in disordered media: statistical mechanisms, models and physical applications*. Phys. Rep. **195**, 127–293 (1990). (Cited on pages [22](#), [81](#), [82](#), [83](#), [86](#) and [88](#).)
- [Bow75] R. Bowen, *Equilibrium states and the ergodic theory of Anosov diffeomorphisms*, volume 470 of Lecture notes in mathematics. (Springer-Verlag, Berlin, 1975). (Cited on page [9](#).)
- [Bow79] R. Bowen, *Invariant measures for Markov maps of the interval*. Commun. Math. Phys. **69**, 1–17 (1979). (Cited on page [40](#).)
- [Boy79] A. Boyarski and M. Scarowsky, *On a class of transformations which have unique absolutely continuous invariant measures*. Trans. Am. Math. Soc. **255**, 243–242 (1979). (Cited on page [29](#).)
- [Boy88] A. Boyarski, *A matrix method for estimating the Lyapunov exponent of one-dimensional systems*. J. Stat. Phys. **50**, 213–229 (1988). (Cited on page [29](#).)
- [Bra00a] A.C. Branka, *Nosé-Hoover chain method for nonequilibrium molecular dynamics simulation*. Phys. Rev. E **61**, 4769–4773 (2000). (Cited on pages [175](#), [176](#), [177](#) and [207](#).)

- [Bra00b] A.C. Branka and K.W. Wojciechowski, *Generalization of Nosé and Nosé-Hoover isothermal dynamics*. Phys. Rev. E **62**, 3281–3292 (2000). (Cited on pages [175](#), [176](#), [177](#) and [207](#).)
- [Bre96] W. Breymann, T. Tél and J. Vollmer, *Entropy production for open dynamical systems*. Phys. Rev. Lett. **77**, 2945–2948 (1996). (Cited on pages [10](#), [57](#), [128](#), [185](#), [186](#), [189](#) and [191](#).)
- [Bre98] W. Breymann, T. Tél and J. Vollmer, *Entropy balance, time reversibility, and mass transport in dynamical systems*. Chaos **8**, 396–408 (1998). (Cited on pages [10](#), [14](#), [57](#), [128](#), [151](#), [183](#), [186](#) and [230](#).)
- [Bri95] J. Bricmont, *Science of chaos or chaos in science?* Phys. Mag. **17**, 159–212 (1995). (Cited on page [130](#).)
- [Bri96] N.V. Brilliantov, F. Spahn, J.-M. Hertzsch and Th. Pöschel, *Model for collisions in granular gases*. Phys. Rev. E **53**, 5382–5392 (1996). (Cited on page [215](#).)
- [Bri01] M.E. Briggs, J.V. Sengers, M.K. Francis, P. Gaspard, R.W. Gammon, J.R. Dorfman and R.V. Calabrese, *Tracking a colloidal particle for the measurement of dynamic entropies*. Physica A **296**, 42–59 (2001). (Cited on pages [12](#), [86](#) and [250](#).)
- [Bro84] S.E. Brown, G. Mozurkewich and G. Gruner, *Subharmonic Shapiro steps and Devil’s-staircase behavior in driven charge-density-wave systems*. Phys. Rev. Lett. **52**, 2277–2280 (1984). (Cited on page [11](#).)
- [Bru76] St.G. Brush, *The kind of motion we call heat*, volume 1/2. (North Holland, Amsterdam, 1976). (Cited on pages [17](#) and [133](#).)
- [Bul90a] A. Bulgac and D. Kusnezov, *Canonical ensemble averages from pseudomicrocanonical dynamics*. Phys. Rev. A **42**, 5045–5048 (1990). (Cited on pages [163](#), [175](#), [177](#) and [207](#).)
- [Bul90b] A Bulgac and D. Kusnezov, *Deterministic and time-reversal invariant description of Brownian motion*. Phys. Lett. A **151**, 122–128 (1990). (Cited on pages [175](#), [176](#), [177](#) and [207](#).)
- [Bun80] L.A. Bunimovich and Ya.G. Sinai, *Markov partitions for dispersed billiards*. Comm. Math. Phys. **78**, 247–280 (1980). (Cited on pages [22](#), [53](#), [54](#), [99](#), [106](#), [107](#), [108](#), [144](#), [145](#) and [154](#).)
- [Bun81] L.A. Bunimovich and Ya.G. Sinai, *Statistical properties of Lorentz gas with periodic configuration of scatterers*. Comm. Math. Phys. **78**, 479–497 (1981). (Cited on pages [22](#), [53](#), [54](#), [106](#), [107](#), [108](#), [144](#), [145](#) and [154](#).)
- [Bun91] L.A. Bunimovich, Ya.G. Sinai and N.I. Chernov, *Statistical properties of two-dimensional hyperbolic billiards*. Russ. Math. Surveys **46**, 47–106 (1991). (Cited on pages [22](#), [106](#), [107](#), [108](#), [144](#), [145](#) and [154](#).)
- [Bun96] L.A. Bunimovich and H. Spohn, *Viscosity for a periodic two disk fluid: an existence proof*. Commun. Math. Phys. **176**, 661–680 (1996). (Cited on pages [144](#), [225](#) and [249](#).)

- [Bun03a] L.A. Bunimovich, *Deterministic walks in random environments*. in print for the Physica D Special Issue Ref. [Kla03b], 2003. (Cited on page 81.)
- [Bun03b] L.A. Bunimovich and M.A. Khlabystova, *One-dimensional Lorentz gas with rotating scatterers: exact solutions*. J. Stat. Phys. **112**, 1207–1218 (2003). (Cited on page 213.)
- [Cec03] F. Cecconi, M. Falcioni, A. Vulpiani and D. del Castillo-Negrete, *The origin of diffusion: the case of non chaotic systems*. Physica D **180**, 129–139 (2003). (Cited on pages 12 and 250.)
- [Cen00] M. Cencini, M. Falcioni, E. Olbrich, H. Kantz and A. Vulpiani, *Chaos or noise: Difficulties of a distinction*. Phys. Rev. E **62**, 427–437 (2000). (Cited on pages 12, 86 and 250.)
- [Cha70] S. Chapman and T.G. Cowling, *The mathematical theory of non-uniform gases*. (Cambridge University Press, Cambridge, 1970). (Cited on page 144.)
- [Che89] Q. Chen and J.D. Meiss, *Flux, resonances and the Devil’s staircase for the sawtooth map*. Nonlinearity **39**, 347–356 (1989). (Cited on page 31.)
- [Che90] Q. Chen, I. Dana, J.D. Meiss, N.W. Murray and I. C. Percival, *Resonances and transport in the sawtooth map*. Physica D **46**, 217–240 (1990). (Cited on page 31.)
- [Che93a] N.I. Chernov, G.L. Eyink, J.L. Lebowitz and Ya.G. Sinai, *Derivation of Ohm’s law in a deterministic mechanical model*. Phys. Rev. Lett. **70**, 2209–2212 (1993). (Cited on pages 14, 148, 150, 151, 153, 154, 155, 158, 159, 186, 188, 189 and 191.)
- [Che93b] N.I. Chernov, G.L. Eyink, J.L. Lebowitz and Ya.G. Sinai, *Steady-state electrical conduction in the periodic Lorentz gas*. Comm. Math. Phys. **154**, 569–601 (1993). (Cited on pages 14, 148, 150, 151, 153, 154, 155, 158, 159, 188, 189 and 191.)
- [Che94] N.I. Chernov, *Statistical properties of the periodic Lorentz gas. Multidimensional case*. J. Stat. Phys. **74**, 11–53 (1994). (Cited on pages 53, 54, 106, 107 and 108.)
- [Che95a] Ch.-Ch. Chen, *Diffusion coefficient of piecewise linear maps*. Phys. Rev. E **51**, 2815–2822 (1995). (Cited on pages 11, 26 and 82.)
- [Che95b] N.I. Chernov and J.L. Lebowitz, *Stationary shear flow in boundary driven Hamiltonian systems*. Phys. Rev. Lett. **75**, 2831–2834 (1995). (Cited on pages 13, 14, 15, 128, 151, 194, 207, 210, 225, 227, 229 and 230.)
- [Che97] N.I. Chernov and J.L. Lebowitz, *Stationary nonequilibrium states in boundary-driven Hamiltonian systems: Shear flow*. J. Stat. Phys. **86**, 953–990 (1997). (Cited on pages 13, 14, 15, 128, 151, 194, 207, 210, 225, 227, 229 and 230.)
- [Che99] N.I. Chernov, *Decay of correlations and dispersing billiards*. J. Stat. Phys. **94**, 513–556 (1999). (Cited on pages 106, 107, 108, 144, 145 and 154.)
- [Che02] A.V. Chechkin, V.Yu. Gonchar, J. Klafter, R. Metzler and L.V. Tanatarov, *Stationary states of non-linear oscillators driven by Lévy noise*. Chem. Phys. **284**, 233–251 (2002). (Cited on page 240.)

-
- [Che03] A.V. Chechkin, J. Klafter, V.Yu. Gonchar, R. Metzler and L.V. Tanatarov, *Bifurcation, bimodality, and finite variance in confined Lévy flights*. Phys. Rev. E **67**, 010102(R)/1–4 (2003). (Cited on page [240](#).)
- [Chi79] B.V. Chirikov, *A universal instability of many-dimensional oscillator systems*. Phys. Rep. **52**, 263–379 (1979). (Cited on page [73](#).)
- [Cho98] Ph. Choquard, *Variational principles for thermostatted systems*. Chaos **8**, 350–357 (1998). (Cited on pages [14](#), [169](#) and [170](#).)
- [Cic80] G. Ciccotti and A. Tenenbaum, *Canonical ensemble and nonequilibrium states by molecular dynamics*. J. Stat. Phys. **23**, 767–772 (1980). (Cited on pages [13](#), [128](#), [194](#), [210](#) and [226](#).)
- [Cil98] S. Ciliberto and C. Laroche, *An experimental test of the Gallavotti-Cohen fluctuation theorem*. J. Phys. IV France **8**, 215–219 (1998). (Cited on page [15](#).)
- [Cir82] M. Cirillo and N.F. Pedersen, *On bifurcations and transition to chaos in a Josephson junction*. Phys. Lett. **90A**, 150–152 (1982). (Cited on page [11](#).)
- [Cla93] I. Claes and C. Van den Broeck, *Dispersion of particles in periodic media*. J. Stat. Phys. **70**, 1215–1231 (1993). (Cited on page [11](#).)
- [Cla00] I. Claus and P. Gaspard, *Microscopic chaos and reaction-diffusion processes in the periodic Lorentz gas*. J. Stat. Phys. **101**, 161–186 (2000). (Cited on page [21](#).)
- [Cla01] I. Claus and P. Gaspard, *Fractals and dynamical chaos in a two-dimensional Lorentz gas with sinks*. Phys. Rev. E **63**, 036227/1–10 (2001). (Cited on page [21](#).)
- [Cla02] I. Claus and P. Gaspard, *The fractality of the relaxation modes in reaction-diffusion systems*. Physica D **168–169**, 266–291 (2002). (Cited on pages [10](#), [21](#), [190](#) and [191](#).)
- [Cla03] I. Claus, P. Gaspard and H. van Beijeren, *Fractals and dynamical chaos in a random 2D Lorentz gas with sinks*. in print for the Physica D Special Issue Ref. [[Kla03b](#)], 2003. (Cited on page [21](#).)
- [Coh92] E.G.D. Cohen et al., *Round table discussion (II): Irreversibility and Lyapunov spectra*. in: M. Mareschal and B.L. Holian, Eds., Microscopic simulations of complex hydrodynamic phenomena, volume 292 of NATO ASI Series B: Physics, pages 327–343, Plenum Press, New York, 1992. (Cited on pages [182](#), [192](#), [194](#) and [195](#).)
- [Coh95] E.G.D. Cohen, *Transport coefficients and Lyapunov exponents*. Physica A **213**, 293–314 (1995). (Cited on pages [14](#), [151](#), [152](#), [224](#), [225](#) and [231](#).)
- [Coh97] E.G.D. Cohen, *Dynamical ensembles in statistical mechanics*. Physica A **240**, 43–53 (1997). (Cited on page [225](#).)
- [Coh98] E.G.D. Cohen and L. Rondoni, *Note on phase space contraction and entropy production in thermostatted Hamiltonian systems*. Chaos **8**, 357–365 (1998). (Cited on pages [10](#), [128](#), [129](#), [148](#), [150](#), [159](#), [202](#) and [207](#).)

- [Coh99] E.G.D. Cohen and G. Gallavotti, *Note on two theorems in nonequilibrium statistical mechanics*. J. Stat. Phys. **96**, 1343–1349 (1999). (Cited on page [15](#).)
- [Coh02] E.G.D. Cohen and L. Rondoni, *Particles, maps and irreversible thermodynamics*. Physica A **306**, 117–128 (2002). (Cited on page [10](#).)
- [Cvi92] P. Cvitanović, P. Gaspard and Th. Schreiber, *Investigation of the Lorentz gas in terms of periodic orbits*. Chaos **2**, 85–90 (1992). (Cited on pages [22](#), [102](#) and [191](#).)
- [Cvi95] P. Cvitanović, J.-P. Eckmann and P. Gaspard, *Transport properties of the Lorentz gas in terms of periodic orbits*. Chaos, Solitons and Fractals **6**, 113–120 (1995). (Cited on pages [102](#) and [191](#).)
- [Cvi00] P. Cvitanović, *Chaotic field theory: a sketch*. Physica A **288**, 61–80 (2000). (Cited on pages [11](#) and [86](#).)
- [Cvi03] P. Cvitanović, R. Artuso, R. Mainieri, G. Tanner and G. Vattay, *Chaos: classical and quantum*. (Niels Bohr Institute, Copenhagen, 2003). webbook under www.nbi.dk/ChaosBook/. (Cited on pages [11](#), [17](#), [26](#), [81](#) and [191](#).)
- [Dae99] D. Daems and G. Nicolis, *Entropy production and phase space volume contraction*. Phys. Rev. E **59**, 4000–4006 (1999). (Cited on pages [129](#), [186](#), [195](#), [208](#) and [230](#).)
- [Dan89a] I. Dana, *Hamiltonian transport on unstable periodic orbits*. Physica D **39**, 205–235 (1989). (Cited on page [249](#).)
- [Dan89b] I. Dana, N.W. Murray and I.C. Percival, *Resonances and diffusion in periodic Hamiltonian maps*. Phys. Rev. Lett. **65**, 1693–1697 (1989). (Cited on page [249](#).)
- [Dav79] P.J. Davis, *Circulant matrices*. (Wiley Interscience Publ., New York, 1979). (Cited on page [30](#).)
- [Del95a] C. Dellago, L. Glatz and H.A. Posch, *Lyapunov spectrum of the driven Lorentz gas*. Phys. Rev. E **52**, 4817–4826 (1995). (Cited on pages [147](#), [148](#), [153](#), [154](#), [155](#), [157](#), [158](#), [159](#) and [222](#).)
- [Del95b] C. Dellago, L. Glatz and H.A. Posch, *Lyapunov spectrum of the driven Lorentz gas*. Phys. Rev. E **52**, 4817–4826 (1995). (Cited on page [151](#).)
- [Del95c] C. Dellago and H. A. Posch, *Lyapunov exponents of systems with elastic hard collisions*. Phys. Rev. E **52**, 2401–2406 (1995). (Cited on page [81](#).)
- [Del96a] C. Dellago and H.A. Posch, *Lyapunov instability, local curvature, and the fluid-solid phase transition in two-dimensional particle systems*. Physica A **230**, 364–387 (1996). (Cited on page [144](#).)
- [Del96b] C. Dellago, H.A. Posch and W.G. Hoover, *Lyapunov instability in a system of hard disks in equilibrium and nonequilibrium steady states*. Phys. Rev. E **53**, 1485–1501 (1996). (Cited on page [152](#).)

-
- [Del97a] C. Dellago and H.A. Posch, *Lyapunov instability of the boundary-driven Chernov-Lebowitz model for stationary shear flow*. J. Stat. Phys. **88**, 825–842 (1997). (Cited on pages [152](#), [153](#) and [231](#).)
- [Del97b] C. Dellago and H.A. Posch, *Lyapunov spectrum and the conjugate pairing rule for a thermostatted random Lorentz gas: Numerical simulations*. Phys. Rev. Lett. **78**, 211–214 (1997). (Cited on pages [145](#), [152](#), [196](#) and [226](#).)
- [Der83] B. Derrida, *Velocity and diffusion constant of a periodic one-dimensional hopping model*. J. Stat. Phys. **31**, 433–449 (1983). (Cited on page [83](#).)
- [Det95] C.P. Dettmann, G.P. Morriss and L. Rondoni, *Conjugate pairing in the three-dimensional periodic Lorentz gas*. Phys. Rev. E **52**, R5746–R5748 (1995). (Cited on pages [148](#), [151](#), [152](#) and [222](#).)
- [Det96a] C.P. Dettmann and G.P. Morriss, *Crisis in the periodic Lorentz gas*. Phys. Rev. E **54**, 4782–4790 (1996). (Cited on pages [147](#), [148](#), [151](#), [153](#), [154](#) and [155](#).)
- [Det96b] C.P. Dettmann and G.P. Morriss, *Hamiltonian formulation of the Gaussian isokinetic thermostat*. Phys. Rev. E **54**, 2495–2500 (1996). (Cited on pages [14](#) and [170](#).)
- [Det96c] C.P. Dettmann and G.P. Morriss, *Proof of Lyapunov exponent pairing for systems at constant kinetic energy*. Phys. Rev. E **53**, R5545–R5548 (1996). (Cited on page [152](#).)
- [Det97a] C.P. Dettmann and G.P. Morriss, *Hamiltonian reformulation and pairing of Lyapunov exponents for Nose-Hoover dynamics*. Phys. Rev. E **55**, 3693–3696 (1997). (Cited on pages [14](#), [152](#), [169](#) and [170](#).)
- [Det97b] C.P. Dettmann and G.P. Morriss, *Stability ordering of cycle expansions*. Phys. Rev. Lett. **78**, 4201–4204 (1997). (Cited on pages [148](#), [157](#), [158](#) and [159](#).)
- [Det97c] C.P. Dettmann, G.P. Morriss and L. Rondoni, *Irreversibility, diffusion and multifractal measures in thermostatted systems*. Chaos, Solitons and Fractals **8**, 783–792 (1997). (Cited on pages [148](#) and [153](#).)
- [Det99a] C.P. Dettmann, *Hamiltonian for a restricted isoenergetic thermostat*. Phys. Rev. E **60**, 7576–7577 (1999). (Cited on page [170](#).)
- [Det99b] C.P. Dettmann and E.G.D. Cohen, *Microscopic chaos from Brownian motion?* Nature **401**, 875–875 (1999). (Cited on pages [12](#), [86](#) and [250](#).)
- [Det00a] C.P. Dettmann, *The Lorentz gas: a paradigm for nonequilibrium steady states*. in: Hard Ball Systems and the Lorentz Gas, pages 315–366. (2000). see Ref. [[Sza00](#)]. (Cited on pages [12](#), [13](#), [17](#), [127](#), [128](#), [148](#), [149](#), [150](#), [151](#), [154](#), [157](#), [158](#), [163](#), [164](#), [170](#), [185](#), [186](#) and [192](#).)
- [Det00b] C.P. Dettmann and E.G.D. Cohen, *Microscopic chaos and diffusion*. J. Stat. Phys. **101**, 775–817 (2000). (Cited on pages [12](#), [86](#) and [250](#).)
- [Dev89] R.L. Devaney, *An introduction to chaotic dynamical systems*. (Addison-Wesley, Reading, second edition, 1989). (Cited on pages [153](#), [175](#) and [212](#).)

- [dG62] S.R. de Groot and P. Mazur, *Non-equilibrium thermodynamics*. (North Holland, Amsterdam, 1962). reprinted by Dover, New York, 1984. (Cited on pages [132](#) and [150](#).)
- [Die03] P. Dieterich, V. Dreval, R. Preuss, R. Klages and A. Schwab, *Classification of the migratory process on different time-scales - evaluation of the Na+H+ exchanger in MDCK-F cell migration*. in preparation, 2003. (Cited on pages [129](#), [235](#) and [236](#).)
- [Din87] E.J. Ding and P.C. Hemmer, *Exact treatment of mode locking for a piecewise linear map*. J. Stat. Phys. **46**, 99–110 (1987). (Cited on page [45](#).)
- [dM93] W. de Melo and S. van Strien, *One-dimensional dynamics*, volume 25 of *Ergebnisse der Mathematik und ihrer Grenzgebiete, 3.Folge*. (Springer, Berlin, 1993). (Cited on page [40](#).)
- [Dob76a] R. Dobbertin, *On functional relations between reduced distribution functions and entropy production by non-Hamiltonian perturbations*. Physica Scripta **14**, 85–88 (1976). (Cited on page [185](#).)
- [Dob76b] R. Dobbertin, *Vlasov equation and entropy*. Physica Scripta **14**, 89–91 (1976). (Cited on page [185](#).)
- [Dol00] M. Dolowschiak and Z. Kovacs, *Breaking conjugate pairing in thermostated billiards by a magnetic field*. Phys. Rev. E **62**, 7894–7897 (2000). (Cited on pages [152](#), [153](#) and [183](#).)
- [Dor77] J.R. Dorfman and H. van Beijeren, *The Kinetic Theory of Gases*. in: B.J. Berne, Eds., *Statistical mechanics*, volume B, chapter 3, pages 65–179. (Plenum Press, New York, 1977). (Cited on page [35](#).)
- [Dör85] M. Dörfle, *Spectrum and eigenfunctions of the Frobenius-Perron operator of the tent map*. J. Stat. Phys. **40**, 93–132 (1985). (Cited on pages [49](#) and [58](#).)
- [Dor95] J.R. Dorfman and P. Gaspard, *Chaotic scattering theory of transport and reaction-rate coefficients*. Phys. Rev. E **51**, 28–35 (1995). (Cited on pages [10](#), [12](#), [28](#) and [189](#).)
- [Dor99] J.R. Dorfman, *An Introduction to Chaos in Nonequilibrium Statistical Mechanics*. (Cambridge University Press, Cambridge, 1999). (Cited on pages [9](#), [10](#), [11](#), [12](#), [15](#), [17](#), [21](#), [26](#), [28](#), [58](#), [60](#), [74](#), [77](#), [81](#), [93](#), [99](#), [127](#), [144](#), [145](#), [148](#), [158](#), [159](#), [161](#), [162](#), [163](#), [175](#), [183](#), [185](#), [186](#), [187](#), [188](#), [189](#), [194](#) and [212](#).)
- [Dor02] J.R. Dorfman, P. Gaspard and T. Gilbert, *Entropy production of diffusion in spatially periodic deterministic systems*. Phys. Rev. E **66**, 026110/1–9 (2002). (Cited on pages [10](#), [57](#) and [186](#).)
- [Dre88] U. Dressler, *Symmetry property of the Lyapunov spectra of a class of dissipative dynamical systems with viscous damping*. Phys. Rev. A **38**, 2103–2109 (1988). (Cited on pages [14](#) and [152](#).)

-
- [Dru00] P. Drude, *Zur Elektronentheorie der Metalle*. Ann. Phys. **1**, 566–612 (1900). (Cited on page [142](#).)
- [Duf95] N.G. Duffield, J.T. Lewis, N. O’Connell, R. Russell and F. Toomey, *Entropy of ATM Traffic Streams: A Tool for Estimating QoS Parameters*. I.E.E.E. Journal on Selected Areas in Communications **13**, 981–990 (1995). (Cited on page [35](#).)
- [Ebe99] W. Ebeling, F. Schweitzer and B. Tilch, *Active Brownian particles with energy depots modeling animal mobility*. BioSystems **49**, 17–29 (1999). (Cited on pages [129](#), [235](#) and [237](#).)
- [Ebe00] W. Ebeling, *Canonical nonequilibrium statistics and applications to Fermi-Bose systems*. Cond. Matt. Phys. **3**, 285–293 (2000). (Cited on page [238](#).)
- [Ebe01] W. Ebeling and F. Schweitzer, *Swarms of particle agents with harmonic interactions*. Theory in Biosciences **120**, 207–224 (2001). (Cited on page [239](#).)
- [Ebe03] W. Ebeling and G. Röpke, *Statistical mechanics of confined systems with rotational excitations*. in print for the Physica D Special Issue Ref. [[Kla03b](#)], 2003. (Cited on pages [235](#) and [239](#).)
- [Eck85] J.-P. Eckmann and D. Ruelle, *Ergodic theory of chaos and strange attractors*. Rev. Mod. Phys. **57**, 617–656 (1985). (Cited on pages [17](#), [151](#), [152](#), [153](#), [188](#), [189](#), [191](#), [194](#) and [212](#).)
- [Eck99a] J.-P. Eckmann, C.-A. Pillet and L. Rey-Bellet, *Entropy production in non-linear, thermally driven Hamiltonian systems*. J. Stat. Phys. **95**, 305–331 (1999). (Cited on pages [13](#), [129](#), [137](#), [186](#), [208](#) and [226](#).)
- [Eck99b] J.-P. Eckmann, C.-A. Pillet and L. Rey-Bellet, *Non-equilibrium statistical mechanics of anharmonic chains coupled to two heat baths at different temperatures*. Commun. Math. Phys. **201**, 657–697 (1999). (Cited on pages [13](#), [137](#) and [226](#).)
- [Eck00] J.-P. Eckmann and O. Gat, *Hydrodynamic Lyapunov modes in translation-invariant systems*. J. Stat. Phys. **98**, 775–797 (2000). (Cited on page [15](#).)
- [Eck03] B. Eckhardt, E. Hascoet and W. Braun, *Passive fields and particles in chaotic flows*. preprint nlin.CD/0303004, 2003. (Cited on pages [86](#) and [89](#).)
- [Ehr59] P. Ehrenfest and T. Ehrenfest, *The conceptual foundations of the statistical approach in mechanics*. (Cornell Univ. Press, Ithaca, 1959). reprinted by Dover, New York, 2002. (Cited on page [9](#).)
- [Ein05] A. Einstein, *Über die von der molekularkinetischen Theorie der Wärme geforderten Bewegung von in ruhenden Flüssigkeiten suspendierten Teilchen*. Ann. d. Ph. **17**, 549–560 (1905). (Cited on page [26](#).)
- [Els85] Y. Elskens and R. Kapral, *Reversible dynamics and the macroscopic rate law for a solvable Kolmogorov system: the three baker’s reaction*. J. Stat. Phys. **38**, 1027–1049 (1985). (Cited on pages [21](#) and [52](#).)

- [Erd00] U. Erdmann, W. Ebeling, L. Schimansky-Geier and F. Schweitzer, *Brownian particles far from equilibrium*. Eur. Phys. J. B **15**, 105–113 (2000). (Cited on pages [129](#), [235](#), [237](#), [238](#), [239](#) and [241](#).)
- [Erd02] U. Erdmann, W. Ebeling and V.S. Anishchenko, *Excitation of rotational modes in two-dimensional systems of driven Brownian particles*. Phys. Rev. E **65**, 061106–1/9 (2002). (Cited on pages [235](#), [239](#) and [241](#).)
- [Ers93] S.V. Ershov, *Is a perturbation theory for dynamical chaos possible?* Phys. Lett. A **177**, 180–185 (1993). (Cited on pages [49](#) and [58](#).)
- [Eva83a] D.J. Evans, *Computer “experiment” for nonlinear thermodynamics of Couette flow*. J. Chem. Phys. **78**, 3297–3302 (1983). (Cited on pages [13](#), [148](#), [149](#) and [224](#).)
- [Eva83b] D.J. Evans, W.G. Hoover, B.H. Failor, B. Moran and A.J.C. Ladd, *Nonequilibrium molecular dynamics via Gauss’s principle of least constraint*. Phys. Rev. A **28**, 1016–1021 (1983). (Cited on pages [13](#), [149](#) and [174](#).)
- [Eva85a] D.J. Evans, *Response theory as a free-energy extremum*. Phys. Rev. A **32**, 2923–2925 (1985). (Cited on page [185](#).)
- [Eva85b] D.J. Evans and B.L. Holian, *The Nosé-Hoover thermostat*. J. Chem. Phys. **83**, 4069–4074 (1985). (Cited on pages [128](#), [164](#), [165](#), [166](#), [170](#), [173](#) and [174](#).)
- [Eva86] D.J. Evans and G.P. Morriss, *Shear Thickening and Turbulence in Simple Fluids*. Phys. Rev. Lett. **56**, 2172–2175 (1986). (Cited on page [225](#).)
- [Eva90a] D.J. Evans, E.G.D. Cohen and G.P. Morriss, *Viscosity of a simple fluid from its maximal Lyapunov exponents*. Phys. Rev. A **42**, 5990–5997 (1990). (Cited on pages [14](#), [151](#), [152](#), [225](#) and [231](#).)
- [Eva90b] D.J. Evans and G.P. Morriss, *Statistical mechanics of nonequilibrium liquids*. Theoretical Chemistry. (Academic Press, London, 1990). (Cited on pages [9](#), [12](#), [13](#), [14](#), [17](#), [127](#), [128](#), [132](#), [133](#), [149](#), [150](#), [151](#), [153](#), [159](#), [161](#), [162](#), [164](#), [170](#), [185](#), [186](#), [194](#), [219](#), [224](#), [225](#) and [226](#).)
- [Eva93a] D.J. Evans, E.G.D. Cohen and G.P. Morriss, *Probability of second law violations in shearing steady flows*. Phys. Rev. Lett. **71**, 2401–2404 (1993). (Cited on page [15](#).)
- [Eva93b] D.J. Evans and S.S. Sarman, *Equivalence of thermostatted nonlinear response*. Phys. Rev. E **48**, 65–70 (1993). (Cited on page [128](#).)
- [Eva98] D.J. Evans, D.J. Searles, W.G. Hoover, B.L. Holian, H.A. Posch and G.P. Morriss, *Comment on “Modified nonequilibrium molecular dynamics for fluid flows with energy conservation”*. J. Chem. Phys. **108**, 4351–4352 (1998). (Cited on pages [162](#), [176](#) and [177](#).)
- [Eva00] D.J. Evans, E.G.D. Cohen, D.J. Searles and F. Bonetto, *Note on the Kaplan-Yorke dimension and linear transport coefficients*. J. Stat. Phys. **101**, 17–34 (2000). (Cited on pages [14](#), [153](#), [191](#) and [225](#).)

- [Eva02a] D.J. Evans and L. Rondoni, *Comments on the entropy of nonequilibrium steady states*. J. Stat. Phys. **109**, 895–920 (2002). (Cited on pages [128](#), [184](#) and [185](#).)
- [Eva02b] D.J. Evans and D.J. Searles, *The Fluctuation Theorem*. Advances in Physics **51**, 1529–1585 (2002). (Cited on page [15](#).)
- [Eyi92] G.L. Eyink and J.L. Lebowitz, *Generalized Gaussian dynamics, phase-space reduction and irreversibility: a comment*. in: M. Mareschal and B.L. Holian, Eds., Microscopic simulations of complex hydrodynamic phenomena, volume 292 of NATO ASI Series B: Physics, pages 323–326, Plenum Press, New York, 1992. (Cited on pages [182](#), [194](#) and [195](#).)
- [Fal90] K. Falconer, *Fractal geometry*. (Wiley, New York, 1990). (Cited on page [31](#).)
- [Far85] J.D. Farmer, *Sensitive dependence on parameters in nonlinear dynamics*. Phys. Rev. Lett. **55**, 351–354 (1985). (Cited on pages [78](#) and [79](#).)
- [Far99] Z. Farkas, P. Tegzes, A. Vukics and T. Vicsek, *Transitions in the horizontal transport of vertically vibrated granular layers*. Phys. Rev. E **60**, 7022–7031 (1999). (Cited on pages [12](#), [23](#), [117](#) and [249](#).)
- [Fei78] M.J. Feigenbaum, *Quantitative universality for a class of nonlinear transformations*. J. Stat. Phys. **19**, 25–52 (1978). (Cited on page [78](#).)
- [Fei79] M.J. Feigenbaum, *The universal metric properties of nonlinear transformations*. J. Stat. Phys. **21**, 669–706 (1979). (Cited on page [78](#).)
- [Fei83] M.J. Feigenbaum, *Universal behavior in non-linear systems*. Physica D **7**, 16–39 (1983). (Cited on page [78](#).)
- [Fes02] R. Festa, A. Mazzino and D. Vincenzi, *Lorenz deterministic diffusion*. Europhys. Lett. **60**, 820–826 (2002). (Cited on page [73](#).)
- [Fis73] M.E. Fisher, M.N. Barber and D. Jasnow, *Helicity modulus, superfluidity, and scaling in isotropic systems*. Phys. Rev. A **8**, 1111–1124 (1973). (Cited on page [36](#).)
- [Fle92] R. Fleischmann, T. Geisel and R. Ketzmerick, *Magnetoresistance due to chaos and nonlinear resonance in lateral surface superlattices*. Phys. Rev. Lett. **68**, 1367–1370 (1992). (Cited on pages [143](#) and [249](#).)
- [Fle95] R. Fleischmann et al., *Chaos und fraktale Energiespektren in Antidot-Gittern*. Physikalische Blätter **51**, 177–182 (1995). (Cited on page [249](#).)
- [For87] G.W. Ford and M. Kac, *On the quantum Langevin equation*. J. Stat. Phys. **46**, 803–810 (1987). (Cited on pages [13](#) and [134](#).)
- [For03] C. Forster, R. Hirschl, H.A. Posch and W.G. Hoover, *Perturbed phase-space dynamics of hard-disk fluids*. in print for the Physica D Special Issue Ref. [\[Kla03b\]](#), 2003. (Cited on page [14](#).)
- [Fra90] K. Franke and H. Gruler, *Galvanotaxis of human granulocytes: electric field jump studies*. Europ. Biophys. J. **18**, 335–346 (1990). (Cited on pages [129](#) and [235](#).)

- [Fra91] M. Franaszek, *Influence of noise on the mean lifetime of chaotic transients*. Phys. Rev. A **44**, 4065–4067 (1991). (Cited on pages [11](#), [86](#) and [87](#).)
- [Fuj82] H. Fujisaka and S. Grossmann, *Diffusion in discrete nonlinear dynamical systems*. Z. Physik B **48**, 261–275 (1982). (Cited on pages [21](#), [22](#), [26](#), [27](#), [30](#), [73](#), [74](#), [75](#), [78](#), [81](#), [82](#), [84](#), [93](#) and [95](#).)
- [Ful75] P. Fulde, L. Pietronero, W. R. Schneider and S. Strässler, *Problem of Brownian motion in a periodic potential*. Phys. Rev. Lett. **35**, 1776–1779 (1975). (Cited on page [11](#).)
- [Gal77] F. Galton, *Typical laws of heredity*. Nature **15**, 492–495, 512–514, 532–533 (1877). (Cited on pages [10](#), [127](#) and [142](#).)
- [Gal95a] G. Gallavotti and E.G.D. Cohen, *Dynamical ensembles in nonequilibrium statistical mechanics*. Phys. Rev. Lett. **74**, 2694–2697 (1995). (Cited on page [15](#).)
- [Gal95b] G. Gallavotti and E.G.D. Cohen, *Dynamical ensembles in stationary states*. J. Stat. Phys. **80**, 931–970 (1995). (Cited on page [15](#).)
- [Gal96a] G. Gallavotti, *Equivalence of dynamical ensembles and Navier-Stokes equations*. Phys. Lett. A **223**, 91–95 (1996). (Cited on page [128](#).)
- [Gal96b] G. Gallavotti, *Extension of Onsager’s reciprocity to large fields and the chaotic hypothesis*. Phys. Rev. Lett. **77**, 4334–4337 (1996). (Cited on page [15](#).)
- [Gal97] G. Gallavotti, *Dynamical ensembles equivalence in fluid mechanics*. Physica D **105**, 163–184 (1997). (Cited on page [128](#).)
- [Gal98] G. Gallavotti, *Chaotic dynamics, fluctuations, nonequilibrium ensembles*. Chaos **8**, 384–393 (1998). (Cited on pages [14](#) and [15](#).)
- [Gal99] G. Gallavotti, *Statistical mechanics - a short treatise*. (Springer, Berlin, 1999). Chapter 9. (Cited on pages [9](#), [12](#), [13](#), [14](#), [15](#), [17](#), [127](#), [133](#), [185](#), [186](#) and [187](#).)
- [Gal03] G. Gallavotti, *Nonequilibrium thermodynamics?* preprint cond-mat/0301172, 2003. (Cited on pages [9](#), [15](#), [128](#), [150](#), [187](#) and [195](#).)
- [Gan71] F.R. Gantmacher, *Matrizenrechnung*, volume 2. (VEB Deutscher Verlag der Wissenschaften, Berlin, 3rd edition, 1971). (Cited on page [30](#).)
- [Gar02] P. Garbaczewski and R. Olkiewicz, Eds. *Dynamics of dissipation*, volume 597 of Lecture Notes in Physics, Springer, Berlin, 2002. (Cited on pages [10](#), [17](#), [183](#), [270](#), [279](#) and [288](#).)
- [Gas] P. Gaspard and R. Klages. unpublished. (Cited on pages [67](#), [69](#), [70](#) and [71](#).)
- [Gas71] D. Gass, *Enskog theory for a rigid disk fluid*. J. Chem. Phys. **54**, 1898–1902 (1971). (Cited on page [227](#).)
- [Gas90] P. Gaspard and G. Nicolis, *Transport properties, Lyapunov exponents, and entropy per unit time*. Phys. Rev. Lett. **65**, 1693–1696 (1990). (Cited on pages [10](#), [28](#) and [189](#).)

-
- [Gas92a] P. Gaspard, *Diffusion, effusion, and chaotic scattering*. J. Stat. Phys. **68**, 673–747 (1992). (Cited on pages [10](#), [11](#), [21](#), [28](#), [30](#), [54](#), [55](#), [58](#), [60](#), [93](#) and [183](#).)
- [Gas92b] P. Gaspard, *Diffusion in uniformly hyperbolic one-dimensional maps and Appell polynomials*. Phys. Lett. A **168**, 13–17 (1992). (Cited on pages [28](#) and [30](#).)
- [Gas92c] P. Gaspard and F. Baras, *Dynamical Chaos underlying diffusion in the Lorentz Gas*. in: M. Mareschal and B.L. Holian, Eds., Microscopic simulations of complex hydrodynamic phenomena, volume 292 of NATO ASI Series B: Physics, pages 301–322, Plenum Press, New York, 1992. (Cited on pages [10](#), [22](#), [27](#), [28](#) and [189](#).)
- [Gas93] P. Gaspard, *What is the role of chaotic scattering in irreversible processes?* Chaos **3**, 427–442 (1993). (Cited on pages [10](#), [21](#), [28](#), [30](#), [54](#), [55](#), [56](#), [183](#) and [189](#).)
- [Gas95a] P. Gaspard, *Chaos, fractals, and transport properties: A new insight into nonequilibrium statistical mechanics and Irreversibility*. in: Y. Aizawa, S. Saito and K. Shiraiwa, Eds., Dynamical Systems and Chaos, volume 2, pages 55–68, World Scientific, Singapore, 1995. (Cited on pages [21](#), [54](#), [55](#) and [56](#).)
- [Gas95b] P. Gaspard and F. Baras, *Chaotic scattering and diffusion in the Lorentz gas*. Phys. Rev. E **51**, 5332–5352 (1995). (Cited on pages [10](#), [22](#), [107](#), [145](#), [158](#), [189](#) and [191](#).)
- [Gas95c] P. Gaspard and J.R. Dorfman, *Chaotic scattering theory, thermodynamic formalism, and transport coefficients*. Phys. Rev. E **52**, 3525–3552 (1995). (Cited on pages [10](#), [28](#) and [189](#).)
- [Gas96] P. Gaspard, *Hydrodynamic modes as singular eigenstates of the Liouvillian dynamics: Deterministic diffusion*. Phys. Rev. E **53**, 4379–4401 (1996). (Cited on pages [53](#), [54](#), [57](#), [102](#), [145](#), [153](#), [154](#) and [158](#).)
- [Gas97a] P. Gaspard, *Chaos and hydrodynamics*. Physica A **240**, 54–67 (1997). (Cited on page [57](#).)
- [Gas97b] P. Gaspard, *Entropy production in open volume-preserving systems*. J. Stat. Phys. **88**, 1215–1240 (1997). (Cited on pages [10](#), [57](#), [129](#), [183](#), [185](#), [186](#) and [208](#).)
- [Gas98a] P. Gaspard, *Chaos, scattering, and statistical mechanics*. (Cambridge University Press, Cambridge, 1998). (Cited on pages [9](#), [10](#), [11](#), [12](#), [14](#), [17](#), [21](#), [22](#), [26](#), [28](#), [53](#), [74](#), [77](#), [81](#), [99](#), [102](#), [127](#), [128](#), [129](#), [144](#), [145](#), [151](#), [152](#), [153](#), [154](#), [158](#), [162](#), [175](#), [182](#), [183](#), [185](#), [186](#), [187](#), [188](#), [189](#), [190](#), [191](#), [208](#) and [212](#).)
- [Gas98b] P. Gaspard, M.E. Briggs, M.K. Francis, J.V. Sengers, R.W. Gammons, J.R. Dorfman and R.V. Calabrese, *Experimental evidence for microscopic chaos*. Nature **394**, 865–868 (1998). (Cited on pages [12](#), [86](#) and [250](#).)
- [Gas98c] P. Gaspard and R. Klages, *Chaotic and fractal properties of deterministic diffusion-reaction processes*. Chaos **8**, 409–423 (1998). (Cited on pages [11](#), [16](#), [21](#), [40](#), [41](#), [51](#), [74](#), [77](#), [94](#), [96](#), [98](#), [123](#), [158](#) and [183](#).)

- [Gas01] P. Gaspard, I. Claus, T. Gilbert and J.R. Dorfman, *Fractality of the hydrodynamic modes of diffusion*. Phys. Rev. Lett. **86**, 1506–1509 (2001). (Cited on pages [10](#), [190](#) and [191](#).)
- [Gas02a] P. Gaspard, *Dynamical theory of relaxation in classical and quantum systems*. in: Dynamics of dissipation, pages 111–163. (2002). see Ref. [[Gar02](#)]. (Cited on page [10](#).)
- [Gas02b] P. Gaspard and I. Claus, *Chaos and fractals in dynamical models of transport and reaction*. Philos. Trans. Roy. Soc. London Series A **360**, 303–315 (2002). (Cited on page [21](#).)
- [Gas03] P. Gaspard, G. Nicolis and J.R. Dorfman, *Diffusive Lorentz gases and multibaker maps are compatible with irreversible thermodynamics*. Physica A **323**, 294–322 (2003). (Cited on pages [10](#), [182](#) and [183](#).)
- [Gei82] T. Geisel and J. Nierwetberg, *Onset of diffusion and universal scaling in chaotic systems*. Phys. Rev. Lett. **48**, 7–10 (1982). (Cited on pages [11](#), [21](#), [22](#), [26](#), [73](#), [74](#), [75](#), [81](#), [86](#), [92](#) and [95](#).)
- [Gei84] T. Geisel and S. Thomaes, *Anomalous diffusion in intermittent chaotic systems*. Phys. Rev. Lett. **52**, 1936–1939 (1984). (Cited on page [26](#).)
- [Gei85] T. Geisel, J. Nierwetberg and A. Zacherl, *Accelerated diffusion in Josephson junctions and related chaotic systems*. Phys. Rev. Lett. **54**, 616–619 (1985). (Cited on pages [26](#) and [249](#).)
- [Gei90] T. Geisel, J. Wagenhuber, P. Niebauer and G. Obermair, *Chaotic dynamics of ballistic electrons in lateral superlattices and magnetic fields*. Phys. Rev. Lett. **64**, 1581–1584 (1990). (Cited on pages [143](#) and [249](#).)
- [Ger73] G. Gerlich, *Die verallgemeinerte Liouville-Gleichung*. Physica **69**, 458–466 (1973). (Cited on pages [127](#), [162](#) and [185](#).)
- [Ger99] A. Gervois, D. Iagolnitzer, M. Moreau and Y. Pomeau, Eds. *Statistical Physics - invited papers from STATPHYS 20*, volume 263 of Physica A, North Holland, Amsterdam, 1999. (Cited on pages [9](#) and [130](#).)
- [Gib60] J.W. Gibbs, *Elementary Principles of Statistical Mechanics*. (Dover, New York, 1960). (Cited on page [9](#).)
- [Gil99a] T. Gilbert and J.R. Dorfman, *Entropy production: from open volume-preserving to dissipative systems*. J. Stat. Phys. **96**, 225–269 (1999). (Cited on pages [10](#), [57](#), [128](#), [151](#), [153](#), [183](#), [186](#), [187](#) and [190](#).)
- [Gil99b] T. Gilbert, C.D. Ferguson and J.R. Dorfman, *Field driven thermostated systems: A nonlinear multibaker map*. Phys. Rev. E **59**, 364–371 (1999). (Cited on pages [128](#), [153](#), [158](#), [183](#) and [190](#).)
- [Gil00a] T. Gilbert and J.R. Dorfman, *Entropy production in a persistent random walk*. Physica A **282**, 427–449 (2000). (Cited on pages [10](#), [57](#), [183](#), [186](#) and [190](#).)

- [Gil00b] T. Gilbert, J.R. Dorfman and P. Gaspard, *Entropy production, fractals, and relaxation to equilibrium*. Phys. Rev. Lett. **85**, 1606–1609 (2000). (Cited on pages [10](#), [57](#), [183](#) and [186](#).)
- [Gil01] T. Gilbert, J.R. Dorfman and P. Gaspard, *Fractal dimensions of the hydrodynamic modes of diffusion*. Nonlinearity **14**, 339–358 (2001). (Cited on pages [10](#), [14](#), [128](#), [183](#), [188](#), [189](#), [190](#), [191](#) and [192](#).)
- [Gil04] T. Gilbert and J.R. Dorfman, *On the parametric dependences of a class of nonlinear singular maps*. Discr. Contin. Dyn. Syst. B **4**, 391–406 (2004). (Cited on pages [21](#), [47](#), [158](#) and [183](#).)
- [Gle88] J. Gleick, *Chaos - Making a New Science*. (Penguin, New York, 1988). (Cited on page [17](#).)
- [Gle93] P. Glendinning and C. Sparrow, *Prime and renormalisable kneading invariants and the dynamics of expanding Lorenz maps*. Physica D **62**, 22–50 (1993). (Cited on page [27](#).)
- [Gol85] S. Goldstein, C. Kipnis and N. Ianiro, *Stationary states for a mechanical system with stochastic boundary conditions*. J. Stat. Phys. **41**, 915–939 (1985). (Cited on pages [128](#), [194](#) and [195](#).)
- [Gra99] P. Grassberger and T. Schreiber, *Microscopic chaos from Brownian motion?* Nature **401**, 875–876 (1999). (Cited on pages [12](#), [86](#) and [250](#).)
- [Gra02] P. Grassberger, W. Nadler and L. Yang, *Heat conduction and entropy production in a one-dimensional hard-particle gas*. Phys. Rev. Lett. **89**, 180601/1–4 (2002). (Cited on pages [12](#) and [250](#).)
- [Gre84] C. Grebogi, E. Ott, S. Pelikan and J.A. Yorke, *Strange attractors that are not chaotic*. Physica D **13**, 261–268 (1984). (Cited on page [153](#).)
- [Gri89] M. Grilli and E. Tosatti, *Exact canonical averages from microcanonical dynamics for quantum systems*. Phys. Rev. Lett. **62**, 2889–2892 (1989). (Cited on page [251](#).)
- [Gro] J. Groeneveld. unpublished. (Cited on pages [21](#), [36](#), [39](#), [41](#) and [47](#).)
- [Gro81] J. Groeneveld, J. Jurkiewics and C.P. Korthals Altes, *Twist as a probe for phase structure*. Physica Scripta **23**, 1022–1031 (1981). (Cited on page [36](#).)
- [Gro82] S. Grossmann and H. Fujisaka, *Chaos-induced diffusion in nonlinear discrete dynamics*. Phys. Rev. A **26**, 1779–1782 (1982). (Cited on pages [21](#), [22](#), [26](#), [27](#), [30](#), [73](#), [74](#), [75](#), [78](#), [81](#), [82](#) and [84](#).)
- [Gro83] S. Grossmann and S. Thomae, *Shape dependence of correlation times in chaos-induced diffusion*. Phys. Lett. A **97**, 263–267 (1983). (Cited on pages [21](#), [26](#), [27](#), [73](#), [74](#) and [75](#).)
- [Gro02] J. Groeneveld and R. Klages, *Negative and nonlinear response in an exactly solved dynamical model of particle transport*. J. Stat. Phys. **109**, 821–861 (2002). (Cited on pages [11](#), [16](#), [21](#), [33](#), [36](#), [46](#), [74](#), [77](#), [82](#), [83](#), [88](#), [89](#), [90](#), [94](#), [123](#), [158](#) and [159](#).)

- [Gro03] R. Grochowski, S. Strugholtz, P. Walzel and C.A. Krülle, *Granular Transport on Vibratory Conveyor*. *Chemie Ingenieur Technik* **75**, 1103 (2003). (Cited on pages [12](#) and [249](#).)
- [Gro04] R. Grochowski, P. Walzel, M. Rouijaa, C.A. Krülle and I. Rehberg, *Reversing a granular flow on a vibratory conveyor*. *Appl. Phys. Lett.* **84**, 1019–1022 (2004). (Cited on pages [12](#) and [249](#).)
- [Gru94] H. Gruler and A. de Boisfleury-Chevance, *Directed cell movement and cluster formation: physical principles*. *J. Phys. I: France* **4**, 1085–1105 (1994). (Cited on page [235](#).)
- [Guc90] J. Guckenheimer and P. Holmes, *Nonlinear Oscillations, Dynamical Systems, and Bifurcations of Vector Fields*, volume 42 of Applied mathematical sciences. (Springer, Berlin, 3rd edition, 1990). (Cited on pages [23](#), [27](#), [118](#) and [153](#).)
- [Gup94] D. Gupalo, A.S. Kaganovich and E.G.D. Cohen, *Symmetry of Lyapunov spectrum*. *J. Stat. Phys.* **74**, 1145–1159 (1994). (Cited on page [152](#).)
- [Ham90] I.P. Hamilton, *Modified Nosé-Hoover equation for a one-dimensional oscillator: enforcement of the virial theorem*. *Phys. Rev. A* **42**, 7467–7470 (1990). (Cited on pages [175](#), [177](#) and [207](#).)
- [Hän96] P. Hänggi and R. Bartussek, *Brownian rectifiers: how to convert Brownian motion into directed transport*. in: J. Parisi, S. C. Müller and W. Zimmermann, Eds., *Nonlinear physics of complex systems - current status and future trends*, Springer-Series 'Lecture notes in physics'. (Springer, 1996). (Cited on page [11](#).)
- [Hao89] Bai-Lin Hao, *Elementary symbolic dynamics and chaos in dissipative systems*. (World Scientific, Singapore, 1989). (Cited on page [45](#).)
- [Har] T. Harayama. unpublished. (Cited on pages [102](#) and [105](#).)
- [Har94] R.S. Hartmann, K. Lau, W. Chou and T.D. Coates, *The fundamental motor of the human neutrophil is not random: evidence for local non-Markov movement in neutrophils*. *Biophys. J.* **67**, 2535–2545 (1994). (Cited on pages [129](#) and [235](#).)
- [Har01] T. Harayama and P. Gaspard, *Diffusion of particles bouncing on a one-dimensional periodically corrugated floor*. *Phys. Rev. E* **64**, 036215/1–16 (2001). (Cited on pages [11](#), [117](#), [123](#) and [158](#).)
- [Har02] T. Harayama, R. Klages and P. Gaspard, *Deterministic diffusion in flower-shaped billiards*. *Phys. Rev. E* **66**, 026211/1–7 (2002). (Cited on pages [11](#), [16](#), [22](#), [105](#), [123](#) and [158](#).)
- [Has09] F. Hasenöhr, Eds., *Wissenschaftliche Abhandlungen von L. Boltzmann*, volume 2. (J.A. Barth Verlag, Leipzig, 1909). (Cited on page [140](#).)
- [Hat84] M. Hata and M. Yamaguti, *The Takagi function and its generalization*. *Japan J. Appl. Math.* **1**, 183–199 (1984). (Cited on page [57](#).)

-
- [Hau87] J.W. Haus and K. W. Kehr, *Diffusion in regular and disordered lattices*. Phys. Rep. **150**, 264–406 (1987). (Cited on pages [81](#) and [83](#).)
- [Heg96] H. Hegger, B. Huckestein, K. Hecker, M. Janssen, A. Freimuth, G. Reckziegel and R. Tuzinski, *Fractal Conductance Fluctuations in Gold Nanowires*. Phys. Rev. Lett. **77**, 3885–3888 (1996). (Cited on pages [12](#) and [250](#).)
- [Hes90] S. Hess and W. Loose, *Flow properties and shear-induced structural changes in fluids: a case study on the interplay between theory, simulation, experiment and application*. Ber. Bunsenges. Phys. Chem. **94**, 216–222 (1990). (Cited on page [225](#).)
- [Hes96a] S. Hess, *Constraints in molecular dynamics, nonequilibrium processes in fluids via computer simulations*. in: K.H. Hoffmann and M. Schreiber, Eds., Computational physics, pages 268–293, Springer, Berlin, 1996. (Cited on pages [12](#), [13](#), [17](#), [127](#), [133](#), [148](#), [149](#), [164](#), [165](#), [224](#) and [225](#).)
- [Hes96b] S. Hess, M. Kröger, W. Loose, C. Pereira Borgmeyer, R. Schramek, H. Voigt and T. Weider, *Simple and complex fluids under shear*. in: K. Binder and G. Ciccotti, Eds., Monte Carlo and Molecular Dynamics of Condensed Matter Systems, volume 49 of IPS Conf. Proc., pages 825–841, Bologna, 1996. (Cited on pages [13](#), [148](#), [165](#), [224](#) and [225](#).)
- [Hes97] S. Hess, C. Aust, L. Bennett, M. Kröer, C. Pereira-Borgmeyer and T. Weider, *Rheology: from simple and to complex fluids*. Physica A **240**, 126–144 (1997). (Cited on pages [13](#), [165](#) and [225](#).)
- [Hes02] S. Hess and G.P. Morriss, *Regular and chaotic rotation of a polymer molecule subjected to a shear flow*. preprint, 2002. (Cited on page [176](#).)
- [Hes03] S. Hess, *Construction and test of thermostats and twirlers for molecular rotations*. Z. Naturforsch. **58a**, 377–391 (2003). (Cited on page [176](#).)
- [Hol86] B.L. Holian and W.G. Hoover, *Numerical test of the Liouville equation*. Phys. Rev. A, 4229–4237 (1986). (Cited on pages [163](#), [164](#), [166](#), [173](#) and [175](#).)
- [Hol87] B.L. Holian, W.G. Hoover and H.A. Posch, *Resolution of Loschmidt's paradox: the origin of irreversible behavior in reversible atomistic dynamics*. Phys. Rev. Lett. **59**, 10–13 (1987). (Cited on pages [14](#), [148](#), [149](#), [151](#), [153](#), [166](#), [172](#), [185](#) and [194](#).)
- [Hol95] B.L. Holian, A.F. Voter and R. Ravelo, *Thermostatted molecular dynamics: How to avoid the Toda demon hidden in Nosé-Hoover dynamics*. Phys. Rev. E **52**, 2338–2347 (1995). (Cited on pages [148](#), [149](#), [166](#) and [173](#).)
- [Hoo75] W.G. Hoover and W.T. Ashurst, *Nonequilibrium Molecular Dynamics*. in: H. Eyring and D. Henderson, Eds., Theoretical Chemistry, volume 1, Academic Press, New York, 1975. (Cited on pages [224](#) and [226](#).)
- [Hoo82] W.G. Hoover, A.J.C. Ladd and B. Moran, *High-strain-rate plastic flow studied via nonequilibrium molecular dynamics*. Phys. Rev. Lett. **48**, 1818–1821 (1982). (Cited on pages [13](#), [149](#), [174](#) and [224](#).)

- [Hoo84] W.G. Hoover, B. Moran and J.M. Haile, *Homogeneous periodic heat flow via nonequilibrium molecular dynamics*. J. Stat. Phys. **37**, 109–121 (1984). (Cited on page [226](#).)
- [Hoo85] W.G. Hoover, *Canonical dynamics: equilibrium phase-space distributions*. Phys. Rev. A **31**, 1695–1697 (1985). (Cited on pages [13](#), [163](#), [164](#), [166](#), [170](#), [173](#) and [175](#).)
- [Hoo86] W.G. Hoover and K.W. Kratky, *Heat conductivity of three periodic hard disks via nonequilibrium molecular dynamics*. J. Stat. Phys. **42**, 1103–1114 (1986). (Cited on page [226](#).)
- [Hoo87] W.G. Hoover and H.A. Posch, *Direct measurement of equilibrium and nonequilibrium Lyapunov spectra*. Phys. Lett. A **123**, 227–230 (1987). (Cited on pages [14](#) and [185](#).)
- [Hoo88a] W.G. Hoover, B. Moran, C.G. Hoover and D.J. Evans, *Irreversibility in the Galton board via conservative and quantum Hamiltonian and Gaussian dynamics*. Phys. Lett. A **133**, 114–120 (1988). (Cited on pages [14](#), [148](#), [153](#), [154](#), [155](#) and [170](#).)
- [Hoo88b] W.G. Hoover, C.G. Tull and H.A. Posch, *Negative Lyapunov exponents for dissipative systems*. Phys. Lett. A **131**, 211–215 (1988). (Cited on page [152](#).)
- [Hoo89a] W.G. Hoover, *Generalization of Nosé’s isothermal molecular dynamics: Non-Hamiltonian dynamics for the canonical ensemble*. Phys. Rev. **40**, 2814–2815 (1989). (Cited on pages [175](#) and [207](#).)
- [Hoo89b] W.G. Hoover and B. Moran, *Phase-space singularities in atomistic planar diffusive flow*. Phys. Rev. A **40**, 5319–5326 (1989). (Cited on pages [148](#), [153](#), [154](#) and [155](#).)
- [Hoo91] W.G. Hoover, *Computational statistical mechanics*, volume 11 of Studies in modern thermodynamics. (Elsevier, Amsterdam, 1991). (Cited on pages [9](#), [12](#), [13](#), [14](#), [127](#), [153](#), [163](#), [164](#) and [175](#).)
- [Hoo92] W.G. Hoover and B. Moran, *Viscous attractor for the Galton board*. Chaos **2**, 599–602 (1992). (Cited on pages [148](#), [153](#), [156](#) and [157](#).)
- [Hoo94] W.G. Hoover and H.A. Posch, *Second-law irreversibility and phase-space dimensionality loss from time-reversible nonequilibrium steady-state Lyapunov spectra*. Phys. Rev. E **49**, 1913–1920 (1994). (Cited on page [153](#).)
- [Hoo96a] W.G. Hoover and B.L. Holian, *Kinetic moments method for the canonical ensemble distribution*. Phys. Lett. **211**, 253–257 (1996). (Cited on pages [164](#), [175](#), [176](#) and [207](#).)
- [Hoo96b] W.G. Hoover, O. Kum and H.A. Posch, *Time-reversible dissipative ergodic maps*. Phys. Rev. E **53**, 2123–2129 (1996). (Cited on pages [14](#), [149](#) and [183](#).)
- [Hoo97] W.G. Hoover and O. Kum, *Ergodicity, mixing, and time reversibility for atomistic nonequilibrium steady states*. Phys. Rev. E **56**, 5517–5523 (1997). (Cited on pages [148](#), [149](#), [156](#), [164](#), [175](#), [176](#), [177](#) and [207](#).)

- [Hoo98a] W.G. Hoover, D.J. Evans, H.A. Posch, B.L. Holian and G.P. Morriss, *Comment on "Toward a statistical thermodynamics of steady states"*. Phys. Rev. Lett. **80**, 4103 (1998). (Cited on page [162](#).)
- [Hoo98b] W.G. Hoover and H.A. Posch, *Chaos and irreversibility in simple model systems*. Chaos **8**, 366–373 (1998). (Cited on pages [183](#) and [184](#).)
- [Hoo98c] W.G. Hoover and H.A. Posch, *Multifractals from stochastic many-body molecular dynamics*. Phys. Lett. A **246**, 247–251 (1998). (Cited on pages [128](#), [148](#), [153](#), [194](#) and [195](#).)
- [Hoo99] W.G. Hoover, *Time reversibility, computer simulation, and chaos*. (World Scientific, Singapore, 1999). (Cited on pages [9](#), [10](#), [12](#), [13](#), [14](#), [17](#), [127](#), [132](#), [136](#), [148](#), [150](#), [151](#), [153](#), [155](#), [162](#), [164](#), [170](#), [185](#), [186](#), [194](#), [224](#) and [226](#).)
- [Hoo01] W.G. Hoover, C.G. Hoover and D.I. Isbister, *Chaos, ergodic convergence, and fractal instability for a thermostated canonical harmonic oscillator*. Phys. Rev. E **63**, 026209–1/5 (2001). (Cited on pages [175](#) and [177](#).)
- [Hoo02a] W.G. Hoover, 2002. private communication. (Cited on page [219](#).)
- [Hoo02b] W.G. Hoover, H.A. Posch, K. Aoki and D. Kusnezov, *Remarks on non-Hamiltonian statistical mechanics: Lyapunov exponents and phase-space dimensionality loss*. Europhys. Lett. **60**, 337–341 (2002). (Cited on pages [172](#), [226](#) and [232](#).)
- [Hoo02c] W.G. Hoover, H.A. Posch, C. Forster, C. Dellago and M. Zhou, *Lyapunov modes of two-dimensional many-body systems; soft disks, hard disks, and rotors*. J. Stat. Phys. **109**, 765–776 (2002). (Cited on page [14](#).)
- [Hoo03] W.G. Hoover, K. Aoki, C.G. Hoover and S.V. De Groot, *Time-reversible deterministic thermostats*. in print for the Physica D Special Issue Ref. [[Kla03b](#)], 2003. (Cited on pages [128](#) and [226](#).)
- [Hop37] E. Hopf, *Ergodentheorie*. (Springer, Berlin, 1937). (Cited on page [182](#).)
- [Hsu85] C.S. Hsu and M.C. Kim, *Construction of maps with generating partitions for entropy evaluation*. Phys. Rev. A **31**, 3253–3265 (1985). (Cited on page [29](#).)
- [Hua87] K. Huang, *Statistical mechanics*. (Wiley, New York, 1987). (Cited on pages [9](#), [17](#), [132](#), [150](#) and [162](#).)
- [Hub80] B.A. Huberman, J.P. Crutchfield and N.H. Packard, *Noise phenomena in Josephson junctions*. Appl. Phys. Lett. **37**, 750–752 (1980). (Cited on page [73](#).)
- [Hub90] J.H. Hubbard and Sparrow C., *The classification of topologically expansive Lorenz maps*. Comm. Pure Appl. Math. **43**, 431–443 (1990). (Cited on page [27](#).)
- [Huf01] L. Hufnagel, R. Ketzmerick and M. Weiss, *Conductance fluctuations of generic billiards: Fractal or isolated?* Europhys. Lett. **54**, 703–708 (2001). (Cited on pages [12](#) and [250](#).)

- [Iba96] H. Ibach and H. Lüth, *Solid state physics*. (Springer, Berlin, 1996). (Cited on page [142](#).)
- [Ito81] R. Ito, *Rotation sets are closed*. Math. Proc. Cambr. Phil. Soc. **89**, 107–110 (1981). (Cited on page [35](#).)
- [JA01] J.C. Vallejo J. Aguirre and M.A.F. Sanjuan, *Wada basins and chaotic invariant sets in the Hnon-Heiles system*. Phys. Rev. E **64**, 066208/1–11 (2001). (Cited on page [112](#).)
- [Jac78] M.V. Jacobson, *Topological and metric properties of one-dimensional endomorphisms*. Soviet. Math. Dokl. **19**, 1452–1456 (1978). (Cited on page [78](#).)
- [Jac81] E. Ben Jacob, Y. Braiman, R. Shainsky and Y. Imry, *Microwave induced "Devil's staircase" structure and chaotic behavior in current-fed Josephson junctions*. Appl. Phys. Lett. **38**, 822–824 (1981). (Cited on page [11](#).)
- [Jar00] C. Jarzynski, *Hamiltonian derivation of a detailed fluctuation theorem*. J. Stat. Phys. **98**, 77–102 (2000). (Cited on page [15](#).)
- [Jel88a] J. Jellinek, *Dynamics for nonconservative systems: ergodicity beyond the microcanonical ensemble*. J. Phys. Chem. **92**, 3163–3173 (1988). (Cited on pages [175](#), [176](#) and [194](#).)
- [Jel88b] J. Jellinek and R. S. Berry, *Generalization of Nosé's isothermal molecular dynamics*. Phys. Rev. A **38**, 3069–3072 (1988). (Cited on pages [175](#) and [176](#).)
- [Jel89] J. Jellinek and R. S. Berry, *Generalization of Nosé's isothermal molecular dynamics: necessary and sufficient conditions of dynamical simulations of statistical ensembles*. Phys. Rev. A **40**, 2816–2818 (1989). (Cited on pages [175](#) and [207](#).)
- [Jep03] O. Jepps, D.J. Evans and D.J. Searles, *The fluctuation theorem and Lyapunov weights*. in print for the Physica D Special Issue Ref. [[Kla03b](#)], 2003. (Cited on page [15](#).)
- [Jun96] P. Jung, J. G. Kissner and P. Haenggi, *Regular and chaotic transport in asymmetric periodic potentials: inertia ratchets*. Phys. Rev. Lett. **76**, 3436–3439 (1996). (Cited on pages [11](#) and [249](#).)
- [Jus01] W. Just, H. Kantz, C. Rödenbeck and M. Helm, *Stochastic modelling: replacing fast degrees of freedom by noise*. J. Phys. A: Math. Gen. **34**, 3199–3213 (2001). (Cited on page [136](#).)
- [Jus03] W. Just, K. Gelfert, N. Baba, A. Riegert and H. Kantz, *Elimination of fast chaotic degrees of freedom: on the accuracy of the Born approximation*. J. Stat. Phys. **112**, 277–292 (2003). (Cited on page [136](#).)
- [Kan98] H. Kantz and E. Olbrich, *The transition from deterministic chaos to a stochastic process*. Physica A **253**, 105–117 (1998). (Cited on page [86](#).)

- [Kan03] H. Kantz, W. Just, N. Baba, K. Gelfert and A. Riegert, *Replacing fast chaotic degrees of freedom by noise: a formally exact result*. in print for the Physica D Special Issue Ref. [Kla03b], 2003. (Cited on page 136.)
- [Kar00] J. Karkheck, Eds. *Dynamics: Models and Kinetic Methods for Non-equilibrium Many Body Systems*, volume 371 of NATO Science Series E: Applied Sciences, Kluwer, Dordrecht, 2000. (Cited on pages 10 and 17.)
- [Kat95] A. Katok and B. Hasselblatt, *Introduction to the Modern Theory of Dynamical Systems*, volume 54 of Encyclopedia of Mathematics and its Applications. (Cambridge University Press, Cambridge, 1995). (Cited on page 27.)
- [Keh98] K.W. Kehr, *Diffusion of particles on lattices*. in: R. Haberlandt J. Kaerger, P. Heitjans, Eds., *Diffusion in condensed matter*, pages 265–305, Vieweg, Braunschweig, 1998. (Cited on pages 81 and 83.)
- [Ket96] R. Ketzmerick, *Fractal conductance fluctuations in generic chaotic cavities*. Phys. Rev. B **54**, 10841–10844 (1996). (Cited on pages 12 and 250.)
- [Kla] R. Klages. unpublished. (Cited on pages 11, 21, 36, 44, 47, 88, 89, 90, 91, 92, 202, 206, 216 and 242.)
- [Kla95] R. Klages and J.R. Dorfman, *Simple maps with fractal diffusion coefficients*. Phys. Rev. Lett. **74**, 387–390 (1995). (Cited on pages 11, 16, 21, 25, 26, 35, 36, 40, 44, 58, 73, 74, 82, 83, 86, 88, 94, 97, 123 and 158.)
- [Kla96] R. Klages, *Deterministic diffusion in one-dimensional chaotic dynamical systems*. (Wissenschaft & Technik-Verlag, Berlin, 1996). (Cited on pages 11, 17, 21, 22, 25, 26, 27, 28, 35, 36, 40, 41, 44, 48, 58, 59, 60, 67, 73, 75, 77, 82, 83, 86, 88, 89, 91, 93, 94, 95, 96, 97, 98, 123, 158, 189 and 190.)
- [Kla97] R. Klages and J.R. Dorfman, *Dynamical crossover in deterministic diffusion*. Phys. Rev. E **55**, R1247–R1250 (1997). (Cited on pages 11, 21, 22, 25, 27, 28, 36, 40, 61, 82, 91 and 95.)
- [Kla99a] R. Klages and J.R. Dorfman, *Simple deterministic dynamical systems with fractal diffusion coefficients*. Phys. Rev. E **59**, 5361–5383 (1999). (Cited on pages 11, 21, 25, 26, 28, 35, 36, 40, 44, 58, 73, 74, 82, 83, 86, 88, 94, 97, 123, 158, 189 and 190.)
- [Kla99b] R. Klages and K. Rateitschak. unpublished, 1999. (Cited on pages 202 and 212.)
- [Kla00a] R. Klages and C. Dellago, *Density-dependent diffusion in the periodic Lorentz gas*. J. Stat. Phys. **101**, 145–159 (2000). see also chao-dyn/9910038 for further details. (Cited on pages 11, 22, 54, 93, 99, 100, 101, 102, 103, 105, 107, 110, 111, 112, 113, 123, 147, 158 and 159.)
- [Kla00b] R. Klages, K. Rateitschak and G. Nicolis, *Thermostating by deterministic scattering: construction of nonequilibrium steady states*. Phys. Rev. Lett. **84**, 4268–4271 (2000). (Cited on pages 16, 127, 128, 130, 153, 211, 212, 215, 217, 219, 220, 221 and 222.)

- [Kla02a] R. Klages, *Comment on “Analysis of chaotic motion and its shape dependence in a generalized piecewise linear map”*. Phys. Rev. E **66**, 018201/1–3 (2002). (Cited on pages [11](#), [21](#), [22](#), [25](#), [40](#), [75](#), [95](#), [123](#) and [158](#).)
- [Kla02b] R. Klages, *Suppression and enhancement of deterministic diffusion in disordered dynamical systems*. Phys. Rev. E **65**, 055203(R)/1–4 (2002). (Cited on pages [11](#), [16](#), [22](#), [81](#), [88](#), [89](#) and [196](#).)
- [Kla02c] R. Klages, *Transitions from deterministic to stochastic diffusion*. Europhys. Lett. **57**, 796–802 (2002). (Cited on pages [11](#), [16](#), [22](#), [81](#), [84](#), [85](#) and [196](#).)
- [Kla02d] R. Klages and N. Korabel, *Understanding deterministic diffusion by correlated random walks*. J. Phys. A: Math. Gen. **35**, 4823–4836 (2002). (Cited on pages [11](#), [16](#), [22](#), [25](#), [58](#), [74](#), [75](#), [93](#), [101](#), [105](#), [107](#), [114](#), [122](#), [123](#), [147](#) and [158](#).)
- [Kla03a] R. Klages and T. Klauß, *Fractal fractal dimensions of deterministic transport coefficients*. J. Phys. A: Math. Gen. **36**, 5747–5764 (2003). (Cited on pages [11](#), [21](#), [31](#), [46](#), [59](#), [73](#), [82](#), [88](#) and [123](#).)
- [Kla03b] R. Klages, H. van Beijeren, J.R. Dorfman and P. Gaspard, Eds. *Microscopic chaos and transport in many-particle systems*, Physica D, North Holland, Amsterdam, 2003. see http://www.mpipks-dresden.mpg.de/~chaotran/proceedings/chaotran_proc.html, to be published as a Special Issue in Physica D. (Cited on pages [17](#), [255](#), [260](#), [261](#), [265](#), [267](#), [275](#), [276](#), [277](#), [278](#), [282](#), [286](#), [290](#), [294](#) and [296](#).)
- [Klu90] R. Kluiving, H. W. Capel and R. A. Pasmantier, *Phase-transition-like phenomenon in a piecewise linear map*. Physica A **164**, 593–624 (1990). (Cited on pages [49](#) and [58](#).)
- [Kog83] H. Koga, H. Fujisaka and M. Inoue, *Anomalous enhancement of the diffusion coefficient near the intermittency transition*. Phys. Rev. A **28**, 2370–2373 (1983). (Cited on page [73](#).)
- [Kor02] N. Korabel and R. Klages, *Fractal structures of normal and anomalous diffusion in nonlinear nonhyperbolic dynamical systems*. Phys. Rev. Lett. **89**, 214102/1–4 (2002). (Cited on pages [11](#), [16](#), [58](#), [59](#), [73](#), [94](#), [96](#), [98](#), [123](#) and [158](#).)
- [Kor03] N. Korabel and R. Klages, *Fractality of deterministic diffusion in the nonhyperbolic climbing sine map*. in print for the Physica D Special Issue Ref. [[Kla03b](#)], 2003. (Cited on pages [11](#), [58](#), [73](#), [79](#), [94](#), [96](#) and [98](#).)
- [Kov88] Z.J. Kovalik, M. Franaszek and P. Pieranski, *Self-reanimating chaos in the bouncing-ball system*. Phys. Rev. A **37**, 4016–4022 (1988). (Cited on pages [23](#) and [118](#).)
- [Koz99] Z. Koza, *General technique of calculating the drift velocity and diffusion coefficient in arbitrary periodic systems*. J. Phys. A: Math. Gen. **32**, 7637–7651 (1999). (Cited on page [11](#).)

-
- [Kub92] R. Kubo, M. Toda and N. Hashitsume, *Statistical Physics*, volume 2 of Solid State Sciences. (Springer, Berlin, 2 edition, 1992). (Cited on pages [13](#), [134](#) and [159](#).)
- [Kur98] J. Kurchan, *Fluctuation theorem for stochastic dynamics*. J. Phys. A: Math. Gen. **31**, 3719–3729 (1998). (Cited on page [15](#).)
- [Kus90] D. Kusnezov, A. Bulgac and W. Bauer, *Canonical ensembles from chaos*. Ann. Phys. **204**, 155–185 (1990). (Cited on pages [153](#), [163](#), [166](#), [173](#), [175](#), [177](#) and [207](#).)
- [Kus92] D. Kusnezov and A. Bulgac, *Canonical ensembles from chaos, 2.: constrained dynamic-systems*. Ann. Phys. **214**, 180–218 (1992). (Cited on page [170](#).)
- [Kus93] D. Kusnezov, *Quantum ergodic wavefunctions from a thermal non-linear Schrödinger equation*. Phys. Lett. A **184**, 50–56 (1993). (Cited on pages [163](#) and [251](#).)
- [Kus95] D. Kusnezov, *Dimensional loss in nonequilibrium quantum systems*. Phys. Rev. Lett. **74**, 246–249 (1995). (Cited on page [251](#).)
- [Kus02] D. Kusnezov, E. Lutz and K. Aoki, *Non-equilibrium statistical mechanics of classical and quantum systems*. in: Dynamics of dissipation, pages 83–108. (2002). see Ref. [[Gar02](#)]. (Cited on pages [163](#), [172](#), [195](#), [219](#), [226](#), [232](#) and [251](#).)
- [Lad85] A.J.C. Ladd and W.G. Hoover, *Lorentz gas shear viscosity via nonequilibrium molecular dynamics and Boltzmann’s equation*. J. Stat. Phys. **38**, 973–988 (1985). (Cited on page [225](#).)
- [Lai03] B.B. Laird and B.J. Leimkuhler, *Generalized dynamical thermostating technique*. Phys. Rev. E **68**, 016704/1–6 (2003). (Cited on pages [164](#), [175](#) and [176](#).)
- [Lan08] P. Langevin, *Sur la théorie du mouvement brownien*. C.R. Acad. Sci. (Paris) **146**, 530–533 (1908). see also the English translation in Am. J. Phys. **65**, 1079 (1997). (Cited on pages [13](#), [127](#) and [133](#).)
- [Lar03] H. Larralde, F. Leyvraz and C. Mejia-Monasterio, *Transport properties of a modified Lorentz gas*. J. Stat. Phys. **113**, 197–231 (2003). (Cited on pages [148](#), [182](#), [213](#), [214](#), [226](#) and [249](#).)
- [Las94] A. Lasota and M.C. Mackey, *Chaos, Fractals, and Noise*, volume 97 of Applied mathematical sciences. (Springer, Berlin, 2nd edition, 1994). (Cited on page [28](#).)
- [Lat97] A. Latz, H. van Beijeren and J.R. Dorfman, *Lyapunov spectrum and the conjugate pairing rule for a thermostatted random Lorentz gas: Kinetic theory*. Phys. Rev. Lett. **78**, 207–210 (1997). (Cited on pages [14](#), [145](#), [152](#) and [196](#).)
- [Leb59] J.L. Lebowitz, *Stationary nonequilibrium Gibbsian ensembles*. Phys. Rev. **114**, 1192–1202 (1959). (Cited on page [57](#).)
- [Leb78] J.L. Lebowitz and H. Spohn, *Transport properties of the Lorentz gas: Fourier’s law*. J. Stat. Phys. **19**, 633–654 (1978). (Cited on pages [128](#), [194](#), [210](#) and [226](#).)

- [Leb98] P. Leboeuf, *Normal and anomalous diffusion in a deterministic area-preserving map*. Physica D **116**, 8–20 (1998). (Cited on page [249](#).)
- [Leb99] J.L. Lebowitz and H. Spohn, *A Gallavotti-Cohen-type symmetry in the large deviation functional for stochastic dynamics*. J. Stat. Phys. **95**, 333–365 (1999). (Cited on page [15](#).)
- [Lep00] S. Lepri, L. Rondoni and G. Benettin, *The Gallavotti-Cohen fluctuation theorem for a nonchaotic model*. J. Stat. Phys. **99**, 857–872 (2000). (Cited on pages [12](#), [15](#) and [250](#).)
- [Lep03] S. Lepri, S. Livi and A. Politi, *Thermal conduction in classical low-dimensional lattices*. Phys. Rep. **377**, 1–80 (2003). (Cited on page [226](#).)
- [Lev89] R.W. Leven, B.-P. Koch and B. Pompe, *Chaos in dissipativen Systemen*. (Vieweg, Braunschweig, 1989). (Cited on page [153](#).)
- [L’H93] I. L’Heureux and I. Hamilton, *Canonically modified Nosé-Hoover equation with explicit inclusion of the virial*. Phys. Rev. E **47**, 1411–1414 (1993). (Cited on pages [175](#), [177](#) and [207](#).)
- [Lic92] A.J. Lichtenberg and M.A. Lieberman, *Regular and chaotic dynamics*, volume 38 of Applied Mathematical Sciences. (Springer, New York, 2nd edition, 1992). (Cited on pages [23](#), [74](#), [81](#) and [118](#).)
- [Lie92] S.Y. Liem, D. Brown and J.H.R. Clarke, *Investigation of the homogeneous-shear nonequilibrium-molecular-dynamics method*. Phys. Rev. A **45**, 3706–3713 (1992). (Cited on pages [128](#) and [224](#).)
- [Lie99a] E. Lieb, *Some problems in statistical mechanics that I would like to see solved*. Physica A **263**, 491–499 (1999). (Cited on page [13](#).)
- [Lie99b] E.H. Lieb and J. Yngvason, *The physics and mathematics of the second law of thermodynamics*. Phys. Rep. **310**, 1–96 (1999). (Cited on page [130](#).)
- [Lio38] J. Liouville, *Sur la théorie de la variation des constantes arbitraires*. J. Math. Pures Appl. **3**, 342–349 (1838). (Cited on pages [127](#) and [162](#).)
- [Liu00] Y. Liu and M.E. Tuckerman, *Generalized Gaussian moment thermostating: a new continuous dynamical approach to the canonical ensemble*. J. Chem. Phys. **112**, 1685–1700 (2000). (Cited on pages [175](#) and [207](#).)
- [Llo94] J. Lloyd, L. Rondoni and G.P. Morriss, *Breakdown of ergodic behavior in the Lorentz gas*. Phys. Rev. E **50**, 3416–3421 (1994). (Cited on pages [147](#), [148](#), [153](#), [154](#), [155](#) and [156](#).)
- [Llo95] J. Lloyd, M. Niemeyer, L. Rondoni and G.P. Morriss, *The nonequilibrium Lorentz gas*. Chaos **5**, 536–551 (1995). (Cited on pages [147](#), [148](#), [151](#), [153](#), [154](#), [155](#), [156](#), [157](#), [158](#) and [159](#).)

-
- [Loo90] W. Loose and S. Hess, *Shear-induced ordering revisited*. in: M. Mareschal, Eds., *Microscopic Simulations of Complex Flows*, volume 236 of NATO Asi Series B, Plenum Press, New York, 1990. (Cited on page [225](#).)
- [Lor05] H.A. Lorentz, *The motion of electrons in metallic bodies*. Proc. Roy. Acad. Amst. **7**, 438–453 (1905). (Cited on pages [10](#), [99](#), [127](#) and [142](#).)
- [Lor91] A. Lorke, J.P. Kotthaus and K. Ploog, *Magnetotransport in two-dimensional superlattices*. Phys. Rev. B **44**, 3447–3450 (1991). (Cited on page [143](#).)
- [Luc93] J.M. Luck and A. Mehta, *Bouncing ball with a finite restitution: Chattering, locking, and chaos*. Phys. Rev. E **48**, 3988–3997 (1993). (Cited on pages [23](#) and [118](#).)
- [Lue93] A. Lue and H. Brenner, *Phase flow and statistical structure of Galton-board systems*. Phys. Rev. E **47**, 3128–3144 (1993). (Cited on pages [148](#), [153](#) and [156](#).)
- [Lyo85] S. K. Lyo and P. M. Richards, *Diffusion in a linear lattice with correlated random rates satisfying detailed balance*. Phys. Rev. B **32**, 301–304 (1985). (Cited on page [83](#).)
- [Mac59] J.A. MacLennan Jr., *Statistical mechanics of the steady state*. Phys. Rev. **115**, 1405–1409 (1959). (Cited on page [57](#).)
- [Mac83] J. Machta and R. Zwanzig, *Diffusion in a periodic Lorentz gas*. Phys. Rev. Lett. **50**, 1959–1962 (1983). (Cited on pages [22](#), [100](#), [107](#), [109](#), [110](#), [121](#), [144](#) and [158](#).)
- [Mac84] R.S. MacKay, J.D. Meiss and I.C. Percival, *Transport in Hamiltonian systems*. Physica D **13**, 55–81 (1984). (Cited on page [31](#).)
- [Mae99] C. Maes, *The fluctuation theorem as a Gibbs property*. J. Stat. Phys. **95**, 367–392 (1999). (Cited on page [15](#).)
- [Mae03a] C. Maes and K. Netocny, *Time-reversal and entropy*. J. Stat. Phys. **110**, 269–310 (2003). (Cited on pages [186](#) and [230](#).)
- [Mae03b] C. Maes, K. Netocny and M. Verschuere, *Heat conduction networks*. J. Stat. Phys. **111**, 1219–1244 (2003). (Cited on page [226](#).)
- [Man82] B.B. Mandelbrot, *The fractal geometry of nature*. (W.H. Freeman and Company, San Francisco, 1982). (Cited on pages [31](#) and [98](#).)
- [Mar86] S. Martin and W. Martienssen, *Circle maps and mode locking in the driven electrical conductivity of Barium Sodium Niobate crystals*. Phys. Rev. Lett. **52**, 1522–1525 (1986). (Cited on page [11](#).)
- [Mar89] J.M. Martinis and R.L. Kautz, *Classical phase diffusion in small hysteretic Josephson junctions*. Phys. Rev. Lett. **63**, 1507–1510 (1989). (Cited on page [11](#).)
- [Mar92a] M. Mareschal and B.L. Holian, Eds. *Microscopic simulations of complex hydrodynamic phenomena*, volume 292 of NATO ASI Series B: Physics, Plenum Press, New York, 1992. (Cited on pages [14](#) and [17](#).)

- [Mar92b] G.J. Martyna, M.L. Klein and M. Tuckerman, *Nosé-Hoover chains: the canonical ensemble via continuous dynamics*. J. Chem. Phys. **97**, 2635–2643 (1992). (Cited on pages [164](#), [175](#), [176](#), [177](#) and [207](#).)
- [Mar97] M. Mareschal, Eds. *The microscopic approach to complexity in non-equilibrium molecular simulations*, volume 240 of Physica A, North Holland, Amsterdam, 1997. (Cited on pages [14](#) and [17](#).)
- [Mar03] M. Mareschal and S. McNamara, *Lyapunov hydrodynamics in the dilute limit*. in print for the Physica D Special Issue Ref. [[Kla03b](#)], 2003. (Cited on page [15](#).)
- [Mat97] H. Matsuoka and R.F. Martin, *Long-time tails of the velocity autocorrelation functions for the triangular periodic Lorentz gas*. J. Stat. Phys **88**, 81–103 (1997). (Cited on pages [22](#) and [144](#).)
- [Mat01] L. Matyas, T. Tel and J. Vollmer, *Multibaker map for shear flow and viscous heating*. Phys. Rev. E **64**, 056106/1–11 (2001). (Cited on pages [10](#), [57](#) and [225](#).)
- [Mat03] L. Matyas and R. Klages, *Irregular diffusion in the bouncing ball billiard*. in print for the Physica D Special Issue Ref. [[Kla03b](#)], 2003. (Cited on pages [12](#), [16](#), [22](#) and [117](#).)
- [Max79] J.C. Maxwell, *On Boltzmann's Theorem on the average distribution in a system of material points*. Cam. Phil. Trans. **12**, 547 (1879). (Cited on page [140](#).)
- [Max65a] J.C. Maxwell, *Illustrations of the dynamical theory of gases*. in: S.G. Brush, Eds., Kinetic Theory, volume 1, pages 148–171, Pergamon Press, Oxford, 1965. (Cited on page [9](#).)
- [Max65b] J.C. Maxwell, *On the dynamical theory of gases*. in: S.G. Brush, Eds., Kinetic Theory, volume 2, pages 23–87, Pergamon Press, Oxford, 1965. (Cited on page [9](#).)
- [McN01] S. McNamara and M. Mareschal, *Origin of the hydrodynamic Lyapunov modes*. Phys. Rev. E **64**, 051103/1–14 (2001). (Cited on page [15](#).)
- [Meh90] A. Mehta and J.M. Luck, *Novel temporal behavior of a nonlinear dynamical system: The completely inelastic bouncing ball*. Phys. Rev. Lett. **65**, 393–396 (1990). (Cited on pages [23](#) and [118](#).)
- [Mei92] J.D. Meiss, *Symplectic maps, variational principles, and transport*. Rev. Mod. Phys. **64**, 795–848 (1992). (Cited on pages [31](#), [152](#), [168](#), [183](#) and [212](#).)
- [Men01] D. Mentrup and J. Schnack, *Nosé-Hoover dynamics for coherent states*. Physica A **297**, 337–347 (2001). (Cited on pages [163](#) and [251](#).)
- [Men03] D. Mentrup and J. Schnack, *Nosé-Hoover sampling of quantum entangled distribution functions*. Physica A **326**, 370–383 (2003). (Cited on pages [163](#) and [251](#).)
- [Met73] N. Metropolis, M.L. Stein and P.R. Stein, *On finite limit sets for transformations on the unit interval*. J. Combin. Theor. **15**, 25–44 (1973). (Cited on page [78](#).)

- [Met00] R. Metzler and J. Klafter, *The random walk's guide to anomalous diffusion: a fractional dynamics approach*. Phys. Rep. **339**, 1–77 (2000). (Cited on page [133](#).)
- [Mil98a] L. Milanovic, H.A. Posch and W.G. Hoover, *Lyapunov instability of two-dimensional fluids: Hard dumbbells*. Chaos **8**, 455–461 (1998). (Cited on page [14](#).)
- [Mil98b] L.J. Milanovic, H.A. Posch and W. Thirring, *Statistical mechanics and computer simulation of systems with attractive positive power-law potentials*. Phys. Rev. E **57**, 2763–2775 (1998). (Cited on page [140](#).)
- [Mil02] L. Milanovic and H.A. Posch, *Localized and delocalized modes in the tangent-space dynamics of planar hard dumbbell fluids*. J. Molec. Liqu. **96-97**, 221–244 (2002). (Cited on page [14](#).)
- [Mir83] R.F. Miracky, J. Clarke and R.H. Koch, *Chaotic noise observed in a resistively shunted self-resonant Josephson tunnel junction*. Phys. Rev. Lett. **50**, 856–859 (1983). (Cited on page [11](#).)
- [Mir85] R.F. Miracky, M.H. Devoret and J. Clarke, *Deterministic hopping in a Josephson circuit described by a one-dimensional mapping*. Phys. Rev. A **31**, 2509–2519 (1985). (Cited on page [73](#).)
- [Mis89] M. Misiurewicz, *Persistent rotation intervals for old maps*. in: Dynamical Systems and Ergodic Theory, volume 23 of Banach Center Publications, pages 119–124. (Polish Scientific Publishers, Warszawa, 1989). (Cited on page [27](#).)
- [MM01] C. Mejia-Monasterio, H. Larralde and F. Leyvraz, *Coupled normal heat and matter transport in a simple model system*. Phys. Rev. Lett. **86**, 5417–5420 (2001). (Cited on pages [148](#), [213](#), [226](#) and [249](#).)
- [Mor87a] B. Moran and W.G. Hoover, *Diffusion in a periodic Lorentz gas*. J. Stat. Phys. **48**, 709–726 (1987). (Cited on pages [14](#), [147](#), [148](#), [153](#), [154](#), [155](#), [157](#), [158](#) and [159](#).)
- [Mor87b] G.P. Morriss, *The information dimension of the nonequilibrium distribution function*. Phys. Lett. A **122**, 236–240 (1987). (Cited on pages [14](#), [153](#) and [225](#).)
- [Mor89a] G.P. Morriss, *Dimensional contraction in nonequilibrium systems*. Phys. Lett. A **134**, 307–313 (1989). (Cited on pages [14](#), [152](#), [153](#), [156](#), [225](#) and [231](#).)
- [Mor89b] G.P. Morriss, *Phase-space singularities in a planar Couette flow*. Phys. Rev. A **39**, 4811–4816 (1989). (Cited on pages [14](#), [153](#), [225](#) and [231](#).)
- [Mor89c] G.P. Morriss, D.J. Evans, E.G.D. Cohen and H. van Beijeren, *Linear response of phase-space trajectories to shearing*. Phys. Rev. Lett. **14**, 1579–1582 (1989). (Cited on pages [159](#) and [225](#).)
- [Mor94] G.P. Morriss and L. Rondoni, *Periodic orbit expansions for the Lorentz gas*. J. Stat. Phys. **75**, 553–584 (1994). (Cited on pages [22](#) and [158](#).)
- [Mor96a] G.P. Morriss, C.P. Dettmann and D.J. Isbister, *Field dependence of Lyapunov exponents for nonequilibrium systems*. Phys. Rev. E **54**, 4748–4754 (1996). (Cited on pages [147](#), [148](#), [151](#), [152](#) and [222](#).)

- [Mor96b] G.P. Morriss and L. Rondoni, *Equivalence of "nonequilibrium" ensembles for simple maps*. Physica A **233**, 767–784 (1996). (Cited on pages [128](#) and [190](#).)
- [Mor98] G.P. Morriss and C.P. Dettmann, *Thermostats: Analysis and application*. Chaos **8**, 321–336 (1998). (Cited on pages [12](#), [13](#), [14](#), [17](#), [127](#), [132](#), [148](#), [149](#), [150](#), [151](#), [152](#), [153](#), [154](#), [155](#), [156](#), [164](#), [169](#) and [170](#).)
- [Mor99] G.P. Morriss and L. Rondoni, *Definition of temperature in equilibrium and nonequilibrium systems*. Phys. Rev. E **59**, R5–R8 (1999). (Cited on page [132](#).)
- [Mor02] G.P. Morriss, *Conjugate pairing of Lyapunov exponents for isokinetic shear flow algorithms*. Phys. Rev. E **65**, 017201/1–3 (2002). (Cited on page [152](#).)
- [MT99] C.J. Mundy M.E. Tuckerman and G.J. Martyna, *On the classical statistical mechanics of non-Hamiltonian systems*. Europhys. Lett. **45**, 149–155 (1999). (Cited on page [162](#).)
- [Mun00] C.J. Mundy, S. Balasubramanian, K. Bagchi, M.E. Tuckerman, G.J. Martyna and M.L. Klein, *Nonequilibrium molecular dynamics*, volume 14 of Reviews in Computational Chemistry, chapter 5. (Wiley-VCH, New York, 2000). (Cited on pages [12](#), [13](#), [127](#), [162](#), [164](#), [175](#), [224](#) and [225](#).)
- [Nic96] G. Nicolis and D. Daems, *Nonequilibrium thermodynamics of dynamical systems*. J. Phys. Chem. **100**, 19187–19191 (1996). (Cited on pages [186](#), [195](#) and [208](#).)
- [Nic98] G. Nicolis and D. Daems, *Probabilistic and thermodynamic aspects of dynamical systems*. Chaos **8**, 311–320 (1998). (Cited on pages [17](#), [186](#), [195](#), [208](#) and [230](#).)
- [Nie98] S. Nielsen and R. Kapral, *Coloring a Lorentz gas*. J. Chem. Phys. **109**, 6460–6468 (1998). (Cited on page [21](#).)
- [Nos84a] S. Nosé, *A molecular dynamics method for simulations in the canonical ensemble*. Mol. Phys. **52**, 255–268 (1984). (Cited on pages [13](#), [14](#), [164](#), [165](#), [169](#), [170](#) and [174](#).)
- [Nos84b] S. Nosé, *A unified formulation of the constant temperature molecular dynamics methods*. J. Chem. Phys. **81**, 511–519 (1984). (Cited on pages [13](#), [14](#), [164](#), [166](#), [169](#), [170](#) and [173](#).)
- [Nos91] S. Nosé, *Molecular dynamics simulations at constant temperature and pressure*. in: M. Meyer and V. Pontikis, Eds., Computer Simulation in material science, pages 21–41. (Kluwer Academic Publishers, Netherlands, 1991). (Cited on pages [13](#), [133](#), [166](#), [170](#), [173](#) and [194](#).)
- [Nos93] S. Nosé, *Dynamical behavior of a thermostated isotropic harmonic oscillator*. Phys. Rev. E **47**, 164–177 (1993). (Cited on pages [164](#), [166](#), [170](#), [173](#) and [175](#).)
- [Ott93] E. Ott, *Chaos in Dynamical Systems*. (Cambridge University Press, Cambridge, 1993). (Cited on pages [17](#), [27](#), [28](#), [31](#), [73](#), [78](#), [144](#), [152](#), [153](#), [155](#), [183](#), [188](#), [191](#), [212](#) and [241](#).)

-
- [Pan02a] D. Panja, *An elementary proof of Lyapunov exponent pairing for hard-sphere systems at constant kinetic energy*. J. Stat. Phys. **109**, 705–727 (2002). (Cited on page [152](#).)
- [Pan02b] D. Panja and R. van Zon, *Lyapunov exponent pairing for a thermostatted hard-sphere gas under shear in the thermodynamic limit*. Phys. Rev. E **65**, 060102(R)/1–4 (2002). (Cited on page [152](#).)
- [Pan02c] D. Panja and R. van Zon, *Pairing of Lyapunov exponents for a hard-sphere gas under shear in the thermodynamic limit*. Phys. Rev. E **66**, 021101/1–12 (2002). (Cited on page [152](#).)
- [Pat88] R.K. Pathria, *Statistical mechanics*, volume 45 of International series in natural philosophy. (Pergamon press, Oxford, 1988). (Cited on pages [9](#), [13](#), [127](#), [133](#), [134](#), [158](#) and [162](#).)
- [Pei92] H.-O. Peitgen, H. Jürgens and D. Saupe, *Chaos and Fractals*. (Springer-Verlag, Berlin, 1992). (Cited on pages [27](#) and [31](#).)
- [Pen79] O. Penrose, *Foundations of statistical mechanics*. Rep. Prog. Phys. **42**, 1937–2006 (1979). (Cited on pages [9](#), [12](#), [13](#) and [185](#).)
- [Pet94] J. Petracic, D.J. Isbister and G.P. Morriss, *Correlation dimension of the sheared hard-disk Lorentz gas*. J. Stat. Phys. **76**, 1045–1063 (1994). (Cited on pages [153](#) and [225](#).)
- [Pie83] P. Pieranski, *Jumping particle model. Period doubling cascade in an experimental system*. J. Physique **44**, 573–578 (1983). (Cited on pages [23](#) and [118](#).)
- [Pie88] P. Pieranski, *Direct evidence for the suppression of period doubling in the bouncing-ball model*. Phys. Rev. A **37**, 1782–1785 (1988). (Cited on pages [23](#) and [118](#).)
- [Poi54] H. Poincaré, *Oeuvres I*. (Gauthier-Villiar, Paris, 1954). (Cited on page [35](#).)
- [Poo96] L. Poon, J. Campos, E. Ott and C. Grebogi, *Wada basin boundaries in chaotic scattering*. Int. J. Bif. Chaos **6**, 251–265 (1996). (Cited on page [112](#).)
- [Pop98] M.N. Popescu, Y. Braiman, F. Family and H.G.E. Hentschel, *Quenched disorder enhances chaotic diffusion*. Phys. Rev. E **58**, R4057–R4059 (1998). (Cited on page [81](#).)
- [Pop00] M.N. Popescu, C.M. Arizmendi, A.L. Salas-Brito and F. Family, *Disorder Induced Diffusive Transport in Ratchets*. Phys. Rev. Lett. **85**, 3321–3324 (2000). (Cited on page [81](#).)
- [Pos86] H.A. Posch, W.G. Hoover and F.J. Vesely, *Canonical dynamics of the Nosé oscillator: stability, order, and chaos*. Phys. Rev. A **33**, 4253–4265 (1986). (Cited on pages [164](#), [170](#) and [175](#).)
- [Pos87] H.A. Posch and W.G. Hoover, *Direct measurement of equilibrium and nonequilibrium Lyapunov spectra*. Phys. Lett. A **123**, 227–230 (1987). (Cited on pages [151](#), [153](#) and [156](#).)

- [Pos88] H.A. Posch and W.G. Hoover, *Lyapunov instability of dense Lennard-Jones fluids*. Phys. Rev. A **38**, 473–482 (1988). (Cited on pages [14](#), [132](#), [151](#), [152](#), [153](#), [156](#), [164](#), [167](#), [172](#), [174](#), [177](#), [185](#) and [219](#).)
- [Pos89] H.A. Posch and W.G. Hoover, *Equilibrium and nonequilibrium Lyapunov spectra for dense fluids and solids*. Phys. Rev. A **39**, 2175–2188 (1989). (Cited on pages [14](#), [153](#), [156](#), [164](#), [165](#), [172](#), [174](#), [209](#), [219](#), [224](#), [225](#) and [231](#).)
- [Pos97] H.A. Posch and W.G. Hoover, *Time-reversible dissipative attractors in three and four phase-space dimensions*. Phys. Rev. E **55**, 6803–6810 (1997). (Cited on pages [153](#), [156](#), [164](#), [175](#), [176](#), [177](#) and [207](#).)
- [Pos98] H.A. Posch and W.G. Hoover, *Heat conduction in one-dimensional chains and nonequilibrium Lyapunov spectrum*. Phys. Rev. E **58**, 4344–4350 (1998). (Cited on pages [128](#), [153](#), [194](#), [195](#) and [226](#).)
- [Pos00a] H.A. Posch and R. Hirschl, *Simulation of billiards and of hard body fluids*. in: Hard Ball Systems and the Lorentz Gas, pages 279–314. (2000). see Ref. [[Sza00](#)]. (Cited on page [14](#).)
- [Pos00b] H.A. Posch, R. Hirschl and W.G. Hoover, *Multifractal phase-space distributions for stationary nonequilibrium systems*. in: J. Karkheck, Eds., Dynamics: Models and Kinetic Methods for Non-equilibrium Many Body Systems, volume 371 of NATO Science Series E: Applied Sciences, pages 169–189, Kluwer, Dordrecht, 2000. (Cited on pages [194](#) and [195](#).)
- [Pos03] H.A. Posch and W.G. Hoover, *Large-system phase-space dimensionality loss in stationary heat flows*. in print for the Physica D Special Issue Ref. [[Kla03b](#)], 2003. (Cited on pages [172](#), [226](#) and [232](#).)
- [Pre92] W.H. Press, B.P. Flannery, S.A. Teukolsky and W.T. Vetterling, *Numerical recipes in FORTRAN*. (Cambridge University Press, 2nd edition edition, 1992). (Cited on page [211](#).)
- [Pre02] A. Prevost, D.A. Egolf and J. Urbach, *Forcing and velocity correlations in a vibrated granular monolayer*. Phys. Rev. Lett. **89**, 084301/1–4 (2002). (Cited on pages [12](#), [23](#), [117](#), [118](#) and [249](#).)
- [Rad96] G. Radons, *Suppression of chaotic diffusion by quenched disorder*. Phys. Rev. Lett. **77**, 4748–4751 (1996). (Cited on pages [11](#), [22](#), [81](#), [82](#), [84](#), [91](#) and [196](#).)
- [Rad97] G. Radons, *The thermodynamic formalism of random walks: Relevance for chaotic diffusion and multifractal measures*. Phys. Rep **290**, 67–79 (1997). (Cited on page [11](#).)
- [Rad99] G. Radons, *Disorder phenomena in chaotic systems*. Adv. Solid State Physics **38**, 439–451 (1999). (Cited on pages [11](#), [22](#), [81](#), [82](#) and [84](#).)
- [Rad03] G. Radons, *Anomalous Transport in Disordered Dynamical Systems*. in print for the Physica D Special Issue Ref. [[Kla03b](#)], 2003. (Cited on pages [11](#), [22](#), [81](#), [82](#) and [84](#).)

- [Ram86] J.D. Ramshaw, *Remarks on entropy and irreversibility in non-Hamiltonian systems*. Phys. Lett. A **116**, 110–114 (1986). (Cited on page 162.)
- [Ram02] J.D. Ramshaw, *Remarks on non-Hamiltonian statistical mechanics*. Europhys. Lett. **59**, 319–323 (2002). (Cited on pages 127, 162 and 163.)
- [Rat00a] K. Rateitschak, R. Klages and WG. Hoover, *The Nose-Hoover thermostated Lorentz gas*. J. Stat. Phys. **101**, 61–77 (2000). see also chao-dyn/9912018 for further details. (Cited on pages 16, 128, 130, 153, 165, 166, 167, 170, 171, 172, 173, 174, 204, 205, 206 and 219.)
- [Rat00b] K. Rateitschak, R. Klages and G. Nicolis, *Thermostating by deterministic scattering: the periodic Lorentz gas*. J. Stat. Phys. **99**, 1339–1364 (2000). (Cited on pages 16, 127, 128, 130, 140, 153, 158, 211, 212, 213, 214, 215, 217, 219, 220, 221 and 222.)
- [Rat01] K. Rateitschak, *Construction of nonequilibrium steady states: thermostating by deterministic scattering*. PhD thesis, Université Libre de Bruxelles, Faculté de Sciences, Center for Nonlinear Phenomena and Complex Systems, 2001. (Cited on page 130.)
- [Rat02] K. Rateitschak and R. Klages, *Lyapunov instability for a periodic Lorentz gas thermostated by deterministic scattering*. Phys. Rev. E **65**, 036209/1–11 (2002). (Cited on pages 16, 128, 130, 153, 212, 217, 218, 219, 220, 222 and 223.)
- [Rec80] A.B. Rechester and R.B. White, *Calculation of turbulent diffusion for the Chirikov-Taylor model*. Phys. Rev. Lett. **44**, 1586–1589 (1980). (Cited on page 249.)
- [Rec81] A.B. Rechester, M.N. Rosenbluth and R.B. White, *Fourier-space paths applied to the calculation of diffusion for the Chirikov-Taylor model*. Phys. Rev. A **23**, 2664–2672 (1981). (Cited on page 249.)
- [Rei65] F. Reif, *Fundamentals of statistical and thermal physics*. (McGraw-Hill, Auckland, 1965). see also the amended German translation: Statistische Physik und Theorie der Wärme, 3rd edition, de Gruyter, Berlin, 1987. (Cited on pages 9, 13, 17, 127, 131, 132, 133, 134, 151, 158, 162, 214 and 241.)
- [Rei94] P. Reimann, *Suppression of deterministic diffusion by noise*. Phys. Rev. E **50**, 727–735 (1994). (Cited on pages 11, 22, 73, 74, 75, 86, 87 and 92.)
- [Rei96a] P. Reimann, *Noisy one-dimensional maps near a crisis .1. Weak Gaussian white and colored noise*. J. Stat. Phys. **82**, 1467–1501 (1996). (Cited on pages 11, 22, 86, 87 and 92.)
- [Rei96b] P. Reimann, *Noisy one-dimensional maps near a crisis .2. General uncorrelated weak noise*. J. Stat. Phys. **85**, 403–425 (1996). (Cited on pages 11, 22, 86, 87 and 92.)
- [Rei98] P. Reimann, *Comment on "Toward a statistical thermodynamics of steady states"*. Phys. Rev. Lett. **80**, 4104 (1998). (Cited on page 162.)

- [Rei02] P. Reimann, *Brownian motors: noisy transport far from equilibrium*. Phys. Rep. **361**, 57–265 (2002). (Cited on pages [11](#) and [249](#).)
- [Rie00] J.P. Rieu, A. Upadhyaya, J.A. Glazier, N.B. Ouchi and Y. Sawada, *Diffusion and deformations of single Hydra cells in cellular aggregates*. Biophys. J. **79**, 1903–1914 (2000). (Cited on page [235](#).)
- [Ris96] D. Risso and P. Cordero, *Two-dimensional gas of disks: thermal conductivity*. J. Stat. Phys. **82**, 1453–1466 (1996). (Cited on page [227](#).)
- [Rob92] J.A.G. Roberts and G.R.W. Quispel, *Chaos and time-reversal symmetry: order and chaos in reversible dynamical systems*. Phys. Rep. **216**, 63–177 (1992). (Cited on pages [60](#), [61](#) and [183](#).)
- [Ron00a] L. Rondoni and E.G.D. Cohen, *Gibbs entropy and irreversible thermodynamics*. Nonlinearity **13**, 1905–1924 (2000). (Cited on page [10](#).)
- [Ron00b] L. Rondoni, T. Tél and J. Vollmer, *Fluctuation theorems for entropy production in open systems*. Phys. Rev. E **61**, R4679–R4682 (2000). (Cited on pages [15](#) and [183](#).)
- [Ron02a] L. Rondoni, *Deterministic thermostats and fluctuation relations*. in: Dynamics of dissipation, pages 35–61. (2002). see Ref. [[Gar02](#)]. (Cited on pages [12](#), [13](#), [15](#), [17](#), [127](#), [129](#), [149](#), [164](#), [170](#), [184](#) and [207](#).)
- [Ron02b] L. Rondoni and E.G.D. Cohen, *On some derivations of irreversible thermodynamics from dynamical systems theory*. Physica D **168-169**, 341–355 (2002). (Cited on page [10](#).)
- [Rou04] M. Rouijaa, C.A. Krülle, I. Rehberg, R. Grochowski and P. Walzel, *Transportverhalten und Strukturbildung granularer Materie auf Schwingförderern*. Chemie Ingenieur Technik **76**, 62–65 (2004). (Cited on pages [12](#) and [249](#).)
- [Rue71] D. Ruelle and F. Takens, *On the nature of turbulence*. Commun. Math. Phys. **20**, 167–192 (1971). (Cited on page [153](#).)
- [Rue78] D. Ruelle, *Thermodynamic Formalism*, volume 5 of Encyclopedia of mathematics and its applications. (Addison-Wesley, Reading, Mass., 1978). (Cited on page [9](#).)
- [Rue89] D. Ruelle, *The thermodynamic formalism for expanding maps*. Commun. Math. Phys. **125**, 239–262 (1989). (Cited on page [40](#).)
- [Rue96] D. Ruelle, *Positivity of entropy production in nonequilibrium statistical mechanics*. J. Stat. Phys. **85**, 1–23 (1996). (Cited on pages [13](#), [14](#), [128](#), [185](#), [186](#), [188](#), [189](#) and [191](#).)
- [Rue97a] D. Ruelle, *Entropy production in nonequilibrium statistical mechanics*. Commun. Math. Phys. **189**, 365–371 (1997). (Cited on pages [14](#) and [185](#).)
- [Rue97b] D. Ruelle, *Positivity of entropy production in the presence of a random thermostat*. J. Stat. Phys. **86**, 935–951 (1997). (Cited on pages [14](#) and [195](#).)

- [Rue99a] D. Ruelle, *Gaps and new ideas in our understanding of nonequilibrium*. Physica A **263**, 540–544 (1999). (Cited on page 13.)
- [Rue99b] D. Ruelle, *Smooth dynamics and new theoretical ideas in nonequilibrium statistical mechanics*. J. Stat. Phys. **95**, 393–468 (1999). (Cited on pages 9, 12, 13, 14, 15, 17, 127, 128, 152, 165, 185, 186 and 187.)
- [Rue03] D. Ruelle, *Extending the definition of entropy to nonequilibrium steady states*. Proc. Natl. Acad. Sci. **100**, 3054–3058 (2003). (Cited on pages 14 and 185.)
- [Rug97] H.H. Rugh, *Dynamical approach to temperature*. Phys. Rev. Lett. **78**, 772–775 (1997). (Cited on page 132.)
- [Sac98] A.S. Sachrajda, R. Ketzmerick, C. Gould, Y. Feng, P.J. Kelly, A. Delage and Z. Wasilewski, *Fractal conductance fluctuations in a soft-wall stadium and a Sinai billiard*. Phys. Rev. Lett. **80**, 1948–1951 (1998). (Cited on pages 12 and 250.)
- [Sak02] H. Sakaguchi, *Chaotic diffusion of particles with finite mass in oscillating convection flows*. Phys. Rev. E **65**, 067201/1–3 (2002). (Cited on page 73.)
- [San92] A. Santos, V. Garzó and J.J. Brey, *Comparison between the homogeneous-shear and the sliding-boundary methods to produce shear flow*. Phys. Rev. A **46**, 8018–8020 (1992). (Cited on pages 128 and 224.)
- [Sar92] S.S. Sarman, D.J. Evans and G.P. Morriss, *Conjugate-pairing rule and thermal-transport coefficients*. Phys. Rev. E **45**, 2233–2242 (1992). (Cited on pages 152, 225 and 231.)
- [Sar98] S.S. Sarman, D.J. Evans and P.T. Cummings, *Recent developments in non-Newtonian molecular dynamics*. Phys. Rep. **305**, 1–92 (1998). (Cited on pages 13, 128, 151, 152, 164, 225 and 226.)
- [Sch78] T. Schneider and E. Stoll, *Molecular-dynamics study of a three-dimensional one-component model for distortive phase transitions*. Phys. Rev. B **17**, 1302–1322 (1978). (Cited on pages 13 and 194.)
- [Sch82] M. Schell, S. Fraser and R. Kapral, *Diffusive dynamics in systems with translational symmetry: A one-dimensional-map model*. Phys. Rev. A **26**, 504–521 (1982). (Cited on pages 21, 22, 26, 31, 73, 74, 75, 78, 81 and 95.)
- [Sch89] H.G. Schuster, *Deterministic chaos*. (VCH Verlagsgesellschaft mbH, Weinheim, 2nd edition, 1989). (Cited on pages 11, 17, 144, 153, 175, 183 and 212.)
- [Sch93] M. Schienbein and H. Gruler, *Langevin equation, Fokker-Planck equation and cell migration*. Bull. Math. Biol. **55**, 585–608 (1993). (Cited on pages 129 and 235.)
- [Sch94] F. Schweitzer and L. Schimansky-Geier, *Clustering of “active” walkers in a two-component system*. Physica A **206**, 359–379 (1994). (Cited on page 235.)
- [Sch98] F. Schweitzer, W. Ebeling and B. Tilch, *Complex motion of Brownian particles with energy depots*. Phys. Rev. Lett. **80**, 5044–5047 (1998). (Cited on pages 129, 235 and 237.)

- [Sch01] F. Schweitzer, W. Ebeling and B. Tilch, *Statistical mechanics of canonical-dissipative systems and applications to swarm dynamics*. Phys. Rev. E **64**, 021110/1–12 (2001). (Cited on page [239](#).)
- [Sch03] J. Schumacher and B. Eckhardt, *Fluctuations of energy injection rate in a shear flow*. in print for the Physica D Special Issue Ref. [[Kla03b](#)], 2003. (Cited on page [15](#).)
- [Sea98] D.J. Searles, D.J. Evans and D.J. Isbister, *The conjugate-pairing rule for non-Hamiltonian systems*. Chaos **8**, 337–349 (1998). (Cited on pages [14](#), [152](#), [177](#), [219](#), [225](#) and [231](#).)
- [Sei33] W. Seidel, *Note on a metrically transitive system*. Proc. Nat. Acad. Sci. **19**, 453–456 (1933). (Cited on page [182](#).)
- [Ser01] A. Sergi and M. Ferrario, *Non-Hamiltonian equations of motion with a conserved energy*. Phys. Rev. E **64**, 056125/1–9 (2001). (Cited on pages [170](#), [175](#), [176](#) and [207](#).)
- [Ser03] A. Sergi, *Non-Hamiltonian equilibrium statistical mechanics*. Phys. Rev. E **67**, 021101/1–7 (2003). (Cited on pages [127](#), [162](#), [163](#) and [170](#).)
- [SG95] L. Schimansky-Geier, M. Mieth, H. Rost and H. Malchow, *Structure formation by active Brownian particles*. Phys. Lett. A **207**, 140–146 (1995). (Cited on page [235](#).)
- [Sin70] Ya.G. Sinai, *Dynamical systems with elastic reflections. Ergodic properties of dispersing billiards*. Russ. Math. Surv. **25**, 137–189 (1970). (Cited on pages [108](#) and [144](#).)
- [Sin91] Ya.G. Sinai, Eds., *Dynamical systems*. Number 1 in: Advanced series in nonlinear dynamics. (World Scientific, 1991). (Cited on page [9](#).)
- [Sin00] Ya.G. Sinai, Eds., *Dynamical systems, ergodic theory and applications*. Encyclopaedia of mathematical sciences. (Springer, Berlin, 2nd edition, 2000). (Cited on page [9](#).)
- [Sma80] S. Smale, *The mathematics of time*. (Springer, Berlin, 1980). (Cited on page [13](#).)
- [Sta89] J. Stachel, Eds., *The collected papers of Albert Einstein*, volume 2. (Princeton University Press, Princeton, 1989). (Cited on pages [26](#) and [133](#).)
- [Ste79] W.-H. Steeb, *Generalized Liouville equation, entropy, and dynamic systems containing limit cycles*. Physica **95A**, 181–190 (1979). (Cited on pages [127](#), [162](#) and [185](#).)
- [Ste80] W.-H. Steeb, *A comment on the generalized Liouville equation*. Found. Phys. **10**, 485–493 (1980). (Cited on pages [127](#) and [162](#).)
- [Sto91] C.L. Stokes and S.K. Williams D.A. Lauffenburger, *Migration of individual microvessel endothelial cells: stochastic model and parameter measurement*. J. Cell Science **99**, 419–430 (1991). (Cited on pages [129](#) and [235](#).)

-
- [Sto94] R. Stoop, *Bivariate free energy and anomalous diffusion*. Europhys. Lett. **25**, 99–104 (1994). (Cited on page 11.)
- [Sto95a] R. Stoop, *The diffusion-related entropy function: the enhanced case*. Europhys. Lett. **29**, 433–438 (1995). (Cited on page 11.)
- [Sto95b] R. Stoop, *Thermodynamic approach to deterministic diffusion of mixed enhanced-dispersive type*. Phys. Rev. Lett. **52**, 2216–2219 (1995). (Cited on page 11.)
- [Sto95c] R. Stoop, W.-H. Steeb and G. Radons, *A new characterization of deterministic diffusion: Diffusion-related entropy functions*. Phys. Lett. A **202**, 195–200 (1995). (Cited on page 11.)
- [Stu99] A.M. Stuart and J.O. Warren, *Analysis and experiments for a computational model of a heat bath*. J. Stat. Phys. **97**, 687–723 (1999). (Cited on pages 13 and 134.)
- [Sza00] D. Szasz, Eds., *Hard-Ball Systems and the Lorentz gas*, volume 101 of Encyclopedia of mathematical sciences. (Springer, Berlin, 2000). (Cited on pages 10, 17, 127, 145, 263, 286 and 292.)
- [Tan02a] T. Taniguchi, C.P. Dettmann and G.P. Morriss, *Lyapunov spectra of periodic orbits for a many-particle system*. J. Stat. Phys. **109**, 747–764 (2002). (Cited on page 15.)
- [Tan02b] T. Taniguchi and G.M. Morriss, *Master equation approach to the conjugate pairing rule of Lyapunov spectra for many-particle thermostated systems*. Phys. Rev. E **66**, 066203/1–11 (2002). (Cited on page 152.)
- [Tan02c] T. Taniguchi and G.P. Morriss, *Stepwise structure of Lyapunov spectra for many-particle systems using a random matrix dynamics*. Phys. Rev. E **65**, 056202/1–15 (2002). (Cited on page 15.)
- [Tan02d] K.I. Tanimoto, T. Kato and K. Nakamura, *Phase dynamics in SQUID's: Anomalous diffusion and irregular energy dependence of diffusion coefficients*. Phys. Rev. B **66**, 012507/1–4 (2002). (Cited on pages 11, 73 and 249.)
- [Tas94] S. Tasaki and P. Gaspard, *Fractal distribution and Fick's law in a reversible chaotic system*. in: M. Yamaguti, Eds., *Towards the Harnessing of Chaos*, pages 273–288. (Elsevier, Amsterdam, 1994). (Cited on pages 54 and 57.)
- [Tas95] S. Tasaki and P. Gaspard, *Fick's law and fractality of nonequilibrium stationary states in a reversible multibaker map*. J. Stat. Phys. **81**, 935–987 (1995). (Cited on pages 21, 54, 57 and 183.)
- [Tas99] S. Tasaki and P. Gaspard, *Thermodynamic behavior of an area-preserving multibaker map*. Theoret. Chem. Acc. **102**, 385–396 (1999). (Cited on pages 10, 57, 183 and 186.)
- [Tas00] S. Tasaki and P. Gaspard, *Entropy production and transports in a conservative multibaker map with energy*. J. Stat. Phys. **101**, 125–144 (2000). (Cited on pages 10, 57, 183 and 186.)

- [Tel96] T. Tel, J. Vollmer and W. Breymann, *Transient chaos: The origin of transport in driven systems*. Europhys. Lett. **35**, 659–664 (1996). (Cited on pages [10](#), [14](#), [57](#), [128](#), [153](#), [183](#), [190](#) and [191](#).)
- [Tel98] T. Tel, P. Gaspard and G. Nicolis, Eds. *Chaos and irreversibility*, volume 8 of Chaos, American Institute of Physics, College Park, 1998. (Cited on pages [14](#) and [17](#).)
- [Tel00] T. Tel and J. Vollmer, *Entropy balance, multibaker maps, and the dynamics of the Lorentz gas*. in: Hard Ball Systems and the Lorentz Gas, pages 367–420. (2000). see Ref. [[Sza00](#)]. (Cited on pages [10](#), [57](#), [128](#), [148](#), [153](#), [158](#), [183](#), [186](#), [187](#), [190](#) and [230](#).)
- [Tel01] T. Tel, J. Vollmer and L. Matyas, *Shear flow, viscous heating, and entropy balance from dynamical systems*. Europhys. Lett. **53**, 458–464 (2001). (Cited on page [225](#).)
- [Tel02] T. Tel, J. Vollmer and L. Matyas, *Comments on the paper ‘Particles, maps and irreversible thermodynamics’ by E.G.D. Cohen and L.Rondoni, Physica A 306 (2002) 117*. Physica A **323**, 323–326 (2002). (Cited on page [10](#).)
- [Ten82] A. Tenenbaum, G. Ciccotti and R. Gallico, *Stationary nonequilibrium states by molecular dynamics. Fourier’s law*. Phys. Rev. A **25**, 2778–2787 (1982). (Cited on pages [13](#), [128](#), [194](#), [210](#) and [226](#).)
- [Tho83] S. Thomae, *Chaos-induced diffusion*. in: C. Benedek et al., Eds., Statics and Dynamics of nonlinear systems, pages 204–210, Springer, Berlin, 1983. (Cited on page [27](#).)
- [Til99] B. Tilch, F. Schweitzer and W. Ebeling, *Directed motion of Brownian particles with internal energy depot*. Physica A **273**, 294–314 (1999). (Cited on pages [129](#), [235](#), [237](#) and [239](#).)
- [Tol38] R.C. Tolman, *The principles of statistical mechanics*. (Oxford University Press, New York, 1938). reprinted by Dover, New York, 1979. (Cited on page [9](#).)
- [Tri95] C. Tricot, *Curves and fractal dimension*. (Springer, Berlin, 1995). (Cited on page [31](#).)
- [Tse94] H.C. Tseng, H.J. Chen, P.C.Li, W.Y.Lai, C. H.Chou and H. W.Chen, *Some exact results for the diffusion coefficients of maps with pruning cycles*. Phys. Lett. A **195**, 74–80 (1994). (Cited on pages [11](#), [26](#) and [82](#).)
- [Tse99] H.-C. Tseng and H.-J. Chen, *The effects of quenched disorder on the chaotic diffusion for simple maps*. Int. J. Mod. Phys. **13**, 83–95 (1999). (Cited on pages [81](#) and [82](#).)
- [Tse00] H.-C. Tseng, P.-R. Huang, H.-J. Chen and C.-K. Hu, *The diffusion behavior of a simple map with periodic quenched disorder*. Physica A **281**, 323–336 (2000). (Cited on pages [81](#) and [82](#).)

-
- [Tuc97] M.E. Tuckerman, C.J. Mundy and M.L. Klein, *Toward a statistical thermodynamics of steady states*. Phys. Rev. Lett. **78**, 2042–2045 (1997). (Cited on page 162.)
- [Tuc98a] M.E. Tuckerman, C.J. Mundy, S. Balasubramanian and M.L. Klein, *Response to “Comment on ‘Modified nonequilibrium molecular dynamics for fluid flows with energy conservation’ ”*. J. Chem. Phys. **108**, 4353–4354 (1998). (Cited on page 162.)
- [Tuc98b] M.E. Tuckerman, C.J. Mundy and M.L. Klein, *Reply to comments on “Toward a statistical thermodynamics of steady states”*. Phys. Rev. Lett. **80**, 4105–4106 (1998). (Cited on page 162.)
- [Tuc00] M.E. Tuckerman and G.J. Martyna, *Understanding modern molecular dynamics: techniques and applications*. J. Phys. Chem. B **104**, 159–178 (2000). (Cited on pages 12, 14, 133, 162, 165, 176 and 207.)
- [Tuf92] N.B. Tuffillaro, T. Abbott and J. Reilly, *An experimental approach to nonlinear dynamics and chaos*. (Add. Wesley Publ., New York, 1992). (Cited on pages 23, 118 and 119.)
- [Uff01] J. Uffink, *Bluff your way in the Second Law of Thermodynamics*. Stud. Hist. Philos. M. P. **32B**, 305–394 (2001). (Cited on page 17.)
- [Upa01] A. Upadhyaya, J.P. Rieu, J.A. Glazier and Y. Sawada, *Anomalous diffusion and non-Gaussian velocity distributions of Hydra cells in cellular aggregates*. Physica A **293**, 549–558 (2001). (Cited on page 235.)
- [Van92] W.N. Vance, *Unstable periodic orbits and transport properties of nonequilibrium steady states*. Phys. Rev. Lett. **69**, 1356–1359 (1992). (Cited on pages 14, 148, 151, 153, 157 and 191.)
- [vB95] H. van Beijeren and J.R. Dorfman, *Lyapunov exponents and KS entropy for the Lorentz gas at low densities*. Phys. Rev. Lett. **74**, 4412–4415 (1995). (Cited on pages 14, 81, 145 and 196.)
- [vB96] H. van Beijeren, J.R. Dorfman, E.G.D. Cohen, H.A. Posch and C. Dellago, *Lyapunov exponents from kinetic theory for a dilute, field-driven Lorentz gas*. Phys. Rev. Lett. **77**, 1974–1977 (1996). (Cited on pages 14, 152 and 196.)
- [vB97] H. van Beijeren, J.R. Dorfman, H.A. Posch and C. Dellago, *Kolmogorov-Sinai entropy for dilute gases in equilibrium*. Phys. Rev. E **56**, 5272–5277 (1997). (Cited on pages 14, 145 and 196.)
- [vB98] H. van Beijeren, A. Latz and J.R. Dorfman, *Chaotic properties of dilute two- and three-dimensional random Lorentz gases: Equilibrium systems*. Phys. Rev. E **57**, 4077–4094 (1998). (Cited on pages 14, 81, 145, 152 and 196.)
- [vB00a] H. van Beijeren and J.R. Dorfman, *On thermostats and entropy production*. Physica A **279**, 21–29 (2000). (Cited on page 208.)
- [vB00b] H. van Beijeren, A. Latz and J.R. Dorfman, *Chaotic properties of dilute two- and three-dimensional random Lorentz gases. II. Open systems*. Phys. Rev. E **63**, 016312/1–14 (2000). (Cited on pages 14, 152 and 196.)

- [Vis03a] S. Viscardy and P. Gaspard, *Viscosity in molecular dynamics with periodic boundary conditions*. Phys. Rev. E **68**, 041204/1–10 (2003). (Cited on page 249.)
- [Vis03b] S. Viscardy and P. Gaspard, *Viscosity in the escape-rate formalism*. preprint cond-mat/0309432, to appear in Phys. Rev. E, 2003. (Cited on page 249.)
- [vK71] N. van Kampen, *The case against linear response theory*. Physica Norvegica **5**, 279–284 (1971). (Cited on page 159.)
- [vK92] N. van Kampen, *Stochastic processes in physics and chemistry*. (North Holland, Amsterdam, 1992). (Cited on pages 26, 27, 28, 35, 127, 133, 138 and 141.)
- [Vol97] J. Vollmer, T. Tél and W. Breymann, *Equivalence of irreversible entropy production in driven systems: an elementary chaotic map approach*. Phys. Rev. Lett. **79**, 2759–2762 (1997). (Cited on pages 10, 57, 128, 151, 183, 186, 190 and 230.)
- [Vol98] J. Vollmer, T. Tél and W. Breymann, *Entropy balance in the presence of drift and diffusion currents: an elementary chaotic map approach*. Phys. Rev. E **58**, 1672–1684 (1998). (Cited on pages 10, 57, 128, 183, 186, 190 and 230.)
- [Vol00] J. Vollmer, T. Tél and L. Matyas, *Modeling thermostating, entropy currents, and cross effects by dynamical systems*. J. Stat. Phys. **101**, 79–105 (2000). (Cited on pages 10, 57, 128 and 183.)
- [Vol02] J. Vollmer, *Chaos, spatial extension, transport, and non-equilibrium thermodynamics*. Phys. Rep. **372**, 131–267 (2002). (Cited on pages 10, 17, 57, 61, 128, 148, 153, 158, 183, 186, 187, 190 and 230.)
- [Vol03] J. Vollmer, T. Tel and W. Breymann, *Dynamical-system models of transport: chaos characteristics, the macroscopic limit, and irreversibility*. in print for the Physica D Special Issue Ref. [Kla03b], 2003. (Cited on pages 10, 57, 128, 151, 183, 186 and 190.)
- [vZ98] R. van Zon, R. van Beijeren and C. Dellago, *Largest Lyapunov Exponent for many particle systems at low densities*. Phys. Rev. Lett. **80**, 2035–2038 (1998). (Cited on page 14.)
- [vZ99] R. van Zon, *Kinetic approach to the Gaussian thermostat in a dilute sheared gas in the thermodynamic limit*. Phys. Rev. E **60**, 4158–4163 (1999). (Cited on page 128.)
- [Wac99] R. Wackerbauer, *When noise decreases deterministic diffusion*. Phys. Rev. E **59**, 2872–2879 (1999). (Cited on pages 11, 86 and 87.)
- [Wag99] C. Wagner, R. Klages and G. Nicolis, *Thermostating by deterministic scattering: Heat and shear flow*. Phys. Rev. E **60**, 1401–1411 (1999). (Cited on pages 16, 128, 130, 177, 194, 195, 210, 211, 212, 215, 219, 224, 226, 227, 228, 229 and 230.)
- [Wag00] C. Wagner, *Lyapunov instability for a hard-disk fluid in equilibrium and nonequilibrium thermostated by deterministic scattering*. J. Stat. Phys. **98**, 723–742 (2000). (Cited on pages 16, 128, 153, 177, 212, 224, 231, 232 and 233.)

-
- [Wan66] G.H. Wannier, *Statistical Physics*. (Dover, New York, 1966). (Cited on pages 9 and 151.)
- [Wan02] G.M. Wang, E.M. Sevick, E. Mittag, D.J. Searles and D.J. Evans, *Experimental demonstration of violations of the second law of thermodynamics for small systems and short time scales*. Phys. Rev. Lett. **89**, 050601/1–4 (2002). (Cited on page 15.)
- [War95] S. Warr and J.M. Huntley, *Energy input and scaling laws for a single particle vibrating in one dimension*. Phys. Rev. E **52**, 5596–5601 (1995). (Cited on page 121.)
- [Wax54] N. Wax, *Selected papers on noise and stochastic processes*. (Dover, New York, 1954). (Cited on pages 13, 26, 27, 127, 133, 134 and 141.)
- [Wei86] G.H. Weiss, *Overview of theoretical models for reaction rates*. J. Stat. Phys. **42**, 3–36 (1986). (Cited on page 54.)
- [Wei91] D. Weiss, M.L. Roukes, A. Menschig, P. Grambow, K. von Klitzing and G. Weimann, *Electron pinball and commensurate orbits in a periodic array of scatterers*. Phys. Rev. Lett. **66**, 2790–2793 (1991). (Cited on pages 12, 143 and 249.)
- [Wei94] G.H. Weiss, *Aspects and applications of the random walk*. (North-Holland, Amsterdam, 1994). (Cited on pages 81 and 83.)
- [Wei95] D. Weiss and K. Richter, *Antidot-Übergitter: Flippern mit Elektronen*. Physikalische Blätter **51**, 171–176 (1995). (Cited on pages 12 and 249.)
- [Wei97] D. Weiss, G. Lutjering and K. Richter, *Chaotic electron motion in macroscopic and mesoscopic antidot lattices*. Chaos, Solitons and Fractals **8**, 1337–1357 (1997). (Cited on pages 12, 143 and 249.)
- [Wei00] S. Weiss, D. Koelle, J. Müller, R. Gross and K. Barthel, *Ratchet effect in dc SQUIDS*. Europhys. Lett. **51**, 499–505 (2000). (Cited on pages 11 and 249.)
- [Wie01] J. Wiersig and K.-H. Ahn, *Devil's staircase in the magnetoresistance of a periodic array of scatterers*. Phys. Rev. Lett. **87**, 026803/1–4 (2001). (Cited on pages 12 and 249.)
- [Wig92] S. Wiggins, *Chaotic transport in dynamical systems*, volume 2 of Interdisciplinary Applied Mathematics. (Springer, New York, 1992). (Cited on page 31.)
- [Win92] R.G. Winkler, *Extended-phase-space isothermal molecular dynamics: canonical harmonic oscillator*. Phys. Rev. A **45**, 2250–2255 (1992). (Cited on pages 175, 176 and 207.)
- [Win95] R.G. Winkler, V. Kraus and P. Reineker, *Time reversible and phase-space conserving molecular dynamics at constant temperature*. J. Chem. Phys. **102**, 9018–9025 (1995). (Cited on pages 175, 176 and 207.)
- [Woj98] M.P. Wojtkowski and C. Liverani, *Conformally symplectic dynamics and symmetry of the Lyapunov spectrum*. Commun. Math. Phys. **194**, 47–60 (1998). (Cited on page 152.)

- [Woj02] D.K. Wojcik and J.R. Dorfman, *Quantum multibaker maps: extreme quantum regime*. Phys. Rev. E **66**, 36110/1–16 (2002). (Cited on pages [183](#) and [249](#).)
- [Woj03a] D.K. Wojcik and J. R. Dorfman, *Crossover from diffusive to ballistic transport in periodic quantum maps*. in print for the Physica D Special Issue Ref. [[Kla03b](#)], 2003. (Cited on page [249](#).)
- [Woj03b] D.K. Wojcik and J.R. Dorfman, *Diffusive-ballistic crossover in 1D quantum walks*. Phys. Rev. Lett. **90**, 230602/1–4 (2003). (Cited on pages [183](#) and [249](#).)
- [Wol85] A. Wolf, J.B. Swift, H.L. Swinney and J.A. Vastano, *Determining the Ljapunov exponents from a time series*. Physica D **16**, 285–317 (1985). (Cited on page [152](#).)
- [Yor85] J.A. Yorke, C. Grebogi, E. Ott and L. Tedeschini-Lalli, *Scaling behavior of windows in dissipative dynamical systems*. Phys. Rev. Lett. **54**, 1095–1098 (1985). (Cited on page [78](#).)
- [You02] L.-S. Young, *What are SRB measures, and which dynamical systems have them?* J. Stat. Phys. **108**, 733–754 (2002). (Cited on pages [9](#) and [187](#).)
- [Zha92] K. Zhang and K. Zhang, *Mechanical models of Maxwell’s demon with noninvariant phase volume*. Phys. Rev. A **46**, 4598–4605 (1992). (Cited on pages [207](#) and [226](#).)
- [Zwa73] R. Zwanzig, *Nonlinear generalized Langevin equations*. J. Stat. Phys. **9**, 215–220 (1973). (Cited on pages [13](#) and [134](#).)
- [Zwa82] R. Zwanzig, *Non-Markoffian diffusion in a one-dimensional disordered lattice*. J. Stat. Phys. **28**, 127–133 (1982). (Cited on page [83](#).)
- [Zwa01] R. Zwanzig, *Nonequilibrium statistical mechanics*. (Oxford University Press, Oxford, 2001). (Cited on pages [13](#), [127](#), [134](#) and [135](#).)

Declaration

Herewith I declare that this habilitation thesis was written only by myself and without any other auxiliary means than those indicated in my work. Passages that have been included, word for word or according to their contents, from other sources have been marked respectively. As far as the research presented in this thesis was performed together with other colleagues or coworkers, I have included respective hints.

I did not attempt any habilitation at another university up to now.

I have filed for a police document that shall be sent to the faculty in due time.

Erklärung

Hiermit erkläre ich, dass ich meine Habilitationsschrift selbst und ohne andere als die darin angegebenen Hilfsmittel angefertigt habe. Wörtlich oder inhaltlich übernommene Stellen wurden als solche gekennzeichnet. Gemeinschaftliche Arbeiten wurden ebenfalls als solche explizit angegeben.

Ein früheres Habilitationsgesuch an einer anderen Universität ist nicht erfolgt.

Ein der Fakultät zu übersendendes polizeiliches Führungszeugnis wurde bei der zuständigen Meldestelle beantragt.